

LOW CYCLE FATIGUE OF FPSO SHIP STRUCTURE

BY

AHMED MEGHARBI

**A THESIS SUBMITTED FOR THE DEGREE OF DOCTOR OF
PHILOSOPHY (PhD) AT NEWCASTLE UNIVERSITY**

**SCHOOL OF MARINE SCIENCE AND TECHNOLOGY, FACULTY
OF SCIENCE, AGRICULTURE AND ENGINEERING**



December 2014

DEDICATION

To my father who was always proud of his son and consistent in his follow-up of my research progress over the years until he passed away on 19th July 2010, and to my beloved mother who always remembers me in her prayers; may Allah grant here long, blessed and healthy life.

"My Lord, have mercy upon them as they brought me up [when I was] little." 17-24

ABSTRACT

The phenomenon of low cycle fatigue (LCF) is characterised by high stress range, close to or above yield, and relatively low number of cycles to failure, typically below 10^4 . In the case of tankers and Floating, Production, Storage and Offloading units (FPSO), nominal stress amplitudes lower than the yield stress may result in plastic strains due to the high stress concentrations that are typical in many of the hulls' structural details. FPSOs are more susceptible to damage due to LCF compared to tankers, cargo and other ocean going ships. The main reasons are; the unique structure of FPSO in terms of the presence of internal turret and topsides load which affects the structural response of FPSO to dynamic and quasi-static loads, the frequent loading and unloading patterns of FPSO (i.e. unlike oil tankers which are either in full load or ballast condition) which causes the FPSO to experience the maximum hogging and sagging still water bending moment every single cycle and the condition of the sea at which the FPSO is operating (site specific environment) where even benign condition may subject the FPSO to extremely diverse wave induced loads.

An increasing number of FPSOs are being used in the oil and gas industry due to the practical advantages they offer as compared to fixed installations, however, many FPSO show signs of cracks at critical locations in the first five years of service. It is believed that this is primarily due to LCF. It is therefore imperative to address LCF at the design stage. Finite Element Analysis (FEA) has been used to demonstrate that extremely high stress levels, exceeding three times the yield stress of the material, may occur at some critical locations during FPSO operations. Due to this 'new' form of damage in ship structures classification societies, shipyards and other organizations are addressing the issue of LCF by issuing various guidance notes and recommended practices in order to assess the damage due to LCF.

This research contains a very extensive and useful literature review of the state-of-the-art in LCF assessment methods available in literature and various class societies. Representative operational loading conditions (most onerous) have been presented for LCF Assessment of FPSO. LCF tests of typical longitudinal attachment were performed. This important structural element is seldom tested compared to the transverse attachment or cruciform. Experimental and numerical results compare well. A novel method of predicting LCF life has been proposed and a new S-N curve is proposed to be used for LCF assessment.

ACKNOWLEDGMENT

All praise is due to ALLAH and may the peace and blessings be upon his prophet Mohammad.

Special thanks are due to:

My mentor at BP Shipping Technical Authority (former line manager at Lloyd's Register), Dr Alwyn Mcleary who was behind the choice of the research topic and for his guidance and support.

My tutors Professor Bob Dow and Dr Yongchang Pu at Newcastle University who played a crucial role in this research with their guidance and support.

My mentors at Lloyd's Register, Dr Helena Polezhayeva, Principal Specialist at London Design Support Structural Analysis Services and Dr Mohammed Sarumi, Lead Structures and Pipeline Specialist at the FE Modelling Team, Aberdeen. I acknowledge the efforts of both who devoted their time towards this research and played a major mentoring role.

I would like to express my gratitude to Dr Min Xie, Satheesh Manayankath, Mozahid Sufyan and Dr Harvinder Sehmi who assisted at different stages towards my understanding of the topic, Naval Architect terminology and relevant software. Also, I would like to express my gratitude and appreciation to Dr Manoj Kumar who coordinated the fatigue testing and also for his advice and support.

I am also indebted to my lovely wife Rabiaa for her exceptional support, encouragement and patience and my children Mohammad, Mahmood, Fatima, Al-Houssen, Al-Hassan and Mohsen who kept me smiling even in difficult times.

Thanks are also due to my brothers, sisters and extended family in Libya.

DECLARATION

All work included in this research is believed to be original work of the author unless stated otherwise.

.....

Table of Contents

1	Chapter 1. Introduction	26
1.1	Research Background and Subject Matter	26
1.2	Objectives and Methodology	27
1.3	Thesis Scope and Structure	27
1.4	Phenomenon of LCF	28
1.5	Failures Caused by LCF.....	29
1.6	Introduction to FPSO	31
1.6.1	<i>Marine/Oil and Gas</i>	31
1.6.2	<i>FPSO Construction Type</i>	32
1.6.3	<i>Difference between an Oil Tanker and a FPSO.....</i>	34
1.6.3.1	<i>FPSO Structure</i>	34
1.6.3.2	<i>Fatigue Hot Spots and Critical locations.....</i>	37
1.6.3.3	<i>The Effects of conversion on fatigue</i>	39
1.6.4	<i>Loading and Strength of FPSO vs. Oil Tankers.....</i>	41
1.6.4.1	<i>Static and dynamic loads</i>	41
1.6.4.2	<i>Still Water Bending Moment</i>	42
1.6.4.3	<i>Vertical Wave Bending Moment.....</i>	44
1.6.4.4	<i>Combined SWBM and VWBM.....</i>	45
1.7	Fatigue Analysis.....	47
1.8	Conclusions.....	48
2	CHAPTER 2: Literature Review	51
2.1	Introduction.....	51
2.1.1	<i>Notch Effect, Energy Criteria and Cyclic Deformation.....</i>	52
2.1.1.1	Elastic plastic stress strain relations	55
2.1.1.2	Notch correction for uniaxial loading	56
2.1.1.3	Neuber's Rule	57
2.1.1.3.1	Neuber's Rule and Ramberg Osgood relations combined	59
2.1.2	<i>Factors Affecting LCF</i>	60
2.1.3	<i>Fatigue Life Prediction</i>	61
2.1.4	<i>Combined HCF and LCF</i>	66
2.1.5	<i>Testing of Welded Joints</i>	69
2.1.6	<i>Reliability</i>	74
2.2	The Fundamental Theory of LCF	74

2.2.1	<i>Stress concentration factor (SCF)</i>	74
2.2.2	<i>Fatigue notch factor</i>	76
2.2.3	<i>Approximations</i>	83
2.2.3.1	<i>Example of Local stress strain value according to Neuber</i>	87
2.2.4	<i>Cyclic Loading</i>	90
2.2.4.1	<i>Cyclic Strain Hardening and Softening Materials</i>	90
2.2.4.2	<i>Application of Cyclic Strain Approach to ship structural detail</i>	92
2.2.4.3	<i>Cyclic stress strain diagram</i>	99
2.2.4.4	<i>Bauschinger effect</i>	100
2.2.5	<i>Material Fatigue Criteria</i>	108
2.2.6	<i>Strain Life Criteria</i>	110
2.2.7	<i>Fatigue Life Prediction</i>	113
2.2.7.1	<i>General</i>	113
2.2.7.2	<i>Material Notch Sensitivity</i>	120
2.2.8	<i>Cumulative Fatigue</i>	121
2.2.8.1	<i>Rain flow counting method</i>	125
2.2.9	<i>Laws governing HCF and LCF</i>	128
2.3	<i>The Phenomena of LCF in a Ship Structure</i>	129
2.3.1	<i>Fatigue Damage</i>	129
2.3.2	<i>Main factors affecting fatigue damage</i>	131
2.3.2.1	<i>Service loading</i>	133
2.3.2.2	<i>Residual welding stresses</i>	135
2.4	<i>LCF Assessment</i>	141
2.4.1	<i>Work of ISSC Committee Ill.2: Fatigue and Fracture</i>	141
2.4.1.1	<i>Probabilistic Approach</i>	145
2.4.1.1.1	<i>Probabilistic S – N Approach</i>	145
2.4.1.1.2	<i>Probabilistic Fracture Mechanics Approach</i>	145
2.4.1.1.3	<i>Multiaxial Fatigue</i>	145
2.4.1.2	<i>Fatigue analysis methodologies used for Stress Response Assessment</i>	145
2.4.1.3	<i>Additional Rules and Recommendations for FPSOs</i>	146
2.4.1.4	<i>Methods to Calculate Damage due to combined Low Frequency and High Frequency load</i>	147
2.4.1.4.1	<i>Combined Spectrum Method</i>	147
2.4.1.4.2	<i>Modified Combined Spectrum Method</i>	148
2.4.1.4.3	<i>Simplified Analytical Method</i>	148

2.4.1.5	Benchmark Studies	149
2.4.1.6	HSE LCF Review.....	151
2.4.2	<i>Local Approaches (State of the Art)</i>	151
2.4.2.1	Global and local approaches	155
2.4.2.2	Notch root approach.....	156
2.4.2.3	Comparison of Approaches.....	158
2.4.2.4	Peculiarities of welded structures.....	159
2.4.2.5	Structural stress and strain approaches	159
2.4.2.5.1	Structural strain approach according to Haibach	159
2.4.2.5.2	Structural stress approach according to Dijkstra and Gurney	159
2.4.2.6	Structural stress concept codified procedure.....	162
2.4.2.6.1	Internal linearization	163
2.4.2.6.2	Modified internal linearization.....	164
2.4.2.6.3	Unconventional structural stress concept.....	165
2.4.2.7	Notch stress or strain codified procedure.....	166
2.4.2.7.1	Modification of the notch stress concept in IIW Recommendations	167
2.5	Conclusions.....	169
3	CHAPTER 3: LCF in IIW (State of the Art)	171
3.1	IIW HCF	171
3.1.1	<i>Effective Notch Stress (HCF)</i>	172
3.2	Effective Notch Strain (LCF).....	177
3.3	Effective Notch Strain Application.....	182
3.4	Conclusion	184
4	CHAPTER 4: LCF in Class Societies (State of the Art)	187
4.1	DNV, Daewoo Shipbuilding & Marine Engineering Co., Ltd (DSME) and Inha University.....	187
4.1.1	<i>Strain Life Method</i>	188
4.1.2	<i>Equivalent Elastic Notch Stress and Pseudo Stress</i>	188
4.1.3	<i>Plasticity Correction</i>	189
4.2	S-N Curve Applied for LCF.....	190
4.3	Lloyd's Register and Glasgow & Strathclyde Universities	194
4.3.1	<i>Simplified LCF Assessment</i>	194
4.3.2	<i>LCF Fatigue Damage</i>	195
4.3.3	<i>Combining LCF and HCF</i>	199
4.4	Class Societies LCF Procedures Overview.....	199

4.4.1	<i>American Bureau of Shipping</i>	199
4.4.1.1	<i>Loading Conditions</i>	199
4.4.1.2	<i>Load Cases</i>	200
4.4.1.3	<i>Structural Details</i>	200
4.4.1.3.1	<i>Loads considered for High Cycle (Dynamic Loads)</i>	200
4.4.1.3.2	<i>Loads considered for Low Cycle (Static Loads)</i>	200
4.4.1.3.3	<i>Loading Conditions Selected for LCF</i>	200
4.4.1.3.4	<i>Hot spot stress</i>	201
4.4.1.4	<i>Stress Range Calculations</i>	202
4.4.1.4.1	<i>Elastic Hot Spot Stress</i>	202
4.4.1.4.2	<i>Pseudo Hot Spot Stress</i>	204
4.4.1.4.3	<i>Low Cycle S-N Curve and Damage Calculation</i>	205
4.4.1.5	<i>Combined Low Cycle and High Cycle Fatigue Damage</i>	206
4.4.2	<i>Bureau Veritas</i>	207
4.4.2.1	<i>Loading Conditions</i>	207
4.4.2.2	<i>Load Cases</i>	207
4.4.2.3	<i>Elementary Stress Range Calculations</i>	207
4.4.2.3.1	<i>Nominal Stress Range</i>	207
4.4.2.3.2	<i>Hot Spot Stress Range</i>	208
4.4.2.3.3	<i>Notch Stress Range</i>	208
4.4.2.4	<i>Low Cycle S-N Curve and Damage Calculation</i>	209
4.4.3	<i>Det Norske Veritas</i>	211
4.4.3.1	<i>Loading Conditions</i>	211
4.4.3.2	<i>Load Cases</i>	214
4.4.3.3	<i>Stress Range Calculations</i>	214
4.4.3.3.1	<i>Hot Spot Stress</i>	214
4.4.3.3.2	<i>Pseudo Hot Spot Stress</i>	215
4.4.3.3.3	<i>Low Cycle S-N Curve and Damage Calculation</i>	217
4.4.3.4	<i>Combined Low Cycle and High Cycle Fatigue Damage</i>	217
4.4.3.5	<i>Other Factors</i>	218
4.4.4	<i>Limitations</i>	219
4.4.5	<i>Lloyd's Register</i>	219
4.4.5.1	<i>Loading Conditions</i>	219
4.4.5.2	<i>Load Cases</i>	220
4.4.5.3	<i>Stress Range Calculations</i>	220

4.4.5.3.1	<i>Pseudo Hot Spot Stress</i>	220
4.4.5.3.2	<i>Low Cycle S–N Curve and Damage Calculation</i>	220
4.4.5.4	<i>Combined Low Cycle and High Cycle Fatigue Damage</i>	221
4.5	Class Societies LCF Procedures Summary	223
4.5.1.1	<i>Representative Operational Loading Conditions for LCF</i>	224
4.5.1.1.1	<i>Approach</i>	226
4.5.1.1.2	<i>Objective</i>	226
4.5.1.1.3	<i>Case Study</i>	226
4.5.1.1.3.1	<i>FPSO I</i>	227
4.5.1.1.3.2	<i>FPSO II</i>	230
4.5.1.2	<i>Representative Loading Conditions in Class Society Rules</i>	232
4.5.1.2.1	<i>Lloyd’s Register (LR)</i>	232
4.5.1.2.2	<i>American Bureau Of Shipping ABS-FPI (2009)</i>	233
4.5.1.2.3	<i>Det Norske Veritas DNV-CN-30.7 (2010)</i>	234
	Six load conditions may be considered for LCF assessment for vessels with one centreline bulkhead; these are presented in Table 19:	234
4.5.1.2.4	<i>Bureau Veritas BV-Part-D-Ch1-Sec7 (2007)</i>	237
4.5.1.3	<i>Summary of Operational (Hull) Loading Conditions Considered For LCF According to Class Societies</i>	237
4.5.1.4	<i>Summary of Operational (Hull) Loading Conditions According to Case Study</i> 238	
4.5.1.5	<i>Recommendations</i>	238
4.6	Conclusions	239
5	CHAPTER 5: LCF Tests	241
5.1	Literature Review	241
5.1.1	<i>Ship Structure Committee (SSC-137)</i>	241
5.1.2	<i>Fatigue Process</i>	241
5.1.3	<i>Effects of material texture on fatigue</i>	242
5.1.4	<i>HSE LCF Review</i>	242
5.1.4.1	<i>TWI</i>	242
5.1.4.1.1	<i>Transverse butt weld</i>	242
5.1.4.1.2	<i>Longitudinal fillet weld</i>	244
5.1.4.1.3	<i>Transverse (non-load carrying fillet weld)</i>	246
5.1.4.1.4	<i>Transverse (load carrying fillet weld)</i>	247
5.2	Class Societies and Shipyards	248
5.3	Full Scale Testing	249

5.4	IIW (HCF).....	250
5.5	LCF Tests in LR Southampton Facilities.....	251
5.5.1	<i>Introduction</i>	251
5.5.2	<i>Specimens and Material</i>	251
5.5.3	<i>Some basic definitions</i>	254
5.5.4	<i>Test Programme and Conditions</i>	254
5.5.4.1	Type A - Longitudinal Attachment (Larger Specimen)	254
5.5.4.2	Type B - Base Metal Specimen (BMS) – Smooth Round Type	256
5.5.4.3	Type C - Deposit Metal Specimen (DMS) – Smooth Round Type	256
5.5.5	Type A Test Procedures	257
5.5.6	Results - Type A Tests	258
5.5.6.1	A1 and A2 Tests (Monotonic).....	258
5.5.6.1.1	Monotonic Test Validation.....	263
5.5.6.2	A3 and A4 Tests.....	264
5.5.6.3	A5 Test	265
5.5.6.4	A6 Test	266
5.5.6.5	A7 Test	269
5.5.6.6	Data Processing.....	270
5.5.7	Results - Type B Tests	272
5.5.7.1	B1 Test (Monotonic).....	272
5.5.7.2	B2 Test (Monotonic).....	273
5.5.8	Results - Type C Tests	275
5.5.8.1	C1 Test (Monotonic)	275
5.5.8.2	C2 Test (Monotonic)	275
5.5.8.3	Type B and C Tests (Hysteresis)	277
5.5.8.4	LCF Tests Type B and C Specimens	277
5.5.8.5	Type B and C LCF Tests	278
5.6	Conclusions.....	279
6	CHAPTER 6: LCF Novel Approach.....	281
6.1	Proposed LCF Assessment Methodology	281
6.1.1	<i>Novel Approach</i>	282
6.1.2	<i>Novel approach applied to LCF test results</i>	287
6.1.3	<i>Novel approach applied to nonlinear FEA</i>	289
6.1.3.1	<i>Transverse (Cruciform) Attachment Model</i>	290
6.1.3.1.1	<i>FE Model (Transverse Attachment)</i>	295

6.1.3.1.2	<i>FE Model (Transverse Attachment – Boundary Conditions)</i>	295
6.1.3.1.3	<i>Non Linear Analysis Results (Transverse Attachment)</i>	297
6.1.3.2	<i>FE Model (Longitudinal Attachment)</i>	301
6.1.3.2.1	<i>FE Model (Longitudinal Attachment – Boundary Conditions)</i>	302
6.1.3.2.2	<i>Non Linear Analysis Results (Longitudinal Attachment)</i>	304
6.1.3.3	<i>Discussion</i>	307
6.2	<i>Comparison with Coffin-Manson</i>	309
6.3	<i>Summary</i>	309
6.4	<i>Benefits of this method</i>	311
6.5	<i>Conclusions</i>	311
7	CHAPTER 7: Conclusions and Recommendations	313
7.1	<i>Conclusions</i>	313
7.2	<i>Recommendations and Future work</i>	315
8	References	318
9	Appendixes	324

List of Figures

Figure 1: Prestige after hull separation (ABS-SSC, 2002).....	30
Figure 2: Ship types (Molland, 2008)	32
Figure 3: Floating Offshore Asset Scope, Lloyd's Register EMEA.....	32
Figure 4: FPSO conversion and new build in the last decade.....	33
Figure 5: Anonymous Typical FPSO General Arrangement	35
Figure 6: Anonymous Typical FPSO General Arrangement	35
Figure 7: Anonymous Typical FPSO General Arrangement	35
Figure 8: Typical midship section nomenclature (ShipRight, 2004)	36
Figure 9: Typical transverse bulkhead nomenclature (ShipRight, 2004).....	36
Figure 10: Welded hopper knuckle connection (ShipRight-3, 2004)	37
Figure 11: Radiused hopper knuckle connection (ShipRight-3, 2004)	38
Figure 12: Bulkhead stool to inner bottom connection (ShipRight-3, 2004).....	38
Figure 13: Longitudinal end connection (ShipRight-3, 2004)	39
Figure 14: e.g. Turret port side – Yield Strength 235N/mm ² (View on Moonpool) (Client-Report-GA, 2002)	40
Figure 15: SWBM variation at midsection of FPSO (Sun and Bai, 2003)	42
Figure 16: Modelling long-term SWBM variability (Huang and Moan, 2005).....	43
Figure 17: Modelling short-term SWBM variability (Huang and Moan, 2005)	44
Figure 18: Long-term VWBM variability (sagging or hogging)	45
Figure 19: Model of combined SWBM and VWBM (Huang and Moan, 2005).....	45
Figure 20: Location of hotspots in bottom detail (Raji, 2010).....	47
Figure 21: Schematic, showing process zone embedded within cyclic plastic zone and associated energy expenditure (Skelton et al., 1998).....	52
Figure 22: Different phases of the fatigue life (Wilczynski and Mróz, 2007)	54
Figure 23: Fatigue Loading (Wilczynski and Mroz 2007).....	56
Figure 24: Graphical interpretation of Neuber rule and Molski–Glinka method for uniaxial loading (Wilczynski and Mróz, 2007)	57
Figure 25: Graphical representation of Neuber rule for uniaxial LCF (Wilczynski and Mróz, 2007)	59
Figure 26: Manson–Coffin fatigue life curve represented by equation (Eq.6) axes in log scale (Seweryn et al., 2008).....	63
Figure 27: Hysteresis loop plastic strain energy density Δw^p is dissipated in a load cycle and elastic strain energy density Δw^{e+} referred to as the tension half cycle (Seweryn et al., 2008)..	64
Figure 28: Multilinear representation of the Ramberg–Osgood curve and the traces of the plastic surfaces at $\sigma_3 = 0$ plane (Seweryn et al., 2008).....	65
Figure 29: Schematic representation of combined HCF and LCF cycle (Byrne et al., 2003)....	66
Figure 30: Fatigue crack growth rate regimes for HCF and LCF loadings (Byrne et al., 2003)	67
Figure 31: Schematic representations of the repeated stress time sequences used in prior overload experiments (Byrne et al., 2003).....	68
Figure 32: Weldment fatigue specimen type (Madi et al., 2004).....	70
Figure 33: Welded joint specimen used in the literature (Madi et al., 2004).....	70
Figure 34: Control of welded joint specimen tests (Madi et al., 2004).....	71
Figure 35: Test at room temperature with three extensometers (Madi et al., 2004)	71
Figure 36: Strain measurements for the butt-welded tube (Madi et al., 2004).....	72
Figure 37: Crack localization for the tube (Madi et al., 2004).....	73

Figure 38: Definition of J_f (Madi et al., 2004)	73
Figure 39: Fatigue damage zone in a stress concentration area (Petinov, 2003)	75
Figure 40: Typical fatigue curves: material – solid line, structural element – dashed line (Petinov, 2003).....	77
Figure 41: Fatigue notch factor of welded joints (transverse fillet and butt welds ; nlc : non – load – carrying) as function of the stress concentration factor under the condition of constant notch sensitivity ranges ; after Sunamoto et al. (Radaj et al., 2006).....	77
Figure 42: Similar specimens of different sizes (Petinov, 2003)	78
Figure 43: ‘Process Zone’ and stress distributions in dimensionless form (Petinov, 2003)	79
Figure 44: Notches in a rectangular (left) and circular (right) cross sections (Petinov, 2003)	80
Figure 45: Plastic strain localization along the corner edge of deck opening in a steel model with rounded (left) and elliptic (right) corners, plotted against applied load, tons, Solid lines – loading, dashed lines – unloading (Petinov, 2003)	82
Figure 46: Stress and strain concentration factors depending on the nominal stress left – stress patterns in a plate with a circular hole, right – stress and strain concentration versus nominal stress (Petinov, 2003).....	85
Figure 47: Local strain ranges based on Stowell and Neuber formulae and their FEM evaluation for an Aluminium alloy (AlMg61). Solid lines – monotonous loading at $\sigma_{max} = 72$ MPa ; dashed lines – cyclic loading at $\Delta\sigma = 107.1$ MPa (Petinov, 2003)	87
Figure 48: Edge distribution for a scallop under axial loading (Fricke and Paetzold, 1995).....	88
Figure 49: Example of local stress strain values according to Neuber (Fricke and Paetzold, 1995)	89
Figure 50: e.g. Cyclic Strain Hardening Material - 304 stainless steel (Manson, 1964).....	90
Figure 51: e.g Cyclic Strain Softening Material - 4340 steel (Manson, 1964)	91
Figure 52: Distribution of amplitudes of the applied load (F , σ_e , σ_n) (Fricke and Paetzold, 1987)	92
Figure 53: Relationship between applied load and local strain (Fricke and Paetzold, 1987)	93
Figure 54: Relationship between damage parameter and crack initiation life (Fricke and Paetzold, 1987)	93
Figure 55: Large scale test model of the longitudinal stiffener / transverse web intersection (Fricke and Paetzold, 1987)	94
Figure 56: Elastic strain distribution and yield curves for the notch root subjected to cyclic loading (Fricke and Paetzold, 1987)	95
Figure 57: Determination of the theoretical elastic notch stress σ_e for a structural detail in a double bottom (Fricke and Paetzold, 1987)	96
Figure 58: Unit load cases for a structural detail in a double bottom (Fricke and Paetzold, 1987)	96
Figure 59: Theoretical elastic stress distribution σ_e for two realistic load cases (Fricke and Paetzold, 1987)	97
Figure 60: Crack initiation life N_e for specimens of normal strength steel (NS 24), Grade A (Fricke and Paetzold, 1987)	98
Figure 61: Relationship between fatigue life N_e and elastic notch stress amplitude σ_e for simplified load histories (Fricke and Paetzold, 1987).....	99
Figure 62: Strain hardening under compression following unloading after tensile plastic deformation (Petinov, 2003)	100
Figure 63: Cyclic diagram in a reversed loading test (Petinov, 2003)	101
Figure 64: The plastic strain range, $\Delta\epsilon_{pl}$, in LCF (Ashby and Jones, 2002)	102

Figure 65: Cyclic hardening: (a) testing under control of load (stress) amplitude, (b) testing under strain range control (Petinov, 2003).....	104
Figure 66: Generalization of cyclic curves: left – the common point for all of diagram is the load reverse point, right – superposition of diagrams (Petinov, 2003)	105
Figure 67: Cyclic stress / strain ranges and development of damage to microstructure (Petinov, 2003)	107
Figure 68: Specimens for fatigue testing of materials: top – for cyclic torsion tests, bottom – for axial cyclic load or strain range control testing (Petinov, 2003).....	108
Figure 69: Actual and ‘design’ S–N curves (Petinov, 2003)	109
Figure 70: Method of predicting axial fatigue life based on ductility, fracture strength and ultimate strength (Manson, 1964)	114
Figure 71: Fracture stress against function of true ductility and ultimate strength (Manson, 1964)	115
Figure 72: Relation between plastic strain ductility and cycles to failure (Manson 1964)	118
Figure 73: Ratio of elastic strain range to σ_u / E against cycles to failure (29 materials) (Manson, 1964)	118
Figure 74: Model for method of universal slopes (Manson, 1964).....	119
Figure 75: Comparison of predicted and experimental axial fatigue life for low – alloy and high – strength steels (Manson, 1964)	119
Figure 76: Comparison of predicted and experimental axial fatigue life for stainless steels and high – temperature alloys (Manson, 1964)	120
Figure 77: Axial strain – cycling – fatigue behaviour of 29 materials (Manson, 1964)	121
Figure 78: Cyclic strain hardening under two – level fatigue tests (Manson, 1964).....	122
Figure 79: Cyclic Strain hardening under multilevel fatigue tests (Manson, 1964)	123
Figure 80: Cyclic Strain softening under multilevel fatigue tests (Manson, 1964)	124
Figure 81: Cumulative fatigue damage obtained by strain cycling of smooth specimens (Manson, 1964)	125
Figure 82: Variable Stress Diagram prepared for Assessing Cumulative Damage (Shigley et al., 2003)	126
Figure 83: Initiation controlled HCF - Basquin's Law (Ashby and Jones, 2002)	128
Figure 84: Initiation controlled LCF- the Coffin Manson Law (Ashby and Jones, 2002)	129
Figure 85: A series of grains with well-developed slip bands and non-propagating cracks observed in the vicinity of the principal crack (Petinov, 2003)	130
Figure 86: Slip band formation: a – slip scheme at monotonous loading, b – slip progress at cyclic loading c – taper section of a slip band in copper after 2×10^5 cycles (Petinov, 2003) ...	131
Figure 87: Definition of the local stress at the bracket toe (Petinov, 2003).....	132
Figure 88: Stress concentration at the bracket end (Petinov, 2003).....	134
Figure 89: Stress concentration in the side shell plating at the side opening (Petinov, 2003) .	135
Figure 90: Mean stress in the cyclic loading; schematic representation of a load cycle comprising the constant (mean) stress (Petinov, 2003)	136
Figure 91: Goodman's Rule - the effect of tensile mean stress on initiation controlled fatigue (Ashby and Jones, 2002).....	137
Figure 92: Endurable nominal stress amplitude of welded joints made of structural steels dependent on mean stress (Haigh diagram); after Haibach (Radaj et al., 2006).....	138
Figure 93: Relaxation residual welding stresses in a stress concentration area (Petinov, 2003)	139

Figure 94: Formation of effective (non – relaxed) residual stresses in a hull structural detail (Petinov, 2003).....	140
Figure 95: Crack tip plastic zone (Petinov, 2003).....	140
Figure 96: Distance of the read out points (ROPs) from the hot spot used in Osawa’s method (ISSC, 2009)	150
Figure 97: Classification of local concepts of fatigue assessment of welded joints (Radaj et al., 2009)	151
Figure 98: Micro and macro phenomena of material fatigue (Radaj, 1996).....	153
Figure 99: Parameter governing fatigue failure (Radaj et al., 2006).....	154
Figure 100: Global and local approaches for describing the fatigue strength (Radaj, 1996)...	156
Figure 101: Comparison specimen for simulating the cyclic stress strain and crack initiation behaviour at the notch root (Radaj, 1996).....	157
Figure 102: Three types of fatigue – critical weld toes (types A, B, C) in plate – type reference structure proposed by Fricke (Radaj et al., 2006)	161
Figure 103: Strain gauge positioning for the hot spot stress determination in plate – type structures (Radaj et al., 2006)	162
Figure 104: Two procedures to obtain the hot spot structural stress: codified procedure of linear extrapolation (σ_{hs}) and procedure based on strain at distance d from the weld toe after Haibach (σ_{sH}) (Radaj et al., 2009)	163
Figure 105: Linear extrapolation of surface stresses (Radaj et al., 2009)	164
Figure 106: Internal linearization of the structural stresses as proposed by Dong et al. for single-sided weld (a), edge weld (b) and double-sided weld (c) resulting in the hot spot structural stress σ_{hs} ; cross-sections (a, c) and front view (b) (Radaj et al., 2009)	165
Figure 107: Stress distributions (b, c) calculated by the finite element method for a reference structural detail (a) with non-load-carrying fillet welds (double-sided transverse attachment joint; weld toe radius ρ); after Xiao and Yamada (redrawn with restriction to weld toe angle $\theta = 45^\circ$) (Radaj et al., 2009).....	166
Figure 108: Definition of the maximum notch stress σ_k in comparison to the hot spot structural stress σ_{hs} and Haibach’s structural stress σ_{sH} (Radaj et al., 2009).....	167
Figure 109: Limitation to the design S–N curve FAT 225 (relating to reference notch radius $\rho_r = 1.0$ mm) by FAT 160 x K_w with weld notch factor $K_w \geq 1.6$; according to the IIW recommendations (Radaj et al., 2009)	168
Figure 110: Fictitious notch rounding graph according to Hobbacher, 1996 (Fricke, 2010b). 173	173
Figure 111: Actual notch with stress averaging over ρ^* (Sonsino, 2009)	174
Figure 112: Substitute notch with fictitious notch radius resulting in σ_{av} (Sonsino, 2009).....	174
Figure 113: The hot spot stress location at the toe of a weld (Schijve, 2012)	177
Figure 114: Definition of effective stress-strain range (Saiprasertkit et al., 2011).....	178
Figure 115: Relationship between effective notch strain and fatigue life (Saiprasertkit et al., 2011)	179
Figure 116: Concept proposed by (Saiprasertkit et al., 2011).....	179
Figure 117: Application of proposed method to experimental results (Saiprasertkit et al., 2011)	182
Figure 118: Investigated Structure (Fricke et al., 2013)	183
Figure 119: Observed cracks (Fricke et al., 2013)	183
Figure 120: S–N curve for effective strain range (Fricke et al., 2013)	184
Figure 121: Actual, Equivalent Elastic and Pseudo Stress (Urm et al., 2004b).....	189
Figure 122: S–N curve in low cycle region (Wang et al., 2006).....	190

Figure 123: Test specimen from TWI (1974) (Wang et al., 2006)	191
Figure 124: Testing specimen presented in Heo et al. (2004) (Wang et al., 2006).....	191
Figure 125: Strain-life curve (Wang et al., 2006)	192
Figure 126: Fatigue design S–N curves for weld details of materials stated below (PD5500, 2011)	193
Figure 127: LCF Damage at BHS6 (Raji, 2010).....	196
Figure 128: Location of hotspots in bottom detail (Raji, 2010).....	196
Figure 129: LCF S–N Curve 1 (Raji, 2010).....	197
Figure 130: LCF S–N Curve 2 (Raji, 2010).....	198
Figure 131: LCF S–N Curve 3 (Raji, 2010).....	199
Figure 132: Sample Functions of S_w and S_B (ABS-SBFA, 2010)	202
Figure 133: A Single Loading/Offloading Cycle (ABS-SBFA, 2010)	203
Figure 134: k_e as a Function of S_E (ABS-SBFA, 2010)	205
Figure 135: LCF Design Curve (ABS-SBFA, 2010)	206
Figure 136: Operation scenarios, full load – ballast (DNV-CN-No.30.7, 2010)	212
Figure 137: Operation scenarios, ballast - full load – alternate load conditions (DNV-CN-No.30.7, 2010)	213
Figure 138: The combined fatigue criteria (DNV-CN-No.30.7, 2010).....	218
Figure 139: Frequency of observed draughts at Fwd end for FPSO I during loading (Pre Discharge)	228
Figure 140: Frequency of observed draughts at Aft end for FPSO I during loading (Pre Discharge)	229
Figure 141: Frequency of observed draughts at Fwd end for FPSO I after offloading (Post-Discharge)	229
Figure 142: Frequency of observed draughts at Aft end for FPSO I after offloading (Post-Discharge)	230
Figure 143: Frequency of observed draughts at Fwd end for FPSO II during loading/offloading	231
Figure 144: Frequency of observed draughts at Aft end for FPSO II during loading/offloading	232
Figure 145: Endurance data for transverse butt welds ($R=0$) (HSE-Review, 2004).....	243
Figure 146: Endurance data for transverse butt welds ($R=-1$) (HSE-Review, 2004).....	244
Figure 147: Endurance data for longitudinal fillet welded attachments (load control) (HSE-Review, 2004)	245
Figure 148: Endurance data for longitudinal fillet welded attachments (displacement control) (HSE-Review, 2004).....	246
Figure 149: Endurance data for transverse non load-carrying fillet welds (HSE-Review, 2004)	247
Figure 150: Endurance data for transverse load-carrying fillet welds (HSE-Review, 2004)...	248
Figure 151: Mild steel grade A panel.....	252
Figure 152: Longitudinal Attachment Specimen	252
Figure 153: Uniform Gage Section Test Specimen	253
Figure 154: Strain gauge locations for Type A static tests	254
Figure 155: Strain gauge locations for Type A other tests.....	255
Figure 156: Test A1 and A2, nominal stress and strain	259
Figure 157: Test A1 Set up	259
Figure 158: Test A2 Set up	260

Figure 159: Test A2, local strain range close to weld toes	261
Figure 160: Test A2, local strain range away to weld toes	262
Figure 161: Test Validation 1.25mm Displacement	264
Figure 162: Test A4 results	265
Figure 163: A5 specimen, failure at weld toes.....	266
Figure 164: Test A6 Displacement vs. Nominal Strain Range	267
Figure 165: Test A6 Displacement vs. Nominal Stress Range	267
Figure 166: Test A6 Displacement vs. Number of Cycles to Failure	268
Figure 167: Test A7 Strain range, % (max & min) vs. no. of cycles	270
Figure 168: Test A7 Load, Newton (max & min) vs. no. of cycles N	271
Figure 169: Test A7 Nominal Stress range, MPa vs. LogN.....	271
Figure 170: Test A7 Strain range, % (max & min) vs. LogN	272
Figure 171: Test A7 Load applied vs. strain range (cyclic diagram)	272
Figure 172: Type B and C Test set up.....	273
Figure 173: Monotonic test B1	273
Figure 174: Monotonic test B2	274
Figure 175: Comparison of monotonic tests type B.....	274
Figure 176: Monotonic test C1	275
Figure 177: Monotonic test C2	276
Figure 178: Comparison of monotonic tests type C.....	276
Figure 179: Type B and C specimens: Hysteresis Loop	277
Figure 180: Type B and C specimens: Stress strain curves of stated specimens	278
Figure 181: Type B and C specimens: S-N Curve data (strain curves)	279
Figure 182: Stress strain– Neuber and Ramberg Osgood relationships	282
Figure 183: S-N D Curve	285
Figure 184: S-N Curves in pseudo stress range	286
Figure 185: S-N Curves in elasto-plastic stress range.....	287
Figure 186: Test Results and S-N design Curves – Pseudo Elastic Stress.....	288
Figure 187: Test Results and S-N design Curves – Elasto-Plastic Notch Stress.....	289
Figure 188: Transverse (Cruciform) Attachment Full Model Dimensions	290
Figure 189: Stress strain curve of base metal.....	292
Figure 190: Stress strain curve of deposit metal (Weld).....	294
Figure 191: Flow stress data used in the analysis	294
Figure 192: Transverse (crucifix) attachment quarter model 0mm radius general view	295
Figure 193: Transverse (crucifix) attachment quarter model 1mm radius general view	296
Figure 194: Transverse (crucifix) attachment quarter model 0mm radius close view	296
Figure 195: Transverse (crucifix) attachment quarter model 1mm radius close view	297
Figure 196: Transverse (Cruciform) Attachment Nonlinear FEA Results vs DSME test results	299
Figure 197: Transverse (crucifix) attachment model 0mm radius 1 st principal stress distribution	299
Figure 198: Transverse (crucifix) attachment model 1mm radius 1 st principal stress distribution	300
Figure 199: Transverse (crucifix) attachment model 0mm radius 1st principal maximum stress at weld toe	300
Figure 200: Transverse (crucifix) attachment model 1mm radius 1 st principal maximum stress at weld toe.....	301

Figure 201: Longitudinal Attachment Full Model Dimensions	302
Figure 202: Longitudinal attachment quarter model 0mm radius general view	302
Figure 203: Longitudinal attachment quarter model 1mm radius general view	303
Figure 204: Longitudinal attachment quarter model 0mm radius close view	303
Figure 205: Longitudinal attachment quarter model 1mm radius close view	304
Figure 206: Longitudinal Attachment Test Results vs TWI and Nonlinear FEA LQM	305
Figure 207: Longitudinal attachment model 0mm 1 st principal stress distribution.....	305
Figure 208: Longitudinal attachment model 1mm 1 st principal stress distribution.....	306
Figure 209: Longitudinal attachment model 0mm 1 st principal maximum stress at the weld toe	306
Figure 210: Longitudinal attachment model 1mm 1 st principal maximum stress at the weld toe	307
Figure 211: LQM 1mm results compared with Coffin-Manson	309
Figure 212: Comparison of pseudo results for both transverse and longitudinal attachments.	310
Figure 213: Comparison of elastic plastic results for both transverse and longitudinal attachments	310

List of Tables

Table 1: FPSO Survey Statistics in the last Decade	33
Table 2: Wave damage and low cycle damage for different sea scatter diagrams. Raji (2010). 47	
Table 3: Petinov approximation of local strain at various stress concentrations	86
Table 4: Materials for Axial LCF Investigation. Manson (1964).....	116
Table 5: Material Variables in Axial LCF Investigation. Manson (1964)	117
Table 6: Example stress amplitude and midrange components (Shigley et al., 2003)	127
Table 7: Influence parameters controlling cyclic crack initiation. Radaj (1996)	153
Table 8: Influence parameters controlling cyclic crack propagation. Radaj (1996)	153
Table 9: Structural stress at hot spots in elastic range. Fricke et al., (2013)	184
Table 10: Details of fatigue design curves PD5500 (2011)	194
Table 11: Class societies LCF procedure's high level summary	224
Table 12: Loading Conditions for FPSO service. LR-Report (2008)	225
Table 13: General particulars of FPSOs.	227
Table 14: Observed draughts for FPSO I before discharge	227
Table 15: Observed draughts for FPSO I after discharge	228
Table 16: FPSO II Range of Draught Occurrence.....	231
Table 17: Design Load Combinations Static & Dynamic (Sea-going load cases) LR-Report (2007).....	233
Table 18: ABS Representative loading conditions for LCF.....	234
Table 19: DNV Representative loading conditions for LCF (1)	235
Table 20: DNV Representative loading conditions for LCF (2)	236
Table 21: DNV Representative loading conditions for LCF (3)	236
Table 22: BV Representative loading conditions for LCF.....	237
Table 23: Mild steel grade A panel Details	253
Table 24: Approximate initial gauge locations for Test A1	260
Table 25: Approximate initial gauge locations for Test A2.....	261
Table 26: Displacement measure beyond which strain gauges stop recording	262
Table 27: Initial displacement measure.....	263
Table 28: Type A test results.....	269
Table 29: Tensile information for the BMS	275
Table 30: Tensile information for the DMS.....	277
Table 31: Type B and C LCF test results	278
Table 32: Stress strain relationship example	285
Table 33: Mild steel Grade A flow stress data (Wang et al., 2006)	291
Table 34: Deposit Metal Cyclic Properties Urm et al., (2004b).....	293
Table 35: Transverse (Cruciform) Attachment Nonlinear FEA Results	298
Table 36: Longitudinal Attachment Nonlinear FEA Results	304

NOMENCLATURE

Roman

ABS	American Bureau of Shipping
Aft	Aft ward
BV	Bureau Veritas
BS	British Standard PD5500
BMS	Base Metal Specimen
CSR	Common structural rules
CQM	Crucifix quarter model
DFF	Design fatigue factor
DLA	Dynamic loading approach
DNV	Det Norske Veritas
DSME	Daewoo Shipbuilding & Marin Engineering Co., Ltd
DMS	Deposit Metal Specimen (Weld)
FAT	Fatigue class
FDA	Fatigue design assessment
FDPSO	Floating, drilling, production, storage, and offloading unit
FEA	Finite element analysis
FEM	Finite element method
FPI	Floating production installation
FPU	Floating production unit
FPS	Floating production system
FPSO	Floating production storage and offloading unit
Fwd	Forward
FWS	Fillet Weld Specimen
GL	Germanischer Lloyd
HAZ	Heat affected zone
HCF	High cycle fatigue

HISC	Hydrogen induced stress cracking
HSE	Health and safety executive
HSS	Hot spot stress
ISSC	International ship and offshore structures congress
IACS	International association of class societies
IIW	International institute of welding
N	Newton (Load or Force)
N	Number of Cycles to Failure (S-N Curve)
NK	Nippon Kaiji Kyokai
NS	North Sea
LCF	Low cycle fatigue
LR	Lloyd's Register
LSA	Local strain approach
LQM	Longitudinal quarter model
RINA	Registro Italiano Navale
RS	Russian Maritime Register of Shipping
R	Stress Ratio ($\sigma_{\min} / \sigma_{\max}$)
S-N	Cyclic stress (S) against the logarithmic scale of the number of cycles to failure (N)
SSC	Ship structure committee
SWBM	Still water bending moment
SWLE	Still water load effect
TAPS	Trans-Alaska pipeline system
TWI	Technical welding institute
UTS	Ultimate Tensile Strength
VLCC	Very large crude oil carriers
VWBM	Vertical wave bending moment
WA	West Africa

K'	Cyclic strength coefficient
n'	Cyclic strain hardening exponent
K_w	Fatigue notch factor
s	Factor for stress multiaxiality and strength criterion
q	Notch sensitivity factor
K_f	Notch factor
r	Notch root radius
K_e	Plasticity correction factor
SCF	Stress concentration factor
K_t	Theoretical stress concentration factor
E	Young modulus
Greek	
ϵ -N	Cyclic strain (ϵ) against the logarithmic scale of the number of cycles to failure (N)
σ	Actual stress in the elasto plastic state
ϵ	Actual strain in the elasto plastic state
$\Delta\sigma$	Actual stress range
$\Delta\epsilon$	Actual strain range
ρ	Actual or effective or fictitious notch radius
Δw^{e+}	Elastic strain energy density of tension (half cycle)
β	Empirical parameter
ψ	Factor due to stress redistribution
ρ_f	Fictitious radius
σ^e	Local elastic stress state at the notch root
ρ^*	Micro-structural support length
α	Material constant
γ	Material parameter
σ_n	Nominal stress

ε_n	Nominal strain
$\Delta\sigma_n$	Nominal linear elastic stress
$\Delta\varepsilon_n$	Nominal linear elastic strain
λ	Non-linearity correction factor
Δw^p	Plastic strain energy density (per load cycle)
K_σ	Stress concentration factor
K_ε	Strain concentration factor
Δw^t	Strain energy density

Chapter 1

Introduction

1 Chapter 1. Introduction

This chapter provides a description of the research background, objectives and methodology, an outline of the thesis structure, an introduction to the phenomenon of low cycle fatigue (LCF) and the susceptibility of Floating Production Storage and Offloading (FPSO) units to LCF.

1.1 Research Background and Subject Matter

The author's research on fatigue started in the summer of 2004 with Lloyd's Register EMEA following a request of a Procedure for the Fatigue Assessment of Pressure Vessels. This was part of the Honours Degree Project that he conducted with the Robert Gordon University in Aberdeen, Scotland. A procedure was developed together with software to carry out fatigue assessment as per the British Standard PD5500 "Specification for unfired, fusion welded pressure vessels". Based on this study a thesis titled 'Accumulated Fatigue Assessment in Pressure Vessels' (Megharbi, 2005) was prepared, in which high cycle fatigue (HCF) was investigated and reference to LCF was made. Furthermore, recommendations were made for more research on strain based life prediction. In November 2006 the author's research on LCF started as requested by Lloyd's Register EMEA to address the LCF phenomena for FPSO ship structures. Since 2008 to date the author had the privilege to work in the Integrity Engineering Services Department of Lloyd's Register in the floating structures team with some expert naval architects specialised in ship survey, hydrodynamics and fatigue analysis. In the past six years the author was the project engineer responsible for the structural integrity management of two FPSOs and one semi-submersible.

Lloyd's Register (LR) is the first classification society in the world formed in 1760 followed by Bureau Veritas (BV) in 1828, Det Norske Veritas (DNV) in 1864, Registro Italiano Navale (RINA) in 1861, Germanischer Lloyd (GL) in 1867, Nippon Kaiji Kyokai (NK) in 1899 and the Russian Maritime Register of Shipping (RS) in 1913. A classification society is a non-governmental organization that establishes and maintains technical standards for the construction and operation of ships and offshore structures. The societies also verify that construction is according to these standards and carry out regular surveys and/or in service inspection to ensure compliance with the standards. Classification societies always seek to improve their rules and regulations; shipyards are also required to investigate any new type of damage in ship structures to guarantee they produce high quality products. Several reported damages in ship structure were

suspected to be caused by LCF as primary reason. Accordingly, both class societies and shipyards were and are still interested in investigating LCF. The suspicion is due to the fact that some cracks were observed within five years of delivery. Urm et al., (2004b)

1.2 Objectives and Methodology

The current research aims to:

1. Review LCF assessment methods available in the literature and adopted by class societies such as ABS, BV, DNV, and LR,
2. To carry out experimental and numerical analyses to assess LCF in standard structural details such as the cruciform and longitudinal attachment,
3. To develop a method of predicting number of cycles to failure due to LCF,
4. To develop a method of combining HCF and LCF,
5. To compare results with the available experimental data.

Other research objectives include:

1. Demonstrating the importance of LCF assessment focusing on failures caused by LCF (some examples of failures).
2. Identifying difference in terms of loading/offloading between FPSO Ship structure and conventional oil tankers.
3. The mechanism driving LCF (including material consideration).
4. Justifying (or otherwise) the use of the S-N approach for LCF assessment.

The above objectives will be addressed in the following chapters.

1.3 Thesis Scope and Structure

This thesis is devoted entirely to the study of LCF in FPSO ship structure. Topics relevant to it are also discussed. The thesis consists of seven chapters; literature review is mainly covered in Chapter 2, however, some other literature review is included in other chapters as applicable. Outlines of the main topics discussed in each Chapter are as follows:

Chapter 1 – general introduction to the research background and subject matter, objectives, thesis scope and structure, introduction to LCF and Floating Production Storage and Offloading (FPSO) units.

Chapter 2 – covers LCF in literature, LCF of ship structure and the state-of-the-art in fatigue assessment of welded Joints.

Chapter 3 – covers the state-of-the-art in LCF assessment methods proposed by the International Institute of Welding (IIW).

Chapter 4 – covers the state-of-the-art in LCF assessment methods recommended by class societies.

Chapter 5 – covers LCF Testing.

Chapter 6 – proposes a novel LCF assessment method and numerical analysis (FEA).

Chapter 7 – covers conclusions derived from the research, findings and recommendations for future work

At the beginning of each chapter an executive summary of the main topics covered in the chapter will be presented. At the end of each chapter a conclusion section of the main concepts/findings to be considered is highlighted.

1.4 Phenomenon of LCF

In the early 1960's, the analyses of fatigue in ship structures based on reported fatigue cracks attracted attention to LCF. It was recognised that at nominal stress amplitudes lower than the yield stress, plastic strains may occur due to high stress concentrations typical for many hull structural details. It was also necessary to assess the damage due to moderate and relatively low stress amplitudes dominating the actual load histories. These considerations resulted in development of the local strain (low cycle format) approach to fatigue of ship hull and marine structures Petinov (2003).

LCF generally refers to the cycle range below 10^4 cycles. This range is not covered by existing fatigue curves available in many ship classification societies. LCF is normally expressed in terms of total strain range rather than stress range because the local fatigue sensitive zone that is subject to high stress level is experiencing strain controlled conditions rather than load or stress controlled conditions. In other words plasticity occurs at notched areas such as toe of weld. Urm et al., (2004b)

LCF life is divided into the nucleation of single or multicracks, the growth and coalescence of these cracks and the growth of the resulting crack to final failure. It was reported that over 80% of the entire LCF life was spent in the growth and coalescence

of multicracks before the formation of a fatal crack (Kim et al., 2004) (Stolarz, 1997) (Stolarz et al., 2001).

LCF in FPSOs is mainly associated with continuous production and periodic offloading. It is now the subject of research conducted by some classification societies because of increased interest from ship owners and operators. Although some believe that the effect is moderate in some parts of the structure, it is found to significantly contribute to fatigue life in other areas of the structure. Raji (2010)

According to Lloyd's Register Floating Offshore Installation (FOI) ship units guidance on calculation ShipRight-FOI (2008), LCF is defined as fatigue damage arising from changes in the stress level caused by loading and unloading of the unit. The number of cycles in the design life is relatively small but the induced stress range can be significant.

Various class societies, shipyards, the IIW and other academic researchers are the main stakeholders in LCF research. However the IIW appears to be taking the lead in terms of the latest developments which will be discussed later in chapter 3.

1.5 Failures Caused by LCF

Finding a historical record of a ship structural failure or accident that has been attributed directly to LCF was a challenging task. This is because the available historical record of infamous fatigue failures are to do with trains, planes or oil platforms and also because most of the accidents involving ships are mainly due to grounding, capsizing, collision, fire and cargo shifting (Bamitabh, 2013). None of these are directly related to fatigue which is an accumulative process by its nature. However, LCF may have been the initial cause of some of these accidents. Moreover, the lack of record of stress ranges from these failures made it even more difficult to analyse.

Petinov (2003) stated that detailed descriptions of the failure origin (configuration of the critical element, origin's location, etc.) in structural elements is typically missing. Even in very good reports such as Jordan and Cochran (1978), Sipes (1990), etc., fatigue damages were described too vaguely. Only for the platform 'Alexander Kielland' the initial failure due to fatigue was well documented and analysed extensively. Efficiency of structural fatigue models can be assessed using properly documented and published results of full scale or model fatigue tests of ship structures.

The complete hull failure in the single hull tanker Prestige in 2002 may be attributed fully or partially to LCF. According to the Ship Structure Committee (SSC) report ABS-SSC (2002) the cause of the initial damage is not known. It is worth mentioning that the previous captain complained about numerous structural deficiencies within the ship and he resigned in protest (Wikipedia, 2013b). ABS report ABS-SSC (2002) acknowledged that some as-built structural details failed the 2003 ABS requirements for fatigue, but ABS maintains that this is not a probable cause of the hull failure, as the Prestige operated in a gentler environment than the criteria were developed for, and “most of the side longitudinal having insufficient fatigue life were renewed at the 4th and 5th Special Hull Surveys”. The ABS’s conclusion was “flooding in the ship’s starboard #2 Aft and #3 wing tanks caused a 25 degree list, which was counter ballasted by flooding #2 Aft port and #3 port ballast tanks. This resulted in an overstressed hull girder which failed after six days of exposure to heavy seas, causing the ship to break in two and sink” as shown in **Figure 1**. ABS concluded that “the sustained dynamic wave loading for the period while the Prestige was under tow subsequent to the initial casualty was the direct cause of the ultimate disintegration of the hull structure and subsequent sinking of the vessel”. ABS-SSC (2002)



Figure 1: Prestige after hull separation (ABS-SSC, 2002)

More recently, a significant number of indications (i.e. cracks) were reported in a purpose built twenty year old FPSO operating at the North Sea. These defects were reported in all cargo tanks at hopper knuckle weld connection between the longitudinal

bulkheads (inboard and outboard) and the inner bottom (tank top). Several entire sections of defected structural detail were cropped and replaced. Following a survey performed by a third party, three samples were sent for investigation; sample A with longitudinal cracking along weld repair performed at yard, sample B with longitudinal cracking along the original weld and sample C with cracking in the weld metal. The results were as follows: the appearance of the cracks in samples A and B was consistent with hydrogen induced stress cracking. This was supported by high hardness levels in the heat affected zones (HAZ) and a significant amount of martensite in the HAZ of welds in all the investigated samples. The appearance of the crack in the weld metal of sample C was consistent with a fatigue crack propagated from a lack of root fusion (DNV-Report, 2011).

The available reports attributed the cracks to loss of plate thickness due to widespread corrosion, Hydrogen Induced Stress Cracking (HISC) or lack of root fusion. However, there is no evidence of widespread corrosion. Also, HISC usually occurs due to sustained high loads in the presence of hydrogen. In this case, the structure is exposed to cyclic loading and the presence of hydrogen is speculative. A closer examination of the details and loading would suggest that LCF is involved. The location of the cracks at the hopper knuckle is likely to see high stress concentrations and plasticity. This, coupled with the relatively low number of cycles to failure, makes LCF the most likely cause of failure.

1.6 Introduction to FPSO

1.6.1 *Marine/Oil and Gas*

The Floating Production Storage and Offloading (FPSO) units is a member of a wider family in marine industry as shown in **Figure 2** and one member of the family of the Floating Production Systems in Oil and Gas as shown in **Figure 3**. FPSOs make up almost 70% of all floating systems in the world. Huang et al., (2005) The increasing number of FPSOs being used in the oil and gas industry is due to the practical advantages they offer as compared to fixed installations.

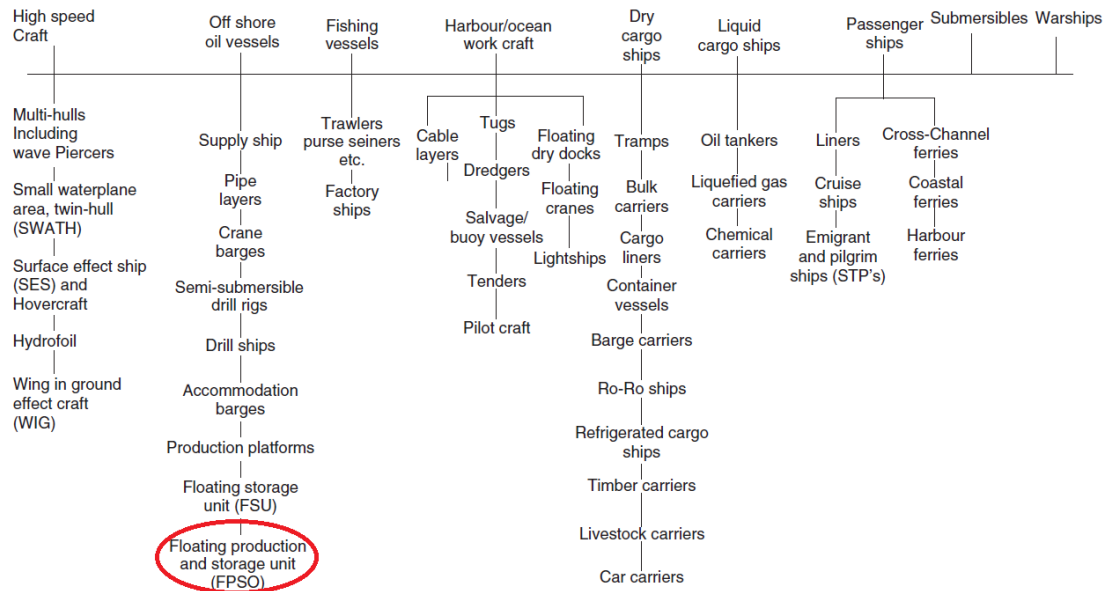


Figure 2: Ship types (Molland, 2008)

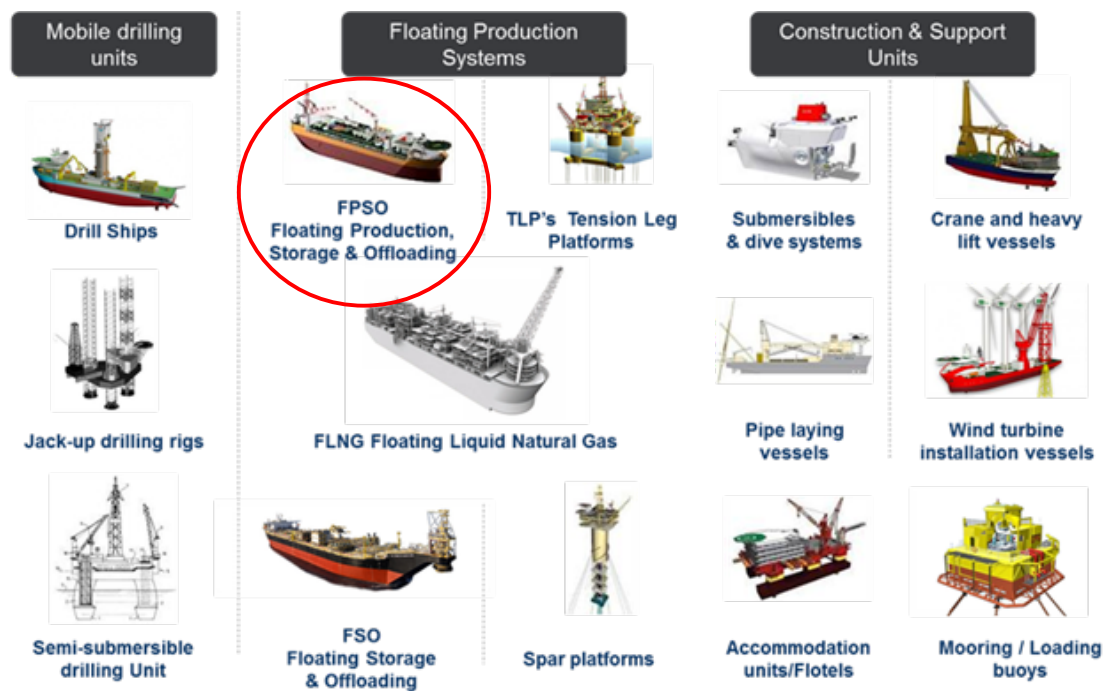


Figure 3: Floating Offshore Asset Scope, Lloyd's Register EMEA

1.6.2 FPSO Construction Type

FPSO units are either new build, converted or unconventional. Most of the existing converted FPSOs are from very large crude oil carriers (VLCCs) Raji et al., (2009), Unconventional FPSOs (i.e. not ship-type FPSO) such as Sevan SSP are not considered in this research. Some converted FPSOs such as the AZURITE floating, drilling,

production, storage, and offloading (FDPSO) vessel include drilling facilities. Based on the worldwide survey of FPSO units (Mahoney and Supan, 2012) carried out in the last 10 years; between 51% and 64% of 153 FPSO's are conversions and between 36% and 49% are new builds. **Table 1** details the number of producing FPSOs and relevant percentages in the last decade excluding the year 2008 where only semi Floating Production Systems (FPS) and Floating Production Units (FPU) survey were carried out (i.e. no FPSO survey carried out).

Table 1: FPSO Survey Statistics in the last Decade

Year	No. of FPSO	New build	%	Conversion	%
2003	118	52	44	66	56
2004	116	47	41	69	59
2005	148	72	49	76	51
2006	157	70	45	87	55
2007	155	64	41	91	59
2009	181	67	37	114	63
2010	186	67	36	119	64
2011	158	60	38	98	62
2012	156	58	37	98	63

Figure 4 shows the relative increase of converted FPSOs and the relative decrease of new build FPSOs during the last decade. The author's observation of the relative increase of the converted FPSOs is purely due to feasibility reasons i.e. it is more cost effective to convert an ocean going ship into a FPSO than to build a FPSO.

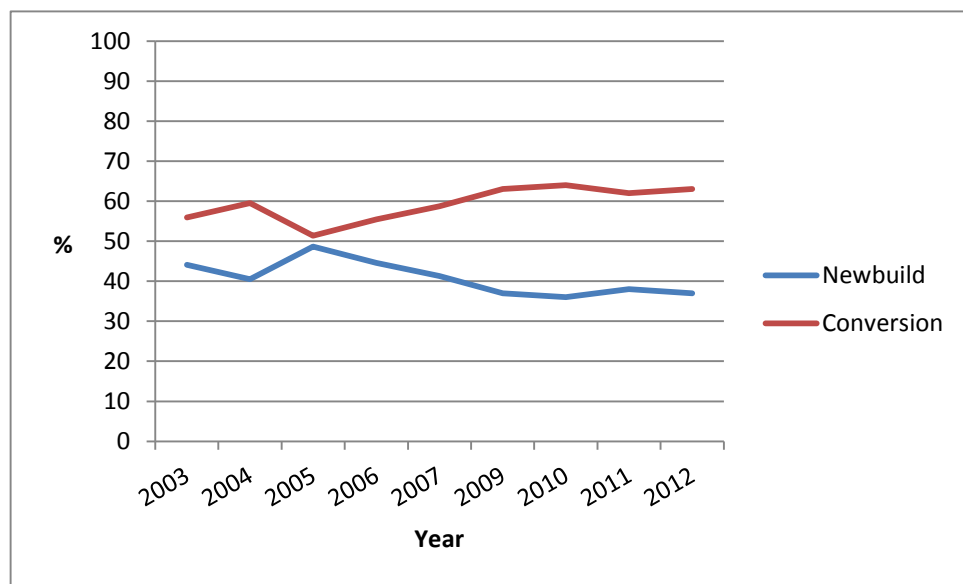


Figure 4: FPSO conversion and new build in the last decade

1.6.3 Difference between an Oil Tanker and a FPSO

The operation of FPSOs is not the same as oil tankers and the expectations of the oil and gas industry are not the same as the expectations of tanker industry. From the economic point of view, the costs of lost production time in FPSO are much higher than tanker off hire costs. Tankers normally dry dock for survey and repairs every five years, FPSO survey and repair is more expensive as this is done on site. Furthermore, tanker owners pay for steel weight of the hull structure twice, once at build and second as fuel during the tanker life. On the other hand FPSO owners only pay once (at build) for steel weight of the hull structure, hence there is less advantage in reducing the steel weight. Bamford et al., (2007)

Additional differences between tankers and FPSOs may be summarized as follows:

1. All oil tankers are new built
2. Most FPSOs are converted from oil tankers
3. A FPSO is stationed in a specific site using a mooring system
4. Risers are attached to the FPSO hull
5. A FPSO is normally designed to have no dry docking during its service period
6. A FPSO has in addition topside facilities
7. A FPSO has in addition turret facilities
8. A FPSO is subjected to site specific environmental conditions
9. A FPSO operates at constantly changing drafts due to frequent loading and offloading cycles

1.6.3.1 FPSO Structure

Hull structure is designed and build entirely to ship rules for converted FPSOs (i.e. former oil tankers) and for new build FPSOs because FPSO rules are extensively based on ship rules for the hull structure. Bamford et al., (2007)

FPSO hull structure is similar to trading tanker hull structure. The major difference is the extra topside equipment and structure as well as the turret structure and mooring arrangement on the FPSO.

Some anonymous typical FPSO structures presented in **Figures 5-7** show various internal turret locations.

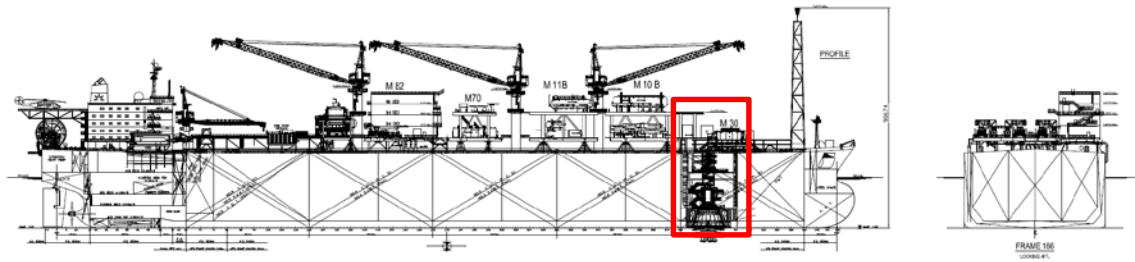


Figure 5: Anonymous Typical FPSO General Arrangement

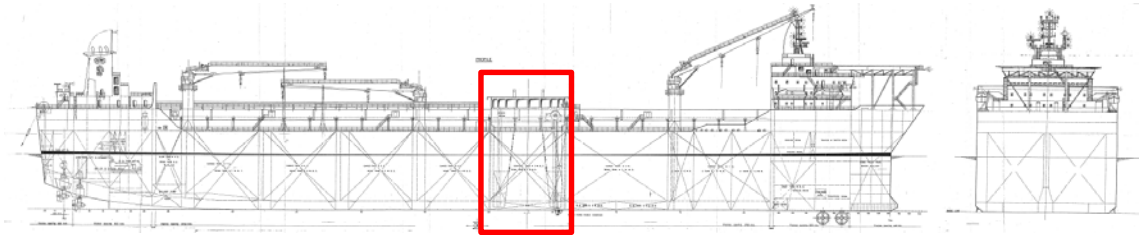


Figure 6: Anonymous Typical FPSO General Arrangement

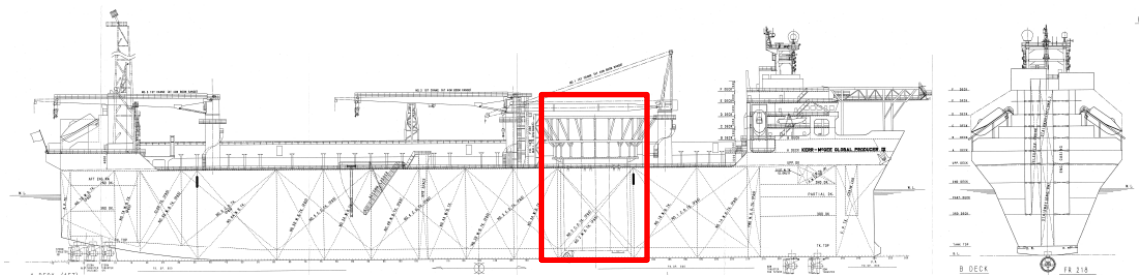


Figure 7: Anonymous Typical FPSO General Arrangement

Figures 8 and 9 outline the common terminology used to describe various parts of the hull in class societies and in this thesis.

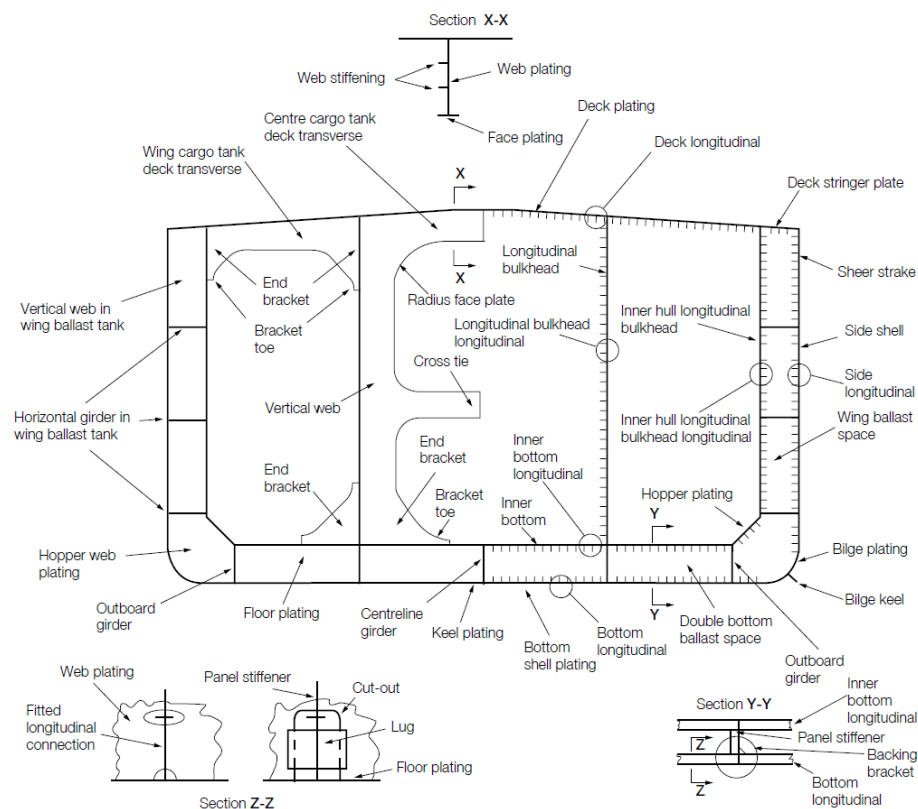


Figure 8: Typical midship section nomenclature (ShipRight, 2004)

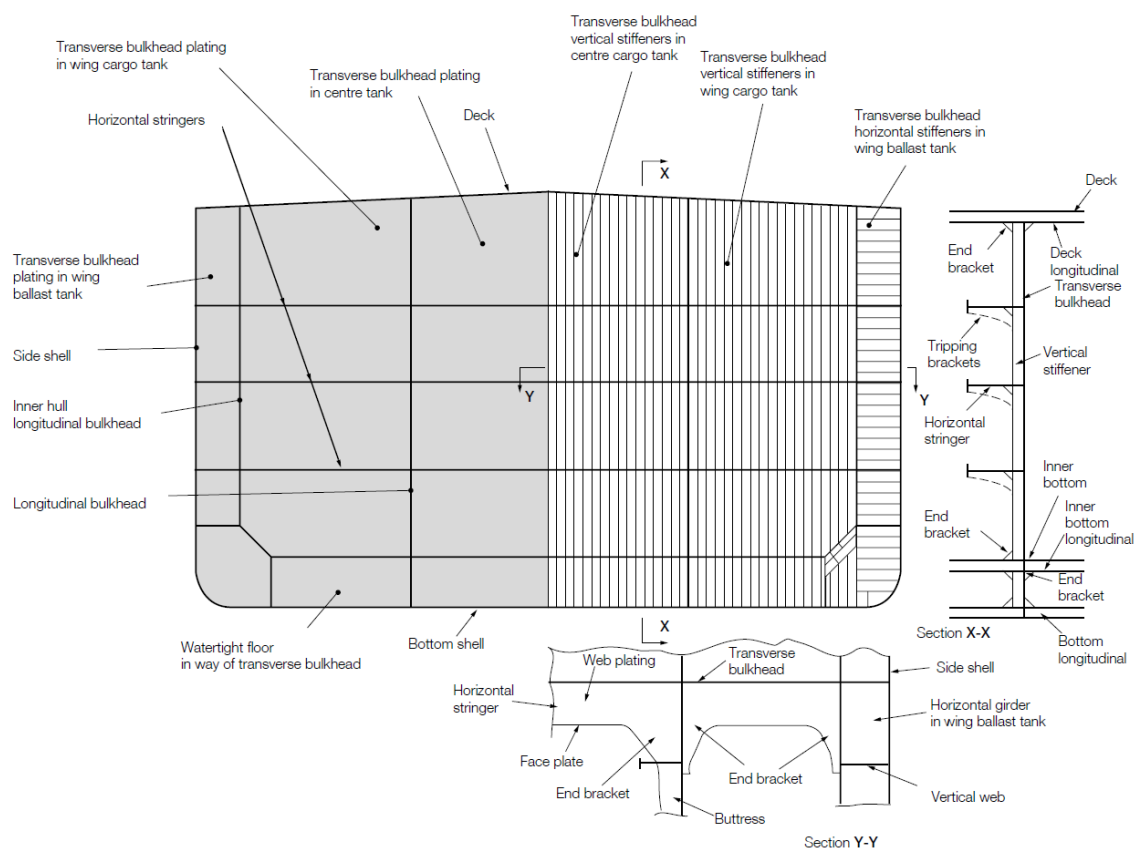


Figure 9: Typical transverse bulkhead nomenclature (ShipRight, 2004)

1.6.3.2 Fatigue Hot Spots and Critical locations

During the ship's life, it should be recognized that as a result of poor workmanship, deficient material, collision damage, etc., structural failure may occur in areas not identified as fatigue hot spots. For example specific longitudinal stiffener end connections which fatigue analysis indicates may be susceptible to fatigue failure (LR-Hull-Inspection-Guide, 2007). The critical location is the structural detail where the stress field is expected to have a complex behaviour under cyclic loading. In general, this location of a structural detail will be in way of a stress concentration, structural discontinuity and at the toe of the weld (ShipRight-3, 2004). Some examples of the critical structural details which should be considered in LCF are:

1. Welded hopper knuckle connection, **Figure 10**
2. Radiused hopper knuckle connection, **Figure 11**
3. Bulkhead stool to inner bottom connection, **Figure 12**
4. Longitudinal end connection, **Figure 13**

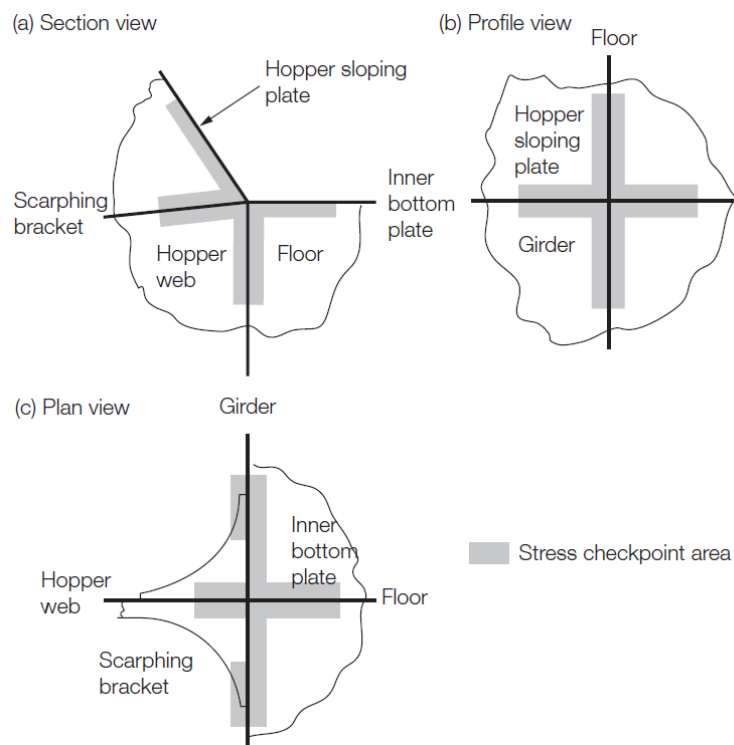


Figure 10: Welded hopper knuckle connection (ShipRight-3, 2004)

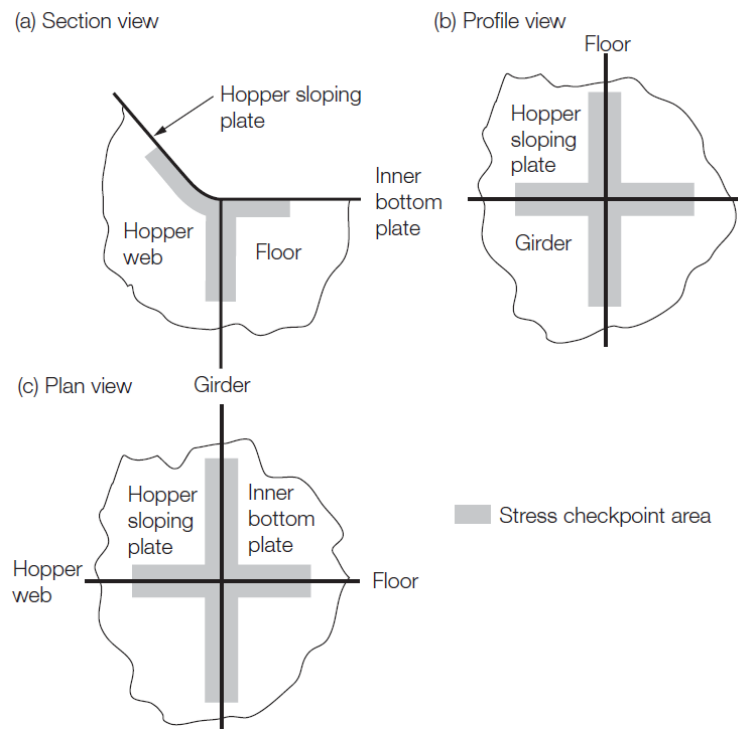


Figure 11: Radiused hopper knuckle connection (ShipRight-3, 2004)

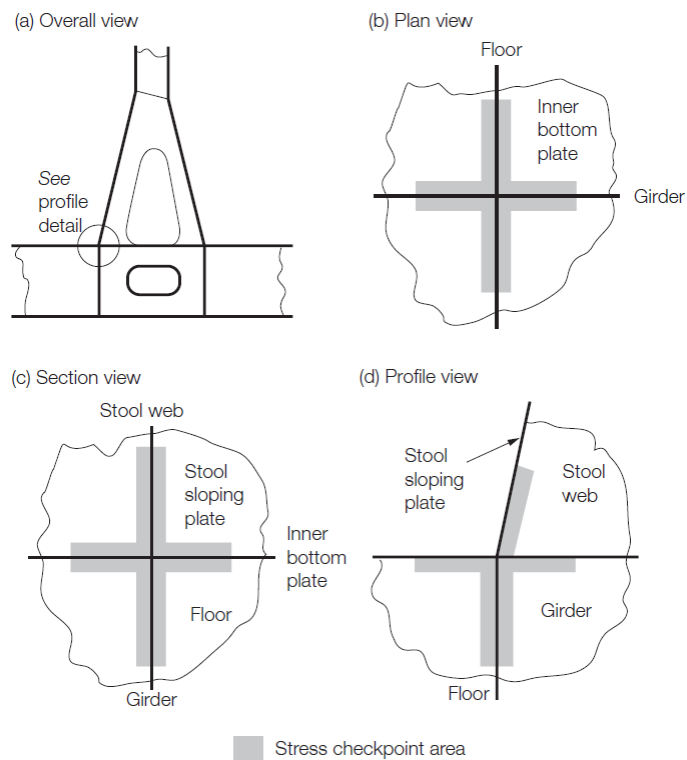


Figure 12: Bulkhead stool to inner bottom connection (ShipRight-3, 2004)

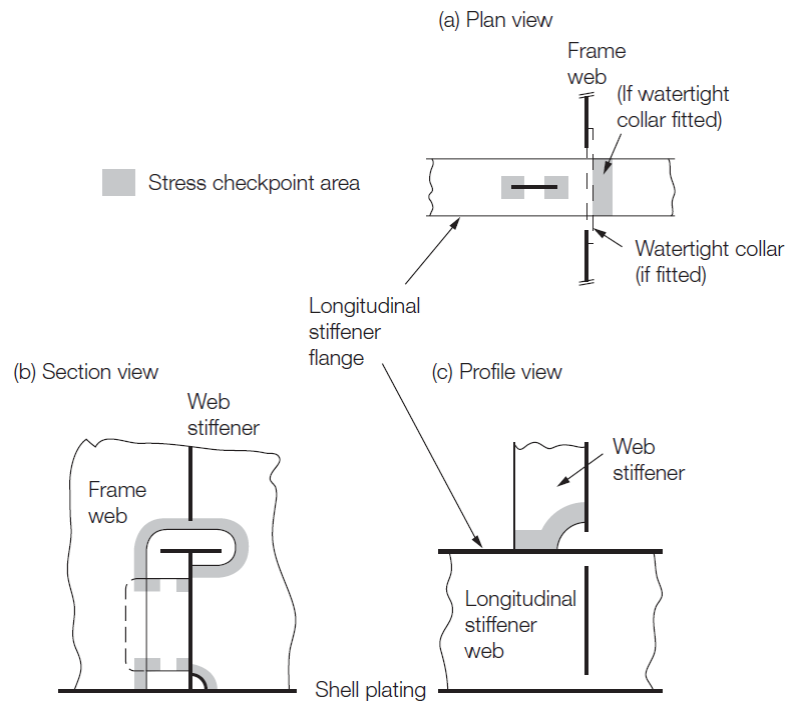


Figure 13: Longitudinal end connection (ShipRight-3, 2004)

1.6.3.3 *The Effects of conversion on fatigue*

From the fatigue point of view; the inherited accumulated fatigue over the years of the ocean going ship will be added to the specific and unique FPSO fatigue accumulations at a fixed location. Especially with the tonnes of extra steel added as topsides and the internal turret added as a modification to the primary hull structure. This combination is not favoured by fatigue. The Kuito FPSO may be a good example to quote as the primary cause of cracking according to the ABS report (470 crack defects were reported after conversion) was the fatigue damage sustained during its 10.5 years of trade on the Trans-Alaska Pipeline System (TAPS) trade route (ABS-OMAE-FPSO, 2004).

However, the author is of the opinion that the primary cause of fatigue damage in the Kuito's case is LCF due to either; frequent loading and unloading which is the major cause of damage in benign locations (Bamford and Stewart, 2007) or due to both frequent loading and unloading together with wave induced loads even when the extreme value of vertical wave bending moment (VWBM) is small. The reason being that wave induced loads are a rapid time variant process and its maxima meet the maxima of still water bending moment (SWBM) with a greater probability, resulting in higher combination factors. Huang et al., (2005) Therefore, although Kuito FPSO was operating in benign conditions (in Block 14) which may appear less onerous particularly

when considering HCF, this may not be the case in LCF. This is because even in benign environments the FPSO may experience extremely diverse wave induced loads which is more onerous for LCF.

The turret cavity or Moonpool modification in **Figure 14** refers to the vessel structure within the turret cavity and the access space between the turret and cavity. This structure is prone to ovality due to dynamic loading and can be subjected to fatigue cracking particularly in conversions where the turret alignment and vessel structure surrounding the turret is less likely to be adequate (HSE-2001/73, 2001).

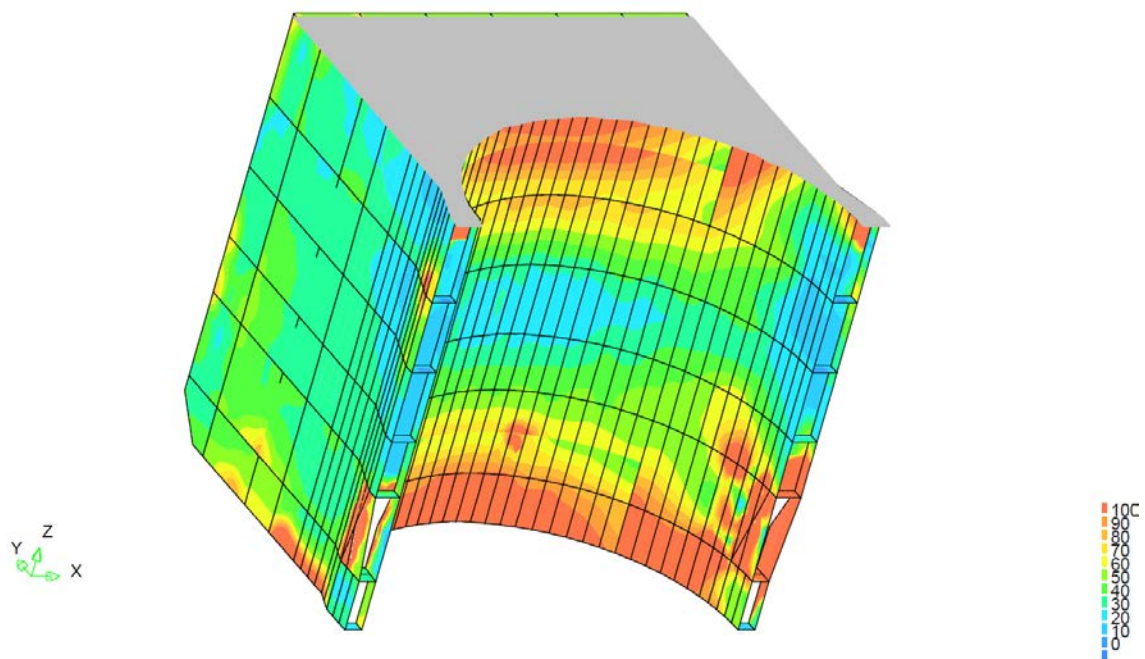


Figure 14: e.g. Turret port side – Yield Strength 235N/mm^2 (View on Moonpool) (Client-Report-GA, 2002)

It is typical for the hull of a trading tanker to be reassessed when converted to FPSO for the following reasons (ShipRight-FOI, 2008):

1. Loads from Topsides equipment on upper deck,
2. Integration of the mooring system of an internal turret,
3. Redefinition of loading limitations as a tanker (e.g. Still Water Bending Moment and Shear Forces)
4. Corrosion in excess of that permitted for a trading tanker.

1.6.4 Loading and Strength of FPSO vs. Oil Tankers

FPSOs operate in a different way from oil tankers. This is because cargo is continuously being loaded and unloaded which means that still water loads vary constantly (i.e. FPSO hull structure being repeatedly in sagging and hogging conditions). This also results in varying pressure differences on the bulkheads. Furthermore, topside weight and the presence of the turret result in a distribution of weight that is different from an oil tanker. The additional volume at the ends of the FPSOs combined with limited ballast tanks can create still water bending moments significantly larger than traditional oil tankers. Moreover, because FPSOs are operating in different areas with harsh and benign conditions, extremely diverse wave induced loads are experienced. Huang et al., (2005)

The key design driver for oil tankers is the longitudinal strength whereas both longitudinal and transverse strengths are key drivers in FPSO design. This is due to the fact that for a FPSO it cannot be assumed that all the ballast tanks will be full and all cargo tanks empty at light drafts. In addition, it cannot be assumed that all ballast tanks will be empty and all cargo tanks full at deep drafts. Furthermore, even in benign environments, FPSOs can experience significant roll responses which cause the transverse structure to rack. Bamford et al., (2007)

1.6.4.1 Static and dynamic loads

Petinov (2003) Hull structures are subjected, apart from wave induced and vibratory forces, to constant and slowly varying loads and stresses due to static loads (the hydrostatic pressures, the weight of hull structure, machinery, storage, cargoes, etc.). In addition, the self-balancing stresses due to a temperature gradient and residual stresses imposed on the structure during production should also be considered to complete the loading history. For example, hull girder bottom members are loaded by wave-induced global bending, lateral pressures, inertial and static loads. At the same time they are flexed under external hydrostatic and hydrodynamic pressure, static and inertial loads from inside.

Petinov (2003) The loads imposed on a hull structure can be grouped into dynamic (rapidly alternating) and quasi-static (relatively slowly varying) groups. The latter is complemented by the stresses due to the difference in ambient and hull steel temperatures and by the residual welding stresses. The thermal stress can be subdivided

into slowly varying ones which depend on air-water average temperatures (varying seasonally along the ship routes), diurnal variations depending on the air water temperature difference and due to the hull structure's exposure to solar radiation. The latter group develops mainly in relatively calm and moderate seas and may be regarded in the long term representation as complementing the alternating load history. Therefore, the attention is focused on the effects of quasi-static loads and residual stresses on fatigue behaviour of structural components under wave-induced loads.

1.6.4.2 Still Water Bending Moment

The still water bending moment (SWBM) on an oil tanker is due to the ship's lightweight, deadweight and buoyancy but in a FPSO the SWBM varies much more frequently from one load condition to another. This variation of load conditions is due to loading patterns and human action. The number of its load condition is far more than that of oil tanker. The SWBM variation at midship section of a FPSO with different load conditions is illustrated in **Figure 15** (Sun and Bai, 2003).

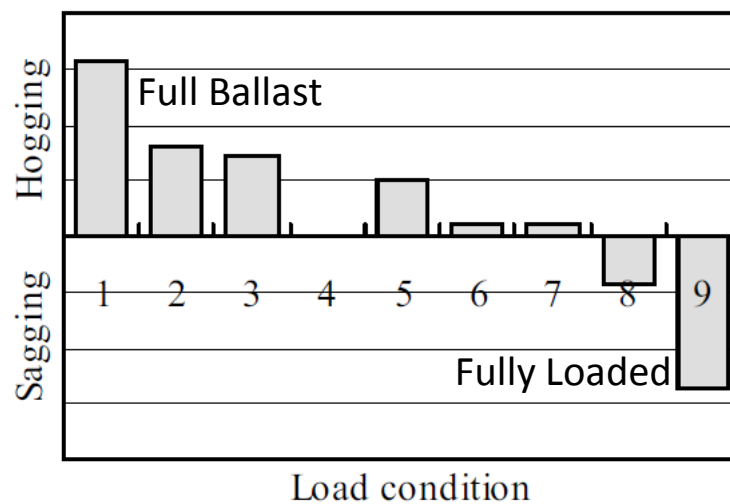


Figure 15: SWBM variation at midsection of FPSO (Sun and Bai, 2003)

The still water load due to gravity and buoyancy contributes to around 50% of the total global hull girder load for oil tankers. This is less for FPSOs operating in the North Sea. Due to frequent loading and unloading the still water load effect (SWLE) in FPSOs is different from oil tankers. Topside loads on a FPSO combined with the presence of the internal turret may result in an uneven time fraction in hogging and sagging of an FPSO. This has a direct effect on the combined sagging and hogging extreme bending

moments. Moreover, in every single loading and unloading cycle the FPSO will experience maximum bending moments for both hogging and sagging. The variation in the maximum SWBM over different cycles describes the long term variation of SWBM as shown in **Figure 16**. The variation in the SWBM in one cycle describes the short term variation of SWBM as shown in **Figure 17**. This is due to difference in weight distribution which changes the buoyancy resulting in changes in SWBM. Two types of weight distribution variations exist; one where loading positions remain unchanged but the cargo or weight varies and the second is where the loading positions change. Huang et al., (2005)

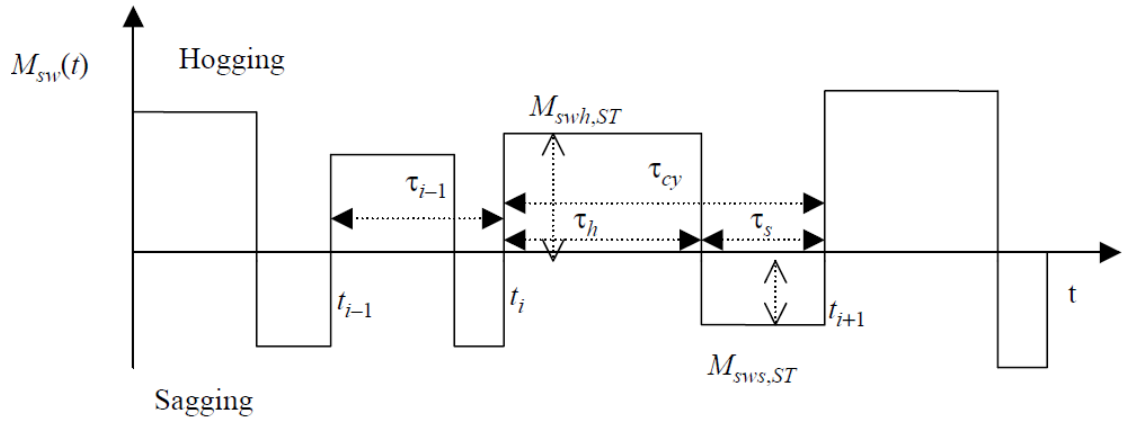


Figure 16: Modelling long-term SWBM variability (Huang and Moan, 2005)

Figure 16 shows the proposed model consisting of a Poisson point process for the renewal time of successive cycles, with a mean occurrence rate of $\nu_{cy}=1/E[\tau_{cy}]$, where $E[\tau_{cy}]$ is the mean value of the duration τ_{cy} for any one cycle. At each renewal instant, the SWBM is successively modelled by two square waves. Their heights $M_{swh,ST}$ and $M_{sws,ST}$ correspond to the maximum intensities of hogging and sagging SWBM in one cycle, i.e. random variables with a distribution. Their random widths τ_h and τ_s are the durations of hogging and sagging, and are assumed to follow exponential distributions.

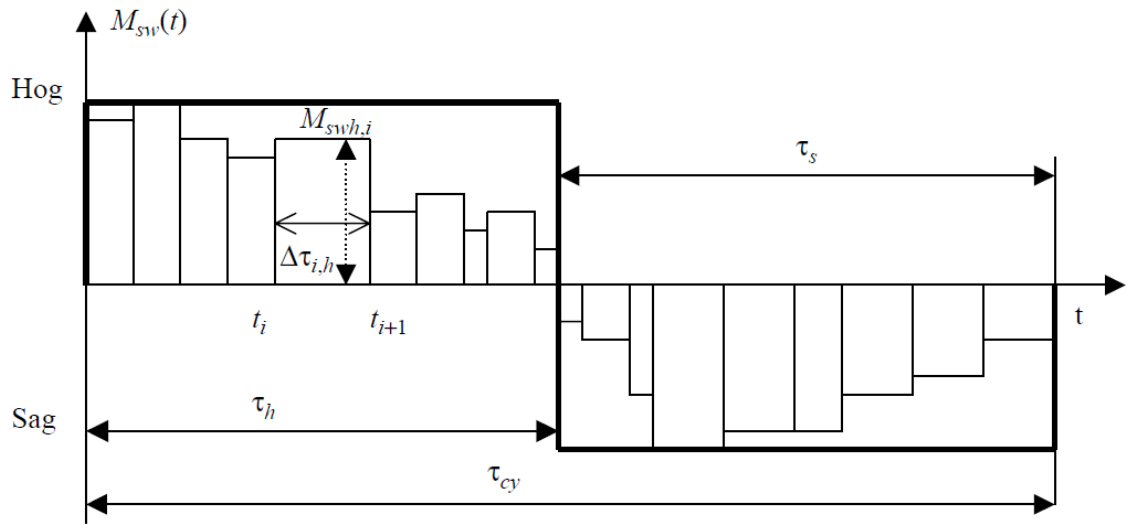


Figure 17: Modelling short-term SWBM variability (Huang and Moan, 2005)

Figure 17 is assumed for a loading–offloading cycle. In this model, any rectangle stands for one of the above-defined load conditions, its height $M_{sw,i}$ ($M_{sws,i}$ and $M_{swh,i}$ refer to sagging and hogging) stands for the intensity of SWBM under the i th load condition, its width $\Delta\tau_i$ ($\Delta\tau_{i,h}$ and $\Delta\tau_{i,s}$ refer to hogging and sagging durations) stands for the duration of the corresponding load condition, while t_i is the renewal instant of load conditions.

1.6.4.3 Vertical Wave Bending Moment

In the long term range, wave elevation is a non-stationary process modelled by taking wave elevation as a sequence of discrete short periods of stationary Gaussian waves characterised by parameters such as significant wave height and average period. Short term VWBM corresponds to a steady (random) sea state which is considered stationary with duration of several hours. Long term statistics are derived by using the total probability theorem for all short term sea states over the relevant long term scatter diagram. Long term VWBM is then modelled as a Poisson square wave process as shown in **Figure 18**.

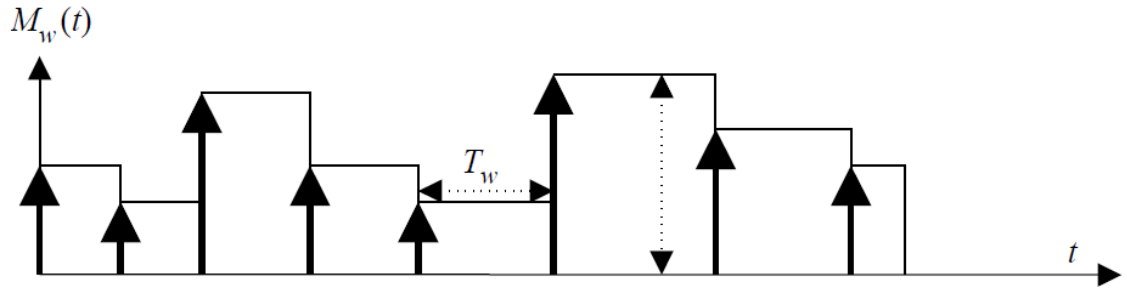


Figure 18: Long-term VWBM variability (sagging or hogging)

Where

M_w is the peak of each individual VWBM,

T_w is the mean long-term peak values of VWBM

1.6.4.4 Combined SWBM and VWBM

The load combination method is based on load models and the correlation between loads. The assumption of independence between still water and wave induced bending moments is adopted for oil tankers but not for a FPSO yet, this is because no information about this correlation is available yet. Therefore, independence between the SWBM and VWBM is assumed. The combination of hull girder bending moments needs to be achieved separately for hogging and sagging, as shown in **Figure 19**. Huang et al., (2005)

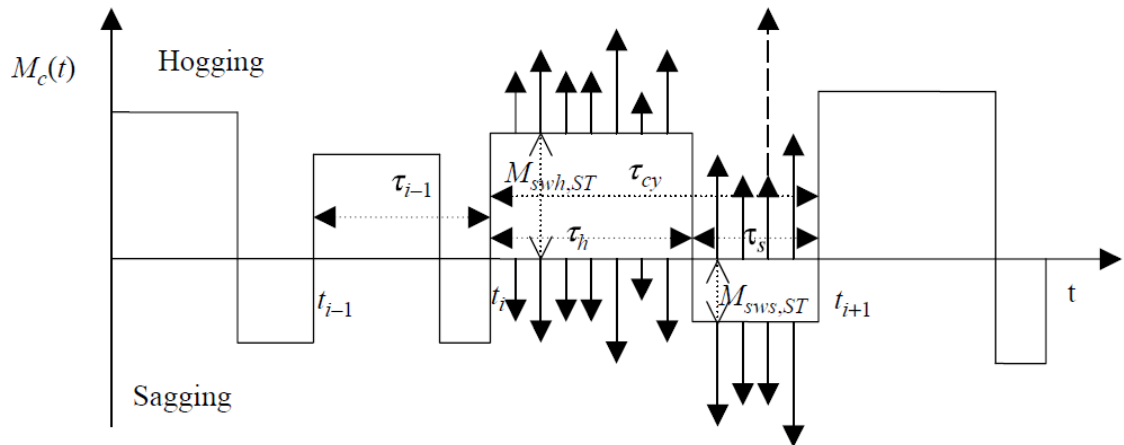


Figure 19: Model of combined SWBM and VWBM (Huang and Moan, 2005)

Load combination factors of VWBM are larger than those for SWBM because wave induced load is generally larger than still water load in harsh conditions. For a FPSO operating in the North Sea, the combined load is dominated by VWBM (primary load effect) and the corresponding SWBM is considered the secondary load effect. For a FPSO operating in West Africa (i.e. benign waters) still water load is dominant and the combination factor of VWBM is the most significant although the extreme values of VWBM are small. This is because wave induced load is a rapid time variant process and its maxima meets the maxima of SWBM with a greater probability resulting in higher combination factors. The SWBM combination factor is mainly dominated by its relative magnitude to wave induced load. For wave induced load with a rapid time variation; the VWBM combination factor is determined, not only by its relative magnitude to still water load, but also its time variation. The fast time variation of VWBM will result in an increase in the corresponding combination factor, despite its smaller relative magnitude in some conditions. For instance, in benign waters, the wave induced load is much smaller than the still water load, but with larger combination factors. Huang et al., (2005)

The previous statement is supported by a recent conclusion of LCF assessment of a single hull FPSO module by Raji (2010) who stated that LCF damage is more significant when the FPSO is in benign waters than when it is located in rough seas, see **Table 2**. For example, at location BHS1 (Bottom Detail - **Figure 20**), the ratio of the LCF damage to the wave fatigue damage is 1:300 when the FPSO is in the North Sea (NS) and approximately 1:56 when the FPSO is located in the seas of West Africa (WA). Another example, at location BHS3 (Bottom Detail - **Figure 20**), the ratio of the LCF damage to the wave fatigue damage is 1:600 when the FPSO is in the NS and approximately 1:124 when the FPSO is located in the seas of WA. This shows that LCF damage will play a more critical role on the cumulative damage and fatigue life when the FPSO is located in the WA.

Table 2: Wave damage and low cycle damage for different sea scatter diagrams. Raji (2010)

	North Sea (NS)		West Africa (WA)	
	HCF Damage	LCF Damage	HCF Damage	LCF Damage
BHS1	1.44	0.0048	0.236	0.00421
BHS2	2.33	0.0754	0.349	0.0960
BHS3	3.42	0.0055	0.557	0.0045
BHS4	0.90	0.0026	0.170	0.00066
BHS5	1.52	0.1510	2.270	0.1330
BHS6	1.15	0.1880	1.660	0.1750

Note: BHS6 location is shown in 4.3.2 Bottom Detail **Figure 128**

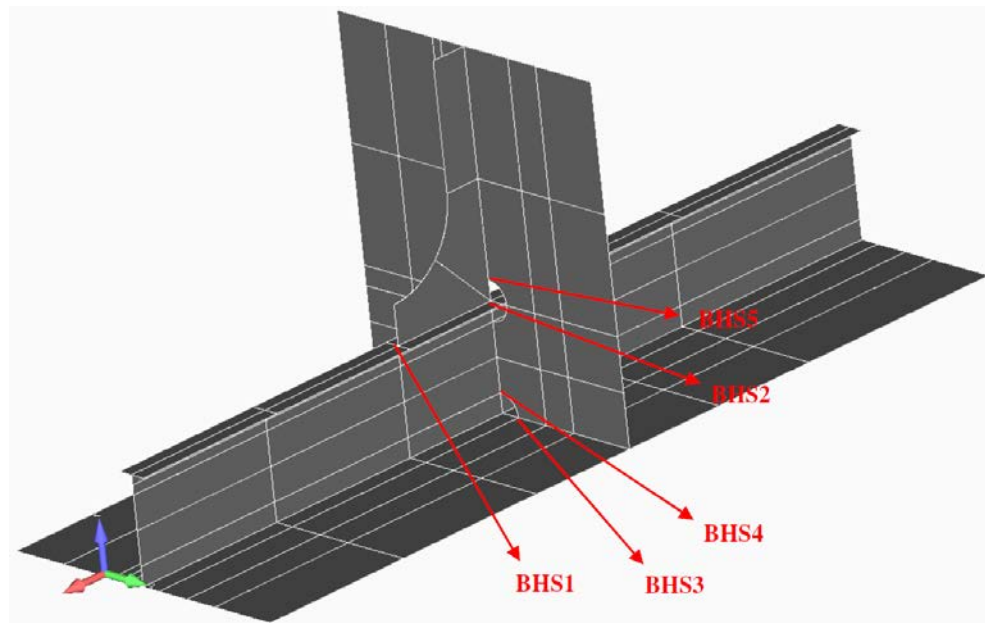


Figure 20: Location of hotspots in bottom detail (Raji, 2010)

1.7 Fatigue Analysis

In the case of oil tankers the minimum design life is 25 years with a sailing life of 50% full load, 50% in ballast and 15% life moored in a harbour. In common structural rules (CSR) fatigue requirement, the load assessment is based on the expected stress history for a trading tanker which is characterized by dynamic load values with 10^{-4} probability of occurrence during the design life. The load history of each structural member is represented by the Weibull probability distribution of the corresponding stresses

calibrated using spectral fatigue analysis. Only the wave induced loads are considered. Other cyclic loading such as slamming, low cycle (high stress range due to loading and unloading), or vibration induced fatigue are not considered. Bamford et al., (2007)

The common structural rules approach to fatigue analysis cannot be applied to FPSOs. A FPSO is at sea 100% of the time, undergoing many intermediate loading conditions between full and ballast conditions. LCF is more significant due to frequent loading and unloading, and different environmental loads and associated heading probabilities. The application of deterministic fatigue methods to FPSO hull structure is questionable because spectral fatigue analysis would be necessary to calibrate the deterministic method. The importance of LCF for FPSOs will complicate the fatigue analysis especially for benign environments and for conversions it is necessary to account for the fatigue damage accumulated during the trading life as a tanker. Spectral fatigue analysis using voyage simulation software to model trading tanker service is recommended and is already routinely used for the screening of FPSO conversion candidates. Site specific fatigue analysis is required for both new builds and conversions. Two design approaches are available; local and global. The local design approach focuses on making local improvements to reduce the stress where fatigue life is too low (toe grinding is an extreme example of this). This approach minimizes steel weight but increases the costs of design and production. The global approach focuses on making global improvements to reduce the stress in areas where fatigue lives are too low (prohibiting the use of high tensile steel is an extreme example of this approach). This approach reduces design and production cost but increases steel weight. Bamford et al., (2007)

1.8 Conclusions

1. LCF is believed to be the primary reason for several reported damages in ship structures
2. Quasi-static loading due to loading and unloading of cargo and ballast is the single most significant load case causing LCF
3. FPSOs are more susceptible to LCF for three main reasons: one, the unique structure of FPSO in terms of the presence of internal turret and topside loads which affects the structural response of FPSO to dynamic and quasi-static loads; two, the frequent loading and unloading patterns of a FPSO (i.e. unlike oil tankers which are either in full load or ballast condition) which causes the FPSO to experience the maximum hogging and sagging still water bending moment in

every single cycle; three, the condition of the sea at which the FPSO is operating (site specific environment), even benign condition may subject the FPSO to extremely diverse wave induced loads.

Chapter 2

Literature Review

2 CHAPTER 2: Literature Review

This chapter provides a literature review of LCF divided into three main categories following the introduction, these are; the fundamental theory of LCF, the phenomena of LCF in a ship structure and LCF assessment.

2.1 Introduction

Most of the available literature discusses LCF in terms of either material behaviour or modelling and prediction of LCF life in rotating or tubular structures. These are typically at room temperature or at high temperatures (i.e. creep) and are therefore not directly relevant to the research topic (i.e. steel for ship structure). However, including such literature in the review may help to shed some light on some of the fundamental aspects of LCF. LCF has been studied in other areas of engineering including:

1. Power generating facilities (Earthman, 1991)
2. Aeronautical applications (Luquiau et al., 1997)
3. Nuclear design codes (Mathew et al., 2008)
4. Structural materials (Matsuzuki and Horibe, 2009)
5. Aluminium foams (Ingraham et al., 2009)
6. Automotive and aerospace industries (Begum et al., 2009) (Mo et al., 2010)
7. Non-linear ultrasonic technique (Palit Sagar et al., 2011)
8. Railway applications (Šamec et al., 2011)
9. Piping systems in nuclear power plants (Yu et al., 2012)

LCF has been directly or indirectly covered in literature in different contexts or themes which the author has classified into seven main categories as follows:

1. Fatigue mechanism
2. Notch effect, energy criteria and cyclic deformation
3. Effects of various parameters on LCF
4. Prediction, assessment and damage accumulation
5. Application of combined HCF and LCF
6. Testing of welded joints
7. Reliability analysis

Each of the stated main categories will be highlighted and discussed in the following sections.

2.1.1 Notch Effect, Energy Criteria and Cyclic Deformation

Skelton et al., (1998) stated that when an energy value for crack initiation is known from LCF tests with a constant strain range at elevated temperature, an estimate of linear elastic fracture mechanics (LEFM) crack growth rates may be obtained from equations. These equations are based on the energy required to fail a process zone at the crack tip, **Figure 21**. During fatigue cycling (reversed load cycling), a contained yield region at the crack tip is forced into alternate tension/compressive yields by the surrounding elastic matrix.

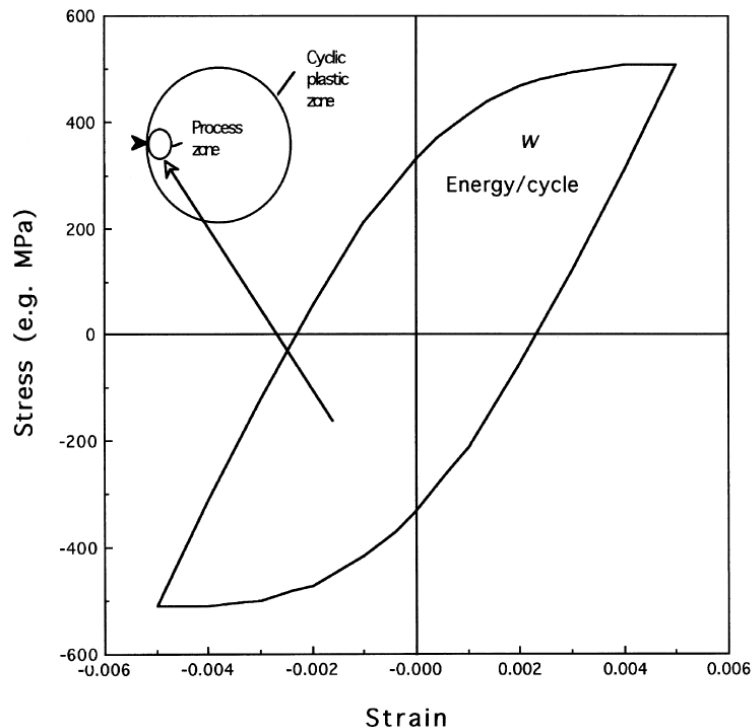


Figure 21: Schematic, showing process zone embedded within cyclic plastic zone and associated energy expenditure (Skelton et al., 1998)

Bentachfine et al., (1999) proposed a new method to determine the notch effect in LCF. This method needs a fatigue reference curve expressed in terms of the strain energy density range versus the number of cycles to failure and to compute the strain energy density range distribution at notch tip. This method is based on the volumetric approach of the fatigue initiation area with a pseudo effective distance. This distance represents the beginning of the pseudo singularity of the strain energy density range at the notch tip. They also studied the ‘hot spot approach’. This was developed by improving Dowling’s method. It uses more appropriate relationships, between the elastoplastic

stress and strain concentration factors and the elastic one, than Neuber's rule. They concluded that this method overestimates the number of cycles to failure because the Neuber's rule underestimates the notch effect and ignores the necessity of a fatigue process volume. Furthermore, it has been noticed that the notch effect does not disappear in LCF by plastic relaxation and remain a problem for some structural components exhibiting a complex geometry.

Yang et al., (2003) investigated fatigue characterization of 63Sn/37Pb solder material at varying loading rates and dwell times at room temperature both experimentally and analytically. Based on the experimental results, the time-dependent deformation and damage models are established, and the cyclic failure criteria under different loading conditions were proposed. These models can be used to predict the ratchetting deformation and failure behaviour, and the strain rate-dependent low cyclic fatigue life of the solder material. In addition, the effects of dwell time on LCF of the materials can also be taken into account.

Yoon et al., (2004) investigated the overlay model (distributed element model) of cyclic deformation which is considered to be physically motivated and has definite advantages over the classical models as it could describe qualitatively a variety of effects that the classical models are not able to describe. This model successfully describes the deformation behaviour of a material that obeys Masing's hypothesis. However, there are many materials that do not satisfy Masing's hypothesis, and show cyclic hardening or cyclic softening and strain range dependence. Masing's hypothesis is that the shape of the cyclic stress strain hysteresis loop should be geometrically similar to the monotonic stress strain curve magnified by a scale factor of two. The discrepancy between Masing's hypothesis and the real material behaviour is due to considerable changes in the hysteresis loop e.g. cyclic hardening or cyclic softening and strain range dependence. (Yoon et al., 2004) modified the overlay model to consider the characteristics in the cyclic deformation behaviour of non-Masing material, this is observed through LCF tests of 316L and 429EM stainless steel. The prediction by the modified overlay model shows good agreement with the actual hysteresis loops at a wide range of strain amplitudes and temperatures.

Wilczynski et al., (2007) concluded in their literature review that the fatigue analysis is assisted by finite element modelling technology, different approximation concepts, or continuum damage mechanics. They also concluded that the optimal design for the low

cycle regime does not seem to be considered so far. In other words the theoretical understanding of LCF is at the early stages of its development. They also showed how proper shape modification of notches or element boundaries can significantly increase the number of cycles corresponding to crack initiation or ultimate member failure. Shape optimization computational technology is used to maximize the life-time of notched structural components in the LCF regime. The presented approach is composed of three steps: (1) stress-strain calculation using notch correction and plasticity models; (2) estimation of the critical plane to assess potential fatigue life spans; and (3) formulation of the optimization problem with a constraint set on the number of cycles corresponding to crack initiation.

The modes of failure of structural members can be classified in the following categories:

1. Failure by excessive deflection
2. Failure by yielding at ordinary temperatures (plasticity) or elevated temperatures (creep)
3. Failure by fracture:
 - a. Sudden fracture of brittle materials
 - b. Fracture of cracked structural components
 - c. Progressive fracture (fatigue)
 - d. Time dependent fracture at elevated temperature

The total fatigue life with the number of cycles N_f of structural detail is given as a sum of two portions. The first one corresponds to the initiation stage N_i (fatigue crack initiation), the second part corresponds to the subsequent fatigue crack propagation N_p , as illustrated in **Figure 22**. The stress concentration factor K_t is an important parameter for prediction of crack initiation. The stress intensity factors K_i ($i = I, II, III$ crack modes) are used for prediction of crack growth. Wilczynski et al., (2007)

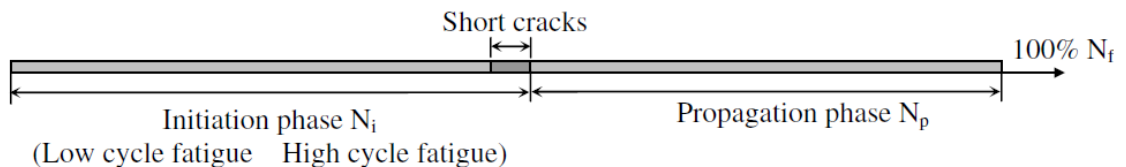


Figure 22: Different phases of the fatigue life (Wilczynski and Mróz, 2007)

When the elastic local stress and strain exceed the elastic limit, an elasto plastic stress evolution occurs. The crack initiation is then dependent on the plastic dissipated energy and the stress at the notch root. In order to maximize the critical number of cycles corresponding to crack initiation a rational design of notch shape is required. Wilczynski et al., (2007)

The four major approaches used to design against fatigue failure are:

1. Stress life (S–N) model (stress based approach)
2. Local strain life (ϵ –N) model which is a strain based approach or local strain approach (LSA)
3. The fatigue crack growth (da/dN - ΔK) model (fracture mechanics approach) where ‘a’ is the half crack length and ΔK is the stress intensity factor range
4. The two stage model (i.e. combining models 2 and 3) in order to incorporate both fatigue crack formation (nucleation) and fatigue crack growth

Fatigue crack initiation life predictions for notched specimens or components based on the LSA require fatigue data obtained from simple uniaxial unnotched specimen tests. It is assumed that smooth and notched specimens with the same local strain range experience the same number of cycles to fatigue failure. Local strain range is estimated using any of following methods:

1. Experimental tests using strain gauges
2. Numerical methods like elasto-plastic finite or boundary element analyses
3. Using approximate elasto-plastic stress strains relations like notch correction (NC) rules, known also as notch stress-strain conversion (NSSC) rules

2.1.1.1 Elastic plastic stress strain relations

It is assumed that the lifetime operating loads are either known or have been specified as a design condition. In certain components the operating load history is almost uniform with small variation from cycle to cycle, but in most cases the real load histories vary in both shape and magnitude with time. The loading history could be a superposition of deterministic or stochastic loads. In most cases fatigue loading is multiaxial (see **Figure 23**) which means that stresses vary across and along the structural component. Wilczynski et al., (2007)

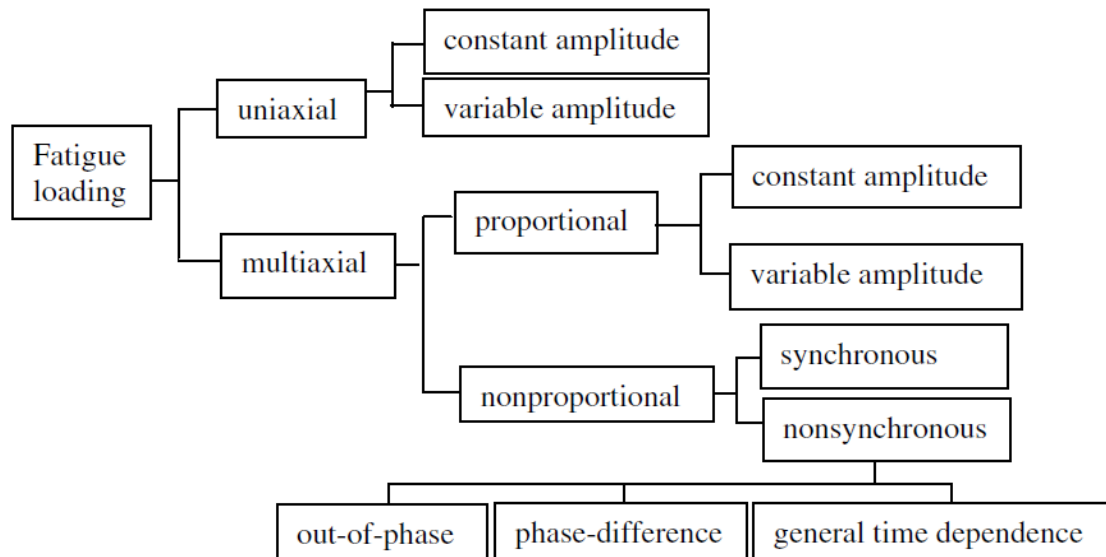


Figure 23: Fatigue Loading (Wilczynski and Mroz 2007)

2.1.1.2 Notch correction for uniaxial loading

Failures of structural components often initiate in regions of stress concentrations. Hence, fatigue initiation and crack growth require an accurate knowledge of local notch tip stresses and strains. These quantities can be determined using the time consuming finite element method or practical less complex approaches are often used for complex loading histories. The most popular in literature are the Neuber's rule and Molski and Glinka method. Wilczynski et al., (2007) These methods have the following assumptions:

1. remote stresses are elastic
2. notch tip strains are elastic plastic
3. notch tip behaviour is largely controlled by the surrounding elastic field

The difference between the two methods is illustrated in **Figure 24**, the total energy density obtained from a linear elastic solution is equal to the total energy density obtained from an elastic plastic analysis (Neuber) and the strain energy density obtained from a linear elastic solution is equal to the strain energy density obtained from an elastic plastic analysis (Molski and Glinka).

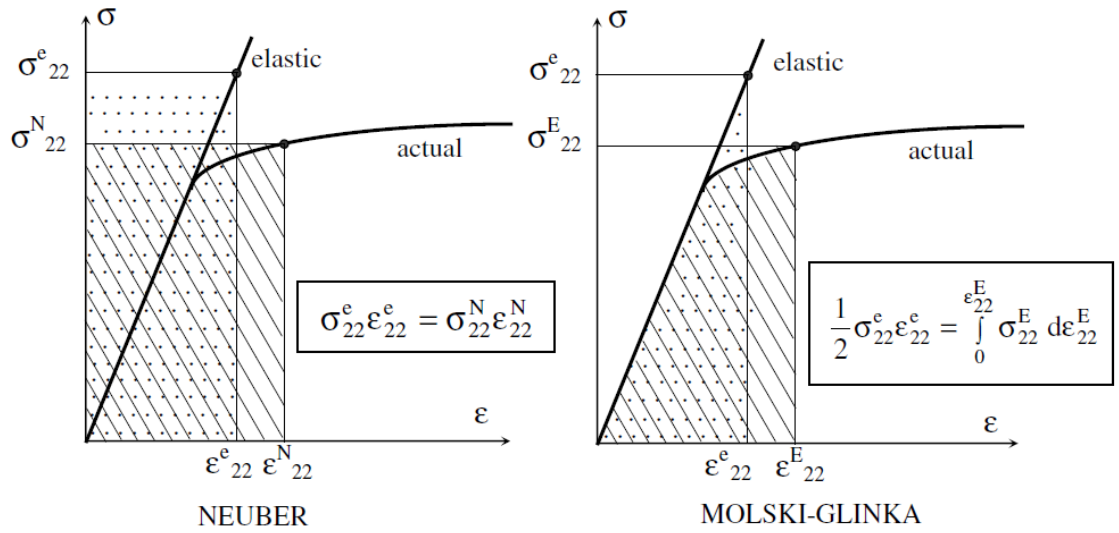


Figure 24: Graphical interpretation of Neuber rule and Molski–Glinka method for uniaxial loading (Wilczynski and Mróz, 2007)

In **Figure 24** the superscripts represent (e) Hypothetical linear elastic stress strain for both Neuber and Molski-Glinka , (N) actual elastic plastic stress strain for Neuber and (E) actual elastic plastic stress strain for Molski-Glinka

2.1.1.3 Neuber's Rule

In the elastic stress range, the stress concentration factor K_σ is equal to the strain concentration factor K_ϵ . This is not valid in elasto-plastic stress range. After yielding, K_ϵ increases while K_σ decrease. Wilczynski et al., (2007) Neuber concluded that the theoretical stress concentration factor K_t in a notched specimen under tension or shear is the geometric mean of the stress and strain concentration in an elastic element:

$$K_t = \sqrt{K_\sigma K_\epsilon}$$

$$\text{Or} \quad \epsilon_\sigma = K_t^2 \epsilon_n \sigma_n$$

$$\text{Or} \quad \epsilon_\sigma = \frac{(K_t \sigma_n)^2}{E} \quad \text{Eq.1}$$

Where

$$K_t = \frac{\sigma^e}{\sigma_n}$$

$$K_\sigma = \frac{\sigma}{\sigma_n}$$

$$K_{\varepsilon} = \frac{\varepsilon}{\varepsilon_n}$$

and σ^e is the local elastic stress state at the notch root, σ_n , ε_n are the nominal stress and strain, σ , ε or σ_{hs} , ε_{hs} denote the actual stress and strain in the elasto plastic state (actual stress and strain in the hot spot) and E is the Young modulus. The stress concentration factor K or K_t is sometimes replaced by the notch factor K_f . The Neuber rule can be more generally interpreted as the equivalence of scalar product of stress and strain in elastic and elasto plastic states:

$$\sigma^e \varepsilon^e = \sigma \varepsilon \quad \text{Eq.2}$$

And when $\sigma^e = K_t \sigma_n$, $\varepsilon^e = K_t \varepsilon_n$ the equality (3) is equivalent to (1)

When the notch root satisfies the condition of elastic deformation, equation (Eq.3) can be extended to cyclic loading:

$$\Delta \sigma^e \Delta \varepsilon^e = \Delta \sigma \Delta \varepsilon \quad \text{or} \quad K_t^2 \Delta \sigma_n \Delta \varepsilon_n = \Delta \sigma \Delta \varepsilon \quad \text{Eq.3}$$

Where $\Delta \sigma$, $\Delta \varepsilon$, $\Delta \sigma_n$, $\Delta \varepsilon_n$ are actual stress and strain range and nominal linear elastic stress and strain, respectively.

Combination of Neuber's equation (Eq.1) or (Eq.3) with the Ramberg Osgood stress strain relations:

$$\varepsilon = \frac{\sigma}{E} + \left(\frac{\sigma}{K'} \right)^{1/n'} = \varepsilon^e + \varepsilon^p$$

$$\Delta \varepsilon = \frac{\Delta \sigma}{E} + 2 \left(\frac{\Delta \sigma}{2K'} \right)^{1/n'} = \Delta \varepsilon^e + \Delta \varepsilon^p \quad \text{Eq.4}$$

Where K' and n' are the cyclic strength coefficient and cyclic strain hardening exponent (material coefficients), respectively, is shown in **Figure 25**.

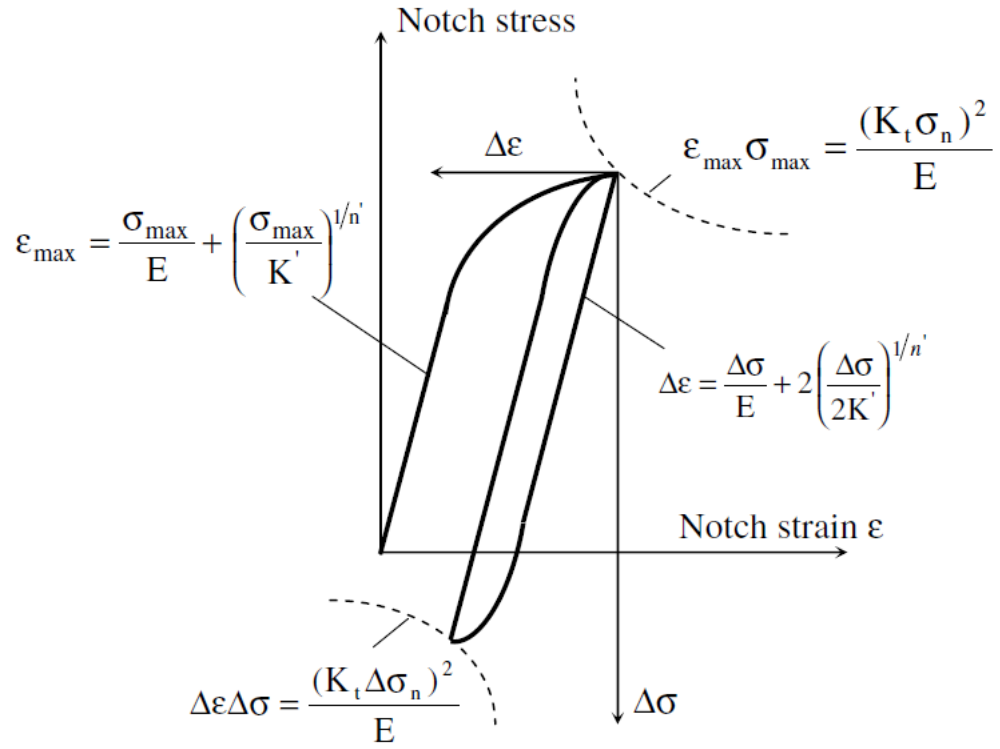


Figure 25: Graphical representation of Neuber rule for uniaxial LCF (Wilczynski and Mróz, 2007)

For Molski–Glinka model and Notch Correction rules for multiaxial loading please refer to Wilczynski et al., (2007)

2.1.1.3.1 Neuber's Rule and Ramberg Osgood relations combined

Combination of Neuber's rule with the Ramberg Osgood stress strain relations is further illustrated by the author as follows:

Ramberg Osgood

$$\varepsilon = \frac{\sigma_{hs}}{E} + \left(\frac{\sigma_{hs}}{K'} \right)^{1/n'} \quad \text{Eq. 5}$$

Neuber

$$K_t^2 \sigma_n \varepsilon_n = \sigma_{hs} \varepsilon$$

Substitute for ε in Neuber's

$$K_t^2 \sigma_n \varepsilon_n = \sigma_{hs} \left(\frac{\sigma_{hs}}{E} + \left(\frac{\sigma_{hs}}{K'} \right)^{1/n'} \right) \quad \text{Eq. 6}$$

$$\text{Now } E = \frac{\sigma_n}{\varepsilon_n} \quad \varepsilon_n = \frac{\sigma_n}{E}$$

Substitute for ε_n

$$K_t^2 \frac{\sigma_n^2}{E} = \frac{\sigma_{hs}^2}{E} + \sigma_{hs} \left(\frac{\sigma_{hs}}{K'} \right)^{1/n'} \quad \text{Eq. 7}$$

2.1.2 Factors Affecting LCF

A number of variables influencing LCF have been covered in literature; including:

1. Porosity and crack initiation, e.g. of powder processed titanium during LCF (Gerard and Koss, 1990), e.g. of cast SiC particulate-reinforced Al–Si alloy composite (Li et al., 2000)
2. Biaxial non-proportional loading, e.g. of a magnesium-lithium alloy (Bentachfine et al., 1996)
3. History effects, e.g. in polycrystalline copper during constant and variable amplitude testing I - Wavy dislocation glide behaviour (Christ et al., 1995)
4. Influence of environment on LCF damage, e.g. in Ti6Al4V and Ti 6246 titanium alloys (Demulsant and Mendez, 1996), e.g. of 2024-T351 and 7075-T651 Aluminium alloys (Lee et al., 2009)
5. Influencing parameters on martensite transformation during LCF for steel AISI 321 (Grosse et al., 2006)
6. Residual stress and plastic strain amplitude, e.g. of austenitic stainless steel AISI 304 (Nikitin and Besel, 2008)
7. Strain amplitude controlled fatigue behaviour, e.g. of pure copper with ultra large grain size (Huang et al., 2012)
8. High temperature LCF behaviour of:
 - a. IN-100 superalloy I and II (Reger and Remy, 1988)
 - b. Ferritic steel forging (Choudhary et al., 1991)
 - c. AISI type 316LN base metal, 316LN-316 weld joint and 316 all-weld metal (Valsan et al., 1992)
 - d. Ti alloys and stainless steel (Mendez, 1999)
 - e. Ti-48Al-2W-0.5Si gamma titanium aluminide (Recina and Karlsson, 1999)

- f. Aluminium alloy (Al–12Si–CuMgNi) (Eswara Prasad et al., 2000)
- g. Modified 9Cr–1Mo ferritic steel (Nagesha et al., 2002)
- h. 316L(N) stainless steel (Srinivasan et al., 2003)
- i. Sn–Ag eutectic solder (Kanchanomai and Mutoh, 2004)
- j. Ni-base superalloy M963 (He et al., 2005)
- k. Titanium aluminide Ti–24Al–15Nb–1Mo alloy (Cao et al., 2006)
- l. Soldering alloys 96.5Sn–3.5Ag (Boulaajaj et al., 2008)
- m. Superalloy IN718 (Praveen and Singh, 2008)
- n. 316 stainless steel welds (Goyal et al., 2009)
- o. An aircraft APU exhaust duct flange (Kim et al., 2012)

2.1.3 Fatigue Life Prediction

Kim et al., (2004) developed a microstructural model for predicting LCF life by modifying Tomkins equation for stage I crack growth by using the ‘equivalent crack’ concept in order to account for multiple cracks initiating and growing at the same time and also by considering damage accumulation from multiple cracking. In order to calculate the length of a fatal crack, statistical analysis was performed considering the distribution of multiple short cracks and a Weibull distribution function. Experimental LCF tests for steels with three different grain sizes were carried out to verify the suggested model. The predicted curve was in good agreement with the experimental data.

Medekshas and Balina (2006) attempted to assess LCF strength of notched components which are used in the practical design procedures for the fatigue life prediction. The Von Mises stress, historically used as a multiaxial design parameter and in the design codes of pressure vessels, has been used here in order to verify its applicability. Moreover, several multiaxial LCF parameters have been proposed without sufficient verification due to two main reasons:

1. The lack of the multiaxial LCF experimental data
2. Due to the variety of these parameters including material constants which hamper the use of the parameters.

The assessment is based on both the finite element method analysis and on numerous experimental data obtained by LCF testing of two alloyed steels and two titanium alloys. Specimens of various shapes (cylinder, plate) with theoretical stress concentration factors ranging from 1.39 to 7.8 as well as smooth ones were used. The

investigation concluded that the stress concentration factor K_t predetermines stress or strain cycling in the concentration zone, and the cyclic life may be predicted using Von Mises stress or strain. The assessment also concluded:

1. Data from LCF tests of smooth specimens can be used for cyclic strength calculations of components with stress concentration. This requires the use of the stabilized cyclic stress strain curve and Neuber's rule. The calculated Von Mises stresses and strains in a concentration zone can be considered LCF fracture criteria.
2. During stress or strain controlled elastic-plastic cyclic loading, the loading conditions, at the stress concentration zone, depend on the theoretical stress concentration factor K_t . In other words, the value of this factor predetermines the loading mode (stress or strain controlled cycling) dominating the concentration zone.
3. For the materials investigated; at moderate values of theoretical stress concentration factor ($K_t = 1.39 - 2.0$) in the concentration zone (localized stress and strain level), stress cycling is dominating and the stress amplitude σ_i may be used as the fracture criterion. At higher values of the factor ($K_t > 2.3$) in the concentration zone, strain cycling is dominating and the strain amplitude ε_i may be used as the fracture criterion. However, for some intermediate K_t values, no specific loading mode dominates in the notch.

The author recommends the use of the fatigue notch factor instead of the theoretical stress concentration factor as it underestimates the allowable stresses Petinov (2003).

Seweryn et al., (2008) presented the description of damage accumulation for analysis of fatigue life of structural elements under torsion. Damage accumulation rule has been formulated incrementally and connected with a monotonic work hardening curve. The proposed model of damage accumulation enables the definition of the number of cycles or the time of safe application of complex fatigue loads to arbitrarily shaped machine components.

Fatigue life in the range of constant amplitude loading (multiaxial) is often described using a range of strain equivalent $\Delta\varepsilon_{eq}$. An example of such models is Manson–Coffin equation (**Figure 26**), modified later by Morrow:

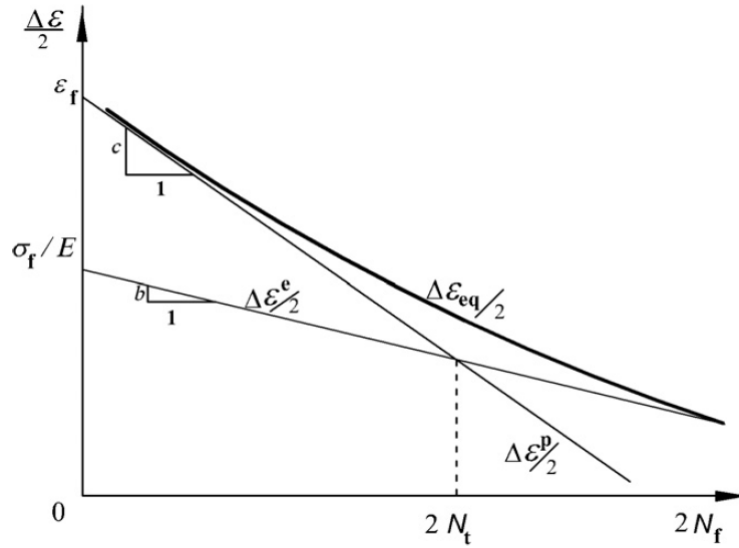


Figure 26: Manson–Coffin fatigue life curve represented by equation (Eq.6) axes in log scale (Seweryn et al., 2008)

The base to formulate criteria to predict LCF life in the range of multiaxial loading is given by equation (Eq.8):

$$\frac{\Delta \varepsilon_{eq}}{2} = \frac{\sigma'_f}{E} (2N_f)^b + \varepsilon'_f (2N_f)^c \quad \text{Eq.8}$$

Where σ'_f , b denote the coefficient and exponent of the elastic fatigue life curve, respectively, ε'_f , and c denote the coefficient and exponent of the plastic fatigue life curve and N_f denotes the number of cycles to failure.

Seweryn et al., (2008) mentioned numerous energy criteria and corresponding assessments of fatigue strength are based on the concept of energy dissipated in the material exercising variable loads. Garud proposed a criterion of damage accumulation under complex low cycle loads using increment of plastic strain energy density over a load cycle. Gołos' and Ellyn presented a hypothesis (**Figure 27**) based on a damage accumulation parameter represented by strain energy density Δw^t which is defined as the sum of plastic strain energy density Δw^p (per load cycle) and elastic strain energy density Δw^{e+} of tension (half cycle):

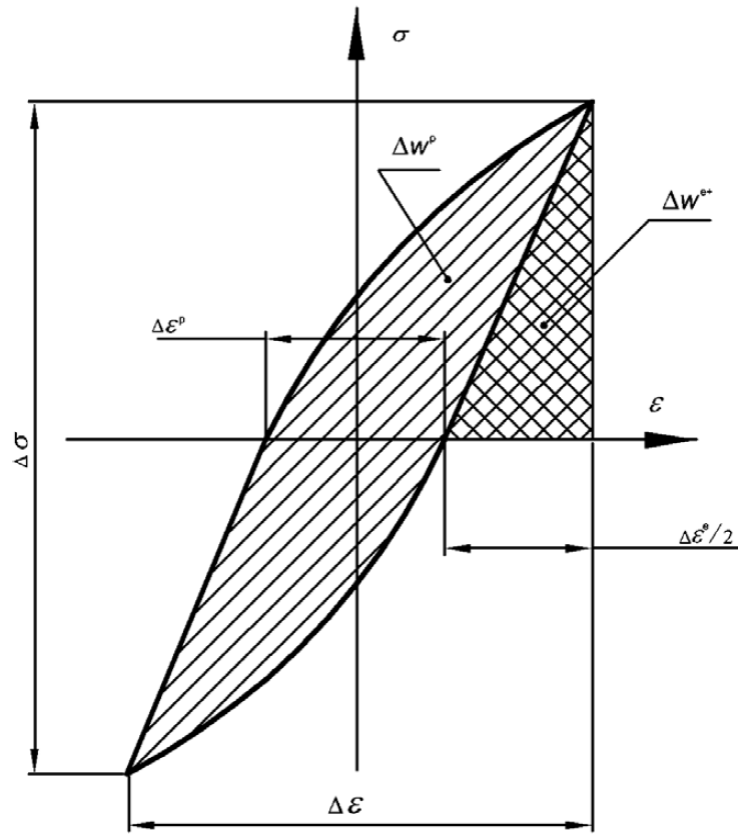


Figure 27: Hysteresis loop plastic strain energy density Δw^p is dissipated in a load cycle and elastic strain energy density Δw^{e+} referred to as the tension half cycle (Seweryn et al., 2008)

Numerous criteria for LCF loads associated with a critical plane are based on strain conditions. In such cases, damage accumulation is estimated using mean and maximum values or amplitudes of normal and shear strains related to the plane. The critical plane on which the critical condition is satisfied corresponds to the representative plane. This approach was first proposed by Findley et al. Seweryn et al., (2008) postulated that the maximum shear plane denotes the representative plane. This is where a combination of range of normal and shear strain components was assumed as the damage accumulation parameter. Strain criteria associated with the critical plane were also formulated by Leese and Morrow, Brown and Miller, Kandil et al., Jacquelin, Socie, Fatemi and Socie, and Zhang et al. Seweryn et al., (2008)

Fatigue damage accumulation for low cycle loads is also estimated by means of energy density related to the critical plane (Glinka et al., Lagoda and Varvani-Farahani). In this criterion the scalar strain energy density is implemented for damage estimation and the

main idea of the approach focuses on the specification of components of the stress and strain vectors associated with a physical plane. An alternative formulation of energy (i.e. stress-strain) condition associated with the critical plane was presented by Chu et al. and Glinka et al. Some of these criteria have been evaluated by Han et al. Seweryn et al., (2008)

Although numerous methods for the prediction of damage accumulation under complex low cycle loads are available, none has gained general acceptance. Therefore the applications were confined to experimentally investigated cases. Seweryn et al., (2008)

Seweryn et al., (2008) proposed a new model of damage accumulation under multiaxial low cycle loads. The numerical algorithm consists of two calculation blocks. The first transforms the analysed load history into the actual stress and strain paths (**Figure 28**) and incorporates constitutive relations together with kinematics hardening law formulated in accordance with Mroz-Garud multisurface model. The second block (containing the damage accumulation function and the material failure criteria) is designed for estimating variations of the measure of damage accumulation. The actual history of stresses and strains links the two units. Obtained in the first unit, it forms the basic set of input data necessary for the fatigue life predictions assessed in the second unit.

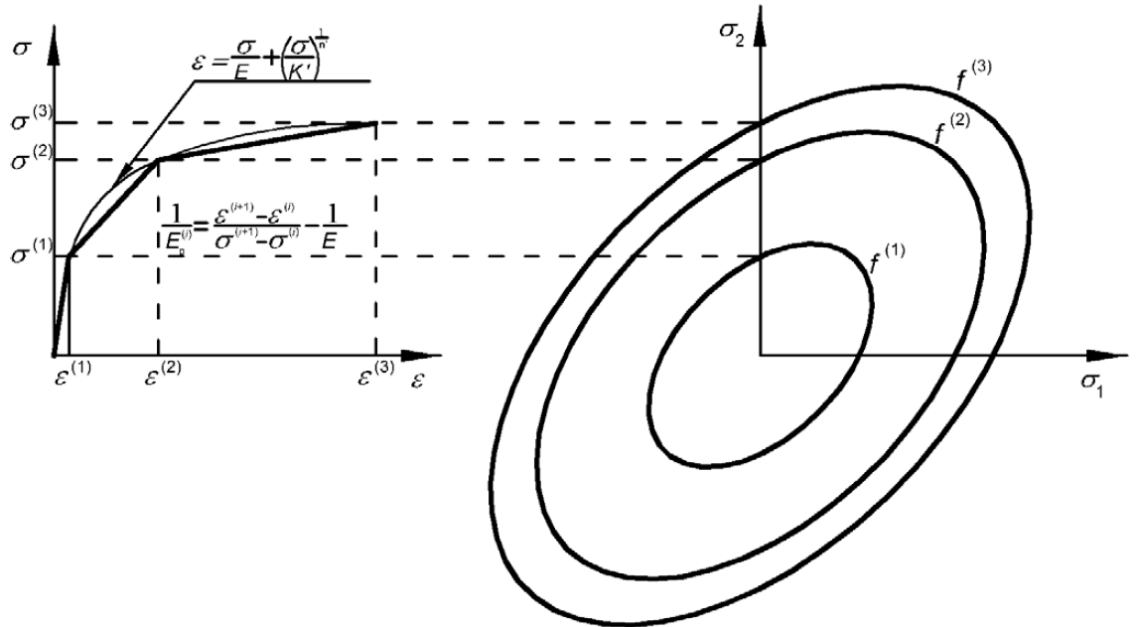


Figure 28: Multilinear representation of the Ramberg–Osgood curve and the traces of the plastic surfaces at $\sigma_3 = 0$ plane (Seweryn et al., 2008)

The process of damage accumulation in materials subjected to variable loads is a complex phenomenon. It occurs in different forms, distinguished for high and LCF loads. In the course of the high cycle loads the micro plastic defects introduce the major contribution to the damage accumulation, while under LCF loads the process is governed by plastic deformations inducing micro plastic defects. Seweryn et al., (2008)

2.1.4 Combined HCF and LCF

Byrne et al., (2003) studied fatigue crack growth rates in forged Ti–6Al–4V aero engine disc material, under combined LCF and HCF at room temperature. In specific terms the influence of single and block overloads due to LCF loading on HCF crack growth behaviour. HCF is a major design issue as it leads to more vibration and less damping in aero engine and civil engine components. When they occur, these high frequency minor cycles will be superimposed on part of each major cycle as shown in **Figure 29**.

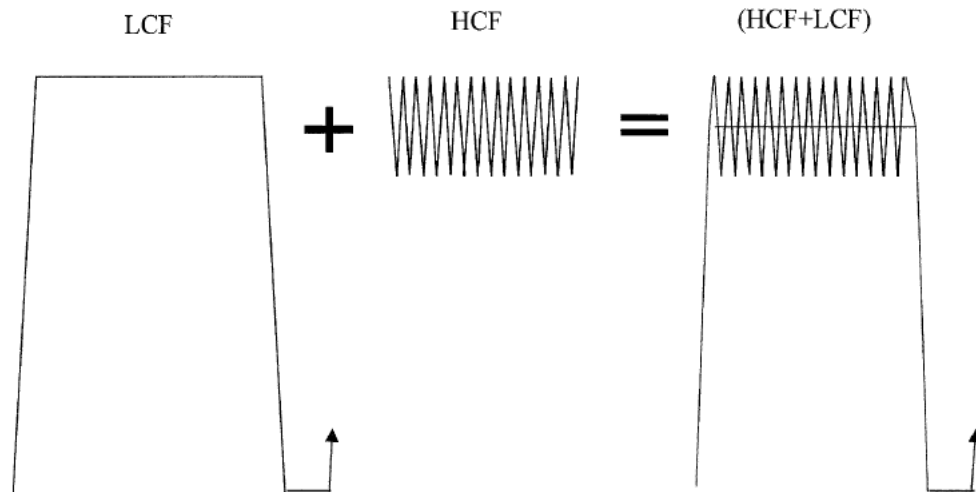


Figure 29: Schematic representation of combined HCF and LCF cycle (Byrne et al., 2003)

(Byrne et al., 2003) Powell et al. have shown that the fatigue crack growth curve for a loading which combines major LCF and minor HCF cycles is characterised by two regimes. These regimes are presented in the diagram of the crack growth increment per loading block (da/dB) versus the total stress intensity range (ΔK_{LCF}) as illustrated in **Figure 30**.

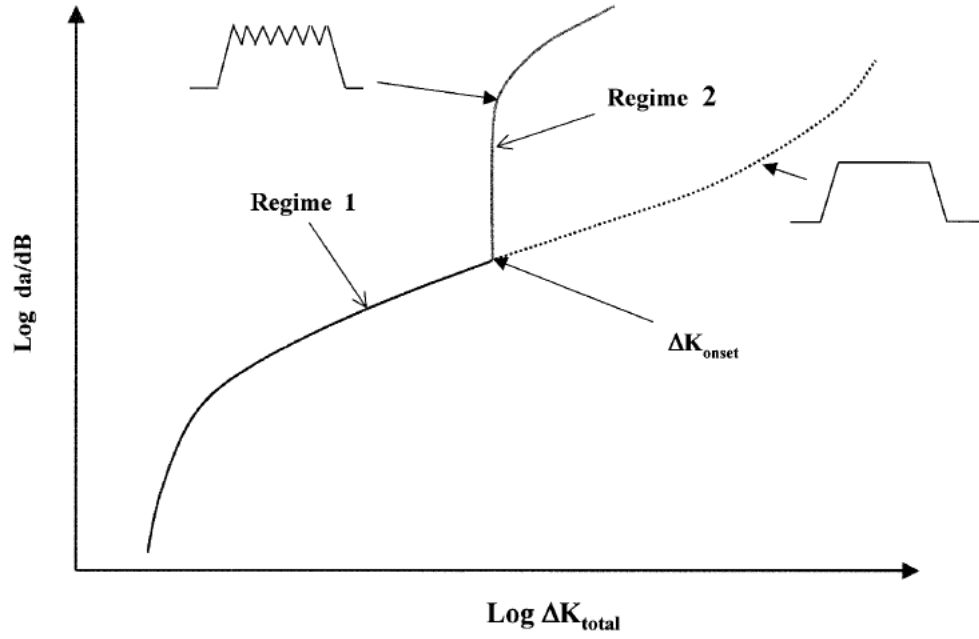


Figure 30: Fatigue crack growth rate regimes for HCF and LCF loadings (Byrne et al., 2003)

At the lower values of ΔK_{total} (regime 1) below the ‘onset’ value of ΔK_{total} , the individual minor cycles do not contribute to the advance of the crack and the growth rates and fractographic appearance correspond to those for LCF loading with the same value of ΔK_{total} .

ΔK_{onset} is the ‘threshold’ for the onset of HCF crack growth under combined HCF and LCF loading. i.e. The value of ΔK_{total} corresponding to the transition between the lower and higher values of stress intensity range.

At the higher values of ΔK_{total} (regime 2), the range of stress intensity associated with the minor (HCF) cycles exceeds the ‘onset’ threshold and each minor cycle contributes to the growth and usually causes the growth rate to increase rapidly, deviating from the response to the application of a discrete LCF loading.

The relationship between ΔK_{HCF} and ΔK_{LCF} where no overloads are presented as:

$$\Delta K_{HCF} = \frac{\Delta K_{LCF} \times (1 - R_{HCF})}{(1 - R_{LCF})} \quad \text{Eq.9}$$

Figure 31 is a schematic representation of HCF and LCF loading patterns used in the tests. HCF cycles loading blocks were preceded by either a single overload cycle or multiple overload cycles. The HCF cycles were sinusoidal stress waves with a

frequency of 157 Hz and stress ratios of $R_{HCF} = 0.7, 0.8$ and 0.9 . A 6.5 s dwell period in the LCF cycle permitted the build-up, application and decay of effectively 1000 HCF cycles. The LCF cycles were trapezoidal stress waves with 1 s rise and fall and dwell at a minimum load of 0.9 s. A stress ratio, R_{LCF} , of 0.01 was used throughout. The magnitude of the overload is indicated by the overload ratio, $T = \text{maximum LCF stress} / \text{maximum HCF stress}$.

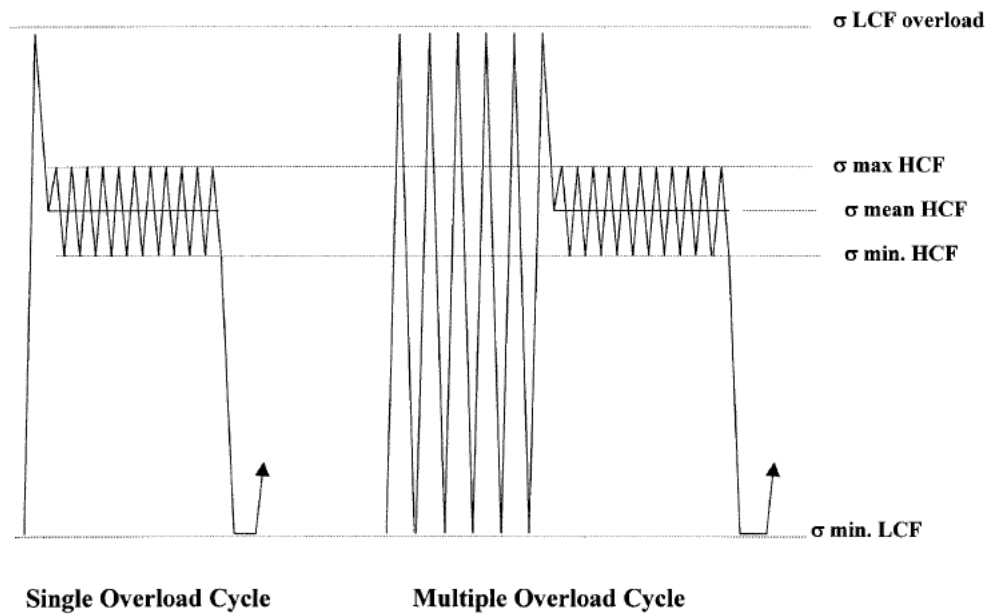


Figure 31: Schematic representations of the repeated stress time sequences used in prior overload experiments (Byrne et al., 2003)

The study observations were:

1. Systematic increases in the applied overload prior to the commencement of the HCF cycles demonstrated a diminution in the contribution of the HCF cycles to crack growth rates and an increase in the stress intensity range at which the HCF cycles begins to contribute to the crack growth rate
2. Increasing the number of prior LCF cycles in the loading block increases the fatigue crack growth rates proportionately prior to the onset of HCF activity and reduces the effect of the HCF cycles after onset
3. For a HCF and to LCF cycle ratio of 1000:1, HCF cycles are suppressed by prior LCF overloads of 100%, 45% and 0% at stress ratios of 0.7, 0.8 and 0.9, respectively

4. The Wheeler overload model gives a reasonable fit to the experimentally determined fatigue crack growth rates after ΔK_{onset} , but an unreliable prediction of ΔK_{onset} using the threshold obtained without any overload influence. A different Wheeler exponent, W , is required for the different combined loading conditions (Byrne et al., 2003)

2.1.5 Testing of Welded Joints

Madi et al., (2004) investigated a reduction life factor (J_f value) that was introduced into the RCC-MR code of the design and construction of fast breeder reactor to account for reduced fatigue strength of welded joints. This reduction factor was investigated using a 'new' experimental approach. This approach simply uses two or three extensometers during the fatigue testing on both the base metal (BM) and weld metal (WM) parts in order to better understand the mechanical behaviours of a welded assembly influenced by the interaction of the different cyclic plastic behaviour of the base metal and weld metal.

The innovative experimental approach is proposed to study the local mechanical behaviour of the welded joint specimens and then determine the J_f parameter. The main advantage of the method is to avoid problems due to the relative stiffness of weld metal (WM) part versus the base metal (BM) part of the specimen. A continuous recording of the stress and strain in the weld allows an estimation of the mechanical behaviour and finally the fatigue life of the joint.

Three different types of uniaxial solid bar specimens are usually used to carry out weldment fatigue data; these are shown in **Figure 32**. The first category of specimens is made up entirely of filler metal taken longitudinally or transversely within the weld. The second type is a welded joint specimen taken transversely across the weld and it comprises the BM, the heat affected zone (HAZ) and the WM. The first category is used to characterize the behaviour and the fatigue life of the filler WM. They are not used to predict the mechanical behaviour of a welded joint. The second category is used to predict the mechanical behaviour of welded joints.

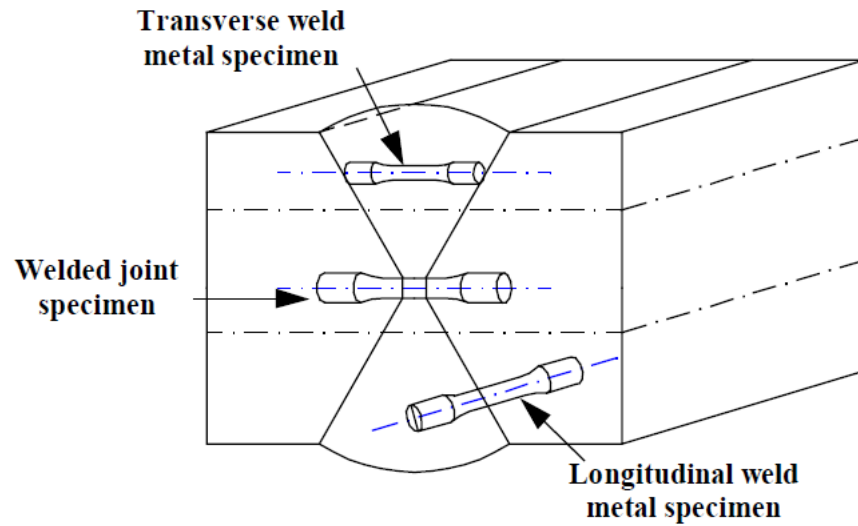


Figure 32: Weldment fatigue specimen type (Madi et al., 2004)

Several laboratories carried out LCF (strain control) testing of welded joint specimens. The gauge length of the extensometer contains a relative proportion of weld as shown in **Figure 33**.

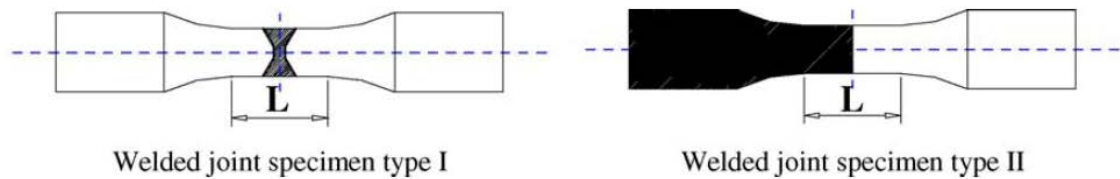


Figure 33: Welded joint specimen used in the literature (Madi et al., 2004)

Madi et al., (2004) proposed that the BM is subjected to controlled strain, and the weld strain is measured with an additional extensometer as shown in **Figure 34**. In this way, it is possible to gain a better picture of the response of an actual welded joint than by tests on welded specimens with a single strain measurement covering only the WM section.

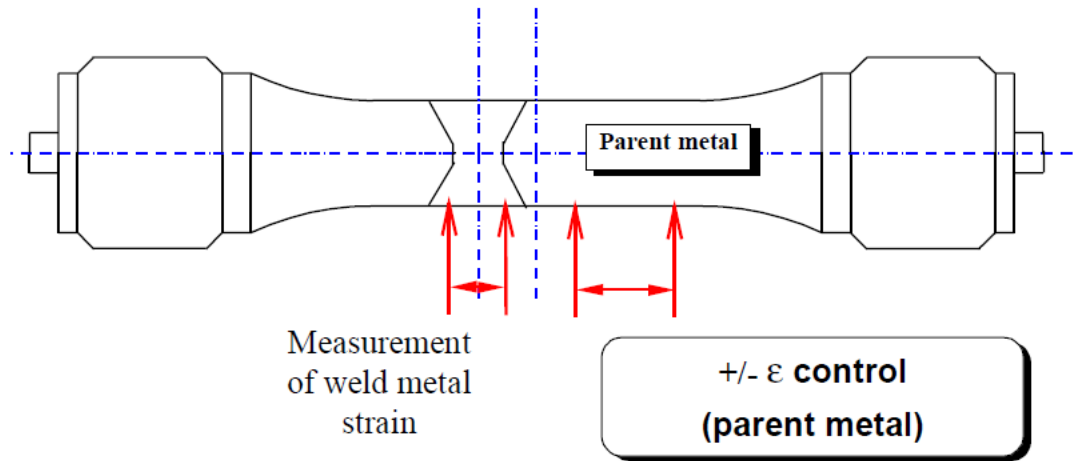


Figure 34: Control of welded joint specimen tests (Madi et al., 2004)

Madi et al., (2004) also tested a specimen with three extensometers as shown in **Figure 35**. During the test the stress evolves, while the strain in the BM remains constant. The strain in the welded joint increases in three stages:

1. Stage I: different fast cyclic hardening of BM and WM. The second being less, it leads to a fast increase of strain in the welded joint
2. Stage II: constant strain rate. Unlike the BM, the weld cyclically softens
3. Stage III: local accumulation of damage in WM leading to the specimen crack

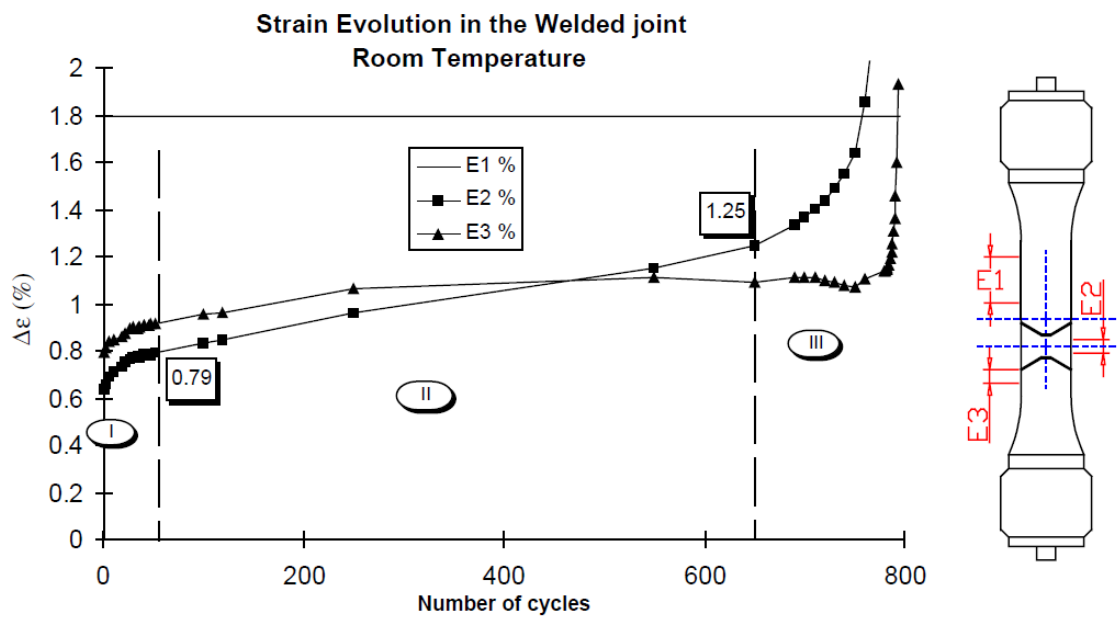


Figure 35: Test at room temperature with three extensometers (Madi et al., 2004)

The new procedure was then performed on welded joint specimens extracted from butt welded pipe connections (uniaxial tensile compressive load), for details please refer to Madi et al., (2004).

The strain histories for the WM part (J1) and the homogeneous part (J2) (**Figure 36**) show that the local behaviour of the weld remains harder than that of the BM. Strain variations of J1 and J2, measured until cycle 400 approximately correlate with those measured in the Bi materials specimens. This shows that the welded specimen results can be transferred to welded structures.

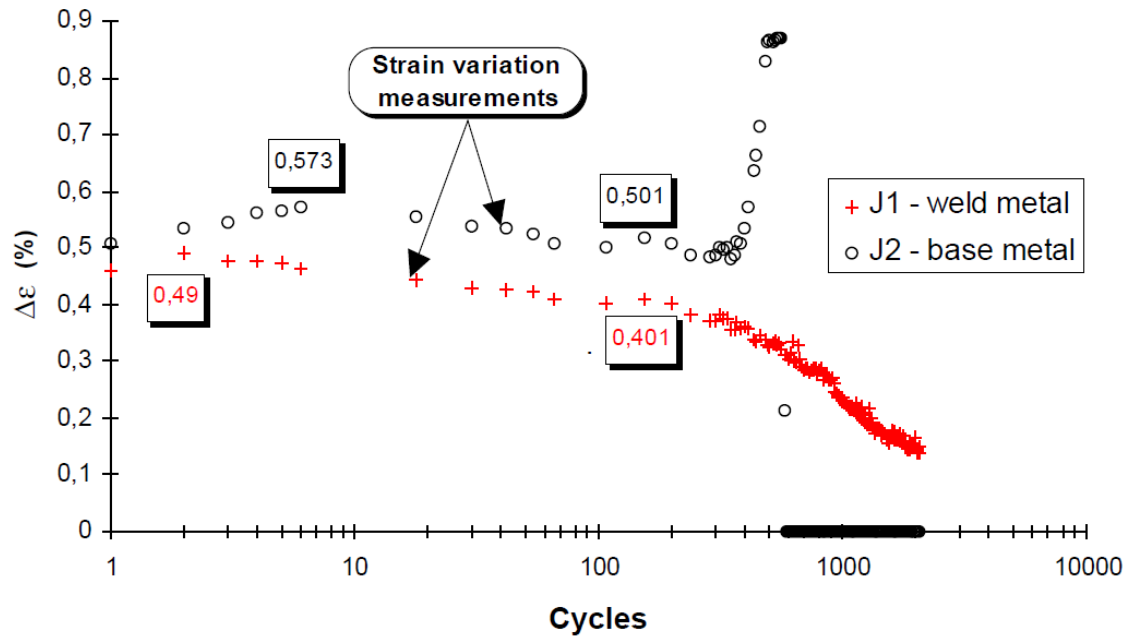


Figure 36: Strain measurements for the butt-welded tube (Madi et al., 2004)

Observations of the crack surface show two different crack initiation zones near the weld depending on the load level. In the homogeneous tube shown in **Figure 37**, the fracture was on the bottom external cross section of the junction between the uniform part and the thicker part. The propagation begins inside out (at the internal surface directed to the external surface). For the welded tube, the fracture was in the weld (in the centre of the structural specimen) and the propagation is directed inside out.

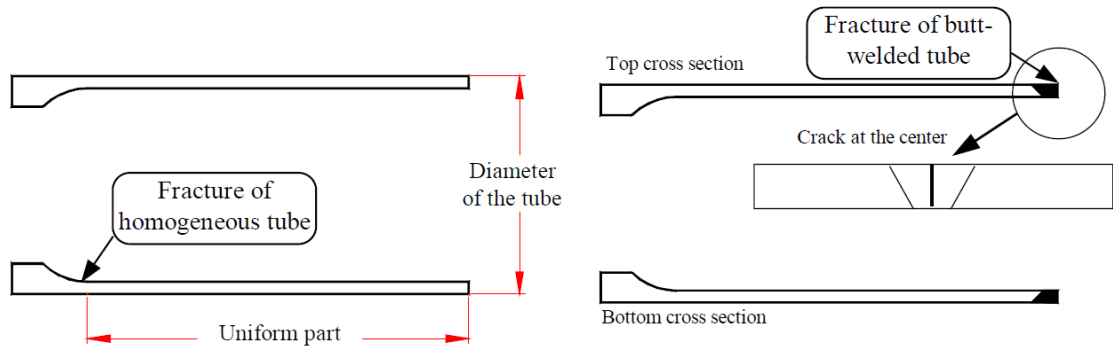


Figure 37: Crack localization for the tube (Madi et al., 2004)

The observations of the fracture topography by scanning electron microscope (SEM) show a multiple crack initiation located on the surface (type I fracture mode). Whereas the strain in the weld is lower than that in the BM, the fracture occurs in the WM. That was also the case for the welded joint specimens broken according to type I fracture mode which implies, in this case, that the reduced fatigue strength of the welded structure is related to a lower strength in fatigue of WM. Madi et al., (2004)

The coefficient J_f , as defined in **Figure 38**, expresses the amplification to be applied to the strain variation occurring in a uniform structural component to obtain the corresponding number of cycles to failure N_r of the weldment component, $\Delta\epsilon_r$, taken from the BM fatigue curve. The applied strain variation in the BM $\Delta\epsilon_i$ is illustrated in **Figure 38**:

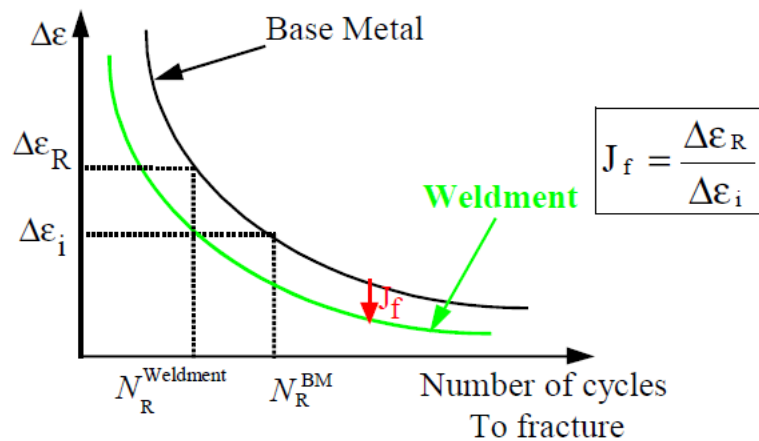


Figure 38: Definition of J_f (Madi et al., 2004)

The results of the dissimilar metal tests show that at low strain loading, representative of loading in service, J_f values are below the value given in RCC-MR (1.25) which is

conservative at such a loading. At higher loading, corresponding to type II fracture, the J_f values are greater than 1.25. These loading levels need to be carefully considered. It is important to note that these results are specific to the X-shaped geometry which results in internal strain. Madi et al., (2004)

It appears that J_f value cannot be considered as a single value for it is influenced by several factors depending on the weldment and on the load level. Hence, the method using life reduction factor J_f is not appropriate for describing fracture mode type II tests as the location of higher stresses and the probable presence of micro cracks at the beginning of the test imply that the propagation phase dominates over the initiation phase. Madi et al., (2004)

Kondo and Okuya (2007) studied the effect of seismic loading on the fatigue strength of welded joints using HCF and variable amplitude fatigue tests after a number of large initial strain cycles (LCF) were performed. The large strain cycles formed a short crack at the toe of the weld due to LCF; this triggered a HCF strength reduction. The HCF limit of welded joints after initial strain cycles is governed by the threshold stress intensity factor of the short crack. The formation of short cracks also enhanced the damage accumulation for subsequent variable amplitude loading.

2.1.6 Reliability

Liu et al., (2005) related LCF life of the aeronautical engine turbine disc structure to the cyclic stress strain level of the disc. He highlighted the significant effect of some variables (such as applied load, working temperature, geometrical dimensions and material properties) on the statistical properties of the stress and the strain of the disc structure and concluded that due to the complicated relationship between the LCF life and the basic random variables, it is very difficult to derive the statistical properties of the LCF life analytically and to analyse the reliability directly. To overcome this difficulty he used finite element analysis as a numerical tool to simulate the turbine disc structure and obtain the probability density distributions of the stress and the strain level at the hot points in the turbine disc structure.

2.2 The Fundamental Theory of LCF

2.2.1 Stress concentration factor (SCF)

SCF is one of the principal factors affecting fatigue behaviour of structures and is used to characterize the local stress. Stress concentration factor was introduced in engineering practice by Inglis in 1913. It relates the maximum local stress (notch stress)

to the nominal stress, which defines the general stress state of a structural detail. The nominal stress may be calculated using the beam theory. Stress concentration depends on the geometry of the element and is influenced by loading mode. In elastic material behaviour stress concentration factor is described as theoretical. In order to evaluate the stress concentration factor, consider a plate with a circular hole loaded uniformly at infinity, i.e. far from the hole, as shown in **Figure 39** and assume that the plane stress for the plate geometry and the loading mode is known, the maximum stress is found in the transverse plane of symmetry at the hole, $\sigma_{y,max}$ in the notched section Petinov (2003).

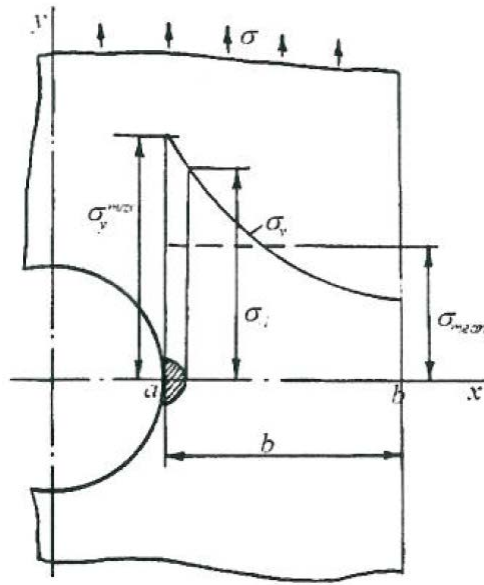


Figure 39: Fatigue damage zone in a stress concentration area (Petinov, 2003)

The stress applied at infinity or the average stress in the notched section, i.e. the nominal stress, may be used as a measure of the stress in the plate. The later, in the notched section, is found as

$$\sigma_n = \frac{\left(\int_0^b \sigma_y(x) dx \right)}{bt} \quad \text{Eq.10}$$

Where $b = B - d$, (B – plate width, d – hole diameter, t – plate thickness).

The theoretical stress concentration factor is

$$K_t = \frac{\sigma_{y,max}}{\sigma_n} \quad \text{Eq.11}$$

Local stress rise makes fatigue damage possible at $\sigma_{y,max} \geq \sigma_{-1}$. However, this condition refers to an infinitely thin film of the material at the hole. In order to create conditions for initiation of the fatigue process elevated stress i.e. $\sigma_y \geq \sigma_{-1}$, should be induced over a set of grains at a certain distance from the hole (shaded area in **Figure 39**). Accordingly, In order to initiate fatigue damage, a nominal stress higher than the presumed by the theoretical stress concentration should be applied and thus the nominal fatigue limit stress of a structural element has to be higher than σ_{-1} / K_t . Experiments confirm this assumption Petinov (2003).

Petinov (2003) stated that the use of stress concentration factors in fatigue assessment should be accompanied by corrections for microplasticity. This is to take into account for the nonlinear material behaviour in fatigue at stress levels of approximately 0.5 of the fatigue limit stress when irregular loading history is assumed.

2.2.2 *Fatigue notch factor*

To define the stress concentration effect in fatigue, Peterson (1974) suggested the ‘fatigue notch factor’ which is defined as the ratio of the material fatigue limit to the fatigue limit of a mechanical (structural) component Petinov (2003). Fatigue notch factor is smaller than the theoretical one.

$$K_f = \frac{\sigma_{-1}^m}{\sigma_{s-1}^m} \leq K_t \quad \text{Eq.12}$$

Where σ_{-1}^m is the fatigue limit of a material obtained by testing the smooth specimens, σ_{s-1}^m is the fatigue limit of a structural detail.

When the nominal stress amplitude increases, the difference between the fatigue curves for the material and for the structural element decreases due to the plasticity as shown schematically in **Figure 40**.

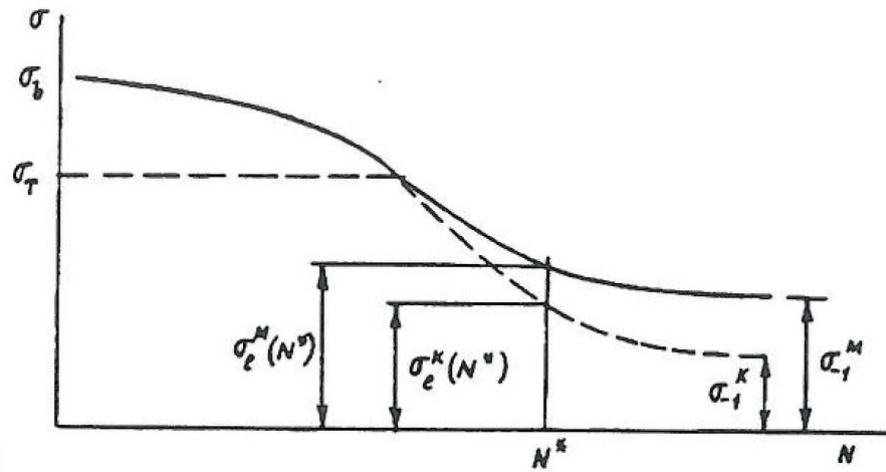


Figure 40: Typical fatigue curves: material – solid line, structural element – dashed line (Petinov, 2003)

The dependency of the fatigue notch factor K_f on the stress concentration factor K_t for welded joints is illustrated in **Figure 41** which is based on material dependent notch sensitivity defined in equation (Eq.23).

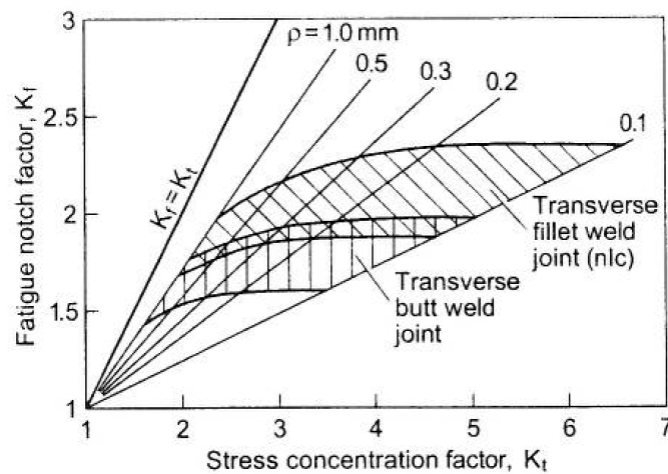


Figure 41: Fatigue notch factor of welded joints (transverse fillet and butt welds ; nlc : non – load – carrying) as function of the stress concentration factor under the condition of constant notch sensitivity ranges ; after Sunamto et al. (Radaj et al., 2006)

Another important influence parameter on the fatigue notch factor and the locally endurable stresses is hardening or softening of the material at the weld notch. The notch stress approach versions according to Lawrence and Radaj recommend the local hardness changes at the notch root to be taken into account when assessing the

endurable notch stresses. Seeger and Sonsino take the hardness changes implicitly into account. Hardness changes relative to the parent material may occur in the heat affected zone (HAZ) and in the fusion zone both without and with filler material. Hardening or softening is dependent on the material composition and the thermal cycles originating from welding Petinov (2003).

Petinov (2003) noted that the use of the theoretical stress concentration factor underestimates the allowable stress. Instead, the fatigue notch factor which was assessed for the whole range of service stresses that can cause damage is preferable.

Petinov (2003) emphasized that only the damage evolution at very short initial cracks may be used to define the fatigue notch factor because only the initial crack is affected by the local stress field. As soon as the crack propagates off the stress concentration site, the corresponding fatigue notch factor becomes less and less indicative of the influence of stress concentration on fatigue strength.

For similar specimens of identical geometry but different sizes fatigue notch factor is different as illustrated in **Figure 42**. The ‘process zone’ and stress distributions in dimensionless form is illustrated in **Figure 43**.

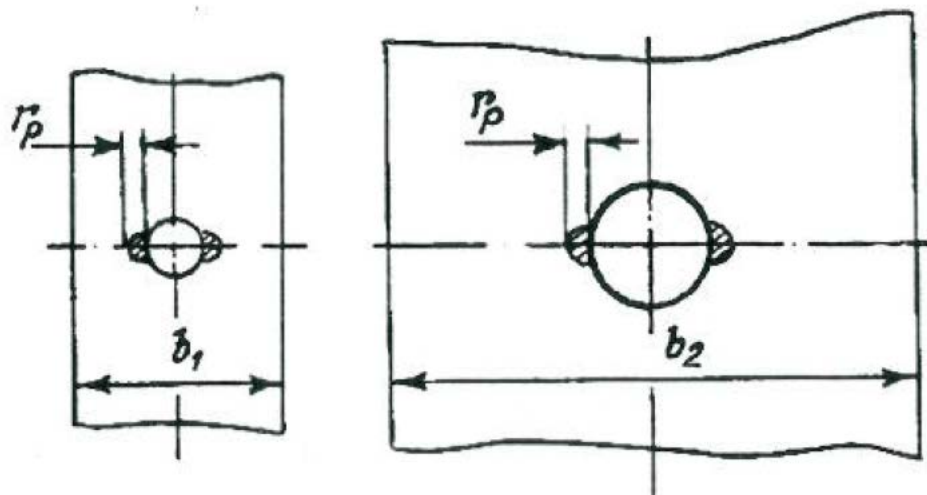


Figure 42: Similar specimens of different sizes (Petinov, 2003)

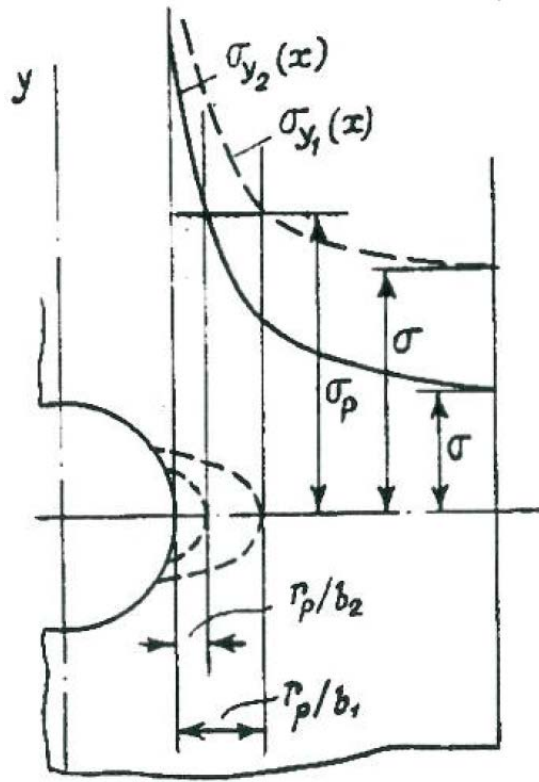


Figure 43: ‘Process Zone’ and stress distributions in dimensionless form (Petinov, 2003)

The influence of stress concentration on the fatigue behaviour of a structural element depends on the sizes of the element and the notch. This is called ‘scale size effect’ and it is observed in fatigue tests of geometrically similar specimens Petinov (2003).

For fatigue strength of welds as a practical applications, a ‘notch sensitivity factor’ is used to express the susceptibility of the fatigue resistance of structural elements to the influence of the stress concentration Petinov (2003). Notch sensitivity factor is defined as:

$$q = \frac{K_f - 1}{K_t - 1} \quad \text{Eq.13}$$

In early fatigue analyses of welds it was assumed that the notch sensitivity factor might be a material constant of the order of 0.8. However, in a more rigorous assessment of fatigue strength of hull structural details; the application of the notch sensitivity technology could be misleading due to the diversity of geometry of notches in structural details and the location of welds with respect to the stress concentration sites and load transition modes Petinov (2003).

Petinov (2003) stated that fatigue notch factor may be applied in the local strain format to modify the failure criterion for HCF and in the case of stress concentrations with small notch root radii, the Peterson's formula may be used:

$$K_f = \frac{1+(K_t-1)}{\left(\frac{1+g}{r}\right)} \quad \text{Eq.14}$$

Where r is the notch root (weld toe), g is the material structural parameter characterizing the size of the high stress notch root zone.

Petinov (2003) stated that extending the Peterson's data to 235 – 390 MPa structural steels makes it possible to define the structural parameter.

Apart from the Peterson equation (Eq. 21); several formulations of fatigue notch factor are known, one of them was derived by Neuber (1934) Petinov (2003):

$$K_f = \frac{1+(K_t-1)}{\left(\frac{1+\pi\left(\frac{\rho}{r}\right)^{1/2}}{(\pi-\omega)}\right)} \quad \text{Eq.15}$$

Where ρ is a material parameter (Neuber's characteristic material particle), r is the notch radius and ω is the groove angle in **Figure 44**.

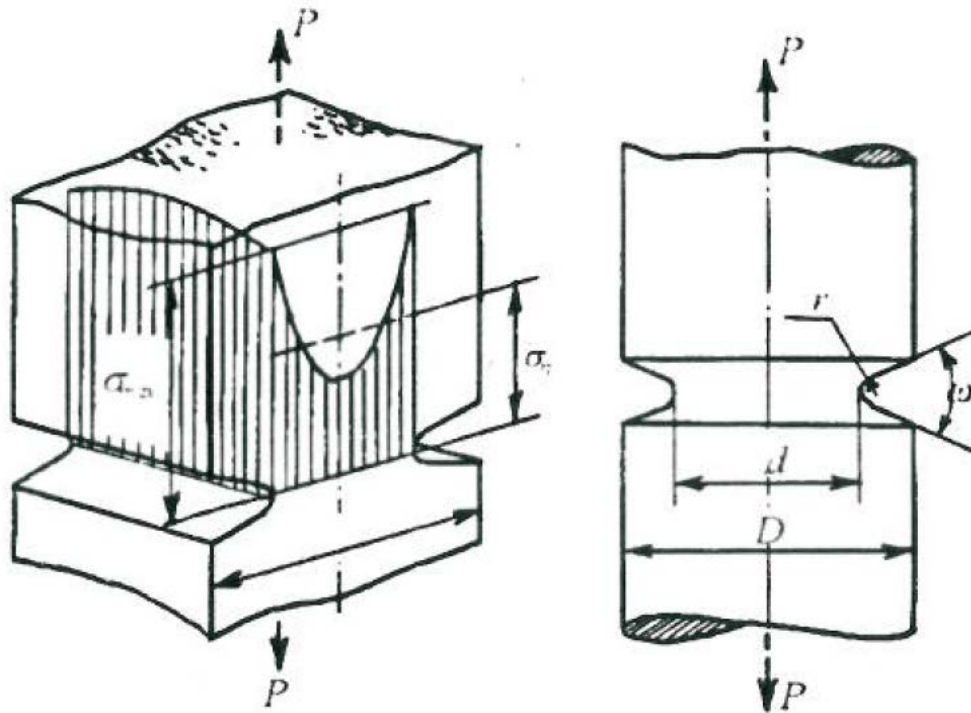


Figure 44: Notches in a rectangular (left) and circular (right) cross sections (Petinov, 2003)

Kudryavtsev (1982) in his studies of short non propagation fatigue cracks suggested a version of Harris' formula Petinov (2003):

$$K_f = K_t - (K_t - 1)^{(-r/\lambda)} \quad \text{Eq.16}$$

Where r is the notch root radius, λ is an empirical parameter assumed as a crack length equivalent to a notch root defect.

Kogaev and Serensen (1962) derived the following equation based on their statistical theory of similitude of fatigue and direct experimental data Petinov (2003):

$$K_f = K_t \left(\frac{\left(1 + \left(\frac{t_s}{44G_s}\right)^k\right)}{\left(1 + \left(\frac{t}{44G}\right)^k\right)} \right) \quad \text{Eq.17}$$

Where t is a dimension of an element's (or specimen) cross section, e.g. plate thickness. $G = (\partial \sigma / \partial x) / \sigma_{\max}$ is the dimensionless gradient of the maximum principal stress at the expected crack nucleation site; for a deep groove $G = 2 / \rho$, k is a form parameter of the failure probability distribution; for Weibull distribution $k = 1 / (1 + m)$, m is the unit volume at a critical location and subscript s is related to a smooth reference specimen.

The onset of plasticity in details with smooth notch geometry such as deck openings is localized and does not follow the elastic strain distribution along the curved edge. This is seen in **Figure 45** where strain distribution under load increments are shown along the curved (rounded and elliptic) hatch corners in a steel deck model. The localization of plasticity is clearly seen in these strain patterns Petinov (2003).

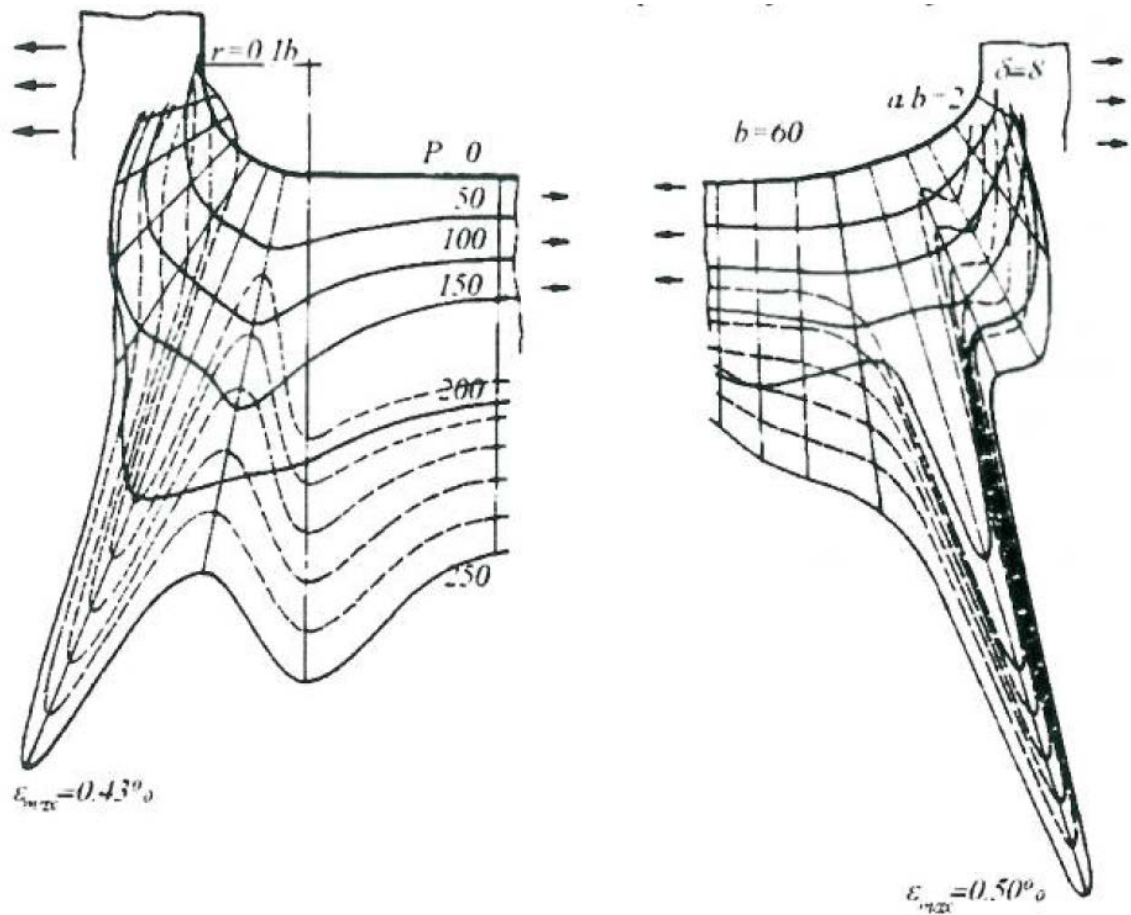


Figure 45: Plastic strain localization along the corner edge of deck opening in a steel model with rounded (left) and elliptic (right) corners, plotted against applied load, tons, Solid lines – loading, dashed lines – unloading (Petinov, 2003)

Local strain measurement at anticipated crack areas in full scale tests is a complicated problem. This is because in welds, the geometry is irregular and the transition from parent to weld material in a cross section of the weld is characterized by a weld toe radius. According to Burnside, et al. (1984), this radius in the welded details of marine structures may usually be around 0.3 mm; Bouchard, et al. (1991) in T welds of plates 26 to 78 mm thick found the weld toe radius ranging from 0.2 to 3.0 mm with mean values of around 0.80 – 1.44 mm. Scorupa (1992) found the representative values of about 0.5 mm. However, regular transition geometry may not be observed in undercuts and welds with excess weld metal and when the transition from parent to weld metal is smooth and the radius is distinct, it may be difficult to find the proper positions for strain gauges and not to miss the maximum strain area even when gauges with 0.2 mm base are applied. A certain complication into analysis of experimental data can stem from material inhomogeneity. If the above problems can be solved, the measured

strains at the weld toe can be used to calculate corresponding stresses applying the cyclic curves for the notch material. However, doesn't allow the assessment and effects of material inhomogeneity Petinov (2003).

Numerical methods and finite element method (FEM) in particular provide the most useful analysis of inelastic stress strain fields in structural details when cyclic properties of the material are known. In FEM, analysis is reduced to a steady state (stabilized) cyclic problem when the detail is analysed under a single load excursion and either the incremental or flow theory of plasticity is applied. Application of a plastic flow theory in FEM allows one to analyse material behaviour under arbitrary varying load patterns starting from the initial loading in the production phase, and to consider superposition of the residual welding stresses and those resulting from the external loading Petinov (2003).

2.2.3 Approximations

Reliable approximations to a steady state cyclic problem may be obtained in engineering analyses by applying empirical or heuristic relationships between elastic plastic stresses and strains at a notch root. In marine applications, the use of Stowell's equation for arbitrary notch geometry was demonstrated by Lida et al, (1981) Petinov (2003). Empirical Stowell's equation gives an estimate of inelastic stress concentration factor for a plate with a central hole under uniaxial tension:

$$K_{\sigma} = 1 + \frac{(K_t - 1)E_s}{E} \quad \text{Eq. 18}$$

Where K_{σ} is the elastic plastic stress concentration factor, $E_s = \frac{\Delta \sigma}{\Delta \epsilon}$ is the secant modulus and $\Delta \sigma$ and $\Delta \epsilon$ are the stress and strain ranges, respectively.

Equation (Eq.25) may be rewritten as:

$$\frac{\Delta \sigma (K_t - 1)}{E \Delta \epsilon} = \frac{\Delta \sigma}{\Delta \sigma_n - 1} \quad \text{Eq. 19}$$

Where $\Delta \sigma_n$ is the nominal stress range, because $K_{\sigma} = \frac{\Delta \sigma}{\Delta \sigma_n}$.

Stowell's formula (19) underestimates the local strain. When the nominal stress increases, the underestimate becomes more pronounced and special procedures should be used within the approach to compensate unavoidable non-conservative fatigue life evaluation Petinov (2003).

Values of theoretical stress concentration factor K_t can be found in literature or calculated using finite element modeling of the detail Petinov (2003). More frequently the inelastic strain and stress concentrations are estimated using the heuristic formula derived by Neuber (1968) as illustrated in 2.1.1.3.

Petinov (2003) explanation of the formula is as follows; assume a thin plate with a central circular hole is loaded at infinity i.e. far enough from the hole (not less than 3 – 4 times the hole diameter to exclude the influence of boundary conditions on the local stress field around the hole and vice versa) with uniformly distributed tensile stresses (**Figure 46**). If the plate thickness is small compared to the hole's radius, the stress state at the highly stressed site is close to the uniaxial one. Assume also that the plate material is elastic – perfectly – plastic without strain hardening beyond the yield point. During the initial stages of loading (as long as the maximum stress does not reach the yield limit) the stress and strain concentration factors are equal. When the nominal stress exceeds a value $\sigma_n = \sigma_y / K_n$, plastic deformation of material begins at the critical point. Since the maximum stress (now equal to the yield limit) doesn't increase anymore, the stress concentration factor decreases. The local strain grows faster than the nominal stress (**Figure 46**) and consequently, the strain concentration factor exceeds the theoretical stress concentration value and continues to increase until the entire section is yielding. This is why the relationship of equation (Eq.1) might be suggested. As a result, equation (Eq.1) may be rewritten in the form:

$$\Delta \sigma \Delta \varepsilon = \frac{(K_t \Delta \sigma_n)^2}{E}$$

Or

$$\Delta \sigma \Delta \varepsilon = \frac{\Delta \sigma^2 e}{E}$$

Where $\Delta \sigma_n$ is the nominal stress used for defining K_t , K_σ and K_ε and $\Delta \sigma_e$ is the local elastic stress range.

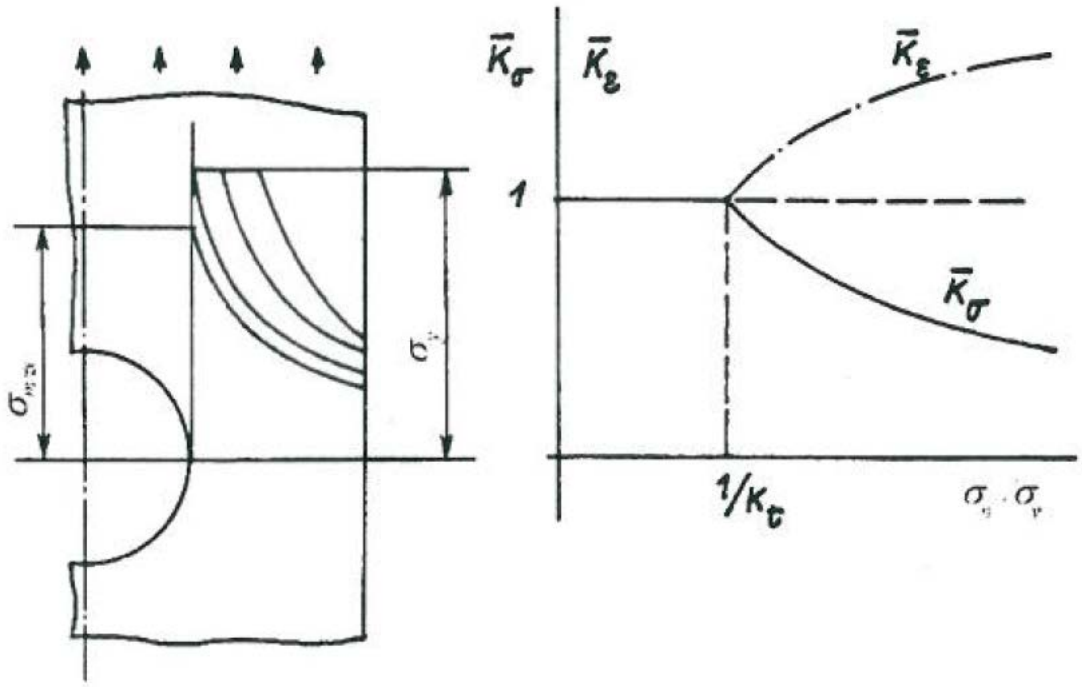


Figure 46: Stress and strain concentration factors depending on the nominal stress left – stress patterns in a plate with a circular hole, right – stress and strain concentration versus nominal stress (Petinov, 2003)

$$\overline{K}_{\sigma} = \frac{K_{\sigma}}{K_t}; \overline{K}_{\varepsilon} = \frac{K_{\varepsilon}}{K_t}$$

Petinov (2003) stated that Neuber's rule equation (Eq.1) was extended to cyclic problems and proved to be reasonable means of evaluating the approximate inelastic notch stresses and strains in fatigue analysis. The approach based on the Neuber equation slightly overestimates local strains at a stress concentration resulting in conservative estimates of fatigue lives that are usually acceptable in engineering evaluations. But when the stress state differs considerably from the uniaxial one at a stress concentration (e.g. in a deep notch where the plate thickness reaches and exceeds the notch root radius), the Neuber equation based approach may not hold.

Duggan (1980) assumed a version of Neuber's formula equation (Eq.1) in the following form Petinov (2003):

$$\Delta \varepsilon = \frac{(K_t \Delta \sigma_n)^2 (1-R)^2 F}{E \Delta \sigma} \quad \text{Eq. 20}$$

Where $R = \frac{\sigma_{\min}}{\sigma_{\max}}$ is the load ratio. F is a correction for the notch scale, stress gradient and stress state at the notch root,

$$F = F\left(\frac{r}{t}, \frac{r}{p}, K_t\right) = A\left(\frac{r^2}{ptK_t}\right)^m \quad \text{Eq. 21}$$

Where $A = 0.924$ and $m = 0.105$ for the high strength steels in aircraft engineering, r is the notch radius, p is a parameter to account for strain distribution at the notch root; it is assumed that at a small distance from the notch root the strains are distributed linearly:

$$\varepsilon(x) = \varepsilon_{max} - p \frac{\partial \varepsilon}{\partial x}$$

t is the plate thickness or a characteristic dimension of a component cross section.

Another approximate relationship was assumed by Petinov (2003) in 1976 based on thorough experimental study of local strain evolution at various stress concentrations, mean stresses and nominal stress amplitudes in hull structural steels. Analysis of cyclic diagrams (strain at notch root vs. nominal stress) revealed similitude of material response regardless of mean stress:

$$\Delta \varepsilon = \left(\frac{K_t \Delta \sigma_n}{E}\right) \left(1 + M_s(r, t) F(\sigma_m) \left(\frac{AK_t \Delta \sigma_n}{\sigma_s - 1}\right)^\beta\right) \quad \text{Eq. 22}$$

Where $M_s(r, t)$ is the notch scale effect correction of the plastic strain component:

$$M_s(r, t) = \frac{M_o}{\left(1 + \left(\frac{a}{t}\right)^s \left(\frac{r}{t}\right)^q\right)}$$

Here M_o , a , s , and q are empirical parameters which were found in **Table 3**:

Table 3: Petinov approximation of local strain at various stress concentrations

Low alloy steel of $\sigma_y = 300$ MPa		Low alloy steel of $\sigma_y = 395$ MPa	
M_o	0.155	M_o	0.107
a	0.24	a	0.203
s	0.30	s	0.25
q	1.50	q	1.20

$F(\sigma_m)$ in Eq.22 is the correction for mean stress effect on the plastic strain range:

$$F(\sigma_m) = 1 + B \sigma_m / (K_t \Delta \sigma_n)$$

where σ_m is the nominal mean stress. A , B , and β are empirical parameters which for these steels are: $A = 1.25$, $B = 2.50$ and $\beta = 1.20$.

Equation (Eq.22) may be used for the same purposes as the other approaches. **Figure 47** illustrates the application of the Stowell and Neuber formulae based approaches and the use of equation (Eq.22) ‘experiment based’ for assessment of local strain in case of structural members with stress concentrations, $K_t = 2 - 4$. The results for the above steels show that the Stowell formula based method may essentially underestimate the local strain in stress concentration zones as compared to the empirical data of equation (Eq.22). On the contrary, the use of Neuber’s formula slightly overestimates the local strain ranges. However, at moderate stress concentrations and nominal stresses, the compared approaches lead to agreeable results.

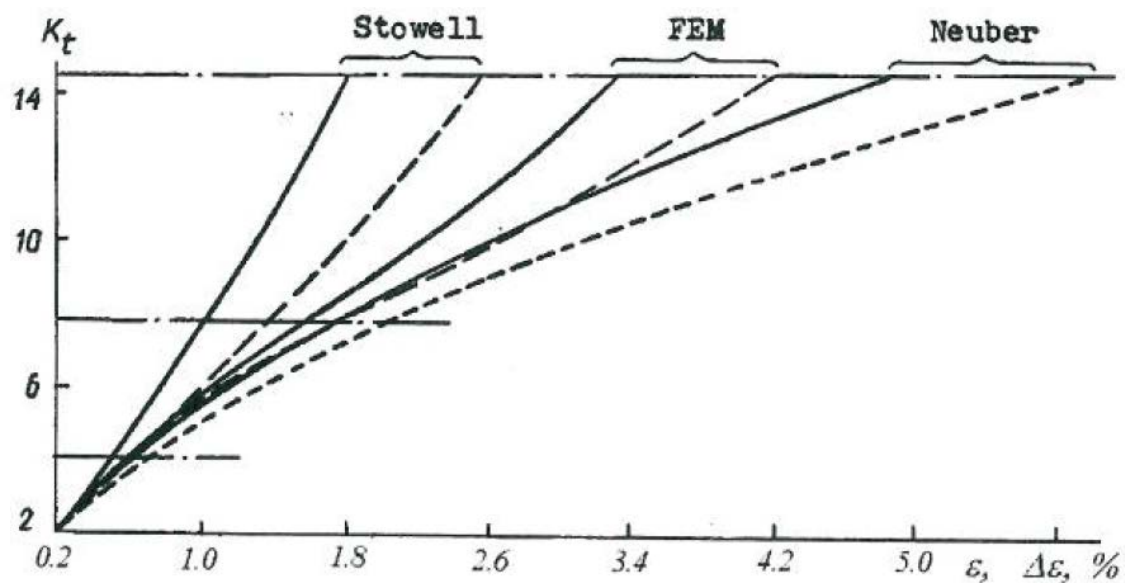


Figure 47: Local strain ranges based on Stowell and Neuber formulae and their FEM evaluation for an Aluminium alloy (AlMg61). Solid lines – monotonous loading at $\sigma_{max} = 72$ MPa ; dashed lines – cyclic loading at $\Delta\sigma = 107.1$ MPa (Petinov, 2003)

2.2.3.1 Example of Local stress strain value according to Neuber

Fricke et al., (1995) analysed a scallop shown in **Figure 48** with the oval elliptical shape because it did show a better performance as a drain hole with only slightly increased local stresses. The maximum nominal stress amplitude is assumed to be $\sigma_{n,a} = 150$ N/mm² in the structure made of normal hull structural steel (NT 24). Since local elastic plastic straining was expected within the highest load cycle, its contribution to total damage was evaluated on the basis of the notch stress approach.

Stress concentration factor, $K_t = 2.16$

Nominal stress amplitude, $\sigma_{n,a} = 150 \text{ N/mm}^2$

Elastic notch stress amplitude, $\sigma_{k,a} = \sigma_{n,a} \times K_t = 324 \text{ N/mm}^2$

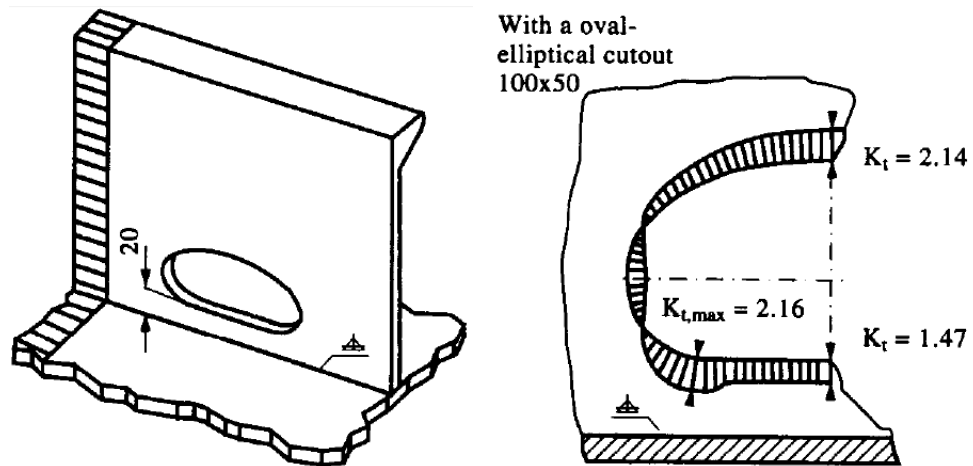


Figure 48: Edge distribution for a scallop under axial loading (Fricke and Paetzold, 1995)

The local notch stress and strain amplitudes have been determined graphically using Neuber's rule, **Figure 49**.

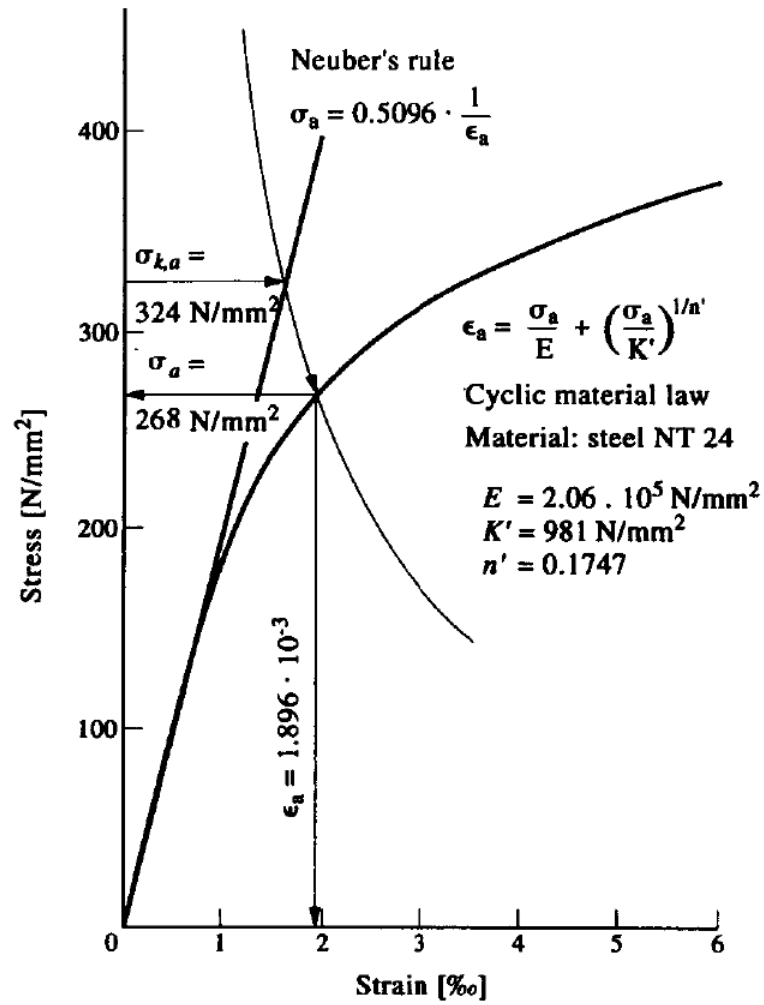


Figure 49: Example of local stress strain values according to Neuber (Fricke and Paetzold, 1995)

Local notch stress amplitude $\sigma_a = 268 \text{ N/mm}^2$

Local notch strain amplitude $\epsilon_a = 1.896 \times 10^{-3}$

The damage parameter according to Smith et al., if zero mean stress is assumed, becomes:

$$P_{\text{SWT}} = \sqrt{\sigma_{\text{max}} \times \epsilon_a \times E} = 324 \text{ N/mm}^2$$

The number N_c of load cycles until crack initiation is according to the damage parameter life curve according to Smith et al. for specimens with thermally cut plate edge:

$$N_c = \left(\frac{P_{\text{SWT}}}{2668}\right)^{-4.812} = 25472 \text{ cycles}$$

Thus, the damage caused by one cycle (to be used in the linear damage calculation) becomes:

$$D_1 = \frac{1}{N_c} = 3.926 \times 10^{-5}$$

2.2.4 Cyclic Loading

2.2.4.1 Cyclic Strain Hardening and Softening Materials

Manson (1964) proposed the concept that cyclic life is related to the plastic strain range in 1952 as a result of his effort to estimate the importance of temperature on the thermal stress fatigue of turbine buckets and more importantly proposed that plastic strain line is linear on log – log coordinates. In 1964 he described the state of the art regarding the basic phenomenon by presenting and discussing the fundamental aspects of investigations conducted in the laboratory at Lewis Research Centre. The Principal Variables Governing Strain Cycling Fatigue Behaviour (Hardening and Softening) are quoted here. When a specimen subject to axial reversed strain cycling (i.e. +ve and –ve strain by reversing the load) requires a different load to accomplish a desired amount of strain. If the load (i.e. stress range – including compression and tension) required to maintain the strain range is ‘greater’ the material is considered Cyclic Strain Hardening Material (**Figure 50**) and if the load required to maintain the strain range is ‘smaller’ the material is considered Cyclic Strain Softening Material (**Figure 51**).

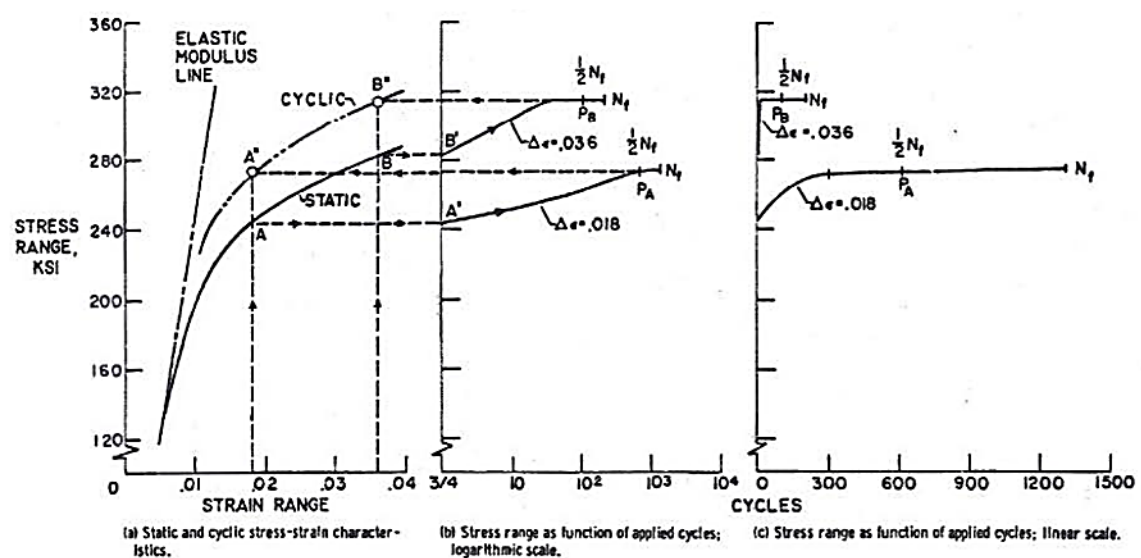


Figure 50: e.g. Cyclic Strain Hardening Material - 304 stainless steel (Manson, 1964)

Asymptotic stress range: (example of cyclic strain hardening) 1st cycle of loading the stress range required to produce a fixed strain range is 0.018 is at point A on S-N curve in **Figure 50** (a). In successive cycles greater stress range is required to maintain the same strain range **Figure 50** (b). After about 600 cycles of loading the stress stabilizes and remains approximately constant for the remainder of the test (about 1400 cycles). Saturation hardening is achieved during the early cycles of loading usually before half the number of cycles to failure **Figure 50** (c) or in other words is the re-plot of **Figure 50** (b) with the cyclic life scale made linear.

Plotting the asymptotic stress range against the applied strain range and repeating the strain cycles increase will result in another S-N curve (cyclic) that is above the initial S-N curve (static), this material exhibit the cyclic strain hardening. Manson (1964)

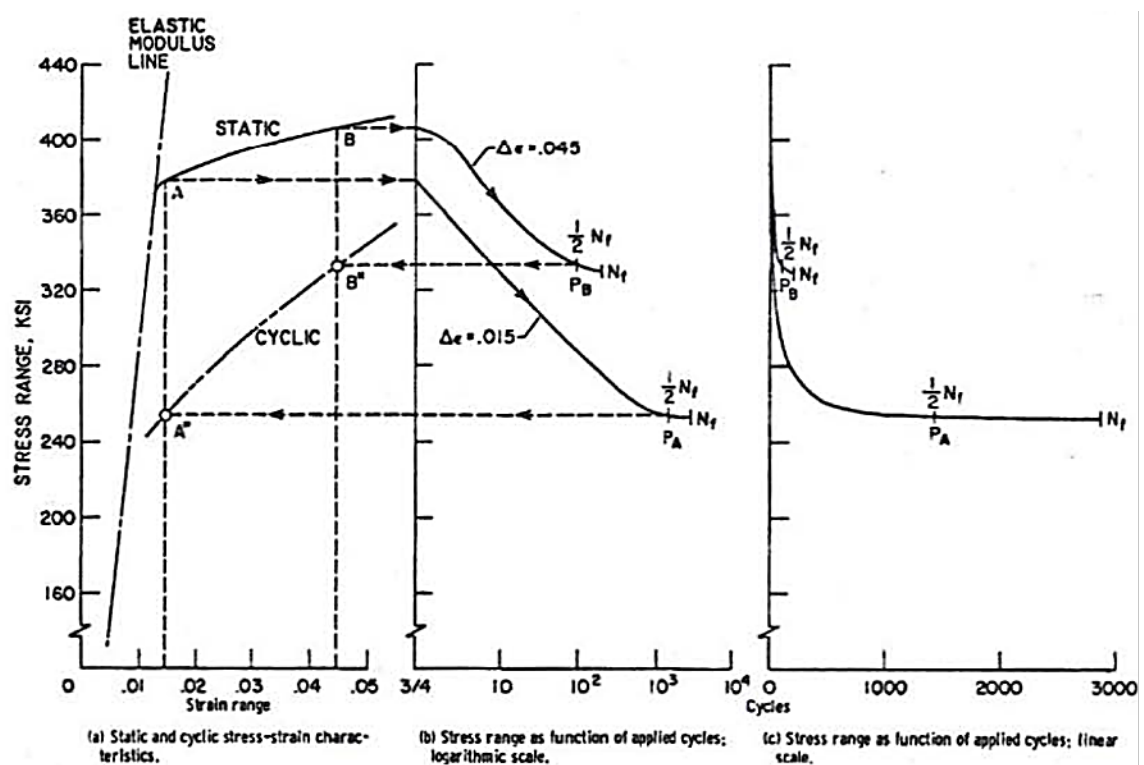


Figure 51: e.g Cyclic Strain Softening Material - 4340 steel (Manson, 1964)

Asymptotic stress range (example of Cyclic strain softening) 1st cycle of loading the stress range required to produce a fixed strain range is 0.015 is at point A on the static S-N curve in **Figure 51** (a) but it quickly diminishes after few cycles to half the stress range at point A'. Here the cyclic S-N curve falls considerable below the static S-N curve.

Plotting the asymptotic stress range against the applied strain range and repeating the strain cycles increase in the same manner described above will result in another S-N curve (cyclic) that is below the initial S-N curve (static), this material exhibit the cyclic strain softening. Manson (1964)

From **Figures 50** and **51**, Manson concluded that Yield Stress is not a property of primary influence on the fatigue characteristics because only very few cycles can drastically change the stress required to produce a given strain; therefore, yield stress can be dismissed as a property of primary importance in governing fatigue life in the low cycle range and he also concluded a crack depth of (0.002 to 0.003 in) started late in the life of the specimen, approximately 65% of the life for the low cycle test and approximately 85% for the high cycle test.

2.2.4.2 Application of Cyclic Strain Approach to ship structural detail

Fricke et al., (1987) stated that cracks were found mainly at the rounded edges of the cutout in the transverse member. These cracks were a major problem for the first super tankers 10 to 20 years ago. Investigations showed that the elastic notch stress can far exceed the yield stress, even at normal service loading. The nonlinear behaviour of the typical mild steel was described in terms of the static and cyclic material laws; for small stress amplitudes ($230 \text{ N/mm}^2 < \sigma_a < 384 \text{ N/mm}^2$), cyclic softening was observed. At high stress amplitudes above $\sigma_a = 384 \text{ N/mm}^2$, cyclic hardening was observed. The elements of the cyclic strain approach for estimating the fatigue life are shown in **Figures 52-54** and step 4.

1. Step 1

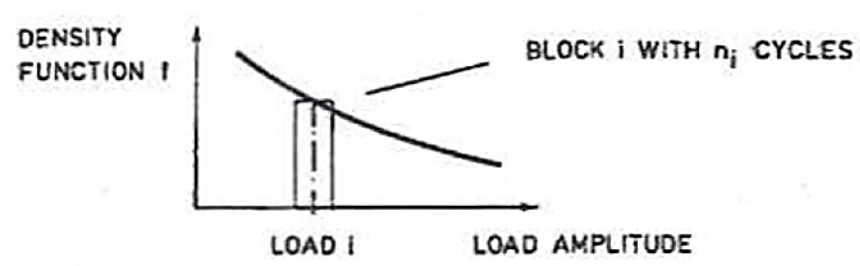


Figure 52: Distribution of amplitudes of the applied load (F , σ_e , σ_n) (Fricke and Paetzold, 1987)

2. Step 2

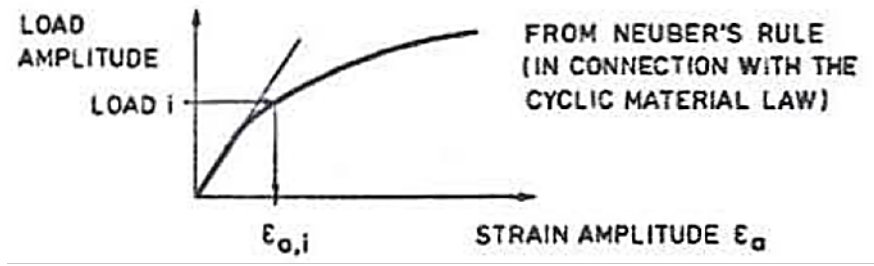


Figure 53: Relationship between applied load and local strain (Fricke and Paetzold, 1987)

3. Step 3

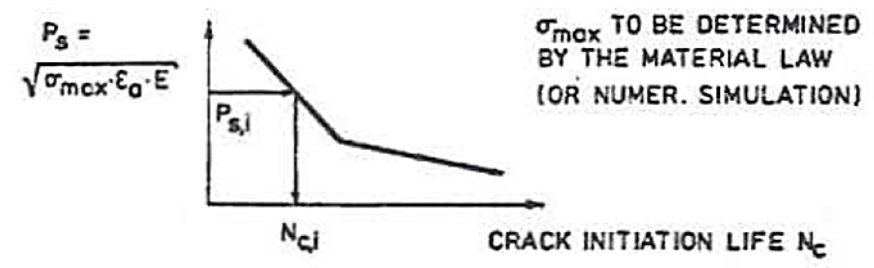


Figure 54: Relationship between damage parameter and crack initiation life (Fricke and Paetzold, 1987)

4. Step 4: Damage accumulation law (Fricke and Paetzold, 1987)

$$\sum \frac{n_i}{N_{c,i}} = 1 \quad \text{Eq. 23}$$

Two examples were used to demonstrate the application of the cyclic strain approach; the first was large scale longitudinal stiffener/transverse web intersection subjected to exponentially distributed load amplitudes and the second example was a longitudinal/floor intersection in a double bottom.

In the first example, **Figure 55**; the correction for yielding in Neuber's rule was not necessary because the transverse web was not highly stressed. The limit load factor K_p (SCF) was found to be about 5. It was observed that in the case of changing load amplitudes, the largest load levels are often not the most damaging ones. The strain calculated by the FE method is smaller than that obtained from the experiment and from Neuber's rule. The latter are in good agreement up to 0.3 percent of strain amplitude.

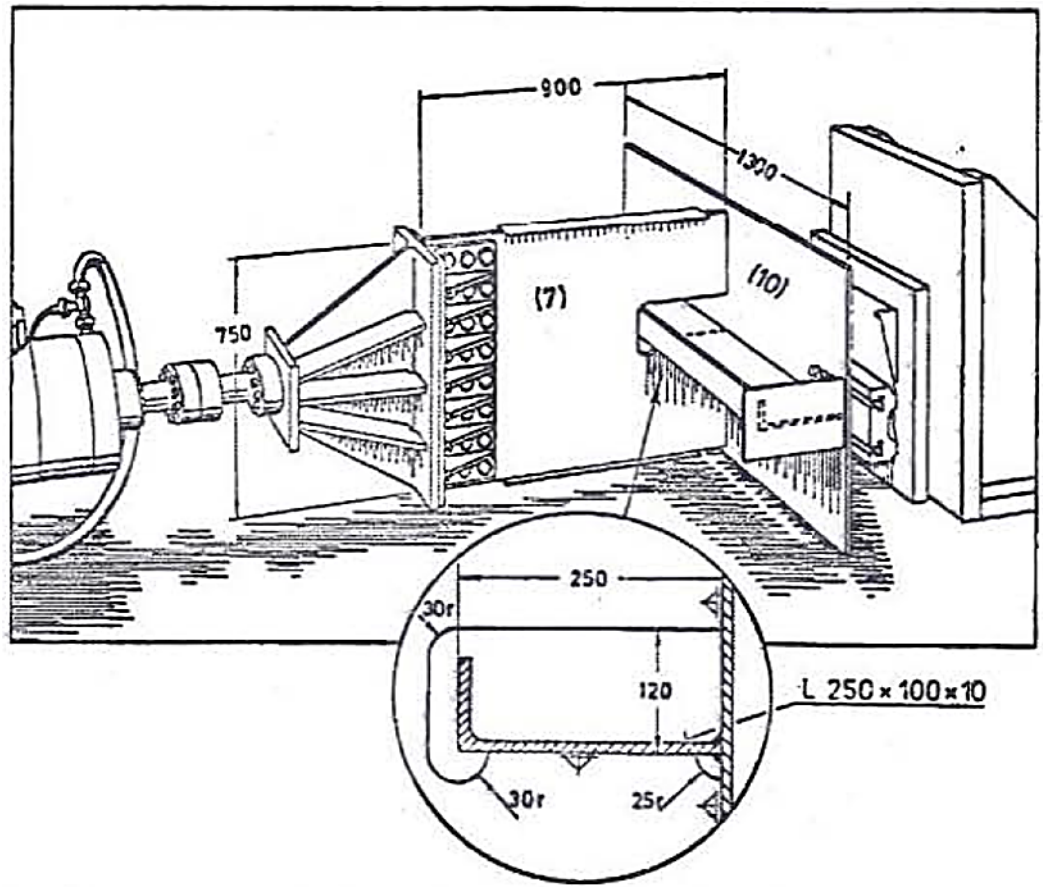


Figure 55: Large scale test model of the longitudinal stiffener / transverse web intersection (Fricke and Paetzold, 1987)

At higher loads; Neuber's solution remains on the safe side as shown in **Figure 56**. A few additional tests were performed with a random loading sequence instead of the blocked sequence. It was observed that the actual crack initiation life in the experiment was shorter than the estimated one. Hence, further research was recommended.

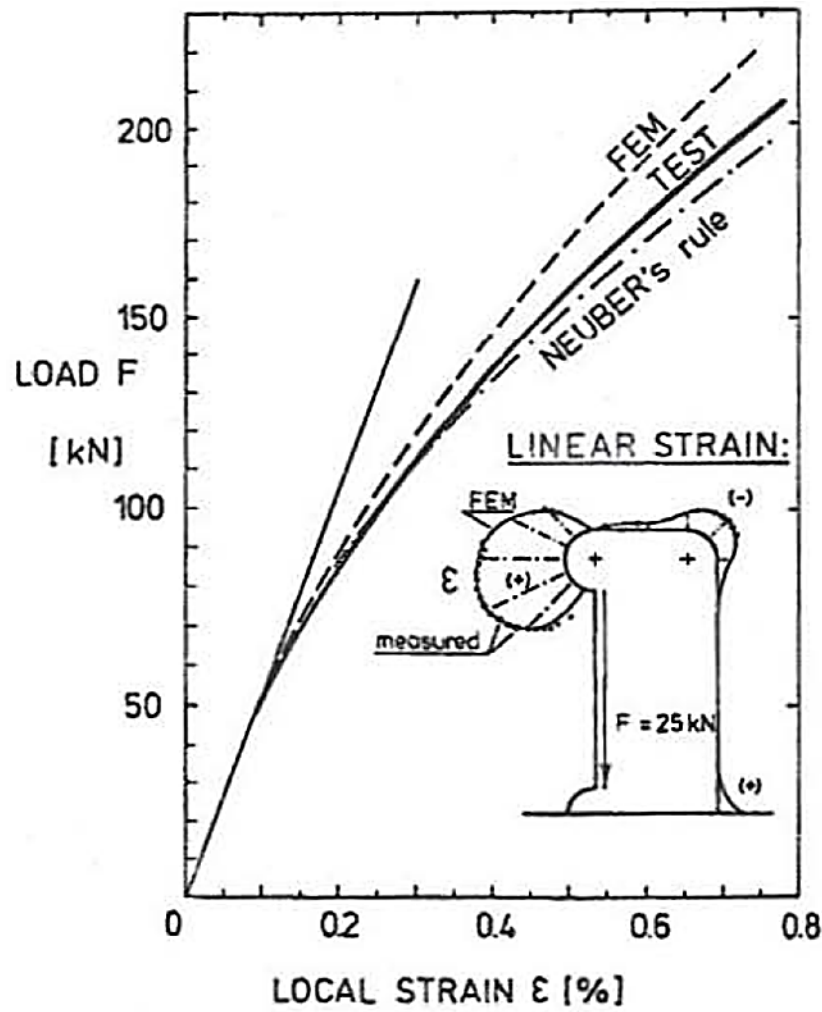


Figure 56: Elastic strain distribution and yield curves for the notch root subjected to cyclic loading (Fricke and Paetzold, 1987)

In the second example, **Figure 57**; a comparison with experimental results was not possible. Two load cases were considered for the ship, ballast on a wave crest and full load in a wave trough. Five load cases were considered for the double bottom floor, these are illustrated in **Figure 58**. Load cases 1 and 2 are loads on the longitudinals due to pressure on the inner and outer bottom plate. Load cases 3 to 5 are the common beam forces and moments N , S , and M .

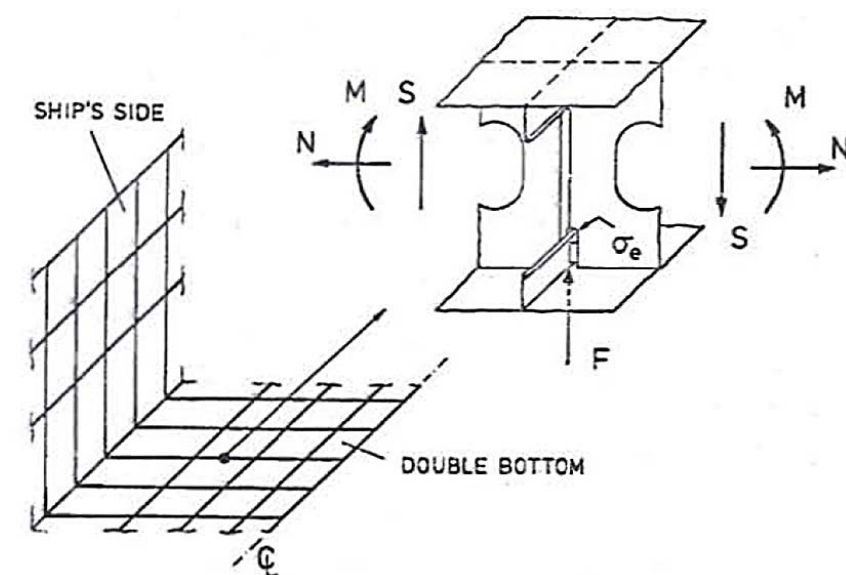


Figure 57: Determination of the theoretical elastic notch stress σ_e for a structural detail in a double bottom (Fricke and Paetzold, 1987)

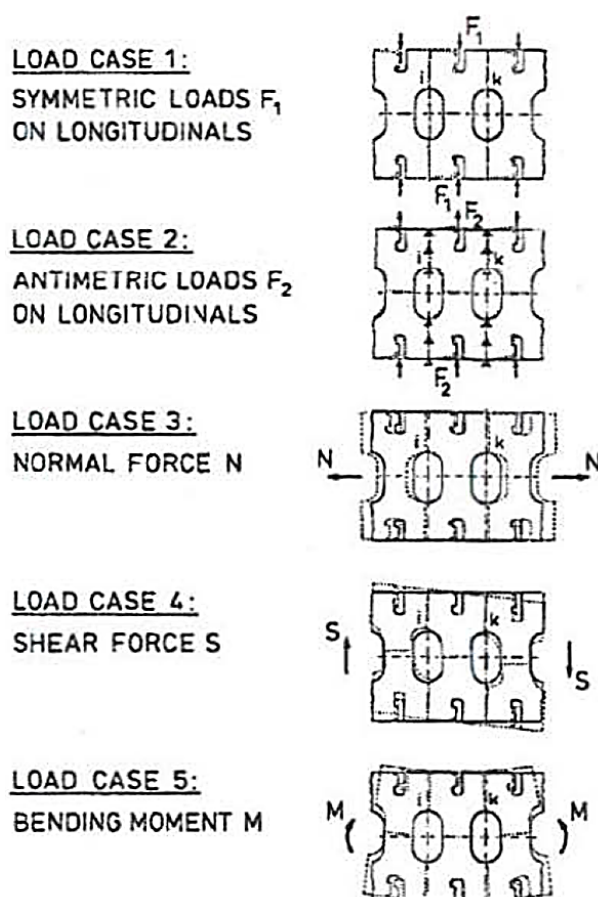


Figure 58: Unit load cases for a structural detail in a double bottom (Fricke and Paetzold, 1987)

The highest stresses occurred at the rounded edges of the cutout as illustrated in **Figure 59**. The difference in stress between the two cases reached a value of more than 900 N/mm². That is nearly four times the minimum yield stress of the normal strength ship structural steel.

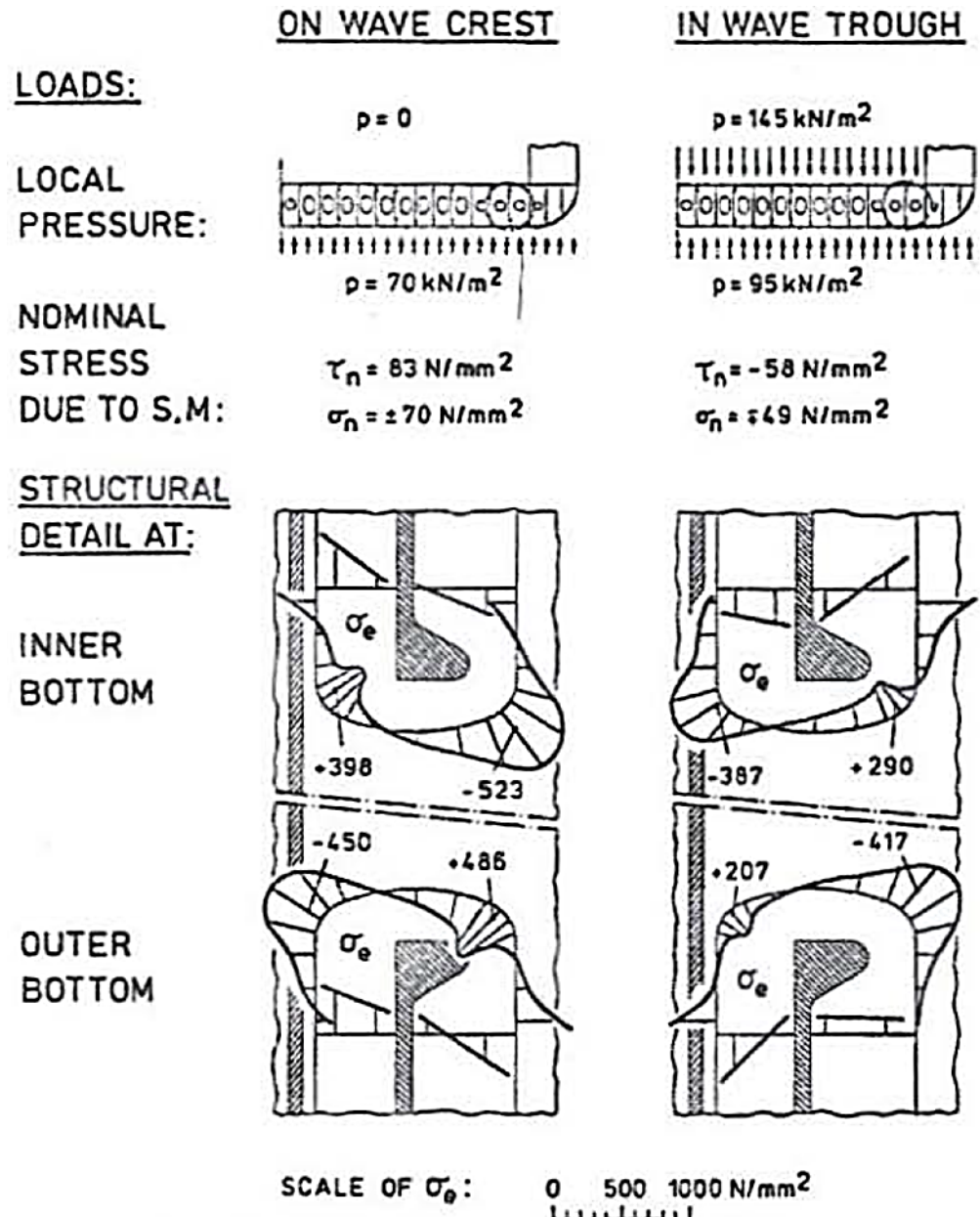


Figure 59: Theoretical elastic stress distribution σ_e for two realistic load cases (Fricke and Paetzold, 1987)

For the structural detail in **Figure 59**, $K_p = 2.94$ was found. The material data for mild steel with a lower yield stress of 290 N/mm² were taken as $K' = 1020 \text{ N/mm}^2$ and $n' =$

0.209. The factor for general yielding varied between 1.1 and 1.2. A value of K_p between 2 and 3 was recommended for similar structures. Neglecting the small wave induced load cycles was justified by the fact that these mainly remain in the elastic region in a bottom structure and the assumption that their contribution to the damage was small in this case. For fatigue life, the damage parameter life curve in **Figure 60** (b) was used, although it was not exactly valid for the material chosen in this example.

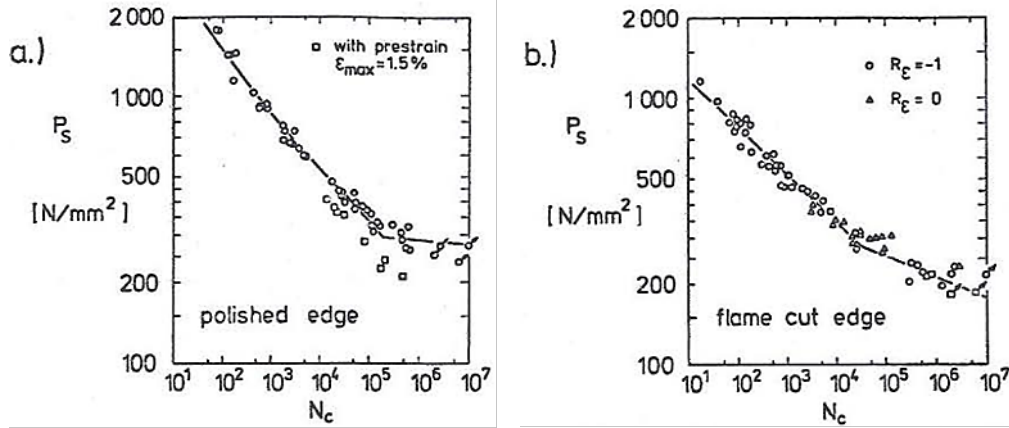


Figure 60: Crack initiation life N_c for specimens of normal strength steel (NS 24), Grade A (Fricke and Paetzold, 1987)

When omitting the influence of mean stress, a crack initiation life of about 1000 voyages was found (i.e. more than the expected number of voyages of a normal merchant ship). It can be seen that far higher stress and strain amplitudes may occur when not only the shear forces S and moment M change their sign, but also the loads due to pressure. In other words, if alternating pressure acts from inside and outside the shell (as in single bottom tankers) cracks at the described details must be expected relatively early in highly stressed transverse webs.

For the estimation of the critical elastic notch stress for simplified load histories Fricke et al., (1987) suggested two simplified probability distributions of the notch stress (as used in the examples); the exponential distribution due to wave induced loads and the constant amplitude loading corresponding to the large load cycles. The mean stress is again assumed to be zero. The crack initiation life N_c can now be estimated directly from the parameter life curve for given amplitudes of the elastic notch stress σ_e . The results are shown in **Figure 61**. The limit load factor (SCF) was set to 2, 3, and infinity. Permissible amplitude of σ_e can be estimated from **Figure 61**. The safety factor must

take into account the unknown scatter of material data because the results are valid only for mild steel and for the specified edge roughness.

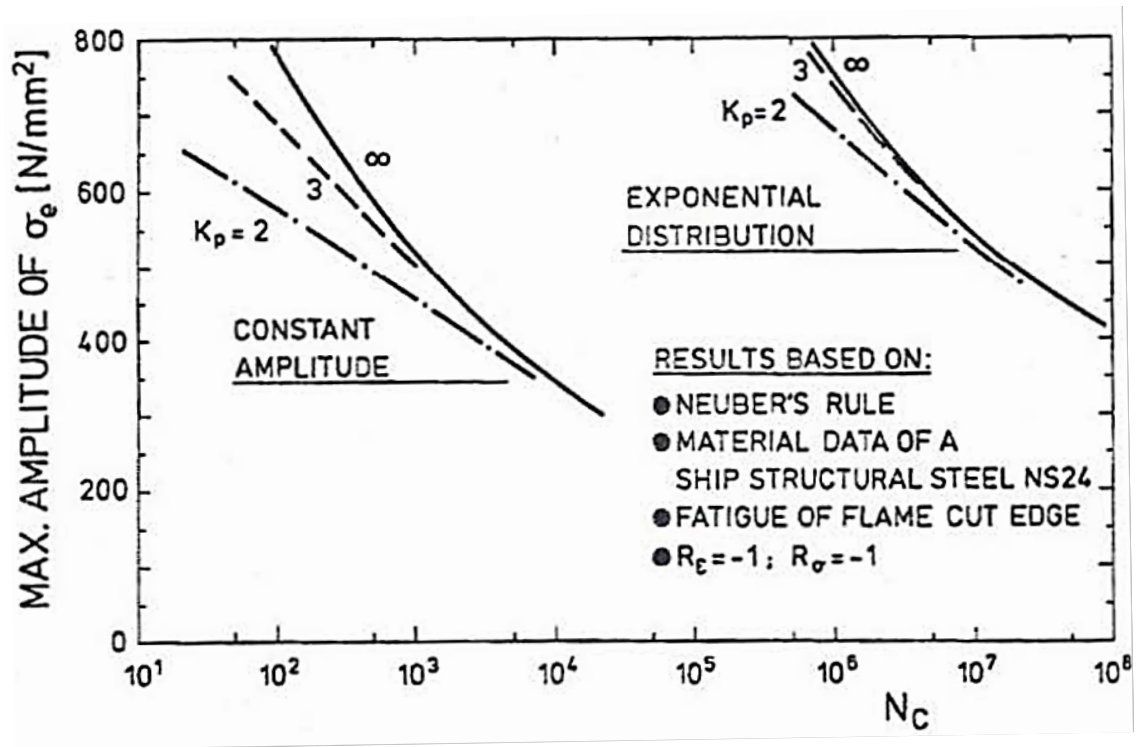


Figure 61: Relationship between fatigue life N_c and elastic notch stress amplitude σ_e for simplified load histories (Fricke and Paetzold, 1987)

2.2.4.3 Cyclic stress strain diagram

Strain hardening microscopic processes was briefly discussed by Petinov (2003) as follows: Assume a standard tensile test to obtain engineering stress strain diagram. If the test is interrupted when the applied stress exceeds the yield point, the specimen is unloaded from state *a* in **Figure 62** and after that the loading is resumed. It may be seen that unloading and the repetitive loading up to the above state reveals almost elastic behaviour of the material. Continuing interceptive loading results in the same stress strain curve obtained in the standard continuous test, although some insignificant discrepancies may be observed, as shown in **Figure 62**. Here the consecutive loading and unloading indicates that higher elastic stress would be necessary to produce additional strain.

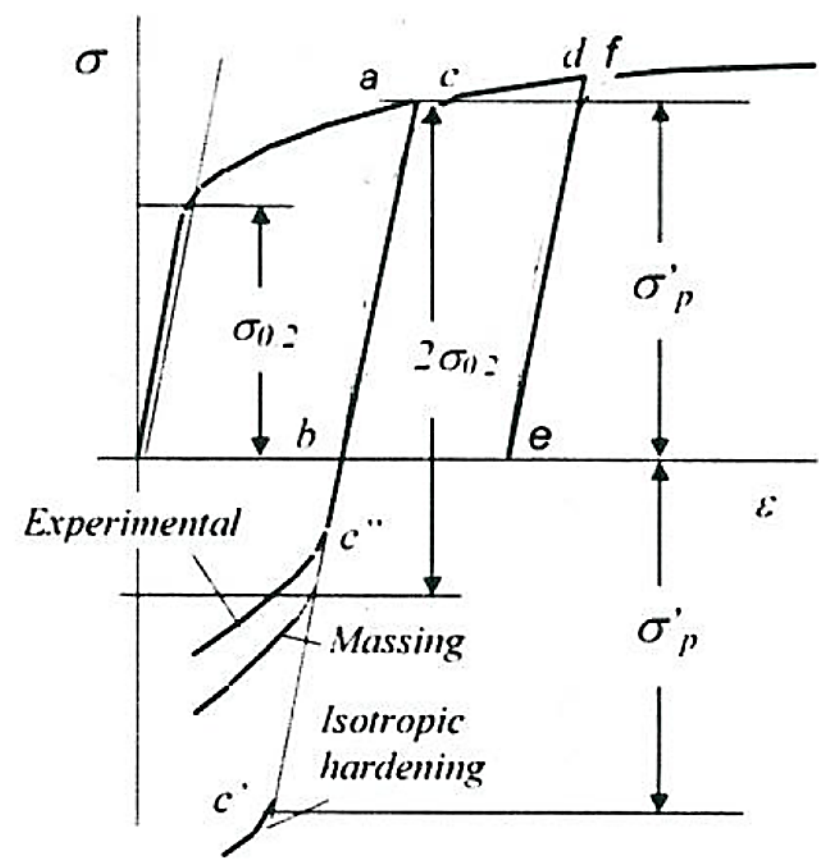


Figure 62: Strain hardening under compression following unloading after tensile plastic deformation (Petinov, 2003)

Material with this type of behaviour is regarded as strain isotropic and this property is used in the isotropic strain hardening theory of plasticity.

2.2.4.4 Bauschinger effect

Petinov (2003) assumed a more complicated test; in its initial phase elastic plastic state is attained under tension and the specimen is unloaded. Loading is then resumed in the opposite direction, compressive loading and different strain hardening properties are revealed. It may happen that the proportionality limit developed in unloading from the state “a” or “d” in tension is not reproduced during the compressive loading. In fact a nonlinear response may be observed at a stress essentially smaller than the stress expected according to the isotropic strain hardening theory ($c'' - d''$ curve in **Figure 63**). Repeating the load excursions between limits “a” and “d” in **Figure 63** would demonstrate that the attained properties would in general characterize the future behaviour of material. These specific features of material response to changes of the load direction in plastic condition are known as the Bauschinger effect. Further

unloading from the d'' in **Figure 63** and resumed tensile loading up to state a defined by strain $\Delta\varepsilon$ as a $b\ c''\ d''$ – curve. Repeating the test in the same fashion one may assume that the material has obtained a new property called the cyclic curve or cyclic stress – strain diagram as seen in either a $b\ c''\ d''$ – curve or $d''\ e''\ a$ – curve.

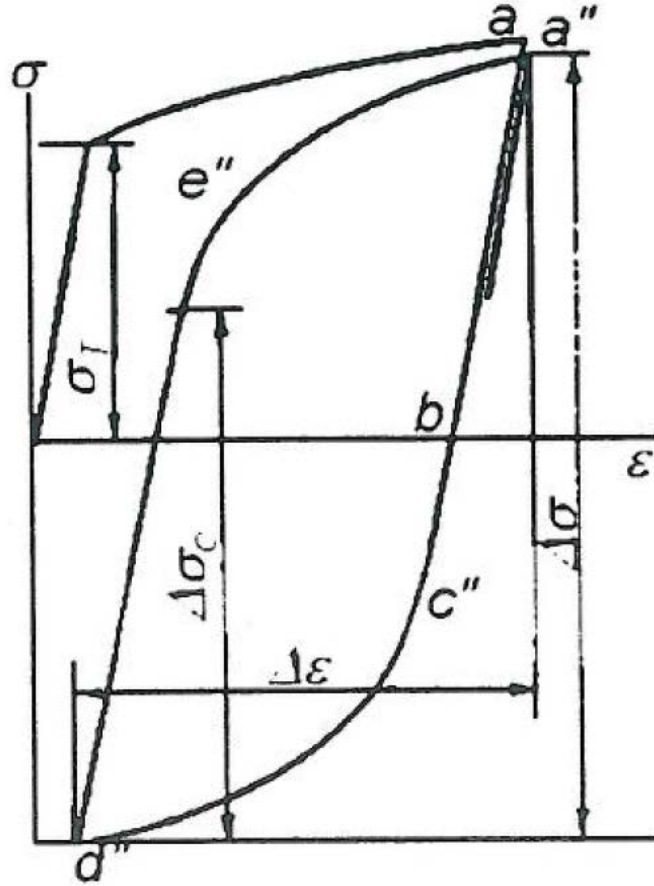


Figure 63: Cyclic diagram in a reversed loading test (Petinov, 2003)

An early prediction of the cyclic curve based on monotonous response data was derived by Massing in 1926 Petinov (2003). It was assumed that the cyclic curve $a\ b\ c''\ d''$ might be plotted by magnifying the stress scale of the initial static curve by two times. Later, Moskvitin (1965) used this assumption for generalizing the incremental theory of plasticity considering the cyclic loading.

Massing rule provides a rough approximation to the actual cyclic curve since resulted from experimental observations. The cyclic proportionality limit specified at a given plastic strain (smaller than the standard 0.2% offset) is not as high as the unidirectional yield stress doubled. Although some promising attempts to predict the cyclic curve based on static tensile data are being made (Hatanaka, 1982), the direct experimental

cyclic curves and approximations of experimental data are preferred for assessing the fatigue properties of materials and structural components Petinov (2003).

As shown schematically in **Figure 63** the parameters of cyclic curve are:

1. The stress range, $\Delta\sigma = \sigma_{\max} - \sigma_{\min}$, where σ_{\max} and σ_{\min} are the maximum and minimum stresses in the loading cycle
2. The total (elastic plus plastic) strain range, $\Delta\epsilon = \epsilon_{\max} - \epsilon_{\min}$, where ϵ_{\max} , ϵ_{\min} – are respectively the maximum and minimum strains corresponding to the above stresses and defining the limits of cyclic curve.

The strain range is a sum of the elastic and plastic components:

$$\Delta\epsilon = \Delta\epsilon_e + \Delta\epsilon_p$$

The plastic strain range is defined also as the plastic hysteresis loop width, $\Delta\epsilon^{pl}$ as in **Figure 64**. In the cyclic test programs either of the above parameters, the stress or strain range may be set controllable, whereas the material response is observed as the behaviour of the “free” parameter. The load and stress controlled test can be used to demonstrate the influence of load / stress ratio, $\sigma_{\min} / \sigma_{\max} = R$, on the fatigue life, fatigue strength and failure mode Petinov (2003).

This influence is related to the effects of mean cyclic stress, $\sigma_m = \frac{(\sigma_{\max} + \sigma_{\min})}{2}$.

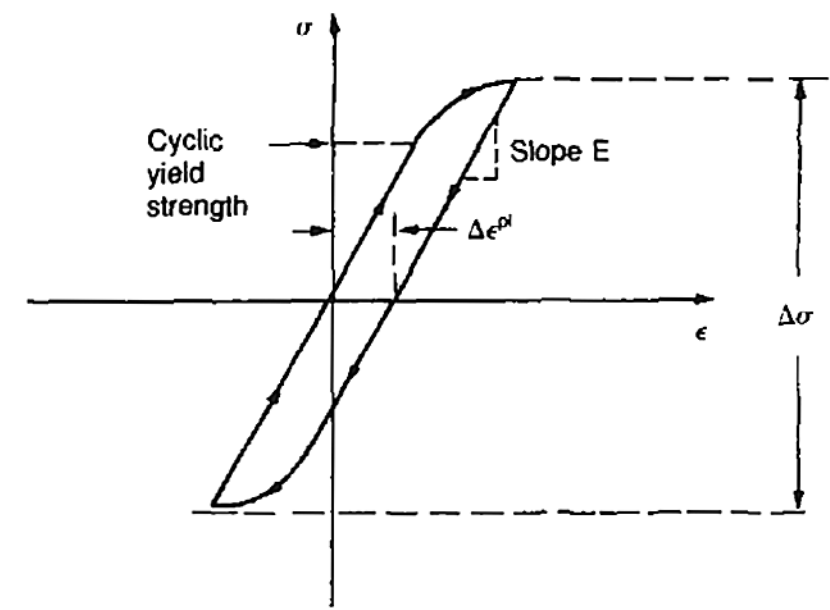


Figure 64: The plastic strain range, $\Delta\epsilon^{pl}$, in LCF (Ashby and Jones, 2002)

Petinov (2003) stated that cyclic diagrams recorded during testing many structural steels reveal a stable character of material resistance and cyclic plasticity within a wide range of load conditions. This fact makes it possible to assume stability of the cyclic curve in successive loading cycles. However, this may be only a first approximation in describing the material behaviour because detailed analysis indicates that the material properties may change in the course of load repetitions. Depending on $\Delta\sigma$ (or $\Delta\epsilon$), σ_{\max} (or σ_{\min}), ϵ_{\max} (or ϵ_{\min}), basic crystalline lattice type and particular alloy composition, specific heat treatment, etc., the inelastic response of material may exhibit unexpected properties.

The two types of cyclic loading that can be realized in laboratory tests are:

1. Cyclic loading; when maximum and minimum stresses (loads) are controlled,
2. Cyclic straining; strain range controlled loading.

Interpretation of the results of such tests for a structural element should be supported by analysis of the local material loading conditions. In case of a non-redundant structure and insignificant stress concentration at the expected failure origin, the loading conditions may be regarded as equivalent to the cyclic loading. If the crack origination is expected in a high stress concentration site and in an excessively redundant structure, the local loading conditions may be attributed to the strain controlled type Petinov (2003).

Petinov (2003) observed that the analysis of the behaviour of materials under the above test conditions reveals the same basis mechanisms of plastic and microplastic deformation but they develop in a different manner. For example a low tensile strength Aluminium alloy hour-glass specimen is subject to cyclic testing with maximum and minimum stresses, as shown in **Figure 65** (a). A typical material response to cyclic loading is a decrease of the hysteresis loop width in every load reversals, especially in the first load reversals. The reduction of plastic response of material results consequently in a decrease of the total strain range coupled by an increase of material stiffness. In the strain controlled tests, **Figure 65** (b) the increase of material stiffness results in an increase of stress range during the succeeding load reversals. This process may be accompanied by a gradual reduction of the plastic strain range, together with an increase of the stress ranges revealing the cyclic strain hardening of the material.

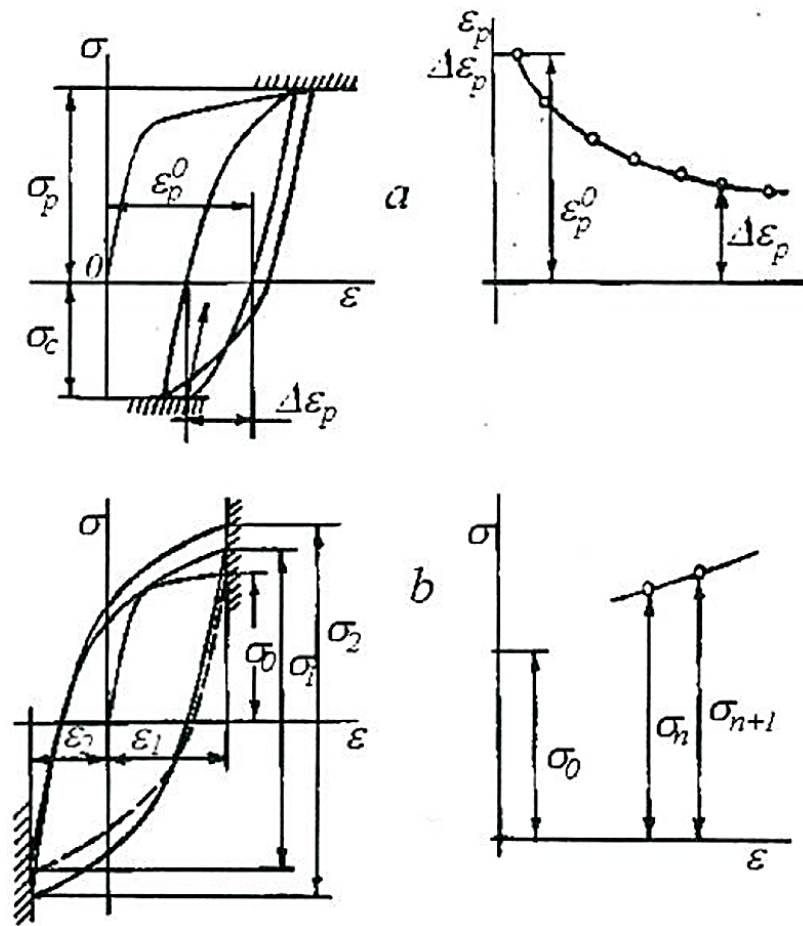


Figure 65: Cyclic hardening: (a) testing under control of load (stress) amplitude, (b) testing under strain range control (Petinov, 2003)

If the test conditions maintain the mean stress (or mean strain) in the load cycle, irreversible plastic strains are accumulated cycle by cycle. This gradual accumulation can result in a quasi-static failure. In structural elements where the fatigue process is concentrated within a small volume, the quasi-static accumulation of plastic strain is limited by the surrounding elastic bulk of material. Fatigue testing of notched specimens reveals insignificant accumulation of plastic strain at the notch root if the nominal stress amplitude does not exceed the elasticity limit stress. Petinov (2003)

In contrast to the above materials, some heat resistant steels reveal the opposite cyclic properties. In stress range controlled tests, the material stiffness gradually decreases and the hysteresis loop widens, what manifests the cyclic strain softening. This type of material behaviour in strain controlled tests reveals a reduction of the stress range in the course of load reversals. Consequently, materials of this group are called cyclically softening. Results of cyclic tests allows one to generalize the cyclic hardening or

softening of materials and to model the essential trends in the material cyclic response Petinov (2003).

Makhutov (1981) suggested for the hysteresis loop width:

$$\text{For cyclically hardening materials} \quad \Delta \overline{\varepsilon}_p = \frac{\Delta \overline{\varepsilon}_{pl}}{n^\alpha} \quad \text{Eq. 24}$$

$$\text{For cyclically softening materials} \quad \Delta \overline{\varepsilon}_p = \Delta \overline{\varepsilon}_{pl}^{\beta(n-1)} \quad \text{Eq. 25}$$

Where $\Delta \overline{\varepsilon}_p$ is the plastic strain range related to elasticity limit state,

$\Delta \overline{\varepsilon}_{pl}$ is the plastic strain in the first load reversal ($n = 1$),

$\Delta \overline{\varepsilon}_{pl}^\alpha$ is a material constant.

β is an empirical parameter.

One way of generalization is shown in **Figure 66** (Left) presumes that the curves are plotted together with a common unloading point. The envelope of the diagram's opposite unloading points forms the generalized cyclic curve. Another way of generalization is shown in **Figure 66** (Right) is based on a common curvature for the family when the superimposed curves do not have a common unloading point. This situation complicates an approximation of the family. Therefore, the first type of generalization of cyclic curves seems to be preferable in fatigue analyses. Petinov (2003)

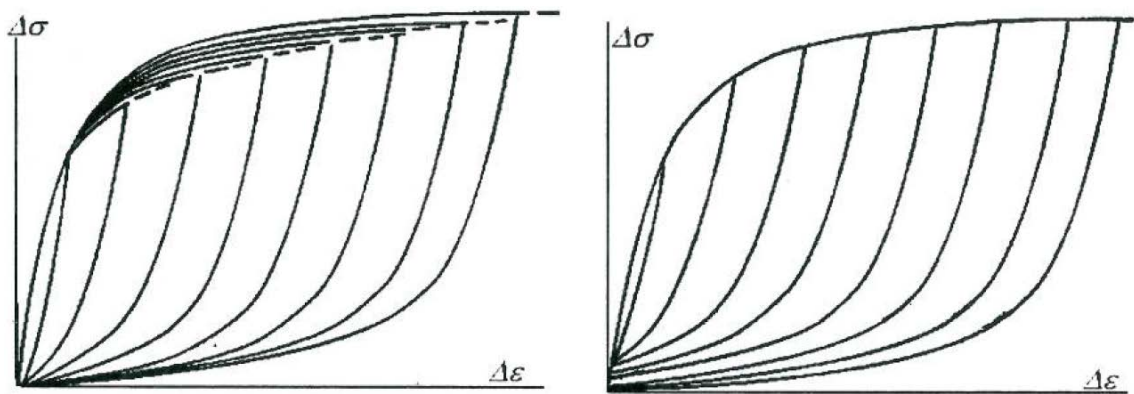


Figure 66: Generalization of cyclic curves: left – the common point for all of diagram is the load reverse point, right – superposition of diagrams (Petinov, 2003)

The experimentally obtained (generalized) cyclic curve may be approximated in a form suitable for an analytical or numerical solution Petinov (2003). For a cyclically stable material, the cyclic curve of which does not differ much from a bilinear one, the Ramberg Osgood equation may be applied:

$$\begin{aligned}\Delta \sigma &= E \Delta \varepsilon & \text{at } \Delta \varepsilon &= \Delta \varepsilon_c \\ \Delta \sigma &= E \Delta \varepsilon - P(\Delta \varepsilon - \Delta \varepsilon_c) & \text{at } \Delta \varepsilon &> \Delta \varepsilon_c\end{aligned}$$

Where $\Delta \varepsilon_c$ is the strain range which corresponds to the cyclic proportionality stress range, P is an experimentally obtained coefficient. In a general case when the bilinear approximation may be inappropriate and a non-stabilized cyclic behaviour should be analysed, a modified Ramberg Osgood equation may be an effective approximation:

$$\Delta \varepsilon = \frac{\Delta \sigma}{E} + K(\Delta \sigma - \Delta \sigma_c)^k \quad \text{Eq. 26}$$

Where K and k are material cyclic hardening parameters. $\Delta \sigma_c$ is the cyclic proportionality stress range.

Serensen et al. (1975) recommended a more general approximation that considers the influence of the mean stress and the cyclic strain hardening or softening. Petinov (2003)

Concluding, it should be noted that evaluation of the cyclic proportionality limit stress, $\Delta \sigma_c$ presents a serious problem that should be noted while analysing experimental stress strain records. Application of 0.02 off set strain is not reasonable because it means neglecting a considerable portion of inelastic strain range. The 0.02 margin should be reduced to a value as small as possible indicating the onset of inelastic deformation in analysing the experimental cyclic diagrams and fatigue under programmed and random loadings. To illustrate this statement, **Figure 67** shows schematically the cyclic stress strain ranges and subsequent development of damage to microstructure. Development of microplasticity in randomly distributed single material elements at low stress ranges does not influence the elastic behaviour of bulk material but clears the way for initiating the fatigue process. Petinov (2003)

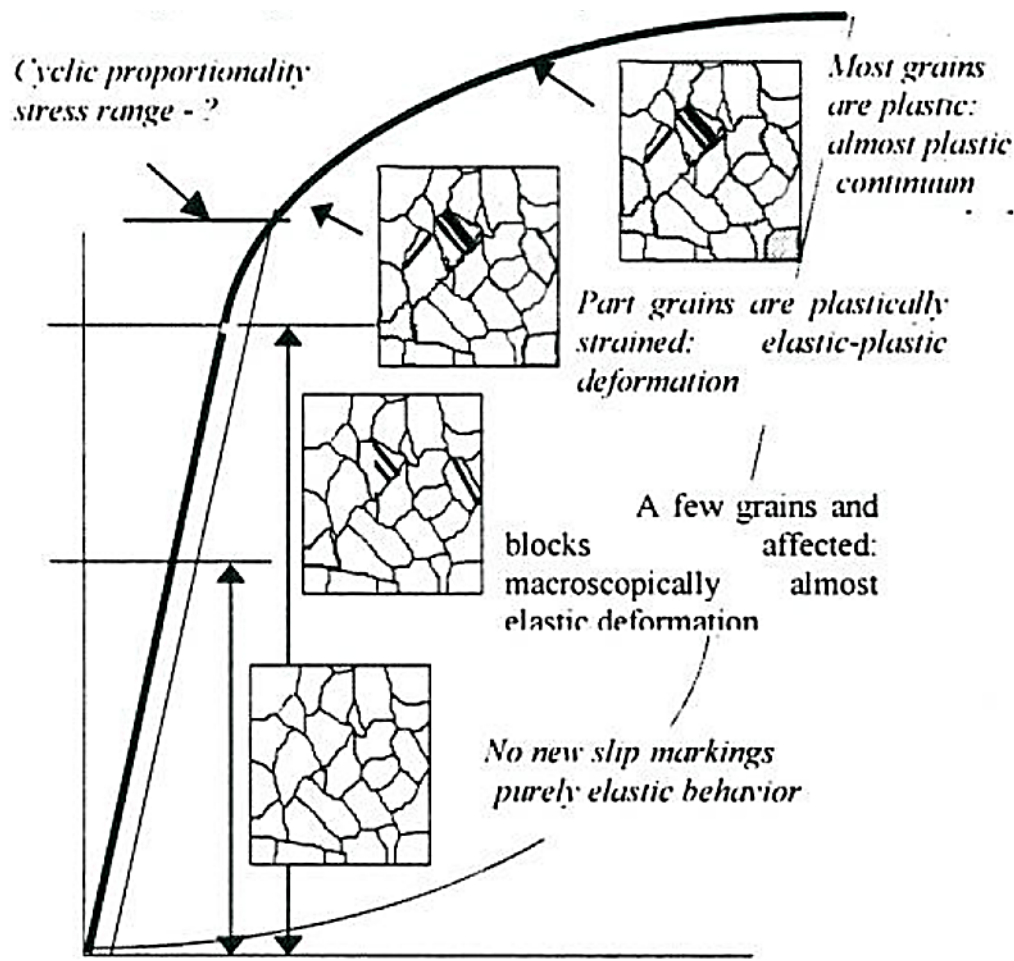


Figure 67: Cyclic stress / strain ranges and development of damage to microstructure (Petinov, 2003)

Petinov (2003) emphasized that information on material behaviour under monotonous and alternating loading should be obtained via testing of specimens with a uniform stress state in the gauge part. This concerns the database of the low cycle (local strain) and inelastic strain energy approaches. The use of the S-N format with basis S-N curves related to typical welded joints does not imply the detailed analysis of the fatigue process at the crack origination location.

Because the effects of sample size and surface conditions of the actual structural components are ambiguous, the volume of the gauge part of a specimen should not be less than the volume of the high stress concentration zone in the hull, e.g. a part of deck plating at the hatch corner, a rounded coming at the hatch, etc. As to the specimen's surface finish, in order to obtain the material cyclic properties, the gauge part should be smooth enough to exclude the deteriorating effects of machine markings. To what extent this corresponds to the surface conditions at the notch root is uncertain. To clear

up this ambiguity from the engineering point of view, comparative studies may be applied. Petinov (2003)

There are two types of specimens and two types of loading which meet the conditions:

1. Thin wall tubular specimen for fully reversing torsional strain / load cycling, a version of which is shown in **Figure 68** (top),
2. Hour glass (or short cylindrical) specimen for reversing axial strain / load testing (**Figure 68**, (bottom)); when misalignment in fixation of the specimen in testing machine may be ignored, short cylindrical axially loaded specimens may be applied. Petinov (2003)

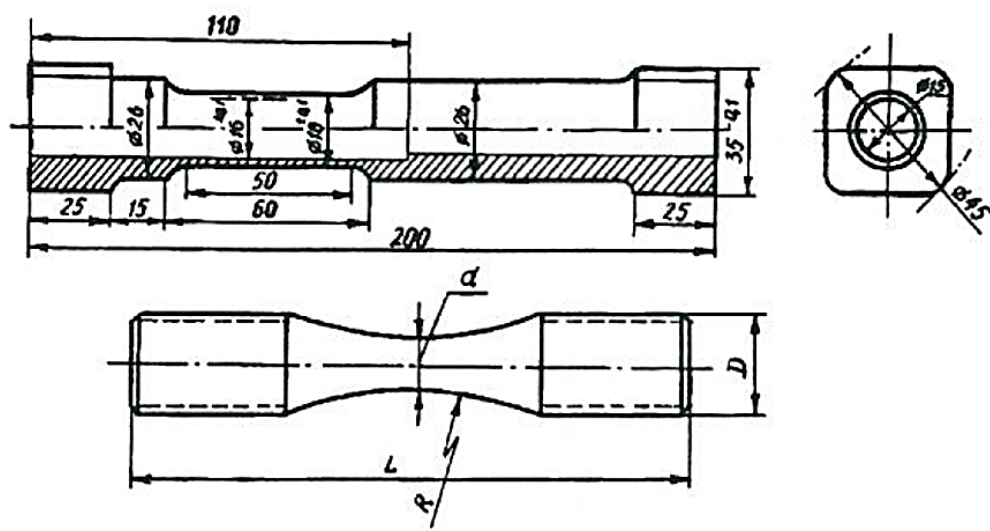


Figure 68: Specimens for fatigue testing of materials: top – for cyclic torsion tests, bottom – for axial cyclic load or strain range control testing (Petinov, 2003)

2.2.5 Material Fatigue Criteria

Petinov (2003) discussed the fatigue criteria of materials in details starting from the most essential phenomena of material resistance to alternating load which is attributed to A. Woehler in 1870. Following his experimental studies on axles of railway carriages he found a relationship between alternating stress amplitude and number of cycles prior to crack initiation or prior to complete failure and also he found a maximum alternating stress that did not result in fatigue failure. This stress amplitude was later named fatigue limit and corresponds to 2 – 5 millions of cycles. Cyclic hardening and softening with sequential changes in the cyclic proportionality limit offer no visible link to the fatigue limit.

Structural steels (unlike Aluminium alloys, copper based alloys) exhibit a well-defined fatigue limit when tested in air not in corrosive environments. The criterion of fatigue failure of material may be assumed in a form of a relationship between one of the hysteresis loop parameters, stress range, strain range, or plastic strain range, and the number of load cycles prior to failure. However, none of these parameters may be considered as the only one representing material cyclic strength. For example, if the stress range is assumed to be the controlled test parameter, one has to keep in mind the variability of other parameters. For this reason the fatigue criteria, in which the number of load cycles prior to material failure is related to either stress or strain range, are provisional. A relatively more advanced representation of the fatigue of materials may be suggested in the form of a cycle by cycle accumulation of inelastic strain energy until it reaches a critical value but because the experimental estimate of this critical value is questionable more simplified approaches are used in engineering applications Petinov (2003).

The most common approach in engineering analysis is the S-N approaches based on relating the number of cycles at a specific failure mode to the applied stress range or stress amplitude and because stress reaching yield limit is usually not allowed in ship hull and marine structures the S-N criterion is limited by its high cycle part on condition $\Delta\sigma < 2\sigma_y$ as illustrated in **Figure 69**. Petinov (2003)

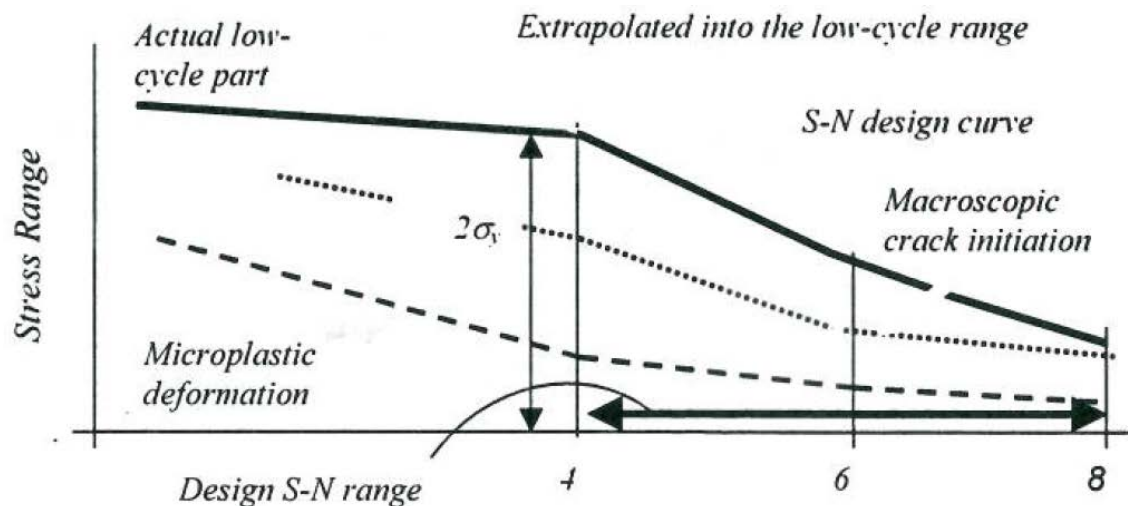


Figure 69: Actual and 'design' S-N curves (Petinov, 2003)

Petinov (2003) emphasized that omitting the low cycle part of S-N curve would automatically result in extrapolating the high cycle approximation further into the low

cycle part in the fatigue strength assessment procedures when linear damage accumulation is applied. This is physically inconsistent with the mechanics of material deformation and fatigue damage. Of the many known approximations of experimental data derived for engineering applications, the most commonly accepted is the Basquin equation (1910), written in the form:

$$N(\sigma) = \frac{C}{\sigma^m} \quad \text{Eq. 27}$$

Where C and m are experimentally obtained coefficients, σ is the stress amplitude.

Weibull (1961) suggested the approximation which also accounts for the endurance limit:

$$\sigma(N) = K(\sigma - \sigma_e)^m$$

Where σ_e is the endurance limit stress, K is the empirical coefficient.

2.2.6 Strain Life Criteria

Petinov (2003) presented the strain life criteria in the most possible simple way which is rather complicated however the criteria was introduced by Coffin (1954) and Manson (1965) who described the relationships between plastic strain range and the number of cycle reversals to material failure in low cycle region at approximately $N < 10^4$ where the stress amplitudes exceed the static yield limit. This is best known as Coffin Manson Relation. Initially, the strain life criterion was derived in order to evaluate the fatigue lives of components in mechanical engineering during cyclic thermal stressing.

The Coffin's plastic strain criterion, obtained from the plastic strain range controlled tests is presented in the form:

$$\Delta \varepsilon_p = CN^{-\alpha} \quad \text{Eq. 28}$$

where $\Delta \varepsilon_p$ is the plastic strain range, C and α are the parameters assumed as the material constants; according to Coffin, $\alpha = 0.5$ and $C = -0.5 \ln(1 - \psi)$ where ψ is the area reduction for the tested materials. Further analyses revealed that the values of these parameters may significantly differ from Coffin's estimates.

Using plastic strain range as an indicator of fatigue damage was regarded as fundamental in attempts to relate the plastic strain range to the changes of dislocation structure per load reversal. Petinov (2003) Petinov also noted that the direct use of criterion in equation (Eq.1) in the fatigue analysis of ship's structural details is barely

feasible for two reasons. First, the definition of the plastic strain and its distinction from the total strain range is complicated. Second, the ship hull and marine structures are infrequently subjected to loads causing plastic strains in notches. For these reasons, equation (Eq.1) is modified so that the strain criterion of fatigue failure should relate the total strain range to the fatigue life of the material. The criterion should cover not only the overloads but also the whole range of excitations capable of producing fatigue damage to a structural detail. Based on Coffin's criterion, several versions of the strain criterion are known to cover both low cycle and HCF. One of the simplest is the engineering criterion suggested by Coffin and Tavernelli (1962);

$$\Delta \varepsilon = \Delta \varepsilon_p + \Delta \varepsilon_e = -0.5 \ln(1 - \phi) N^{-0.5} + \frac{2 \sigma_{-1}}{E} \quad \text{Eq. 29}$$

When experimental data are available for a material, this equation is modified to:

$$\Delta \varepsilon = C N^{-\alpha} + \frac{2 \sigma_{-1}}{E} \quad \text{Eq. 30}$$

Equation (Eq.30) can fit the experimental data in the range of transition between low cycle and HCF when plasticity becomes more a randomly scattered microstructural process and thus, can be applied to the fatigue analyses of ship and marine structures. Petinov (2003) The second term in the right hand part of equation (Eq.30) conditionally presents the elastic strain range. The elastic strain range corresponding to the hysteresis loop may essentially exceed the value of $2 \sigma_{-1} / E$. Consequently, $\Delta \varepsilon_e$ has to be greater than the strain range specified at the fatigue limit. To consider this, Manson (1962) proposed a form of the criterion in which the elastic term is better suitable to the experimental data:

$$\Delta \varepsilon = C N^{-\alpha} + B N^{-\beta} \quad \text{Eq. 31}$$

Here C, B, α and β are the best fit material constants, N is the number of load reversals, i.e. twice the load cycles.

In addition, Manson (1962) introduced the relationships for obtaining these constants from static test characteristics. equation (Eq.30) is frequently presented in the form:

$$\frac{\Delta \varepsilon}{2} = \left(\frac{\sigma'_f}{E} \right) (2N)^\beta + \varepsilon'_f (2N)^\alpha \quad \text{Eq. 32}$$

Where σ'_f and ε'_f are the fatigue strength and fatigue ductility coefficients, respectively.

In 1988 Manson and Muralidharan derived the following expression:

$$\Delta \varepsilon = 0.0266 \varepsilon_f^{0.115} \left(\frac{\sigma_u}{E} \right)^{-0.52} N^{-0.56} + 1.170 \left(\frac{\sigma_u}{E} \right)^{0.832} N^{-0.09}$$

Where σ_u is the ultimate strength of material, $\varepsilon_f = -\ln(1 - \psi)$ is the ductility.

Makhutov (1981) modified equation (Eq.30) into the following form:

$$\Delta \varepsilon = 0.8 \varepsilon^{3/4} N^{1/2} + \left(\frac{2\sigma - 1}{E} \right) \left(\frac{N}{N_0} \right)^{-0.08} \quad \text{Eq. 33}$$

Where $\varepsilon_t = -\ln(1 - \psi)$, N_0 is the number of cycles corresponding to definition of the fatigue limit.

Equation (Eq.31) does not comprise the fatigue limit. Therefore, it can be used in the fatigue analysis of materials which do not reveal this limit or structural steels in aggressive media.

A modified version of equation (Eq.31) was proposed by Kloppel and Klee (1969) who subdivided the elastic strain range and another with the fatigue limit strain:

$$\Delta \varepsilon = CN^{-\alpha} + BN^{-\beta} + \frac{2\sigma - 1}{E} \quad \text{Eq. 34}$$

Constants B and β here are different from those in equation (Eq.31).

Serensen et al., (1975) derived the following versions of the strain life equation corresponding to load controlled test conditions (cyclic loading of an excessively redundant structure):

For fully reversed loading

$$\Delta \varepsilon = -\ln(1 - \phi) N^{-\alpha} + \frac{2\sigma - 1}{E} \quad \text{Eq. 35}$$

For cyclic loading with a constant component

$$\Delta \varepsilon = -0.5 \ln(1 - \phi) (1 - R) AN^{-\alpha} + \frac{2\sigma - 1}{E(1 + \frac{\sigma - 1 F(R)}{\sigma_u})} \quad \text{Eq. 36}$$

Where $R = \sigma_{\min} / \sigma_{\max}$, $F(R) = (1 + R) / (1 - R)$, σ_u is the ultimate tensile strength of the material.

For arbitrarily loaded strain controlled tests, the following form of equation (Eq.44) was assumed:

$$\Delta \varepsilon = -0.5 \ln(1 - \phi) (N + 2F(R))^{-\alpha} + \frac{2 \sigma_{-1}}{E(1 + \frac{\sigma_{-1} F(R)}{\sigma_u})} \quad \text{Eq. 37}$$

For the same loading conditions Duggan (1980) applied the following version of equation (Eq.31) in fatigue analysis of machine components to allow for overloads:

$$\Delta \varepsilon = (C_p - \varepsilon_m) N^{-\alpha} + C_e \left(1 - \left(\frac{\sigma_m}{\sigma_u} \right)^k \right) N^{-\beta} \quad \text{Eq. 38}$$

Where σ_m and ε_m are the constant stress and strain components in a cycle, C_p , C_e , α and β are the parameters to be experimentally obtained.

Petinov (2003) stated that some of the above equations are derived for fatigue analysis mainly in the low cycle region at nominal stresses near elasticity limit or higher, e.g. equation (Eq.35) and equation (Eq.36) and when equation (Eq.31), equation (Eq.34), or equation (Eq.38) are applied as the strain life criteria, iterative procedures should be used in practical calculations of random load fatigue analysis. To avoid these difficulties, equation (Eq.30) might be preferable using experimental evaluation of its constants. Since this equation can be used in the fatigue analysis of structural details, evaluating the fatigue limit should include the influence of principal factors such as stress concentration, stress state at notch root, effects of the size of the stress concentration zone, etc.

Petinov (2003) noted that the material fatigue failure criterion used in the low cycle format, equation (Eq.30), does not consider the effects of microplasticity in a high cycle region and by this, underestimates the material fatigue resistance in the vicinity of the fatigue limit.

Petinov (2003) concluded that an unambiguous definition of the state of damage is needed in any of the above mentioned criteria for fatigue failure and for the number of cycles prior to failure.

2.2.7 Fatigue Life Prediction

2.2.7.1 General

For Fatigue Life Prediction (number of cycle to failure) from a practical point of view Manson (1964) took advantage of the fact that elastic and plastic components are straight lines on log – log coordinates; which means only a few simple tensile tests are needed to establish a correlation between these lines and the properties of materials. This is known as Four Point Correlation Method illustrated in **Figure 70**:

assumption that the total strain range at 10^4 cycles is approximately 1 % for all materials.

Thus, from knowledge of the tensile properties of a material, two points on each of the lines can be determined and the plastic and elastic components plotted. Four Point Correlation Method has one limitation that is it requires knowledge of the true fracture stress which is not always given in the literature and therefore an additional approximation is required. O'Brien suggested a very good approximation where he recommended that the fracture stress (True Stress) could be obtained by multiplying the ultimate tensile strength by the factor $(1 + D)$. Manson (1964)

Thus,

$$\sigma_f = \sigma_u (1 + D) \quad \text{Eq. 39}$$

This relation is valid as seen in **Figure 71** where fracture stress is plotted against the product of $\sigma_u (1 + D)$.

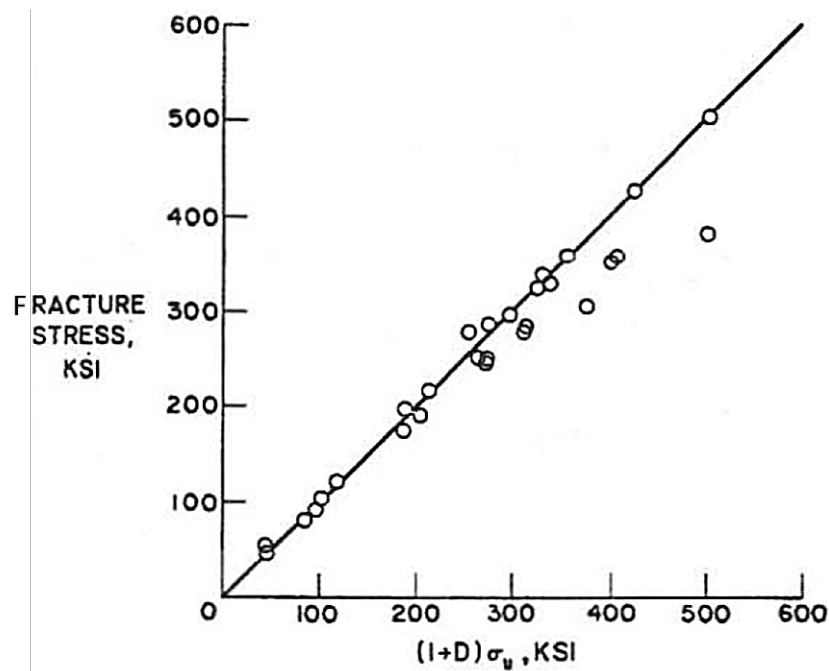


Figure 71: Fracture stress against function of true ductility and ultimate strength (Manson, 1964)

Each data point represents a different material, and the data in general falls close to a 45° line. By using this approximation, only the elastic modulus and two tensile

properties, σ_u and reduction in area (which establishes D), are needed to predict axial fatigue life for a specified strain range.

The validity of this procedure was further investigated by examining a larger number of materials (29) in axial LCF tests. These structural materials are included in **Table 4**.

Table 4: Materials for Axial LCF Investigation. Manson (1964)

4130 Soft	Titanium 6Al-4V
4130 Hard	Titanium 5Al-2.5Sn
4130 X-hard	Magnesium AZ31B-F
4340 Annealed	Aluminium 1100
4340 Hard	Aluminium 5456 H311
304 Annealed	Aluminium 2014 T6
304 Hard	Aluminium 2024 T4
52100 Hard	Aluminium 7075 T6
52100 X-hard	Silver 0.99995 pure
AM 350 Annealed	Beryllium
AM 350 Hard	Inconel X
310 Stainless	A286 aged
Vascomax 300 CVM	A286 34 % cold reduced and aged
Vascojet MA	D 979
Vascojet 1000	

These materials cover a range of variables that might affect fatigue behaviour such as those shown in **Table 5**.

Table 5: Material Variables in Axial LCF Investigation. Manson (1964)

Crystalline structure	Body – centered cubic
	Face – centered cubic
	Close – packed hexagonal
Methods of strengthening	Precipitation hardening
	Hot and cold worked
Reduction in area	1 to 94 %
Tensile strength	16,000 to 413,000 psi
True fracture stress	48,000 to 500,000 psi
Elastic modulus	6.2×10^6 to 42.0×10^6 psi
Notch sensitivity	Notch ductile to very notch sensitive
Stacking – fault energy	Low (steels) to high (Aluminium)
Cyclic behaviour	Strain softening to strain hardening

Manson (1964) also discussed the Universal Slopes Method which is based on the assumption that the slopes of both elastic and plastic lines are the same for all materials (i.e. plastic line assumed to be -0.5 and elastic line assumed to be -0.12). In 1952 when S S Manson first proposed that plastic strain line is linear on log – log coordinates, his proposal was based on very limited experimental data available at that time not enough to justify the assumption of a universal slope for all materials therefore; he suggested that the exponent (slope) would be a material constant. Later, Coffin suggested that the exponent has a universal value of -0.5 for all materials. Based on the indications of conducted tests, Manson is of the view that slopes are different from material to material but if a universal slope is to be assumed then -0.6 would be more representative of all materials.

Figures 72 and 73 show the results of 29 materials represented with a straight line with a slop of -0.6 for plastic and a straight line with a slop of -0.12 for elastic.

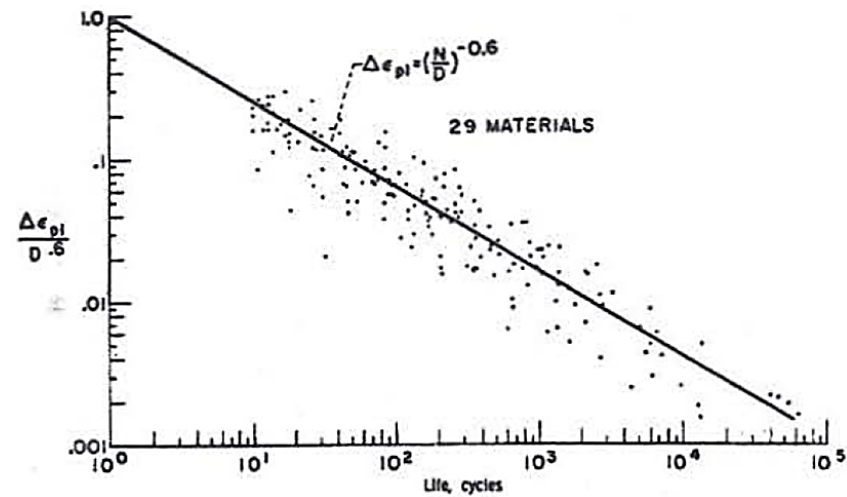


Figure 72: Relation between plastic strain ductility and cycles to failure (Manson 1964)

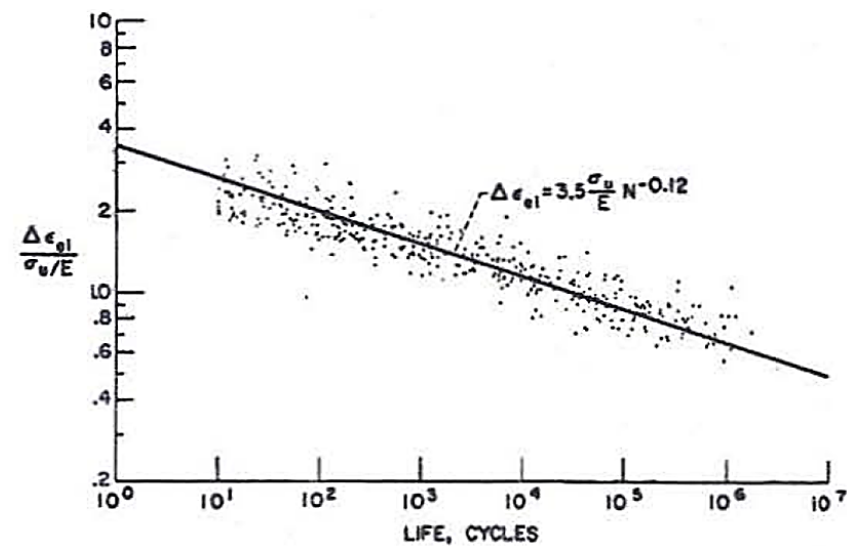


Figure 73: Ratio of elastic strain range to σ_u / E against cycles to failure (29 materials) (Manson, 1964)

The total strain range $\Delta \epsilon$ is presented in **Figure 74**:

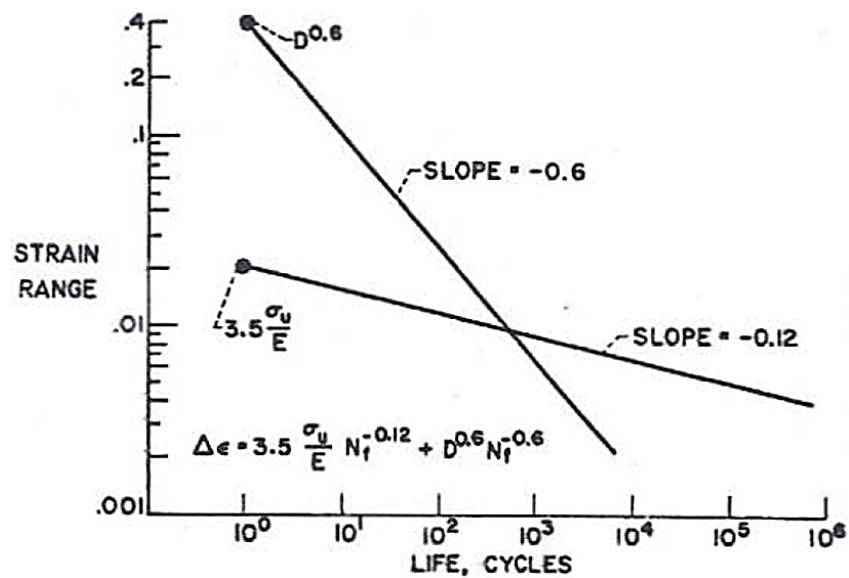


Figure 74: Model for method of universal slopes (Manson, 1964)

Figures 75 and 76 present the actual results of comparison between Experiments and the two Predictions Methods for 29 materials tested.

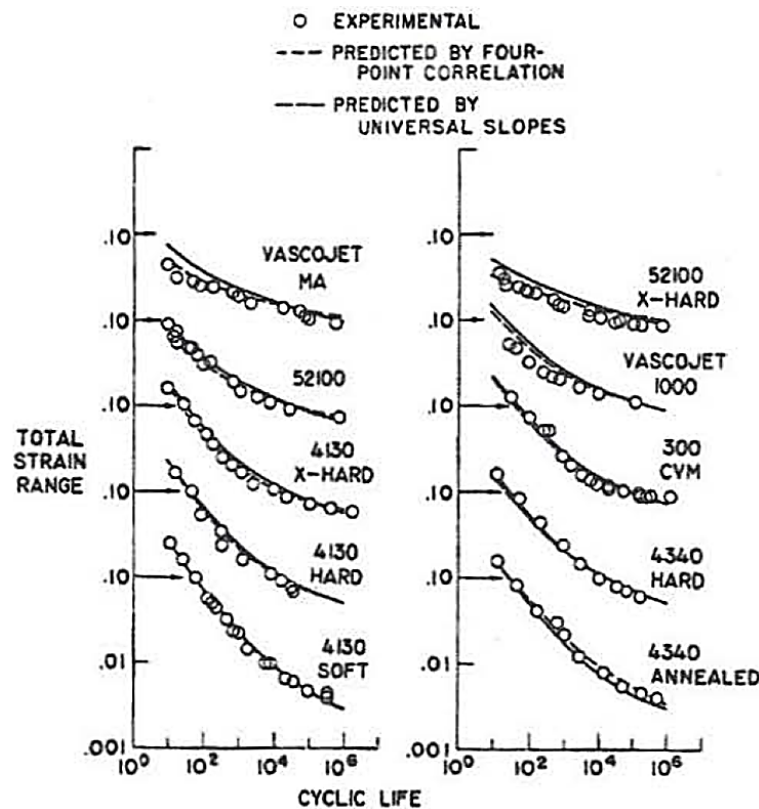


Figure 75: Comparison of predicted and experimental axial fatigue life for low – alloy and high – strength steels (Manson, 1964)

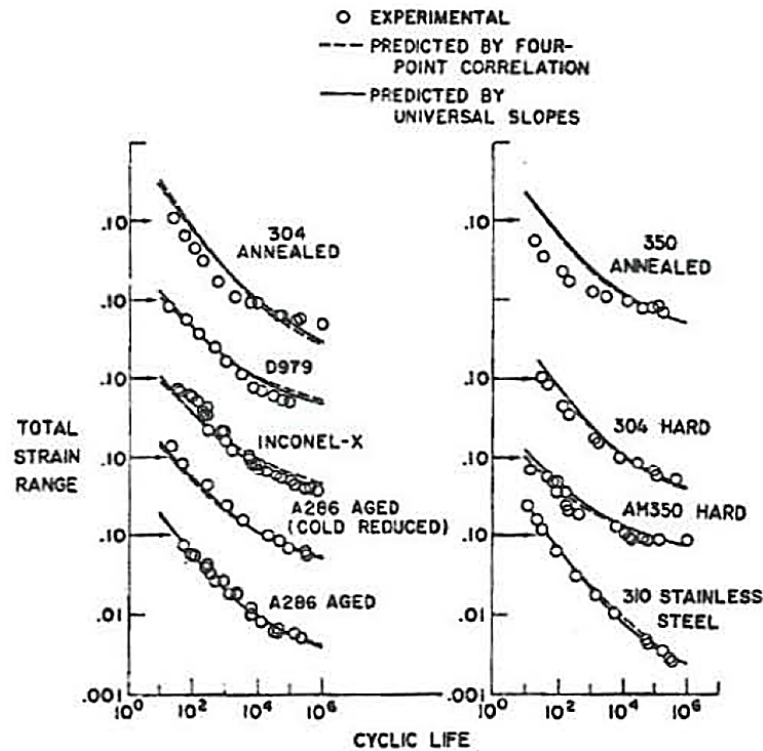


Figure 76: Comparison of predicted and experimental axial fatigue life for stainless steels and high – temperature alloys (Manson, 1964)

2.2.7.2 Material Notch Sensitivity

Manson (1964) also observed that materials sensitive to notches or cracks will not manifest its sensitivity until a crack of significant size develops to alter the stress field. If such a crack does not occur until late in the life of the specimen; the material cannot be sensitive to it until most of the life has already been used. He also concluded that the important feature of axial strain cycling tests of un-notched specimens is the late development of significant cracking therefore, the principal reason why tests of this kind do not reflect notch sensitivity is that cracks of significant size are not present in these materials during the major portion of their life.

According to Coffin et al observations of the specimen surface in some of their tests; when visual cracking occurred, they regarded the test complete i.e. initial cracking is the criterion for failure. Manson however, in all of the tests on the 29 materials; failure was taken as the actual separation of the two halves of the specimen.

Manson's first approximation is that most materials will survive approximately 10,000 cycles of application of a strain range of 1%. Morrow has examined this rule of thumb

in comparison with others and has concluded that a better approximation is the one suggested by Peterson; most materials can withstand 1000 cycles of a strain range of 2% prior to failure. Manson re-examined these two approximations utilizing the results of the 29 materials previously used to relating life to strain range and favoured the 2% rule at 1000 cycles as shown in **Figure 77**.

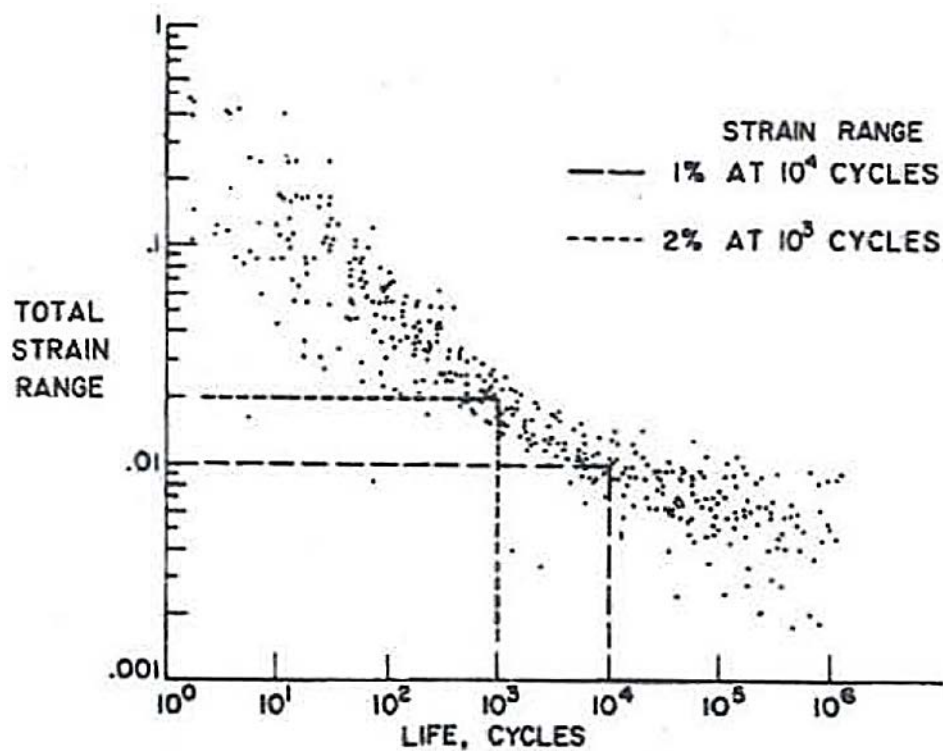


Figure 77: Axial strain – cycling – fatigue behaviour of 29 materials (Manson, 1964)

2.2.8 Cumulative Fatigue

Manson (1964) refers to cumulative fatigue as the behaviour of actual structures operating under a spectrum of loading. This well-known linear damage rule was first proposed by Palmgren and later by Langer and by Miner. It assumes that at any stage of the loading history of the material, the percentage of life used is proportional to the cycle ratio at that loading condition. Thus, if a stress range or strain range is applied for n_1 cycles at a condition where failure would occur if N_1 cycles are applied, the percentage of life used is n_1/N_1 . It is well known that this is just an approximation and may often result in inaccurate predictions of fatigue life. Hence he outlined some of the factors that govern material behaviour under cumulative fatigue loading both in terms of Cyclic Hardening and Softening and Crack Propagation. **Figure 78** presents some results obtained with 2024 – T4 Aluminium under an interrupted loading spectrum.

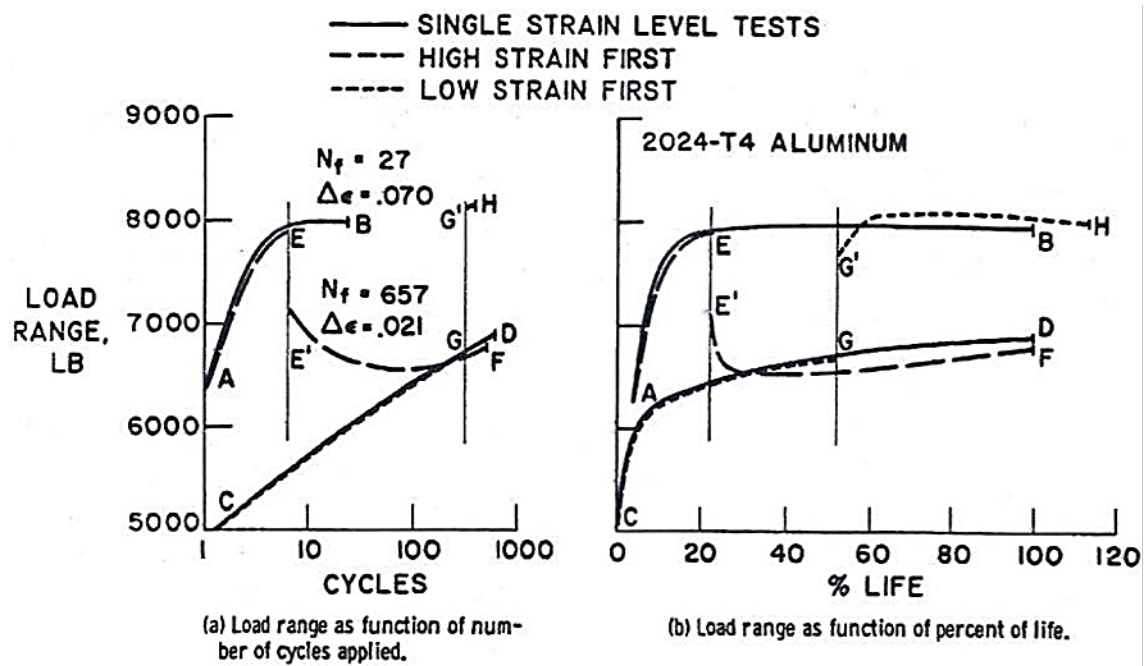


Figure 78: Cyclic strain hardening under two – level fatigue tests (Manson, 1964)

The curve AB represents load range of a test with constant strain range at 0.070 and life of 27 cycles. The curve CD represents load range of a test with constant strain range at 0.021 and life of 657 cycles. If strain range of 0.070 is applied for only 25% of the expected life for this strain level the variation of load range follows the curve AE. If at this time the strain range is changed to 0.021 and maintained until failure occurs, the resulting load range curve is E'F indicating that the material first softens and then hardens. In **Figure 78** (b) the horizontal scale is taken to be percentage of life instead of cyclic life (same phenomena). Initially the hardening from A to E follows the basic curve AB. When the strain range changes to 0.021 the stress range falls within few cycles to the curve CD that corresponds to the same percentage of life that was already used on curve AB. Thus, the curve E'F falls rapidly at first to curve CD but since at 25% of the expected life the curve CD curve E'F indicates the material is still undergoing hardening.

A similar result is obtained if test starts first with the low strain range and then continues at the higher strain level. Manson (1964) To keep the curves separated Manson chosen to illustrate the case in which half of the life is used at the lower strain level followed by straining at the higher level. The first portion of the test is represented by CG which follows CD; the second follows the curve G'H. G'H segment in **Figure**

79 (a) is disconnected from the other curves but when plotted against percentage life in **Figure 79** (b) it rises to the vicinity of curve AB and follows it closely indicating the validity of a linear cumulative life rule when considering the degree of hardening achieved at any point in the history of loading. More extensive tests are shown in **Figure 79** for the same material.

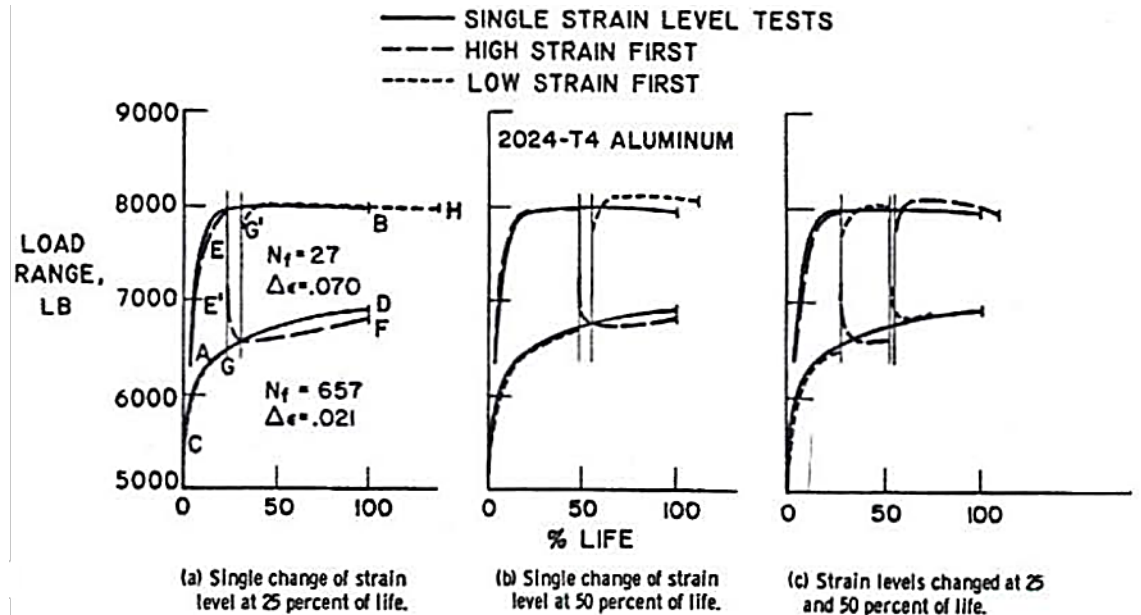


Figure 79: Cyclic Strain hardening under multilevel fatigue tests (Manson, 1964)

In **Figure 79** (a) the results are shown for a change of strain level at approximately 25% of life for both a high and a low strain level test. In **Figure 79** (b) the change is made at approximately 50% of life and in **Figure 79** (c) two changes are introduced; one at approximately 25% and the other at approximately 50% of life. In all cases the tendency is almost identical. Very shortly after the strain range is changed the curve tends to seek a stress level corresponding to the curve for the new strain range at the percentage of life used, regardless of the strain level at which the life fraction was consumed. Thus, the material may require initial softening to approach the necessary curve followed by hardening as it rises along that curve or it may require initial hardening followed by subsequent softening for the same reason. These results imply that at any condition of consumed life based on the linear damage rule the material seeks a specific stress level associated with the cyclic hardening or softening curve connected with its current strain value and consumed life fraction. From **Figures 78** and **79**, Manson observed that at fracture the summation of the ratios is close to unity as indicated by the end points of

the test curves regardless of the sequence of loading. **Figure 80** presents the results of tests of this kind for a strain softening material – titanium alloy.

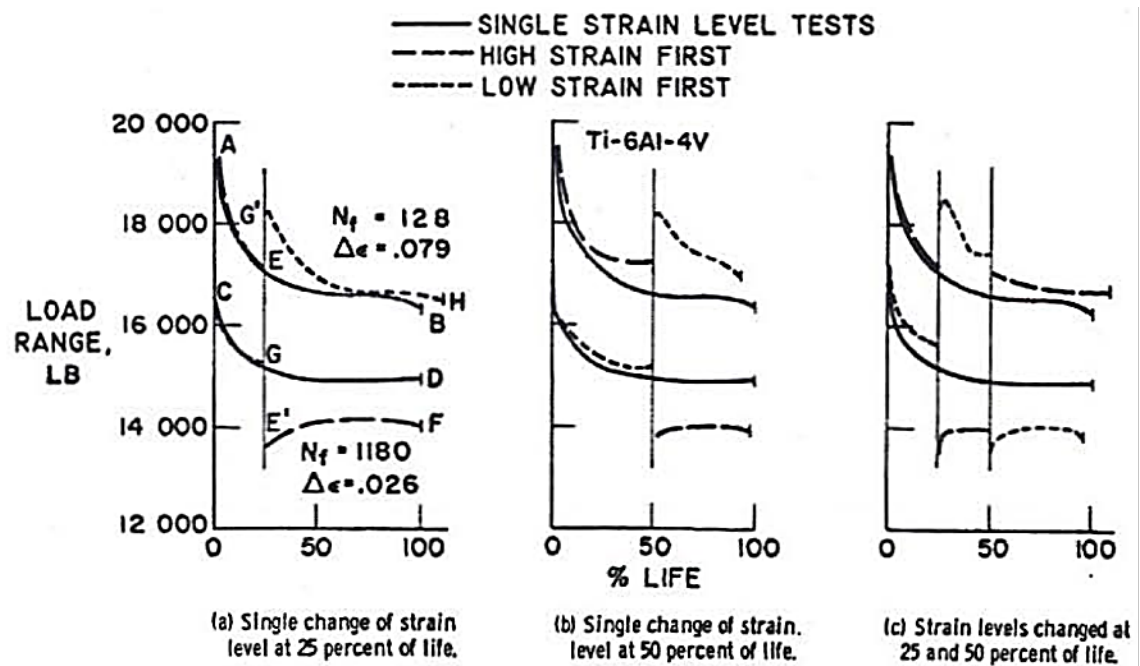


Figure 80: Cyclic Strain softening under multilevel fatigue tests (Manson, 1964)

The basic behaviour is similar to that of strain hardening material previously discussed but when the change is made in strain level the new stress sought by the material does not reach the curve associated with the new strain level.

For example, in **Figure 80** (a) if the high strain is applied for the first 24% of life the curve follows AE. Changing to the lower strain level produces point E' below the curve CD at 25% of life. Further cycling at the lower strain level produces the curve E'F which never reaches the curve CD. This behaviour is characteristic of all the tests shown in this curve and requires further investigation. Manson (1964) A summary of all of these tests on the basis of the linear damage rule is presented in **Figure 81**.

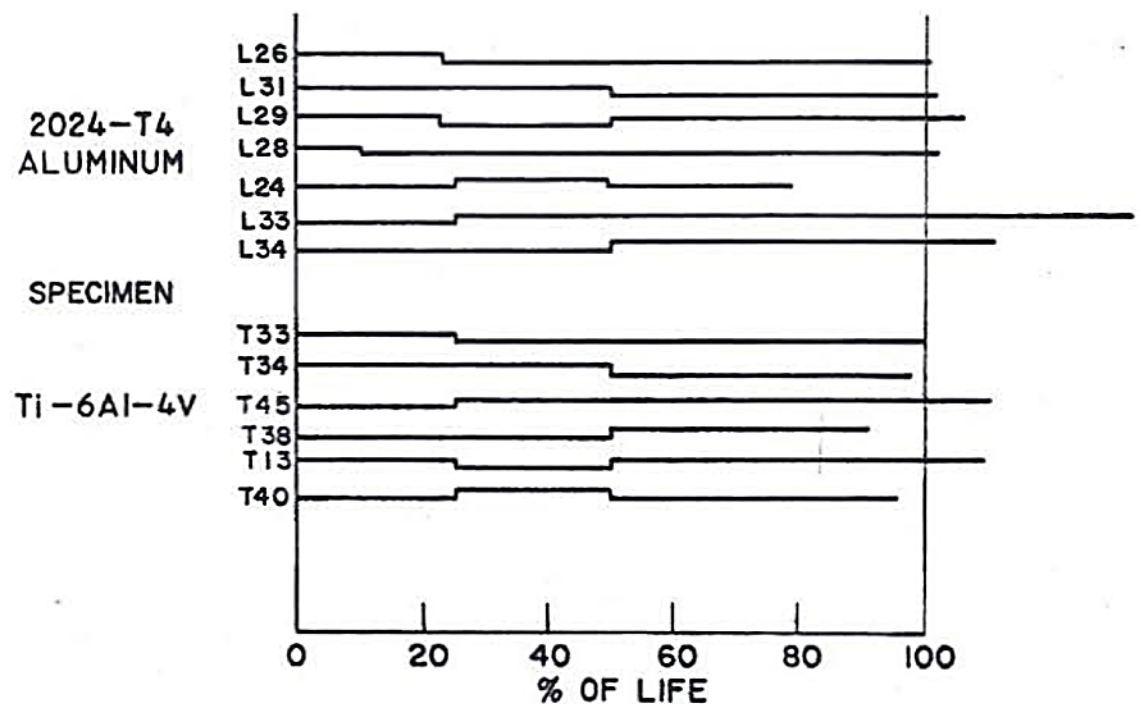


Figure 81: Cumulative fatigue damage obtained by strain cycling of smooth specimens (Manson, 1964)

Each set of horizontal lines represents one of the tests conducted. A step in the line indicates whether the high stress was applied first or last. For example, for specimen L26 first 25% of life was at a higher strain level because this portion of the line is higher than the remaining portion. Fracture is indicated by the end point of each of these lines. For all the tests summarized the cycle ratio lies between approximately 0.8 and 1.3 and is very close to unity for most of the tests. Even the extremes are within the scatter band of expected behaviour in this type of test.

These results imply that the linear damage rule is accurate for these materials under the types of loading used. In these tests the main portion of the life was used in developing a very small crack rather than in propagating the crack. Therefore, as long as the major portion of the life is devoted to crack development the linear damage rule is applicable. This assumption of the validity of the linear damage rule within the crack initiation stage is in the method developed by Grover for the analysis of cumulative fatigue damage. Manson (1964)

2.2.8.1 Rain flow counting method

The rain flow counting technique or reservoir method is basically tracing the assumed stress history for cycle counting by assuming that cycles as reservoirs filled with rain

water, once the reservoir is filled, rain will overflow to the next cycle and so on. To assess the numbers of cycles to failure; the structure detail at the critical location is subjected to a fully reversed stress σ_1 for n_1 cycles, σ_2 for n_2 cycles, e.g. a fully reversed cycle with stresses varying 60,80,40, and 60 kpsi and a second fully reversed cycle -40, -60, -20, and -40 kpsi as shown in **Figure 82** is considered. Shigley et al., (2003)

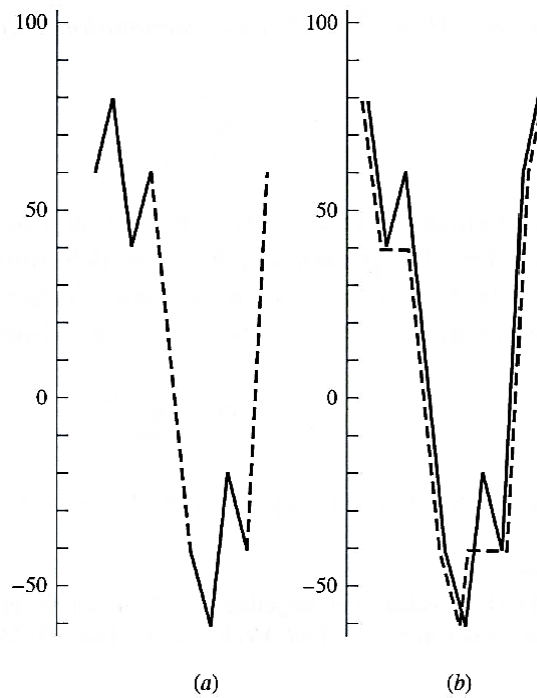


Figure 82: Variable Stress Diagram prepared for Assessing Cumulative Damage (Shigley et al., 2003)

In **Figure 82** (a) the time trace is the solid line plus the dashed line and it begins with 80 kpsi and ends with 80 kpsi. For this to be true we need to acknowledging the existence of a single stress time trace (hidden cycle) shown as the dashed line in **Figure 82** (b). If there are 100 applications of the all positive stress cycle, then 100 applications of the all negative stress cycle, the hidden cycle is applied but once. If the all positive stress cycle is applied alternately with the all negative stress cycle, the hidden cycle is applied 100 times. To ensure that the hidden cycle is not lost, begin on the snapshot with the largest (or smallest) stress and add previous history to the right side, as was done in Figure 73 (b). Characterization of a cycle takes on a max-min-same max (or min-max-same min) form. The hidden cycle is identified first by moving along the dashed line trace in

Figure 82 (b) identifying a cycle with an 80 kpsi max, a 60 kpsi min, and returning to 80 kpsi. Deleting the used part of the trace (the dashed line) leaves a 40, 60, 40 cycle and a -40, -20, -40 cycle.

Since failure loci is expressed in terms of stress amplitude component σ_a and steady component σ_m , the following equations are used to construct the **Table 6** below:

$$\sigma_m = \frac{\sigma_{\max} + \sigma_{\min}}{2} \quad \text{Eq. 40}$$

$$\sigma_a = \left| \frac{\sigma_{\max} - \sigma_{\min}}{2} \right| \quad \text{Eq. 41}$$

Table 6: Example stress amplitude and midrange components (Shigley et al., 2003)

Cycle Number	σ_{\max}	σ_{\min}	σ_a	σ_m
1	80	-60	70	10
2	60	40	10	50
3	-20	-40	10	-30

The most damaging cycle is number 1 which could have been lost.

The fluctuating stress levels on a structure may be time varying. Methods are provided to assess the fatigue damage on a cumulative basis. The Palmgren Mine cycle ratio summation rule (Miner's rule (Eq. 23)) is written as;

$$\sum \frac{n_i}{N_i} = c$$

Where n_i is the number of cycles at stress level σ_i and N_i is the number of cycles to failure at stress level σ_i . The parameter c has been determined by experiment; it is usually found in the range $0.7 < c < 2.2$ with an average value near unity.

Using the deterministic formulation as a linear damage rule:

$$D = \sum \frac{n_i}{N_i} \quad \text{Eq. 42}$$

Where D is the accumulated damage. When $D = c = 1$, failure occurs.

Other methods for counting cycles include:

1. Number of tensile peaks to failure.
2. All maxima above the waveform mean, all minima below.
3. The global maxima between crossings above the mean and the global minima between crossings below the mean.
4. All positive slope crossings of levels above the mean, and all negative slope crossings of levels below the mean.
5. A modification of the preceding method with only one count made between successive crossings of a level associated with each counting level.
6. Each local maxi-min excursion is counted as a half-cycle, and the associated amplitude is half-range.
7. The preceding method plus consideration of the local mean.
8. Rain-flow counting technique.

2.2.9 Laws governing HCF and LCF

For fatigue behaviour of un-cracked components (i.e. No Pre-cracks); HCF is governed by the Basquin's Law stated early in equation (Eq.27) and represented in **Figure 83**.

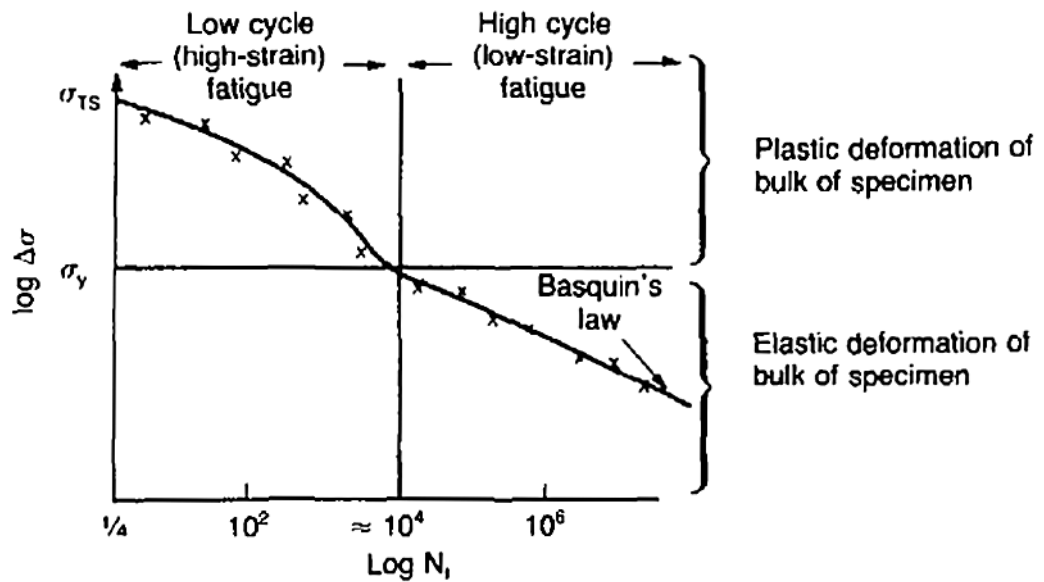


Figure 83: Initiation controlled HCF - Basquin's Law (Ashby and Jones, 2002)

LCF is governed by the Coffin-Manson Law and represented in **Figure 84**. Miner's Rule is damage accumulation law.

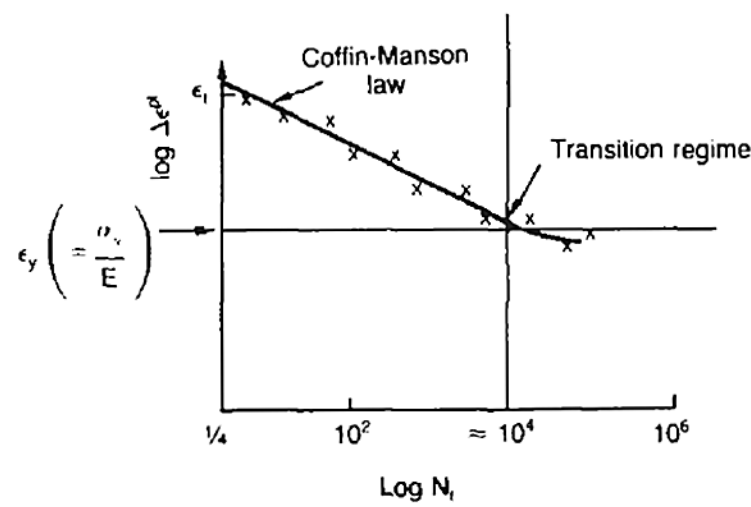


Figure 84: Initiation controlled LCF- the Coffin Manson Law (Ashby and Jones, 2002)

2.3 The Phenomena of LCF in a Ship Structure

2.3.1 Fatigue Damage

Petinov (2003) stated in his book that extensive fatigue testing on structural metals revealed that fatigue cracks initiate at the free surface early in the loading process. Factors such as stress concentration at the surface, material homogeneity, surface treatment, surface grains slip, environment and type of loading are critical for fatigue crack origination pattern at the surface. Early micro structural study on polished and etched surface of a specimen during cyclic loading found the development of slip markings (striations) in individual grains soon after commencement of the test. Striations orientation was approximately to the maximum shear stress plane. Following experimental investigations confirmed these observations.

Also it was found that further cycling loading produces new slip markings in parallel planes, forming slip bands with irreversible slip traces accumulated and further tensile loading would add new slip markings. Some slip bands are intensified under cyclic loading and the process may be transferred into the adjacent grains especially where the slip planes are oriented in favour of slipping. New striations are beginning to form in the initially affected grains. Further loading is accompanied by slip nucleation in new grains, but there also are grains that remain intact throughout the whole fatigue life

span. Coarsened, the slip bands are transformed into micro-tears inwards the grain forming a micro crack that propagates into adjacent grains with intensive slip bands. Breaking through the grain boundary the crack changes its direction to be parallel to the slip plane of the new grain. Petinov (2003)

Figure 85 is a schematic illustration of the slip progress; starting the microscopic crack from a free surface (a) and propagating it through the sub-surface grains (b-c, c-d), macroscopic crack growth commencement from (d) and on e-f, g-h ‘passive’ slip systems.

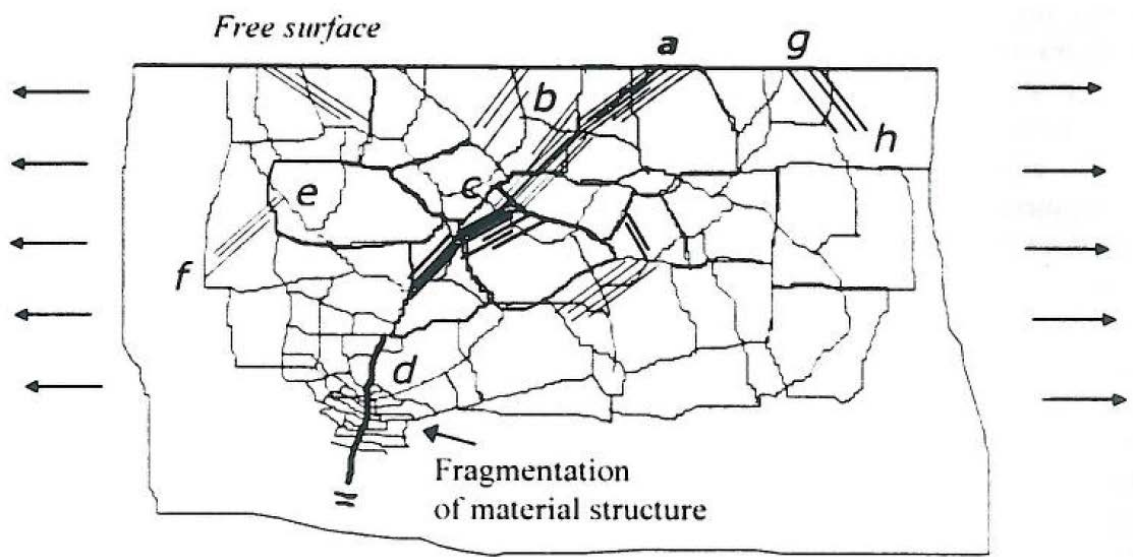


Figure 85: A series of grains with well-developed slip bands and non-propagating cracks observed in the vicinity of the principal crack (Petinov, 2003)

Petinov (2003) mentioned that the mechanisms of plasticity and fatigue damage were studied by Gilman (1959), Forsyth (1969), Ivanova (1979) and many others within the scope of the dislocation theory were it was found that early in the load cycling, the dislocation structure rapidly changes in certain grains with crystallographic planes favourable to slip. The density of dislocations rapidly increases. Consequently, as a result of dislocation displacements towards the free surface of the grains, the slip markings and slip bands are generated in the above planes. Piles of dislocations reach the grain surface form microscopic disturbances, extrusions and intrusions (shallow micro cracks). These surface developments become observable using taper sectioning technique as shown in **Figure 86**. Wood (1963). Piled up at the grain boundaries, at inclusions and twin boundaries, the dislocation arrays can either elevate the local

stresses considerably to trigger slip mechanisms in the adjacent grains, or cause micro – tears which can coalesce with the microcracks generated at the free surface. The increase of the dislocation density results macroscopically in the cyclic strain hardening and in changes in physical characteristics of the material. In initially strengthened material; the onset of cyclic loading (capable of causing the localized plasticity) results in a decrease of efficiency of the microstructural barriers which could prevent the progressive slip. As the reflection of this at the macroscopic level, the cyclic strain softening may be observed.

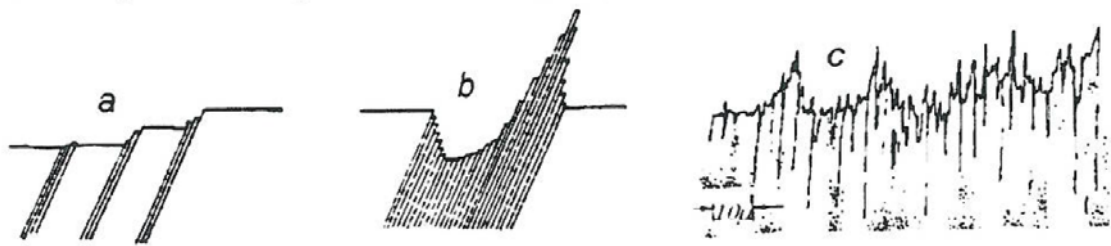


Figure 86: Slip band formation: a – slip scheme at monotonous loading, b – slip progress at cyclic loading c – taper section of a slip band in copper after 2×10^5 cycles (Petinov, 2003)

2.3.2 Main factors affecting fatigue damage

According to Petinov (2003) the bulk material of hull structures is never affected by fatigue. This is because nominal or other characteristic average stresses in structural members in service are relatively small even compared to the fatigue limit of the material. All ship hulls and marine structures are designed to operate within the elastic zone of material behaviour at extreme service conditions. However, some small areas where stresses reaching the yield point may be allowed but this material confined to the stress concentration zone is surrounded by bulk material of a structure which deforms elastically under applied loads.

Therefore, mechanical conditions of alternating loading for a material with stress concentrations are assumed to be strain control conditions. This assumption is important in developing structural fatigue models. In other words, the material fatigue failure criterion has to be consistent with the material failure definition. The most preferred is a macroscopic fatigue crack initiation in a uniformly stressed smooth specimen. Petinov (2003)

According to the local stress raisers mechanical and physical nature, the Fatigue of ship structures is subdivide into micro and macroscopic stress concentrations. Macroscopic (global, structural) stress concentration is due to the geometry of structural details. Therefore, it is attributed to structural design procedures. Micro stress concentration in welded details is related mainly to the fatigue properties of welded joints with inherent flaws regardless of type and weld geometry including residual welding stress influence. Petinov (2003)

Hot spot stress concept used in the fatigue analysis of details where ‘structural stress concentration’ is superimposed on a welded joint may be considered a macro stress concentration and is defined by extrapolating the stress to the weld toe as shown in **Figure 87**. Where; σ_{max} is the maximum stress at the weld toe based on strain measurements or FEM calculations and σ'_{max} is the stress extrapolated to the bracket toe excluding influence of the weld geometry. Petinov (2003)

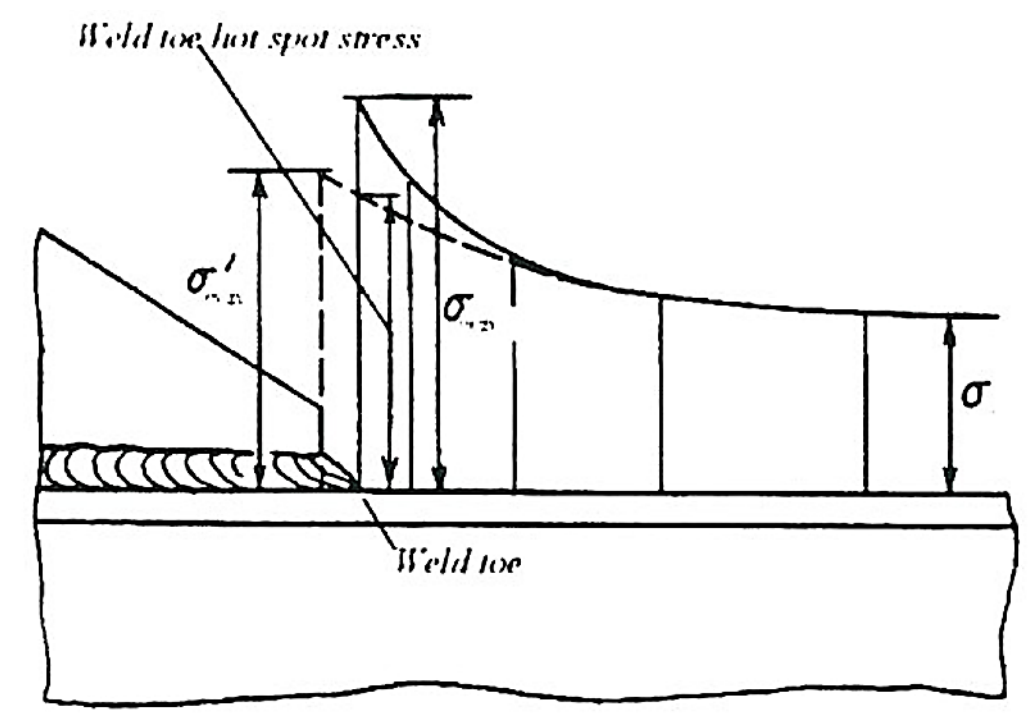


Figure 87: Definition of the local stress at the bracket toe (Petinov, 2003)

This approach to fatigue strength assessment of structural details sounds simple but in reality complications and drawbacks arise from selection of an appropriate S – N curve. The very idea of superimposing the structural stress concentration (hot spot stress) over

the weld is the most important drawback because it implies the multiplication of stress concentration factors, which is incorrect since the stress field of superimposed notches is specific for the combined geometry and cannot be subdivided into elementary stress fields due to nonlinearity even when material deforms linearly. The onset of local plasticity introduces an additional nonlinearity. Petinov (2003)

The argument in favour of the hot spot stress concept based on occasional agreement between test and calculation results may be regarded as the efficiency of an approximate rule which may be accepted under certain conditions, when the effects of the mentioned nonlinearities are comparable to the scatter of test results. When a welded detail is subjected to a complex loading progression under which the principal stress vector may rotate, the hot spot stress approach fails to accommodate the test results. Petinov (2003)

2.3.2.1 Service loading

Service loading of ship hull and marine structures may be grouped into categories with respect to the nature of the components and types of structural response. One category is formed when the loads produce similar deformations of a detail type. This can be seen in **Figure 88** for the weld toe material at a bracket connecting an inner bottom longitudinal and a transverse bulkhead stiffener. The loading conditions for this detail are the same regardless of whether it is due to vertical and horizontal hull girder bending or local bending of the double bottom structure under inertia and hydrodynamic loads. Petinov (2003)

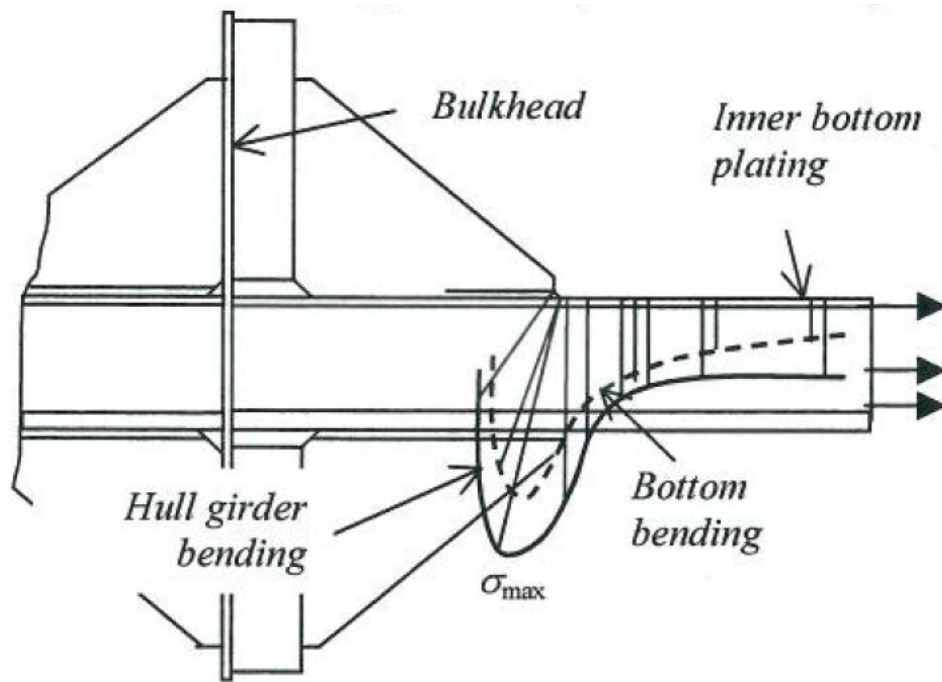


Figure 88: Stress concentration at the bracket end (Petinov, 2003)

Another category is the combined loading; for example, the stresses in the side shell plating at the side opening (**Figure 89**) are due to the hull bending in the vertical plane and due to the shear type deformation in the same plane. The bending induced maximum stress is located at the opening corners where the longitudinal edge begins to curve into the vertical edge and the shear induced maximum stress is concentrated further along the curved edge. Petinov (2003)

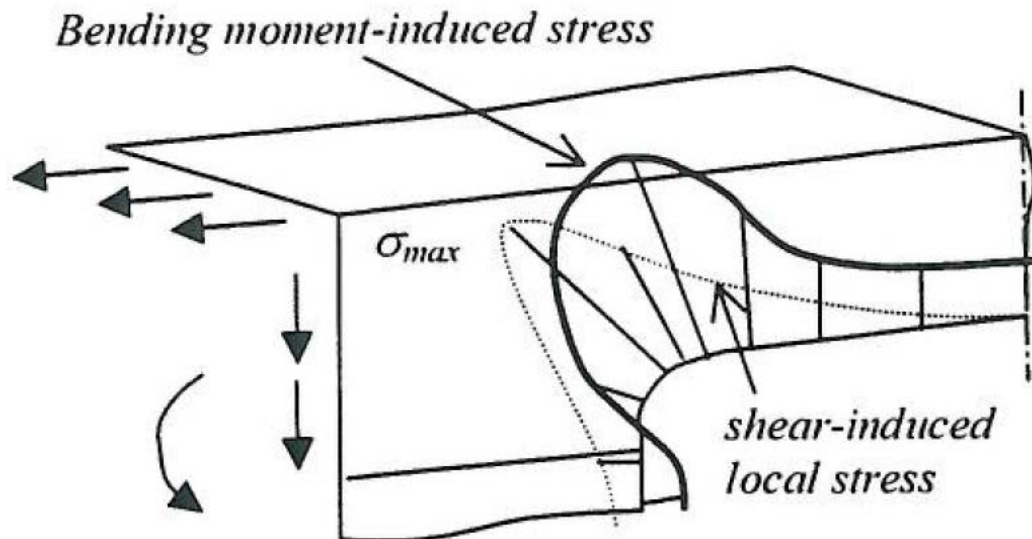


Figure 89: Stress concentration in the side shell plating at the side opening (Petinov, 2003)

2.3.2.2 Residual welding stresses

Residual welding stresses affect the crack initiation and propagation periods. In crack initiation; the effects of welding are due to pre-strain of material in critical sites induced by high local stresses and material plasticity, as well as due to the partial residual stress relaxation caused by the high stress concentration in the heat affected and fusion zones and subsequent plastic straining of material at occasional overloads. Residual welding stress relaxation under irregular service loading with long periods of moderate and calm sea conditions is a gradual stress field transformation rather than an abrupt change at commencement of the cyclic loading. The rate of the residual welding stress relaxation and the magnitude of the remaining un-relaxed stress taken as the mean stress shown in **Figure 90**, remain uncertain. When the crack initiation is related to the early stages of macroscopic crack growth, the mean stress effect on fatigue life is insignificant since the initiation mechanisms are mainly dependent on load range and the decision of whether or not to account for the mean stress in fatigue assessment depends on the degree of approximation in the fatigue model. Petinov (2003)

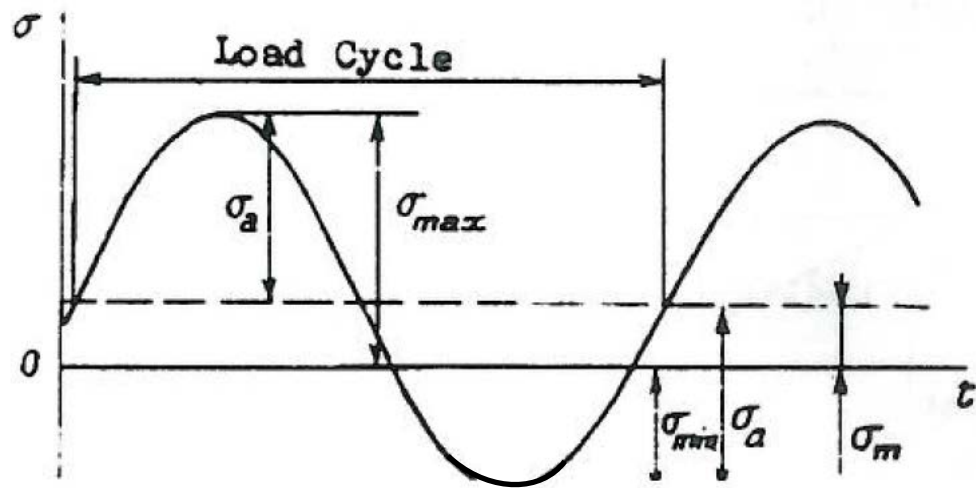


Figure 90: Mean stress in the cyclic loading; schematic representation of a load cycle comprising the constant (mean) stress (Petinov, 2003)

When material is subjected to a mean tensile stress (i.e. $\sigma_m > 0$) the stress range must be decreased to preserve the same N_f according to Goodman's Rule (**Figure 91**)

$$\Delta \sigma_{\sigma_m} \approx \Delta \sigma_0 \left(1 - \frac{\sigma_m}{\sigma_{TS}} \right) \quad \text{Eq. 43}$$

Where

$\Delta \sigma_0$ is the cyclic stress range for failure in N_f cycles under zero mean stress, and $\Delta \sigma_{\sigma_m}$ is the same thing for a mean stress of σ_m .

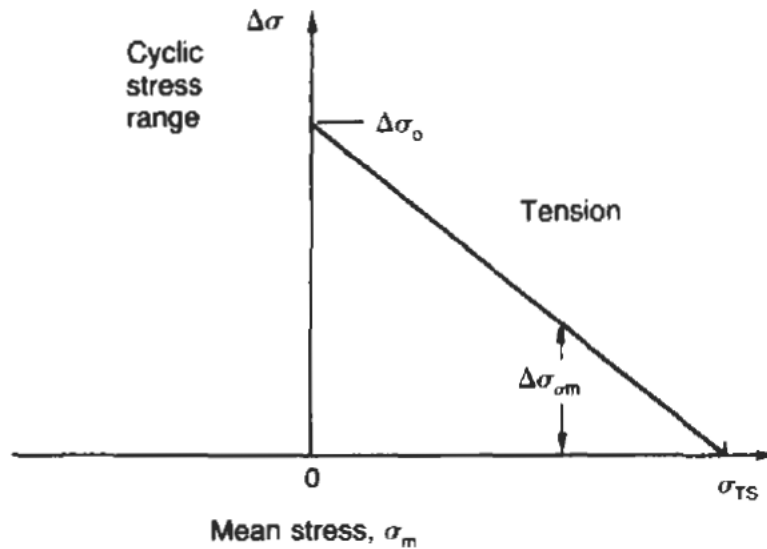


Figure 91: Goodman's Rule - the effect of tensile mean stress on initiation controlled fatigue (Ashby and Jones, 2002)

Goodman's Rule is empirical, and does not always work, that is why tests simulating service conditions must be carried out, and the results used for the final design. But preliminary designs are usually based on this rule. Ashby and Jones (2002)

In terms of stress vs. fatigue life (number of load cycles), the fatigue limit of a structural element may be defined, by applying Goodman's formula:

$$\sigma_e^{(s)} = \frac{\left(1 - \frac{K_t \sigma_m}{\sigma_u}\right) \sigma_{-1}}{K_f} \quad \text{Eq. 44}$$

Where K_f is the fatigue notch factor and the product $K_t \sigma_m$ is assumed to be the local mean stress.

However, if plastic deformations take place at the notch root under combined constant and variable stress components, assumption in equation (Eq.16) becomes invalid. Petinov (2003)

An example of the influence of mean and residual stresses is longitudinally welded girders where the residual stresses in the weld reach the yield limit and the fatigue failures start from imperfections in this area. Stress relieved or post weld treated welded joints with compressive residual stresses in the critical area allow higher permissible

stresses which depend on the stress ratio R ($\sigma_{\min} / \sigma_{\max}$). This is illustrated in the Haigh diagram **Figure 92**. Definite functional relationships are recommended by Eurocode 3, IIW design recommendations, German guideline - Fracture Mechanics Proof of Strength for Engineering Components – (FKM) and by Haibach. In IIW fatigue design recommendations, the influence of the mean nominal stress σ_{nm} on the endurable nominal stress range (or amplitude) is assumed to be independent of σ_{nm} in general but a fatigue enhancement factor can be introduced in certain cases. Stress relieved welded components allow a fatigue enhancement factor rising linearly up to 1.6 between $R = 0.5$ and $R = -1$. Radaj et al., (2006)

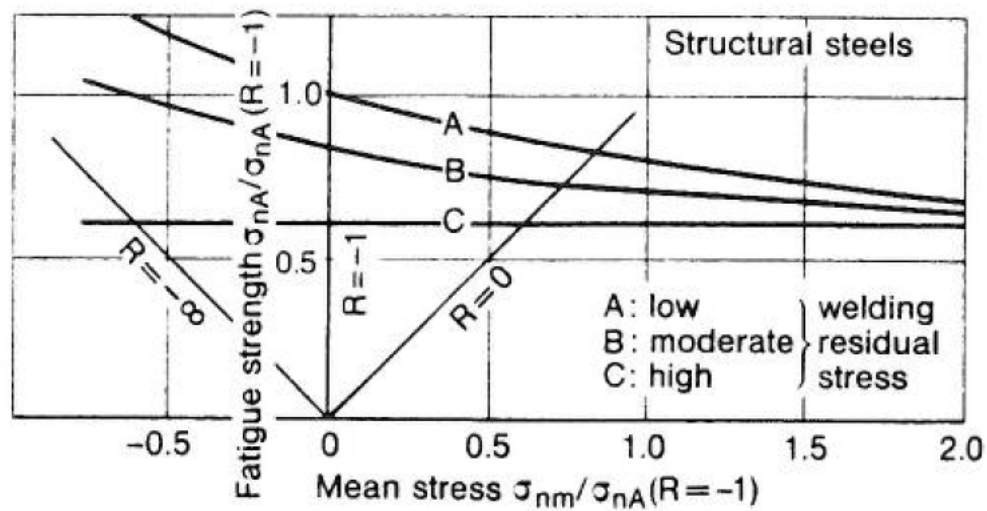


Figure 92: Endurable nominal stress amplitude of welded joints made of structural steels dependent on mean stress (Haigh diagram); after Haibach (Radaj et al., 2006)

Petinov (2003) presented schematically, the process of mean stress relaxation in **Figure 93**. Assuming a structural detail under cyclic loading in which the nominal strain is transformed at the stress concentration site into the local strain range $\Delta \epsilon$; the constant tensile or residual tensile stress produces a local tensile strain that is ‘assumed’ proportional to the theoretical stress concentration factor, i.e. is equal to $K_t \sigma_m / E$. If the combined constant and alternating stresses provide the conditions for local plasticity, the local stress increase at the notch root is limited according to the static stress strain diagram ($f-o'-a'$). Due to Bauschinger effect, unloading may result in a nonlinear diagram ($a' - b'$) that depends on stress concentration, nominal stress and material properties. At the proceeding reloading ($b-c$) under fixed local strain range conditions, the maximum stress decreases with the same result on mean stress, and so on.

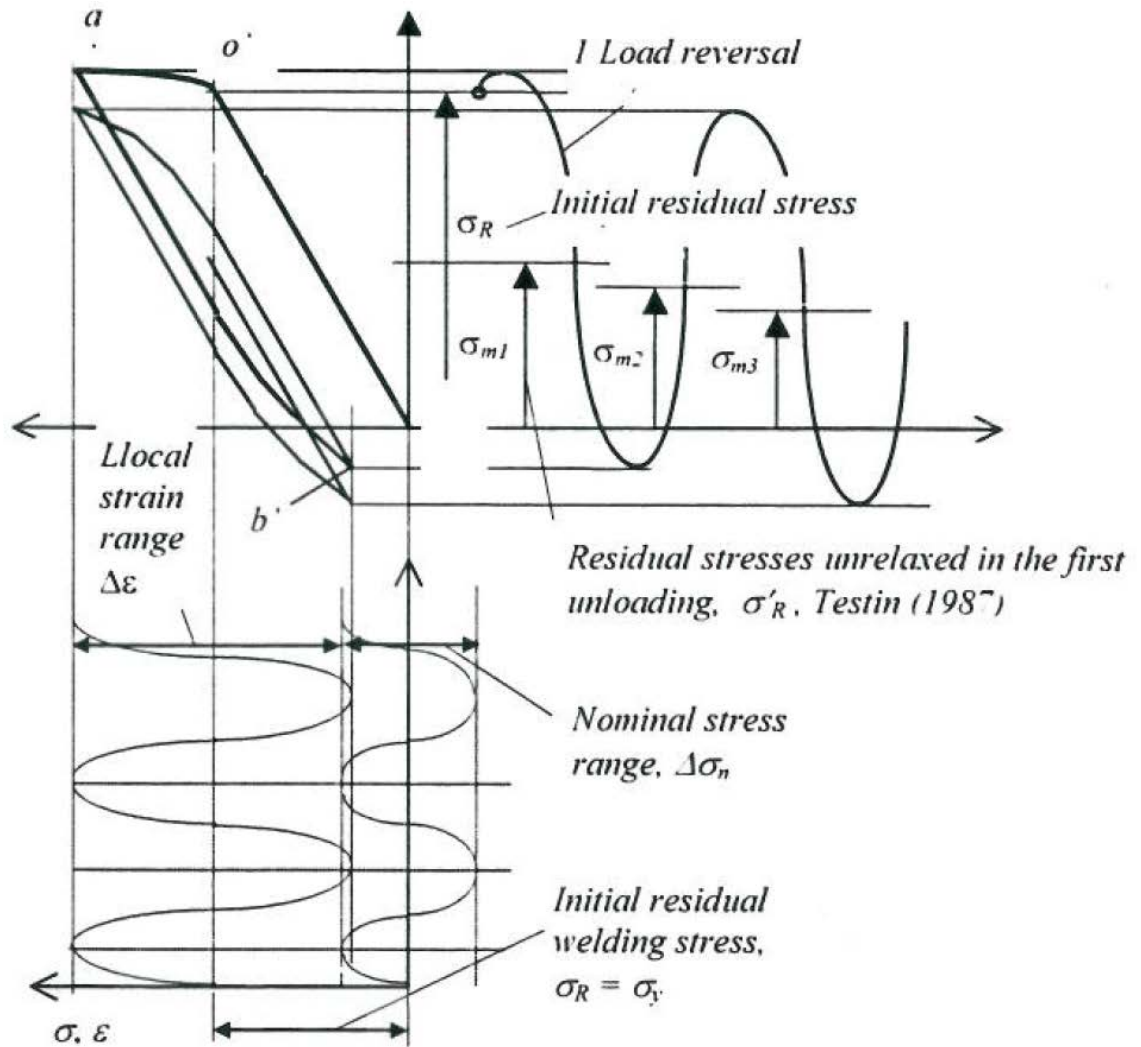


Figure 93: Relaxation residual welding stresses in a stress concentration area (Petinov, 2003)

Petinov (2003) stated that for a cyclically hardening material (e.g Aluminium alloys) the mean stress relaxation process is compensated by cyclic hardening resulting in higher sensitivity of Aluminium alloys to mean stress compared to mild steels. Respectively, considering the residual stresses relaxation due to material plasticity allows the assumption of a scheme of forming effective (non – relaxed) residual welding stresses in the detail in question, as shown in **Figure 94**.

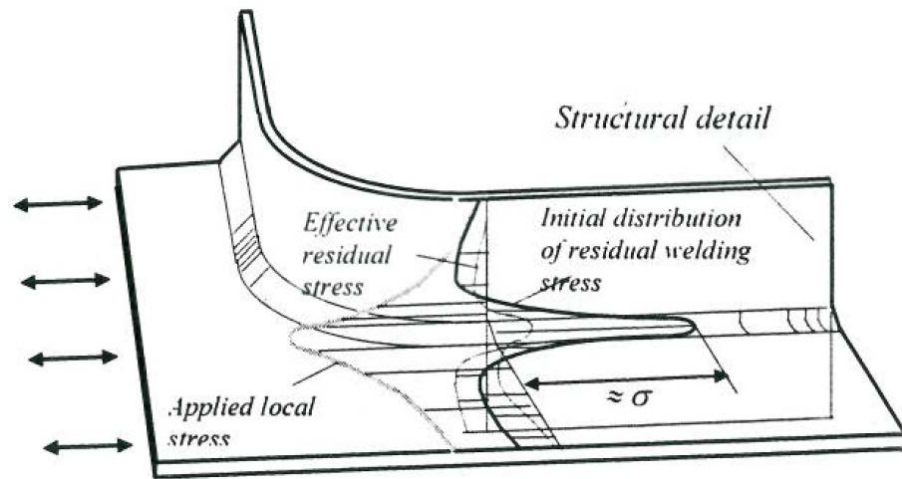


Figure 94: Formation of effective (non – relaxed) residual stresses in a hull structural detail (Petinov, 2003)

The effects of residual stresses upon macroscopic crack propagation are clearer than that in the initiation phase. Residual stresses affect crack opening and conditions for crack growth. At the same time with the crack extension and formation of the plastic zone ahead of the crack tip (**Figure 95**), the residual stresses are redistributed gradually resulting in changes of the crack opening and growth rate. Omitting the effects of residual welding stress may result in non-conservative estimations of fatigue life. Petinov (2003)

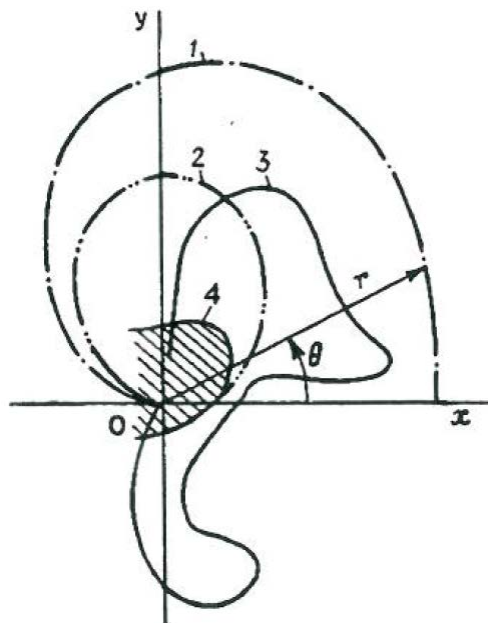


Figure 95: Crack tip plastic zone (Petinov, 2003)

Figure 95 shows the geometry of the crack tip plasticity zone observed experimentally at cycling and at overloads:

1. Plane stress, theoretical estimation,
2. Plane strain, theoretical estimation,
3. Plane stress, experiment, static loading,
4. Plane stress, experiment, cyclic loading.

2.4 LCF Assessment

2.4.1 *Work of ISSC Committee III.2: Fatigue and Fracture*

In a comparative study (including 8 class societies) on ‘fatigue strength assessment procedures used by the classification societies’, the Committee III.2 ‘Fatigue and Fracture’ of the International Ship and Offshore Structures Congress ISSC (2000) have shown in the results of their calculation a relatively short fatigue life of 5.3 years, although the structural detail considered was not prone to fatigue failures. The structural detail was a pad detail on the longitudinal coaming of a Panamax container vessel. This detail was chosen because of the well-defined loading due to hull girder bending and a direct calculation of loads using the spectral method was performed. Fricke et al., (2002)

It is interesting to note that as this observation brings into the reliability of the class society’s calculation results especially for structural details considered prone to fatigue failures. This indicates the acute nature of the conservatism built into the approaches of the main class societies. This conservatism is a typical approach which deemed necessary by class societies, however, also reflects the relatively low level of development in the understanding of LCF. As advancements are made in the study of LCF the class societies will improve to reflect this, removing unnecessary conservatism in the process.

The following is a description of how the four class societies carried out the fatigue assessment according to their procedures:

1. The DNV procedure for fatigue strength assessment is based on hotspot stress approach. Stress concentration factors are obtained from a table of standard details. The stress range is multiplied by a stress concentration factor for the

weld (notch stress) before entering the S-N curve. The calculations only include the stress component from the vertical bending moment as per IACS UR S11, transferred to a probability of 10^{-4} by the Weibull distribution with a shape parameter of 0.93. The stress range is further reduced by a factor of 0.80 to account for worldwide operation. A reduction in life for a plate thickness above 22mm is included.

2. ABS supports both the nominal and the hot spot stress approaches in their simplified fatigue strength assessment method. The fatigue stress ranges are assumed to follow a Weibull probability distribution. For the given detail, the design stress range is the same as that specified by IACS UR S11. The Weibull shape parameter is estimated to be 0.81. The effect of mean stress has been ignored. Basic S–N curves were used to describe the fatigue strength of the details. In order to account for corrosion, a net ship concept was used together with a stress reduction factor of 0.95.
3. In Lloyd’s Register, the ShipRight Fatigue Design Assessment (FDA) Level 3 procedure was applied. FDA Level 3 is a spectral approach where, in this case, a scaled hull form and weight distribution from a similar ship is used for generation of the vertical bending moment response amplitude operator from 2D strip theory. A typical container trade pattern is assumed and a twenty year simulation period with 27% non-sailing days is chosen. The fatigue stress is obtained from a detailed FE model composed of four noded shell elements, representing the geometric stress (hot spot stress) with some embedded notch stress effects. The analysis was performed in house by LR.
4. According to BV rules two load cases should be taken into account: half time in head sea conditions and half time in oblique sea conditions. The stresses are based on the rule bending moment specified by IACS UR S11. The stresses and S-N curve are based on the notch stress approach. The hot spot stress concentration factor was obtained from a finite element calculation, while the notch stress concentration factor was obtained from a table depicting the type of weld and quality of welding. The calculation included the stress component from the IACS head sea vertical bending moment, transferred to a probability of 10^{-5} using a Weibull distribution with a shape parameter of 0.943 combined with a horizontal bending moment. Another combination of vertical and horizontal bending moments provided the oblique seas component. A reduction of life for thickness above 16mm is included as well as a reduction of stress amplitude

when the notch stress amplitude corresponding to a probability of 10^{-5} is above the yield stress. The component of stress above the yield stress was weighted with a compressive stress factor of 0.6.

In ISSC (2009) the international ship and offshore structures congress Committee III.2 reviewed recent works related to fatigue and fracture and described the results of a literature survey of more than 280 references. The review covered LCF as one approach; the other two are high cycle and ultra-high cycle approaches. Life prediction methods which presume homogeneous material (free from cracks, inclusions or defects) can be divided into strain based (LCF) and stress based (HCF) methods. This design approach is normally used in fatigue assessment of local areas where high stress concentrations exist and the material local response is repeated plastic deformation. Stress based approaches use the elastic stress range (or amplitude) as the governing load parameter.

Lotsberg et al (2006) described the methodology developed by DNV in the Recommended Practice DNV-RP-C206 (DNV, 2007) for fatigue design of FPSO units. The methodology is described with a special regard to the hot spot structural stress evaluation method and to the calculation of LCF damage from loading and unloading. Due to large stress cycles which imply local yielding at the hot spot, hot spot stresses calculated from linear elastic analysis are modified by a plasticity correction factor and by a redistribution factor before the S-N curve is entered. In screening the structure of a ship to identify the most critical hot spots, the hot spot structural approach may be advantageously applied, even if considerable plastic local deformations occur.

Boge et al (2007) presented the results of laboratory tests carried out on tubular joints with the aim of investigating the stress life curve in the LCF region. The main purpose of the study is to generate more data for the LCF region of tubular joints and to investigate the effect of mean stress (R ratio) on fatigue strength in this region. The data analysed and compared with published data and with current fatigue design criteria for tubular joints. The comparison shows a common scatter band in the cycle range of 10^4 - 10^5 . The two S-N curves evaluated separately in the low cycle range ($10^3 < N < 10^5$) and in the high cycle range ($10^5 < N < 10^7$) exhibit different slopes. Such a slope discrepancy is explained with the transition from high to low cycle.

Wang et al (2006) proposed a fatigue damage prediction method for welded joints in the LCF regime in ship structures. A literature review of material behaviour under low

cycle large stress range was conducted and the possible approaches to obtain the strain life curve were discussed. In the procedure, the hot spot stress is used and the pseudo hot spot stress range is derived based on elastic hot spot stress range and material stress strain curve with the application of Neuber's hypothesis. A suitable design S-N curve has been derived from tests carried out on non-load carrying fillet joints under strain control condition. Tateishi et al (2007) discussed a local strain based approach to predict the fatigue strength of welded joints in extremely LCF region. LCF tests were conducted on T-shaped welded joints in order to locate crack initiation sites and to obtain the fatigue life. The local strain field around the welded toe was analysed by elasto-plastic FE analysis, and the local strain amplitude at the cracking point was quantified. Extensive research on LCF has revealed that the strain amplitude at the cracked point (local strain) dominates the LCF life.

Robinson and Czyryca (2006) presented HCF and LCF crack growth tests carried out in air and in artificial seawater. The results show that the titanium alloy tested was unaffected by the seawater environment in comparison with the tests carried out in air. Fatigue crack growth tests on titanium alloy weld metal were conducted in air and artificial seawater with and without cathodic protection. The results indicated a minor effect of seawater in increasing crack growth rate of the weld metal. However, the application of a cathodic potential of 0.987 V versus Ag/AgCl reference electrode showed crack growth rates similar to crack growth rate in air. Kim and Paik (2007) studied the corrosion fatigue crack propagation characteristics of TMCP (Thermo-Mechanically Controlled Processed) steel in synthetic seawater to imitate the conditions in seawater ballast tank structures under corrosive environment. The tests were carried out with and without the application of cathodic protection. The fatigue loading test speed was 0.17 Hz corresponding to a typical sea wave period and the stress ratio was $R=0.1$. It was found that the fatigue crack propagation rate of the TMCP steel in synthetic seawater condition was faster than that in air condition by almost a factor of two. It was observed that the fatigue crack propagation rate of TMCP steel in seawater condition with cathodic protection was in between air condition and seawater condition without cathodic protection.

A summary of the relevant topics discussed by the ISSC (2009) review is presented in the following sections:

2.4.1.1 Probabilistic Approach

Two different approaches are often considered to describe the fatigue limit state; S-N curve with Miner's damage accumulation rule or fracture mechanics based approach. The influencing parameters for fatigue are treated as basic variables in the analysis in order to account for uncertainties. Obtaining the statistical information of these variables is one of the main challenges. The requirement of reliable mathematical models to describe the statistical variation, for probability analysis, of the parameters is another challenge due to limited amount of measured data. The appropriate modelling of the structural response due to fatigue loading for both approaches is important.

2.4.1.1.1 Probabilistic S – N Approach

The reanalysis of the existing data showed that fatigue life predictions for offshore structures are mainly dominated by uncertainties in the estimation of nominal stress and stress concentration factor. Other influencing variables are related to the modelling of the fatigue strength with S-N curve and Miner damage summation.

2.4.1.1.2 Probabilistic Fracture Mechanics Approach

Fracture mechanics models are applied to assess structures degrading due to crack growth. One of the main challenges is that the probabilistic fracture mechanical approaches need to be calibrated based on the S-N curves. This is due to the crack initiation and because initial stages are subject to uncertainties (see Table 6 in 2.4.2) which are difficult to quantify.

2.4.1.1.3 Multiaxial Fatigue

The influence of multiaxial fatigue design procedures has advanced in the ship industry by adopting new criteria in the fatigue life prediction models. With the support of the existing computer software capabilities, different interpretations of the critical plane concept (i.e. the material plane which accumulates the most fatigue damage during load cycling and where crack occurrence and initial growth is assumed to take place) has been adopted, implemented and are widely used in multiaxial fatigue assessments.

2.4.1.2 Fatigue analysis methodologies used for Stress Response Assessment.

Among several methodologies that exist to determine long term stress ranges, three have been stated:

1. **Simplified Rule** based analysis which assumes a two parameters (shape and reference stress) Weibull distribution for the long term stress distribution. Stresses are based on analytical formulas or the Finite Element Method.
2. **Spectral Fatigue Analysis Methodology** uses the actual or assumed wave environment encountered by the ship to determine the long term stress range. Linear load effects and the linear stress response is assumed and is performed in the **frequency domain**. Two types of fatigue spectral methodologies exist :
 - a. Full spectral methodology: where all linear loads effects (including phasing between them) are included in the analysis via an integrated hydrodynamic / structural program.
 - b. Load component spectral methodology is proposed by DNV and LR. Here the loads applied on the structure are simplified. All load effects contributing to the total stress can be isolated and the total stress transfer function is obtained by a linear summation of the load transfer function (calculated using hydrodynamic analysis) multiplied by the corresponding stress response per unit load (calculated individually from FE model for each unitary load).
3. **Design Wave approach** is a simplification of the frequency domain analysis. In this approach, each load is defined by an equivalent wave corresponding to a certain probability of exceedance which gives the maximum load response. In practice, several wave frequencies and heading combinations should be analysed for each response studied. The Design Wave Method is generally used to determine rule loads and the Standard Wave data (IACS Rec 34) for North Atlantic Zones is generally the base in most of the classification society rules. Fatigue design codes procedures for FPSOs are based on quasi-static wave loads and on cargo (still water loading) variations because the number of cycles due to the loading / offloading process of the tanks may be high for special details.

2.4.1.3 Additional Rules and Recommendations for FPSOs

Some FPSO details may be subjected to severe stress cycles during loading and unloading e.g. welded bulkheads connections for tanks that experience a full load reversal according to loading steps. A simplified method is proposed in (DNV – RP – C206 (2007)) and (BV rules for FPSOs (2007)) to calculate the damage due to loading / unloading cycles and wave cycles. Alternatively fatigue damage may be obtained by making a **time domain** simulation of the combined stress process and applying the

Rainflow counting method. This method gives a better estimation of fatigue damage if performed rigorously with a sufficient number of time simulations representative of the wave scatter diagram. DNV – RP – C206 (2007)

DNV – RP – C206 (2007) and BV rules for FPSOs (2007) provides design fatigue factor (DFF) on the calculated lifetime of structural details of offshore ships in order to achieve a reliable long term operation of structures that are permanently installed on a field. The factor DFF is considered a safety factor on the calculated fatigue life and is related to the accumulated probability of fatigue failure during the design fatigue life. Both of them require a minimum DFF of 2, or higher, taking into account the consequences of failure and the degree of accessibility for in-service inspection and repair of structural details of offshore ships. Knowing that allowable Miner sum is taken equal to unity divided by DFF, the allowable Miner sum is less than 0.5.

2.4.1.4 Methods to Calculate Damage due to combined Low Frequency and High Frequency load

Several methods are proposed to calculate the damage of structural components subject to combined effect of high frequency loads and low frequency loads. In the Simple Damage Summation Method, high frequency damage and low frequency damage are calculated separately and then added. Simple summation method is non-conservative and shall not be used according to DNV – RP – C206 (2006). The reason being; combined fatigue damage is not equal to the sum of high frequency damage and low frequency damage because of the nonlinear relation of fatigue damage and stress.

2.4.1.4.1 Combined Spectrum Method

In the combined spectrum method, the two stress response spectra (related to low frequency and high frequency) are calculated separately and are added together in order to obtain the combined spectrum. The characteristics of the combined spectrum in terms of standard deviation and up crossing rate are then determined and the damage is calculated using the combined spectrum characteristics. The combined spectrum method is used for the offshore specific interfaces such as risers and mooring lines that are governed by nonlinear dynamics as well as wave hull interactions. The impact of wave and swell directionality on fatigue damage result could be significant in critical structural locations. The combined Spectrum method provides a conservative estimate of the damage with respect to Rainflow counting when responses spectra are independent. In the case of dependent stress response (case of ships subject to

combination of quasi static wave response and springing response), this method is non-conservative.

2.4.1.4.2 Modified Combined Spectrum Method

The combined spectrum method with dual narrow banded correction factor corresponds to a modification of the combined spectrum method mentioned above by multiplying the fatigue damage with a (dual narrow banded) correction factor. DNV – RP – C206 (2006) This method can decrease the conservatism of the combined spectrum method with respect to rainflow counting method and is applicable when frequencies of the two spectra are very distinct i.e. frequency ratio is greater than 4 according to DNV – RP – C206 (2006). The improvement tends to be lost when the low frequency load is strongly dominant. This method is particularly applicable to mooring systems or risers which are subjected to low frequency stresses induced by vessel slow drift motion combined to wave frequency stresses.

2.4.1.4.3 Simplified Analytical Method

The Simplified Analytical Method for calculation of combined fatigue damage requires a damage accumulation law together with a cycle counting method (e.g Rainflow counting). Analytical prediction formulas are proposed by several authors in order to estimate fatigue damage in case of combined low and high frequency loads:

1. Combination of two narrow – banded Gaussian high and low frequency processes with well separated spectra.
2. Combination of a wide band process, where the combined fatigue damage may be evaluated from analytical formulae in order to estimate the expected Rainflow damage.
3. Combination of low and high frequency loads (Gaussian and non-Gaussian) for which the combined fatigue damage is determined from explicit practical formula which is based on the information about individual low frequency and high frequency responses such as individual fatigue damage, mean up crossing frequencies and kurtosis. The numerical simulation showed that the predicted damage due to Gaussian wide band loads obtained by the derived formula is very simple to use and close to the rain flow damage prediction; the ratio of the new formula damage result versus Rainflow damage is included between 0.8 to 1.2. The above formula is derived by considering actual loads as random

processes and not constant amplitude stresses as in the derivation of the DNV's formula. Lotsberg (2005) considered; combination of two equivalent damage constant amplitude stress histories and following the rainflow counting derived a simple formula used now as DNV's rule formula in DNV-RP-C206 (2007). BV Rules for FPSOs (2007) proposed similar approach for evaluating the combined fatigue damage. However, according to the numerical examples results studied by Huang and Moan (2006), DNV's formula may overestimate the combined damage by a factor of 30% up to more than 100%. ISSC (2009)

2.4.1.5 Benchmark Studies

A comparative study on estimation techniques for Structural Hot Spot Stress (HSS) of web stiffened cruciform connections has been carried out to validate the applicability of the shell based HSS determination techniques proposed by Lotsberg et al (2007), Osawa et al (2007) and IACS CSR – B (2005). HSS is derived by one of the four following methods:

1. Conventional linear extrapolation method (0.5t – 1.5t); where stresses are read out from a shell FE model at read out points shifted away from the intersection line by 0.5t and 1.5t where t is the plate thickness. HSS is derived by linear extrapolation over these points away from the intersection.
2. Lotsberg's method (2007); where stresses are read out from a shell FE model at read out point shifted away from the intersection line by the following value:

$$X_{\text{shift}} = \frac{t_1}{2} + X_{\text{wt}} \quad \text{Eq. 45}$$

Where, t_1 is the plate thickness of plate at hot spot area, and x_{wt} is the additional fillet weld leg length, HSS is derived as:

$$\text{HSS} = \sigma_s(x_{\text{shift}}) \times \beta \quad \text{Eq. 46}$$

Where, σ_s is the surface stress at the point shifted away from the intersection line by x, and the correction factor β is given by:

$$\beta = \gamma + \alpha_1 \frac{x_{\text{wt}}}{t_1} + \alpha_2 \left(\frac{x_{\text{wt}}}{t_1} \right)^2 \quad \text{Eq. 47}$$

Coefficients γ , α_1 , α_2 depend on the bevel angle between the main and attachment plates, θ , and they are given as follows:

For $\theta = 135^\circ$ connections, $\gamma = 1.07$, $\alpha_1 = 0.15$, $\alpha_2 = 0.22$,

For $\theta = 120^\circ$ connections, $\gamma = 1.09$, $\alpha_1 = 0.16$, $\alpha_2 = 0.36$,

For $\theta = 90^\circ$ connections, $\gamma = 1.20$, $\alpha_1 = 0.04$, $\alpha_2 = 0.30$,

3. Osawa's method, where stresses are read out from a shell FE model at read out points shifted away from the intersection line by the following values:

$$x_{0.5t} = \frac{t_h}{2} + \Delta, \quad x_{1.5t} = \frac{3t_h}{2} + \Delta \quad \text{Eq. 48}$$

Where, t_h is the plate thickness of the main plate at hot spot area. Offset Δ is given by:

$$\Delta = \frac{t_v}{2} \operatorname{cosec} \phi - \frac{t_h}{2} \cot \phi \quad \text{Eq. 49}$$

Where, t_v is the plate thickness of the attached plate, and ϕ is the angle between the main and attached plates (the supplementary angle of the bevel angle θ , see **Figure 96**). HSS is derived as:

$$\sigma_{\text{hot spot}} = 1.5 \sigma_s(x_{0.5t}) - 0.5 \sigma_s(x_{1.5t}) \quad \text{Eq. 50}$$

Where, $\sigma_s(x)$ is the surface stress at the point shifted away from the intersection line by x .

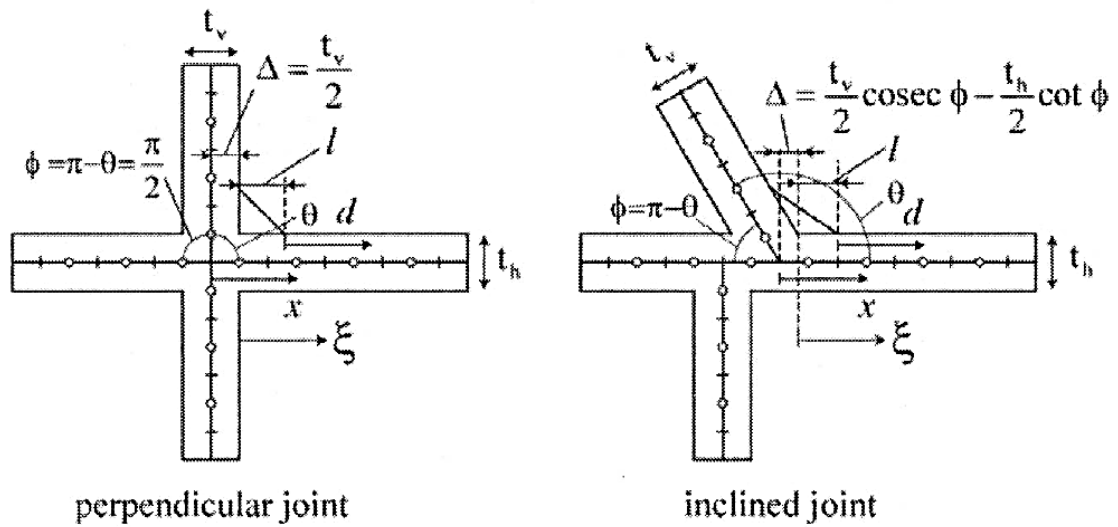


Figure 96: Distance of the read out points (ROPs) from the hot spot used in Osawa's method (ISSC, 2009)

4. CSR – B method; where HSS is derived by modifying method 1 above by the correction factor λ defined as:

$$\lambda = \begin{cases} 0.8 & \phi \leq 75^\circ \\ 0.8 - \frac{0.2}{15} & \phi > 75^\circ \end{cases} \quad \text{Eq. 51}$$

Where, ϕ is the angle between the main and attached plates defined in **Figure 96**.

2.4.1.6 HSE LCF Review

HSE (Health and Safety Executive) study review of LCF resistance (HSE-Review, 2004) is discussed in section 5.1.4 under LCF testing (Chapter 5) because it is more relevant there.

2.4.2 Local Approaches (State of the Art)

In a very comprehensive review Radaj (1996) presented a number of local approaches (**Figure 97**) for assessing the fatigue strength and service life of welded and non-welded structures based on structural stresses, notch stresses and fracture mechanics. For complex structural details when neither a nominal stress nor a design category can be assigned local concepts are applicable. The necessity for the application of local concepts is further justified by the fact that the fatigue process has a local character and cannot be well described by global (nominal) stresses. Radaj et al., (2009)

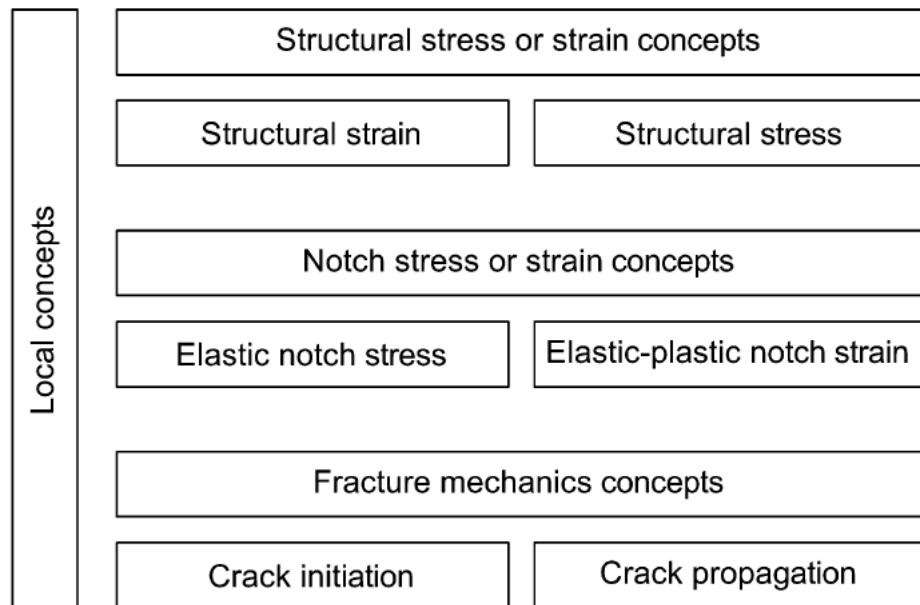


Figure 97: Classification of local concepts of fatigue assessment of welded joints (Radaj et al., 2009)

The initiative behind the review was to present the progress in methods achieved previous years while industrial application was lagging behind. Another reason for the review was the discussions on local approaches to be included in design codes. Radaj defined local approaches as procedures which aim at the design, dimensioning and optimization of structural components on the basis of local stress and strain parameters. Local approaches supplement or substitute nominal stress approach. Radaj stated that because of the fact local approaches are different in terms of variety, state of development, contents and the range of applicability; it is difficult to standardize for industrial application and include into design codes. However, only local approaches trace the parameters which have a decisive influence on the fatigue strength and service life of welded joints whereas global approaches do not separate these parameters. Testing procedures without local approaches are too expensive and time consuming to achieve the aim of an appropriate design. Radaj (1996)

The basics of fatigue assessment procedures lies in the understanding of the micro and macro phenomena of material fatigue, Influence parameters for cyclic crack initiation and Influence parameters for cyclic crack propagation. These parameters dominate an extremely complex physical reality which needs to be controlled by engineers. This microstructural phenomenon (moving dislocations, microcrack initiation on slip bands, further crack growth by local slip mechanisms at the crack tip) schematically shown in **Figure 98** can be approximately described by a macroscopic elastic-plastic stress and strain analysis according to continuum mechanics. The initiation of the crack is determined by the amplitudes of the cyclic stress and strain components at the notch root and the volume of the highly stressed material. The influence parameters controlling the limit values of the stress and strain parameters are summarized in **Table 7**, the number of the influence parameters being handled by the procedure of strength assessment is large and the problem facing engineers is the lacking possibility of decouple the effects of the influence parameters. The crack propagation is determined by the amplitudes of the cyclic stress intensity factor or of the cyclic J-integral at the crack tip. The influence parameters controlling the limit values of the stress and strain parameters at the crack tip are summarized in **Table 8**. Radaj (1996)

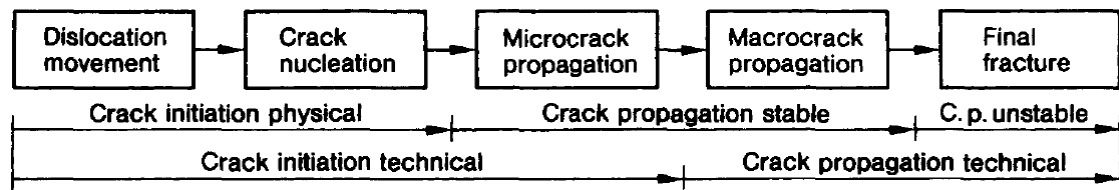


Figure 98: Micro and macro phenomena of material fatigue (Radaj, 1996)

Table 7: Influence parameters controlling cyclic crack initiation. Radaj (1996)

<i>Material</i>	<i>Component</i>	<i>Surface</i>
Type	Shape (notch effect)	Roughness
Alloy	Size (technological, stress-mechanical and statistical size effect)	Hardness
Grain size		Residual stress
Microstructure		
<i>Environment</i>	<i>Loading type</i>	<i>Loading course</i>
Temperature	Mean stress (including residual stress)	Amplitude spectrum
Corrosion	Multiaxiality (including phase angle)	Amplitude sequence
		Mean value sequence
		Rest periods

Table 8: Influence parameters controlling cyclic crack propagation. Radaj (1996)

<i>Material</i>	<i>Component</i>	<i>Crack</i>
Type	Shape	Shape
Alloy	Size (technological, stress-mechanical and statistical size effect)	Size
Grain size		
Microstructure		
<i>Environment</i>	<i>Loading type</i>	<i>Loading course</i>
Temperature	Crack opening mode	Amplitude spectrum
Corrosion	Mean stress intensity	Amplitude sequence
	Multiaxiality (including plate thickness)	Mean value sequence
		Rest periods

In their exceptional book ‘Fatigue Assessment of Welded Joints by Local Approaches’ Radaj et al., (2006) re-presented the parameter governing fatigue as structured according to Haibach (**Figure 99**), based on the main testing and analysis procedures used to obtain the above mentioned critical values for fatigue strength or service life assessments.

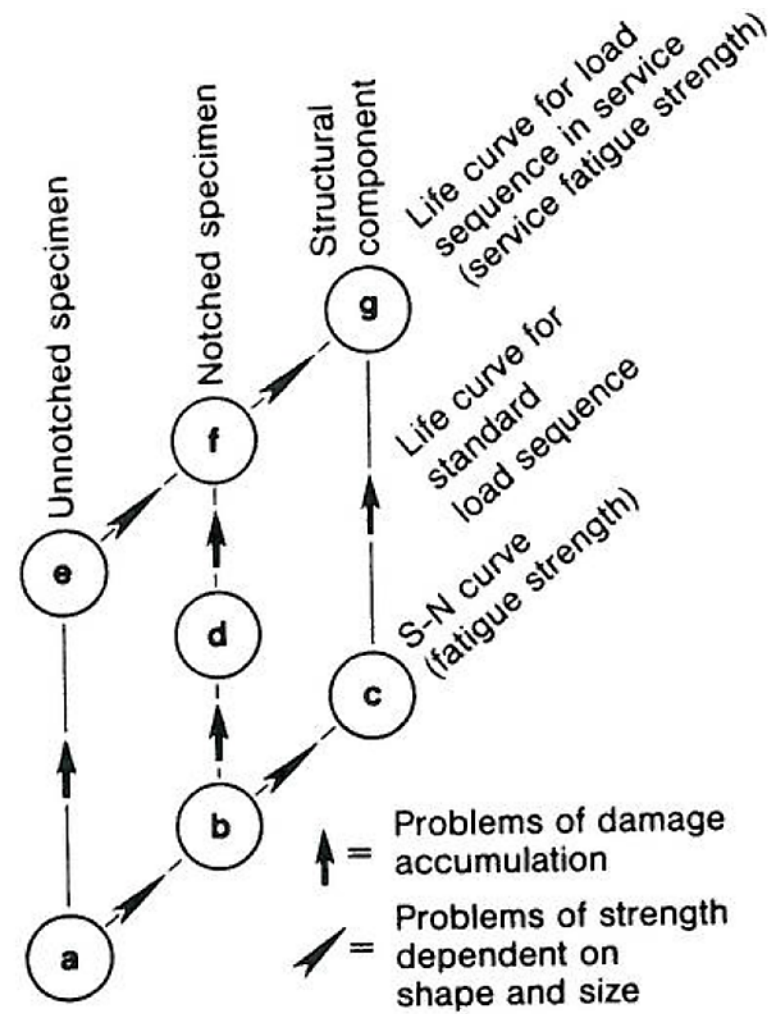


Figure 99: Parameter governing fatigue failure (Radaj et al., 2006)

The description of fatigue strength proceeds from the S–N curve (nominal stress amplitude versus number of cycles) of the unnotched specimen (a). The S–N curve of the notched specimen (b) is gained therefrom by considering the stress concentration factor and the notch radius. Finally, the S–N curve of the structural component (c) results from additionally considering size and surface effects (including residual stresses). This path a–b–c or e–f–g is connected with the problem of strength dependent on shape and size. On the other hand, the fatigue life curve resulting from variable amplitude loading can be derived from the S–N curve resulting from constant amplitude loading by introducing a damage accumulation hypothesis. This is the path a–e, b–f or c–g from conventional fatigue strength to service fatigue strength. The problem of damage accumulation can be partly solved by determining the fatigue life curve of the notched specimen under standard load sequences, path d–f–g instead of c–g. However, this does not mean that every fatigue strength assessment starts with the S–N curve of the

unnotched specimen and ends with the life curve of the structural component. In fact, the S–N curve of the component is often gained proceeding from the S–N curve of the notched specimen. Also, the life curves of structural components are mostly determined without reference to specimen testing. Radaj et al., (2006)

2.4.2.1 Global and local approaches

For practical fatigue assessments many approximate models have been conceived because it is impossible for a physical model to account for all fatigue influencing parameters. The global approach is a valid tool for design and statistical quality control of typical structural details and guidelines are provided in design rules and codes. The local approach is the most suitable for research and calibration purposes and because it is more onerous than the global approach, local approaches are enforced in codes only for unconventional fatigue analyses. ISSC (2009)

Local approaches evolved from global approaches; they supplements, deepen and extend the global approach. Local approach history received some essential development stated by Radaj (1996). He also highlighted that researchers from the USA were leading in LCF strength at elevated temperatures and the application related to the development of the local approach e.g. application of Neuber formula and Paris equation while researchers from Germany were leading in HCF strength especially the determination of the fatigue notch factor of notched specimens. Later on, the main efforts related to the local approach shifted to Germany.

Global approach is nominal stress approach i.e. a strength assessment that proceed directly from nominal stresses derived with the assumption of a constant or linearized stress distribution or from the acting forces and moments. Local approach is a strength assessment that proceeds from local stress and strain parameters. The local fatigue damage process of material includes cyclic crack initiation, cyclic crack propagation and final fracture. Crack initiation is connected with the 'notch root approach' which is based on the stresses and strains at the notch root derived by continuum mechanics. Crack propagation and final fracture are described by the 'fracture mechanics approach'. The strength assessment according to the complete local approach therefore consists of the notch root approach and the fracture mechanics approach. Radaj (1996)

Structural stress approach is an approach between the global and local versions; it emphasizes the stress concentrations caused by the macrogeometry while the actual notch effect is suppressed. According to the local stress and strain parameters chosen

and the type of failure criteria introduced, the most important basic variants of the global and local approach are shown in **Figure 100** each variant characterized by the typical load, stress or strain parameters and the relevant strength diagram. The local quantities result from the global quantities proceeding from the left hand side to the right hand side of the figure by increasingly taking local conditions into account. The following strength diagrams are presented: load S–N curve, nominal stress S–N curves for standardized notch cases, structural stress S–N curve, notch strain S–N curve, Kitagawa diagram (cyclic limit stress over the length of short cracks) and crack propagation rate over the cyclic stress intensity factor of longer cracks. Radaj (1996)

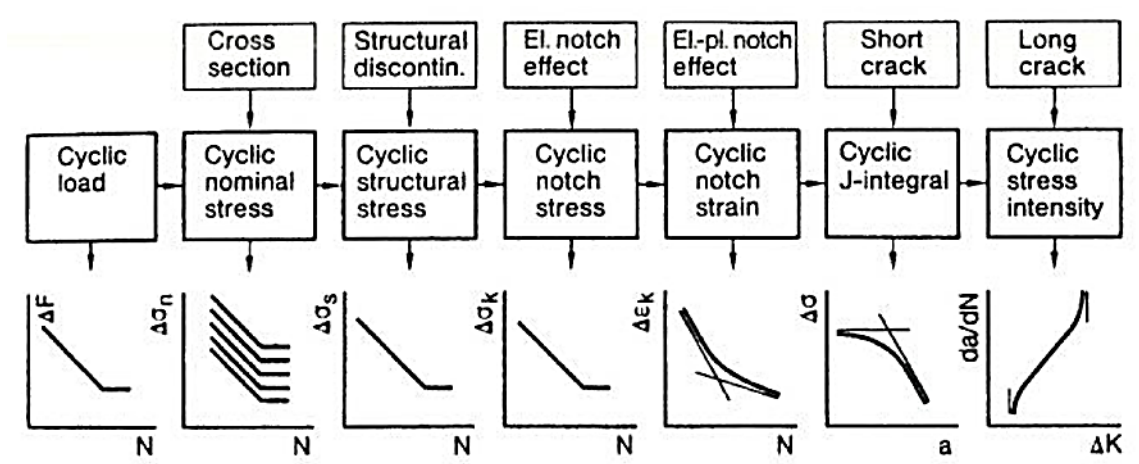


Figure 100: Global and local approaches for describing the fatigue strength (Radaj, 1996)

Figure 100 abbreviations; El. ‘elastic’ and El. pl. ‘elastic-plastic’; with ΔF cyclic load, $\Delta\sigma_0$ cyclic nominal stress, $\Delta\sigma_s$ cyclic structural stress, $\Delta\sigma_k$ cyclic notch stress, $\Delta\epsilon_k$ cyclic notch strain, $\Delta\sigma$ cyclic stress at crack tip, da/dN crack propagation rate, N number of cycles to failure, a crack length and ΔK cyclic stress intensity factor; notch stress intensity approach to be supplemented.

2.4.2.2 Notch root approach

The notch root approach for assessing the fatigue strength and service life up to crack initiation proceeds from the elastic-plastic strain amplitudes at the notch root and compares them with the strain S–N curve of the material in the unnotched comparison specimen shown in **Figure 101**. The idea behind this approach is that the mechanical behaviour of the material at the notch root in respect of local deformation, local damage and crack initiation is similar to the behaviour of axially loaded unnotched or mildly

notched specimen in respect of global deformation, global damage and complete fracture. Radaj (1996)

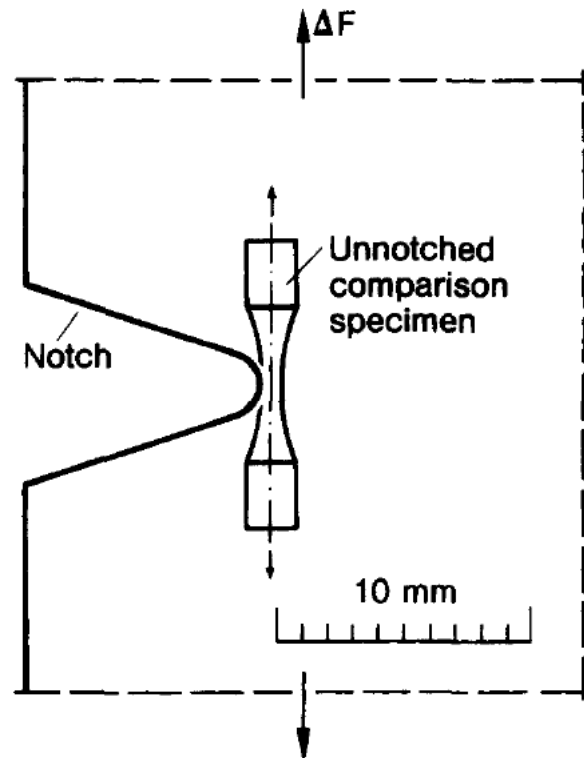


Figure 101: Comparison specimen for simulating the cyclic stress strain and crack initiation behaviour at the notch root (Radaj, 1996)

The stresses and strains at the notch root of the structural component are calculated proceeding from the cyclic stress-strain curve and the macrostructural support formula according to Neuber. The notch root strain can also be measured instead of being calculated. The comparison specimen is required in this case to determine the stresses which are connected with the elastic-plastic strains. Finally, a sequence of hysteresis loops in the stress-strain diagram (i.e. the stress-strain path) results on the basis of the load-time function. The strain S–N curves of the comparison specimen is dependent on the mean stress and can be represented by a single damage parameter S–N curve which counts for mean stress effect. Damage from stress-strain path is determined cycle by cycle, added up and compared with the S–N curve. The damage parameter S–N curve may be used with a factor in order to fit the results from component fatigue tests. The Miner rule may be used proceeding from the strain S–N curve if the strain amplitudes have been evaluated in a spectrum or matrix. The principal direction of the stresses and strains at the notch root changes permanently in the case of complex loading sequences

acting on the component including mean load variation and mutual phase shift. The numerical procedure becomes extremely complicated both in respect of theory and application. The yielding behaviour including hardening and softening under multiaxial, proportional or nonproportional stressing and straining has to be considered. Research has clarified only part of the problem so far. The notch root approach, which requires high expenditure in its general form, is simplified for application. This can be done in different ways. The simplest version of the approach refers to the fatigue strength for infinite life i.e. to constant amplitude loading with fatigue fractures avoided. The assumption is well founded in this case that no appreciable plastic deformation occurs at the notch root i.e. the notch effect of the structural component can be described as linearelastic and set against the endurance limit of the material. Radaj (1996)

The elastic stress concentration factor is dependent on the shape, the dimensions and the loading of the structural component. The fatigue notch factor is derived from introducing an additional microstructural support hypothesis defined for zero mean stress. The endurance limit of the material is taken from an amplitude-mean diagram taking into account roughness, hardness and residual stresses in the surface layer. Von Mises strength hypothesis is used in the case of ductile materials. The fatigue strength for infinite life of the structural component can thus be determined. The notch root approach in this simple form has been successfully applied at first for engine components with an expected infinite life such as crankshafts, connecting rods or gearwheels. The simplified notch root approach referring to the fatigue strength for infinite life can be extended into the high-cycle fatigue strength range referring to finite life without problems. But it will be sufficient in general, to consider the normalized S-N curve of the nominal stress approach as valid which can be based on the fatigue strength for infinite life of the component. The elastic-plastic notch root approach is indispensable on the other hand in the LCF range and for solving problems of service fatigue strength. Radaj (1996)

2.4.2.3 Comparison of Approaches

Radaj (1996) considered the nominal stress approach to be robust and superior to the local approach as far as it is statistically founded, but the robustness is bound to the condition of the structural component and the test specimen in respect to influence parameters. The notch case classification based on the local approach, for example, is well known to the experts. Therefore, the local approach is indispensable as a supplement to the nominal stress approach if structural component and test specimen

differ in respect of individual parameters or where nominal stresses cannot be defined. Structural stress approach has the widest field of application because structural stress analysis is always required as notch stresses and stress intensity factors are based on structural stresses. The move from the structural stress approach to the notch stress approach or further to the fracture mechanics approach is justified if the scatter range of the local notch geometry caused by the manufacturing process is small or if the scatter range can be passed over by a worst case consideration. However, in notch stress approach the scattering of the notch geometry cannot be accurately evaluated and it is not well suited for the notch stress analysis.

2.4.2.4 Peculiarities of welded structures

Welded structures have several peculiarities that further complicates the local approaches which are already complex. These peculiarities often remain unconsidered in the local approaches. Radaj subdivided them into three categories, material mismatch (inhomogeneous), residual stresses of welds and geometry related. The material characteristic values of the base material are used, the effect of residual stresses is roughly taken into account and the worst case of the geometrical notch parameters is considered.

2.4.2.5 Structural stress and strain approaches

2.4.2.5.1 Structural strain approach according to Haibach

Haibach has shown in an early historical contribution that the cyclic elastic plastic strain measured and averaged with a strain gauge of definite length (3 mm) at a definite small distance from the weld toe (2.0-2.5 mm considering the centre of the strain gauge) is well suited to characterize the HCF strength of welded joints independent of joint type, weld shape and type of transverse loading, provided that the fatigue fracture occurs at the weld toe. Radaj (1996)

2.4.2.5.2 Structural stress approach according to Dijkstra and Gurney

According to the procedure proposed by Dijkstra and Gurney et al., the axial surface stresses in the tube are measured at a small and at a larger distance from the weld toe notch and after that linearly extrapolated to the point of notch stress concentration. The structural stress approach combined with the above separation procedure is demonstrated in the design rules for tube structures in offshore engineering. This well founded approach in the HCF range (predominantly elastic behaviour) becomes

questionable when extended to the LCF range (predominantly plastic behaviour). The structural stress approach considered as a procedure which transfers the fatigue strength values of welded specimens to the local design within a structure is also applicable in cases where the structure is analysed according to the plate and shell theory, using simple engineering formulae or more complex finite element methods. However, the theoretical approach suppresses the notch stress completely because of the assumption of linear stress distribution over the plate or shell thickness. According to Radaj, this is a better way to define structural stresses because a single valued solution is possible. The structural stresses determined accordingly are higher than the values gained from linearly extrapolating the measured stress values at the surface. Structural stress calculations which use the measurement related procedure of surface stress extrapolation are sometimes chosen in order to apply the permissible structural stresses from the codes. Radaj (1996)

The structural stress approach as described above has tentatively been applied in ship design also. The global and local geometric shape parameters of the ship structure are a major factor influencing its fatigue strength. They vary to a large extent because each ship is of a singular design. The influence of shape parameters is insufficiently taken into account by the nominal stress approach, whereas the structural stresses reflect the influence. Another field of successful application of the structural stress approach are welded joints with small eccentricities caused by imperfect manufacture (imperfections). The usage in respect of design typical large eccentricities (e.g. cover plate ends on double T-section girders, longitudinal stiffeners, cover plates in general) was less successful. The increase of surface stress at those structural components can be calculated in analogy to the model of elastically supported beam bending. Based on such comparative calculations, the measuring points are recommended at a distance from the weld toe notch of $0.3-1.0t$ (with plate thickness t). These investigations have shown that the linear extrapolation should be supplemented by a quadratic or even cubic term. This means that the stress increase in front of the considered welded joints occurs with various gradients and nonlinearities. A uniform schematic approach seems to be impossible. The structural stress approach of the considered type presupposes a pronounced notch effect at the point of crack initiation. This should be distinguished from a structural stress approach without a notch effect. Crack initiation outside the weld notches in the notch free area of the base metal should be aimed at by appropriate design and production measures. Radaj (1996)

The hot spot structural stress approach for welded tubular joints has been transferred to welded joints of plate – type structures such as cover plate ends, longitudinal and transverse attachments, gusset plates, overlap joints, circular pads and girders with cope holes. Radaj et al., (2006) This transfer was mainly promoted by experts at the IIW. For fatigue critical areas or hot spots, three different configurations may occur, these are classified into different types as shown in **Figure 102**: the weld toes on the plate surface at the ends of attachments (type A), the weld toes on the plate edge at the ends of attachments (type B) and the weld toes on the plate surfaces amid the weld along an attachment (type C). Linear or nonlinear extrapolation of the strains determined in two or three evaluation points on a line normal to the weld is recommended by Niemi and Tanskanen as illustrated in **Figure 103**. The distances of the evaluation points from the weld toe depend on the plate thickness in **Figure 103** (a) and (b). Considering attachments welded to the edge of plate strips (forming in plane notches in **Figure 103** (c)), the plate thickness is no longer a suitable parameter to position the evaluation points for stress extrapolation. In this case, absolute distances for the evaluation points and quadratic extrapolation for the stresses are proposed. The minor influence of plate width on the extrapolated stresses is neglected.

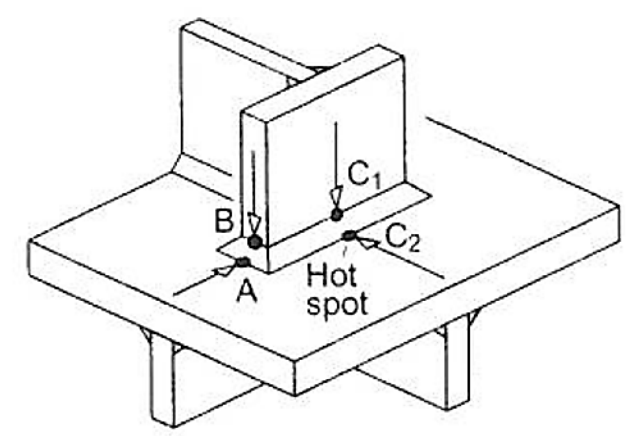


Figure 102: Three types of fatigue – critical weld toes (types A, B, C) in plate – type reference structure proposed by Fricke (Radaj et al., 2006)

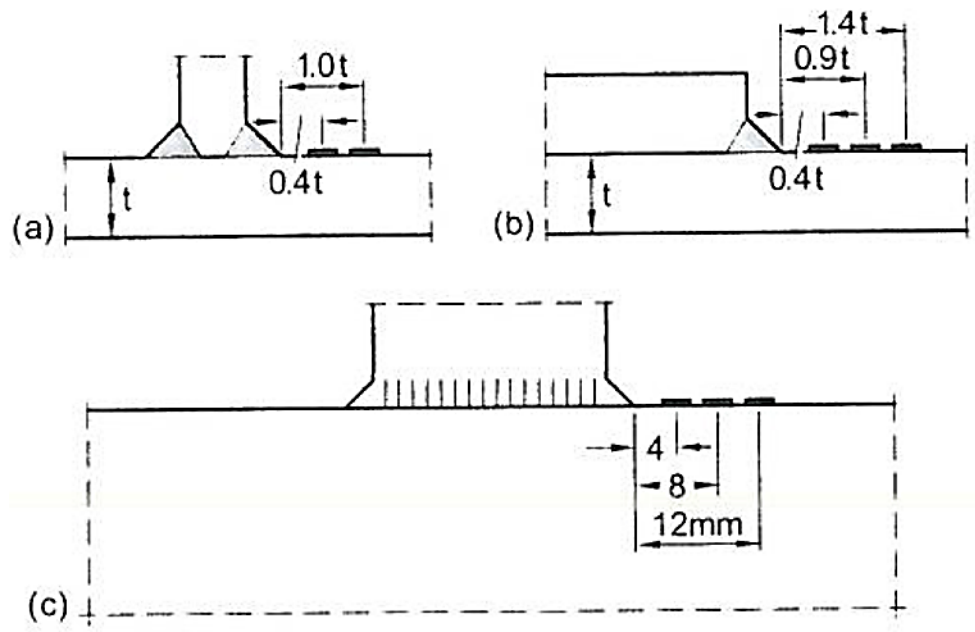


Figure 103: Strain gauge positioning for the hot spot stress determination in plate – type structures (Radaj et al., 2006)

Figure 103 showed arrangement for linear (a) and nonlinear (b) extrapolation of structural stresses on the plate surface of transverse or longitudinal attachments (weld toes of types A and C), and nonlinear extrapolation of structural stresses at the plate edge in the case of edge attachments (weld toe of type B) (c); after Niemi and Tanskanen. Radaj et al., (2006)

2.4.2.6 Structural stress concept codified procedure

The original idea of this concept has been proposed in terms of structural strains. The local strain in front of the weld toe measured by a strain gauge serves as the parameter for fatigue assessment. With the introduction of the finite element method, the structural stress variant which was developed for tubular connections in steel constructions (roofs, bridges, off-shore structures) gained an importance and led to the hot spot structural stress concept as a codified procedure of fatigue assessment. In this method, the surface stresses at prescribed evaluation points in front of the weld seam are linearly extrapolated to the weld toe as shown in **Figure 104**. Later on, the concept was transferred from tubular connections to plate and shell structures of ships. The codified procedure may be supplemented by Haibach's special procedure which is also indicated in **Figure 104**. Radaj et al., (2009)

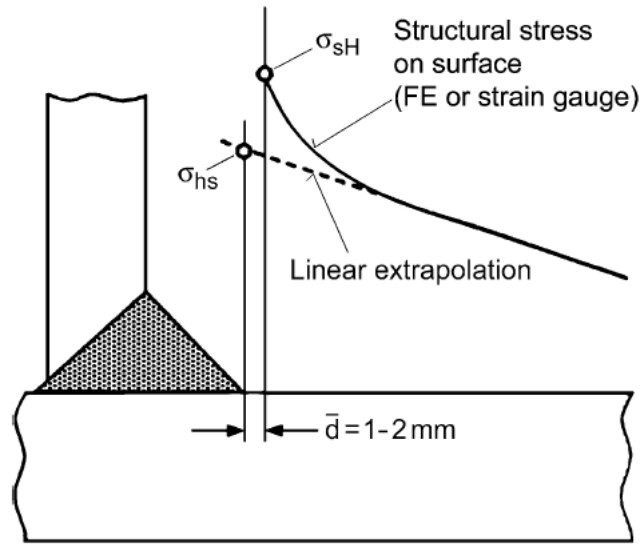


Figure 104: Two procedures to obtain the hot spot structural stress: codified procedure of linear extrapolation (σ_{hs}) and procedure based on strain at distance \bar{d} from the weld toe after Haibach (σ_{sH}) (Radaj et al., 2009)

Radaj et al., (2009) presented four contributions to the structural stress concept. The fourth has not been mentioned because it is related to thin sheet welded joints. The other three are:

2.4.2.6.1 Internal linearization

The conventional method of determining the hot spot structural stress is the linear or nonlinear extrapolation of measured surface stresses to the weld toe (two or three evaluation points at recommended locations). The extrapolation of surface stresses is also applicable based on finite element models shown in **Figure 105** (a). For shell or plate structures the internal linearization of the cross sectional stresses gained from structural analysis offers an alternative as illustrated in **Figure 105** (b). Systematic investigations revealed the need of detailed rules for finite element modelling and stress analysis in order to avoid too large scatter and uncertainties of the results. Radaj et al., (2009)

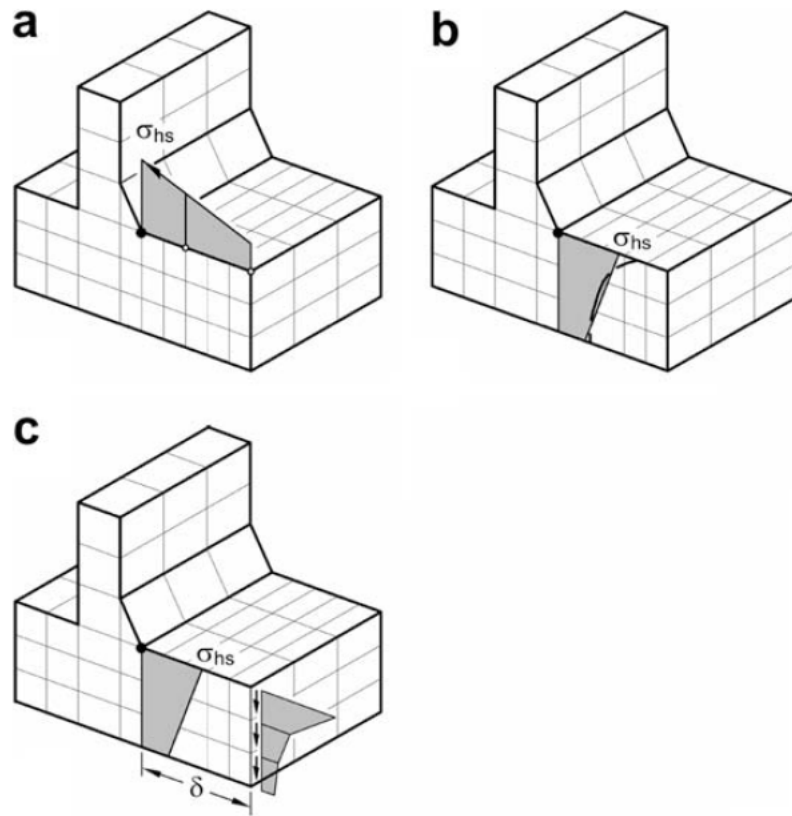


Figure 105: Linear extrapolation of surface stresses (Radaj et al., 2009)

In **Figure 105** (a) and internal linearization of cross-sectional stresses at weld toe (b, c) in a finite element model with hexahedral elements resulting in hot spot structural stress σ_{hs} ; in the variant (c) proposed by Dong et al. normal and shear stresses at distance δ are the basis of σ_{hs}

2.4.2.6.2 Modified internal linearization

The structural stress linearization across the plate thickness has been modified by Dong with the effect that the influence of the stress gradient in the direction of expected crack growth is considered based on a crack propagation approach. The internal linearization across the plate thickness in the case of a single sided weld is shown in **Figure 106** (a). Linearization up to a depth $t_1 < t$ is recommended as in **Figure 106** (b). The depth t_1 is the crack length at failure. For double sided welded joints under symmetrical loading conditions, a linearization across one half of the plate thickness is recommended ($t_1 = t/2$) as in **Figure 106** (c). For the determination of the structural stresses from finite element models, Dong recommends special procedures that are claimed to be mesh insensitive. As the grid point stresses depend on the mesh density close to the notch stress singularity at the weld toe and because these stresses are influenced by the

stresses in the adjacent weld element, they should be evaluated at a distance δ from the weld toe as shown in **Figure 106** (c). Dong's modification has some restrictions as the partial linearization of the structural stresses presumes the definition of fatigue effective reference length across which linearization is performed. This length cannot be uniformly defined but must be derived by individual adjustment to the relevant test results. Radaj et al., (2009)

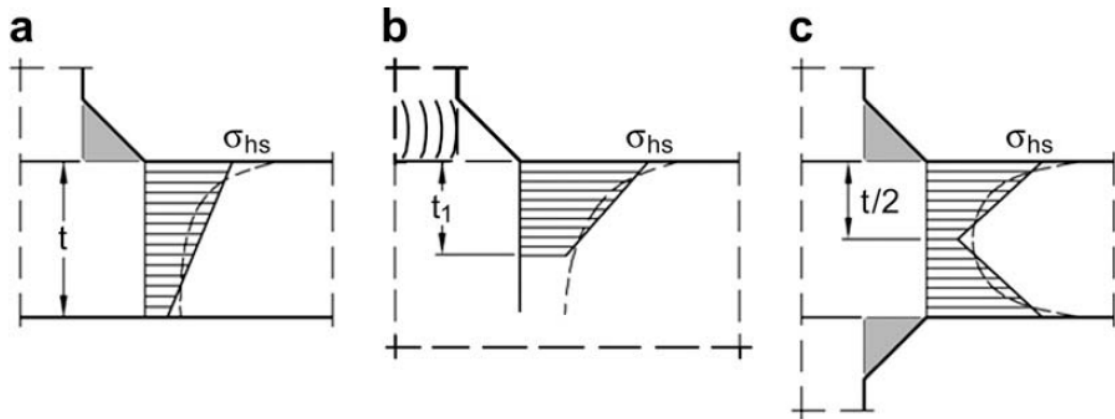


Figure 106: Internal linearization of the structural stresses as proposed by Dong et al. for single-sided weld (a), edge weld (b) and double-sided weld (c) resulting in the hot spot structural stress σ_{hs} ; cross-sections (a, c) and front view (b) (Radaj et al., 2009)

In **Figure 106** monotonic decrease of the original stress (dashed curve); depth t_1 corresponding to a defined damaging crack depth for edge attachments (b)

2.4.2.6.3 Unconventional structural stress concept

In Radaj et al., (2009) Xiao and Yamada proposed the unconventional structural stress concept that considers the structural stress calculated 1 mm below the weld toe (expected crack path) as the relevant fatigue parameter. The approach has been verified by Xiao and Yamada for non-load carrying fillet welds on both sides of transverse and longitudinal attachments. Noh et al. have shown that the concept is applicable also to the fatigue assessment with respect to toe failures of load-carrying fillet welds in cruciform joints considering partial and full penetration welds. The selection of the above mentioned evaluation point 1 mm in depth is based on analysis results for a reference structural detail, a plate of thickness $t = 10$ mm with double sided transverse attachments as shown in **Figure 107** (a). Finite element calculations showed that the local stress at the weld toe of the reference detail drops more rapidly in the thickness direction than on the surface. Whereas on the surface, the local stress increase extends

to a distance of about 2.5 mm in y direction as illustrated in **Figure 107** (b), the local stress has already dropped to nearly the nominal stress 1 mm in depth below the notch surface as illustrated in **Figure 107** (c). It is shown that the stress 1 mm in depth is correlated with the short crack propagation phase. The concept is not applicable to weld root failures.

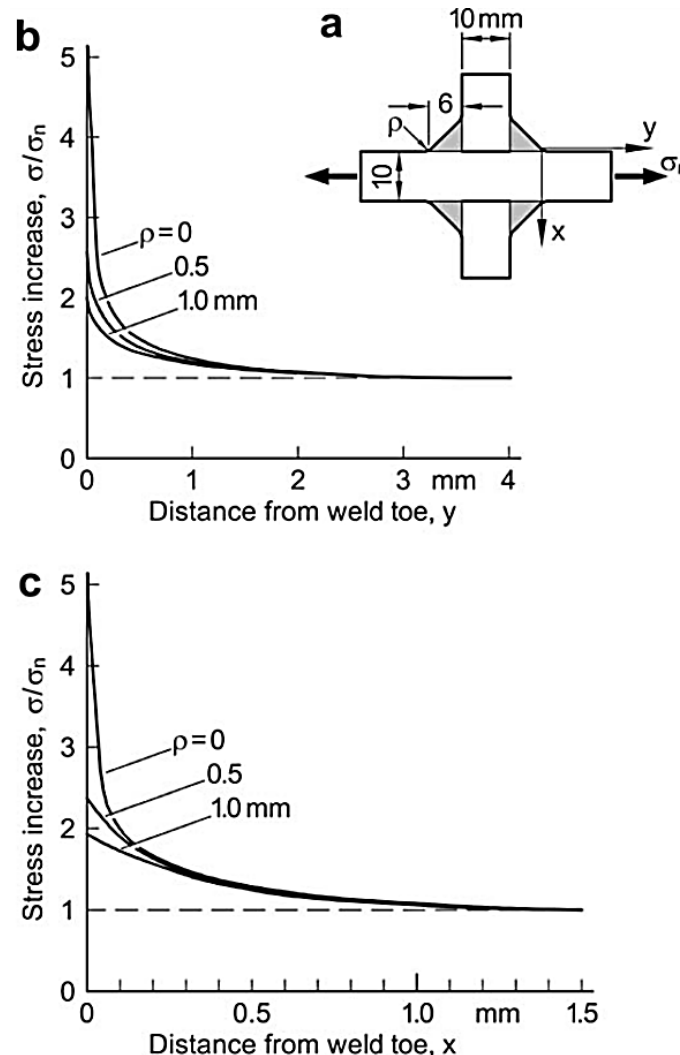


Figure 107: Stress distributions (b, c) calculated by the finite element method for a reference structural detail (a) with non-load-carrying fillet welds (double-sided transverse attachment joint; weld toe radius ρ); after Xiao and Yamada (redrawn with restriction to weld toe angle $\theta = 45^\circ$) (Radaj et al., 2009)

2.4.2.7 Notch stress or strain codified procedure

Radaj et al., (2009) presented another four contributions to the notch stress concept. Three have not been mentioned because they are related to thin sheet, spot welded joints and aluminium alloys. The one we are interested in is the:

2.4.2.7.1 Modification of the notch stress concept in IIW Recommendations

Notch stress or strain concepts use the maximum elastic notch stresses or elastic plastic notch strains to assess the fatigue strength as shown in **Figure 108** (showing stresses only). These stresses or strains can be calculated for the sharp or mild notches at the weld toe, weld root or nugget edge where the structural stresses have already been defined. The elastic notch stress concepts were originally restricted to the HCF range. The elastic plastic notch strain concepts apply to the medium cycle and LCF range. The elastic notch stress concept for welded joints is based on the early work of Mattos and Lawrence (notch support effect according to Peterson: critical distance approach) and of Radaj (notch support effect according to Neuber: fictitious notch rounding). The concept was modified by Olivier et al. (statistical evaluations) and extended by Sonsino (highly stressed material volume, multiaxial strength criteria). The elastic notch stress concept has been successfully applied to welded joints in steels and in aluminium alloys. The elastic plastic notch strain concept for welded joints (also early proposed by Mattos and Lawrence), is based on developments for non-welded components loaded predominantly in the LCF range, incorporating Neuber's simple equation (Neuber's rule) which relates the elastic plastic notch strain to the notch stress in case of local yielding at the notch. Radaj et al., (2009)

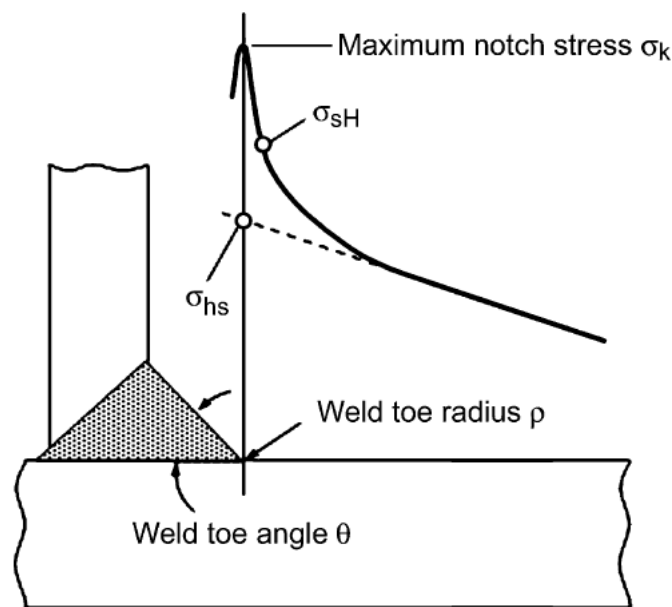


Figure 108: Definition of the maximum notch stress σ_k in comparison to the hot spot structural stress σ_{hs} and Haibach's structural stress σ_{sH} (Radaj et al., 2009)

The elastic notch stress concept has originally been proposed for application in the HCF range. It is extended for application in the medium cycle and LCF range by the IIW recommendations. A uniform reference notch radius $\rho_r = 1 \text{ mm}$ at sharp weld notches for plate thickness $t \geq 5 \text{ mm}$ is combined with the design S–N curve FAT 225 for welded joints in steel. This extension may result in non-conservative results in case of mild weld notches. The approved modification of the IIW recommendations confines the applicability of the S–N curve FAT 225 by prescribing a minimum fatigue notch factor $K_w = 1.6$, at the weld toe or root and by proving additionally that the parent material outside the weld notch provides a sufficient fatigue strength with respect to the structural stress there. For LCF, the design S–N curve (**Figure 109**) FAT 225 must be limited by FAT $160 \times K_w$ (with $K_w \geq 1.6$). Radaj et al., (2009)

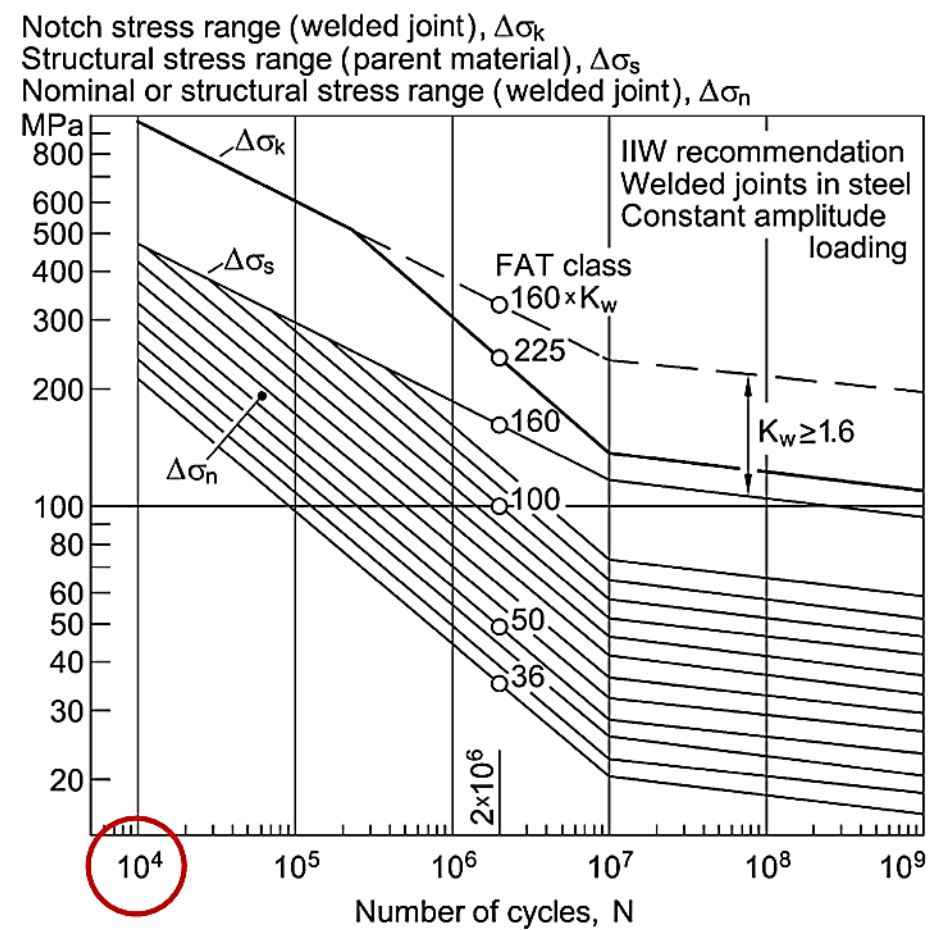


Figure 109: Limitation to the design S–N curve FAT 225 (relating to reference notch radius $\rho_r = 1.0 \text{ mm}$) by FAT $160 \times K_w$ with weld notch factor $K_w \geq 1.6$; according to the IIW recommendations (Radaj et al., 2009)

The limitation is given by transformation of the curve FAT 160 relating to the parent material into the local system. For this, the weld notch factor K_w of the weld under consideration has to be derived as the ratio of the maximum notch stress σ_k for $\rho_r = 1$ mm to the relevant hot spot structural stress σ_s . The described procedure corresponds to performing two assessments independently and using the less conservative result: weld notch stress (according to $K_w \geq 1.6$) compared with the curve FAT 225 and relevant structural stress outside the weld notch compared with the curve FAT 160. Radaj et al., (2009)

Here, it is important to highlight that the FAT 225 is relatively covering the medium fatigue range i.e. not the LCF range since the threshold is 10^4 and also the fact that its application is confined by the minimum fatigue notch factor.

2.5 Conclusions

1. The elastic-plastic notch root approach is indispensable for solving problems of service fatigue strength in the LCF range.
2. The elastic plastic notch strain concept for welded joints is based on developments for non-welded components loaded predominantly in the LCF range, incorporating Neuber's rule which relates the elastic plastic notch strain to the notch stress in case of local yielding at the notch.
3. The well founded approach of structural stress or hot spot stress in the HCF range (predominantly elastic behaviour) is questionable when extended to the LCF range (predominantly plastic behaviour).
4. IIW recommendations confines the applicability of the S–N curve FAT 225 by prescribing a minimum fatigue notch factor $K_w = 1.6$ and for LCF, the design S–N curve FAT 225 must be limited by $FAT\ 160 \times K_w$ (with $K_w \geq 1.6$).
5. IIW recommendations FAT 225 covers the medium fatigue range not the low cycle range i.e. below the threshold of 10^4 .

Chapter 3

International Institute of Welding (IIW)

3 CHAPTER 3: LCF in IIW (State of the Art)

This chapter is an outline of the state-of-the-art for LCF assessment in the International Institute of welding (IIW) and may be considered as a supplement to chapter two.

3.1 IIW HCF

The recommendations of the International Institute of Welding (IIW) on fatigue of welded components and structures and on the effect of weld imperfections in respect to fatigue have been published firstly in 1996 then updated in 2006. The code covered component testing, nominal stress, structural stress, notch stress method and fracture mechanics assessment procedures. The update of the recommendations covered some main areas such as structural hot-spot stress allowing for an economic and coarser meshing in finite element analysis, extension of effective notch stress concept to welded aluminium structures and numerical assessment of post weld treatments for improving fatigue properties. Hobbacher (2009)

In fatigue assessment; fatigue actions and fatigue resistance are related by an appropriate assessment procedure. It must be ensured that all three elements (actions, resistance and assessment procedure) correspond. Hobbacher (2008) Three procedures may be distinguished:

1. Procedures based on S-N curves, such as
 - a. Nominal stress approach,
 - b. Structural hot spot stress approach,
 - c. Effective notch stress approach.
2. Procedures based on fatigue crack propagation considerations.
3. Direct experimental approach by fatigue testing of components or entire structures.

These approaches differ mainly in the stress used in the assessment, IIW (International Institute of Welding) most recent published guideline Fricke (2010a) outlined and described various approaches for fatigue strength assessment applicable to weld toe and weld root failure. IIW definitions are as follows:

1. Nominal stress approach, based on the stress disregarding any stress increase due to the structural detail or the weld; in the case of weld root failure, a special nominal stress in the weld has to be used.
2. Structural stress approach, based on the stress containing only the stress increase due to the structural geometry, but not due to the local weld geometry; the

approach has firstly been developed for weld toe failures, but has been extended to some cases with weld root fatigue at fillet welds, using a linearized stress in the weld.

3. Effective notch stress approach, based on the local stress at the rounded weld toe or weld root notch, assuming ideal-elastic material behaviour and microstructural support effects to a certain extent.
4. Stress intensity approach, using the notch stress intensity factor (N-SIF) of the weld toe with zero radius as fatigue parameter; for the weld root, the stress intensity factor for crack tips is used.
5. Crack propagation approach, using Paris law for determining the fatigue life of a propagating crack; while the actual non-fused part is considered as initial crack at the weld root, an initial crack depth must be assumed for the weld toe.

Due to the vastness of the topic only 3rd approach will be investigated in this research following the literature review as this is the most advanced and latest development in the author's view, however, reference will be made to other approaches where required. For example class society's common use of the 2nd approach.

3.1.1 *Effective Notch Stress (HCF)*

The Effective Notch Stress (ENS) concept in simple terms means that the geometry of the toe is replaced by a rounded notch with a specific radius ρ . The stress concentration factor K_t is then calculated by FE analysis. These K_t values are used to evaluate the stress distribution at the toe of welds in a structure. Schijve (2012)

Notch stress approach considers increase in local stress at the notch due to weld toe and/or weld root based on theory of elasticity i. e. without consideration of elastic-plastic material behaviour. Fricke (2010b) The micro-structural support effect of inhomogeneous material structure can be taken into account by different hypotheses in the (elastic) notch stress approach:

1. Stress gradient approach. Siebel and Stieler (1955)
2. Stress averaging approach, proposed by Neuber (1937, 1946 and 1968)
3. Critical distance approach. Peterson (1959)
4. Highly stressed volume approach. Kuguel, (1961) and Sonsino (1994 and 1995).

Only last three hypotheses have found wide application to welded joints. The stress averaging approach is mainly used in the form of fictitious notch rounding illustrated in **Figure 110** known also as effective notch stress approach, while the critical distance

approach employs the ratio of a material constant and the notch radius to reduce the elastic stress concentration factor K_t to the fatigue notch factor K_f .

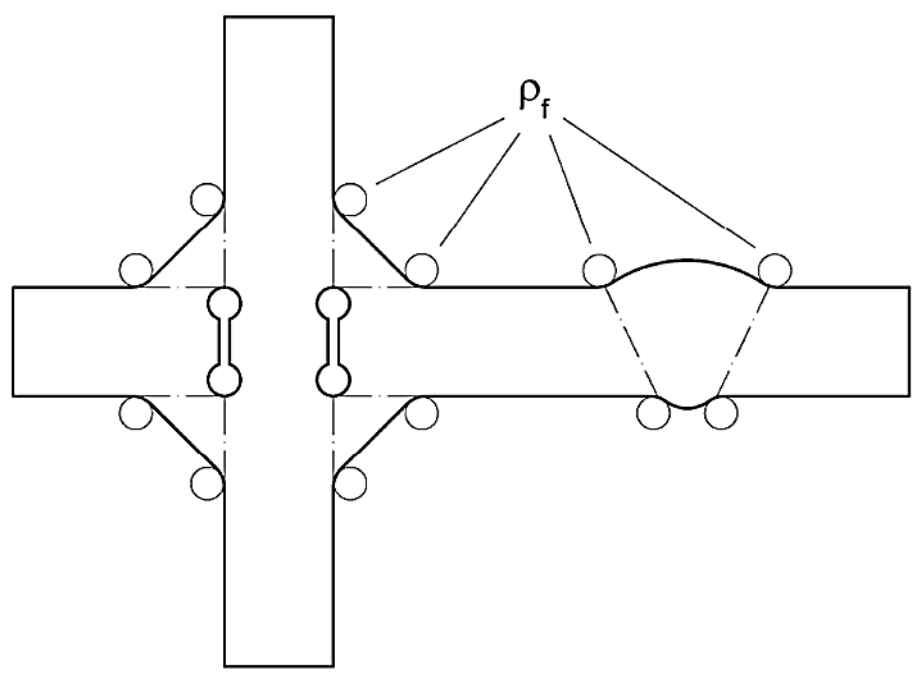


Figure 110: Fictitious notch rounding graph according to Hobbacher, 1996 (Fricke, 2010b)

The basic idea behind this approach is that the stress reduction in a notch due to averaging the stress over a certain depth can alternatively be achieved by a fictitious enlargement of the notch radius.

Neuber (1968) proposed the following formula for the fictitious radius ρ_f :

$$\rho_f = \rho + s \cdot \rho^* \quad \text{Eq. 52}$$

Where

- ρ = actual notch radius
- s = factor for stress multiaxiality and strength criterion
- ρ^* = micro-structural support length

Neuber's microstructural concept illustrated in **Figures 111** and **112** is the theoretical background of the reference radii method. Substitute notch with fictitious notch radius results in average notch stress σ_{av} gained by the integration of the stress distribution in the real notch (Sonsino, 2009).

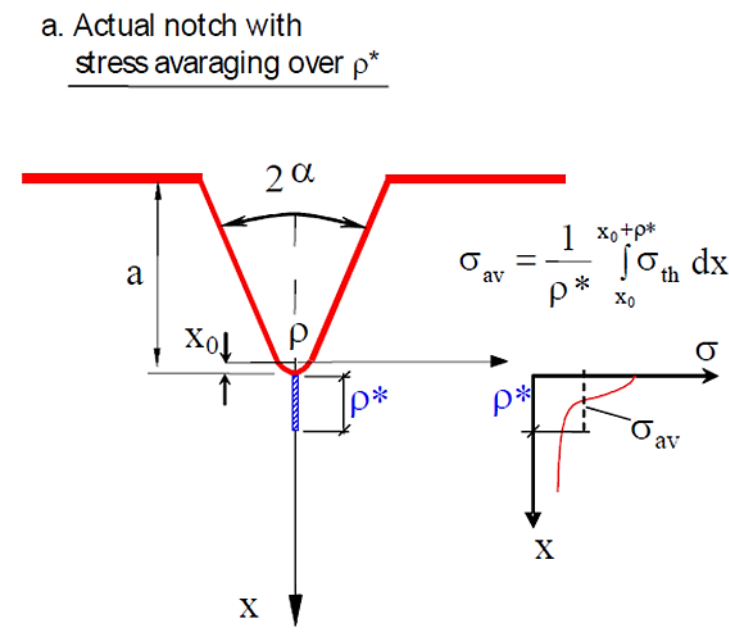


Figure 111: Actual notch with stress averaging over ρ^* (Sonsino, 2009)

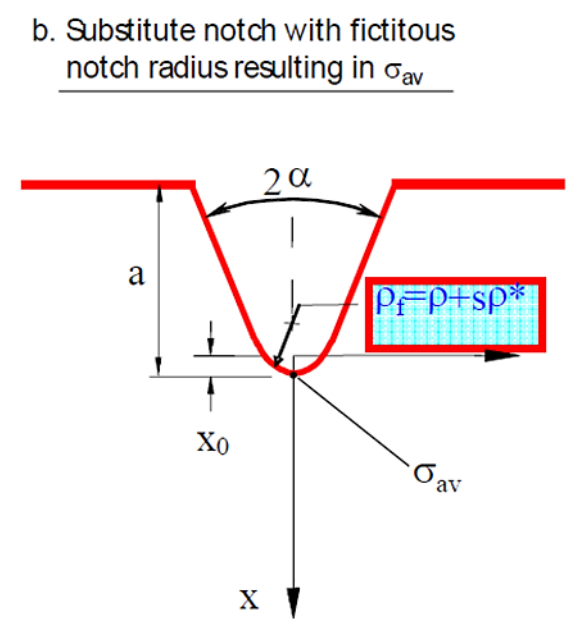


Figure 112: Substitute notch with fictitious notch radius resulting in σ_{av} (Sonsino, 2009)

In his proposed approach for welded joints Radaj (1990) assumed the factor s to be 2.5 for plane strain conditions at the roots of sharp notches. This factor results in an increase of the actual radius by 1 mm to obtain the fictitious radius ρ_f . For typical welds in (low strength) steel $\rho^* = 0.4$ mm (for cast steel in welded zone). The worst case scenario (conservative) in Radaj's applied approach, he assumed an actual radius of zero so that the fictitious radius is 1 mm. The rounding approach is applied to both the weld

toe and the weld root and because stress analysis results in fatigue effective stress, the approach is called Effective Notch Stress Approach.

Berto et al., (2012) evaluated the multiaxiality factor s for V-notches with root hole subjected to in-plane shear loading using three different methods. They applied the fictitious notch rounding concept for the first time to this geometrical configuration. The values of s for pointed V-notches determined by three different methods have been found to be almost the same and mainly dependent on the notch opening angle. The values of the multiaxiality factor s have been validated by FE analysis results and it has been highlighted that fictitious notch rounding is a procedure well suited only for engineers' preliminary strength assessments because effects of nearby boundaries, loading and support conditions and cross-sectional weakening may deteriorate the results. As soon as FE models are available, direct notch stress averaging over the microstructural support length in the critical direction (for 2D) or strain energy density evaluation over a control volume (for 3D) should be preferred.

In order to establish guidelines for modelling structures, Fricke (2006) performed a round robin numerical analysis on three welded details using the effective notch stress approach. A cruciform joint with non-load carrying fillet welds in one load case and load carrying in the other. A T-joint of rectangular hollow section (RHS) members and fillet-welded end connection of a RHS joint being prone to fatigue failure at the weld root with nonfused root faces. The results of the analysis were element size along the circumference of the rounded notch should not be larger than 0.25 mm and principal stress gives good estimates of fatigue lives on the basis of FAT 225 for structure details where fatigue tests are available.

In contrast to widely applied nominal and structural hot-spot stress approaches, notch stress approach can explicitly consider the shape of the weld. Fricke and Kahl (2007) introduced techniques for measuring the weld profile for different bracket connections. The effective notch stress is then analysed using finite-element FE sub-models of the coarse bracket models. The fatigue test results are compared with design S-N curves based on computed effective notch stresses as well as with the structural hot-spot stresses derived from the coarse models and the result was notch stress approach predicts better the different fatigue behaviour of structural variants.

Because fatigue crack propagation analysis is considered to be effective in evaluating fatigue strength in load carrying cruciform welded joints which are prone to cracks in weld roots Mori and Myoken (2008) compared fatigue crack propagation analysis with

effective notch stress concept using load carrying cruciform welded joint and concluded that the fatigue strength obtained using effective notch stress approach:

1. ≈ 0.6 to 0.8 times higher compared to fatigue test results while fatigue strength estimated by crack propagation analysis agrees well with fatigue test results.
2. ≈ 0.75 to 1.5 times high compared to fatigue crack propagation analysis.
3. Gives appropriate estimation for influence of cross plate thickness and weld shape on fatigue strength.
4. Underestimates the influence of weld size and weld penetration depth on fatigue strength.
5. Overestimation the influence of main plate thickness and bi-axial load on fatigue strength.

In order to determine the effective notch stress using FEA, IIW recommendations state that element sizes not more than $1/6$ of the radius when using linear elements and $1/4$ of the radius when using high order elements Hobbacher (2008), this has been examined in 6.2.1 and the author is of the opinion that as long as the mesh is fine enough at the stress concentration area and nonlinear analysis is carried out, element order has little influence on the results.

Schijve (2012) reviewed the effective notch stress concept for fatigue prediction of welded joints and considered it to be the most recent model for fatigue assessment of welded joints. However, he proposed a modified version of the effective notch stress and recommended further research for his proposal. The proposal is that ρ should depend on a characteristic ratio of two dimensions ρ/h where h is defined in **Figure 113**. He also recommended that a handbook be issued with calculated effective K_t values for a variety of welded configurations with various dimensions. The review made some important statement/conclusions such as:

1. Theoretical stress concentration K_t value should be based on the maximum principal tensile stress.
2. The theoretical stress concentration K_t (calculated by FE analysis for the effective notch radius ρ) gives a direct numerical indication of the stress distribution and should be preferred for the assessment of the fatigue quality of different configurations of the welded structures instead of the FAT values in the IIW document which are associated with S–N curves.

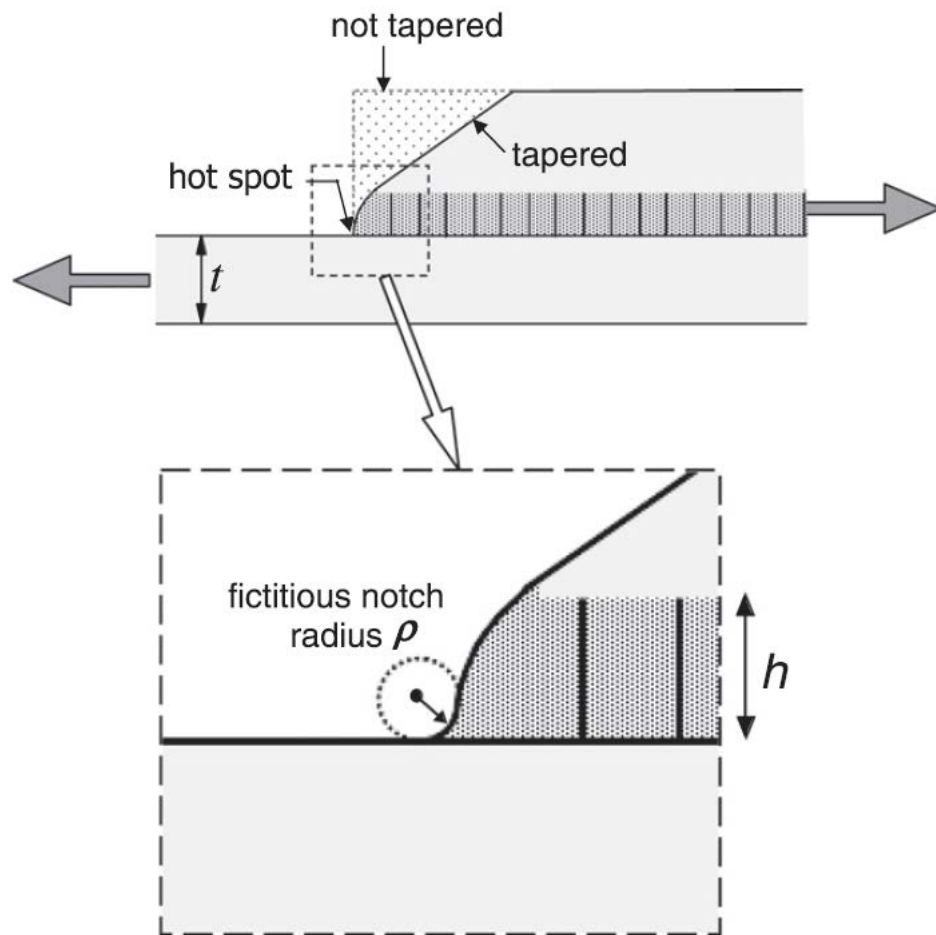


Figure 113: The hot spot stress location at the toe of a weld (Schijve, 2012)

3.2 Effective Notch Strain (LCF)

The author considers this to be the most recent advance in LCF where Saiprasertkit et al., (2011) examined effective notch strain in elastic and elasto-plastic condition for load carrying cruciform welded joints and proposed a correlation between effective notch strain range and nominal strain range. This study concluded that strength mis-matching between deposit metal and base metal has significant influence on LCF strength and negligible influence on HCF strength. Effective notch strain can be used to evaluate fatigue strength for specimens with different incomplete penetration ratio and strength mis-matching from low to HCF regions and finally this correlation is valid for fatigue assessment from low to HCF regions regardless of the weld geometry and the strength mis-matching.

In this assessment the maximum value of equivalent total strain range calculated in the element along the notch was used as the effective notch strain range. The equivalent total strain is the summation of the elastic and plastic component as shown in **Figure**

114 and equation (Eq.51). The elastic component can be calculated by dividing the equivalent stress range given in equation (Eq.52) with Young's modulus. The plastic component can be calculated by equation (Eq.53).

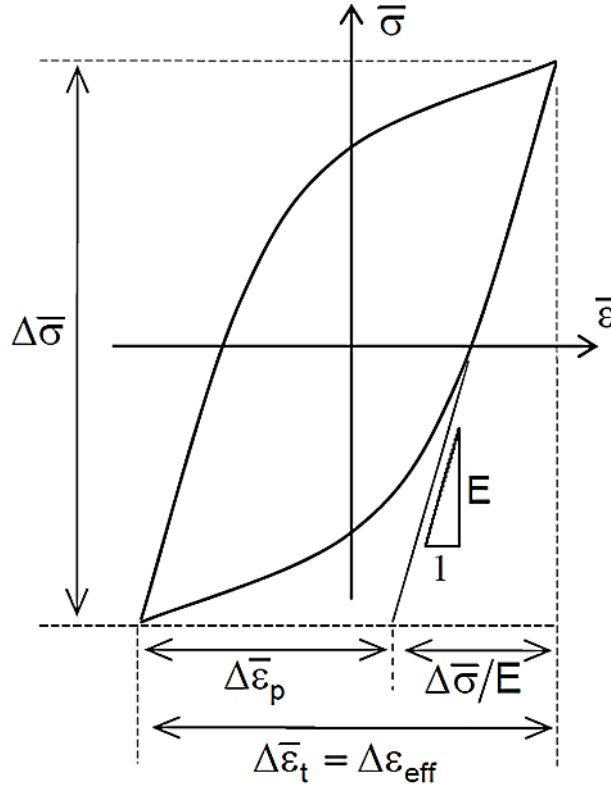


Figure 114: Definition of effective stress-strain range (Saiprasertkit et al., 2011)

$$\Delta \varepsilon_{\text{eff}} = \Delta \varepsilon_t = \frac{\Delta \bar{\sigma}}{E} + \Delta \varepsilon_p \quad \text{Eq. 53}$$

$$\Delta \bar{\sigma} = \sqrt{\frac{1}{2} \left[(\Delta \sigma_x - \Delta \sigma_y)^2 + (\Delta \sigma_y - \Delta \sigma_z)^2 + (\Delta \sigma_z - \Delta \sigma_x)^2 + 6 (\Delta \tau_{xy}^2 + \Delta \tau_{yz}^2 + \Delta \tau_{zx}^2) \right]} \quad \text{Eq.54}$$

$$\Delta \varepsilon_p = \frac{1}{3} \sqrt{2 \left[(\Delta \varepsilon_{p,x} - \Delta \varepsilon_{p,y})^2 + (\Delta \varepsilon_{p,y} - \Delta \varepsilon_{p,z})^2 + (\Delta \varepsilon_{p,z} - \Delta \varepsilon_{p,x})^2 + \frac{3}{2} (\Delta \gamma_{p,xy}^2 + \Delta \gamma_{p,yz}^2 + \Delta \gamma_{p,zx}^2) \right]} \quad \text{Eq.55}$$

Where, $\Delta \sigma$ is the normal stress range, $\Delta \tau$ is the shear stress range, $\Delta \varepsilon_p$ is the normal plastic strain range, $\Delta \gamma_p$ is the shear plastic strain range, the subscript of x, y and z are x, y and z direction, $\Delta \varepsilon_{\text{eff}}$ is the effective notch strain range, $\Delta \varepsilon_t$ is the equivalent total strain range, $\Delta \bar{\sigma}$ is the equivalent stress range and $\Delta \varepsilon_p$ is the equivalent plastic strain range.

Figure 115 shows the relationship between the effective notch strain range calculated from equation (Eq.53) and the fatigue life. The effective notch strain range was obtained

at the weld root. Consequently, the proposed effective notch strain can be successfully used to evaluate the fatigue strength of the load carrying cruciform joints from low to HCF region, regardless of the material mis-matching and the incomplete penetration size.

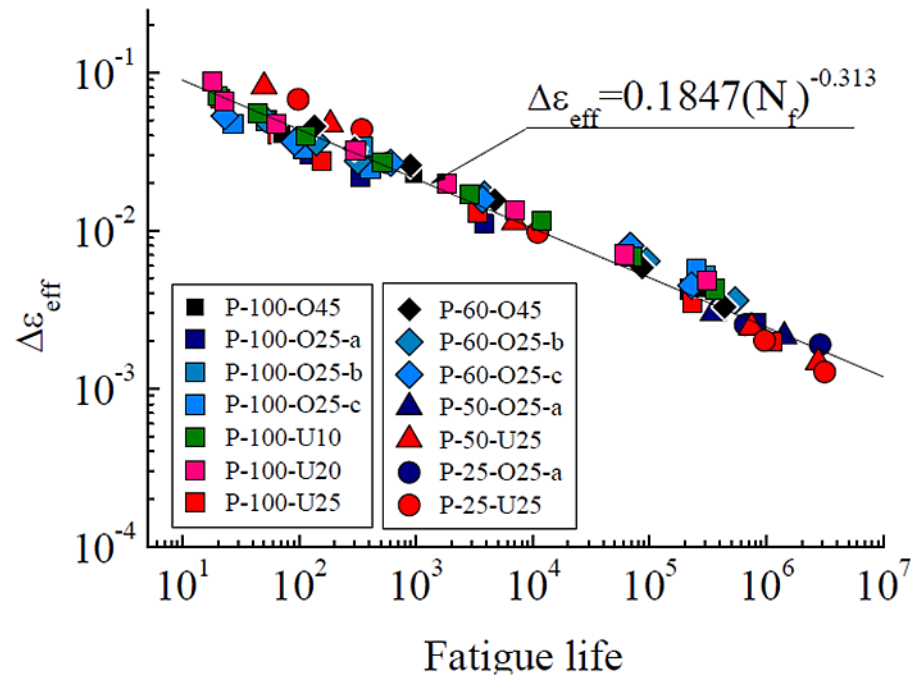


Figure 115: Relationship between effective notch strain and fatigue life (Saiprasertkit et al., 2011)

The concept of the proposed method for estimating effective notch strain is illustrated in **Figure 116**.

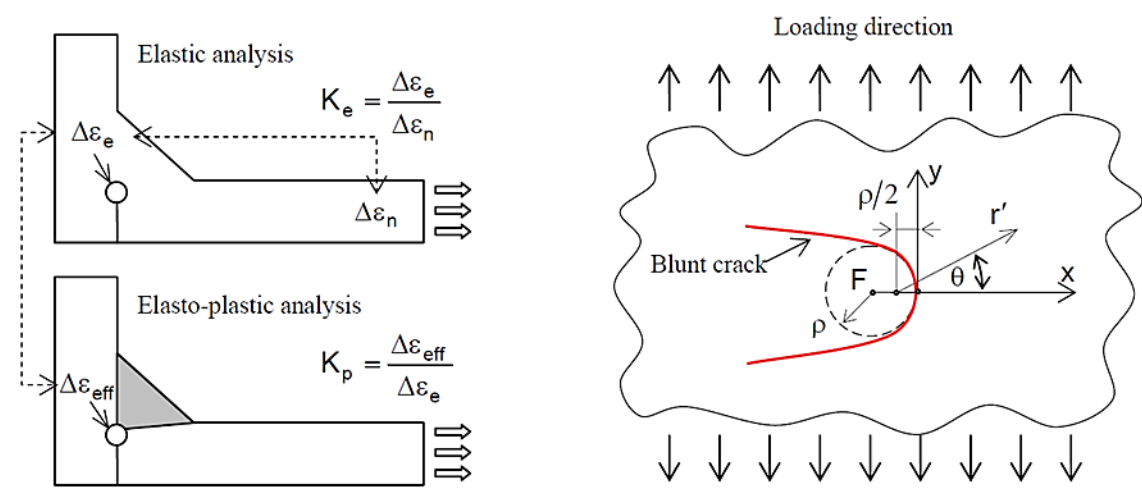


Figure 116: Concept proposed by (Saiprasertkit et al., 2011)

The method predicts effective notch strain range from nominal strain range by elastic analysis using two factors, K_e and K_p . K_e is the ratio between strain range (obtained at the effective notch in elastic analysis) and the nominal strain range (calculated from the nominal stress range in elastic analysis). K_p is the relationship between effective notch strain range and elastic local strain range. By establishing the formulae for K_e and K_p , the effective notch strain range can be determined from the nominal strain range.

$$\Delta \varepsilon_{\text{eff}} = K_p \times K_e \times \Delta \varepsilon_n \quad \text{Eq. 56}$$

Where, $\Delta \varepsilon_{\text{eff}}$ is the effective notch strain range, $\Delta \varepsilon_e$ is the elastic local strain range and $\Delta \varepsilon_n$ is the nominal strain range.

The estimation formula for K_e is derived as follows; Effective notch acts as a blunt crack **Figure 116**. Mode I stress field for a crack in the infinite plate can be expressed as follows:

$$\begin{Bmatrix} \sigma_x \\ \sigma_y \\ \tau_{xy} \end{Bmatrix} = \frac{K_I}{\sqrt{2\pi r'}} \begin{Bmatrix} -\cos \frac{3\theta}{2} \\ \cos \frac{3\theta}{2} \\ -\sin \frac{3\theta}{2} \end{Bmatrix} + \frac{K_I}{\sqrt{2\pi r'}} \cos \frac{\theta}{2} \begin{Bmatrix} 1 - \sin \frac{\theta}{2} \sin \frac{3\theta}{2} \\ 1 + \sin \frac{\theta}{2} \sin \frac{3\theta}{2} \\ \sin \frac{\theta}{2} \cos \frac{3\theta}{2} \end{Bmatrix} + \dots \quad \text{Eq. 57}$$

Where, K_I is the stress intensity factor, θ and r' are indicated in **Figure 116**. At the crack tip where $\theta=0$, $r'=p/2$ (p is the radius at the tip), equation (Eq.57) is reduced to,

$$\sigma_y = \sigma_{\text{max}} = \frac{2K_I}{\sqrt{\pi p}} \quad \text{Eq. 58}$$

Where, σ_{max} is the maximum stress at crack tip. Considering the stress intensity factor of load carrying cruciform joints,

$$K_I = M_K \sigma_n \sqrt{\pi a \sec\left(\frac{\pi a}{w}\right)} \quad \text{Eq. 59}$$

$$M_K = A_0 + A_1 \left(\frac{2a}{w}\right) + A_2 \left(\frac{2a}{w}\right)^2 \quad \text{Eq. 60}$$

$$A_0 = 0.956 - 0.343 \left(\frac{H}{t_p}\right)$$

$$A_1 = -1.219 + 6.210 \left(\frac{H}{t_p}\right) - 12.220 \left(\frac{H}{t_p}\right)^2 + 9.704 \left(\frac{H}{t_p}\right)^3 - 2.741 \left(\frac{H}{t_p}\right)^4$$

$$A_2 = 1.954 - 7.938 \left(\frac{H}{t_p} \right) + 13.299 \left(\frac{H}{t_p} \right)^2 - 9.541 \left(\frac{H}{t_p} \right)^3 + 2.513 \left(\frac{H}{t_p} \right)^4$$

Where, H is the weld leg size, 2a is the crack length, w=2H+tp (tp is the plate thickness of the loading plate) and σ_n is the nominal stress. From equation (Eq.59) and equation (Eq.60), given

$$\sigma_{\max} = 2M_K \sigma_n \sqrt{\left(\frac{a}{\rho} \right)} \sqrt{\sec\left(\frac{\pi a}{w} \right)} \quad \text{Eq. 61}$$

K_e is expressed as:

$$K_e = \frac{\Delta \varepsilon_e}{\Delta \varepsilon_n} = \frac{\sigma_{\max}}{\sigma_n} = 2M_K \sqrt{\left(\frac{a}{\rho} \right)} \sqrt{\sec\left(\frac{\pi a}{w} \right)} \quad \text{Eq. 62}$$

Where, the crack tip radius is 1.0mm for the effective notch.

The estimation formula for K_p is derived as follows; Considering influencing parameters as plate thickness, weld leg size, incomplete penetration ratio and matching ratio on the relationship between effective notch strain range and elastic local strain range together with fitting the relationship with formula by regression analyses. K_p is expressed as:

$$K_p = \frac{\Delta \varepsilon_{\text{eff}}}{\Delta \varepsilon_e} = \alpha + \beta (\Delta \varepsilon_e)^{\gamma-1} \quad \text{Eq. 63}$$

Where α is a material constant, β is an empirical parameter and γ is a material parameter.

Hence; the correlation is

$$\Delta \varepsilon_{\text{eff}} = K_p \times K_e \times \Delta \varepsilon_n = \left(2M_K \sqrt{\left(\frac{a}{\rho} \right)} \sqrt{\sec\left(\frac{\pi a}{w} \right)} \right) (\alpha + \beta (\Delta \varepsilon_e)^{\gamma-1}) \times \Delta \varepsilon_n \quad \text{Eq. 64}$$

The proposed formula can be applied to both the elasto-plastic and elastic regions, because K_p is 1.0 in the elastic conditions ($\Delta \varepsilon_{\text{eff}} = \Delta \varepsilon_e$), meaning the formula is consistent with the previously proposed formula in terms of the stress concentration factor.

The proposed formula was verified as the nominal strain range at the loading plate (obtained from the elastic analysis) were substituted into equation (Eq.64) and the resulting effective notch strain range is plotted against the fatigue test results in **Figure 115**, along with the fitted curve and the lower bound from **Figure 117**.

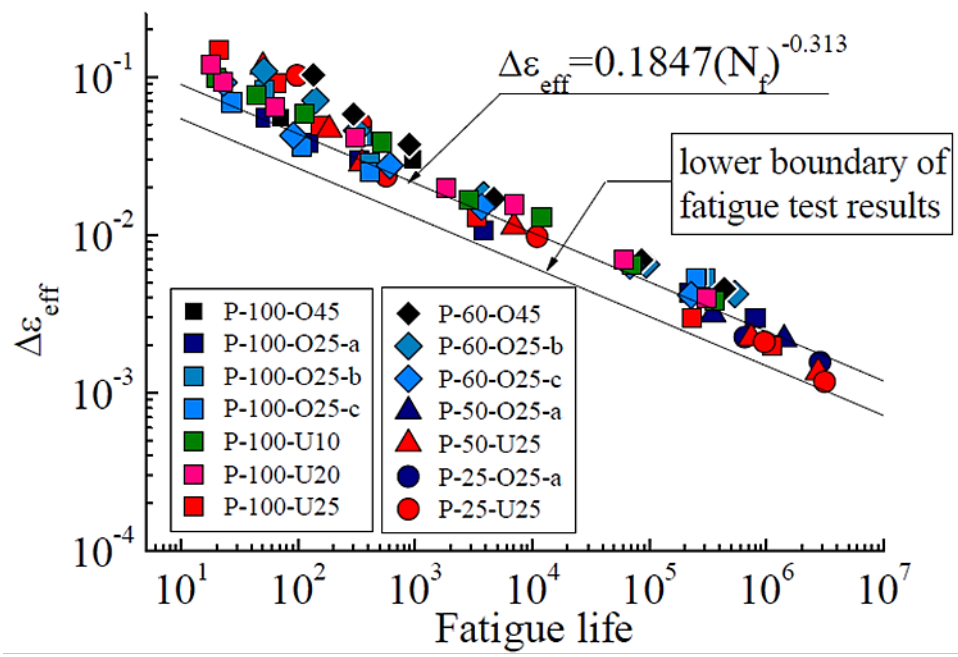


Figure 117: Application of proposed method to experimental results (Saiprasertkit et al., 2011)

3.3 Effective Notch Strain Application

More recently, Fricke et al., (2013) carried out experimental and numerical analysis of LCF on Web Frame Corner in ships. This analysis was based on the correlation previously discussed. This is perhaps the most advanced experimental and numerical analysis in LCF testing. Their conclusion is that high elastic plastic stresses and strains occur in front of the critical weld toe i.e. in the base metal. A brief description of the experimental and numerical analysis is presented here:

With the objective of a practical design procedure, the IIW commission XIII carried out experimental LCF test on a large scale mild steel web frame corner shown in **Figure 118**.

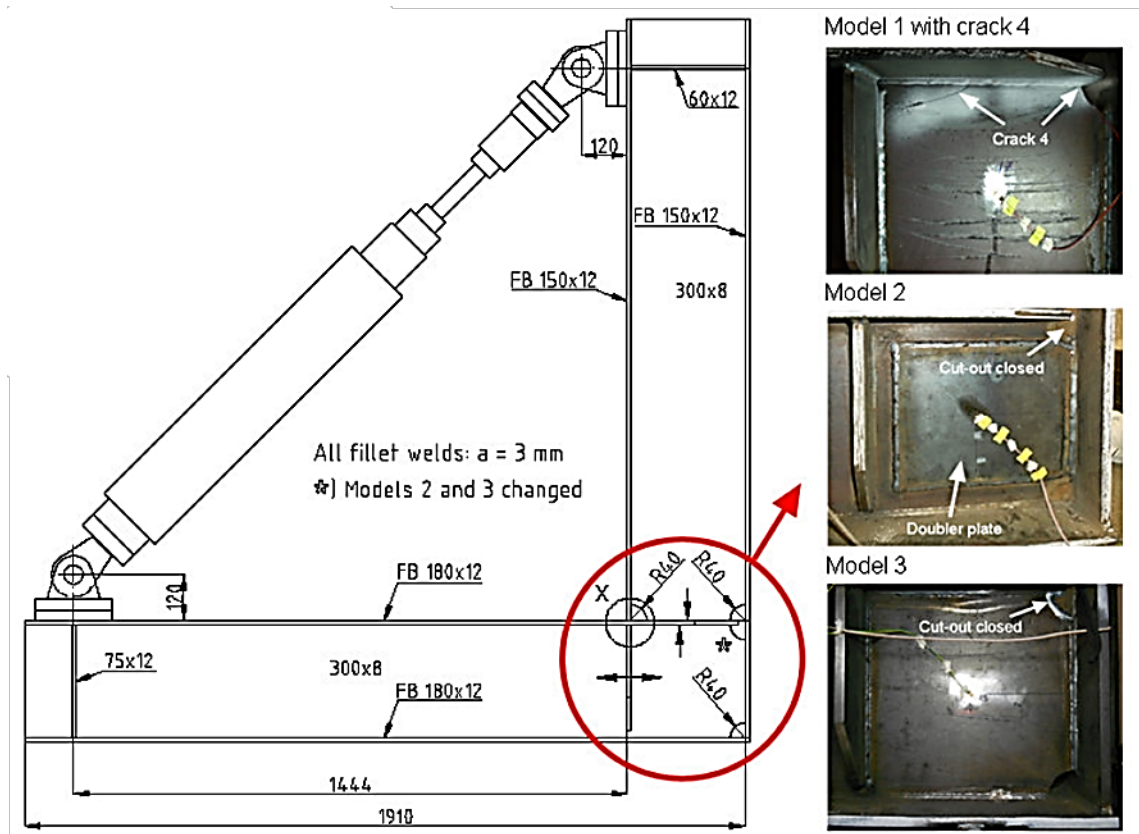


Figure 118: Investigated Structure (Fricke et al., 2013)

The test showed that the most critical crack at upper weld toe (crack 2 at HS2) presented in **Figure 119**. Crack 1 at lower weld toe and crack 3 at scallop initiated earlier, but were less critical.

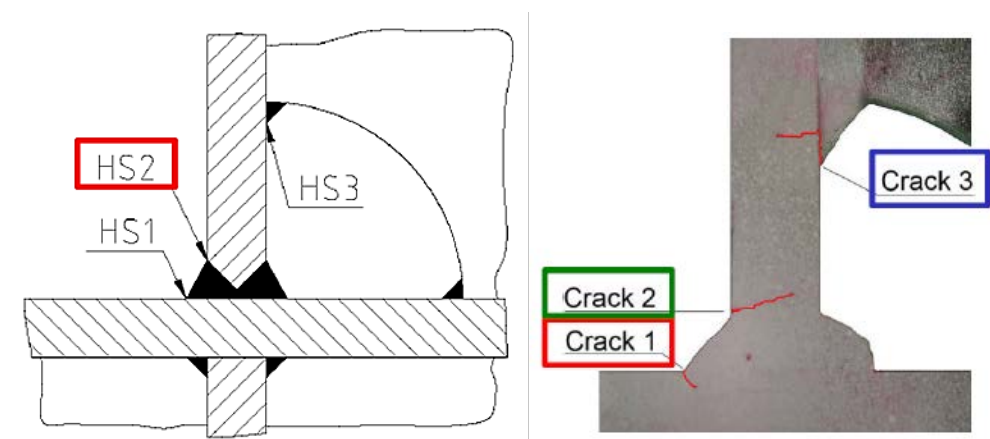


Figure 119: Observed cracks (Fricke et al., 2013)

In the linear FE analysis, extrapolation of stresses was over $(0.4 \times t)$ and $(1 \times t)$ in front of weld toe, the largest structural stress is at HS2. The structural stress at hot spots in elastic range for 25 kN load are presented in **Table 9**:

Table 9: Structural stress at hot spots in elastic range. Fricke et al., (2013)

Hot Spot	Model 1		Model 2		Model 3	
	σ_{HS} (MPa)	SCF	σ_{HS} (MPa)	SCF	σ_{HS} (MPa)	SCF
HS1	103	2.4	96	2.2	104	2.4
HS2	174	3.5	156	3.1	172	3.4
HS3	138	2.8	138	2.8	137	2.8

In the nonlinear FE analyses, the cyclic properties of the base metal, weld metal and HAZ are assumed to be the same for simplification.

For the assessment of notch strain; load carrying cruciform joints with elastic-plastic strain were tested with 1mm radius at the notch at HS2 with local mesh of 0.2mm element size. For S–N curve of effective notch strain range, equations (Eq.53, Eq.54 and Eq.55) were used. The failure criterion was 5 % strain drop.

The S–N curve for effective strain range is presented in **Figure 120**:

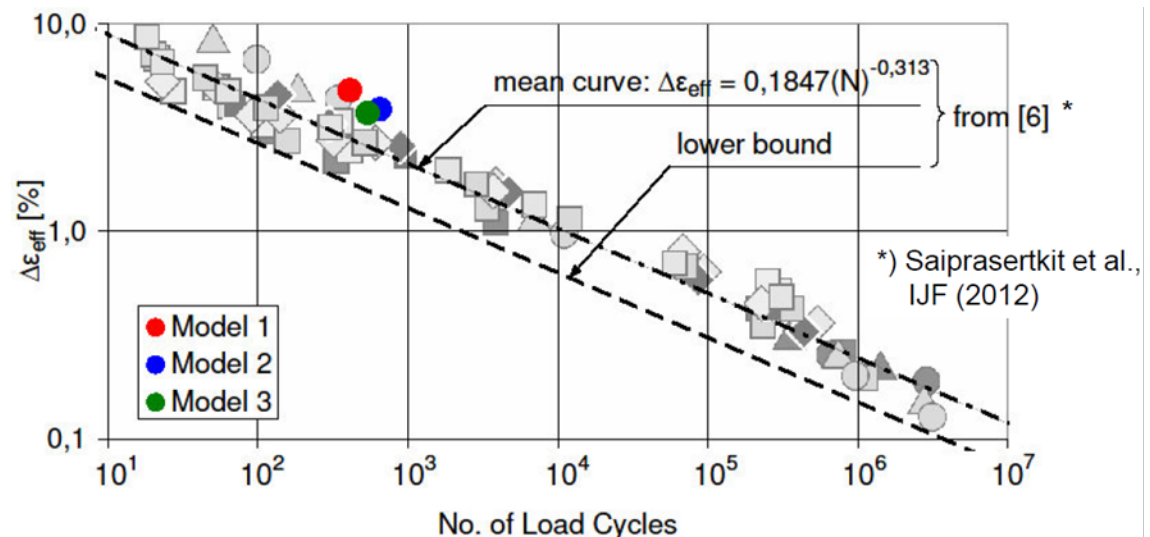


Figure 120: S–N curve for effective strain range (Fricke et al., 2013)

3.4 Conclusion

1. In contrast to widely applied nominal and structural hot-spot stress approaches, notch stress approach can explicitly consider the shape of the weld.

2. The effective notch stress concept for fatigue prediction of welded joints is considered to be the most recent model for fatigue assessment of welded joints.
3. The effective notch strain approach adopted by IIW in LCF assessment has established correlation between effective notch strain range and nominal strain range. The study concluded that strength mis-matching between deposit metal and base metal has significant influence on LCF strength and negligible influence on HCF strength.
4. The use of transverse attachment as a test specimen for LCF assessment is very common both on small and large scale.
5. The effective notch stress (fictitious radius) originally used for HCF can be adopted for LCF.

Chapter 4

Classification Societies

4 CHAPTER 4: LCF in Class Societies (State of the Art)

This chapter reviews the state-of-the-art in LCF assessment procedures recommended by four class societies. The approach is to map and compare their procedure. This chapter may be used in the future as the foundation of the common LCF assessment procedure for FPSO and may be put forward for the International Association of Class Societies (IACS) once the FPSO common structure rule becomes a reality. Two case studies were considered and representative loading conditions for LCF assessment has been presented.

4.1 DNV, Daewoo Shipbuilding & Marine Engineering Co., Ltd (DSME) and Inha University

In a joint project between DNV (Korea and Norway), DSME (Korea), Inha University and Inha College (Korea); fatigue tests in high stress and low cycle regime were carried out on base metal as well as welded joints to unveil LCF performance. Also a simplified procedure has been developed to assess LCF strength of ship structures using pseudo elastic stress range. The following are some summaries of the main findings/conclusions of the study:

LCF assessment procedures for ship structures have not been developed in class societies due to a number of reasons stated by (Urm et al., 2004a), these are:

1. Cyclic stress-strain curves for steel materials and weld metal commonly used for new building of ships are not available.
2. A procedure to obtain the damage due to LCF is not available.
3. A procedure to combine damages due to HCF and LCF is not available.
4. Strain-cycle curves or stress-cycle curves are not developed for low cycle high stress regions below 10^4 cycles.

Urm et al., (2004a) suggested that two options are available to express fatigue life in low cycle regime; the strain life curve or the equivalent elastic notch stress and pseudo stress. The first option is preferred by researchers but the second is the one used in industry by many design codes for the following reasons:

1. Most ship designers are familiar with the use of notch stress range for fatigue strength evaluation since S–N curves are widely used.

2. It is time consuming to derive the strain concentration factors of many features of the ship structure while it is more convenient to use the existing stress concentration factors available within the common design codes.
3. It is convenient to combine the fatigue damage due to LCF with HCF.

Urm et al., (2004a) outlined the most vulnerable critical locations for LCF in bulk carriers as:

1. Web stiffeners on top of bottom and inner bottom longitudinals.
2. Heel and end connections of horizontal stringers in transverse bulkheads to longitudinal bulkhead.
3. Lower stool connection to inner bottom.

Urm et al., (2004a) outlined the load conditions and critical locations to be considered in terms of LCF for tankers as:

1. Longitudinal connections at full load draft and ballast.
2. Lower and upper hopper knuckle connections at shallowest draft and deepest draft.
3. Horizontal stringers of transverse bulkhead at shallowest draft and deepest draft.

4.1.1 Strain Life Method

This is the most preferred method of assessment of LCF by researchers. The basic assumption of strain life method is that smooth specimen (unnotched) tested under strain controlled conditions can simulate fatigue damage at the notch root of actual structural component. i.e. the same amount of fatigue damage is assumed to occur in the material at notch root and in the smooth specimen when both are subjected to identical stress strain conditions. Strain life method is related to crack initiation not crack propagation because strain control assumption is not valid when crack grows to be a larger one. Urm et al., (2004b)

4.1.2 Equivalent Elastic Notch Stress and Pseudo Stress

Pseudo stress is another option that can be used in LCF assessment and it is the most preferred by design codes. Pseudo stress is defined as actual strain times elastic modulus; actual strain is determined by elasto-plastic analysis. **Figure 121** shows actual, equivalent elastic and pseudo stress with its elastic and elasto-plastic stress strain relations. Actual stress is the stress located on the intersection point between Neuber's

curve and actual stress strain curve, B. Pseudo stress goes up to point A. Equivalent elastic stress is obtained by Neuber's rule leading to point C. Urm et al., (2004b)

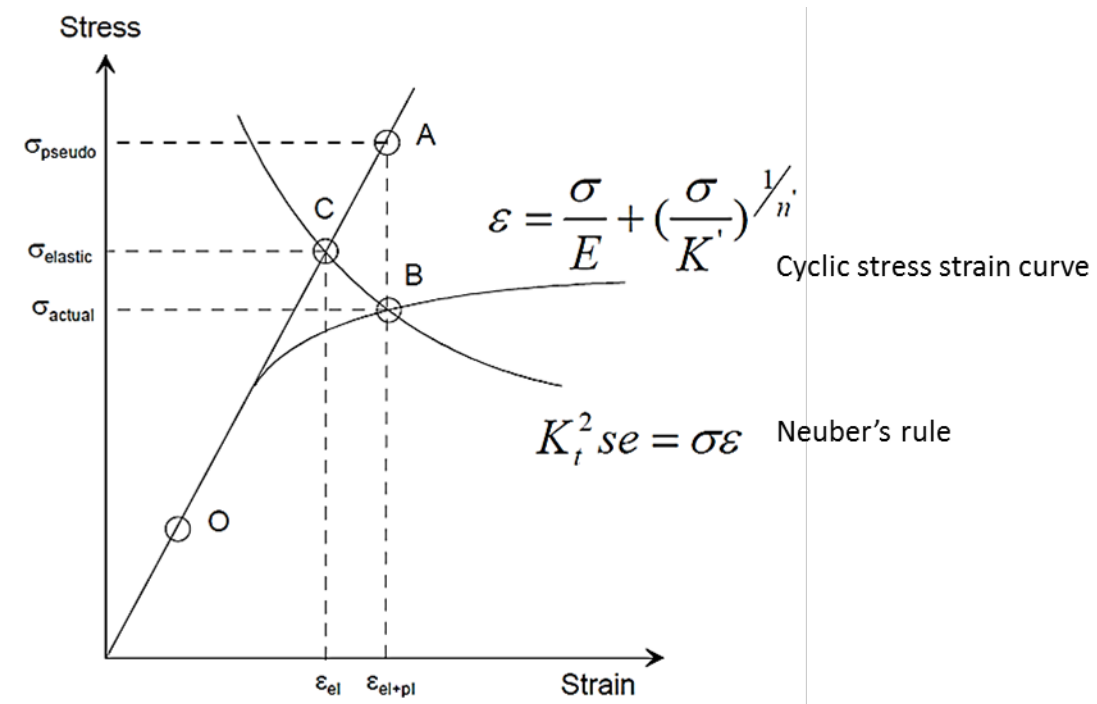


Figure 121: Actual, Equivalent Elastic and Pseudo Stress (Urm et al., 2004b)

Where definition of stresses and strains are as follows (DNV-CN-No.30.7, 2010):

- σ_{pseudo} - Pseudo linear elastic stress
- σ_{elastic} - Linear elastic stress by FEA
- σ_{actual} - Actual stress at hot spot
- $\epsilon_{\text{elastic}}$ - Elastic strain from linear FEA

4.1.3 Plasticity Correction

Urm et al., (2004a) described a simplified approach to obtain the LCF stress range with a plasticity correction factor. The approach is based on converting the total strain to the pseudo elastic stress range using the concept of a plasticity correction factor. The calculated stress ranges (from the simplified approach or the linear elastic finite element analysis) is multiplied by the plasticity correction factor to obtain the pseudo elastic stress range. The calculated stress ranges for LCF is corrected using a plasticity correction factor in order to employ the S–N curve instead of a strain cycle curve. The plasticity correction factor, k_e used in BS5500 may be used when the cyclic stress strain

relation is not known. If cyclic stress strain curves are known; Neuber's rule or Glinka's rule can be used for the calculation of plasticity correction factor.

4.2 S-N Curve Applied for LCF

Pseudo hot spot stress vs. number of cycles to failure, with TWI (1974) and Heo et al. (2004) data based on a Neuber correction is shown in **Figure 122**:

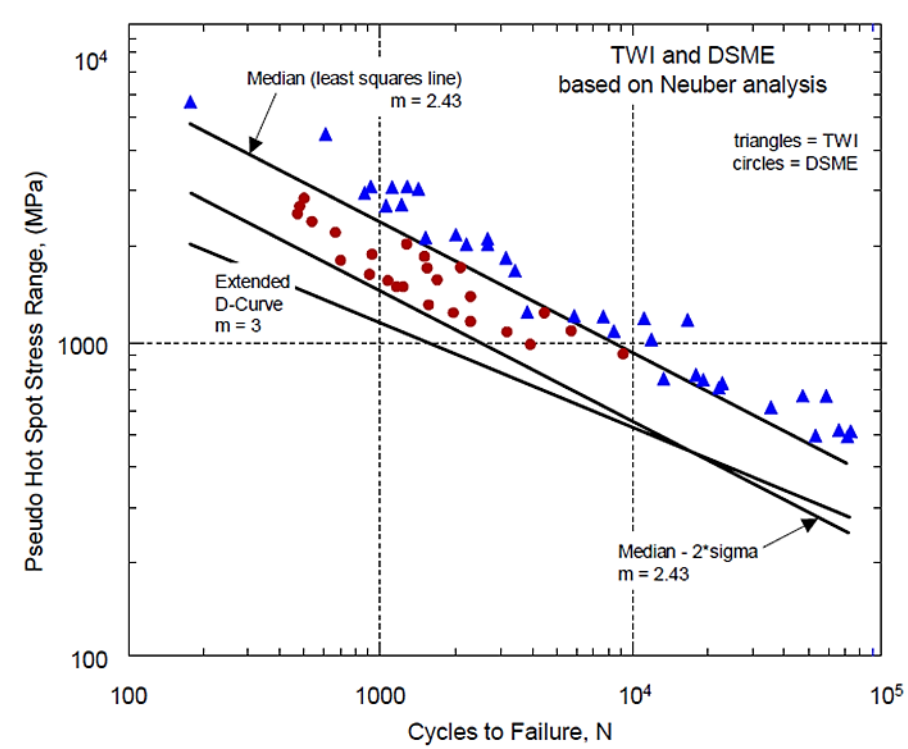


Figure 122: S–N curve in low cycle region (Wang et al., 2006)

TWI used a longitudinal non load carrying fillet weld specimen (SCF 1.55) shown in **Figure 123**:

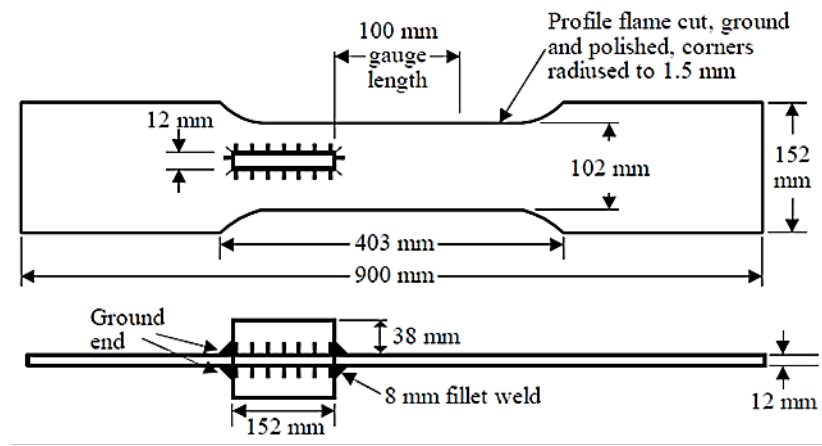


Figure 123: Test specimen from TWI (1974) (Wang et al., 2006)

The final failure was taken as the point at which a sudden drop occurred in the cyclic tensile load. The D curve is also plotted in **Figure 122** for reference. The median of the pooled TWI and DSME data is calculated based on least square fit. A design curve is normally defined as the median curve minus two standard deviations. For low cycle region, $N < 10^4$, using D curve, as a design S–N curve for LCF, yields conservative results. Heo et al. (2004) test data is based on fatigue testing of a non-load-carrying partially penetrated cruciform fillet joint (SCF 1.28), as shown in **Figure 124**:

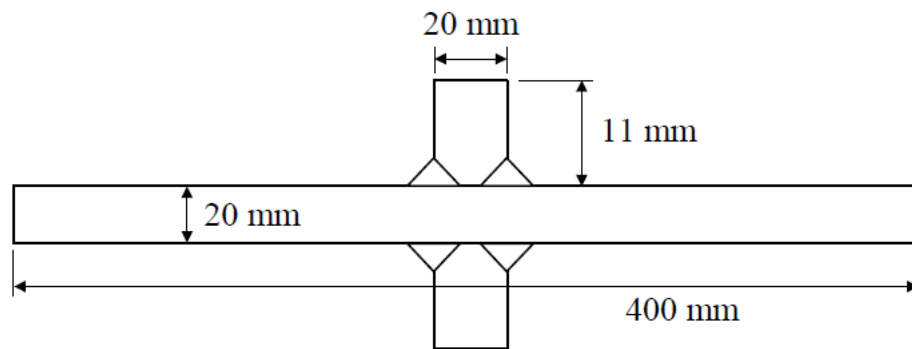


Figure 124: Testing specimen presented in Heo et al. (2004) (Wang et al., 2006)

The test was carried out under strain control condition and strain ratio was set to be zero which means strain value fluctuates between zero and specified maximum value (tension cycles only or half cycle, i.e. no compression). Test was stopped when the load dropped down to 50% of initial value which corresponded to small amount of crack propagation. The inverse slope of the median 2 standard deviation curve is 2.43.

From **Figure 125** showing the Park Lawrence model (strain life curves for HAZ) and the experimental data in **Figure 122**, Wang et al observed that there is a tendency for the S–N curve to have a curvature that bends upwards in the area where cycle to failure is below 1000. It will be ideal that this tendency be reflected in the design S–N curve for LCF, although using D curve would be conservative, modifying D curve for cycles to failure less than 1000 may complicate the damage model calculation. Wang et al., (2006)

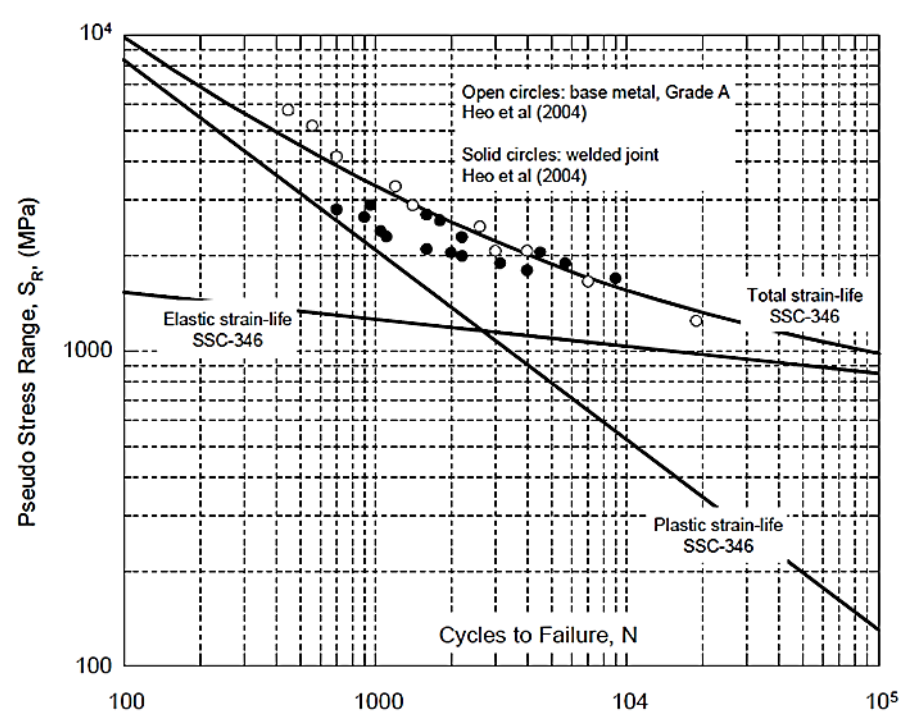


Figure 125: Strain-life curve (Wang et al., 2006)

In the British standard, the design S–N curves for the assessment of weld details in **Figure 126** have been derived from fatigue test data obtained from welded specimens. These welded specimens were fabricated to normal standards of workmanship and tested under load control or, for applied strains exceeding yield (LCF), under strain control. Continuity from low cycle regime to high cycle regime is achieved by expressing the low cycle data in terms of pseudo elastic stress range (i.e. strain range multiplied by elastic modulus). Regression analysis of the fatigue test data gave the

mean S–N curve and standard deviation of log N. The curves in **Figure 126** are two standard deviations below the mean, representing approximately 97.7 % probability of survival.

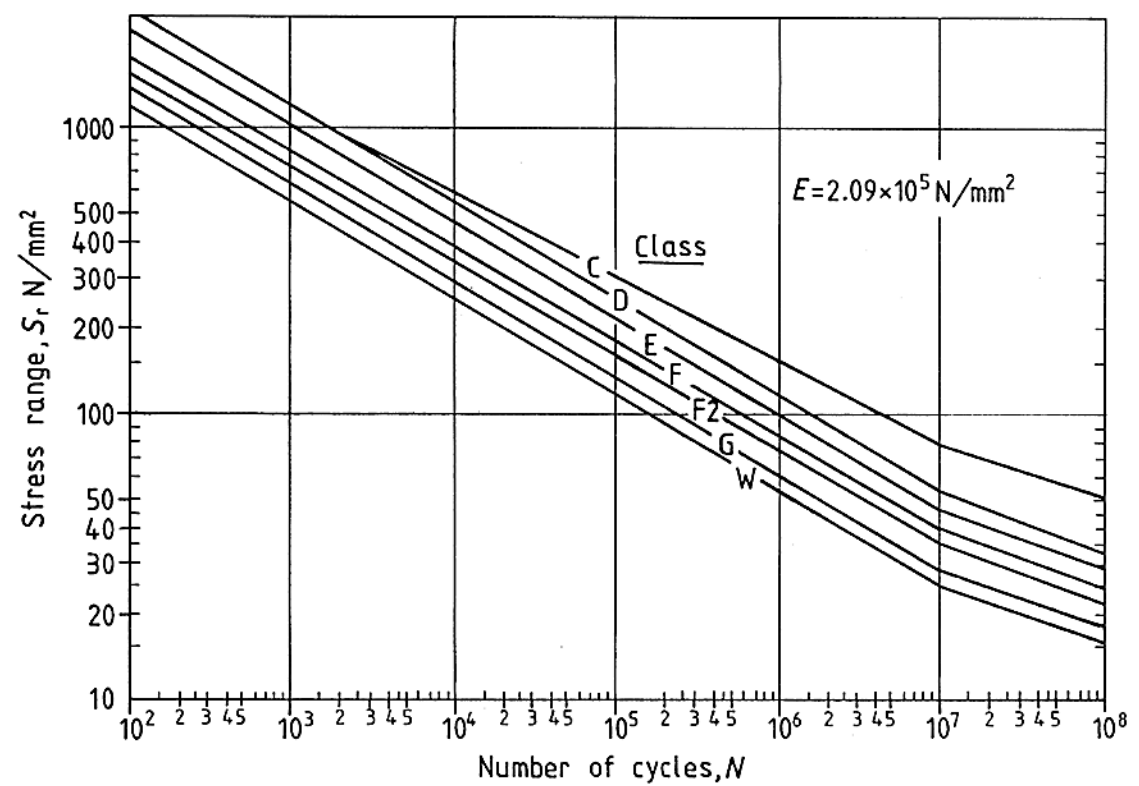


Figure 126: Fatigue design S–N curves for weld details of materials stated below (PD5500, 2011)

The S–N curves in **Figure 126** have the form:

$$S_r^m N = A \quad \text{Eq. 65}$$

Where

S_r is the stress range, m and A are constants given in **Table 10**. Different values apply for lives up to 10^7 cycles and for above 10^7 cycles.

Table 10: Details of fatigue design curves PD5500 (2011)

Class	Constants of S-N curve				Stress range at
	For N < 10 ⁷ cycles		For N > 10 ⁷ cycles		N = 10 ⁷ cycles
	m	A ^a	m	A ^a	N/mm ²
C ^b	3.5	4.22 x 10 ¹³	5.5	2.55 x 10 ¹⁷	78
D	3	1.52 x 10 ¹²	5	4.18 x 10 ¹⁵	53
E	3	6.33 x 10 ¹¹	5	2.29 x 10 ¹⁵	47
F	3	4.31 x 10 ¹¹	5	1.02 x 10 ¹⁵	40
F2	3	2.50 x 10 ¹¹	5	5.25 x 10 ¹⁴	35
G	3	1.58 x 10 ¹¹	5	2.05 x 10 ¹⁴	29
W	3		5	9.77 x 10 ¹³	25

^a For E = 2.09 x 10⁵ N/mm²

^b If S_r > 766 N/mm² or N < 3 380 cycles, use class D curve.

4.3 Lloyd's Register and Glasgow & Strathclyde Universities

In a joint project with the universities of Glasgow and Strathclyde, Lloyd's Register investigated the LCF damage on critical structural details of FPSOs due to the loading and unloading of cargo and ballast. Also, a detailed finite element analysis was performed on a single hull FPSO module to check the LCF strength of highly stressed locations and to provide an insight into the mechanism of loading and offloading. The following are some summaries of the main findings/conclusions of the study:

4.3.1 Simplified LCF Assessment

A simplified LCF assessment based on the stress based approach involves the following six main steps Raji (2010):

1. Selection of the structural details to be analysed,
2. Defining load configuration that is characteristic of a typical loading and unloading cycle experienced by the FPSO,
3. Calculation of still water stresses for each loading condition,
4. Defining stress sequence in a complete loading and unloading cycle and evaluating stress ranges and cycles using counting methods,

5. Evaluation of the pseudo elastic stress ranges using a plasticity correction method in order to employ the S–N curve,
6. Calculation of fatigue damage per cycle based on S–N curve and then the cumulative fatigue damage for the design life based on the number of loading and unloading cycles using Miner’s rule.

All methods recommended by three class societies ABS, DNV and LR for the LCF assessment are variations of the stress based fatigue assessment procedure. Raji also noted that the guidance notes are similar in the use of rain flow counting algorithm, the plasticity correction factor calculations, the use of HCF S –N curve and the use of linear damage law to determine fatigue damage. The major difference noted is in the determination of cumulative fatigue damage. Raji et al., (2009)

The methodologies proposed by the classification societies are all based on the assumption that Miner’s linear damage rule applies and that rainflow analysis is used to identify the stress cycles. The main differences lie in the S-N curve and also the method of accounting for plasticity effects in the calculated stresses. Raji (2010)

4.3.2 LCF Fatigue Damage

ABS, DNV and LR LCF damage rules were compared and the results showed that ABS rule gives the highest fatigue damage for the detail while DNV and LR have similar LCF damage results but are less than the ABS damage values by about 50 % **Figure 127** for structural detail in **Figure 128**.

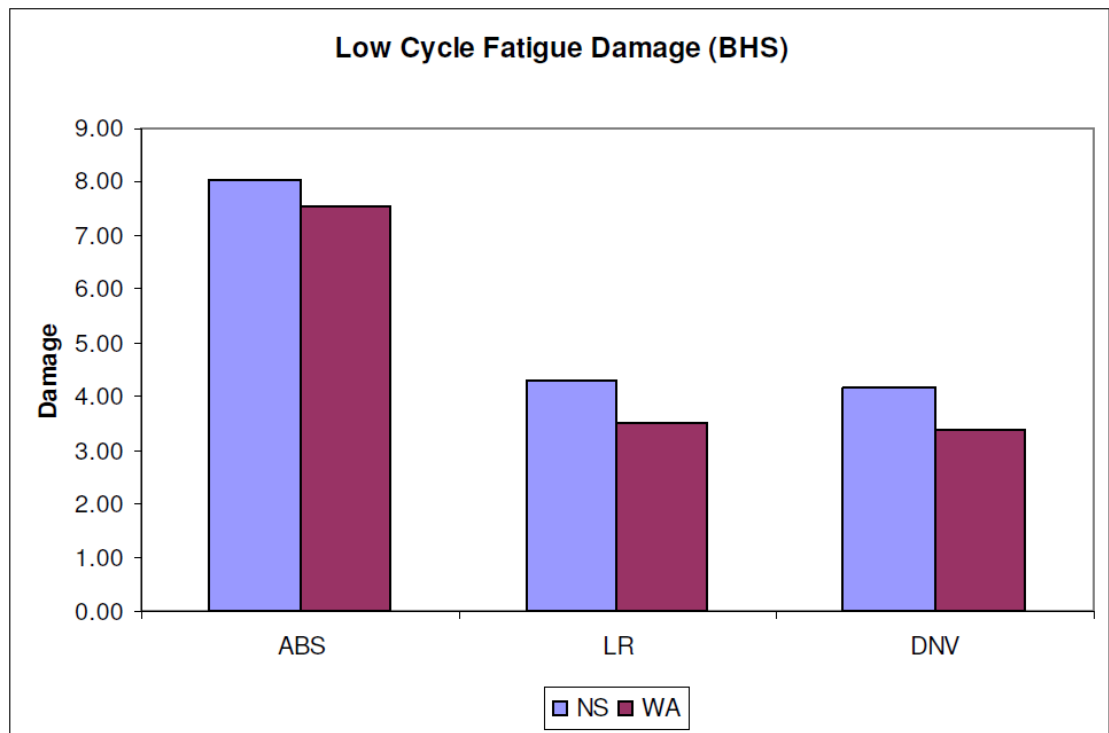


Figure 127: LCF Damage at BHS6 (Raji, 2010)

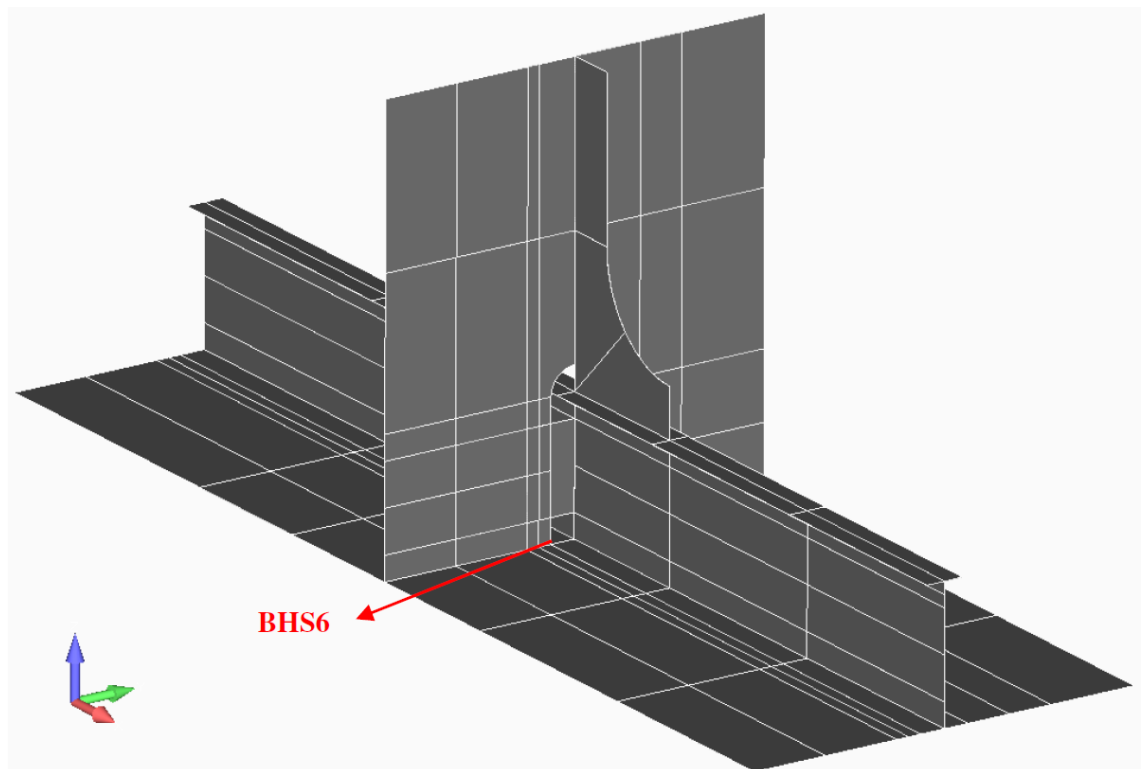


Figure 128: Location of hotspots in bottom detail (Raji, 2010)

Also, the S–N curves did show that irrespective of the large differences obtained in the LCF damage for the different classification societies, the S–N curves produced are quite similar. The higher the stresses in **Figures 129** and **130**, the more the curves converge at a similar value for the number of cycles to failure.

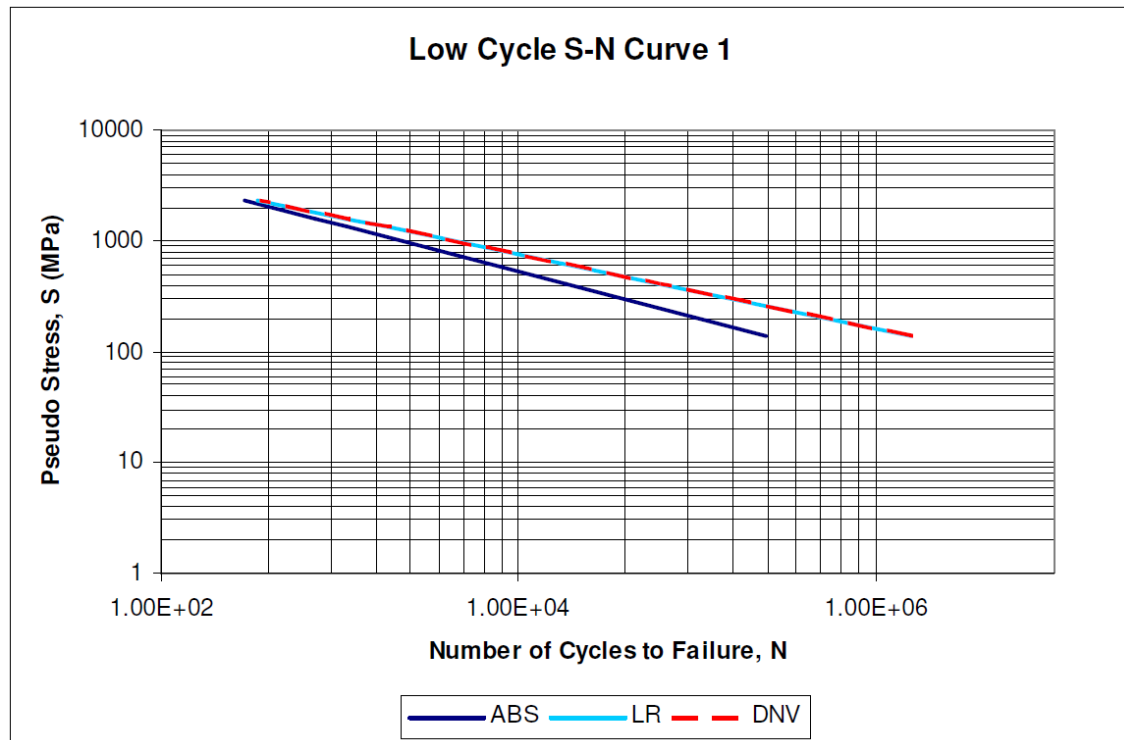


Figure 129: LCF S–N Curve 1 (Raji, 2010)

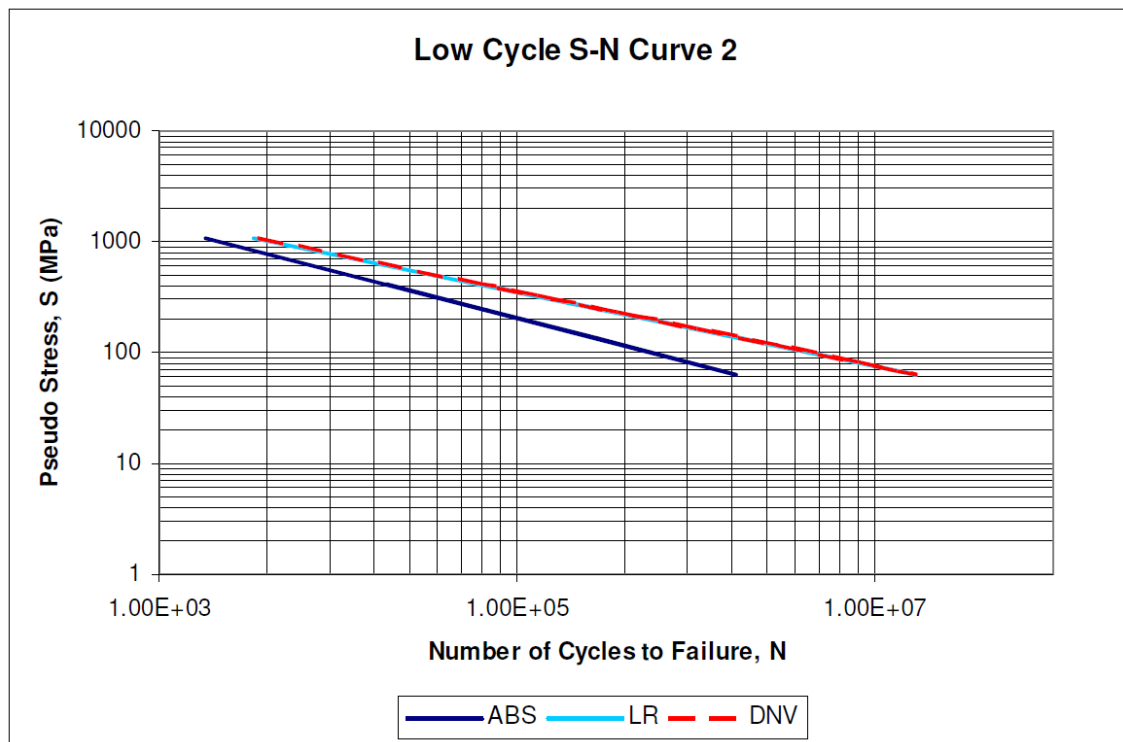


Figure 130: LCF S–N Curve 2 (Raji, 2010)

Figure 131 shows that when the stresses are low, i.e. less than the yield stress of the material, then these curves start to diverge away from an almost uniform solution. Raji (2010)

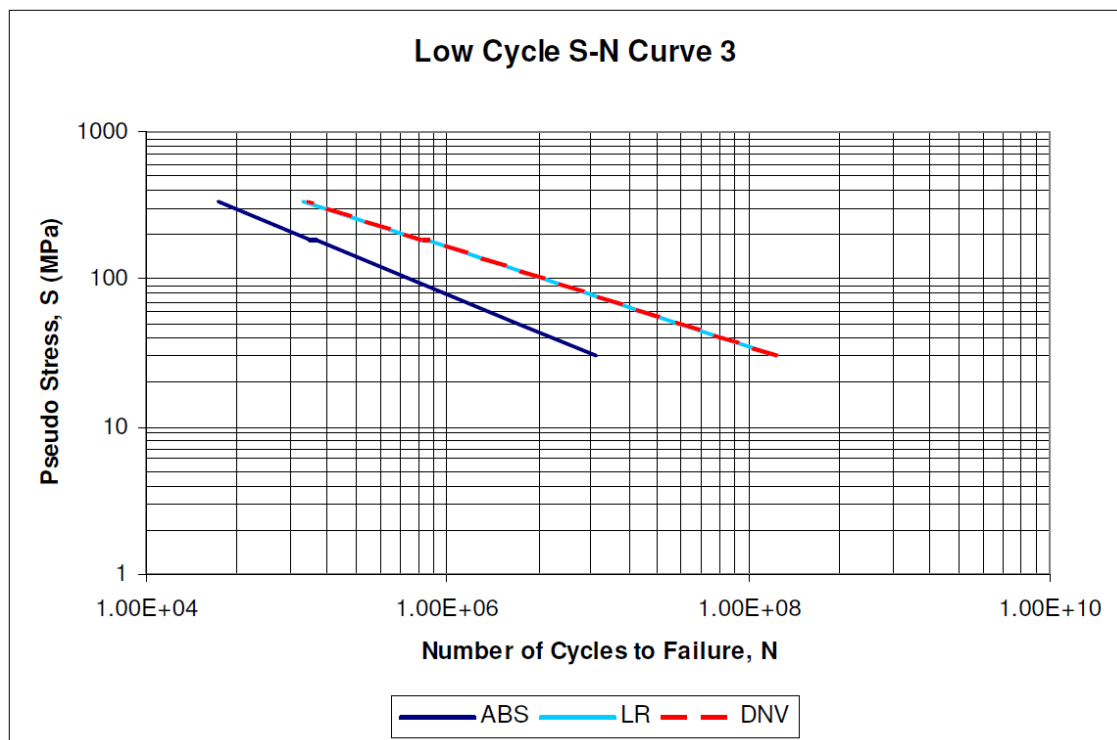


Figure 131: LCF S–N Curve 3 (Raji, 2010)

4.3.3 Combining LCF and HCF

In class society rules, LR and DNV include an adjustment factor to the total damage to account for HCF stresses already included while counting the low cycle stress ranges. ABS considers this adjustment in the form of a constant. This adjustment factor in general, is relatively small value compared to the overall fatigue and may have a negligible effect on the total fatigue damage of the structure. Raji (2010)

4.4 Class Societies LCF Procedures Overview

4.4.1 American Bureau of Shipping

4.4.1.1 Loading Conditions

Four loading conditions may be considered for LCF assessment of FPSO with double hull or double side single bottom; these are:

1. Loading condition 1; 0.4 x scantling draught or actual minimum onsite operating ballast draught if greater than 0.4 x scantling draught but not to exceed 0.6 x scantling draught. This condition is also used for transit condition with actual transit draught between 0.1 x scantling draught and 0.6 x scantling draught.

2. Loading condition 2; 0.57 x scantling draught.
3. Loading condition 3; 0.73 x scantling draught.
4. Loading condition 4; 0.9 x scantling draught or actual maximum onsite operating full load draught if greater than 0.9 x scantling draught.

4.4.1.2 Load Cases

Typical structural analysis is performed with 33 frequencies (0.2 to 1.80 rad/s at a 0.05 increment) and 12 wave headings (0 to 360 degree at a 30-degree increment). Significant reduction in the number of heading angles, hence load cases, to be analysed is possible in the on-site analysis of a FPSO system with a weathervaning turret mooring. A minimum of 5 heading angles, predominant heading and 30 and 60 degrees off either side of predominant heading, is considered sufficient. For example, with 3 basic loading conditions the number of load cases for analysis is $(33 \times 2 \times 5 \times 3) = 990$ instead of 2376.

4.4.1.3 Structural Details

4.4.1.3.1 Loads considered for High Cycle (Dynamic Loads)

1. Hull girder loads (i.e. vertical and horizontal wave bending moments)
2. Dynamic wave pressure
3. Dynamic tank pressure loads resulting from installation motion

4.4.1.3.2 Loads considered for Low Cycle (Static Loads)

1. Static cyclic loads due to cargo loading and offloading

4.4.1.3.3 Loading Conditions Selected for LCF

For locations at longitudinal end connections:

1. Full load condition with design still water bending moment (loading condition 4).
2. Ballast or light draft condition at with design still water bending moment (loading condition 1).

For locations other than longitudinal end connections:

The maximum LCF damage calculated from the following two pairs:

Pair 1

1. Full load condition with design still water bending moment (loading condition 4).
2. Ballast or light draft condition with design still water bending moment (loading condition 1).

Pair 2

1. Intermediate condition with design still water bending moment (loading condition 3)
2. Intermediate condition with design still water bending moment (loading condition 2)

4.4.1.3.4 Hot spot stress

This approach is used for fatigue evaluation of the following details:

1. Connections of Longitudinal Stiffeners to Transverse Web/Floor and to Transverse Bulkhead:
 - ii. Two to three selected side longitudinals in the region from the 1.1 draft to about 1/3 draft in the midship region and also in the region between 0.15L and 0.25L from F.P., respectively,
 - iii. One to two selected longitudinals from each of the following groups:
 - a. Deck longitudinals, bottom longitudinals, inner bottom longitudinals and longitudinals on side longitudinal bulkheads,
 - b. One longitudinal on each of the longitudinal bulkheads within 0.1D from the deck is to be included.
2. Shell, Bottom, Inner Bottom or Bulkhead Plating at Connections to Webs or Floors (for Fatigue Strength of Plating):
 - i. One to two selected locations of side shell plating near the summer load waterline (LWL) amidships and between 0.15L and 0.25L from F.P. respectively,
 - ii. One to two selected locations in way of bottom and inner bottom amidships,
 - iii. One to two selected locations of lower strakes of side longitudinal bulkhead amidships.
3. Connections of the Slope Plate to Inner Bottom and Side Longitudinal Bulkhead Plating at the Lower Cargo Tank Corners:

- i. One selected location amidships at transverse web and between webs, respectively.
4. End Bracket Connections for Transverses and Girders:
 - i. One to two selected locations in midship region for each type of bracket configuration.

4.4.1.4 Stress Range Calculations

4.4.1.4.1 Elastic Hot Spot Stress

The stress considered is the elastic hot spot stress at the toe of the weld and it is assumed that the S–N curve defining fatigue strength is in the pseudo hot spot stress. The stress process **Figure 132**, is considered as a superposition of wave induced stresses (high cycle), $S_W(t)$, and stresses associated with static load (low cycle), $S_B(t)$. The cycles of S_B result from the loading/offloading process. The total stress is:

$$S(t) = S_B(t) + S_W(t) \quad \text{Eq. 66}$$

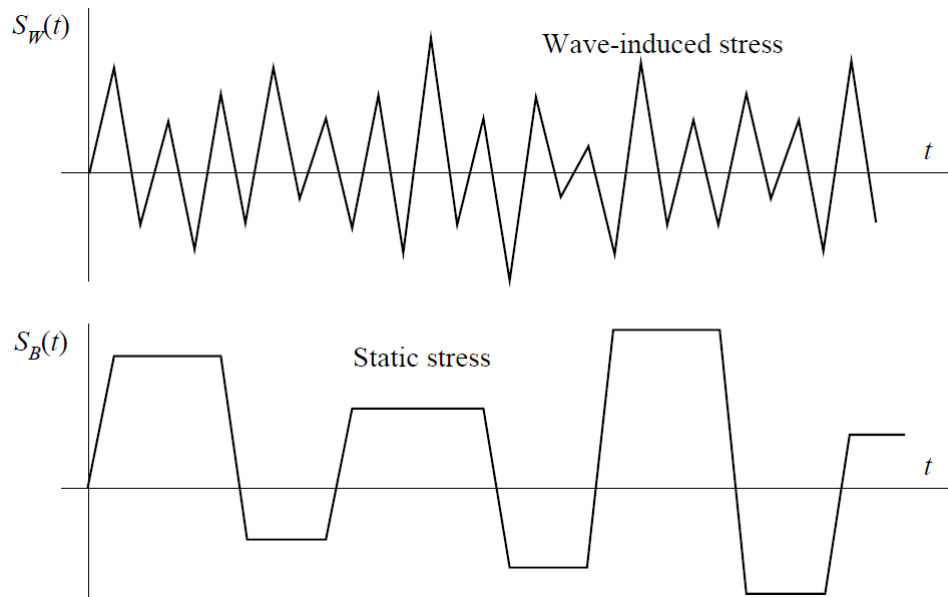


Figure 132: Sample Functions of S_W and S_B (ABS-SBFA, 2010)

In one cycle of the static process, **Figure 133**, the total stress range associated with this cycle is S_E ,

$$S_E = S_B + 0.5(S_M^i + S_M^j) \quad \text{Eq. 67}$$

Where

S_B = static stress range for this cycle

S_M^i = median of the largest stress range of wave induced load for i-th load condition

S_M^j = median of the largest stress range of wave induced load for j-th load condition

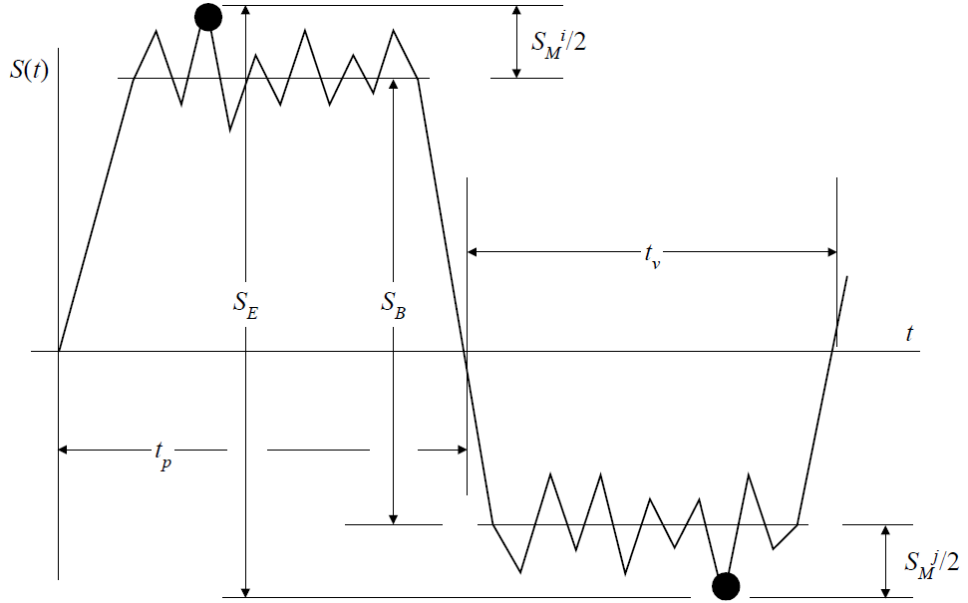


Figure 133: A Single Loading/Offloading Cycle (ABS-SBFA, 2010)

From extreme value theory, the median largest stress range S_M^i in n cycles is given as:

$$\frac{S_M^i}{\delta} = [-\ln(1 - 0.5^{1/n})]^{1/\gamma} \quad \text{Eq. 68}$$

Where

γ and δ are the long term stress shape and scale factors, respectively.

δ can be determined statistically from long term records of stress ranges or can be calculated by the formula:

$$\delta = \frac{S_R}{[\ln(N_s)]^{1/\gamma}} \quad \text{Eq. 69}$$

Where

S_R is the stress range associated with a probability of exceedance of $1/N_s$, and N_s is equal to 10^4 . n may be computed by taking the estimated time for a half cycle divided by the estimated wave period.

The number of cycles for installation's loading and unloading, n_{LCF} , is assumed to be not less than 1200 for 20 years.

Assuming there are 10^8 wave cycles within 20 years, n is then equal to:

$$\frac{10^8}{n_{LCF} \times 2}$$

Note: it is expected that the time in tension will not equal the time in compression. The larger of the two should be selected for conservative analysis.

4.4.1.4.2 Pseudo Hot Spot Stress

To transform elastic hot spot stress range to pseudo hot spot stress range, a plasticity correction factor, k_e , is defined as:

$$k_e = \frac{S_L}{S_E} \quad \text{Eq. 70}$$

Where S_L is the pseudo hot spot stress range.

A plot of k_e as a function of S_E is given, **Figure 134**.

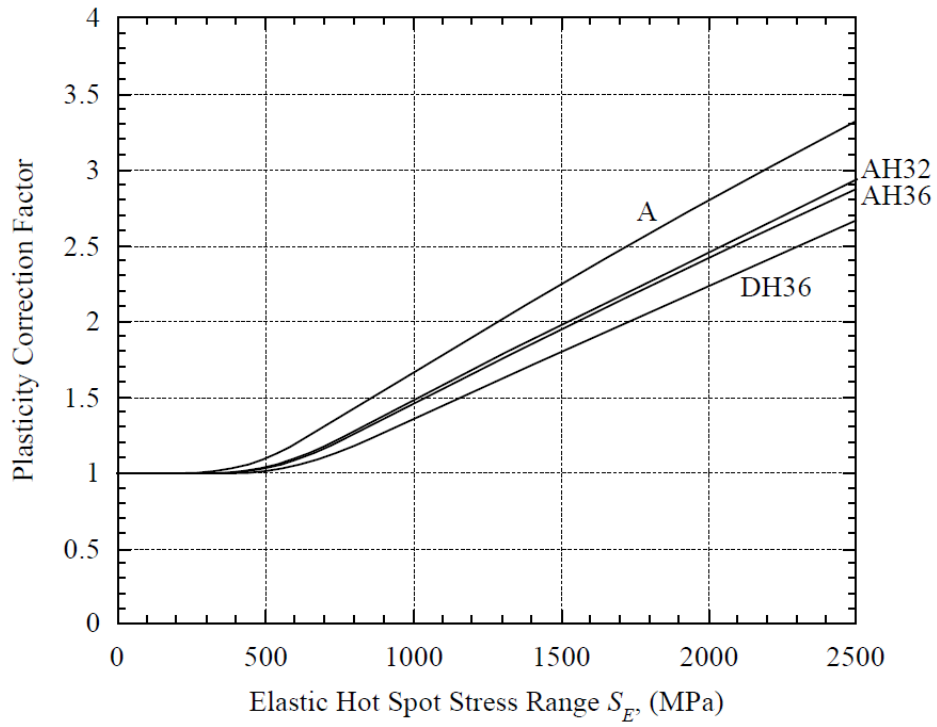


Figure 134: k_e as a Function of S_E (ABS-SBFA, 2010)

An approximate analytical formula derived from the above curves can be used:

$$k_e = 0.5 + k_m S_E$$

k_e should not be less than 1.0,

k_m value of mild steel is 11.20×10^{-4} , other values for various types of steel are given in the code.

4.4.1.4.3 Low Cycle S-N Curve and Damage Calculation

The S-N curve for low cycle region (modified D-Curve) defined in **Figure 135** is given as:

$$NS^q = B \quad \text{for} \quad 100 < N < 10^4$$

Where

$$q = 2.4$$

$$B = 3.51 \times 10^{10} \text{ (MPa)}$$

It is assumed that the LCF design S-N curve is applicable to static induced stresses. Basic application of Miner's rule produces the expression of static stress damage DM_{LCF} is:

$$DM_{LCF} = \frac{N_{LCF} S_L^q}{B} \quad \text{Eq. 71}$$

n_{LCF} is the total cycles of loading/offloading, which is not to be less than 1200 for a ship-type installation to be operated for 20 years.

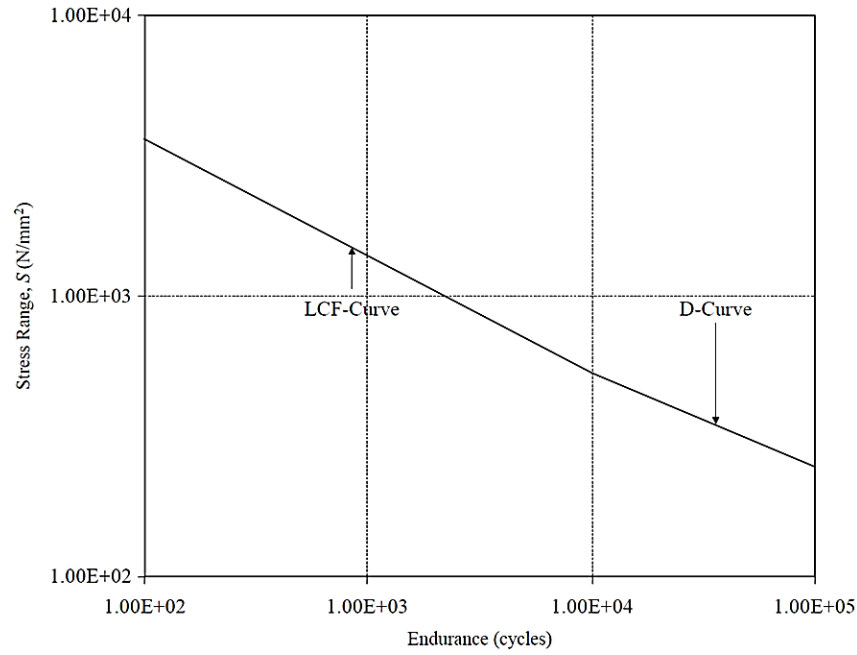


Figure 135: LCF Design Curve (ABS-SBFA, 2010)

4.4.1.5 Combined Low Cycle and High Cycle Fatigue Damage

The total fatigue damage due to both low cycle and high cycle stress can be calculated by:

$$DM_{comb} = \frac{DM_{LCF}^2 + 2 \delta DM_{LCF} DM_{HCF} + DM_{HCF}^2}{\sqrt{DM_{LCF}^2 + DM_{HCF}^2}} \quad \text{Eq. 72}$$

Where

$$\delta = 0.02$$

DM_{LCF} = LCF damage

DM_{HCF} = wave induced HCF damage

Note: for longitudinal stiffener connections, the total fatigue damage due to both low cycle and high cycle stress can be calculated by:

$$DM_{comb} = \frac{(DM_{LCF}^2 + 2 \delta DM_{LCF} DM_{HCF} / \alpha_{Site} + (DM_{HCF} / \alpha_{Site})^2)}{\sqrt{DM_{LCF}^2 + (DM_{HCF} / \alpha_{Site})^2}}$$

Where

α_{Site} = environmental severity factor for the intended site

Where direct calculation of the wave induced loads is not available, the approximation equations with Environmental Severity Factors (ESFs) may be used to calculate the design loads.

4.4.2 Bureau Veritas

4.4.2.1 Loading Conditions

For load model design, on-site condition, four loading conditions are specified for units fitted with one central longitudinal bulkhead and three loading conditions are specified for units fitted with two central longitudinal bulkhead. These are:

1. Loading condition 1; minimum draught T_{mini} ,
2. Loading condition 2; 0.75 x scantling draught,
3. Loading condition 3; 0.9 x scantling draught (not considered for units fitted with two central longitudinal bulkhead,
4. Loading condition 4; maximum draught T .

4.4.2.2 Load Cases

A minimum of 3 internal loading conditions including minimum and maximum draughts, 5 headings and 25 frequencies.

4.4.2.3 Elementary Stress Range Calculations

4.4.2.3.1 Nominal Stress Range

The elementary nominal stress range (N/mm^2) is to be obtained from the following formula:

$$\Delta\sigma_{n,ij} = |\sigma_{n,ij,max} - \sigma_{n,ij,min}| \quad \text{Eq. 73}$$

Where

$\sigma_{n,ij,max}$, $\sigma_{n,ij,min}$ = Maximum and minimum values of the nominal stress, induced by the maximum and minimum loads. i.e. Local lateral pressures (still water pressure and wave pressure) and nominal hull girder normal stresses

i = load case

j = loading condition

4.4.2.3.2 Hot Spot Stress Range

The elementary hot spot stress range (N/mm²) is obtained from the following formula:

$$\Delta\sigma_{S,ij} = |\sigma_{S,ij,max} - \sigma_{S,ij,min}| \quad \text{Eq. 74}$$

Where

$$\Delta\sigma_{S,ij} = K_s \Delta\sigma_{n,ij}$$

$\sigma_{S,ij,max}$, $\sigma_{S,ij,min}$ = Maximum and minimum values of the hot spot stress, induced by the maximum and minimum loads. i.e. local lateral pressures (still water pressure and wave pressure) and nominal hull girder normal stresses

K_s = Stress concentration factor for the relevant detail configuration

$\Delta\sigma_{n,ij}$ = Elementary nominal stress range defined above

4.4.2.3.3 Notch Stress Range

The elementary notch stress range (N/mm²) is obtained from the following formula:

$$\Delta\sigma_{N,ij} = K_{C,ij} \Delta\sigma_{N0,ij} \quad \text{Eq. 75}$$

Where

$$\Delta \sigma_{N0,ij} = 0.7K_F K_m \Delta \sigma_{G,ij}$$

$$K_F = \text{Fatigue notch factor} = \lambda \sqrt{\frac{\theta}{30}}$$

K_m = Stress concentration factor, taking account of misalignment ≥ 1 , defined in **Table 10, Appendix 1**

λ = weld configuration coefficient given in **Table 11, Appendix 1**

θ = Mean weld toe angle (degrees) \geq not less than 30° for butt joints and 45° for T joints or cruciform joints.

For flame cut edges, K_F may be taken equal to the values defined in **Table 12, Appendix 1**, depending on the cutting quality, post treatment and control quality.

$\Delta \sigma_{G,ij}$ = Elementary hot spot stress range

$$K_{C,ij} = \frac{0.4R_{eH}}{\Delta \sigma_{N0,ij}} + 0.6 \quad \text{with} \quad 0.8 \leq K_{C,ij} \leq 1$$

4.4.2.4 Low Cycle S-N Curve and Damage Calculation

The **elementary fatigue damage ratio** is obtained from:

$$D_{ij} = \frac{N_t (\Delta \sigma_{N,ij})^3}{K_p (-\ln p_R)^{3/\xi}} \mu_{ij} \Gamma_C \left[\frac{3}{\xi} + 1 \right] \quad \text{Eq. 76}$$

Where

$\Delta \sigma_{N,ij}$ = Elementary notch stress range, in N/mm² defined above.

$$\mu_{ij} = 1 - \frac{\Gamma_N \left[\frac{3}{\xi} + 1, v_{ij} \right] - \Gamma_N \left[\frac{5}{\xi} + 1, v_{ij} \right] v_{ij}^{-2/\xi}}{\Gamma_C \left[\frac{3}{\xi} + 1 \right]}$$

$$\xi = \xi_0 \left(1.04 - 0.14 \frac{|z - T_1|}{D - T_1} \right) \quad \geq \text{not less than } 0.9 \xi_0$$

$$\xi_0 = \frac{73 - 0.07L}{60} C_{FL} \quad \geq \text{not less than } 0.85$$

T_1 = Draught (m) corresponding to the loading condition (Full load or Ballast)

$$C_{FL} = 1 \text{ or } C_{FL} = \frac{\log[0.2 \log(N_{tFL})]}{\log[0.2 \log(N_t)]}$$

$$v_{ij} = -\left(\frac{S_q}{\Delta \sigma_{N,ij}}\right)^{\xi} \ln p_R$$

$$S_q = (K_p 10^{-7})^{1/3}$$

$$K_p = 5.802 \left(\frac{22}{t}\right)^{0.9} 10^{12}$$

t = Net thickness (mm) of the element under consideration \geq not less than 22 mm

$$N_t = \text{Number of cycles} = N_t = \frac{631 \alpha_0}{T_A} 10^6$$

$$N_{tFL} = \frac{31.55 \alpha_0 T_{FL}}{T_A} 10^6$$

$$\alpha_0 = \text{Sailing factor} = 0.85$$

$$T_A = \text{Average period (seconds)} = 4 \log L$$

$$T_{FL} = \text{Increased design fatigue life (years, 25-40)}$$

$$p_R = 10^{-5}$$

$$\Gamma_N[X + 1, v_{ij}] = \text{Incomplete Gamma function, calculated for } X = \frac{3}{\xi} \text{ or } X = \frac{5}{\xi} \text{ and } = \int_0^{v_{ij}} t^X e^{-t} dt$$

Values of $\Gamma_N[X + 1, v_{ij}]$ are also indicated in **Table 7, Appendix 1**. For intermediate values of X and v_{ij} , Γ_N may be obtained by linear interpolation.

$$\Gamma_C[X + 1] = \text{Complete Gamma function, calculated for } X = \frac{3}{\xi}, = \int_0^{500} t^X e^{-t} dt$$

Values of $\Gamma_C[X + 1]$ are also indicated in **Table 8, Appendix 1**. For intermediate values of X, Γ_C may be obtained by linear interpolation.

The cumulative damage ratio is obtained from the following formula:

$$D = \frac{K_{cor}}{\beta_{IF}} [\alpha D_F + (1 - \alpha) D_B] \quad \text{Eq. 77}$$

Where

α = Coefficient, Part of the ship's life in full load condition, given in **Table 9, Appendix 1** for various ship types.

β_{IF} = Fatigue life improvement factor, generally 2.2, for improvement technique (grinding or others).

D_F = Cumulative damage ratio for ship in Full load condition =

$$D_F = \frac{1}{6}D_{aF} + \frac{1}{6}D_{bF} + \frac{1}{3}D_{cF} + \frac{1}{3}D_{dF}$$

D_B = Cumulative damage ratio for ship in Ballast condition =

$$D_B = \frac{1}{3}D_{aB} + \frac{1}{3}D_{bB} + \frac{1}{3}D_{cB}$$

Where

$D_{aF}, D_{bF}, D_{cF}, D_{dF}$ = Elementary damage ratios for load cases (a,b,c and d) respectively, in Full load condition.

D_{aB}, D_{bB}, D_{cB} = Elementary damage ratios for load cases (a,b and c) respectively, in Ballast condition.

K_{cor} = Corrosion factor = 1.5 for cargo oil tanks and 1.1 for ballast tanks having effective coating protection.

4.4.3 *Det Norske Veritas*

4.4.3.1 *Loading Conditions*

Six load conditions outlined in **Table 19** may be considered for LCF for vessels with a centreline bulkhead, these are:

1. Loading Condition 1; full load T_s , σ_{LC1} ,
2. Loading Condition 2; ballast T_{ball} , σ_{LC2} ,
3. Loading Condition 3; alternate 1, T_{act} , σ_{LC3} ,
4. Loading Condition 4; alternate 2, T_{act} , σ_{LC4} ,
5. Loading Condition 5; alternate 3, T_{act} , σ_{LC5} ,
6. Loading Condition 6; alternate 4, T_{act} , σ_{LC6} ,

Six load conditions outlined in **Table 20** may be considered for LCF for vessels with two longitudinal bulkheads, these are:

1. Loading Condition 7; full load T_s , σ_{LC7} ,
2. Loading Condition 8; ballast T_{ball} , σ_{LC8} ,
3. Loading Condition 9; T_{act} , σ_{LC9} ,
4. Loading Condition 10; T_{act} , σ_{LC10} ,
5. Loading Condition 11; T_{act} , σ_{LC11} ,
6. Loading Condition 12; T_{act} , σ_{LC12} ,

Four load conditions outlined in **Table 21** may be considered for LCF for vessels without longitudinal bulkhead, these are:

1. Loading Condition 13; full load T_s , σ_{LC13} ,
2. Loading Condition 14; ballast T_{ball} , σ_{LC14} ,
3. Loading Condition 15; T_{act} , σ_{LC15} ,
4. Loading Condition 16; T_{act} , σ_{LC16} ,

There are two possible loading and offloading scenarios of a vessel during voyage. These correspond to two stress ranges which shall normally be taken into account at the design stage. These are:

1. Stress range due to full load and ballast as illustrated in **Figure 136** and expressed by the following equation:

$$\Delta\sigma_{LCF}^1 = |\sigma^{full} - \sigma^{ballast}| \quad \text{Eq. 78}$$

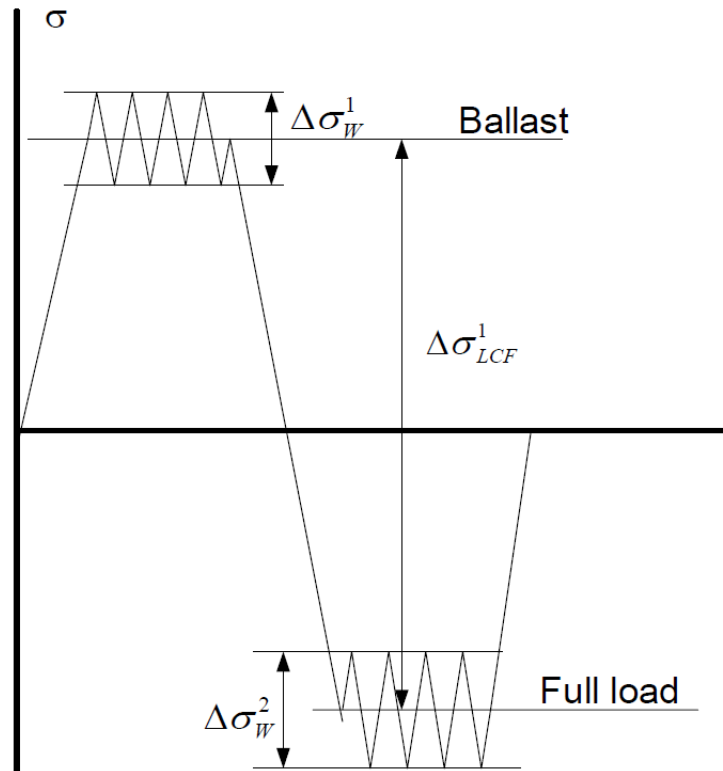


Figure 136: Operation scenarios, full load – ballast (DNV-CN-No.30.7, 2010)

2. Stress range due to two alternate conditions as illustrated in **Figure 137** and expressed by the following equation:

$$\Delta\sigma_{LCF}^2 = |\sigma^{\text{alt } 1} - \sigma^{\text{alt } 2}| \quad \text{Eq. 79}$$

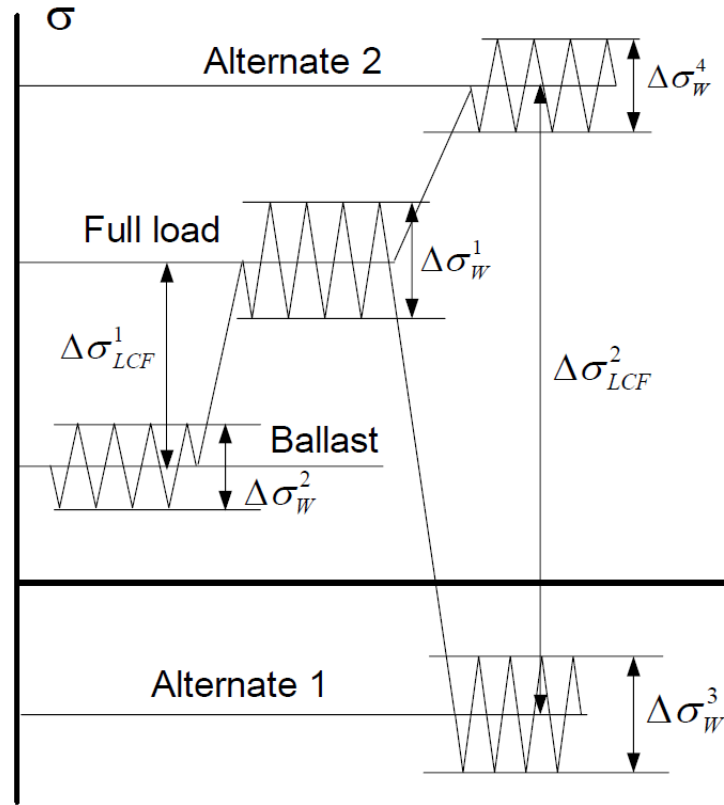


Figure 137: Operation scenarios, ballast - full load – alternate load conditions (DNV-CN- No.30.7, 2010)

The other possible load combinations, e.g. full load to alternate, ballast to alternate, etc. need normally not be taken into account.

The static hot spot surface stress range for LCF is obtained from a combination of load conditions given in **Tables 19-21** and in the code **Table I-3** in **Appendix 2** as applicable.

4.4.3.2 Load Cases

12 wave headings from 0 to 360 degrees with an increment of maximum 30 degrees should be included. For each wave heading 20 to 25 wave frequencies are normally included to properly describe the shape of the transfer function.

4.4.3.3 Stress Range Calculations

4.4.3.3.1 Hot Spot Stress

The hot spot stress range from the wave action can be calculated as:

$$\Delta \sigma_w^i = \Delta \sigma_{HCF}^i 2^{1/h} \left(1 - \frac{\log n_{LCF}}{\log n_0} \right)^{1/h} \quad \text{Eq. 80}$$

Where

$\Delta \sigma_{HCF}^i$ = hot spot HCF stress range corresponding to 10^{-4} probability level for the i-th load condition, based on dynamic pressure components given in this class note for the intended operation route n_0 = number of cycles, 10^8

The static elastic hot spot stress range for the load combination k for LCF calculations is the difference between the hot spot stress components for load condition i and j:

$$\Delta \sigma_{LCF}^k = | \sigma_s^i - \sigma_s^j | \quad \text{Eq. 81}$$

Where

$\Delta \sigma_{LCF}^k$ = static hot spot stress range for the k-th load combination between two load conditions i and j, given in Table I-3

σ_s^i = static hot spot stress amplitude for i-th load condition

σ_s^j = static hot spot stress amplitude for j-th load condition

Thus, combined stress range for, LCF strength assessment which represent a peak to peak stress due to loading and unloading and wave actions is given as below:

$$\Delta \sigma_{comb}^k = \Delta \sigma_{LCF}^k + 0.5(\Delta \sigma_w^i + \Delta \sigma_w^j) \quad \text{Eq. 82}$$

Where

$\Delta \sigma_w^i$ = dynamic stress range at 10^{-4} probability level for the i-th load condition

$\Delta \sigma_w^j$ = dynamic stress range at 10^{-4} probability level for the j-th load condition

4.4.3.3.2 Pseudo Hot Spot Stress

Thus, an effective pseudo stress range for calculation of LCF damage for the k-th load combination can be obtained as:

$$\Delta \sigma_{\text{eff}}^k = \lambda_n \cdot \Delta \sigma_{\text{comb}}^k \quad \text{Eq. 83}$$

Where

λ = Non-linearity correction factor = $k_e \cdot \psi$

$$k_e = \text{Plasticity correction factor} = 1 \quad \text{for} \quad \frac{\Delta \sigma_{\text{comb}}}{\sigma_f} \leq 2$$

$$= a \cdot \Delta \sigma_{\text{comb}} \cdot 10^{-3} + b \quad \text{for} \quad \frac{\Delta \sigma_{\text{comb}}}{\sigma_f} > 2$$

For mild steel $a = 1.16$ and $b = 0.524$.

ψ = Factor due to stress redistribution

$$= 1 \quad \text{if} \quad \frac{\Delta \sigma_{\text{comb}}}{\sigma_f} \leq 2$$

$$= 0.9 \quad \text{for mild steel} \quad \text{if} \quad \frac{\Delta \sigma_{\text{comb}}}{\sigma_f} > 2$$

$$= 0.8 \quad \text{for NV-32 or NV-36 steel} \quad \text{if} \quad \frac{\Delta \sigma_{\text{comb}}}{\sigma_f} > 2$$

σ_f = yield stress

Coefficients for the plasticity correction factor, a and b are given below:

The plasticity correction factor can be obtained from an actual cyclic stress-strain curve and Neuber's rules or non-linear finite element analysis, as shown early in **Figure 121**.

$$k_e = \frac{\sigma_{\text{pseudo}}}{\sigma_{\text{elastic}}}$$

Where

σ_{elastic} = Elastic hot spot stress obtained from linear elastic finite element analysis or a formula

$$\sigma_{\text{pseudo}} = \text{Pseudo linear elastic hot spot stress} = E \cdot \varepsilon_{\text{hs}}$$

For more complex structural connections only part of the region around the hot spot area will be yielding when subjected to large dynamic loads. This can be accounted for by a factor accounting for redistribution of stress and strain. Based on non-linear analysis of actual connections in ship structures a redistribution factor may be introduced.

In order to obtain the plasticity correction factor, a cyclic stress-strain curve for materials should be obtained from tests. If the cyclic stress-strain relation is combined with the Neuber's rule, the Neuber's formula is given using the Ramberg-Osgood relation illustrated before in equation (Eq. 7):

$$\frac{\sigma_n^2 \cdot K^2}{E} = \frac{\sigma_{\text{hs}}^2}{E} + \sigma_{\text{hs}} \cdot \left(\frac{\sigma_{\text{hs}}}{K'} \right)^{1/n}$$

Where

K = stress concentration factor

σ_{hs} = the actual stress in the hot spot

ε_{hs} = the actual strain in the hot spot

E = Young's modulus

n, K' = material coefficients.

The material coefficient K depends on the magnitude of the load and the sharpness of the notch. Coefficients, n and K' are used for derivation of the plasticity correction factors. For mild steel $n = 0.117$ and $K' = 602.8 \text{ N/mm}^2$.

Normally, the Neuber's rule is widely used to obtain the plasticity correction factor, as the rule may give somewhat conservative results. If the plane strain behaviour is relevant, the Glinka rule may be used for derivation of the plasticity correction factor instead of the Neuber's rule.

4.4.3.3.3 Low Cycle S–N Curve and Damage Calculation

A one-slope S–N curve for LCF strength is given as follows:

$$\text{Log } N_k = \text{Log } \bar{a} - m \cdot \text{Log } \Delta \sigma_{\text{eff}}^k \quad \text{Eq. 84}$$

Where

N_k = number of cycles to failure for LCF stress range

$\Delta \sigma_{\text{eff}}^k$ = effective stress range for the k-th load combination

For the basic S–N curve for LCF assessment of welded joints and base metal; $\text{Log } \bar{a}$ is given as 12.164 and $m = 3$ for $10^2 \leq N < 10^4$. This design curve is applicable to both welded joints and base metal for LCF region.

The damage due to LCF is calculated as follows:

$$D_{\text{LCF}} = \sum_1^{n_{\text{LC}}} L_k \cdot D_{\text{LCF}}^k = \sum_1^{n_{\text{LC}}} L_k \cdot \frac{n_{\text{LCF}}}{N_k} \quad \text{Eq. 85}$$

Where

n_{LC} = total number of design load condition

L_k = fraction of load combinations is given in the code.

If a non-linear finite element analysis is carried out directly, the effective pseudo-elastic hot spot stress amplitude can be obtained by multiplying the Young's modulus by the calculated notch strain amplitude.

4.4.3.4 Combined Low Cycle and High Cycle Fatigue Damage

A combined damage ratio due to HCF and LCF shall be satisfied when $D_{\text{LCF}} \geq 0.25$.

$$D_f = \sqrt{D_{\text{HCF}}^2 + \left(\frac{D_{\text{LCF}} - 0.25}{0.75} \right)^2} \leq 1 \quad \text{for } 0.25 \leq D_{\text{LCF}} \leq 1 \quad \text{Eq. 86}$$

Where

D_{HCF} = damage due to HCF based on the 20 years or 25 years design life for NAUTICUS (New building) or CSR respectively.

D_{LCF} = damage due to LCF based on the design cycles, no need to be greater than the maximum design cycles in I-5.

Note that the HCF damage contribution to the combined fatigue damage should be based on minimum design life, 20 years for Nauticus (New building) or 25 years for CSR-notation, even if an extended fatigue design life is required for HCF calculations.

For LCF damage below 0.25, fatigue damage due to HCF shall be satisfied:

$$D_{HCF} \leq 1 \quad \text{for} \quad D_{LCF} < 0.25$$

Figure 138 shows the requirements for the combined fatigue damages.

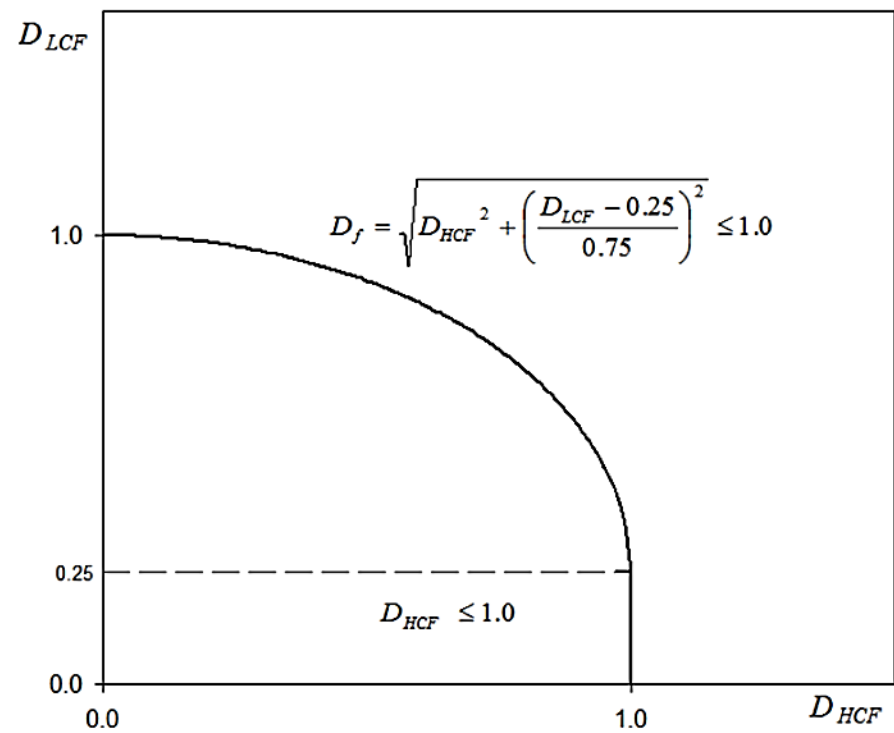


Figure 138: The combined fatigue criteria (DNV-CN-No.30.7, 2010)

4.4.3.5 Other Factors

The following effects, factors and improvements are not accounted for when evaluating damage to due to LCF:

3. Thickness effect,
4. Mean stress for base metal and welded joints,

5. Environmental reduction factor f_e ,
6. Weld improvement.

However, corrosion reduction is applied and S-N curve in air is used.

4.4.4 Limitations

DNV procedure for LCF strength assessment in DNV-CN-No.30.7 (2010) does state the following limitations:

1. New building of steel ship structures,
2. Steel materials with yield stress less than 355 N/mm^2 ,
3. Same LCF performance for base metal and welded joints,
4. The maximum principal stress direction does not change for a load condition.

4.4.5 Lloyd's Register

According to Lloyd's Register; if the number of operating cycles (i.e. loading and unloading) during FPSO service is more than 24 times per annum, the number of operating cycles is defined as High (i.e. may result in significant fatigue damage). If the number of operating cycles (i.e. loading and unloading) during FPSO service is not more than 24 times per annum, the number of operating cycles is defined as Low.

4.4.5.1 Loading Conditions

The FPSO loading conditions used to derive highest stress range from the quasi static (still water) stress cycle will depend on the structural detail to be analysed. Load conditions should be selected to maximise the stress range caused by changes in the unit load condition. This is conservative, as the FPSO may be operated in such a manner that these stress fluctuations are minimised.

Representative loading conditions for all modes of operation are to be assessed including the following:

1. All steps of loading and unloading sequences including intermediate conditions,
2. Inspection and repair loading conditions,
3. Transit loading conditions,
4. Installation loading conditions, and
5. Disconnected loading conditions.

4.4.5.2 Load Cases

Wave frequency; 0.2 rad/s to 1.2 rad/s with 25 regular spaced frequency sampling points. Wave heading; 0° to 180° for ship motions and global hull girder loads, 0° to 360° for hydrodynamic wave pressure in increments of 20°.

4.4.5.3 Stress Range Calculations

4.4.5.3.1 Pseudo Hot Spot Stress

In low-cycle-high-stress region; the hot spot stress to be used with this S–N curve is given by:

$$\Delta\sigma = K_e \cdot \Delta\sigma_{fem} \quad \text{Eq. 87}$$

Where

K_e = plasticity correction

$\Delta\sigma_{fem}$ = stress range obtained from linear fine mesh FE analysis.

The plasticity correction, K_e , will be taken as defined in Annex C of PD 5500 as:

$$k_e = 1 \quad \text{for} \quad \frac{\Delta\sigma_{fem}}{\sigma_y} \leq 2$$

$$k_e = 0.443 \left[\left(\frac{\Delta\sigma_{fem}}{2\sigma_y} \right) - 1 \right]^{0.5} + 1 \quad \text{for} \quad 2 < \frac{\Delta\sigma_{fem}}{\sigma_y} \leq 3$$

$$k_e = 0.823 + 0.164 \frac{\Delta\sigma_{fem}}{\sigma_y} \quad \text{for} \quad \frac{\Delta\sigma_{fem}}{\sigma_y} > 3$$

Where

σ_y = yield stress of material

4.4.5.3.2 Low Cycle S–N Curve and Damage Calculation

Lloyd's Register adopted a hot spot stress approach with the Palmgren-Miner cumulative damage rule to determine the fatigue damage of structural details. The hot spot stress reference mean and design S–N curves are defined as follows:

$$\text{Log } N = \text{Log } K_{hs} - m' \text{Log } (\Delta S) \quad \text{Eq. 88}$$

Where

N = the number of cycles to failure at stress range ΔS

Log K_{hs} = the intercept of the hot spot S-N curve on the Log N-axis

= 12.636 for Fillet weld 'mean curve' and 12.2 for Fillet weld 'design curve'

= 14.033 for Free edge 'mean curve' and 13.625 for Free edge 'design curve'

ΔS = the hot spot stress range obtained using the FE analysis procedure, including any additional stress concentration factors.

m' = the negative slope of the S-N curve

= 3 for Fillet weld

= 3.5 for Free edge

4.4.5.4 Combined Low Cycle and High Cycle Fatigue Damage

Total fatigue damage is calculated as:

$$D_{LCF} + D_{HCF} - D_{HCFadjust}$$

Where

D_{HCF} = damage caused by HCF due to inertial and pressure loads resulting from motion of the unit.

D_{LCF} = damage due to LCF and is given by:

$$D_{LCF} = \sum_{i=1}^n \frac{[K_e(\sigma_{LCi} + 0.5(\sigma_{HCTi} + \sigma_{HCBi}))]^m}{c} \quad \text{Eq. 89}$$

Where

n = number of quasi static "still water" stress cycles

σ_{LCi} = i^{th} highest stress range from the quasi static "still water" stress cycle

σ_{HCTi} = highest wave induced stress range over the duration of the peak of the i^{th} highest quasi static "still water" stress cycle

σ_{HCBi} = highest wave induced stress range over the duration of the trough of the i^{th} highest quasi static "still water" stress cycle

m = slope of the S-N curve for 1 000 cycles

c = intercept of the S-N curve for 1 000 cycles

$D_{HCFadjust}$ = the adjustment to account for HCF cycles which have been included in

D_{LCF}

$$D_{HCFadjust} = \sum_i^n \frac{1}{N(0.5(\sigma_{HCTi} + \sigma_{HCBi}))} \quad \text{Eq. 90}$$

Where

$N(\sigma)$ = Number of cycles obtained from reference S-N curve at stress range σ assuming elastic strain.

$$N(\sigma) = \frac{c}{\sigma^m}$$

σ_{HCTi} and σ_{HCBi} may be calculated based on the combined stress history of the quasi static "still water" stress cycles and the wave induced stress cycles. Where the combined stress history is not known, the highest wave stress range should be assumed to occur in phase with the highest quasi-static stress peak, the second highest wave stress range should be assumed to occur in phase with the highest quasi-static stress trough, the third highest wave stress range should be assumed to occur in phase with the second highest quasi-static stress peak and so on as follows:

$$\sigma_{HCTi} = \sigma_{HCT(2i-1)}$$

$$\sigma_{HCBi} = \sigma_{HC(2i)}$$

Where

σ_{HCK} = the k^{th} highest wave stress range over the design life of the FPSO

In benign or moderate fatigue environments, if the Weibull distribution is known for the long term stress, the long term stress ranges can be determined as follows:

$$\sigma_{HCK} = \sigma_d \left[\frac{\ln(k)}{\ln\left(\frac{t_0}{T_d}\right)} + 1 \right]^{\frac{1}{\gamma}} \quad \text{Eq. 91}$$

Where

T_d = 3155760000 seconds (100 years)

t_0 = mean period stress cycles

γ = shape parameter of Weibull distribution

σ_d = 1 00 year return period stress range.

In a harsh fatigue environment or if the Weibull distribution is not known then the long term stress ranges should be determined using the short term stresses. The stress ranges can be determined from the statistical properties of the stress processes in the collection of 'j' seastates in 'n' possible loading conditions by solving the following for σ_{HCK} :

$$k = \sum_1^n \sum_1^j \left\{ \frac{T_{jn}}{t_{jn}} \cdot e^{-\frac{\sigma_{HCK}^2}{2 \cdot m_{0jn}}} \right\} \quad \text{Eq. 92}$$

Where

t_{jn} = mean period of stress response in sea-state 'j' and loading condition 'n' =

$$2 \pi \sqrt{\left(\frac{m_{0jn}}{m_{2jn}} \right)}$$

T_{jn} = Duration of sea-state 'j' and loading condition 'n' = 10800 seconds (3 hours)

m_{0jn} = zero order moment of stress response spectra in sea-state 'j' and loading condition 'n'.

m_{2jn} = 2nd order moment of stress response spectra in sea-state 'j' and loading condition 'n'.

4.5 Class Societies LCF Procedures Summary

Each class society has its merits and draw backs regarding LCF procedures, some are clear, easy to follow and all relevant instructions are in the same section other are not. Some require more interpretation and engineering judgments other are not. Following the above review of class societies LCF procedure the author had set up some criterion to compare, these may be illustrated in the following **Table 11**:

Table 11: Class societies LCF procedure's high level summary

Class Society	Comparison Criterion								
	A	B	C	D	E	F	G	H	I
ABS	4	5 heading and 33 frequency	Yes		Hot spot stress	Yes	Yes	Yes	Yes
BV	4	5 heading and 25 frequency	No	Fatigue notch factor	Nominal, Hot spot and Notch stress	No	No	No	No
DNV	6	12 heading and 20-25 frequency	Yes	Non-linearity correction factor	Hot spot stress	Yes	Yes	Yes	Yes
LR	Not defined	All heading and 25 frequency	No	HCF adjustment and Weibull distribution assumptions	Hot spot stress	Yes	Yes	Yes	No

A: Loading condition B: Load cases C: Structure details D: Unique E: Stress range approach

F: Plasticity correction G: S-N curve H: Combined LC and HC I: Procedure clarity

4.5.1.1 *Representative Operational Loading Conditions for LCF*

Quasi-static loading due to loading and unloading of cargo and ballast is the single most significant load case causing LCF in FPSOs. The most critical load case generating the maximum stress range is used in LCF assessment and the load case selected is strongly dependent on the ship area under consideration. The loading time of a FPSO is generally between 10 to 14 days, while offloading is carried out within 20 to 24 hours. The sequence and timing of loading and offloading cargo depends entirely on the operator of the FPSO. Raji et al., (2009)

The typical tank loading patterns and hull draft conditions found in FPSOs loading manuals and trim and stability booklet are five to eight representative conditions including major transportation phase(s) for the FPSO ABS-DLA (2001). These are; five after installation:

1. Ballast after offloading (all cargo tanks empty)
2. Second intermediate loading (less than 50% filled)
3. Third intermediate loading (tanks 50% filled)
4. Fourth intermediate loading (more than 50% filled)
5. Full-load before offloading (tanks full)

And one transit:

6. Vessel Loading Pattern and Draft for the voyage from outfitting yard to the installation site

Some of these initial static load cases (2 and 4) were amended in ABS-FPI (2009) ABS-DLA (2010) to be more specific as follows:

1. Ballast or minimum draft condition after offloading
2. Partial load condition (33% full)
3. Partial load condition (50% full)
4. Partial load condition (67% full)
5. Full load condition before offloading
6. Transit load condition
7. Inspection and repair conditions
8. Tank testing condition – during conversion and after construction (periodic survey)

Of these above static load cases one to seven are combined with environmental loading conditions to develop static and dynamic load cases that reflect the maximum loads experienced by each structural component.

Some class societies such as Lloyd's Register have various recommendations for the representative load conditions to be used for Ship-Type FPSO hull; two to seven conditions may be required. These are assigned on the basis of case by case concept. For example; in LR-Report (2009) only two loading conditions were considered; the ballast and full load conditions. However, this was part of the life extension study of a FPSO. In LR-Report (2003) three loading conditions are considered, typically: ballast condition (light load), 50% load and full load condition with an appropriate amount of time at each condition. In LR-Report (2008), four loading conditions were considered as in **Table 12**:

Table 12: Loading Conditions for FPSO service. LR-Report (2008)

Loading Condition	Mean Draught (m)	% of operation
Prosaf Data 1	9.746	10
Prosaf Data 2	10.247	40
Prosaf Data 3	11.649	40
Prosaf Data 4	14.434	10

In LR-Report (2007) seven loading conditions were considered as shown in **Table 17**. DNV-RP-C206 (2006) recommends a minimum of three loading conditions. However, additional loading conditions are required if any of the following three scenarios exist:

1. If the difference in draught between two loading conditions exceed 8m
2. If the dynamic pressure profile would result in a non-conservative evaluation of a side longitudinal
3. If cargo tank configuration is such that full tanks are adjacent to empty tanks

4.5.1.1.1 Approach

The approach taken will be to review a number of class society procedures in terms of the representative loading conditions selected for assessing LCF. Then a review of FPSOs loading manuals in terms of typical tank loading patterns and hull draft conditions will be undertaken. Two FPSOs working in the North Sea will be used as a case study; one with a record of two years drafts during loading and offloading, about 81 loading and offloading cycles; the other will be used to demonstrate the sequence of loading and offloading of one cycle.

4.5.1.1.2 Objective

The objective is to find out which loading condition(s) is more onerous to LCF. In order to do this it is necessary to choose some representative loading conditions. These will be expressed in terms of percentage of scantling draught and percentage of operation under this loading condition. All of this is required in order to implement in Lloyd's Register Fatigue Design Assessment Level 3 (FDA3) software.

4.5.1.1.3 Case Study

Draught data collected from two FPSOs operating in North Sea has been used in this case study to quantify the most frequent draughts during loading and offloading of cargo. The FPSO's general particulars are given in **Table 13**.

Table 13: General particulars of FPSOs.

Item	FPSO I	FPSO II
Overall Length (<i>m</i>)	217.2	257.6
Beam (<i>m</i>)	38.0	41.0
Depth (<i>m</i>)	23.0	23.6
Scantling draught (<i>m</i>)	17.0	16.5

4.5.1.1.3.1 FPSO I

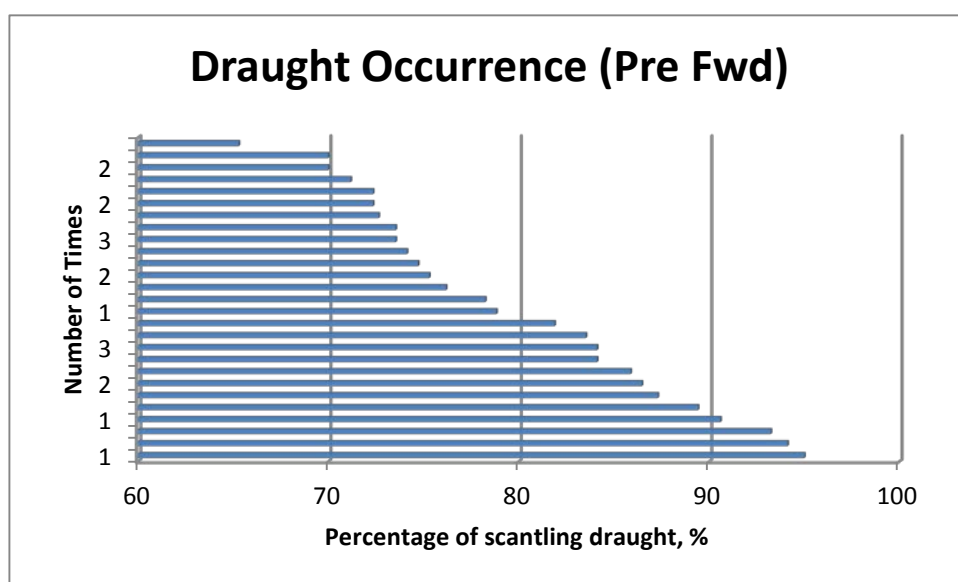
In Client-Report-G3 (2002) loading and offloading data in form of draughts at Forward (Fwd) and Aft ends during loading and after offloading were reviewed for a period of 28 months. During this period, there were 27 loading and offloading cycles, i.e. nearly one loading/offloading cycle every month. The number of occurrence of draughts at Aft and Fwd ends during are presented against percentage of scantling draught in **Table 14** and **Table 15** as well as **Figures 139-142**.

Table 14: Observed draughts for FPSO I before discharge

Range of Draughts (m)	Number of Occurrence	
	Fwd	Aft
10.00 – 10.99	0	0
11.00 – 11.99	3	0
12.00 – 12.99	10	1
13.00 – 13.99	3	5
14.00 – 14.99	6	9
15.00 – 15.99	3	4
16.00 – 16.99	2	8

Table 15: Observed draughts for FPSO I after discharge

Range of Draughts (m)	Number of Occurrence	
	Fwd	Aft
10.00 – 10.99	1	0
11.00 – 11.99	16	0
12.00 – 12.99	5	14
13.00 – 13.99	0	5
14.00 – 14.99	0	3
15.00 – 15.99	0	0
16.00 – 16.99	0	0

**Figure 139:** Frequency of observed draughts at Fwd end for FPSO I during loading (Pre Discharge)

From **Figure 139**, it is clear that the minimum recorded draught of 11.1m (65.0% of scantling draught) was only recorded once as well as the maximum recorded draught of 16.15m (95.0% of scantling draught). The most repeated draughts were 12.3m and 12.35m (72% to 73% of scantling draught).

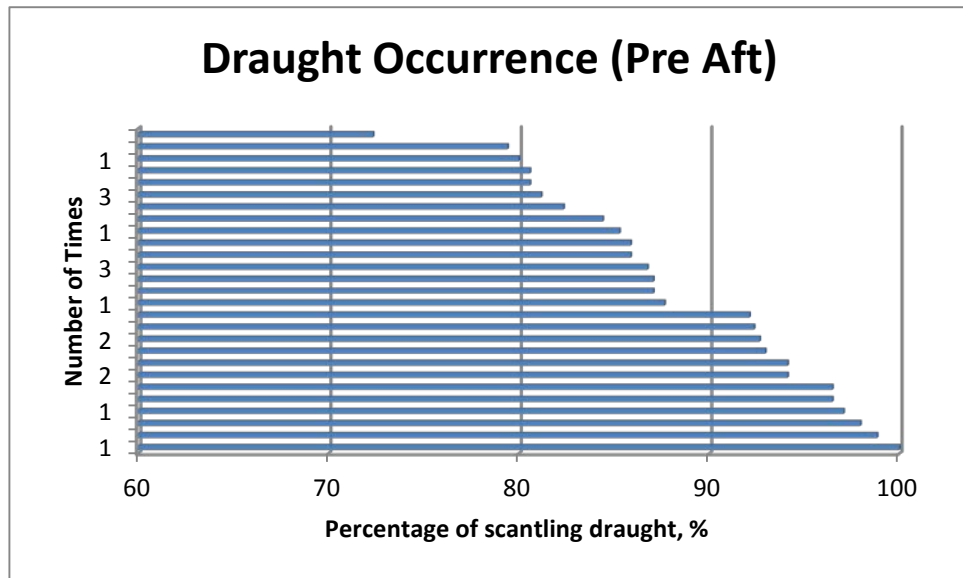


Figure 140: Frequency of observed draughts at Aft end for FPSO I during loading (Pre Discharge)

From **Figure 140**, it is clear that the minimum recorded draught of 12.3m (72.0% of scantling draught) was only recorded once as well as the maximum recorded draught of 17.8m (more than 100% of scantling draught). The most repeated draughts were 14.75, 14.8m, 15.66m, 15.7 and 15.75m (87.0%, 88.0%, 92.0% and 93.0% of scantling draught).

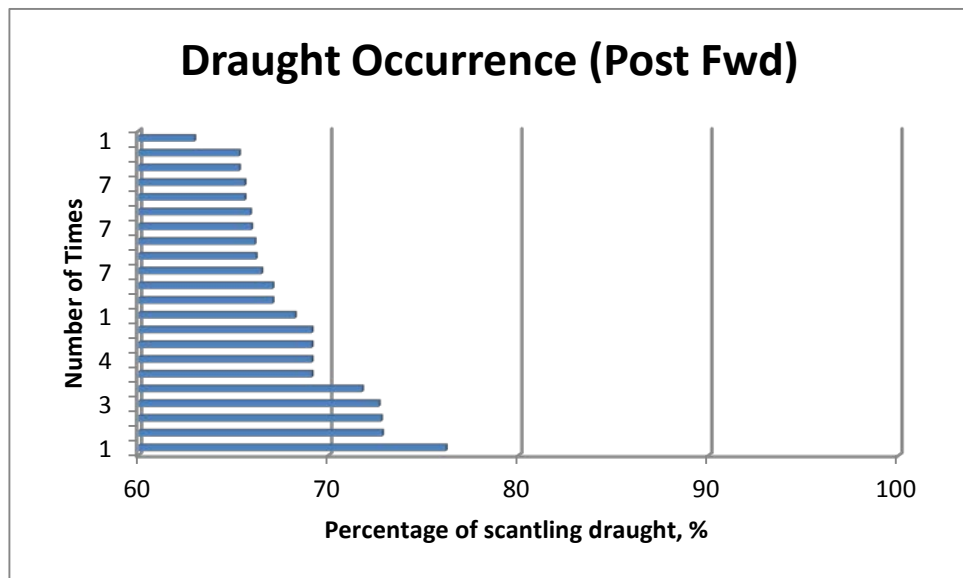


Figure 141: Frequency of observed draughts at Fwd end for FPSO I after offloading (Post- Discharge)

From **Figure 141**, it is clear that the minimum recorded draught of 10.7m (63.0% of scantling draught) was only recorded once as well as the maximum recorded draught of 12.95m (76.0% of scantling draught). The most repeated draughts were 11.1m and 11.2m (65.0% to 66.0% of scantling draught).

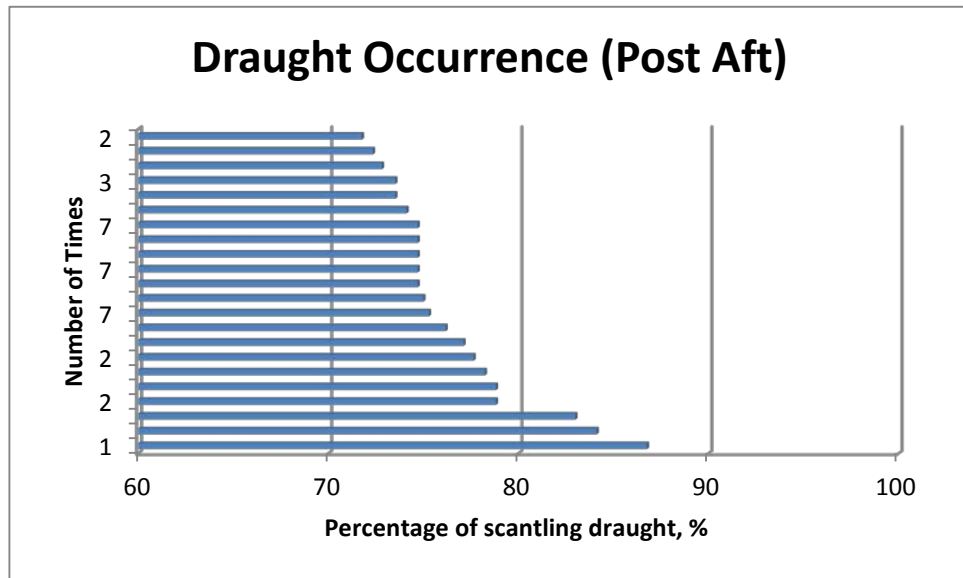


Figure 142: Frequency of observed draughts at Aft end for FPSO I after offloading (Post- Discharge)

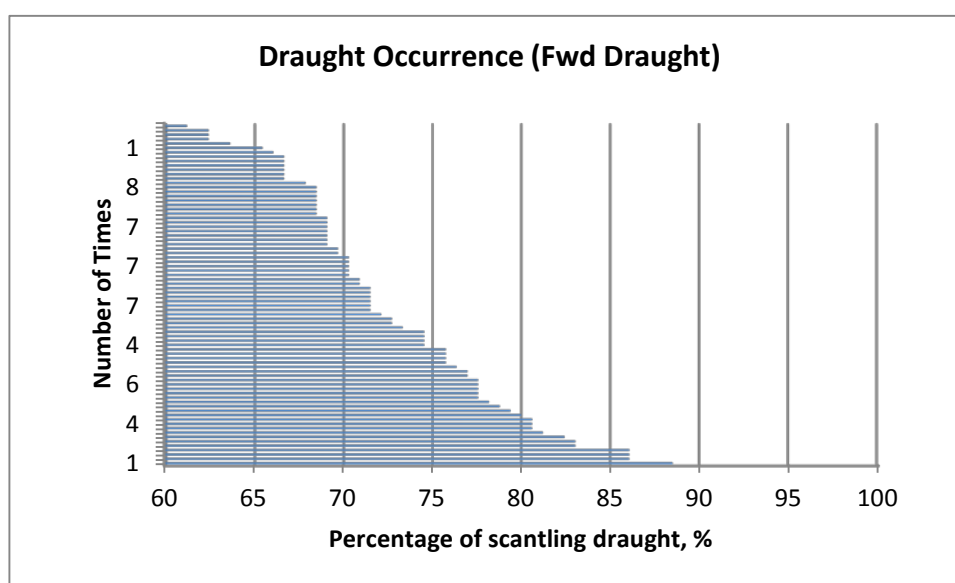
From **Figure 142**, it is clear that the minimum recorded draught of 12.2m (72.0% of scantling draught) was only recorded once as well as the maximum recorded draught of 14.75m (87.0% of scantling draught). The most repeated draughts were 12.7m and 12.75m (about 75.0% of scantling draught).

4.5.1.1.3.2 FPSO II

In Client-Report-G (2009), Loading and offloading data such as Fwd and Aft draughts, bending moment and shear force were reviewed for a period of 21 months (about 40 loading cycles). The loading and offloading occurrence percentage for Aft and Fwd draught is presented in **Table 16** as well as **Figures 143** and **144**.

Table 16: FPSO II Range of Draught Occurrence

Range of Draughts (m)	Number of Occurrence	
	Fwd	Aft
10.00 – 10.99	7	1
11.00 – 11.99	37	19
12.00 – 12.99	20	21
13.00 – 13.99	10	22
14.00 – 14.99	4	15

**Figure 143:** Frequency of observed draughts at Fwd end for FPSO II during loading/offloading

From **Figure 143**, it is clear that the minimum recorded draught of 10.1m (61.0% of scantling draught) was only recorded once as well as the maximum recorded draught of 14.6m (88.0% of scantling draught). The most repeated draughts were 11.3m and 11.4m (68.0% and 69.0% of scantling draught).

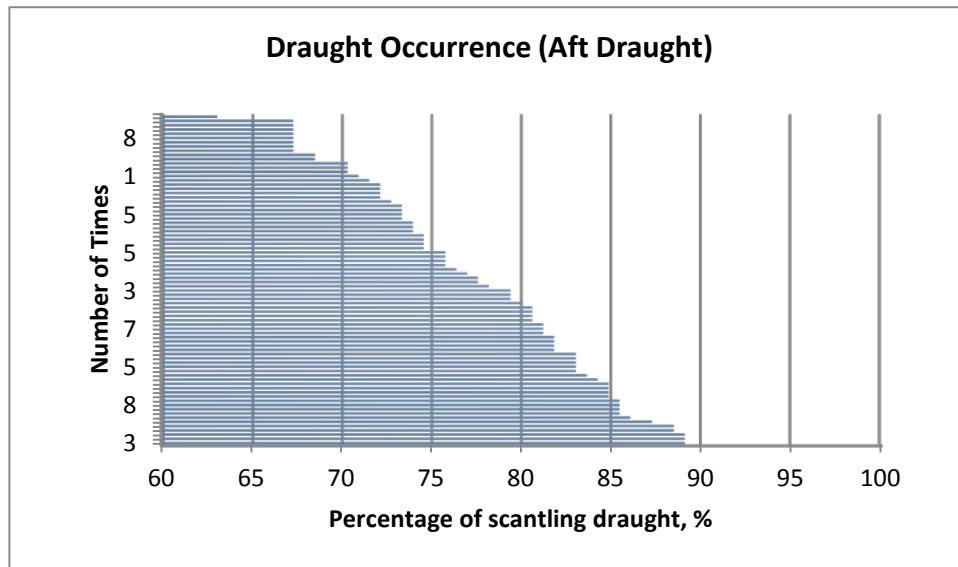


Figure 144: Frequency of observed draughts at Aft end for FPSO II during loading/offloading

From **Figure 144**, it is clear that the minimum recorded draught of 10.4m (63.0% of scantling draught) was only recorded once; the maximum recorded draught of 14.7m (89.0% of scantling draught) was recorded three times. The most repeated draught was 11.1m (67.0% of scantling draught).

4.5.1.2 Representative Loading Conditions in Class Society Rules

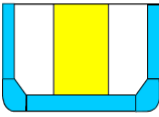
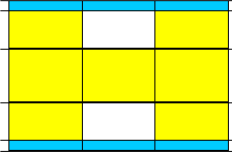
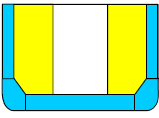
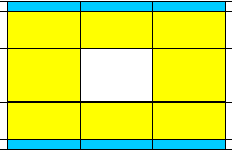
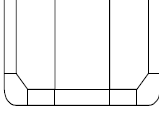
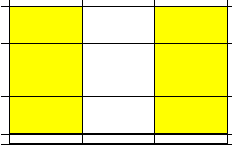
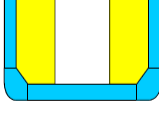
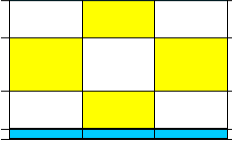
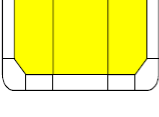
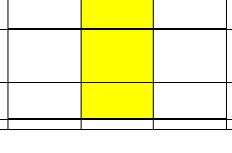
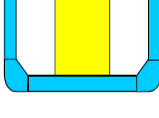
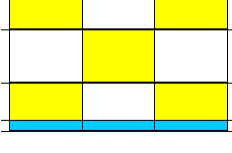
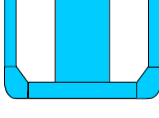
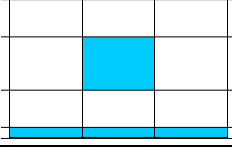
Fatigue assessment is mandatory for design review of FPSO according to the Rules of classification societies. Number of loading conditions in this assessment is selected on case by case basis and kept to a minimum. Normally, this number is in the range of two to seven.

The typical tank loading patterns and hull draught conditions found in FPSO's Loading Manuals and Trim and Stability Booklet are five to eight representative conditions including major transportation phase(s) for the FPSO ABS-DLA (2001).

4.5.1.2.1 Lloyd's Register (LR)

In LR-Report (2007) seven loading conditions were considered as shown in **Table 17** for conversion of a relatively new tanker to FPSO.

Table 17: Design Load Combinations Static & Dynamic (Sea-going load cases) LR-Report (2007)

Loading Condition	Transverse metacentric height and Radius of Gyration	Tank Arrangements	
CSR A I -Mid Side Tanks Empty (0.9 Tsc) & Ballast Tanks Full	GM 10.16m RoG20.3m		
CSR A2 - Mid Centre Tank Empty (0.9 Tsc) & Ballast Tanks Full	GM 9.60m RoG 20.3m		
CSR A3 - Mid All Tanks Abreast Empty (0.55 Tsc)	GM 13.9m RoG 23.2rn		
CSR A4 - Diagonal Mid Centre Tank Empty (0.6 Tsc) & Ballast Tanks Full	GM 8.58m RoG 21.04m		
CSR AS- Mid All Tanks Abreast Full (0.8 Tsc)	GM 9.28m RoG 20.9m		
CSR A6 - Diagnl Mid Centre Tank Full (0.6 Tsc) & Ballast Tanks Full	GM 8.58m RoG 2 1.04m		
CSR A7- Asyrn. Centre & Side Tanks Empty (Tic)	Not Applicable		
CSR AS- Heavy Ballast Condition (Thb)	GM 13.6m RoG 26. 1m		

4.5.1.2.2 American Bureau Of Shipping ABS-FPI (2009)

Four loading conditions may be considered for LCF assessment of FPSO with double hull or double side single bottom; these are presented in **Table 18:**

Table 18: ABS Representative loading conditions for LCF

Loading Condition	Description	Tank Arrangements
Loading condition 1	0.4 x scantling draught ^a	
Loading condition 2	0.57 x scantling draught	
Loading condition 3	0.73 x scantling draught	
Loading condition 4	0.49 x scantling draught	

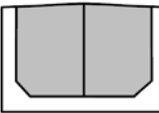
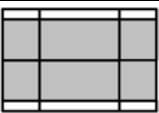
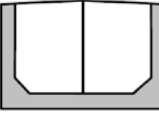
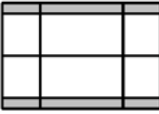
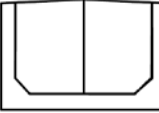
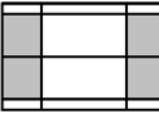
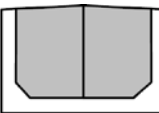
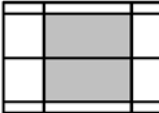
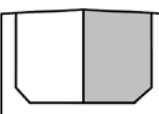
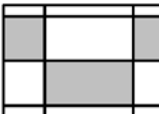
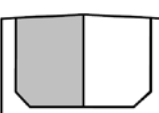
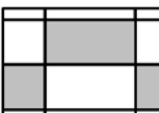
^a actual minimum onsite operating ballast draught if greater than 0.4 x scantling draught but not to exceed 0.6 x scantling draught. This condition is also used for transit condition with actual transit draught between 0.1 x scantling draught and 0.6 x scantling draught.

^b Loading condition 4, Figure 10; 0.9 x scantling draught or actual maximum onsite operating full load draught if greater than 0.9 x scantling draught.

4.5.1.2.3 *Det Norske Veritas DNV-CN-30.7 (2010)*

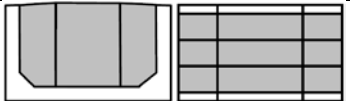
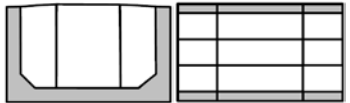
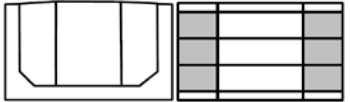
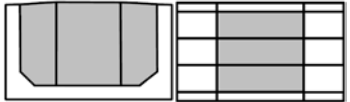
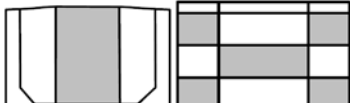

Six load conditions may be considered for LCF assessment for vessels with one centreline bulkhead; these are presented in **Table 19**:

Table 19: DNV Representative loading conditions for LCF (1)

Loading Condition	Description	Tank Arrangements	
Loading condition 1	full load T_s , σ_{LC1}		
Loading condition 2	ballast T_{ball} , σ_{LC2}		
Loading condition 3	alternate 1, T_{act} , σ_{LC3}		
Loading condition 4	alternate 2, T_{act} , σ_{LC4}		
Loading condition 5	alternate 3, T_{act} , σ_{LC5}		
Loading condition 6	alternate 4, T_{act} , σ_{LC6}		

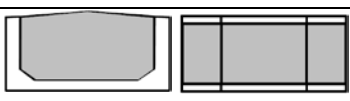



Six load conditions may be considered for LCF assessment for the vessel with two longitudinal bulkheads; these are presented in **Table 20**:

Table 20: DNV Representative loading conditions for LCF (2)

Loading Condition	Description	Tank Arrangements
Loading condition 7	full load T_s , σ_{LC7}	
Loading condition 8	ballast T_{ball} , σ_{LC8}	
Loading condition 9	T_{act} , σ_{LC9}	
Loading condition 10	T_{act} , σ_{LC10}	
Loading condition 11	T_{act} , σ_{LC11}	
Loading condition 12	T_{act} , σ_{LC12}	

Four load conditions may be considered for LCF for vessels without longitudinal bulkhead, these are presented in **Table 21**:

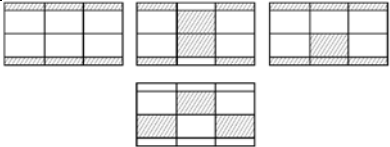
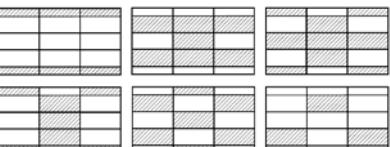
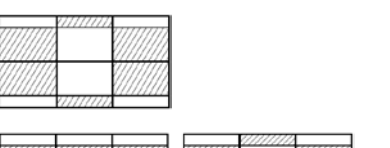

Table 21: DNV Representative loading conditions for LCF (3)

Loading Condition	Description	Tank Arrangements
Loading condition 13	full load T_s , σ_{LC13}	
Loading condition 14	ballast T_{ball} , σ_{LC14}	
Loading condition 15	T_{act} , σ_{LC15}	
Loading condition 16	T_{act} , σ_{LC16}	

4.5.1.2.4 Bureau Veritas BV-Part-D-Ch1-Sec7 (2007)

For on-site condition, four loading conditions are specified for units fitted with one central longitudinal bulkhead and three are specified for units fitted with two central longitudinal bulkheads. These are presented in **Table 22**:

Table 22: BV Representative loading conditions for LCF

Loading Condition	Description	Tank Arrangements
Loading condition 1	minimum draught T_{\min}	
Loading condition 2	0.75 x scantling draught	
Loading condition 3	0.9 x scantling draught ^a	
Loading condition 4	maximum draught T	

^a Not considered for units fitted with two central longitudinal bulkhead.

4.5.1.3 Summary of Operational (Hull) Loading Conditions Considered For LCF According to Class Societies

The common representative loading conditions recommended by class societies for FPSOs are as follows:

1. Ballast condition; this is considered the minimum draught condition where all cargo tanks are empty. ABS considers 0.4 times the scantling draught. ABS-FPI (2009) DNV considers 0.35 times the scantling draught.

2. Full load condition at scantling draught or before offloading where all tanks are full. ABS considers more than 0.9 times the scantling draught. ABS-FPI (2009)

3. Intermediate loading:

For the selection of the intermediate loading case(s). Different class societies have different recommendations for intermediate loading; ABS considers 3 load cases, DNV considers 4 load cases, BV considers 4 load cases and LR considers 2 to 7 load case but only the most representative are mentioned as follows:

- a. Loading condition at 90% of maximum draught (BV)
- b. Loading condition at 75% of maximum draught (BV)
- c. $0.73 \times$ Scantling Draught ABS-FPI (2009)
- d. Tanks are 50% full (LR and ABS)
- e. $0.57 \times$ Scantling Draught ABS-FPI (2009)

4.5.1.4 Summary of Operational (Hull) Loading Conditions According to Case Study

It is clear that the minimum draught condition considered by class societies is not the case in the investigated two FPSOs where minimum draught was always not less than 61.0% of scantling draught. However, it is important to note that contribution of intermediate loading condition in the calculation of fatigue damage is significantly more than those of the ballast and full loading conditions. ABS-FPI (2009) recommends contributions of 15%, 35%, 35% and 15% to the fatigue damage for ballast, two intermediate and full loading conditions respectively.

4.5.1.5 Recommendations

The number of recommended loading conditions to be considered for LCF assessment of an FPSO should be at least four loading conditions. These are:

1. Ballast condition at 10% of operation
2. Full load condition at 10% of operation
3. Loading condition at the most frequent draught below 50% at 40% of operation
4. Loading condition at the most frequent draught above 50% at 40% of operation

4.6 Conclusions

1. The calculated stress ranges for LCF is corrected using a plasticity correction factor in order to employ the S-N curve instead of a strain cycle curve
2. In design S–N curves; continuity from low cycle regime to high cycle regime is achieved by expressing the low cycle data in terms of pseudo elastic stress range (i.e. strain range multiplied by elastic modulus)
3. Despite the large differences in the LCF damage from the different classification societies, the S–N curves produced are quite similar
4. Longitudinal attachment use as a test specimen for LCF assessment is very limited
5. Class societies review presented in this chapter may be used in the future as the foundation of the common LCF assessment procedure for FPSO and may be put forward for the International Association of Class Societies (IACS) once the FPSO common structure rule becomes a reality.
6. Loading and offloading regimes should be strictly according to the FPSO loading manuals, any changes should be absolutely minimal.
7. This is the first time that the assumed onerous loading and unloading configurations in class society rules has been evaluated against actual conditions in operating FPSOs
8. The recommendations contained in the position paper, **Appendix 5**, has been reviewed and approved by LR Global Technology Centre (GTC) in Singapore and it is the subject of a paper to be presented at the 24th International Ocean and Polar Engineering Conference (ISOPE), June 2014 in Busan, South Korea. The position paper is also the basis for a proposal for a Joint Industry Project (JIP) on the quasi-static loading conditions of FPSOs.

Chapter 5

Low Cycle Fatigue Tests

5 CHAPTER 5: LCF Tests

This chapter describes LCF tests of longitudinal attachment specimens made of mild steel (grade A). These tests were carried out at Lloyd's Register Southampton Material Testing Facilities. Also, alongside this, other tests were carried out in order to establish the material properties of base metal and weld metal. Some literature review on LCF tests is included below.

5.1 Literature Review

5.1.1 *Ship Structure Committee (SSC-137)*

Yao and Munse (1961) carried out the oldest available literature review in LCF of metals. Their evaluation of the data on LCF of metals was based on type of test, cyclic rate, stress concentration, crack propagation, material property change and method of analysis. The outcomes of the review at the time were:

1. There was no general analysis applicable to all LCF test conditions
2. The shape of the load time curve is an important factor in analysing LCF tests
3. The extent of the time effect on LCF behaviour, particularly with respect to creep and crack propagation, still remains to be explored
4. The use of strain rather than stress is more desirable in LCF studies of coupon type specimens because of the plastic deformation that takes place during such tests
5. The fatigue hypothesis based on strain, although developed from limited data, exhibits good agreement with the test results and shows some promise of providing a good indication of LCF behaviour for selected loading conditions

Although these stated outcomes were made 52 years ago they are still essentially the same.

5.1.2 *Fatigue Process*

Petinov (2003) stated that when testing a specimen or a structural component; the fatigue process may be conditionally subdivided into three stages. During the first, initiation phase, an intensive slip in single grains prone to shear deformation gives birth to microcracks early in cyclic loading, depending on the applied stress amplitude. Under further cyclic loading one of the microcracks trespasses the threshold at a grain boundary, where the slip systems in adjacent grains are coherent. The slip, intensified in the neighbouring grains, provides conditions for further crack extension. Consecutive

development of a highly localized stress field at the crack tip initiates an intensive fragmentation of material structure and facilitates crack expansion perpendicular to the maximum principal stress. This transition is attributed to stage II of the macroscopic crack formation. Stage II does not reveal a noticeable reduction of the test piece's resistance and distinguishing such a crack would require a special technique or at least a magnifying glass. When the crack is beginning to affect the rigidity of a sample, it may be regarded as the onset of stage III of the process.

5.1.3 *Effects of material texture on fatigue*

Shevandin examined fatigue strength of hull structural steels based on the orientation of specimen to the rolling direction in plates. He found that the fatigue limit obtained in tests of specimens that were cut out of a plate perpendicular to the rolling direction dropped to 40–60 % of the fatigue limit typical for specimens machined from a plate in the rolling direction. He also noted that this effect was less distinct in tests of notched specimens. Petinov (2003)

5.1.4 *HSE LCF Review*

HSE (Health and Safety Executive) study review of LCF resistance, HSE-Review (2004) evaluated the treatment of high stress ranges based on design advice and experimental data available at the time and recommended that restrictions on the applicability of S–N curves in high stress low cycle region due to lack of experimental data should be lifted. These restrictions were in place due to the concern that plasticity effect might cause reduced life. These concerns were not supported by data and the review suggested that fatigue life less than predicted by design curves is possible only under laboratory conditions i.e. would not occur in actual offshore installations.

5.1.4.1 TWI

The TWI (Technical Welding Institute) literature review of LCF test results covered butt welds (Transverse) and fillet welds (Longitudinal) and fillet welds Transverse (load carrying and non-load carrying) as follows:

5.1.4.1.1 Transverse butt weld

These tests by Ida and Radziminiski recorded no failures below 10^4 cycles. Lieurade et al LCF tests with failure criteria of a crack exceeding 5% of nominal section area recorded two cracks initiated at the base metal not the weld. Trufyakov used three grades of steel mild (271MPa), low alloy (458MPa) and high strength (617MPa) in

12mm thick plate containing transverse butt weld. All results for $R=0$, **Figure 145**, lay above Class D design line except few points when maximum stress exceeded $0.8F_y$.

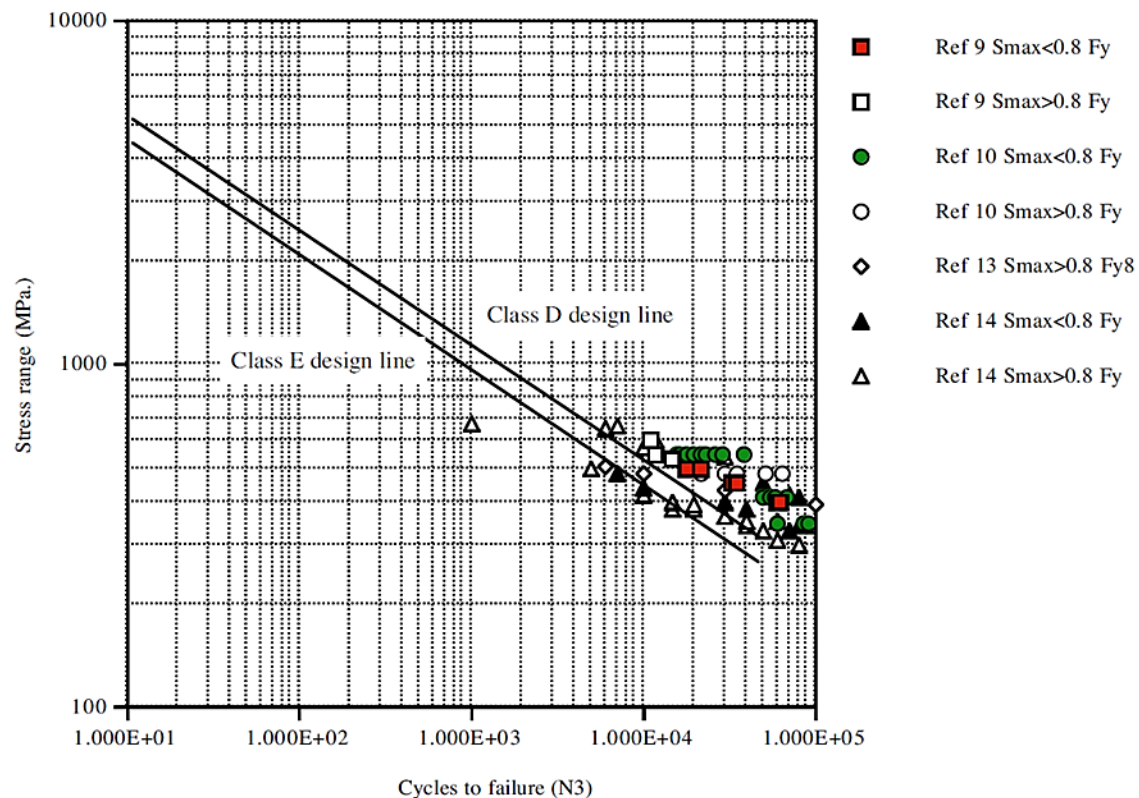


Figure 145: Endurance data for transverse butt welds ($R=0$) (HSE-Review, 2004)

Ferreira et al cruciform joint results, **Figure 146**, recorded all full penetration welds failure in the parent metal and all (except one) of the partial penetration welds failed in the weld itself. A degree of buckling in the specimens was reported. HSE review concluded that Pseudo Elastic stress range is considered suitable for assessing LCF of butt welds.

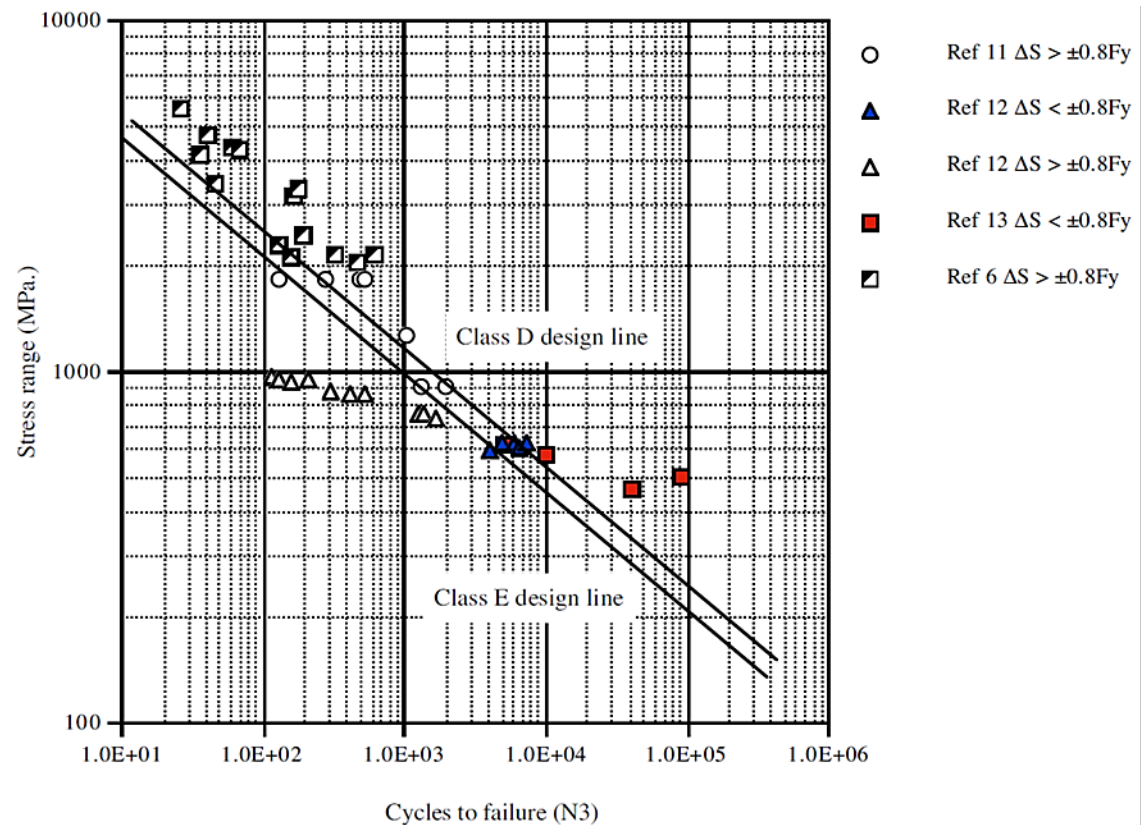


Figure 146: Endurance data for transverse butt welds ($R=-1$) (HSE-Review, 2004)

5.1.4.1.2 Longitudinal fillet weld

In these tests the effect of LCF was more noticeable due to higher SCF at the end of the attachment. Harrison used three medium strength and two high strength steels in his LCF tests under both load and strain control, under load control, **Figure 147**, all material exceeded the class F design line except when the maximum nominal stress exceeded yield stress $1.0F_y$. Under displacement control (strain control), **Figure 148**, all results exceeded class F design line even when the maximum stress range exceeded yield stress $1.6F_y$.

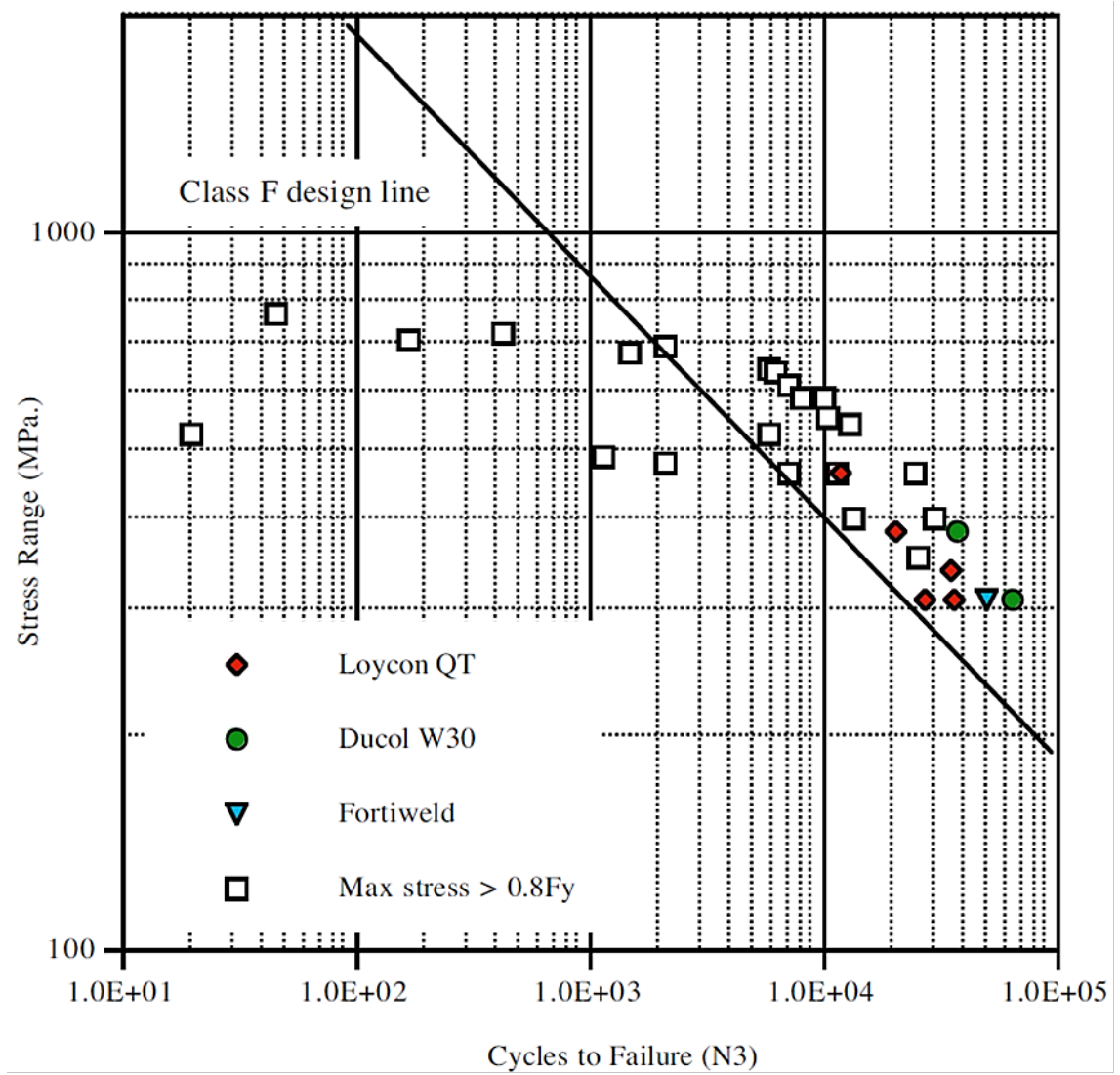


Figure 147: Endurance data for longitudinal fillet welded attachments (load control) (HSE-Review, 2004)

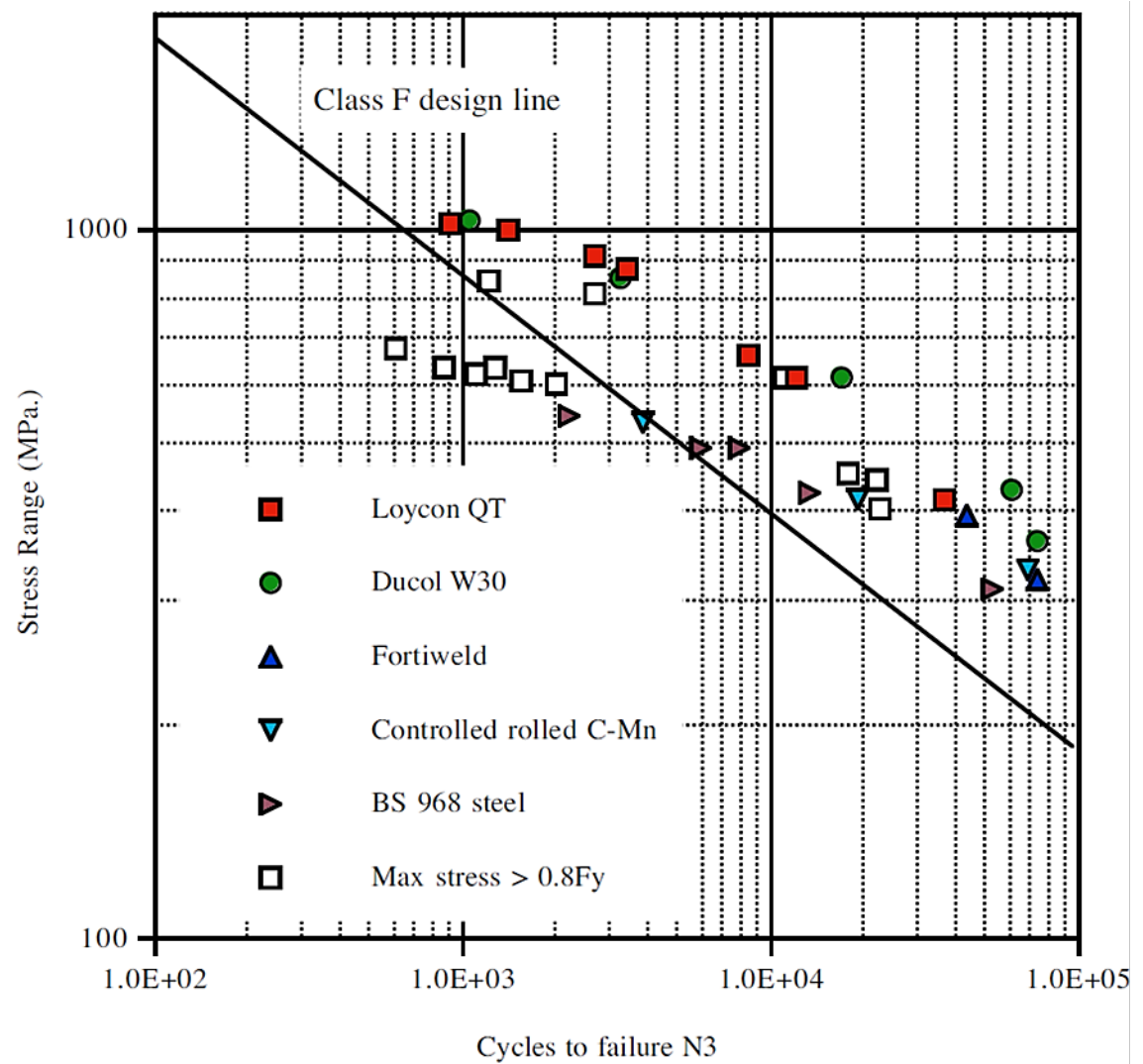


Figure 148: Endurance data for longitudinal fillet welded attachments (displacement control) (HSE-Review, 2004)

5.1.4.1.3 Transverse (non-load carrying fillet weld)

Lieurade investigated LCF behaviour of cruciform joints welded from 12 mm thick E36 and A70 plates with failure criteria defined as; a crack that extends to 5% of the specimen area. Results in **Figure 149** lay well inside Class F design line unless stress ranges exceed 0.8 Fy.

12 mm thick plates with transverse fillet welded attachments were also studied by Trufyakov using low yield point steel M16S mild steel ($F_y=271$ MPa). Fatigue lives at $R=0$ were in the range 3.5×10^4 to 8×10^4 cycles which exceeded Class F design life even though the maximum stress was in excess of 0.8 Fy as seen in **Figure 149**.

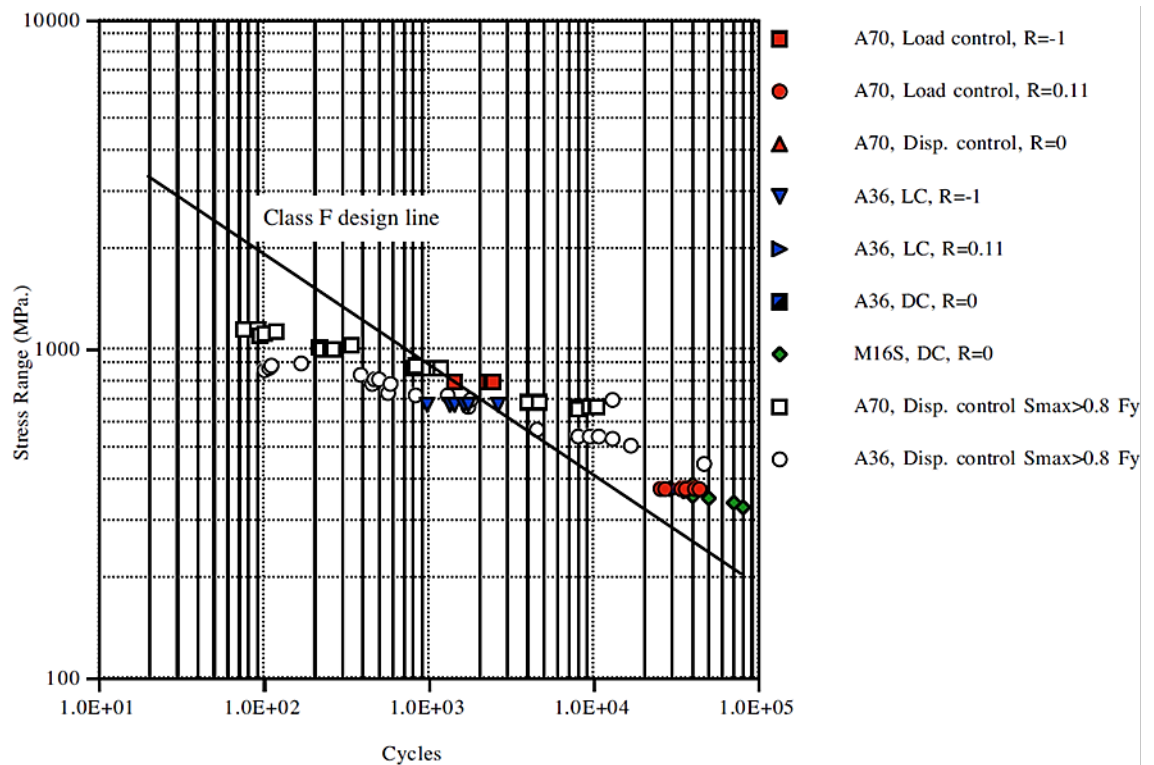


Figure 149: Endurance data for transverse non load-carrying fillet welds (HSE-Review, 2004)

5.1.4.1.4 Transverse (load carrying fillet weld)

Load carrying fillet welds are not normally used in situations where they are likely to be subjected to cyclic loading, full penetration welds being preferred for this detail. However, the data that does exist is summarised in **Figure 150**.

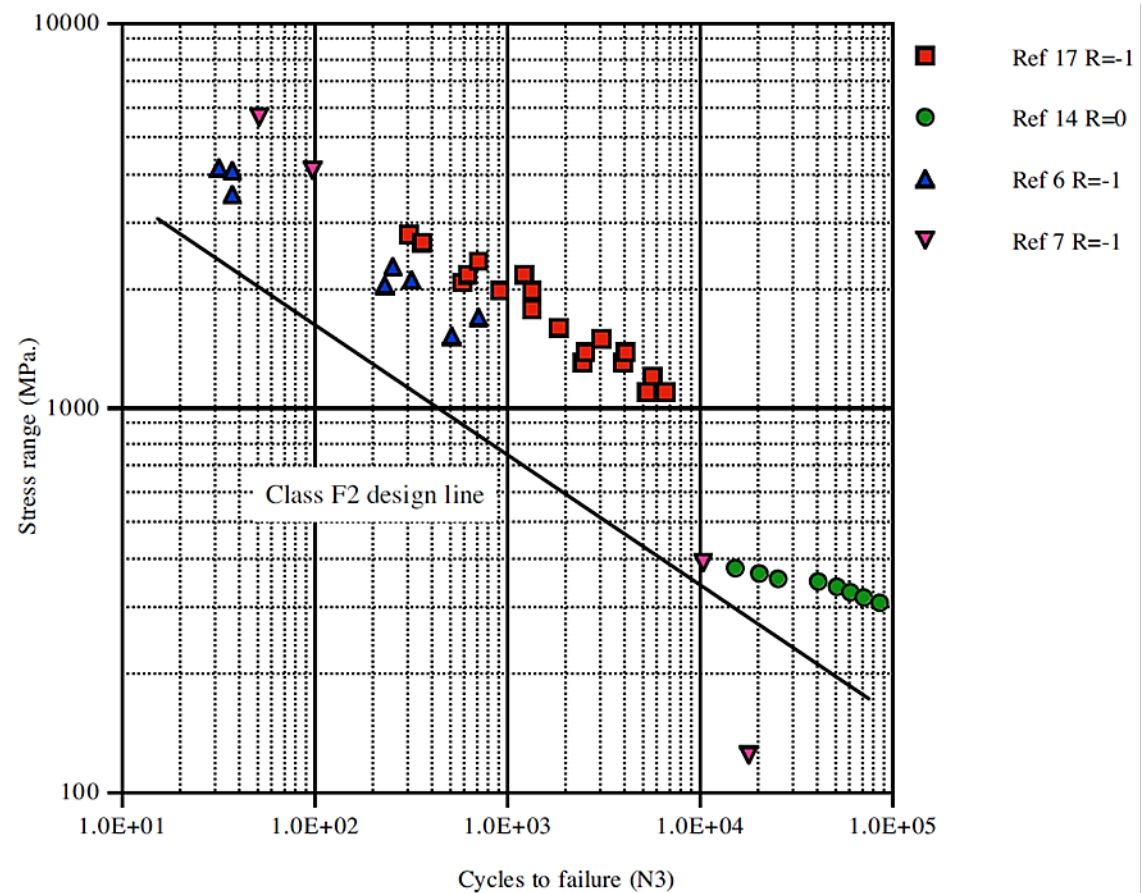


Figure 150: Endurance data for transverse load-carrying fillet welds (HSE-Review, 2004)

The first series of tests considered was conducted by Dunn and Anderson using 12.7 mm plate to BS1501-224-26A LT30 with a low yield stress of 265 MPa. The resulting failures lay well above the relevant Class F2 design line and performed better than Class F. In these tests the pseudo-elastic stress ranges corresponding to the imposed displacements approached 10 Fy indicating substantial reversed plasticity. Also, the resulting fatigue lives were as short as 300 cycles.

A second series of tests were undertaken by Trufyakov using M16S mild steel discussed in a double lap joint configuration. All of the failure points lay above Class F2 design line.

5.2 Class Societies and Shipyards

Heo et al., (2004) in a joint industry project between Daewoo Shipbuilding and Marin Engineering (DSME) and Det Norske Veritas, Korea unveiled the fatigue performances in the high stress and low cycle regime. These tests were carried out at their lab

facilities of naval architecture and ocean engineering in Inha University, Korea. Both base metal (mild steel and high tensile steel) and welded joints (according to the shipyard practice welding procedure) were tested to obtain cyclic and monotonic stress-strain curves. In this study efforts were also made to ‘accurately’ estimate the notch stress-strain state using Neuber’s rule and nonlinear elasto-plastic finite element analysis considering the effect of material inhomogeneity. A number of conclusions were made in this study; the most important are:

1. ‘Simple’ extension of DNV’s high cycle S–N curve to low cycle region is a conservative approach with a condition of keeping its slope as 3.
2. Neuber’s rule is the most conservative in estimating elasto-plastic notch stress-strain state and should be used together with cyclic stress-strain relation of weld metal when dealing with weld toe cracks.

One task of the above mentioned joint industry project (JIP) was to develop LCF ‘Strength Assessment Procedure’ based on Monotonic and cyclic material property tests (Smooth Round Type Specimens) and the fatigue test results (Welded Component Specimens). Urm et al., (2004b) The JIP achieved the following:

1. Described the typical loading conditions to be considered for LCF in oil tankers.
2. Recommended the minimum number of ‘design cycles’ for LCF for different types of ships.
3. Established simple methods to calculate ‘stress components’ due to cargo loading and unloading for longitudinals and by FEA for general details.
4. Proposed S–N curves for LCF for both base metal and welded joints.
5. Provided a method to combine ‘fatigue damage’ due to LCF and due to HCF.

5.3 Full Scale Testing

Aiming at the harmonization of the different approaches for the fatigue strength assessment Fricke and Paetzold (2010) carried out intensive fatigue strength research and investigations in Germany as part of an industry joint project were two ship structure details were selected for full scale tests. The first structural detail type was web frame corners (typical of roll on/roll off ships (ro/ro) ships) from which three models were tested under constant amplitude loading. The second structural detail type was the intersection between longitudinals and transverse web frames (recently showed fatigue failures in containerships). Five models were tested; three under constant and

two under variable amplitude loading. All tests showed long crack propagation phase after first cracks had appeared (20mm failure criterion). For numerical analysis, the structural hot spot stress as well as the effective notch stress approach has been applied. The effective notch stress approach allows the consideration of the weld shape which could partly explain differences in the observed and calculated failure behaviour. Another factor is the distribution of welding induced residual stresses which affected the failure behaviour in the web frame corner. The investigation concluded that computation of effective notch stress in large structures is possible with sub model technique but require more effort than the other techniques. However, it allows the effects of local weld profile and increased weld toe radii to be considered. Also concluded, that failure behaviour of complex structures (determined in numerical analyses) may differ from actual failure behaviour. This is due to varying residual stresses which may cause hot spots to be less critical than assumed for the presence of very high residual stresses.

5.4 IIW (HCF)

Different approaches of fatigue strength assessment of fillet welded joints (Full and Partial) considering effects of weld throat thickness (3 and 7 mm) and load carrying grade were investigated by Fricke and Feltz (2009). They carried out fatigue tests with 12 mm thick lap joints having full-load carrying fillet welds and cover plates where welds carry only part of the load in the plate. Four approaches have been applied to the investigated specimen types and the following conclusions were reached:

1. Joints with large weld throat thickness show crack initiation at the weld toe, while a small weld throat thickness promotes crack initiation from the weld root, particularly with full-load carrying fillet welds.
2. Partial-load carrying fillet welds should be classified as full-load carrying welds because three test series with weld toe failure showed similar characteristic fatigue strengths (FAT-classes) i.e. load carrying grade have no effect on the fatigue strength.
3. The results agree with common joint classification according to nominal stress approach which can also be applied to cases with weld root failure.
4. Structural hot-spot stress approach (applicable to weld toes) yields the same structural stress and strength for partial and full-load carrying fillet welds (non-conservative).

5. Structural stress approach (unconventional) by Xiao/Yamada (applicable to weld toes as well) shows different structural stresses for the specimen types (conservative). The maximum principal stress yields more reasonable results than the directional stress.
6. The modified structural stress approach by Poutiainen (applicable to weld toes) shows larger differences between the different specimens giving conservative results.
7. Effective notch stress approach (applies also to the weld root) shows significant differences between different specimens. The calculated notch stresses correspond to the observed crack initiation site except for the lap joint with 7 mm throat thickness where the stress at the keyhole notch representing the weld root seems to be overestimated.

Fricke and Feltz (2009) stated that all approaches have some shortcomings and that the deviations between fatigue tests and assessment are non-satisfactory.

5.5 LCF Tests in LR Southampton Facilities

5.5.1 Introduction

Following the literature review it was evident that very limited tests were carried out on longitudinal attachment specimen for LCF assessment as compared to the transverse attachment. Both of these are very important component of ship structures. Therefore, the author decided to carry out LCF tests on longitudinal attachment specimen and on uniform gauge section test specimen. Other tests (monotonic and cyclic) were carried out for establishing material properties of both; the Mild Steel Grade A (commonly used in shipyards) as well as the deposit metal used for welding (Bostrand LW1).

5.5.2 Specimens and Material

16 specimens (FWS1 and FWS2) were cut and welded from mild steel grade A panel **Figure 151**. Mild steel grade A was chosen because it is the most common type of construction steel used in shipyards. Material specification including chemical composition of both mild steel grade A and deposit metal Bostrand LW1 are in **Appendix 3**.

The longitudinal attachment specimen dimensions are shown in **Figure 152** and the uniform gauge section test specimen/dimensions are shown in **Figure 153**. Other tests (monotonic and cyclic) were carried out for establishing material properties of both; the

Mild Steel Grade A (commonly used in shipyards) as well as the deposit metal used for welding (Bostrand LW1).

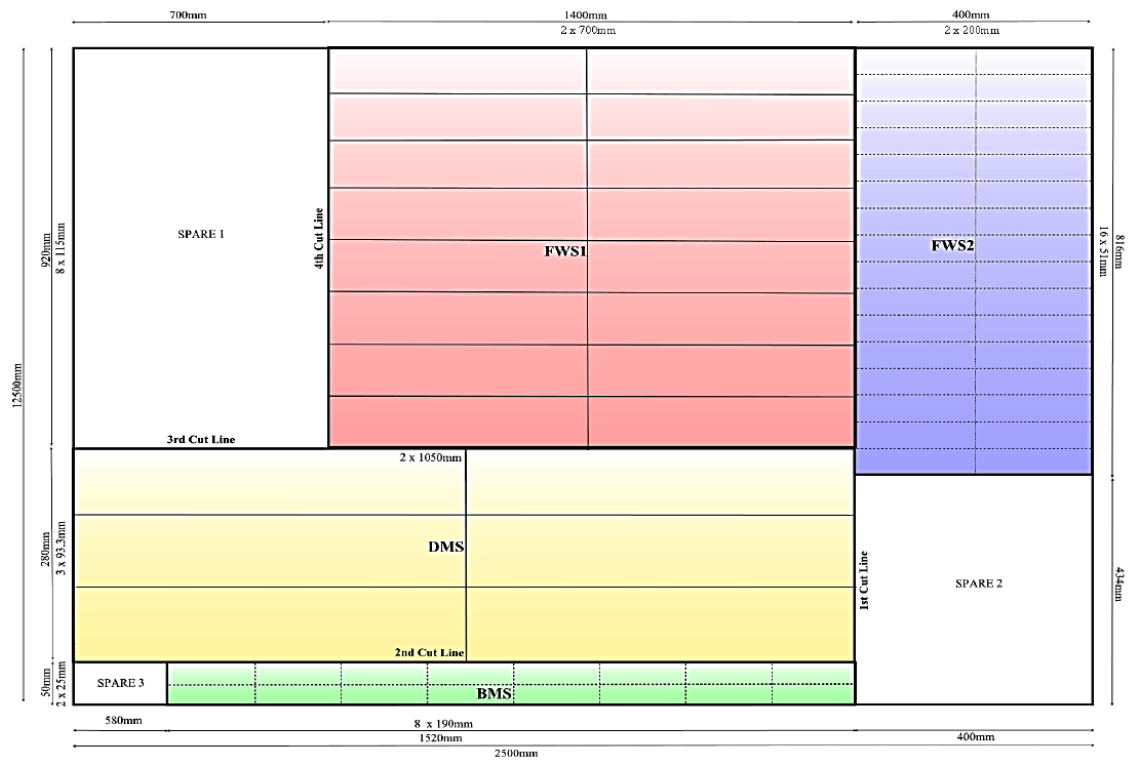


Figure 151: Mild steel grade A panel

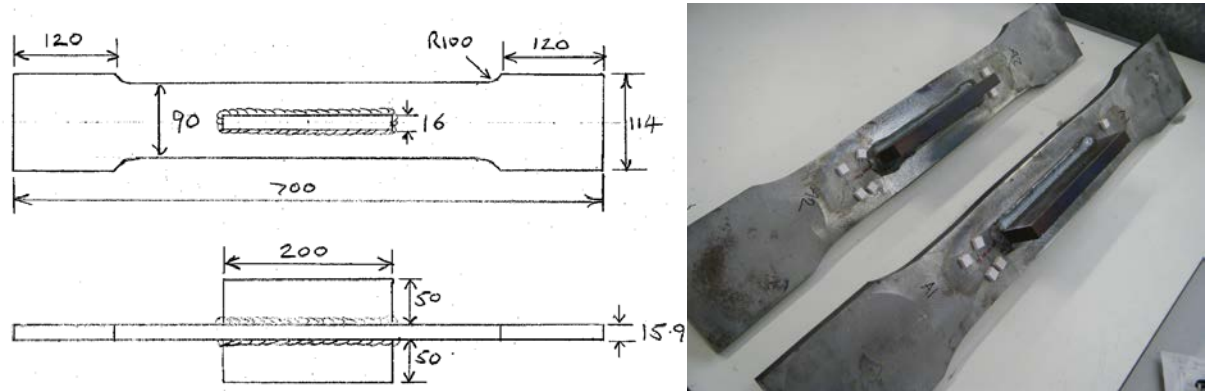


Figure 152: Longitudinal Attachment Specimen

Details of the required numbers of specimen are given in **Table 23**:

Table 23: Mild steel grade A panel Details

Panel	Description	Dimensions (mm)	Sample Size (mm)	Number	Comments
FWS1	Fillet Weld Specimen 1	920 x 1400	115 x 700	16	
FWS2	Fillet Weld Specimen 2	400 x 816	51 x 200	32	2 required for each FWS1
DMS	Deposit Metal Specimen	280 x 2100	93 x 1050	6	
BMS	Base Metal Specimen	50 x 1520	25 x 190	16	
Spare 1	Spare Piece	700 x 920	N/A	1	No need to cut
Spare 2	Spare Piece	400 x 434	N/A	1	No need to cut
Spare 3	Spare Piece	50 x 580	N/A	1	No need to cut

Other specimens were the base metal specimen (BMS) and the weld or deposit mental specimen (DMS) **Figure 153**, 16 base metal specimens were made (cut then machined) from the same panel. Also, 16 weld or deposit metal specimens were made (weld, cut then machined) from the same panel. Both specimen types were designed according to the guidelines of the ASTM E 606 Standard Practice for Strain Controlled Fatigue with testing surface roughness of 0.2- μm .

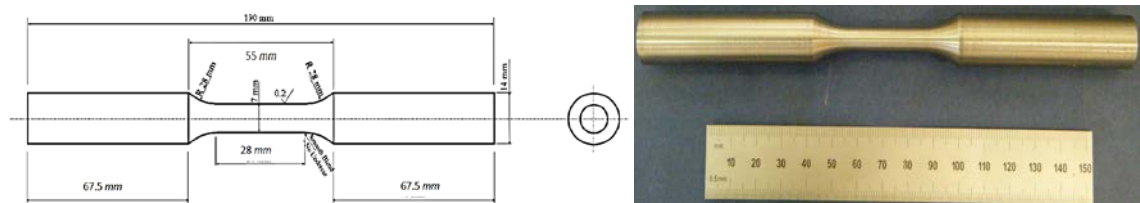


Figure 153: Uniform Gage Section Test Specimen

5.5.3 Some basic definitions

The following principles, terms, laws and conversions are used in this chapter. These are as follows:

Elastic behaviour is governed by **Hooke's Law** $\sigma = E\varepsilon$,

True stress and strain are used for plasticity:

$$\text{True stress } \sigma = \sigma_{\text{Eng}}(1 + \varepsilon_{\text{Eng}}),$$

$$\text{True strain } \varepsilon = \ln(1 + \varepsilon_{\text{Eng}}),$$

Yield criterion; relates multi-axial stress state of structure with uniaxial stress state of test specimen.

Monotonic loading; no unloading takes place during the test,

Cyclic loading; loading reverses direction during the test,

Ratchetting; progressive increase of strain at each cycle,

Shakedown; progressive stabilization of strain at each cycle,

5.5.4 Test Programme and Conditions

The experimental programme may be divided into three categories and these may be summarized as follows:

5.5.4.1 Type A - Longitudinal Attachment (Larger Specimen)

Sample general and close up views of Type A specimen is shown in **Figure 154** as well as strain gauge (SG) locations:

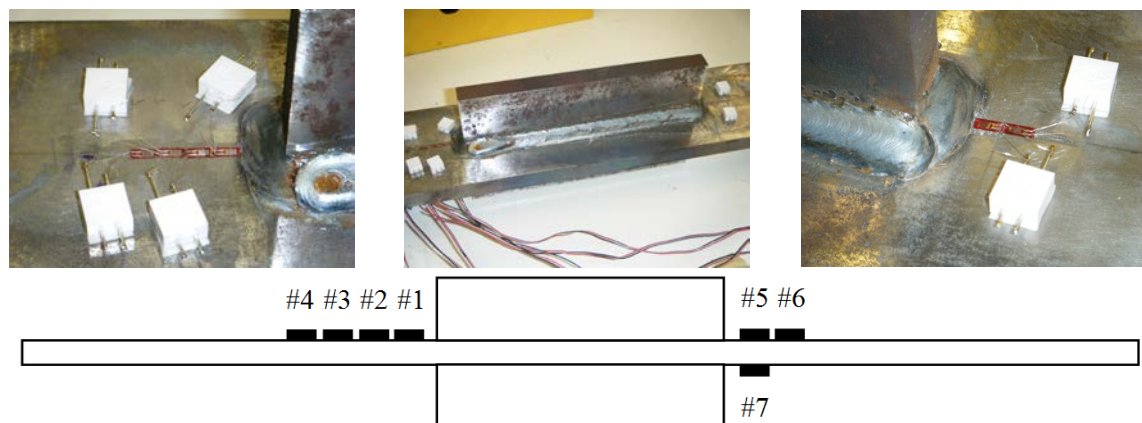


Figure 154: Strain gauge locations for Type A static tests

Where

2mm SG #4 is to measure nominal strain

2mm SG #1, 5 and 7 (as close as possible to weld toe) measuring local strain

Exact location of strain gauges are given in **Table 23** for Test A1 and **Table 24** for Test A2

The SG Locations for Tests A3 to A16 are shown in **Figure 155**:

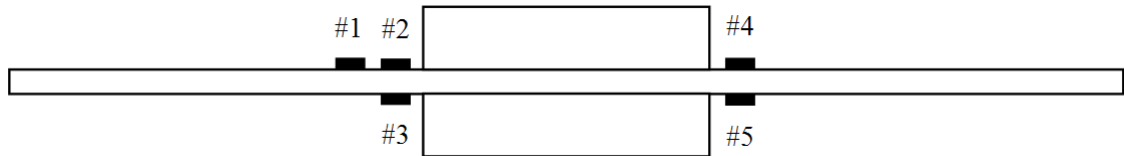


Figure 155: Strain gauge locations for Type A other tests

Where

6mm SG #1 (44mm from weld toe)

2mm SG #2, 3, 4 and 5 (as close as possible to weld toe) measuring local strain

Note: 6mm SG #6 was added on specimen of Test A10 onwards to observe buckling

Test A1 – Quasi Static Test, (Yield Stress and Ultimate Tensile Strength)

Test A2 – Quasi Static Test, (Yield Stress and Ultimate Tensile Strength)

Test A3 – Dynamic LCF, displacement controlled (6mm range) to establish nominal/local strain range

Test A4 – Setup and Dummy Run, strain controlled based on A3

Test A5; +/- 1.1mm displacement control (cycles to failure)

Test A6; +/- 1.3mm displacement control (cycles to failure)

Test A7; +/- 1.4mm displacement control (cycles to failure)

Test A8; +/- 1.5mm displacement control (cycles to failure)

Test A9; +/- 1.6mm displacement control (cycles to failure)

Test A10; +/- 1.7mm displacement control (cycles to failure)

Test A11; +/- 1.8mm displacement control (cycles to failure)

Test A12; +/- 1.9mm displacement control (cycles to failure)

Test A13; +/- 2mm displacement control (cycles to failure)

Test A14; +/- 1.2mm displacement control (cycles to failure)

Test A15; 0-3mm displacement (To assess effect of no compression)

Test A16 – Spare

5.5.4.2 Type B - Base Metal Specimen (BMS) – Smooth Round Type

Note: 25mm extensometer used

Test B1 – Monotonic (tensile diagram recorded)

Test B2 – Monotonic (tensile diagram recorded)

Test B3 – Cyclic (hysteresis diagram recorded)

Note: for B2 and B3, 20 blocks to be used for each test specimen. Each block should contain 40 cycles (20 increasing and 20 decreasing strain ranges). It should take about 10 seconds to complete 1 strain cycle. Strain amplitude range should be from 0.1% to 1.2% with step increment of 0.1%. Urm et al., (2004b) The cyclic diagrams are recorded for each step of the last half-block, and then generalised diagram is developed.

Test B4 – Setup and Dummy Run, strain controlled

Test B5 – Setup and Dummy Run, strain controlled (repeated)

Test B6 – strain level 1, 0.4% strain range (cycles to failure)

Test B7 – strain level 1, 0.4% strain range (cycles to failure)

Test B8 – strain level 2, 0.8% strain range (cycles to failure)

Test B9 – strain level 2, 0.8% strain range (cycles to failure)

Test B10 – strain level 3, 1.2% strain range (cycles to failure)

Test B11 – strain level 3, 1.2% strain range (cycles to failure)

Test B12 – strain level 4, 1.6% strain range (cycles to failure)

Test B13 – strain level 4, 1.6% strain range (cycles to failure)

Test B14 – strain level 5, 2% strain range (cycles to failure)

Test B15 – strain level 5, 2% strain range (cycles to failure)

Test B16 – Spare

5.5.4.3 Type C - Deposit Metal Specimen (DMS) – Smooth Round Type

Note: 25mm extensometer used

Test C1 – Monotonic (tensile diagram recorded)

Test C2 – Monotonic (tensile diagram recorded)

Test C3 – Cyclic (hysteresis diagram recorded)

Note: for C2 and C3, 20 blocks to be used for each test specimen. Each block should contain 40 cycles (20 increasing and 20 decreasing strain ranges). It should take about 10 seconds to complete 1 strain cycle. Strain amplitude range should be from 0.1% to 1.2% with step increment of 0.1%. Urm et al., (2004b) The cyclic diagrams are recorded for each step of the last half-block, and then generalised diagram is developed.

Test C4 – Setup and Dummy Run, strain controlled

Test C5 – Setup and Dummy Run, strain controlled (repeated)

Test C6 – strain level 1, 0.4% strain range (cycles to failure)

Test C7 – strain level 1, 0.4% strain range (cycles to failure)

Test C8 – strain level 2, 0.8% strain range (cycles to failure)

Test C9 – strain level 2, 0.8% strain range (cycles to failure)

Test C10 – strain level 3, 1.2% strain range (cycles to failure)

Test C11 – strain level 3, 1.2% strain range (cycles to failure)

Test C12 – strain level 4, 1.6% strain range (cycles to failure)

Test C13 – strain level 4, 1.6% strain range (cycles to failure)

Test C14 – strain level 5, 2% strain range (cycles to failure)

Test C15 – strain level 5, 2% strain range (cycles to failure)

Test C16 – Spare

5.5.5 Type A Test Procedures

The test methodology is as follows:

1. The specimen, prepared with strain gauges, is loaded into the test machine and the top grip is closed.
2. The position of test machine actuator, the load from the load cell and the measurement from the strain gauges are recorded by a separate data acquisition (DAQ) unit. The position and load from the machine are converted into an analogue signal of +/- 10V to be monitored by the DAQ system. To obtain the best measurement resolution the 10V will not always be scaled to capture the full actuator travel or load cell capacity. Once the

scale has been chosen a datum (or zero point) must be chosen too. To ensure the strain gauges are zeroed at zero strain, this occurs before the bottom grip is closed where the specimen is simply hanging from the top grip. This forms the datum for all of the DAQ channels.

3. The bottom grip is then closed, but some actuator movement may be necessary to ensure the entire specimen tab is in the jaws to prevent slippage during testing. This movement will appear on the DAQ position channel, but does not represent deformation to the specimen.
4. As the grips close a small force (up to 10 kN) may be applied to the specimen. Therefore the first task, after the grips are closed, is to tell the machine to make small actuator movements to bring the load applied to the specimen back to 0 kN.
5. The fatigue test is then started by telling the machine to apply a cyclic waveform of e.g +/- 1.8mm. This runs until failure. The machine does not deviate from this movement for any reason until it is stopped.

5.5.6 Results - Type A Tests

5.5.6.1 A1 and A2 Tests (Monotonic)

Monotonic static tests were performed on 2 specimens with longitudinal attachments. Each specimen was equipped with 7 strain gauges, as indicated in **Figure 154**. These quasi static tests were performed to establish Yield Stress (230 MPa) and Ultimate Strength or Tensile Strength (320 MPa) as shown in **Figure 156**. These tests also help to establish the use of strain gauges at and near the weld toe and the calibration ranges for the various strain gauges. In addition, it provides a correlation between measured displacement and recorded strains by the various strain gauges.

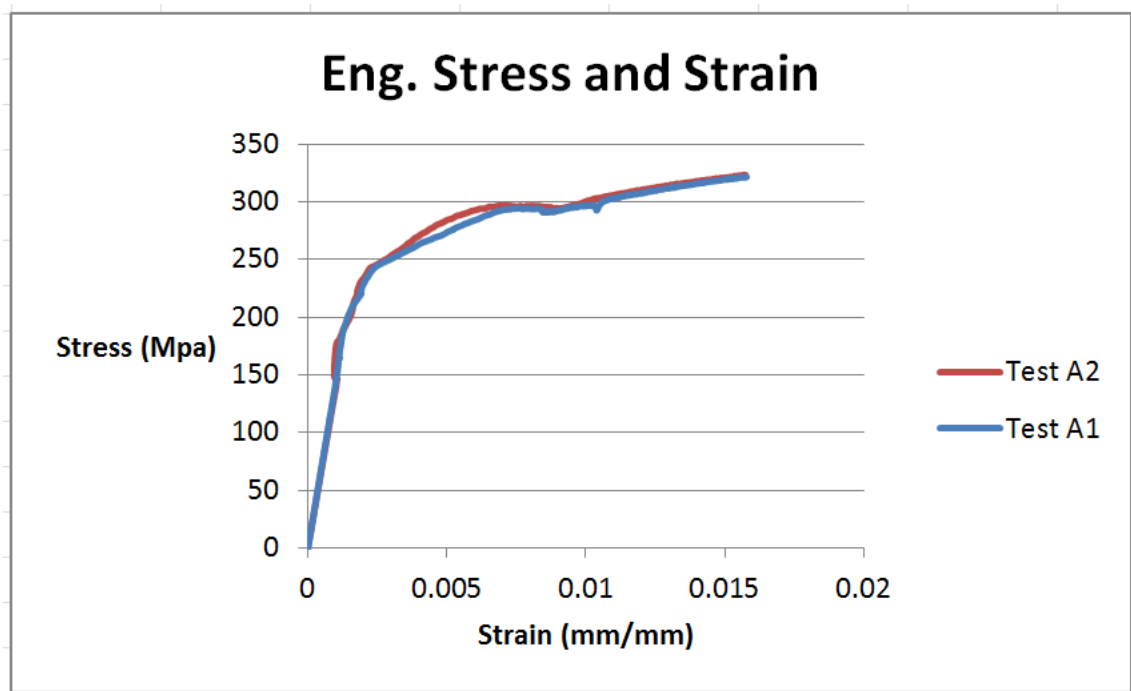


Figure 156: Test A1 and A2, nominal stress and strain

The initial dimension of the uniform cross section is approximately 90.20 mm x 15.9 mm for Test A1, **Figure 157**, and 90.10 mm x 15.95 mm for Test A2, **Figure 158**. Specimen A1 reached about 31mm total displacement and Specimen A2 reached about 28mm total displacement, at which point the machine could no longer apply any further load (630 kN).



Figure 157: Test A1 Set up

The approximate initial gauge locations for Test A1 and A2 are presented in **Tables 24** and **25**.

Table 24: Approximate initial gauge locations for Test A1

Strain Gauge No.	Location (Distance from weld toe) (mm)
1	2.6
2	10
3	17
4	24
5	2.6
6	10.5
7	2.6



Figure 158: Test A2 Set up

Table 25: Approximate initial gauge locations for Test A2

Strain Gauge No.	Location (Distance from weld toe) (mm)
1	2.6
2	9.6
3	16.5
4	24
5	2.6
6	10
7	2.6

Figures 159 and 160 show the local strain recorded in Test A2 with a maximum strain of 1.6% at 6mm displacement.

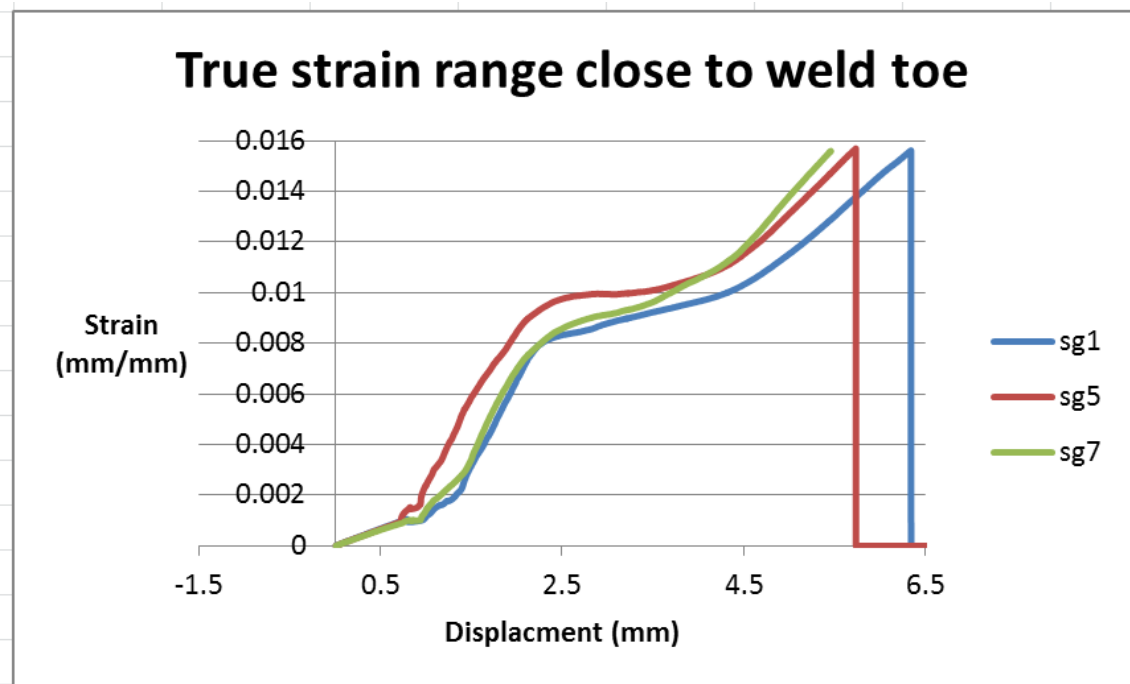


Figure 159: Test A2, local strain range close to weld toes

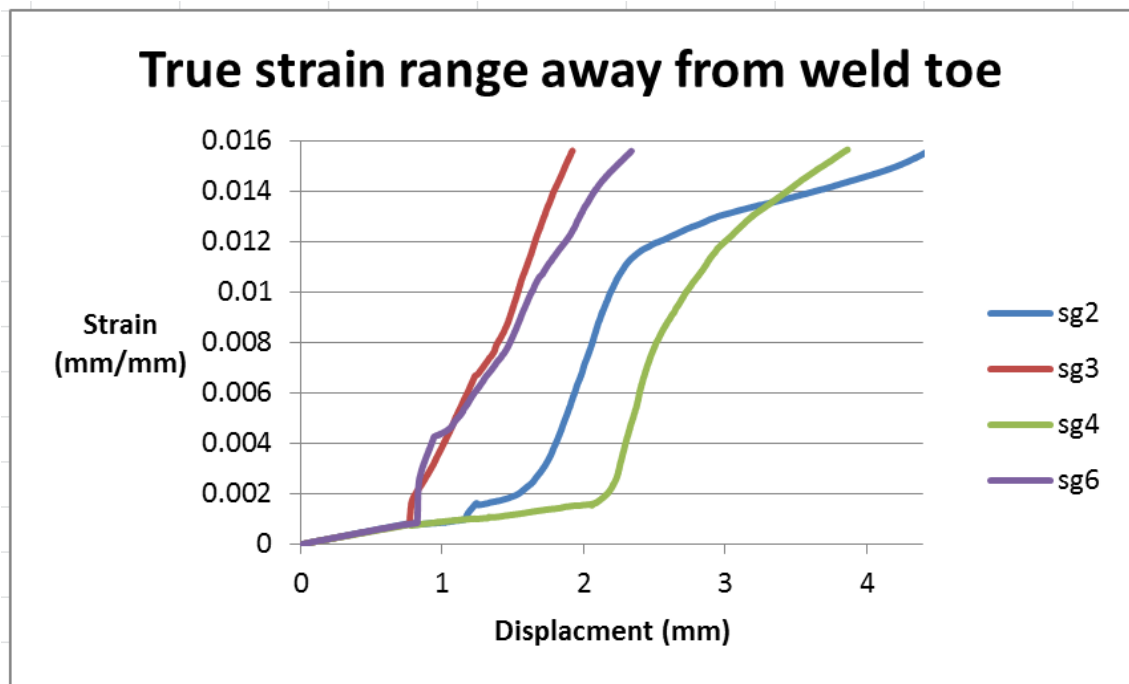


Figure 160: Test A2, local strain range away to weld toes

According to strain Gauges 1, 5 and 7 (closest to weld toe 2.6mm) in both tests the minimum and maximum displacement – local strain relationship is presented in **Tables 26** and **27** as follows:

Table 26: Displacement measure beyond which strain gauges stop recording

Test	Strain Gauge No.	Displacement (mm)	μ strain	Strain %
A1	1	6.26	15784.84	1.6
	5	6.26	15241.94	1.5
	7	5.862	15734.6	1.6
A2	1	6.339	15742.3	1.6
	5	5.733	15820.82	1.6
	7	5.457	15722.56	1.6
Ave		6	15674.51	1.6

Table 27: Initial displacement measure

Test	Strain Gauge No.	Displacement (mm)	μ strain	Strain %
A1	1	1	1227.318	0.1
	5	1	1153.064	0.1
	7	1	1480.552	0.1
A2	1	1	1154.75	0.1
	5	1	2386.969	0.2
	7	1	1397.074	0.1
Ave		1	1466.621	0.1

Therefore, the displacement range to be applied to the longitudinal attachment test A3 and A4 should be +/- 6mm incremental displacement which corresponds to 1.6% local strain range.

5.5.6.1.1 Monotonic Test Validation

A solid finite element model with 45° weld flank angle and 0mm weld toe radius was created and FE analysis was carried out in order to validate the monotonic test and to develop relationship between applied displacement and local strain. For the input, mild steel and deposit metal flow stress data available in literature was used. The numerical results agree well with the test results as shown in **Figure 161** which compares the 0 to 1.25mm range. The difference between the two is explained by the fact that the value of yield stress and hardening parameter used in the FEA were obtained from literature. The actual yield stress in this case is higher while the material exhibits no hardening.

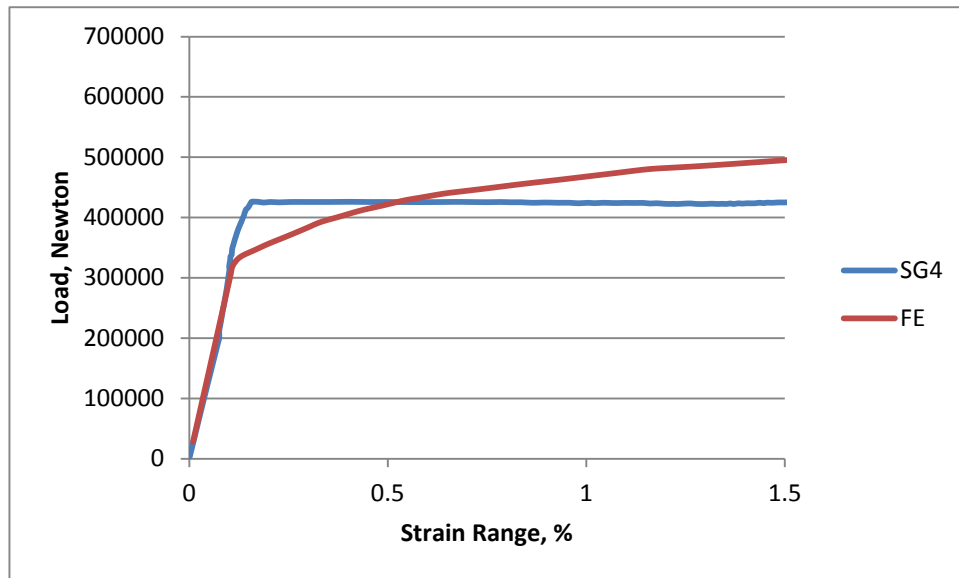


Figure 161: Test Validation 1.25mm Displacement

5.5.6.2 A3 and A4 Tests

The longitudinal attachment was pulled to +6mm in tension at a rate 0.3mm/min (0.05Hz) then unloaded to 0 kN. During the compression cycle buckling of the specimen was observed at 200k Newton (-2mm). Test was stopped as buckling mode of failure is not desired. None of the results were considered.

In A4 test, the longitudinal attachment was repeatedly pulled to +6mm in tension at 0.3mm/min (0.05Hz) then unloaded to 0 kN, results are shown in **Figure 162**. As predicted, the specimen reached about 30mm total displacement, at which point the machine could no longer apply any further load (630 kN).

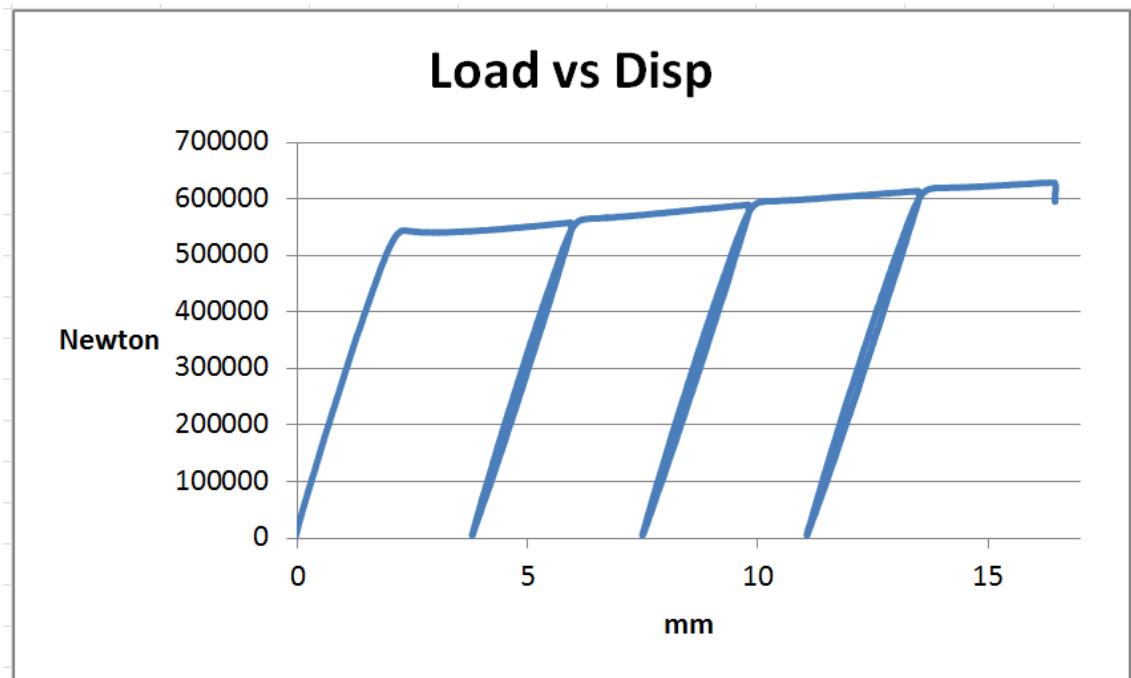


Figure 162: Test A4 results

From test A3 it was clear that the displacement of 6mm caused global plasticity in specimen with longitudinal attachment and because previous specimen did not buckle at -200MPa, we decided to try corresponding +/- 1.1mm (i.e. +1.1mm in tension and -1.1mm in compression), total 2.2mm displacement range with a frequency of 0.2 Hz on Specimen A5.

5.5.6.3 A5 Test

The specimen failed due to LCF after 9500 cycles and the max recorded strain range was 1.4% with no buckling. The specimen failed at weld toe as expected **Figure 163**. For other plots of test A5 please refer to **Appendix 4**. Therefore, test A6 was run with 1.3mm displacement in tension and 1.3mm in compression, 2.6mm in total.



Figure 163: A5 specimen, failure at weld toes

5.5.6.4 A6 Test

Displacement range as a controlled parameter is plotted against nominal stress range, nominal strain range and number of cycles to failure in order to make sure that test conditions remain the same throughout the test. Test A6 diagrams **Figures 164 to 166** have been added here as an example. Test A6 specimen also failed at the weld toe as expected.

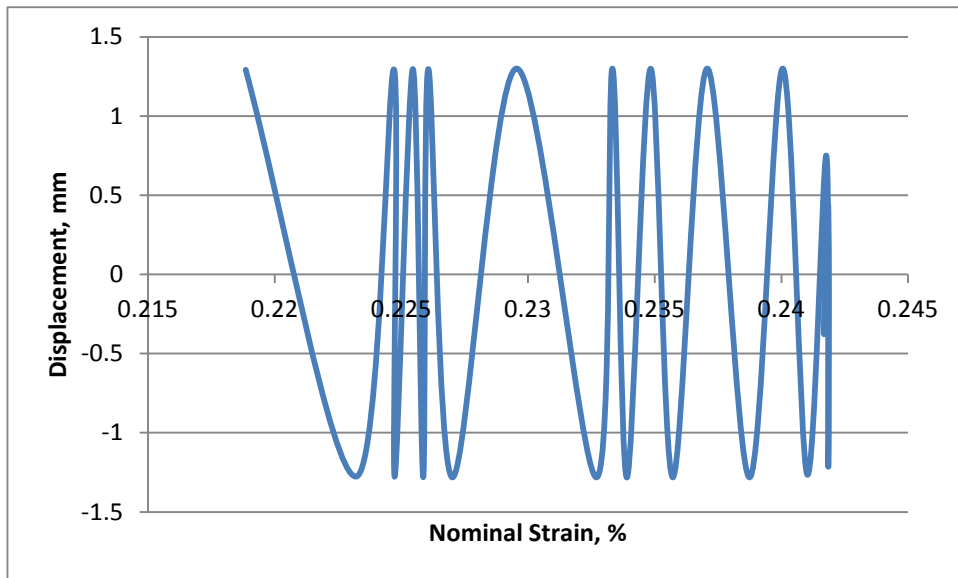


Figure 164: Test A6 Displacement vs. Nominal Strain Range

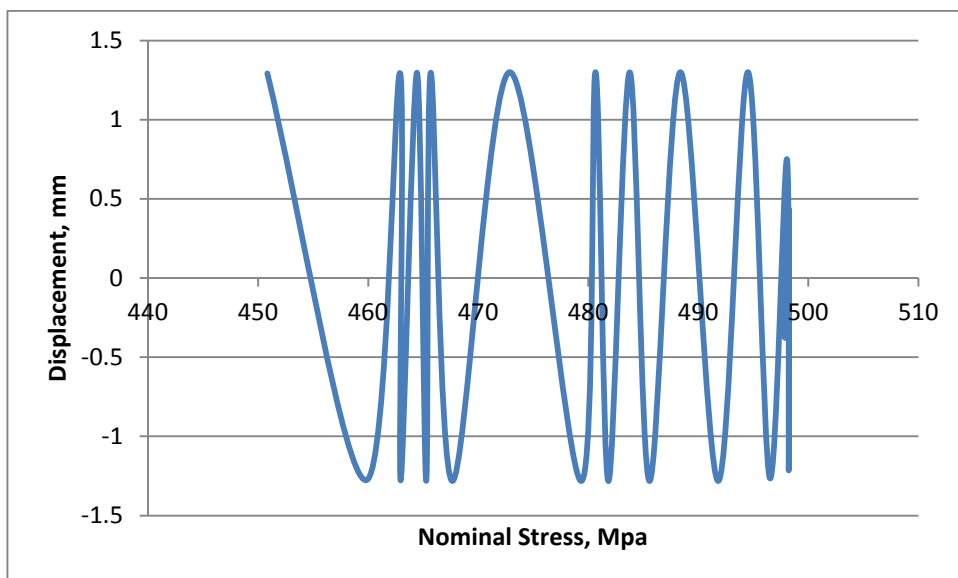


Figure 165: Test A6 Displacement vs. Nominal Stress Range

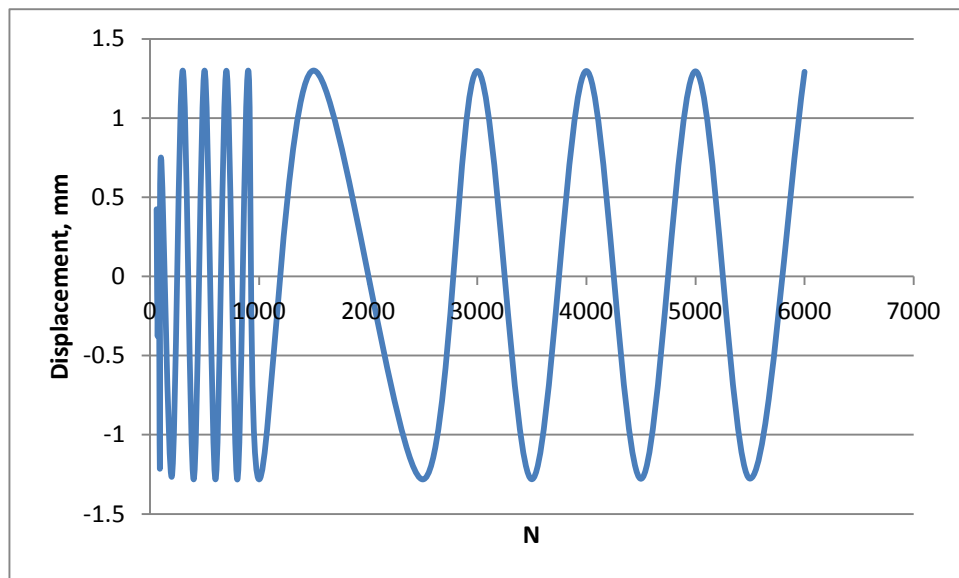


Figure 166: Test A6 Displacement vs. Number of Cycles to Failure

Table 28 below presents a summary of Type A test results. Only Test A7 is presented in this section as an example of the LCF test carried out on the longitudinal attachments. For other Type A Tests results; all relevant data, plots of loading, stress and strain ranges are presented in **Appendix 4**. All the specimens (tests A7 to A13) failed at the weld toe as expected.

Table 28: Type A test results

Test	Frequency, Hz	Displacement, mm	Nominal Stress Range, Mpa	Nominal Strain Range, %	Number of cycles to failure
A1	Unknown	31	293	0.14	N/A
A2	Unknown	28	292	0.14	N/A
A3	0.05	+/-6	Unknown	Unknown	N/A
A4	0.05	+/-6	Unknown	Unknown	N/A
A5	0.2	+/-1.1	421	0.2	9,500
A6	0.25	+/-1.3	498	0.24	6,300
A7	0.25	+/-1.5/1.4	564	0.27	5,000
A8	0.25	+/-1.5	565	0.27	3,600
A9	0.25	+/-1.6	587	0.28	3,070
A10	0.25	+/-1.7	608	0.3	2,150
A11	0.25	+/-1.8	622	0.3	1,200
A12	0.25	+/-1.9	629	0.3	475
A13	0.25	+/-2	628	0.3	450
A14	0.25	+/-1.2	438	0.3	10350
A15	0.25	+/-1.5	533	0.3	4339

5.5.6.5 A7 Test

The specimen failed due to LCF after 5000 cycles and the max recorded strain range was 0.9% as presented in **Figure 167**. No buckling observed and a further strain gauge no. 6 was added to Test A10 specimen onwards in order to capture buckling if it is encountered. **Figures 167-171** illustrate the recorded test variables and observed shakedown and ratcheting (sg1 cyclic diagram).

Analysed cycles have been chosen in semi-log order. Unwanted cycles have been removed; for example cycles where testing is stalled and displacement records are not changing with change in load. For specimen A7 there were 40 records in each cycle (i.e. Zero-positive-zero-negative-zero). Interest is in stable diagram and when cyclic diagram starts changing towards failure. Minimum and maximum range shows the progression of maximum and minimum values of load and strain, and stress and strain ranges with number of cycles. Minimum and maximum values are taken from displacement limit

points. Nominal strain range is calculated as nominal stress range divided by Young Modulus of 206000Mpa.

5.5.6.6 Data Processing

Number of cycles to failure is defined as 20% drop in load or nominal stress or nominal strain range. This point is taken from nominal strain range curve where load/nominal stress/nominal strain range stabilises after 200 cycles to 0.25-0.26% (in case of Test A10). It is clearly visible from diagrams that this range start reducing quickly at the end, 20 % drop will be around 0.2%. This is considered as a failure point for the purpose of obtaining strain-life diagram and number of cycles to failure.

In Test A7 Stress or Strain range plots show when change in displacement range happened, that stable cyclic diagram can be found between 10 and 1000 cycles where the tests conditions are close to controlled strain conditions.

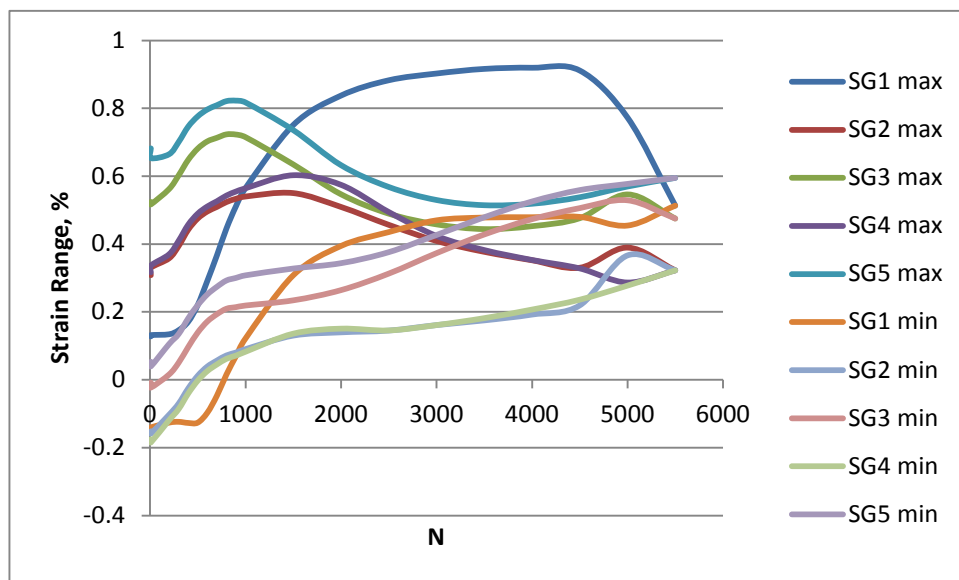


Figure 167: Test A7 Strain range, % (max & min) vs. no. of cycles

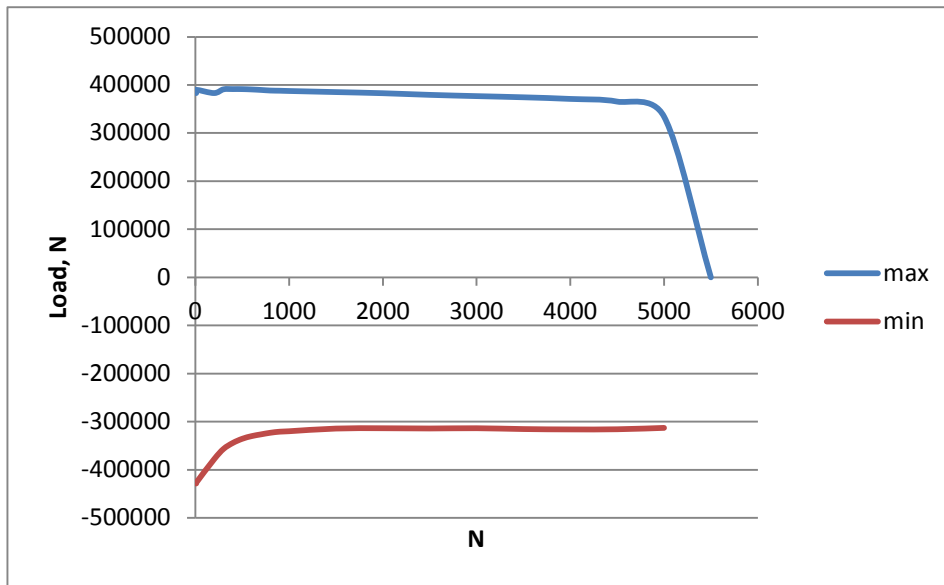


Figure 168: Test A7 Load, Newton (max & min) vs. no. of cycles N

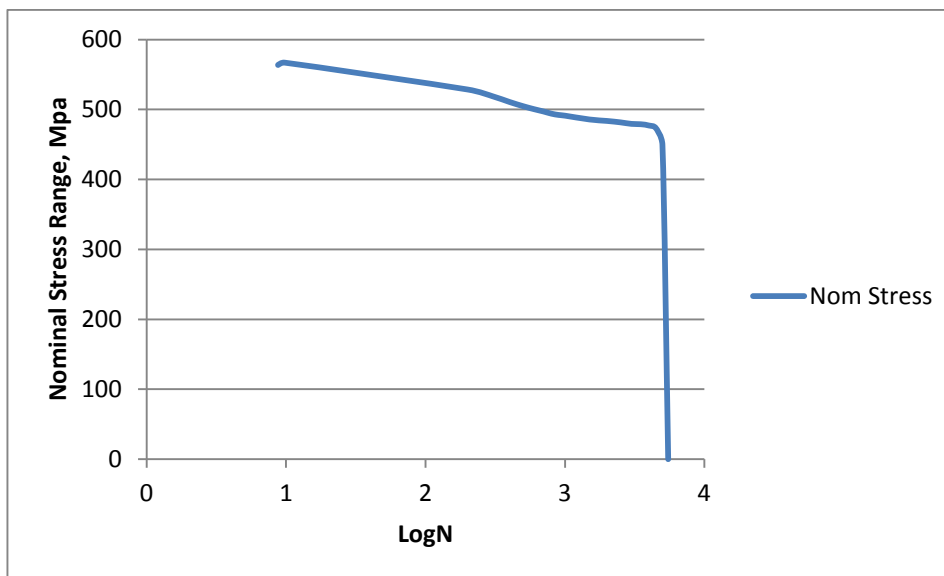


Figure 169: Test A7 Nominal Stress range, MPa vs. LogN

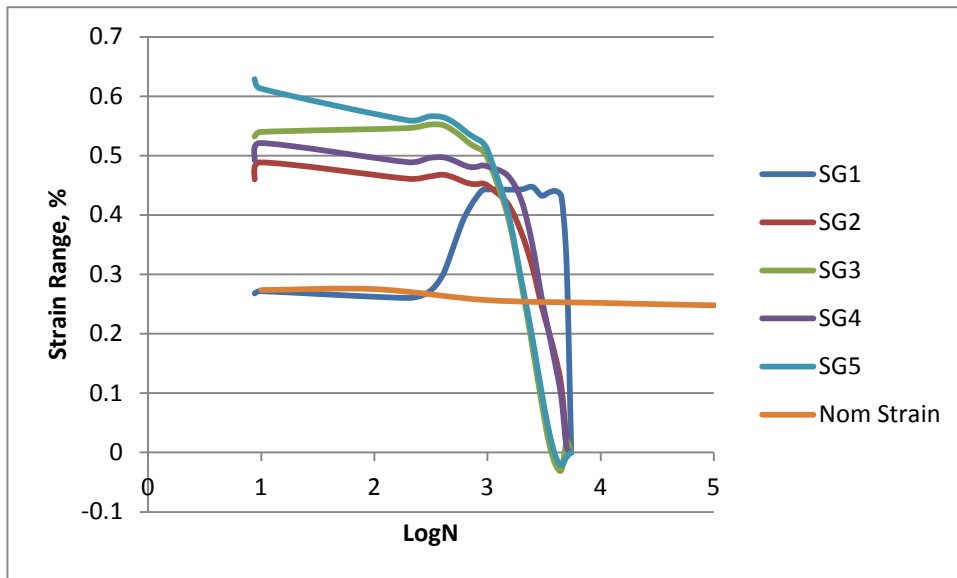


Figure 170: Test A7 Strain range, % (max & min) vs. LogN

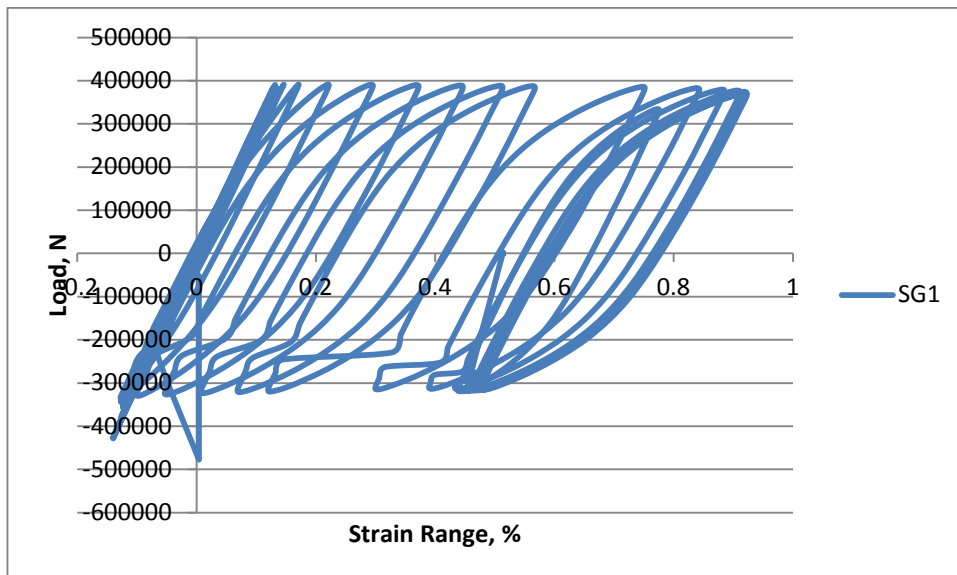


Figure 171: Test A7 Load applied vs. strain range (cyclic diagram)

5.5.7 Results - Type B Tests

5.5.7.1 B1 Test (Monotonic)

Monotonic test carried out to establish tensile data of the base metal used in Type A specimen. Test setup is shown in **Figure 172** and processed results presented in **Table 29**. Stress versus displacement data are plotted in **Figures 173** and **174** for specimen B1 and B2 respectively. Noted slippage of the specimen during first test prior to necking and final fracture **Figure 173**.



Figure 172: Type B and C Test set up

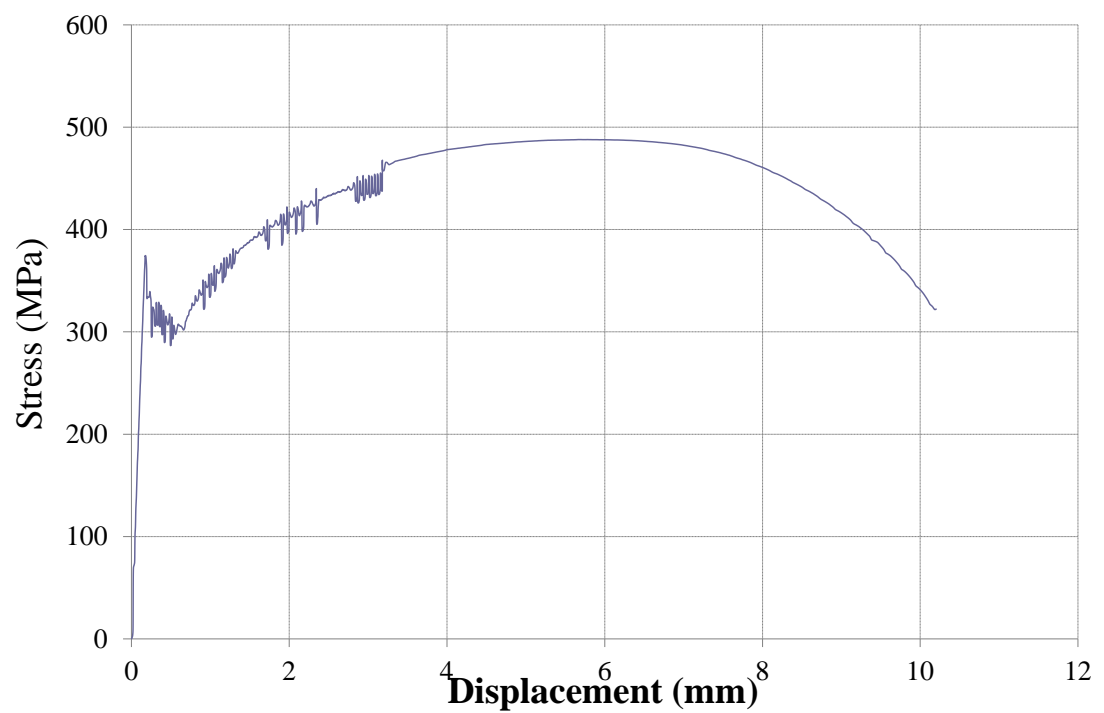


Figure 173: Monotonic test B1

5.5.7.2 B2 Test (Monotonic)

Monotonic test carried out and test results processed, **Figure 174.**

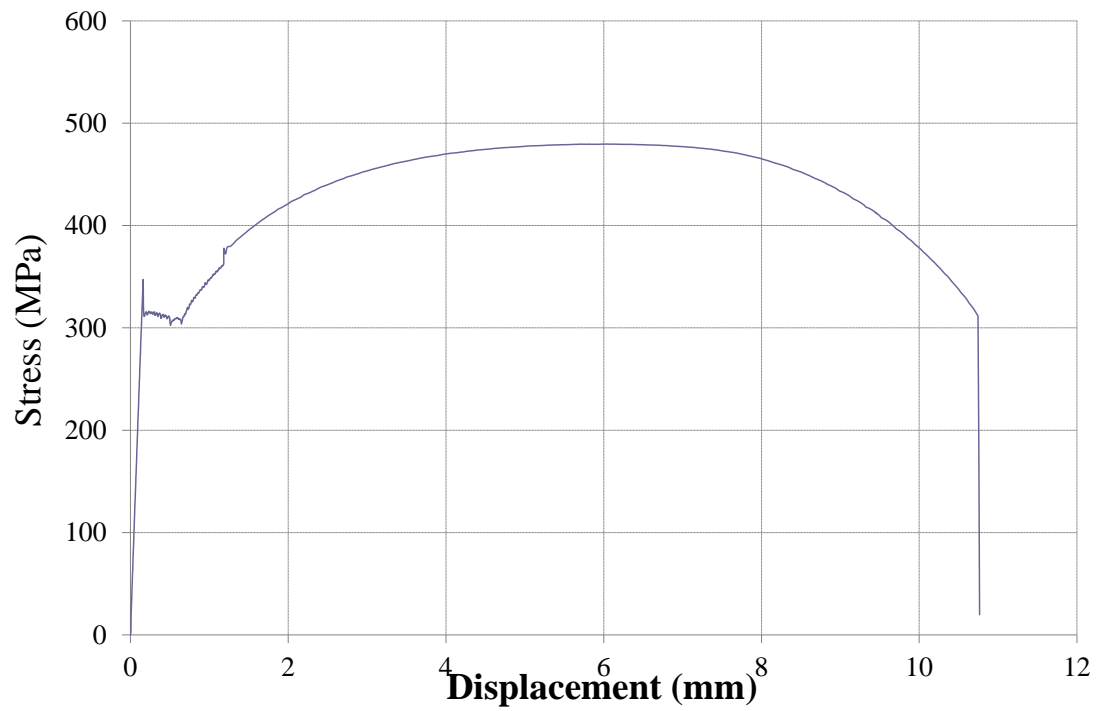


Figure 174: Monotonic test B2

Stress strain curves of B1 and B2 had similar plots as expected **Figure 175**.

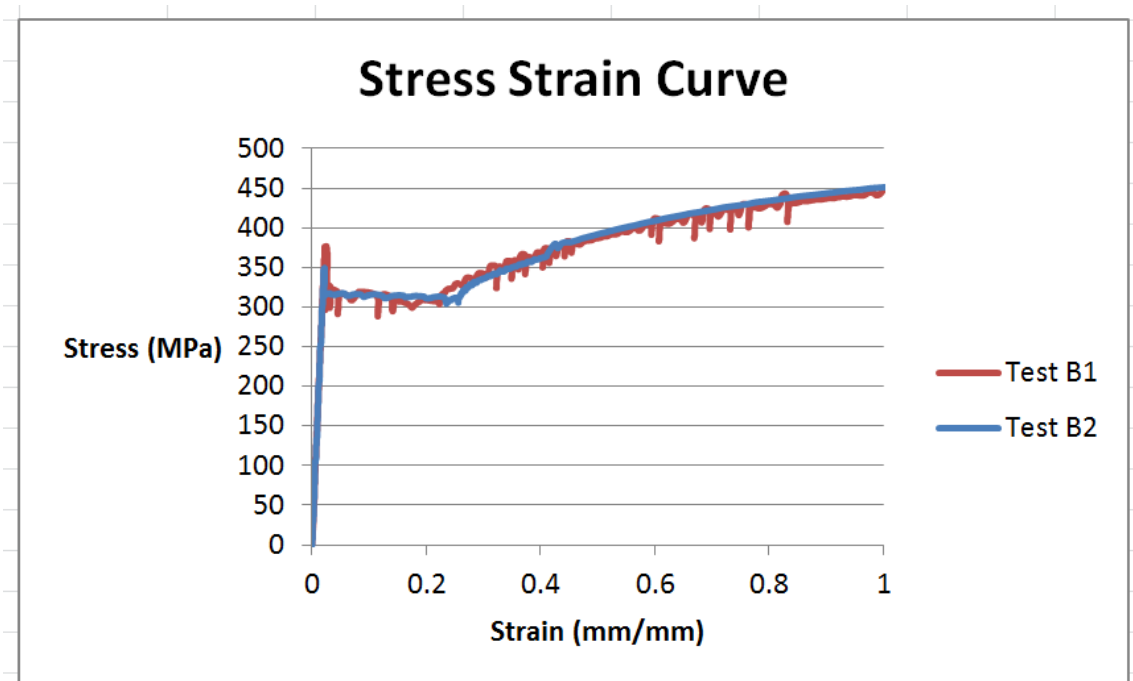


Figure 175: Comparison of monotonic tests type B

Table 29: Tensile information for the BMS

Specimen	Yield Strength, Mpa	UTS, Mpa
BMS1	376.0	455.5
BMS2	349.0	482.5

5.5.8 Results - Type C Tests

5.5.8.1 C1 Test (Monotonic)

Monotonic test carried out to establish tensile data of the weld metal used in Type A specimen. Test setup is the same as the one shown in **Figure 172** and processed results presented in **Table 30**. Stress versus displacement data are plotted in **Figures 176** and **177** for specimen C1 and C2 respectively.

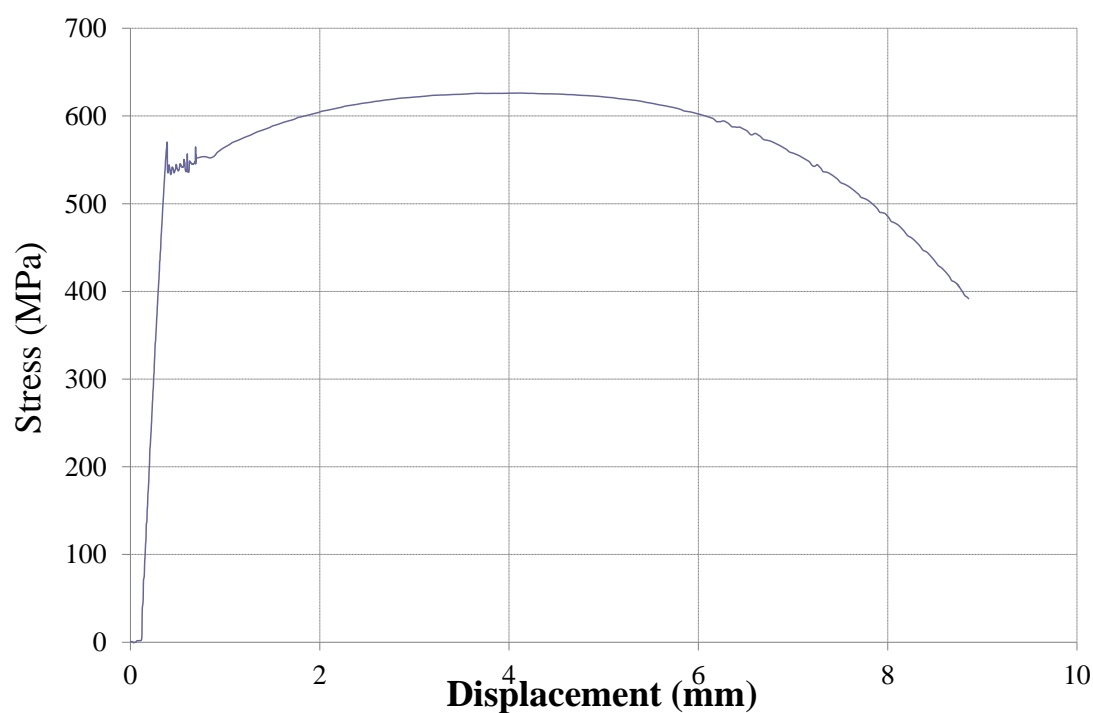


Figure 176: Monotonic test C1

5.5.8.2 C2 Test (Monotonic)

Monotonic test carried out and test results processed, **Figure 177**.

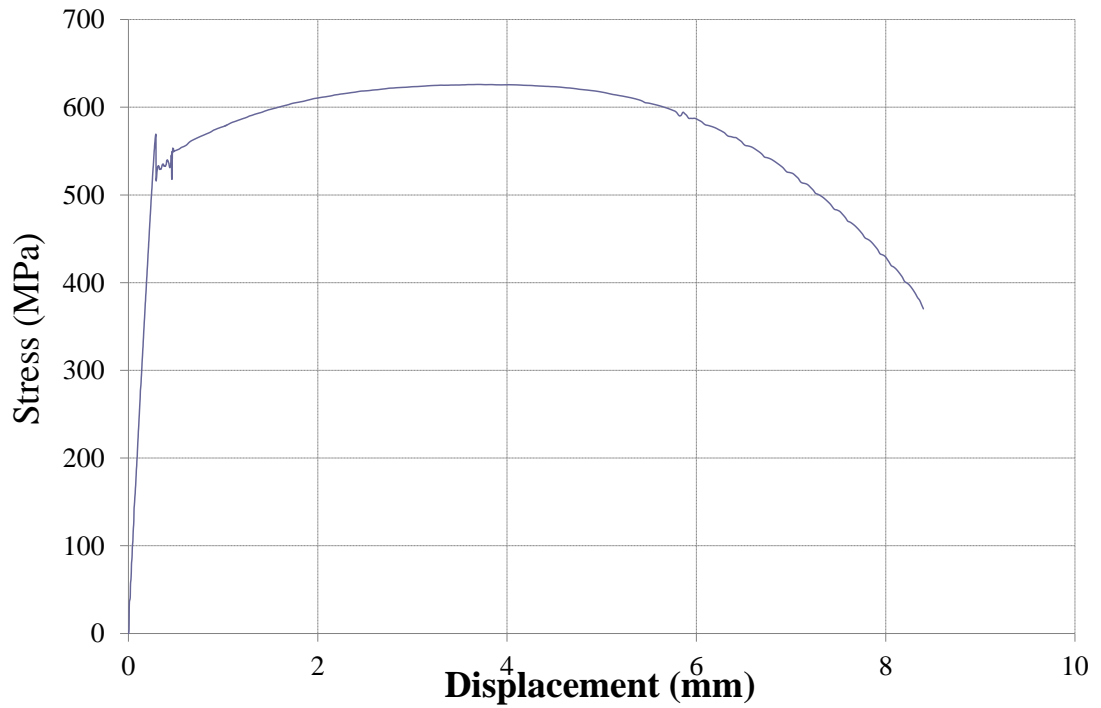


Figure 177: Monotonic test C2

Stress strain curves of C1 and C2 had similar plots as expected **Figure 178**.

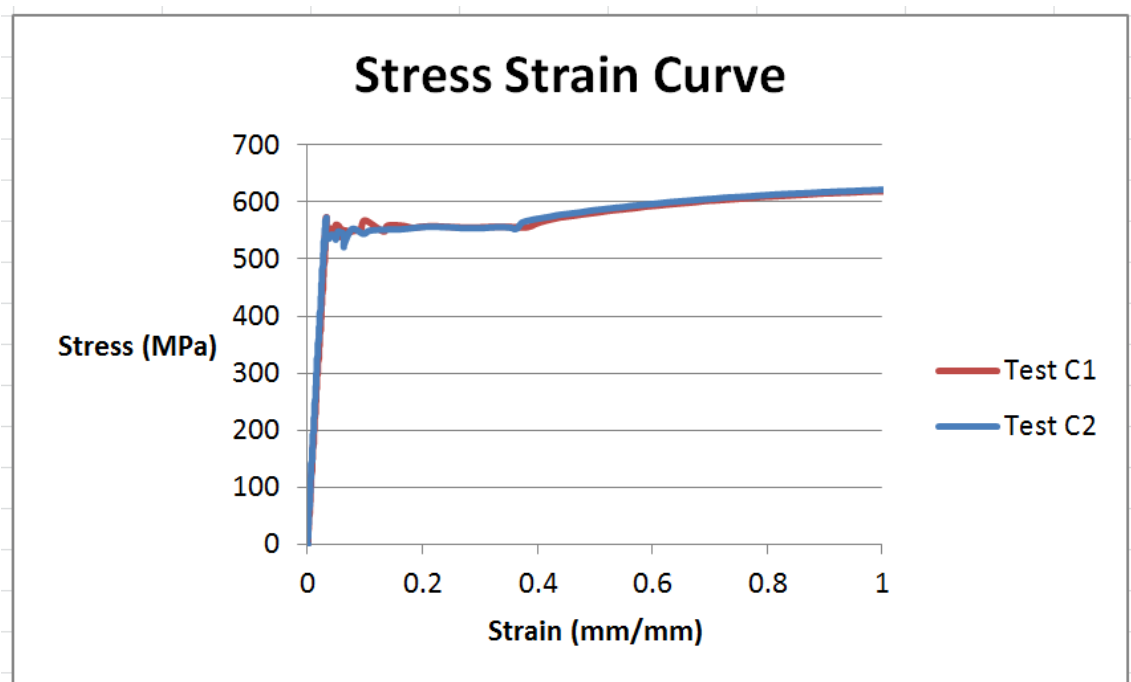


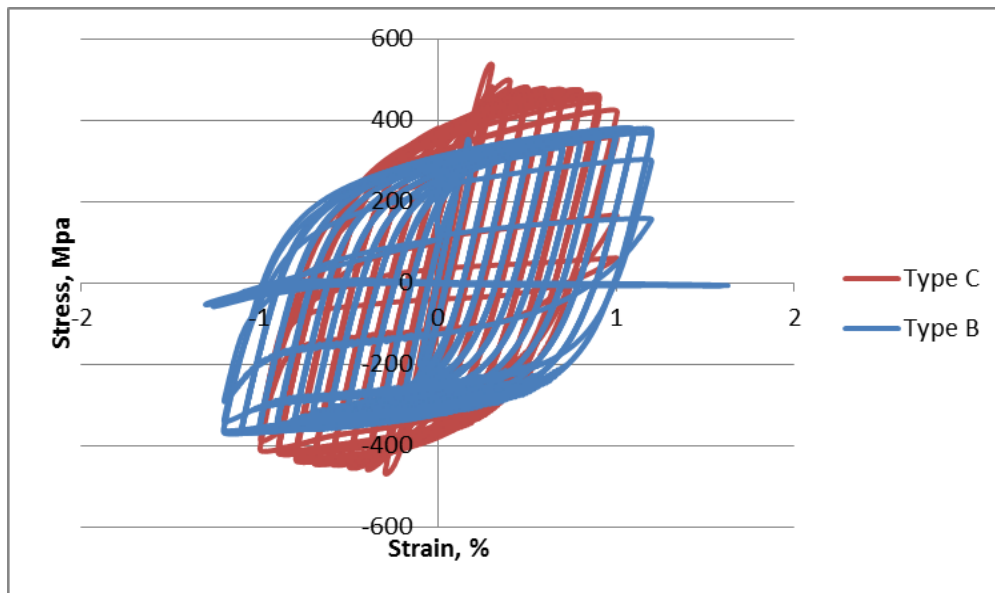
Figure 178: Comparison of monotonic tests type C

Table 30: Tensile information for the DMS

Specimen	Yield Strength, Mpa	UTS, Mpa
DMS1	572.0	629.8
DMS2	572.0	629.7

5.5.8.3 Type B and C Tests (Hysteresis)

This test was carried out in order to establish the stabilized stress strain curve for both the weld metal and the base metal specimens. **Figure 179** presents a comparison of the B specimen and C specimen hysteresis loops; the plots show clearly higher strength of the weld metal over the base metal which is expected purely due to the level of cooling the weld process (runs) is subject to compared to the cooling of the base metal (whole plate).

**Figure 179:** Type B and C specimens: Hysteresis Loop

5.5.8.4 LCF Tests Type B and C Specimens

Those tests were carried out to establish strain life of the base metal. Strain life of the weld metal and the base metal i.e. stress strain curves (40th cycle data) are shown in **Figure 180**.

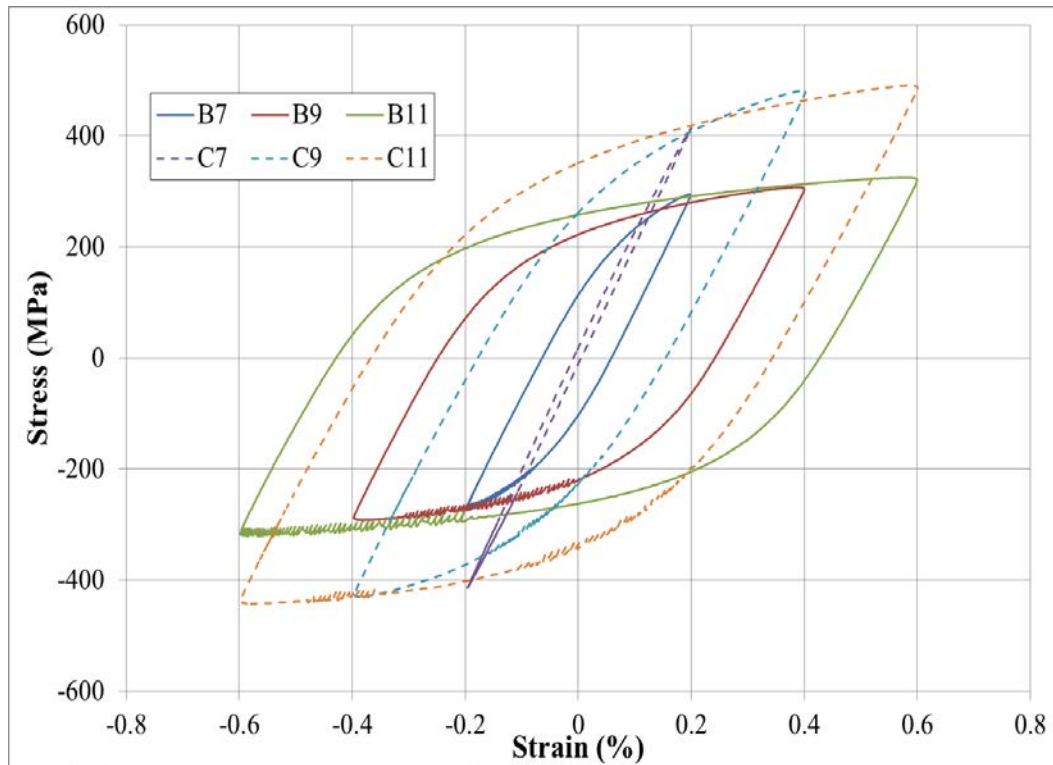


Figure 180: Type B and C specimens: Stress strain curves of stated specimens

5.5.8.5 Type B and C LCF Tests

The LCF tests carried out to Type B and Type C specimens' i.e. round type specimen and presented in **Table 31** below:

Table 31: Type B and C LCF test results

Test number and specimen type	Strain range applied	Number of cycles to failure
B10	+/- 0.6%	550
C10	+/- 0.6%	310
B12	+/- 0.8%	370
C12	+/- 0.8%	252
B14	+/- 1.0%	180
C14	+/- 1.0%	78
B15	+/- 1.0%	153

Figure 181 shows a comparison curves for the number of cycles to failure of both specimens B and specimen C; the plot illustrates the material behaviour of the base

metal compared to weld metal in terms of strain range applied vs number of cycles to failure.

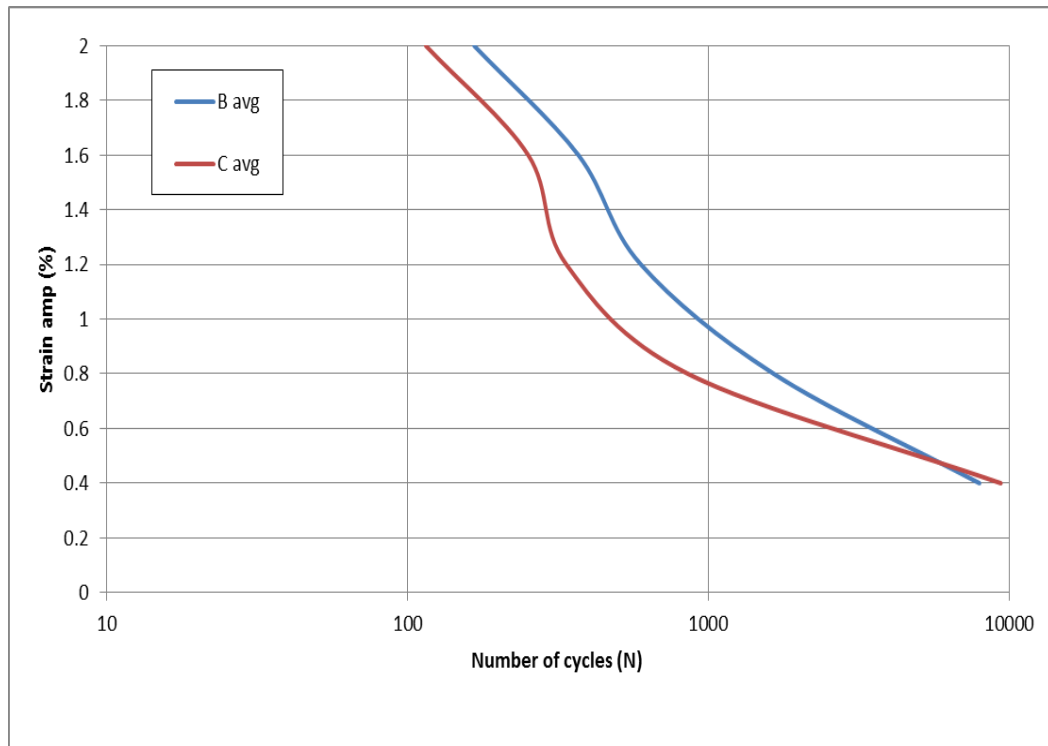


Figure 181: Type B and C specimens: S-N Curve data (strain curves)

Note: A16, B13 and C13 are all spare specimens.

5.6 Conclusions

1. LCF tests of longitudinal attachment specimen have been performed because this important structural element is seldom tested compared to the transverse attachment or cruciform.
2. During tension compression LCF testing buckling mode should be avoided
3. All the specimens failed at weld toes as expected
4. Beyond 2mm displacement and nominal strain range of 0.3% buckling is observed
5. BMS yield stress is 36% smaller than DMS yield stress as expected
6. BMS UTS is 28% smaller than DMS UTS as expected

Chapter 6

LCF Novel Approach

6 CHAPTER 6: LCF Novel Approach

This chapter describes the novel approach proposed by the author for the assessment of LCF. The novel approach has been applied to the two most common structural details of FPSO ship structure, the transverse and the longitudinal attachments, both in terms of FEA and fatigue tests.

6.1 Proposed LCF Assessment Methodology

As illustrated in Chapter 2; the elastic-plastic notch root approach is indispensable for solving problems of service fatigue strength in the LCF range and the well founded approach of structural stress or hot spot stress in the HCF range (predominantly elastic behaviour) is questionable when extended to the LCF range (predominantly plastic behaviour). IIW recommendations confines the applicability of the S–N curve FAT 225 by prescribing a minimum fatigue notch factor $K_w = 1.6$ and for LCF, the design S–N curve FAT 225 must be limited by $FAT\ 160 \times K_w$ (with $K_w \geq 1.6$). IIW recommendations for FAT 225 covers the medium fatigue range not the low cycle range i.e. below the threshold of 10^4 . In Chapter 3; in contrast to the widely applied nominal and structural hot spot stress approaches, notch stress approach 3.1.1 can explicitly consider the shape of the weld and the effective notch stress concept for fatigue prediction of welded joints is considered to be the most recent model for fatigue assessment of welded joints. The strain life method illustrated in 2.2.6 and 4.1.1 is neither practical nor readily available due to lack of material and strain-life data and also cannot be easily added to the HCF damage. In Chapter 4; the calculated stress ranges for LCF is corrected using a plasticity correction factor in order to employ the S–N curve instead of a strain cycle curve and in design S–N curves; continuity from low cycle regime to high cycle regime is achieved by expressing the low cycle data in terms of pseudo elastic stress range (i.e. strain range multiplied by elastic modulus). The corresponding design S–N curves adopted by the different class societies under this method are quite similar, however, they result in significantly large differences in the LCF damage they predict for a given stress range.

Considering the above facts and in order to overcome the disadvantages of the various approaches the author is proposing a novel approach that will utilize the elastic plastic notch root approach, avoid the questionable hot spot stress, explicitly consider the shape of the weld, avoid all approximations and uncertainties of plasticity correction and pseudo elastic stress range.

6.1.1 Novel Approach

The author is proposing the use of elastic-plastic notch stress approach instead of the pseudo elastic stress or the structural hot-spot stress methods. The approach provides for elastic-plastic stress obtained from nonlinear 3D FEA model of the relevant component, explicitly modelling the weld, to be used directly thereby avoiding the questionable hot spot stress and the associated approximations and uncertainties of plasticity correction and pseudo elastic stress range. Where the far-field (nominal) stress can be confidently established and a reliable SCF for the relevant structural detail is known, detailed FEA may not be necessary. The stress range obtained by multiplying the far-field stress by the SCF (i.e. nominal elastic notch stress) can be converted to elastic-plastic notch stress range by the use of Neuber's rule in conjunction with Ramberg Osgood curve for the relevant material.

By using this approach, the pseudo elastic stress range axis (y-axis) in the S-N curve is converted into elastic plastic notch stress. This can be accomplished by utilizing the Ramberg-Osgood and Neuber's relationship as illustrated in **Figure 182**.

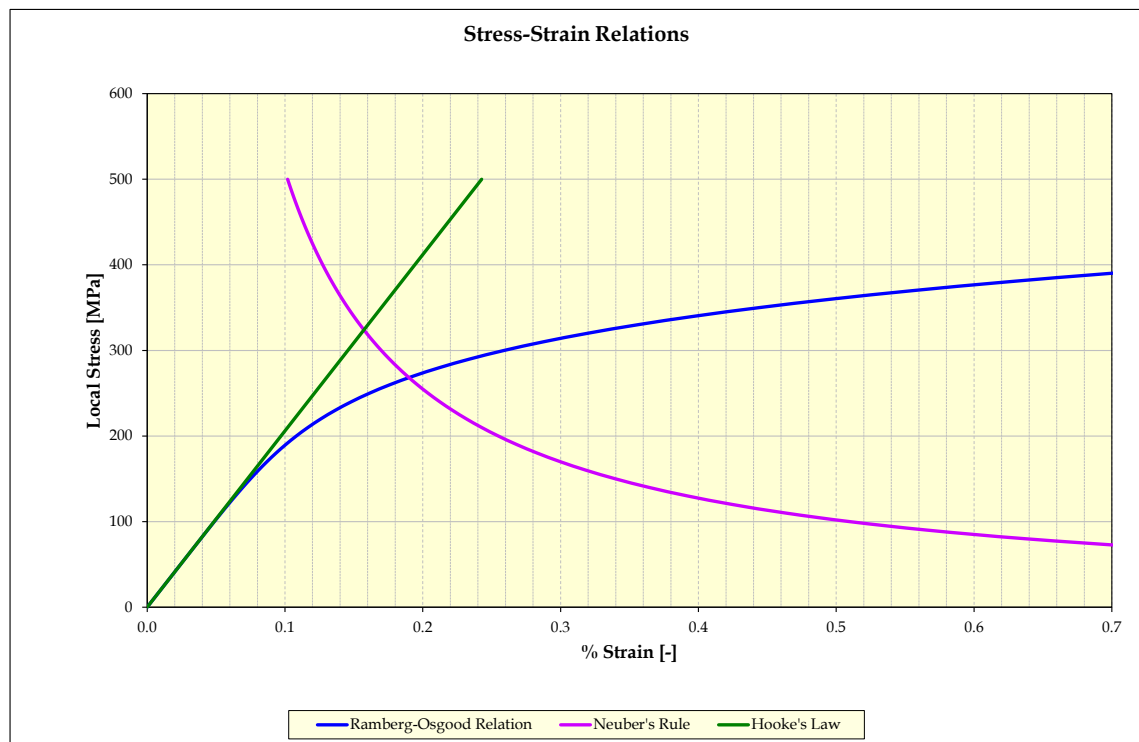


Figure 182: Stress strain– Neuber and Ramberg Osgood relationships

The correlation between elastic plastic stress range and the pseudo elastic stress range as defined by Wang et al., (2006) is as follows:

1. Use of cyclic stress-strain curve (Eq.5) as defined in 2.1.1.3.1
2. Use of Neuber's rule to relate actual and nominal stress and strain both in the elastic and plastic states

$$\sigma_a \varepsilon_a = \frac{S_a^2}{E} \quad \text{Eq. 93}$$

$$S_a = \frac{S_L}{2} \quad \text{Eq. 94}$$

3. Determine actual stress and strain by solving Eq.5 and Eq.93 simultaneously
4. Calculate strain range

$$\varepsilon_R = 2\varepsilon_a \quad \text{Eq. 95}$$

5. Calculate pseudo elastic stress range

$$S_L = E\varepsilon_R \quad \text{Eq. 96}$$

Considering the example of local stress strain value (according to Neuber) as in 2.2.3.1 Neuber's coefficient is defined as

$$\frac{\text{Elastic Notch Stress Amplitude}}{\text{Young's Modulus}} \text{ or } \frac{(\sigma_{k,a})^2}{E} = \frac{\text{Nominal Stress Amplitude} \times K_t}{E}$$

Where

S_a is the elastic stress amplitude = $S_L/2$

S_L is stress associated with LCF

Parameters used in the example below are as follows:

Stress concentration factor,	$K_t = 2.16$
Nominal stress amplitude,	$\sigma_{n,a} = 150 \text{ N/mm}^2$
Elastic notch stress amplitude,	$\sigma_{k,a} = \sigma_{n,a} \times K_t = 324 \text{ N/mm}^2$
Local notch stress amplitude	$\sigma_a = 268 \text{ N/mm}^2$
Local notch strain amplitude	$\varepsilon_a = 1.896 \times 10^{-3}$
Young's Modulus	$E = 2.06 \times 10^5 \text{ N/mm}^2$

Cyclic Strength Coefficient $K' = 981 \text{ N/mm}^2$

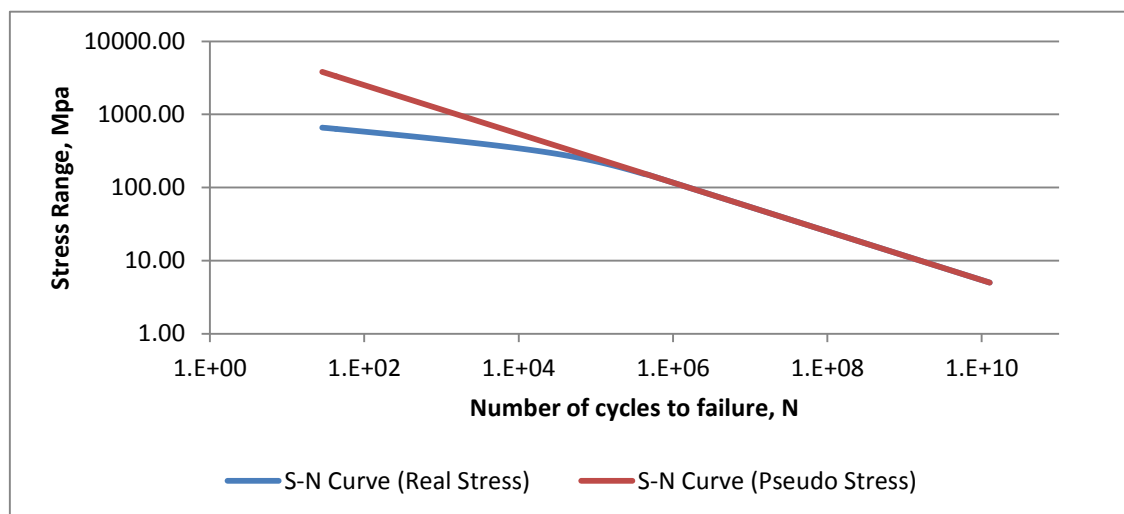
Cyclic Strain Hardening Exponent $n' = 0.1747$

Table 32 presents the above mentioned example with the points of intersection we are interested in.

Table 32: Stress strain relationship example

Stress-Strain Relations	Symbol	Value	Units
<i>Neuber's Rule</i>			
Neuber's Co-efficient	K_neuber	0.5096	MPa
<i>Ramberg-Osgood Relation</i>			
Young's Modulus	E	2.06E+05	MPa
Ramberg K	K_ramberg	9.81E+02	MPa
Ramberg n	n_ramberg	0.1747	-
<i>Hooke's Law</i>			
Peak Stress	stress_peak	400	MPa
Peak Strain	strain_peak	2	%
Output Parameter	Symbol	Value	Units
<i>Point of intersection - Ramberg and Neuber Curves – Elastic Plastic</i>			
Local Stress	σ_a	268.237	MPa
Local Strain	ε_a	0.18998	%
<i>Point of intersection - Neuber and Hooke's Curve – Pseudo</i>			
Local Stress	$\sigma_{k,a}$	324.002	MPa
Local Strain	$\varepsilon_{k,a}$	0.15728	%

By converting the pseudo elastic stress range to elastic plastic notch stress, the BS D curve may be modified (re-defined) in terms of elasto-plastic stress range rather than pseudo stress range as illustrated in **Figure 183**:

**Figure 183:** S-N D Curve

The same modification (re-definition) may be applied to class societies S-N curves such as ABS, DNV, LR mean and LR Design. The advantage of doing so is to overcome the significantly large differences in the LCF damage they predict for a given stress range. This is clearly illustrated in **Figures 184** and **185**.

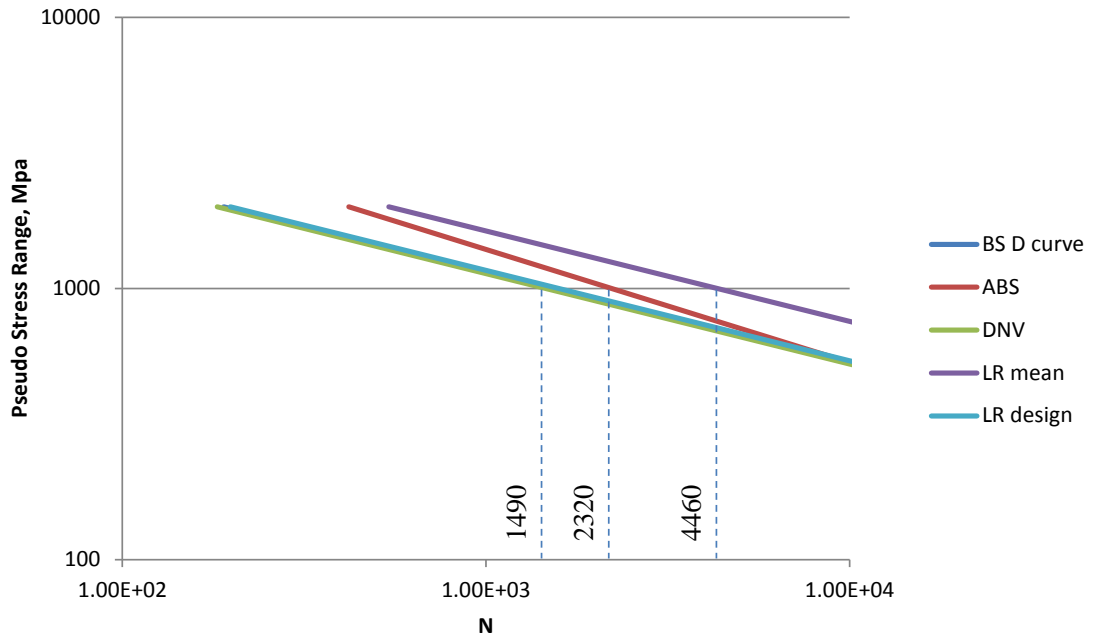


Figure 184: S-N Curves in pseudo stress range

In **Figure 184**, for a given stress range e.g. 1000 Mpa, the number of cycles to failure is significantly different, in this case 1490, 2320 and 4460. On the other hand using the elasto-plastic modified S-N curves, as in **Figure 185**, for a given stress range e.g. 390 MPa, the number of cycles to failure is not significantly different, in this case 3760, 4070 and 8770.

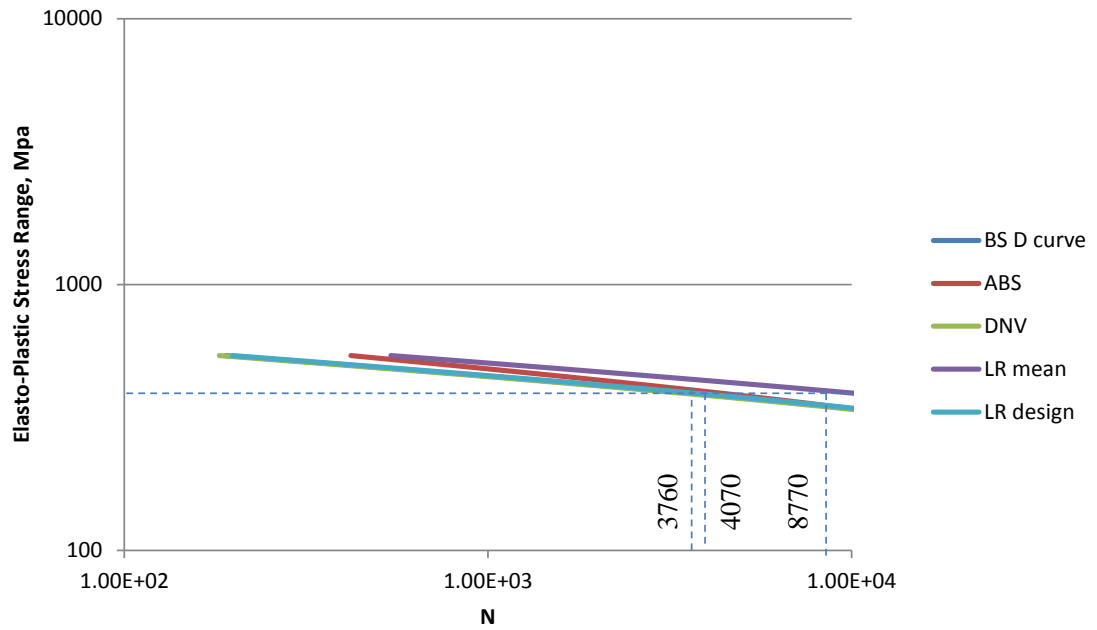


Figure 185: S-N Curves in elasto-plastic stress range

6.1.2 Novel approach applied to LCF test results

This approach can be applied to test results by obtaining local notch stress from farfield stress multiplied by the relevant SCF. Conversely, where local strain measurement at the weld toe is recorded in a test, the local notch stress is obtained by multiplying the notch strain with the Young's modulus to get the notch stress. Using Neuber's rule and the relevant Ramberg Osgood curve, the elastic notch stress is converted to the elasto-plastic notch stress and the number of cycles to failure is read off the modified D curve.

The steps or **procedure** to follow in order to apply the approach may be summarized as follows:

1. Considering the far field stress (nominal stress)
2. Consider the known stress concentration factor (SCF)
3. Multiply the nominal stress by SCF to get the nominal elastic notch stress
4. Use Neuber's rule to convert the nominal elastic notch stress to corresponding elasto-plastic notch stress
5. Use the modified British Standard S-N curve (D Curve) to obtain the number of cycles to failure.

This approach was applied to the available DSME test results, the transverse attachment (cruciform), TWI test results, the longitudinal attachment and the new test results, the longitudinal attachment (Type A) presented in chapter 5. **Figure 186** shows the test results along with the various S-N curves based on pseudo stress while **Figure 187** present the same test results based on the elasto-plastic notch stress method. The latter shows a much better correlation between the various test results as well as the design S-N curves.

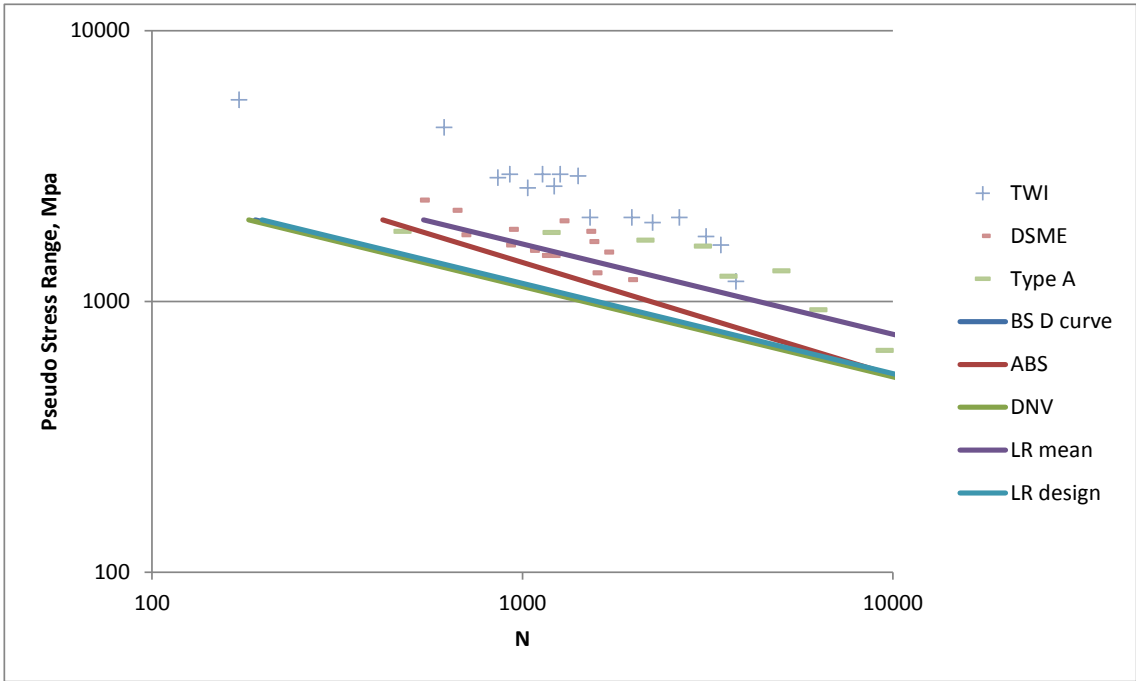


Figure 186: Test Results and S-N design Curves – Pseudo Elastic Stress

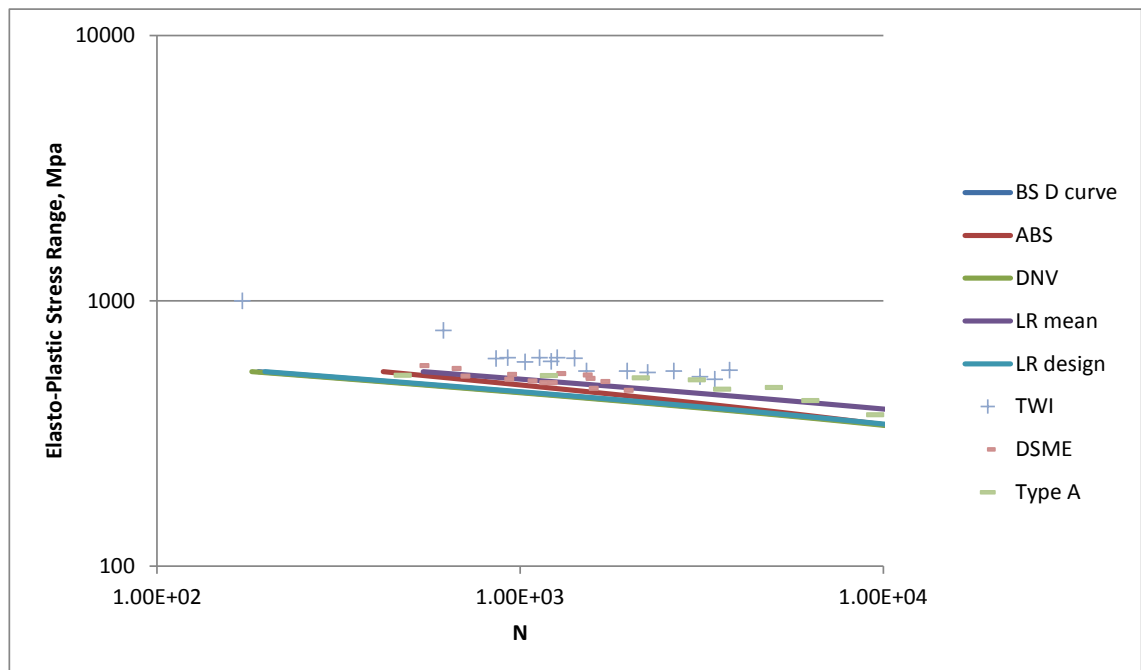


Figure 187: Test Results and S-N design Curves – Elastic-Plastic Notch Stress

6.1.3 Novel approach applied to nonlinear FEA

Nonlinear FEA using elastic-plastic cyclic properties of mild steel base metal and weld metal together with the ‘Effective Notch Stress’ (ENS) method (i.e. 1mm radius at weld toe) was implemented for transverse and longitudinal attachments. The 1st principal stress range obtained from FEA is then used directly to get the number of cycles to failure from the modified D curve.

The key steps may be summarized as follows:

1. Model the Transverse (Cruciform) or Longitudinal Attachment with 1mm or 0mm radius at Weld Toe with 0.25mm mesh density
2. Add the cyclic properties of the base metal and weld deposit metal
3. Apply the correct loading condition (strain or displacement control)
4. Run the nonlinear analysis,
5. Get the results in 1st principal stress range
6. Use the modified British Standard S–N curve (D Curve) to obtain the number of cycles to failure.

6.1.3.1 Transverse (Cruciform) Attachment Model

The transverse (cruciform) attachment quarter model was created in ANSYS as per dimension given in **Figure 188** including 7mm lack of penetration as specified in Urm et al., (2004b). The mesh density was as per the IIW recommendation 0.25mm at the effective notch radius of 1mm or 0mm. Mild steel Grade A flow stress data given in **Table 33** and **Figure 189** were used in the analysis together with Young's Modulus of 210000 MPa for the base metal and Deposit Metal cyclic properties given in **Table 34** and **Figure 190** were used in the analysis together with Young's Modulus of 210000 MPa for the weld metal.

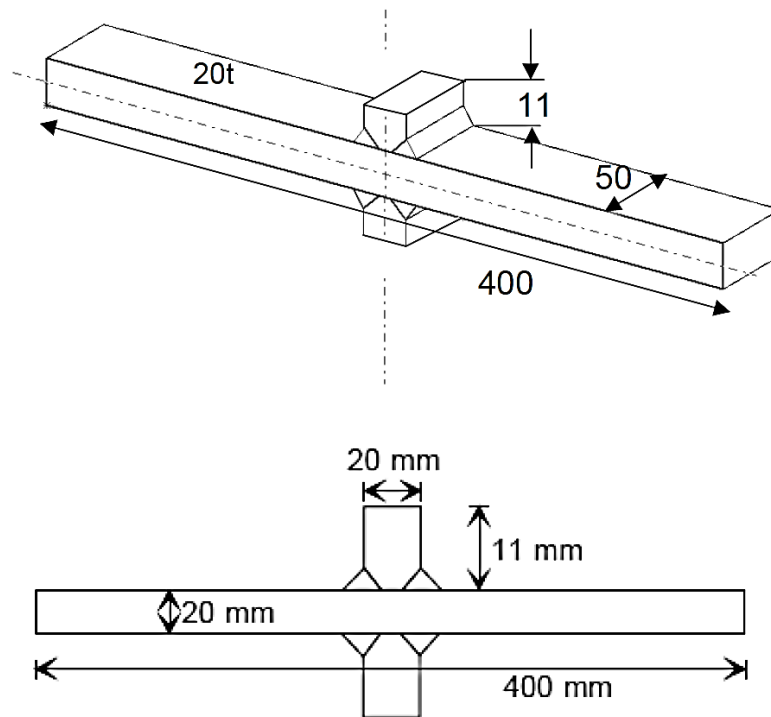


Figure 188: Transverse (Cruciform) Attachment Full Model Dimensions

Table 33: Mild steel Grade A flow stress data (Wang et al., 2006)

Plastic Strain mm/mm	Stress (Pascal)
0.0	2.36E+08
0.001	2.57E+08
0.002	2.80E+08
0.003	2.94E+08
0.004	3.05E+08
0.005	3.13E+08
0.01	3.41E+08
0.02	3.71E+08
0.03	3.90E+08
0.04	4.04E+08
0.05	4.16E+08
0.1	4.52E+08
0.2	4.93E+08
0.3	5.18E+08
0.4	5.36E+08
0.5	5.51E+08
0.6	5.64E+08
0.7	5.74E+08
0.8	5.84E+08
0.9	5.92E+08
1	6.00E+08

Where $K' = 600 \text{ MPa}$ and $n' = 0.123$

Note: Elastic strain of $9.47\text{E-}04$ subtracted prior to input into Ansys.

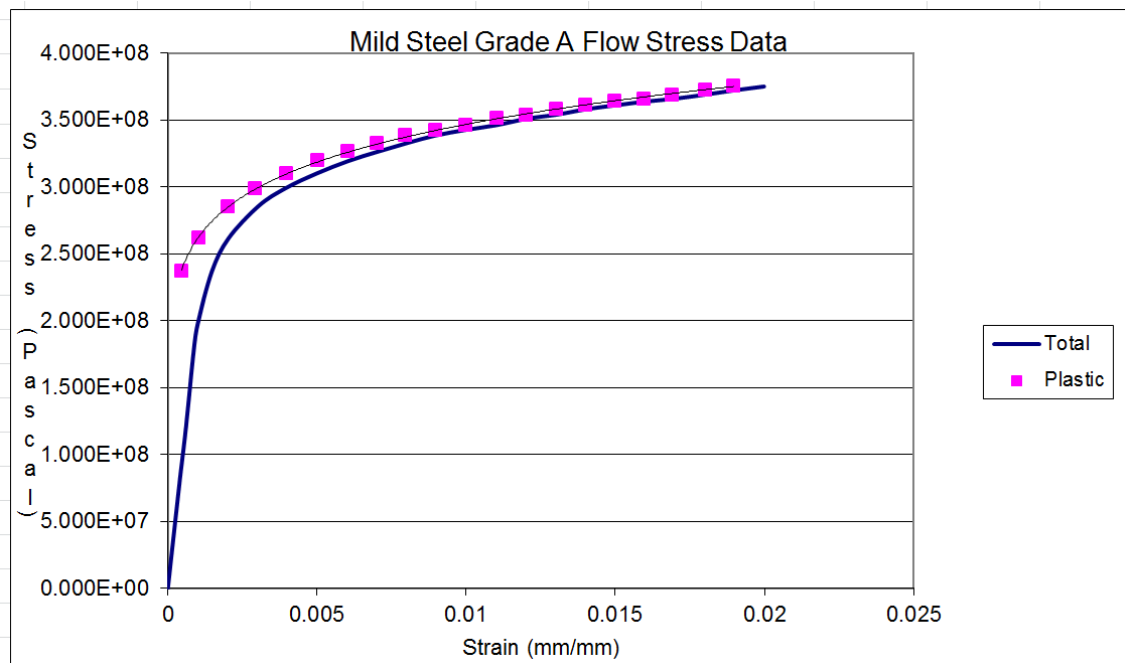


Figure 189: Stress strain curve of base metal

Table 34: Deposit Metal Cyclic Properties Urm et al., (2004b)

Plastic Strain mm/mm	Stress (Pascal)
0.0	3.54E+08
0.001	3.86E+08
0.002	4.20E+08
0.003	4.42E+08
0.004	4.57E+08
0.005	4.70E+08
0.01	5.12E+08
0.02	5.57E+08
0.03	5.86E+08
0.04	6.07E+08
0.05	6.23E+08
0.1	6.79E+08
0.2	7.39E+08
0.3	7.76E+08
0.4	8.04E+08
0.5	8.27E+08
0.6	8.45E+08
0.7	8.61E+08
0.8	8.76E+08
0.9	8.88E+08
1	9.00E+08

Where $K' = 900 \text{ MPa}$ and $n' = 0.123$

Note: Elastic strain of $1.43\text{E-}03$ subtracted prior to input into Ansys.

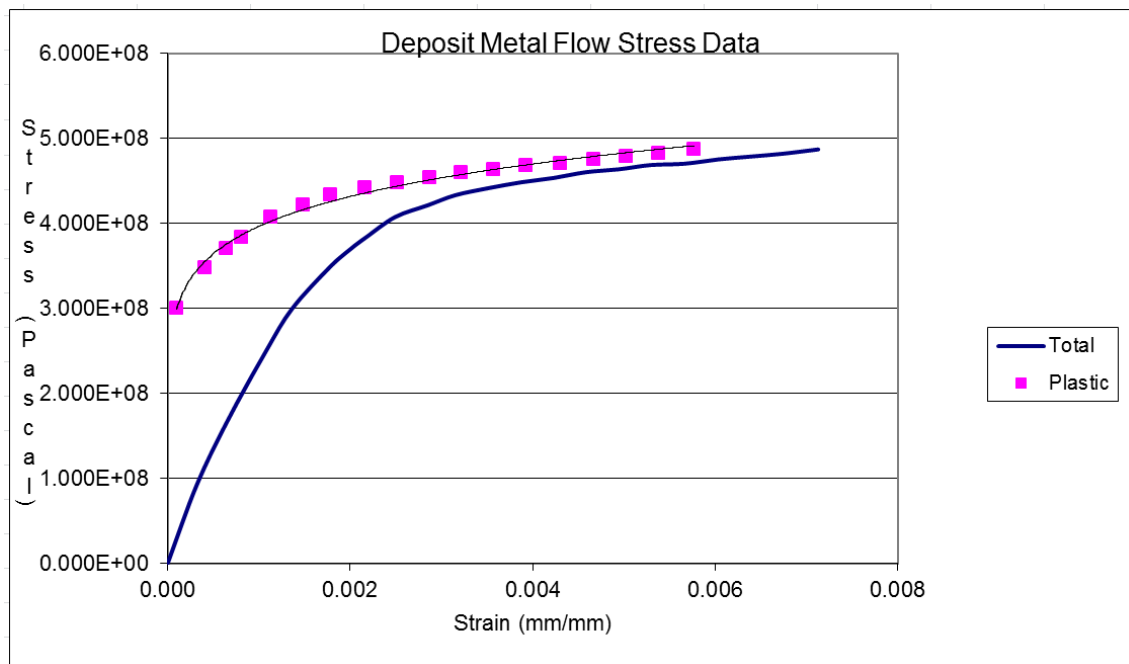


Figure 190: Stress strain curve of deposit metal (Weld)

Figures 188 and 190 cover up to 2.5% of strain range, in order to avoid the extrapolation Ansys will perform to cover the rest of the range up to 100%, Ramberg-Osgood equation and material coefficients n' and K' have been used to develop the full range. The flow stress data used for input into Ansys is shown in **Figure 191**:

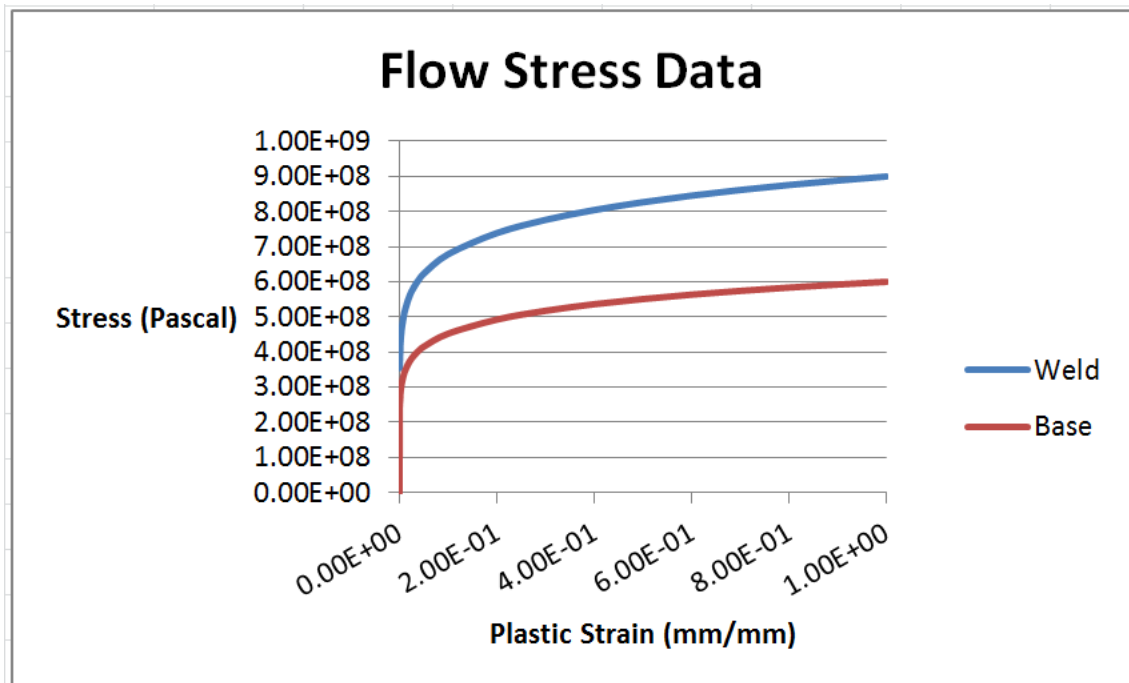


Figure 191: Flow stress data used in the analysis

6.1.3.1.1 FE Model (Transverse Attachment)

4 crucifix quarter models (CQM) were created, 2 with 0mm radius weld toe and 2 with 1mm radius weld toe. Both high order (quadratic) elements Solid 186 (20 nodes) and low order (linear) element Solid 185 (8 nodes) were used in these models to test the IIW recommendation in Hobbacher (2008). Based on the results; the author is of the opinion that as long as the mesh is fine enough at the stress concentration area, in this case 0.1mm and nonlinear analysis is carried out; element order has little influence on the results. Simulation was carried out and results compared with the published results of DSME et al already discussed in 4.1.

6.1.3.1.2 FE Model (Transverse Attachment – Boundary Conditions)

The boundary conditions applied to the quarter model are axial symmetry, half symmetry and free end was bulled.

Figures 192 and 193 are general views of 1mm and 0mm crucifix quarter models.

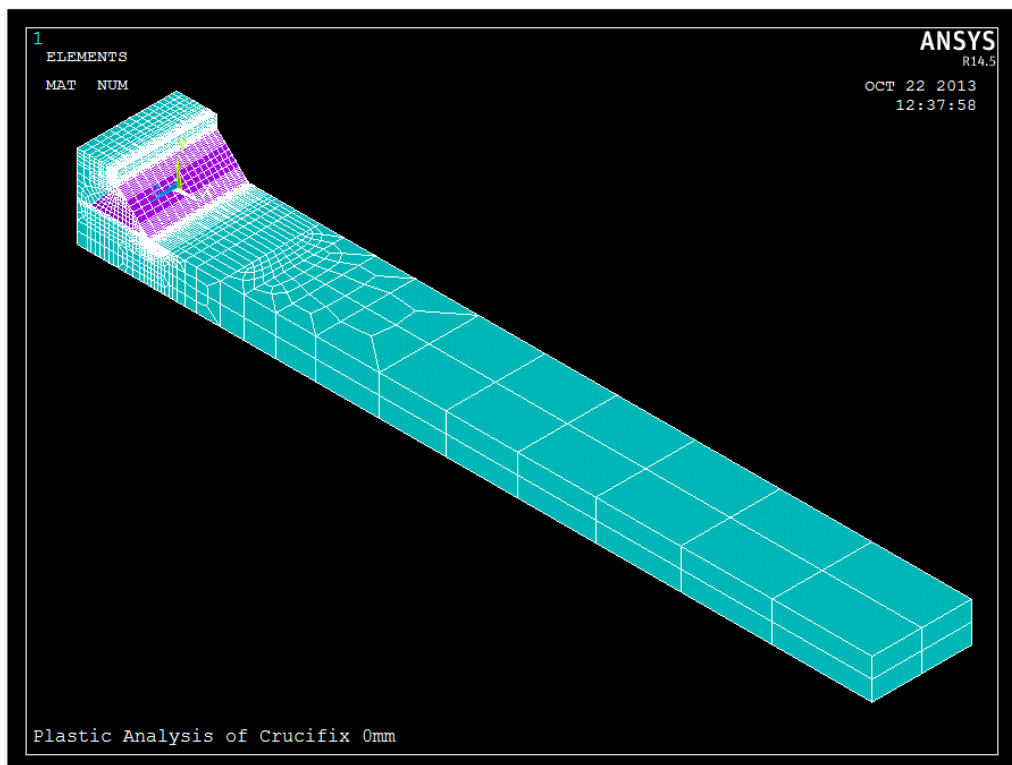


Figure 192: Transverse (crucifix) attachment quarter model 0mm radius general view

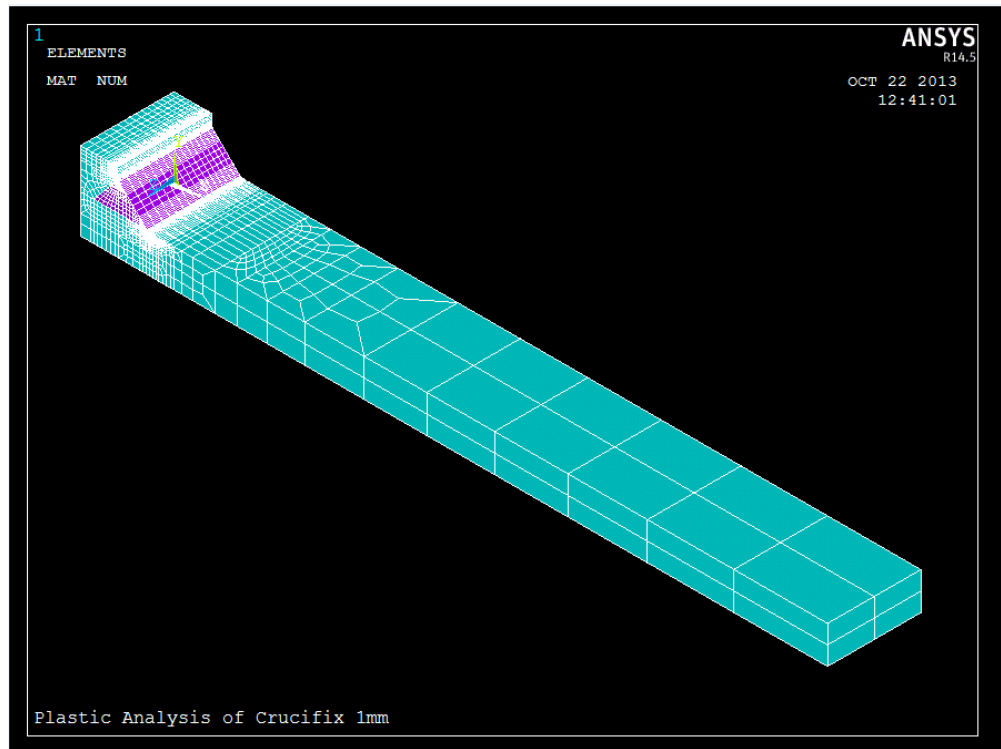


Figure 193: Transverse (crucifix) attachment quarter model 1mm radius general view

Figures 194 and 195 are close up views of the weld toes (1mm and 0mm) of the crucifix quarter models.

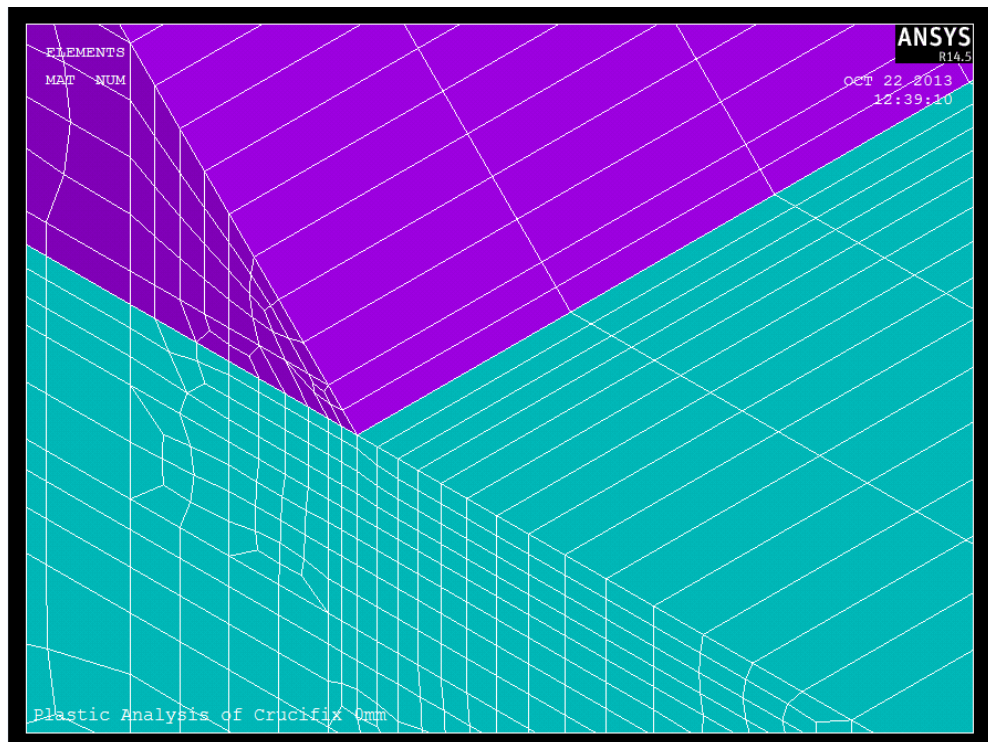


Figure 194: Transverse (crucifix) attachment quarter model 0mm radius close view

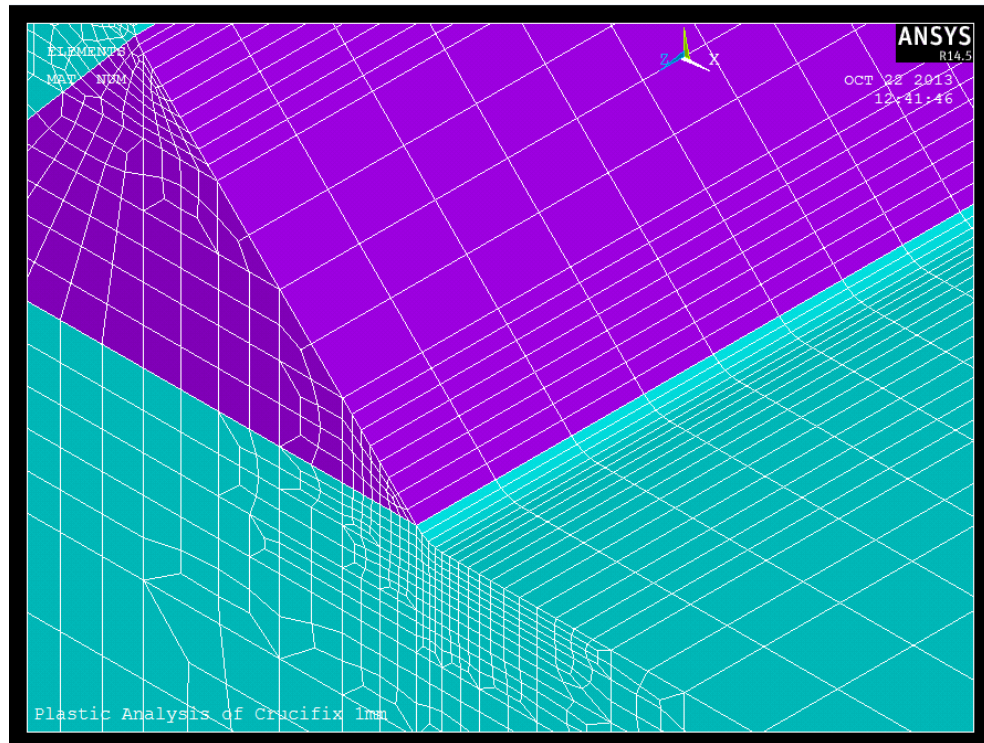


Figure 195: Transverse (crucifix) attachment quarter model 1mm radius close view

6.1.3.1.3 Non Linear Analysis Results (Transverse Attachment)

The 1st principal stress range results (2mm displacements range corresponding to 0.3%-0.9% nominal strain range of both the real test and the FEA) are presented in **Table 35** and **Figure 196**.

Table 35: Transverse (Cruciform) Attachment Nonlinear FEA Results

No. of cycles to Failure as per DSME tests*	Stress range, Mpa		
	Test	FEA	FEA
	DSME*	CQM0mm	CQM1mm
2365	341	507	421
2165	370	528	432
1762	377	552	441
1613	417	565	451
1842	420	565	460
1543	440	565	467
1477	451	564	473
1477	458	564	477
1982	467	564	481
1815	493	564	485
1661	496	564	489
1275	500	564	493
1521	511	564	498
1202	536	564	502

*These data are taken directly/derived from Figure 4 of (Wang et al., 2006)

$$\text{Calculated SCF} = \frac{\sigma_{\text{Peak}}}{\sigma_{\text{Nominal}}} = \frac{565}{346} = 1.6$$

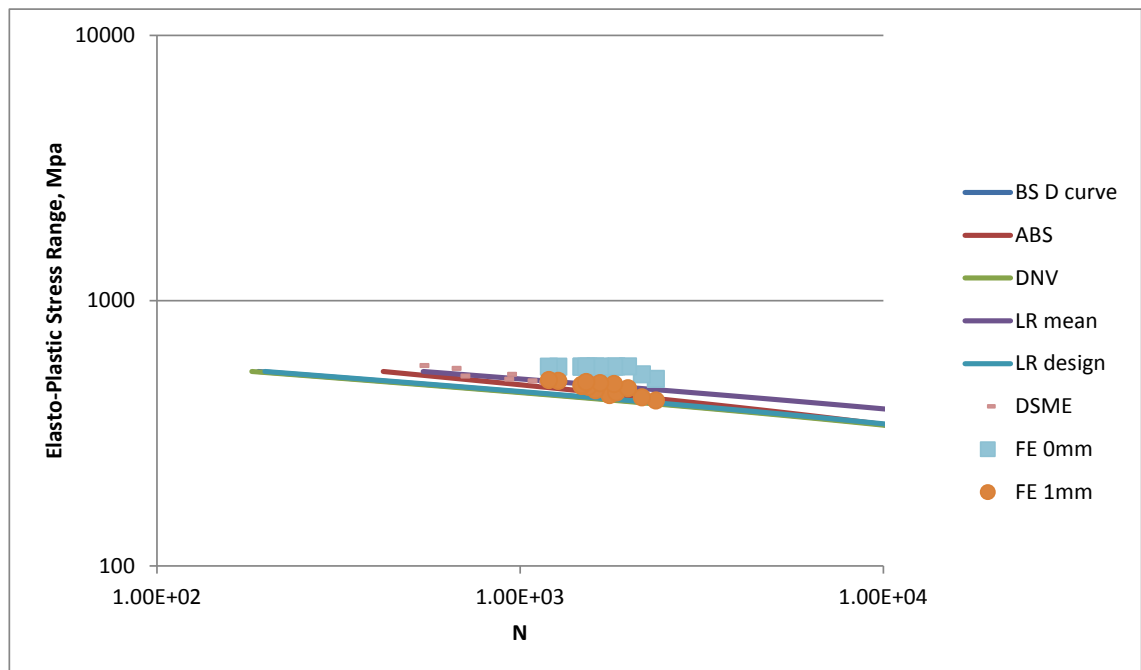


Figure 196: Transverse (Cruciform) Attachment Nonlinear FEA Results vs DSME test results

Some general and close up views of 1st principal stress distribution plots of CQM 0mm and 1mm are presented in **Figures 197- 200**.

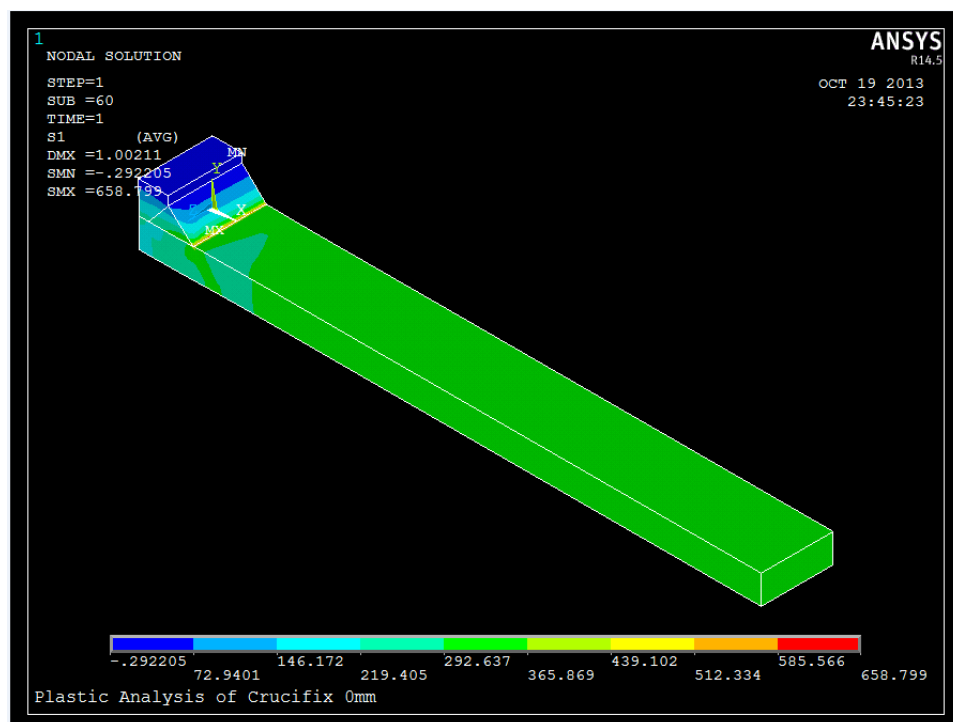


Figure 197: Transverse (crucifix) attachment model 0mm radius 1st principal stress distribution

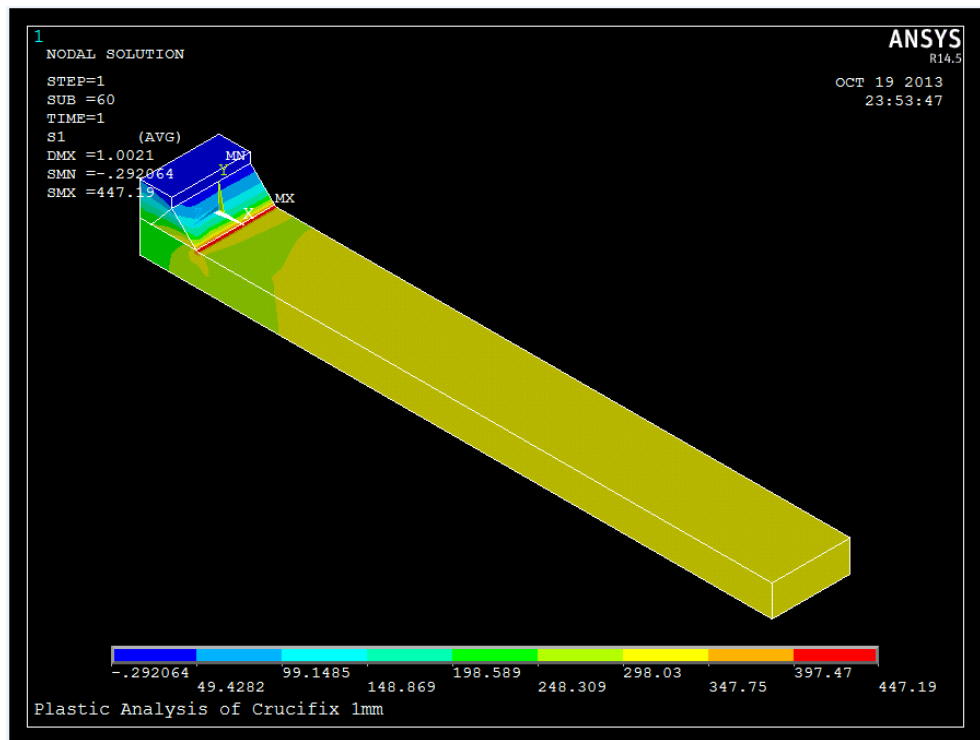


Figure 198: Transverse (crucifix) attachment model 1mm radius 1st principal stress distribution

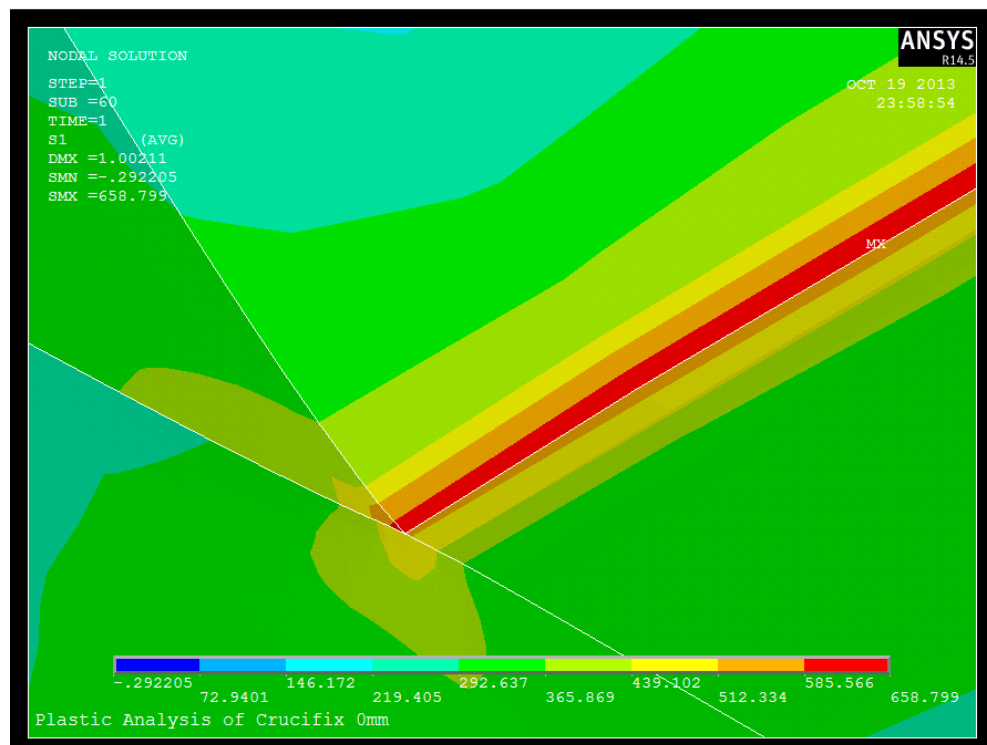


Figure 199: Transverse (crucifix) attachment model 0mm radius 1st principal maximum stress at weld toe

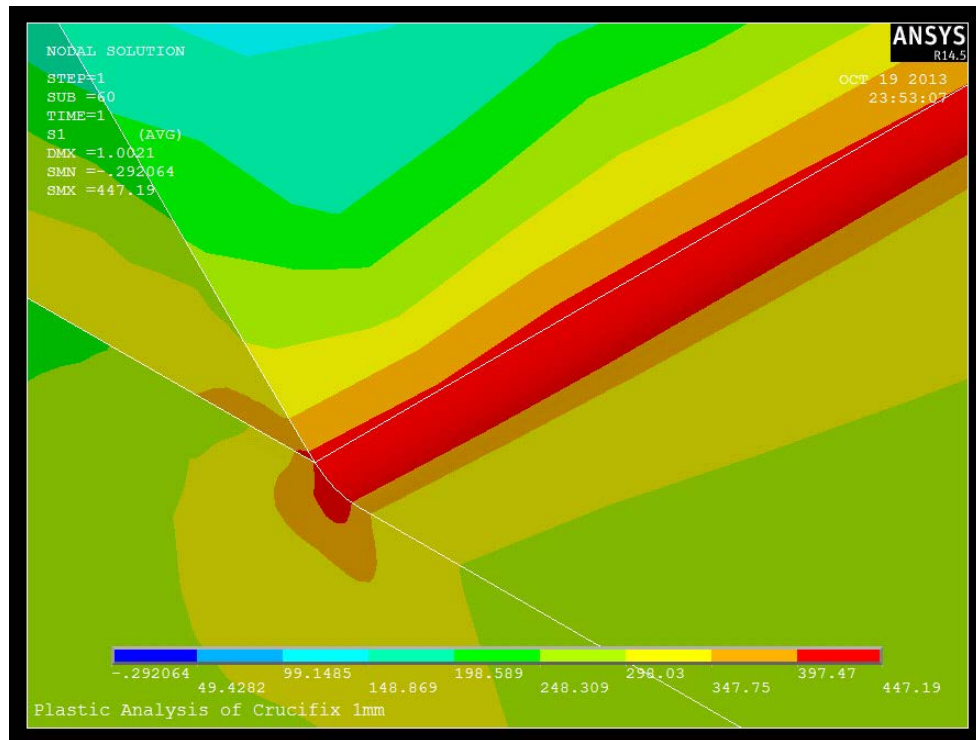


Figure 200: Transverse (crucifix) attachment model 1mm radius 1st principal maximum stress at weld toe

6.1.3.2 FE Model (Longitudinal Attachment)

Two longitudinal quarter model (LQM) were created in ANSYS as per dimension given in **Figure 201**. The mesh density was as per the IIW recommendation 0.25mm at the weld toe. The same flow stress data (as the crucifix) was used for both the base metal and the weld. The two models created, one with 0mm radius weld toe and one with 1mm radius weld toe. Only the low order element Solid 185 (8 nodes) was used in these models to optimize simulation time since mesh was fine enough at the stress concentration area. Simulation was carried out to validate the tests and assess the LCF behaviour in longitudinal attachment. The results of the nonlinear analysis were compared with the results of the tests.

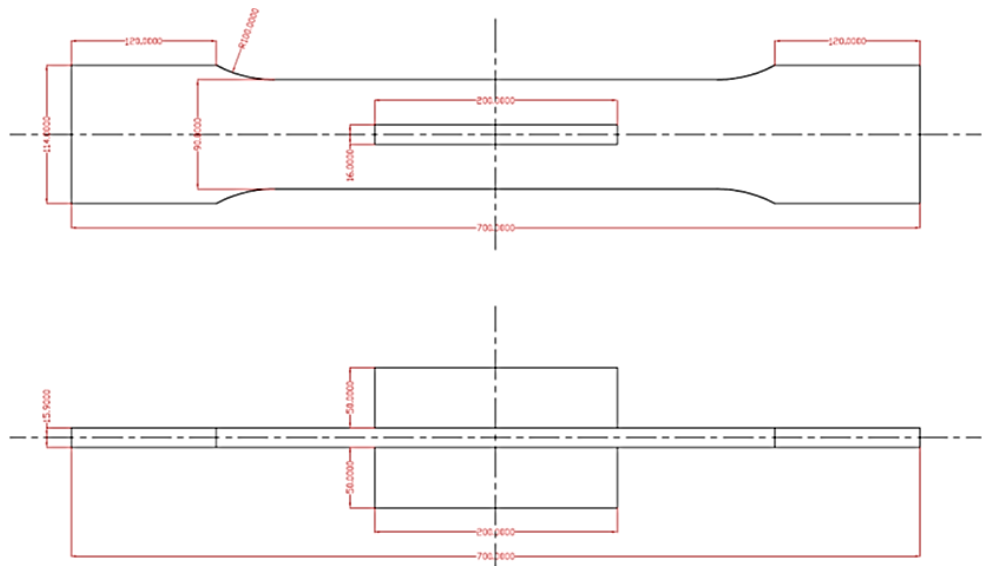


Figure 201: Longitudinal Attachment Full Model Dimensions

6.1.3.2.1 FE Model (Longitudinal Attachment – Boundary Conditions)

The boundary conditions applied to the quarter model are axial symmetry, half symmetry and free end was bulled.

Figures 202 and **203** are general views of 1mm and 0mm longitudinal attachment quarter models.

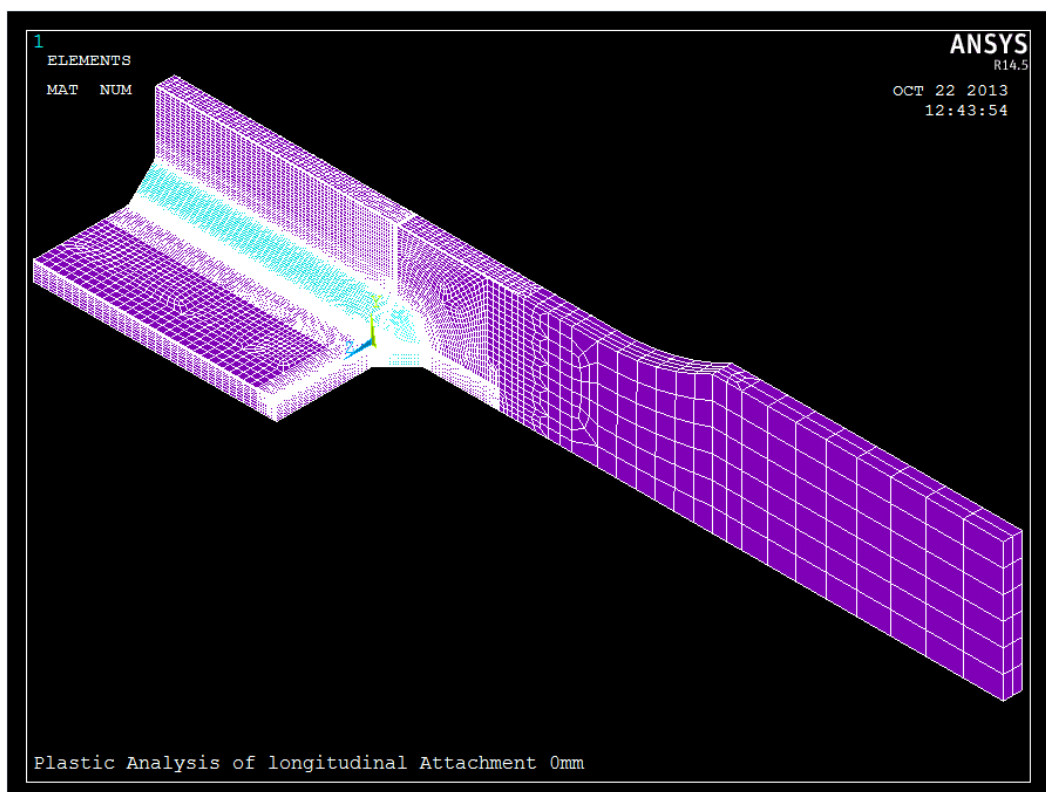


Figure 202: Longitudinal attachment quarter model 0mm radius general view

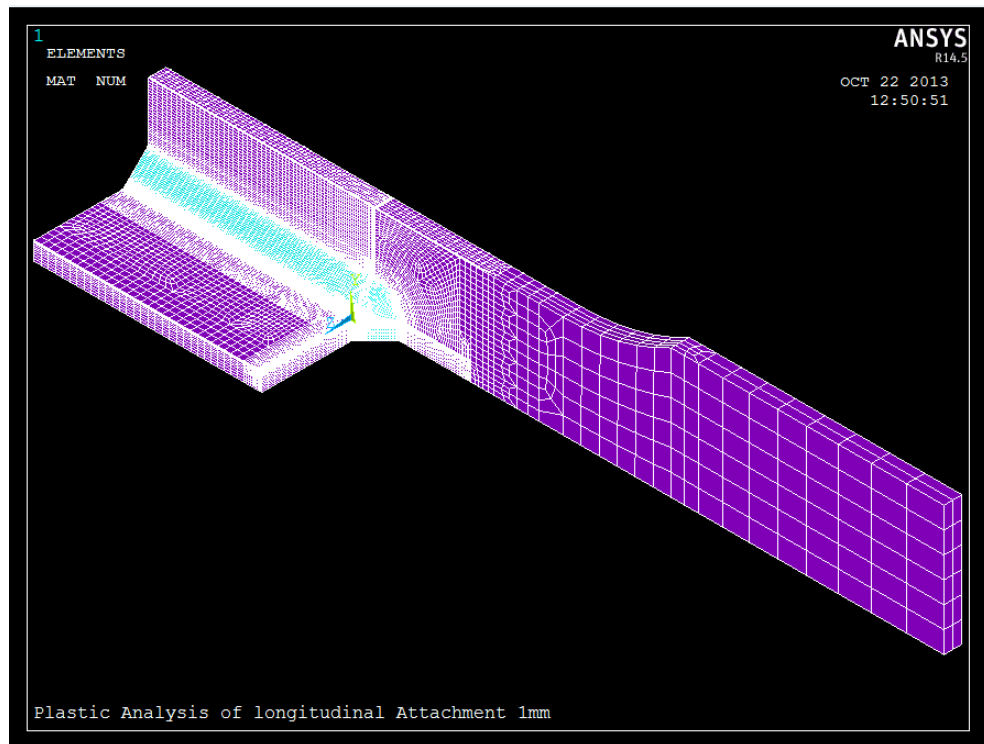


Figure 203: Longitudinal attachment quarter model 1mm radius general view

Figures 204 and 205 are close up views of weld toes (1mm and 0mm) of longitudinal attachment quarter models.

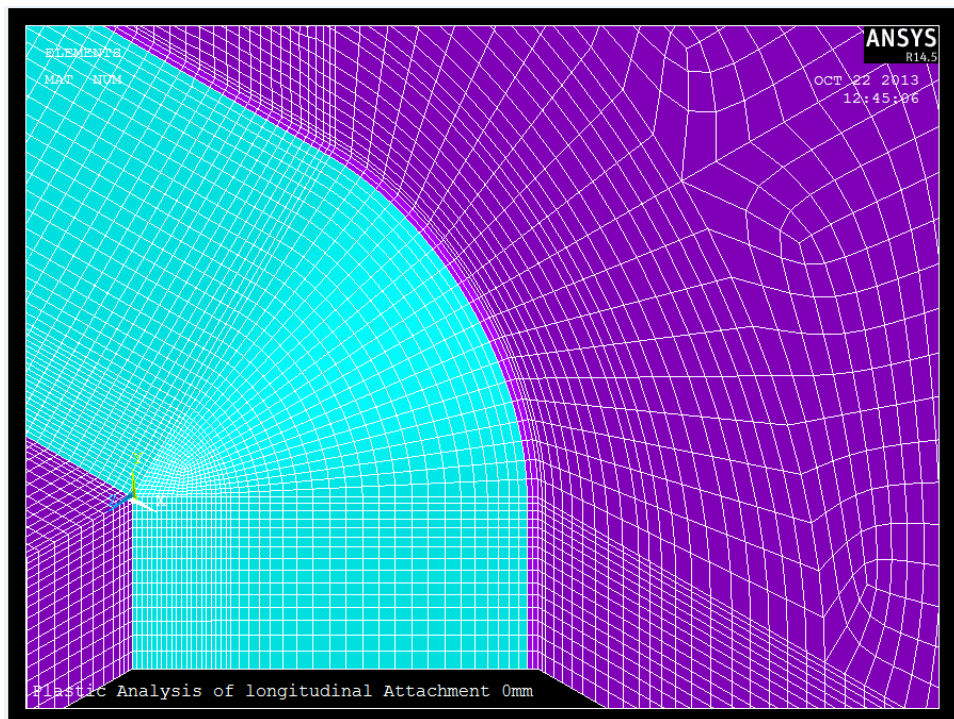


Figure 204: Longitudinal attachment quarter model 0mm radius close view

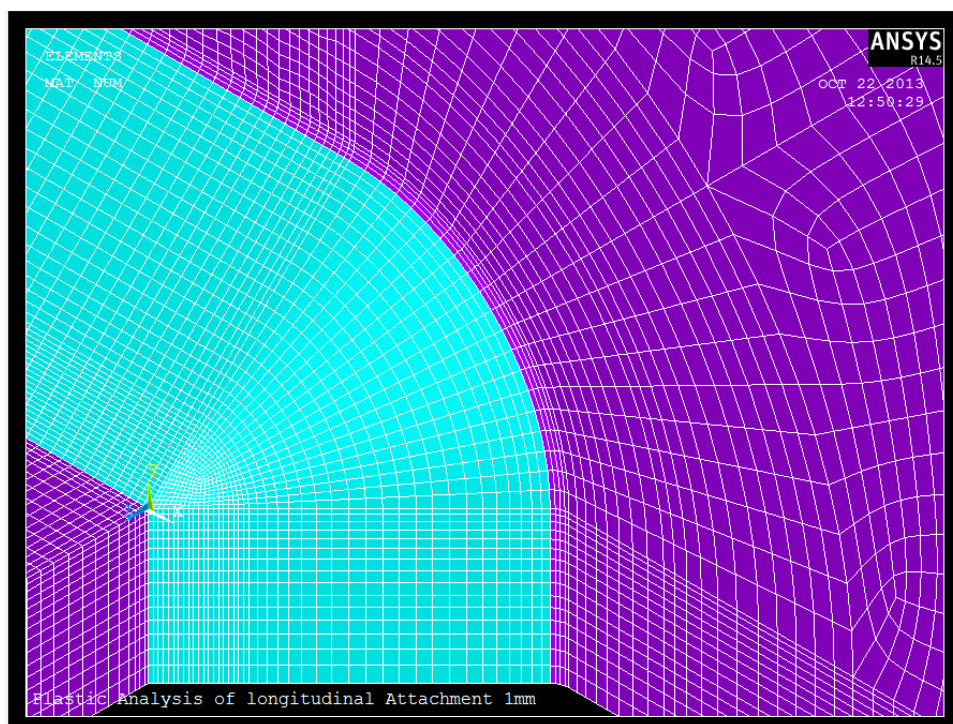


Figure 205: Longitudinal attachment quarter model 1mm radius close view

6.1.3.2.2 Non Linear Analysis Results (Longitudinal Attachment)

The 1st principal stress range results (1.1mm to 1.9mm displacement range corresponding to 0.2%-0.3% nominal strain range of both the real test and the FEA) are presented in **Table 36** and **Figure 206**.

Table 36: Longitudinal Attachment Nonlinear FEA Results

No. of cycles to Failure	Stress range, Mpa		
	Test	FEA	FEA
	Type A	LQM0mm FE	LQM1mm FE
9500	421	533	490
6300	498	544	502
5000	564	548	508
3600	565	553	514
3070	587	556	518
2150	608	560	523
1200	622	563	527
475	629	566	531

$$\text{Calculated SCF} = \frac{\sigma_{\text{Peak}}}{\sigma_{\text{Nominal}}} = \frac{566}{346} = 1.64$$

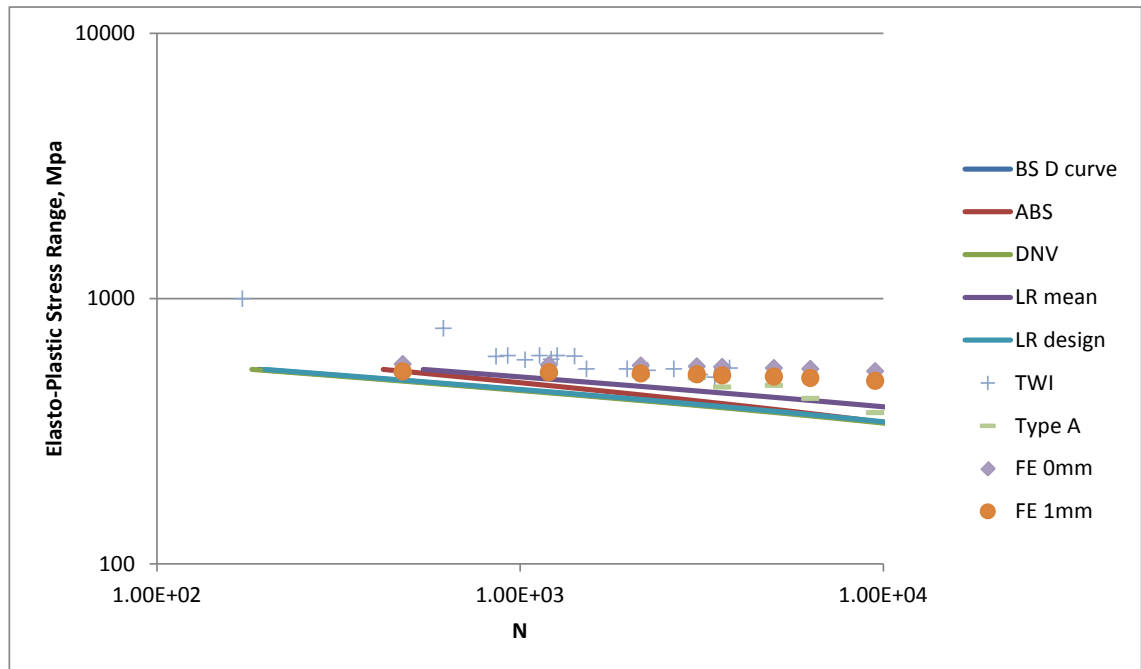


Figure 206: Longitudinal Attachment Test Results vs TWI and Nonlinear FEA LQM

Some general and close up views of plots of LQM 0mm and 1mm 1st principal stress distribution are presented in **Figures 207-210**.

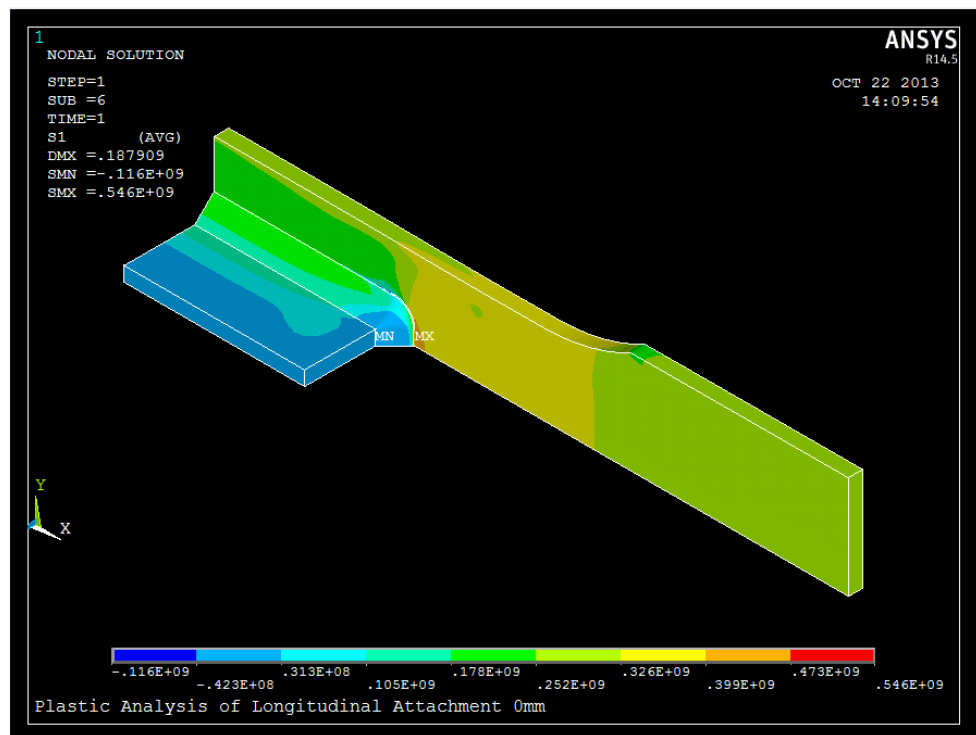


Figure 207: Longitudinal attachment model 0mm 1st principal stress distribution

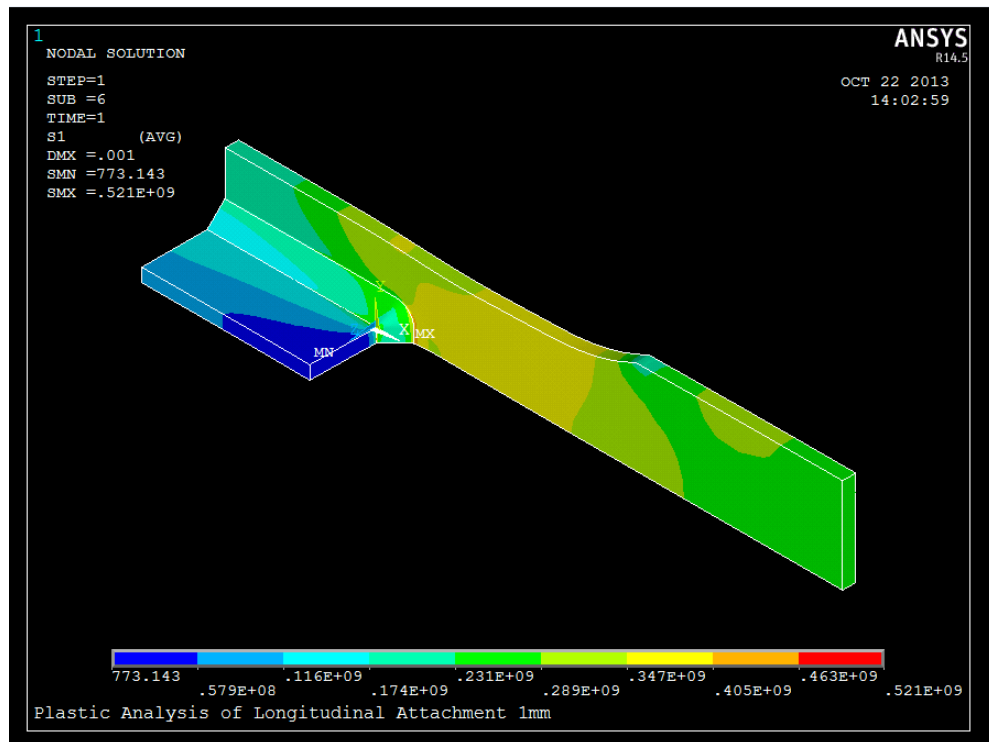


Figure 208: Longitudinal attachment model 1mm 1st principal stress distribution

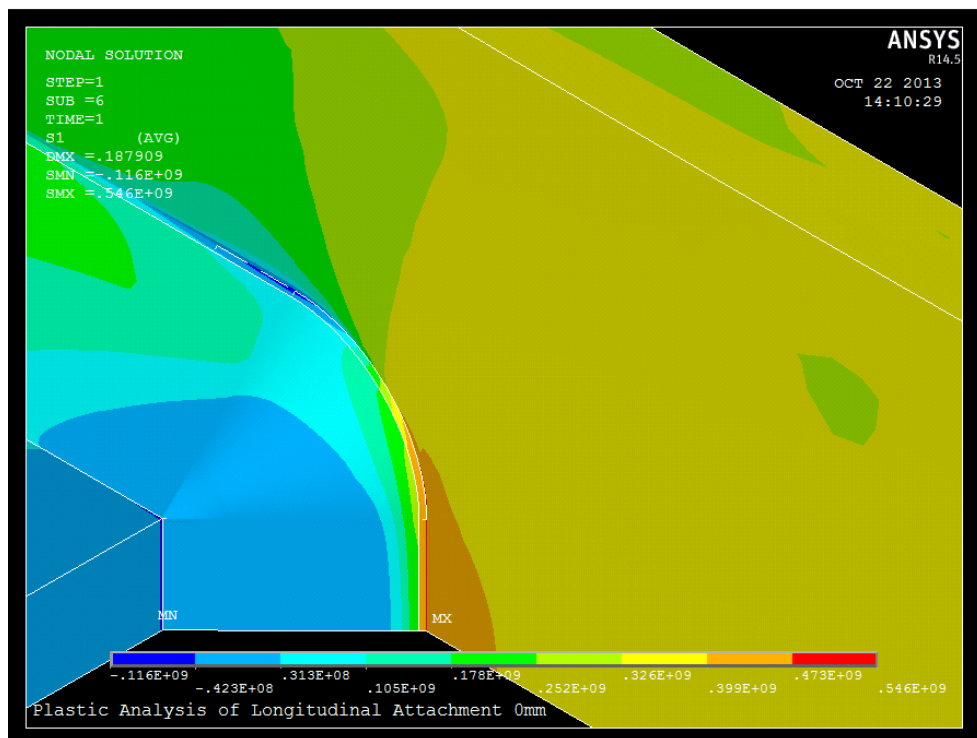


Figure 209: Longitudinal attachment model 0mm 1st principal maximum stress at the weld toe

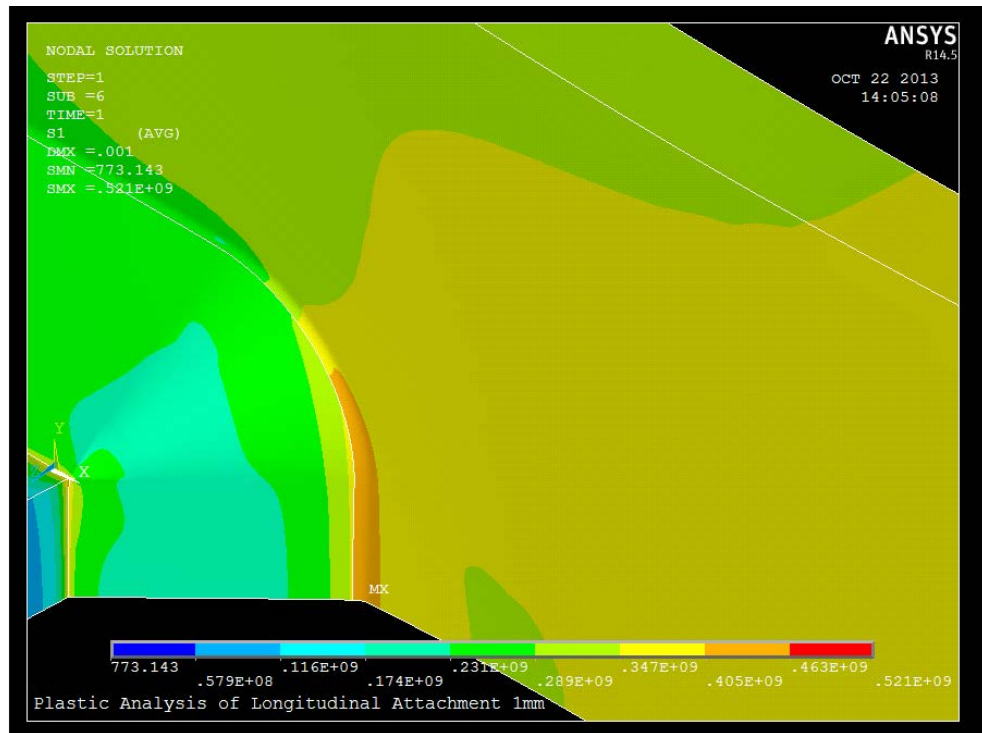


Figure 210: Longitudinal attachment model 1mm 1st principal maximum stress at the weld toe

6.1.3.3 Discussion

If we are to analyse the LCF tests previously mentioned in 4.1; one may summarize that DSME, DNV and Inha University did the following:

1. LCF test carried out on the welded joint (i.e. the crucifix) in order to establish the nominal strain range and number of cycles to failure
2. FEA was used to establish the stress concentration factors
3. Pseudo stress range was calculated
4. Notch stress ranges were calculated using Neuber's rule

The author created the crucifix model discussed in 6.1.3.1 in order to mimic the test and see if the proposed novel method will produce similar results to the tests. To do that the results of the nonlinear FE models (both 0mm and 1mm) were compared to the results of the tests. All results were plotted in **Figure 212** and BS D curve, ABS, DNV, LR mean and LR design curves were used to establish which curve is more realistic.

In **Figure 212**; BS D curve, DNV and LR design are identical in the low cycle region. The number of cycle to failure in the DSME tests together with the 1st principal stress range results from the nonlinear CQM FE models, 0mm weld toe and 1mm weld toe,

were plotted. The results of both models were close to the DSME ones. More importantly, it is clear that the test results and FE results (high stress range) agree well with the S–N curves above 10^3 No. of cycles. This is not so below 10^3 No. of cycles, the reason in the authors view may be attributed to the nature of the S–N curves (i.e. extrapolation) not the results. In reality there is a physical reason for this; that is the ratio of yield stress to the ultimate tensile strength which is around 0.9. In other words the test results do represent the way the material behaves more accurately since S–N curve development is always based on the best fit of a scatter.

Based on this; the author suggests that a knee be introduced in the LCF region i.e. the high stress region similar to the knee between LCF and HCF of the S–N curve.

If we compare the two models' results in **Table 35**, it is clear that the only difference between the two is the peak stress range which is to do with the geometry of the weld toe bearing in mind that both models are identical in everything else (i.e. material properties, flow stress data and loading). The 1mm weld toe is arbitrary (geometric assumption) and is used to avoid the infinite stress (i.e. stress at a point). In fact the 0mm radius model is close to reality and is not artificial, in other words, the 0mm weld toe model must contain the stress driving the crack.

The proposed methodology, based on the elastic-plastic notch stress approach, provides for elastic-plastic stress obtained from nonlinear 3D FEA model of the relevant component, explicitly modelling the weld, to be used directly thereby avoiding the questionable hot spot stress and the associated approximations and uncertainties of plasticity correction and the pseudo elastic stress range. Where the far-field (nominal) stress can be confidently established and a reliable SCF for the relevant structural detail is known, detailed FEA may not be necessary. The stress range obtained by multiplying the far-field stress by the SCF can be converted to elastic-plastic notch stress range by the use of Neuber's rule in conjunction with Ramberg Osgood curve for the relevant material. By using this approach, the pseudo elastic stress range axis in the S–N curve is converted into elastic plastic notch stress. The resulting S–N curve shows a transition between the HCF portion and the low cycle region. Such a re-interpretation of the S–N curve would typically have three segments comprising a straight section below the endurance limit with a transition 'knee' to the HCF region and another transition into the LCF region between 10^4 to 10^5 cycles. The resulting S–N curves show remarkable convergence between the different design S–N curves adopted by the various class

societies and the standard BS S–N curve (D curve). The resulting estimate of the number of cycles to failure, for a given elastic-plastic notch stress range, between the various design S–N curves are very close, thereby providing a more consistent estimate of fatigue life.

6.2 Comparison with Coffin-Manson

As discussed in 6.1, the strain life method illustrated in 2.2.6 and 4.1.1 is neither practical nor readily available due to lack of material and strain-life data and also cannot be easily added to the HCF damage. However, for the benefit of the research a comparison has been carried out between the Coffin-Manson method and the proposed method. **Figure 211** shows correlation between the strain life method results and the proposed method results.

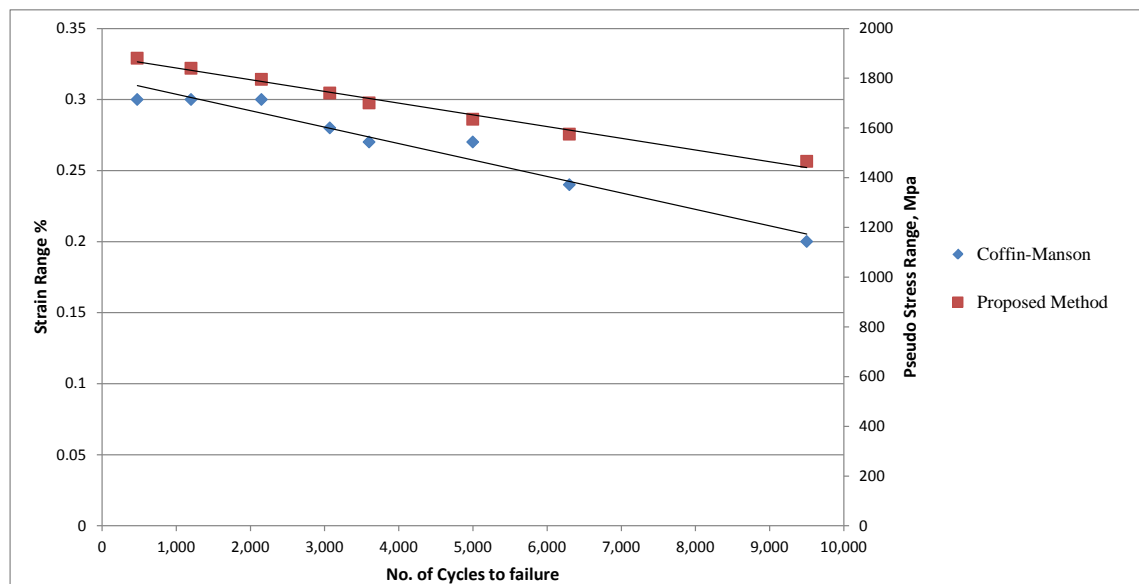


Figure 211: LQM 1mm results compared with Coffin-Manson

6.3 Summary

The results based on the elastic-plastic notch stress approach shows a much better correlation between the FEA results, test data and the various S–N design curves compared to the pseudo elastic stress method. The resulting stresses from the FEA are presented along with the test data and the design S–N curves in **Figures 212** and **213**. In **Figure 212** stress range results have been converted from elastic plastic values to pseudo values and in **Figure 213** stress range results have been converted from pseudo

values to elastic plastic values both using the approach and procedure described in 6.1.1.

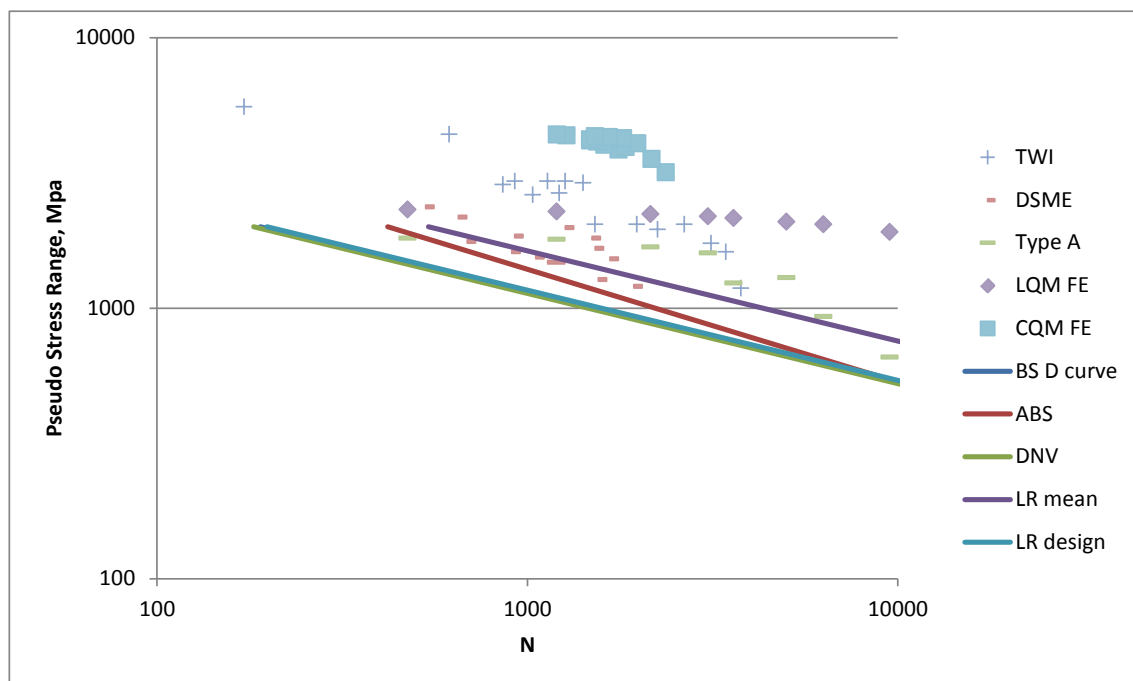


Figure 212: Comparison of pseudo results for both transverse and longitudinal attachments

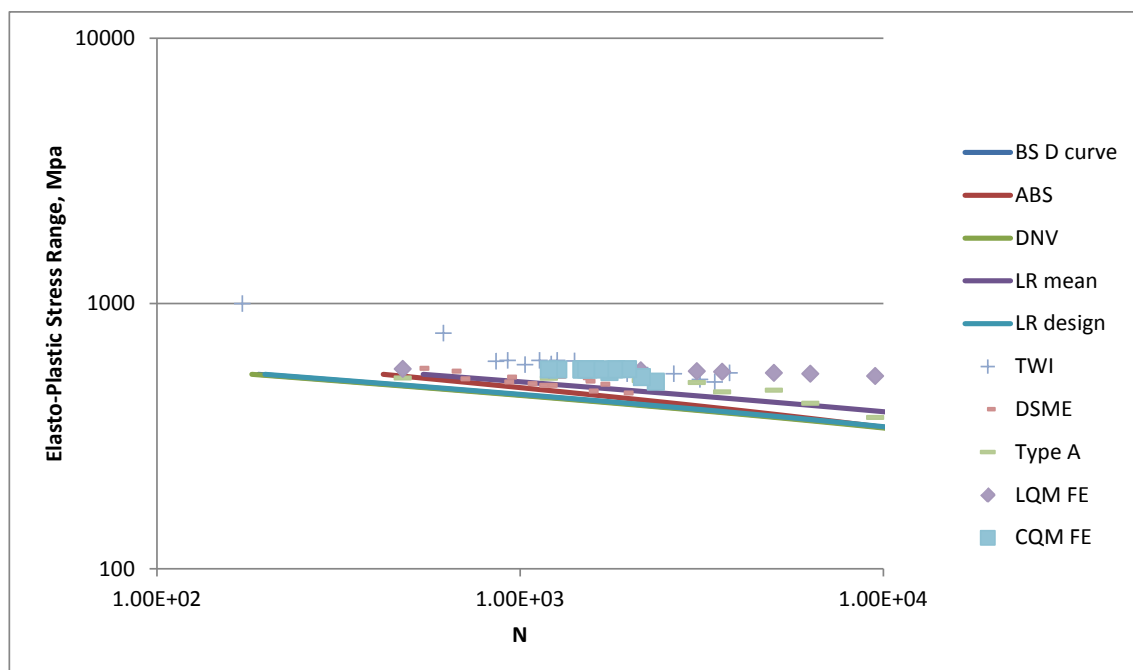


Figure 213: Comparison of elastic plastic results for both transverse and longitudinal attachments

6.4 Benefits of this method

The main benefits of this method can be summarized as follows:

1. Explicitly considers the weld
2. Any stress estimate approach can be used
3. Does not necessarily require FEA
4. Does not use plasticity correction
5. Stress based, hence, HCF and LCF can be added
6. Stress based, hence, can be used in class societies' codes
7. Not limited to research and labs
8. Does not rely on strain S-N curve which is not readily available

6.5 Conclusions

1. The elastic plastic notch stress approach is defined and applied to both test data and FEA
2. The elastic plastic approach overcomes disadvantages of pseudo hot spot stress, plasticity correction and strain life approaches
3. The elastic plastic approach is not limited to FEA
4. The elastic plastic approach steps to use with FEA have been defined
5. The elastic plastic approach steps to use with fatigue tests have been defined
6. Application of the elastic plastic approach to BS S-N curves and CS have been demonstrated
7. Application of the elastic plastic approach to fatigue tests have been demonstrated
8. Application of the elastic plastic approach to FEA have been demonstrated
9. Contrast of 6, 7 and 8 in both nominal elastic notch stress and elasto-plastic have been presented

Chapter 7

Conclusions, Recommendations and Future Work

7 CHAPTER 7: Conclusions and Recommendations

In this chapter, the overall conclusions are presented along with some recommendations and future work.

7.1 Conclusions

This thesis first presents a comprehensive literature review concerning LCF and has identified the current state-of-the-art methodologies in the subject matter. It is the conclusion of this thesis that the available evidence now points clearly to LCF as being the primary reason for several premature damages in critical ship structure components, particularly in FPSOs. These are more susceptible to LCF as compared to other ship types; this is primarily due to the unique structure, frequent loading and unloading patterns and site specific environment. The structure of FPSOs, in terms of internal turret and topside loads, affects the structural response of FPSOs to dynamic and quasi-static loads. Unlike oil tankers, which are either in full load or ballast conditions, FPSOs experience maximum hogging and sagging still water bending moments in every single cycle of loading and unloading. Furthermore, the specific site environment in which FPSOs are moored means that, even in a relatively benign environment, an FPSO may experience extremely diverse wave induced loads. An understanding of the quasi-static loading and unloading of cargo and ballast, the most important of the loading conditions for LCF, is therefore crucial to the design and analysis of FPSOs.

This thesis then presents an assessment of the requirement for the loading conditions of FPSOs by the various class societies and compares these to two case studies of existing FPSOs in the North Sea. This is the first time that the assumed onerous loading and unloading configurations in class society rules has been evaluated against actual conditions in operating FPSOs. It is established in this thesis that the assumed loading conditions in class society rules differ significantly from real life cases. Four more realistic loading conditions have been proposed for the assessment of potential LCF in the design of FPSOs. Those are; Ballast condition at 10% of operation, Full load condition at 10% of operation, Loading condition at the most frequent draught below 50% at 40% of operation and Loading condition at the most frequent draught above 50% at 40% of operation. As a result of this finding, the author was encouraged to present a position paper on the representative operational loading conditions that are most onerous for LCF in FPSOs. The recommendations contained in the position paper has been reviewed and approved by LR Global Technology Centre (GTC) in Singapore

and it is the subject of a paper was presented at the 24th International Ocean and Polar Engineering Conference (ISOPE), June 2014 in Busan, South Korea. The position paper is also the basis for a proposal for a Joint Industry Project (JIP) on the quasi-static loading conditions of FPSOs.

The main issue with loading and offloading is the high stress range they induce in the critical components of FPSOs. This can be close to, above or several times the yield strength of the material, and implies a low number of cycles to failure, typically below 10^4 . The method of assessment of LCF, involving high stress range and low number of cycles to failure, was critically reviewed and a novel approach, which capitalises on existing methods, is proposed. The state-of-the-art is the well founded approach of assessing structural stress or hot spot stress in the HCF range which is predominantly elastic behaviour. This is questionable when extended to the LCF range which is predominantly plastic behaviour. This state-of-the-art method is an alternative to the strain-life method which is not practical or readily available due to lack of material strain-life data. Furthermore, it cannot be easily added to the HCF damage. Under the classical structural stress method, the calculated stress ranges for LCF are corrected using a plasticity correction factor in order to employ the S–N curve instead of a strain cycle curve. The corresponding design S–N curves provide continuity from the low cycle regime to the high cycle regime which is achieved by expressing the low cycle data in terms of pseudo elastic stress range (i.e. strain range multiplied by elastic modulus). Although the design S–N curves produced by the different class societies under this method are quite similar, they result in significantly large differences in the LCF damage they predict for a given stress range.

The proposed methodology for the LCF assessment of FPSOs in this thesis is based on the elastic-plastic notch stress approach. This method provides for elastic-plastic stress obtained from nonlinear 3D FEA model of the relevant component, explicitly modelling the weld, to be used directly thereby avoiding the questionable hot spot stress and the associated approximations and uncertainties of plasticity correction and the pseudo elastic stress range. Where the far-field (nominal) stress can be confidently established and a reliable SCF for the relevant structural detail is known, detailed FEA may not be necessary. The stress range obtained by multiplying the far-field stress by the SCF can be converted to elastic-plastic notch stress range by the use of Neuber's rule in conjunction with Ramberg Osgood curve for the relevant material. By using this approach, the pseudo elastic stress range axis in the S–N curve is converted into elastic

plastic notch stress. The resulting S–N curve shows a transition between the HCF portion and the low cycle region. Such a re-interpretation of the S–N curve would typically have three segments comprising a straight section below the endurance limit with a transition ‘knee’ to the HCF region and another transition into the LCF region between 10^4 to 10^5 cycles. The resulting S–N curves show remarkable convergence between the different design S–N curves adopted by the various class societies and the standard BS S–N curve (D curve). The resulting estimate of the number of cycles to failure for a given elastic-plastic notch stress range between the various design S–N curves are very close, thereby providing a more consistent estimate of fatigue life.

To underpin this approach, test results from the most common structural details prone to LCF damage, namely the longitudinal attachment and the transverse attachment, were analysed in a similar way. By converting the reported pseudo-elastic stresses to elastic-plastic stresses, close correlation were observed between the various tests data and the results of the numerical analyses.

Of the two most common structural details of FPSOs prone to LCF damage, the transverse attachment (cruciform) is the most commonly tested. There are very few published data on the longitudinal attachment. The only available data for which there are sufficient details is the test data published by TWI. This was in relation to half cycle strain control tests. No data was available on full cycle strain control tests for longitudinal attachment. As a result, full cycle strain controlled fatigue tests were performed at Southampton University Lloyd's Register testing facility on a number of longitudinal attachments together with the associated monotonic and cyclic material tests. The results of these tests were analysed in a similar manner with the published data and the results of numerical analyses. These show correlation across the stress ranges.

7.2 Recommendations and Future work

The author recommends the following:

1. Lloyd's Register to adopt the recommended representative load conditions in FDA3
2. Lloyd's Register to consider the novel approach proposed in class rules
3. IACS to consider the harmonization of different FPSO rules into one CSR for FPSOs including LCF assessment procedure
4. Research should be extended to nuclear sector where LCF is more critical.

5. Further publication independently for Chapter two of the thesis in a form of a book in order to benefit a wider audience interested in LCF and to avoid limiting the collected information to only academic arena. This book may be considered a background document for LCF.

References

8 References

- ABS-DLA 2001. Guidance Notes on Safehull-Dynamic Loading Approach for FPSO Systems.
- ABS-DLA 2010. Guide for Dynamic Loading Approach for FPSO Installations.
- ABS-FPI 2009. Floating production installations. *ABS - Guide Notes*, Part 5A, Ch. 3 and Appendix 2.
- ABS-OMAE-FPSO 2004. Structural modifications to the FPSO Kuito cargo tanks. *ABS Technical Papers*, 279-286.
- ABS-SBFA 2010. Spectral-based fatigue analysis for floating production, storage and offloading (FPSO) installations. *ABS - Guide*
- ABS-SSC 2002. PRESTIGE: Complete hull failure in a single-hull tanker. 1-8.
- ASHBY, M. F. & JONES, D. R. H. 2002. *Engineering Materials I*, Butterworth Heinemann.
- BAMFORD, R. J. & STEWART, G. 2007. Application of IACS Common Structural Rules for Oil Tankers to FPSOs. *Offshore Technology Conference*.
- BAMITABH. 2013. *Ship Accident* [Online]. Web Page.
- BEGUM, S., CHEN, D. L., XU, S. & LUO, A. A. 2009. Effect of strain ratio and strain rate on low cycle fatigue behavior of AZ31 wrought magnesium alloy. *Materials Science and Engineering: A*, 517, 334-343.
- BENTACHFINE, S., PLUVINAGE, G., GILGERT, J., AZARI, Z. & BOUAMI, D. 1999. Notch effect in low cycle fatigue. *International Journal of Fatigue*, 21, 421-430.
- BENTACHFINE, S., PLUVINAGE, G., TOTH, L. S. & AZARI, Z. 1996. Biaxial low cycle fatigue under non-proportional loading of a magnesium-lithium alloy. *Engineering Fracture Mechanics*, 54, 513-522.
- BERTO, F., LAZZARIN, P. & RADAJ, D. 2012. Fictitious notch rounding concept applied to V-notches with root holes subjected to in-plane shear loading. *Engineering Fracture Mechanics*, 79, 281-294.
- BOULAAJAJ, A., CABRERA, J. M. & PRADO, J. M. 2008. Effect of initial microstructure, frequency and temperature on the low cycle fatigue behaviour of the soldering alloys 96.5Sn–3.5Ag and 63Sn–37Pb. *Engineering Failure Analysis*, 15, 220-228.
- BV-PART-D-CH1-SEC7 2007. HULL SCANTLINGS.
- BYRNE, J., HALL, R. F. & POWELL, B. E. 2003. Influence of LCF overloads on combined HCF/LCF crack growth. *International Journal of Fatigue*, 25, 827-834.
- CAO, J., BAI, F. & LI, Z. 2006. High temperature low cycle fatigue behavior of titanium aluminide Ti–24Al–15Nb–1Mo alloy. *Materials Science and Engineering: A*, 424, 47-52.
- CHOUDHARY, B. K., BHANU SANKARA RAO, K. & MANNAN, S. L. 1991. High temperature low cycle fatigue properties of a thick-section 9wt.%Cr-1wt.%Mo ferritic steel forging. *Materials Science and Engineering: A*, 148, 267-278.
- CHRIST, H. J., HOFFMANN, G. & ÖTTINGER, O. 1995. History effects in metals during constant and variable amplitude testing I: Wavy dislocation glide behaviour. *Materials Science and Engineering: A*, 201, 1-12.
- CLIENT-REPORT-G3 2002. FPSO Stability Manual.
- CLIENT-REPORT-G 2009. FPSO Cargo Offload Operations.
- CLIENT-REPORT-GA 2002. FPSO Structural Analysis.
- DEMULSANT, X. & MENDEZ, J. 1996. Influence of environment on low cycle fatigue damage in Ti6Al4V and Ti 6246 titanium alloys. *Materials Science and Engineering: A*, 219, 202-211.
- DNV-CN-30.7 2010. FATIGUE ASSESSMENT OF SHIP STRUCTURES.
- DNV-CN-NO.30.7 2010. Fatigue assessment of ship structures. *Det Norske Veritas*, Classification Notes 30.7 Appendix I.
- DNV-REPORT 2011. Failure investigation - Cracks on welds.
- DNV-RP-C206 2006. Fatigue methodology of offshore ships. *Det Norske Veritas*, DNV-RP-C206.
- EARTHMAN, J. C. 1991. Characterization of small crack growth in 12% CrMoV steel under high temperature, low cycle fatigue conditions. *Materials Science and Engineering: A*, 132, 89-95.

- ESWARA PRASAD, N., VOGT, D., BIDLINGMAIER, T., WANNER, A. & ARZT, E. 2000. High temperature, low cycle fatigue behaviour of an aluminium alloy (Al-12Si-CuMgNi). *Materials Science and Engineering: A*, 276, 283-287.
- FRICKE, W. 2006. Round-Robin Study on Stress Analysis for the Effective Notch Stress Approach. *IIW International Institute of Welding*, XIII-2129-06-XV-1223-06.
- FRICKE, W. 2010a. Guideline for the Assessment of Weld Root Fatigue. *IIW International Institute of Welding*, XIII-WG3-12r1-10.
- FRICKE, W. 2010b. IIW Recommendations for the Fatigue Assessment by Notch Stress Analysis for Welded Structures. *IIW International Institute of Welding*, XIII-2240r2-08.
- FRICKE, W., CUI, W., KIERKEGAARD, H., KIHLE, D., KOVAL, M., MIKKOLA, T., PARMENTIER, G., TOYOSADA, M. & YOON, J.-H. 2002. Comparative fatigue strength assessment of a structural detail in a containership using various approaches of classification societies. *Marine Structure*, 15, 1-13.
- FRICKE, W. & FELTZ, O. 2009. Fatigue Tests and Numerical Analyses of Partial-Load and Full-Load Carrying Fillet Welds at Cover Plates and Lap Joints. *IIW International Institute of Welding*, XIII-2278-09-XV-1320-09.
- FRICKE, W., FRIEDRICHS, N., MUSUMECI, L. & PAETZOLD, H. 2013. Experimental and Numerical Analysis of the Low-Cycle Behaviour of a Web Frame Corner in Ships.
- FRICKE, W. & KAHL, A. 2007. Local Stress Analysis and Fatigue Assessment of Bracket Toes Based on Measured Weld Profile. *IIW International Institute of Welding*, XIII-2166-07.
- FRICKE, W. & PAETZOLD, H. 1987. Application of the Cyclic Strain Approach to the Fatigue Failure of Ship Structural Details. *Journal of Ship Research*, 31, 177-185.
- FRICKE, W. & PAETZOLD, H. 1995. Fatigue Strength Assessment of Scallops an Example for the Application of Nominal and Local Stress Approaches. *Marine Structure*, 8, 423-447.
- FRICKE, W. & PAETZOLD, H. 2010. Full-scale fatigue tests of ship structures to validate the S-N approaches for fatigue strength assessment. *Marine Structure*, 23, 115-130.
- GERARD, D. A. & KOSS, D. A. 1990. Porosity and crack initiation during low cycle fatigue. *Materials Science and Engineering: A*, 129, 77-85.
- GOYAL, S., SANDHYA, R., VALSAN, M. & BHANU SANKARA RAO, K. 2009. The effect of thermal ageing on low cycle fatigue behaviour of 316 stainless steel welds. *International Journal of Fatigue*, 31, 447-454.
- GROSSE, M., KALKHOF, D., NIFFENEGGER, M. & KELLER, L. 2006. Influencing parameters on martensite transformation during low cycle fatigue for steel AISI 321. *Materials Science and Engineering: A*, 437, 109-113.
- HE, L. Z., ZHENG, Q., SUN, X. F., GUAN, H. R., HU, Z. Q., TIEU, A. K., LU, C. & ZHU, H. T. 2005. High temperature low cycle fatigue behavior of Ni-base superalloy M963. *Materials Science and Engineering: A*, 402, 33-41.
- HEO, J.-H., KANG, J.-K., KIM, Y., YOO, I.-S., KIM, K.-S. & URM, H.-S. 2004. A Study on the Design Guidance for Low Cycle Fatigue in Ship Structure.
- HOBBACHER, A. F. 2008. Recommendations for fatigue design of welded joints and components. *IIW International Institute of Welding*, IIW-1823-07
- HOBBACHER, A. F. 2009. The new IIW recommendations for fatigue assessment of welded joints and components – A comprehensive code recently updated. *International Journal of Fatigue*, 31, 50-58.
- HSE-2001/73 2001. Failure Modes Reliability and Integrity of Offshore Structures. Annex B, B12.
- HSE-REVIEW 2004. Review of low cycle fatigue resistance. *HSE*, Research Report 207.
- HUANG, H. L., MAO, S. W., GAN, D. & HO, N. J. 2012. The strain amplitude controlled fatigue behavior of pure copper with ultra large grain size. *Materials Science and Engineering: A*.
- HUANG, W. & MOAN, T. 2005. Combination of global still-water and wave load effects for reliability-based design of floating production, storage and offloading (FPSO) vessels. *Applied Ocean Research*, 27, 127-141.
- INGRAHAM, M. D., DEMARIA, C. J., ISSEN, K. A. & MORRISON, D. J. 2009. Low cycle fatigue of aluminum foam. *Materials Science and Engineering: A*, 504, 150-156.

- ISSC 2009. Committee III.2 Fatigue and Fracture. *17th International Ship and Offshore Structures Congress - Seoul, Korea*, 1, 475-585.
- KANCHANOMAI, C. & MUTOH, Y. 2004. Effect of temperature on isothermal low cycle fatigue properties of Sn–Ag eutectic solder. *Materials Science and Engineering: A*, 381, 113-120.
- KASCHNER, G. C. & GIBELING, J. C. 2002. A study of the mechanisms of cyclic deformation in f.c.c. metals using strain rate change tests. *Materials Science and Engineering: A*, 336, 170-176.
- KIM, G.-H., LEE, B.-W., LU, H. & PARK, J.-H. 2012. Failure analysis of an aircraft APU exhaust duct flange due to low cycle fatigue at high temperatures. *Engineering Failure Analysis*, 20, 97-104.
- KIM, H. J., LEE, C. S., PARK, S. H. & SHIN, D. H. 2004. Quantitative analysis on low cycle fatigue damage: a microstructural model for the prediction of fatigue life. *Materials Science and Engineering: A*, 379, 210-217.
- KONDO, Y. & OKUYA, K. 2007. The effect of seismic loading on the fatigue strength of welded joints. *Materials Science and Engineering: A*, 468–470, 223-229.
- LEE, E. U., VASUDEVAN, A. K. & GLINKA, G. 2009. Environmental effects on low cycle fatigue of 2024-T351 and 7075-T651 aluminum alloys. *International Journal of Fatigue*, 31, 1938-1942.
- LI, C., ELLYIN, F., KOH, S. & OH, S. J. 2000. Influence of porosity on fatigue resistance of cast SiC particulate-reinforced Al–Si alloy composite. *Materials Science and Engineering: A*, 276, 218-225.
- LIU, C. L., LU, Z. Z., XU, Y. L. & YUE, Z. F. 2005. Reliability analysis for low cycle fatigue life of the aeronautical engine turbine disc structure under random environment. *Materials Science and Engineering: A*, 395, 218-225.
- LR-HULL-INSPECTION-GUIDE 2007. Hull Inspection Guide. 26-27.
- LR-REPORT 2003. Ship-Type FPSO Hull Structural Appraisal.
- LR-REPORT 2007. FPSO Hull Strength Assessment for FPSO Specific Loading Conditions
- LR-REPORT 2008. FDA2 Fatigue Assessment of the FPSO "Anonymous"
- LR-REPORT 2009. Structural Life Extension Study.
- LUQUIAU, D., FEAUGAS, X. & CLAVEL, M. 1997. Cyclic softening of the Ti-10V-2Fe-3Al titanium alloy. *Materials Science and Engineering: A*, 224, 146-156.
- MADI, Y., MATHERON, P., RECHO, N. & MONGABURE, P. 2004. Low cycle fatigue of welded joints: new experimental approach. *Nuclear Engineering and Design*, 228, 161-177.
- MAHONEY, C. N. & SUPAN, C. 2012. Worldwide Survey of Floating Production Storage and Offloading (FPSO) Units
- MANSON, S. S. 1964. Fatigue: A Complex Subject – Some Simple Approximations. 193-226.
- MATHEW, M. D., KIM, D. W. & RYU, W.-S. 2008. A neural network model to predict low cycle fatigue life of nitrogen-alloyed 316L stainless steel. *Materials Science and Engineering: A*, 474, 247-253.
- MATSUZUKI, M. & HORIBE, S. 2009. Analysis of fatigue damage process in magnesium alloy AZ31. *Materials Science and Engineering: A*, 504, 169-174.
- MEDEKSHAS, H. & BALINA, V. 2006. Assessment of Low Cycle Fatigue Strength of Notched Components. *Materials and Design*, 27, 132–140.
- MEGHARBI, A. 2005. Accumulated Fatigue Assessment in Pressure Vessels. *Thesis for Honours Degree*.
- MENDEZ, J. 1999. On the effects of temperature and environment on fatigue damage processes in Ti alloys and in stainless steel. *Materials Science and Engineering: A*, 263, 187-192.
- MO, D.-F., HE, G.-Q., HU, Z.-F., LIU, X.-S. & ZHANG, W.-H. 2010. Effect of microstructural features on fatigue behavior in A319-T6 aluminum alloy. *Materials Science and Engineering: A*, 527, 3420-3426.
- MOLLAND, T. 2008. *The Marine Engineering Reference Book*, Elsevier Ltd.
- MORI, T. & MYOKEN, M. 2008. Applicability of Effective Notch Stress Conception to Fatigue Strength Evaluation for Cruciform Welded Joints failing from Weld Root. *IIW International Institute of Welding*, XIII-2231-08.

- NAGESHA, A., VALSAN, M., KANNAN, R., BHANU SANKARA RAO, K. & MANNAN, S. L. 2002. Influence of temperature on the low cycle fatigue behaviour of a modified 9Cr–1Mo ferritic steel. *International Journal of Fatigue*, 24, 1285-1293.
- NIKITIN, I. & BESEL, M. 2008. Correlation between residual stress and plastic strain amplitude during low cycle fatigue of mechanically surface treated austenitic stainless steel AISI 304 and ferritic–pearlitic steel SAE 1045. *Materials Science and Engineering: A*, 491, 297-303.
- PALIT SAGAR, S., METYA, A. K., GHOSH, M. & SIVAPRASAD, S. 2011. Effect of microstructure on non-linear behavior of ultrasound during low cycle fatigue of pearlitic steels. *Materials Science and Engineering: A*, 528, 2895-2898.
- PD5500 2011. PD 5500. *British Standard*, Annex C, C/1-C/29.
- PETINOV, S. 2003. Fatigue Analysis of Ship Structures. *Book*.
- PRAVEEN, K. V. U. & SINGH, V. 2008. Effect of heat treatment on Coffin–Manson relationship in LCF of superalloy IN718. *Materials Science and Engineering: A*, 485, 352-358.
- RADAJ, D. 1996. Review of fatigue strength assessment of nonwelded and welded structures based on local parameters. *International Journal of Fatigue*, 18, 153-170.
- RADAJ, D., SONSINO, C. M. & FRICKE, W. 2006. Fatigue Assessment of Welded Joints by Local Approaches.
- RADAJ, D., SONSINO, C. M. & FRICKE, W. 2009. Recent developments in local concepts of fatigue assessment of welded joints. *International Journal of Fatigue*, 31, 2-11.
- RAJI, H. 2010. *Low cycle fatigue in floating production storage and offloading units*. PhD, Universities of Strathclyde.
- RAJI, H., INCECIK, A. & BARLTROP, N. 2009. Low cycle fatigue assessment of an FPSO. *1st International Conference Integrating Structural Analysis, Risk and Reliability*. Glasgow.
- RECINA, V. & KARLSSON, B. 1999. High temperature low cycle fatigue properties of Ti-48Al-2W-0.5Si gamma titanium aluminide. *Materials Science and Engineering: A*, 262, 70-81.
- REGER, M. & REMY, L. 1988. High temperature, low cycle fatigue of IN-100 superalloy I: Influence of temperature on the low cycle fatigue behaviour. *Materials Science and Engineering: A*, 101, 47-54.
- SAIPRASERTKIT, K., HANJI, T. & MIKI, C. 2011. Fatigue strength assessment of load carrying cruciform joints in low and high cycle fatigue region based on effective notch concept. *IIW International Institute of Welding*, XIII-2384-11.
- ŠAMEC, B., POTRČ, I. & ŠRAML, M. 2011. Low cycle fatigue of nodular cast iron used for railway brake discs. *Engineering Failure Analysis*, 18, 1424-1434.
- SCHIJVE, J. 2012. Fatigue predictions of welded joints and the effective notch stress concept. *International Journal of Fatigue*, 45, 31–38.
- SEWERYN, A., BUCZYŃSKI, A. & SZUSTA, J. 2008. Damage accumulation model for low cycle fatigue. *International Journal of Fatigue*, 30, 756-765.
- SHIGLEY, J. E., MISCHE, C. R. & BUDYANAS, R. G. 2003. *Mechanical engineering design* Mc Graw Hill.
- SHIPRIGHT-3, L. 2004. Fatigue Design Assessment Level 3 Procedure. *Lloyd's Register Group*, 1-65.
- SHIPRIGHT-FOI, L. 2008. Floating offshore installation assessment of structures. *Lloyd's Register Group*, Chapter 1-11.
- SHIPRIGHT, L. 2004. Fatigue Design Assessment Level 1 Procedure. *Lloyd's Register Group*, 1-139.
- SKELTON, R. P., VILHELMSSEN, T. & WEBSTER, G. A. 1998. Energy criteria and cumulative damage during fatigue crack growth. *International Journal of Fatigue*, 20, 641-649.
- SONSINO, C. M. 2009. Principles of local stress concepts for the assessment of welded joints. 30-33.
- SRINIVASAN, V. S., VALSAN, M., BHANU SANKARA RAO, K., MANNAN, S. L. & RAJ, B. 2003. Low cycle fatigue and creep–fatigue interaction behavior of 316L(N) stainless

- steel and life prediction by artificial neural network approach. *International Journal of Fatigue*, 25, 1327-1338.
- STOLARZ, J. 1997. Multicracking in low cycle fatigue—a surface phenomenon? *Materials Science and Engineering: A*, 234–236, 861-864.
- STOLARZ, J., MADELAINE-DUPUICH, O. & MAGNIN, T. 2001. Microstructural factors of low cycle fatigue damage in two phase Al–Si alloys. *Materials Science and Engineering*, 275–286.
- SUN, H.-H. & BAI, Y. 2003. Time-variant reliability assessment of FPSO hull girders. *Marine Structures*, 16, 219-253.
- URM, H. S., YOO, I. S., HEO, J. H., KIM, S. C. & LOTSBERG, I. 2004a. Low Cycle Fatigue Strength Assessment for Ship Structures. *9th Symposium on Practical Design of Ships and other Floating Structures*.
- URM, H. S., YOO, I. S., HEO, J. H., KIM, S. C. & LOTSBERG, I. 2004b. Low Cycle Fatigue Strength Assessment for Ship Structures.
- VALSAN, M., RAO, K. B. S., SANDHYA, R. & MANNAN, S. L. 1992. High temperature, low cycle fatigue behaviour of AISI type 316LN base metal, 316LN-316 weld joint and 316 all-weld metal. *Materials Science and Engineering: A*, 149, L9-L12.
- WANG, X., KANG, J., KIM, Y. & WIRSCHING, P. H. 2006. Low cycle fatigue analysis of marine structures. *ABS - OMAE 2006-92268*, 95-99.
- WIKIPEDIA. 2013a. *Classification society* [Online].
- WIKIPEDIA. 2013b. *Prestige oil spill* [Online]. Wikipedia.
- WILCZYNSKI, B. & MRÓZ, Z. 2007. Optimal design of machine components using notch correction and plasticity models. *Computers & Structures*, 85, 1382-1398.
- YANG, X. J., CHOW, C. L. & LAU, K. J. 2003. Time-dependent cyclic deformation and failure of 63Sn/37Pb solder alloy. *International Journal of Fatigue*, 25, 533-546.
- YAO, J. T. P. & MUNSE, W. H. 1961. Low cycle fatigue of metals - Literature review. In: SSC-137, S. S. C. (ed.) *Progress Report*. National Academy of Sciences-National Research Council.
- YOON, S., HONG, S.-G. & LEE, S.-B. 2004. Phenomenological description of cyclic deformation using the overlay model. *Materials Science and Engineering: A*, 364, 17-26.
- YU, D., YU, W., CHEN, G., JIN, F. & CHEN, X. 2012. Role of dynamic strain aging in the tensile property, cyclic deformation and fatigue behavior of Z2CND18.12N stainless steel between 293 K and 723 K. *Materials Science and Engineering: A*, 558, 730-736.

Appendixes

9 **Appendixes**

Appendix 1

Bureau Veritas

Fatigue Check of Structural Detail

Pt B, Ch7, Sec 4

Table 7 : Function $I_N^*[X+1, v_i]$

X	Value of v_i													
	1,5	2,0	2,5	3,0	3,5	4,0	4,5	5,0	5,5	6,0	6,5	7,0	7,5	8,0
2,5	0,38	0,73	1,13	1,53	1,90	2,22	2,48	2,70	2,86	2,99	3,08	3,15	3,20	3,24
2,6	0,38	0,75	1,19	1,63	2,04	2,41	2,71	2,96	3,16	3,31	3,42	3,51	3,57	3,61
2,7	0,39	0,78	1,25	1,73	2,20	2,62	2,97	3,26	3,49	3,67	3,81	3,91	3,99	4,04
2,8	0,39	0,80	1,31	1,85	2,38	2,85	3,26	3,60	3,87	4,09	4,25	4,37	4,46	4,53
2,9	0,39	0,83	1,38	1,98	2,57	3,11	3,58	3,98	4,30	4,56	4,75	4,90	5,01	5,10
3,0	0,39	0,86	1,45	2,12	2,78	3,40	3,95	4,41	4,79	5,09	5,33	5,51	5,65	5,75
3,1	0,40	0,89	1,54	2,27	3,01	3,72	4,35	4,89	5,34	5,70	5,99	6,21	6,37	6,49
3,2	0,40	0,92	1,62	2,43	3,27	4,08	4,81	5,44	5,97	6,40	6,74	7,01	7,21	7,36
3,3	0,41	0,95	1,72	2,61	3,56	4,48	5,32	6,06	6,68	7,20	7,61	7,93	8,17	8,36
3,4	0,41	0,99	1,82	2,81	3,87	4,92	5,90	6,76	7,50	8,11	8,60	8,99	9,29	9,51
3,5	0,42	1,03	1,93	3,03	4,22	5,42	6,55	7,55	8,42	9,15	9,74	10,21	10,57	10,85
3,6	0,42	1,07	2,04	3,26	4,60	5,97	7,27	8,45	9,48	10,34	11,05	11,62	12,06	12,41
3,7	0,43	1,12	2,17	3,52	5,03	6,59	8,09	9,47	10,68	11,71	12,56	13,25	13,79	14,21
3,8	0,43	1,16	2,31	3,80	5,50	7,28	9,02	10,63	12,06	13,28	14,30	15,13	15,80	16,31
3,9	0,44	1,21	2,45	4,10	6,02	8,05	10,06	11,94	13,63	15,09	16,31	17,32	18,12	18,76
4,0	0,45	1,26	2,61	4,43	6,59	8,91	11,23	13,43	15,42	17,16	18,63	19,85	20,83	21,61
4,1	0,45	1,32	2,78	4,80	7,22	9,87	12,55	15,12	17,47	19,54	21,31	22,78	22,98	24,94
4,2	0,46	1,38	2,96	5,20	7,93	10,95	14,05	17,05	19,82	22,29	24,41	26,19	27,65	28,83
4,3	0,47	1,44	3,16	5,63	8,70	12,15	15,73	19,24	22,51	25,45	28,00	30,16	31,93	33,38
4,4	0,48	1,51	3,37	6,11	9,56	13,50	17,64	21,74	25,60	29,10	32,16	34,77	36,94	38,71
4,5	0,49	1,57	3,60	6,63	10,52	15,01	19,79	24,58	29,14	33,31	36,99	40,15	42,79	44,96
4,6	0,49	1,65	3,85	7,20	11,57	16,70	22,23	27,82	33,20	38,17	42,59	46,41	49,63	52,29
4,7	0,50	1,73	4,12	7,82	12,75	18,59	24,98	31,53	37,88	43,79	49,10	53,72	57,65	60,91
4,8	0,52	1,81	4,40	8,50	14,04	20,72	28,11	35,75	43,25	50,29	56,66	62,26	67,05	71,05
4,9	0,52	1,90	4,71	9,25	15,49	23,11	31,64	40,57	49,42	57,81	65,47	72,24	78,08	82,98
5,0	0,53	1,99	5,04	10,07	17,09	25,78	35,65	46,08	56,53	66,52	75,72	83,92	91,03	97,05
5,1	0,55	2,09	5,40	10,97	18,86	28,79	40,19	52,39	64,71	76,61	87,66	97,58	106,3	113,6
5,2	0,56	2,19	5,79	11,95	20,84	32,17	45,34	59,60	74,15	88,32	101,6	113,6	124,2	133,2
5,3	0,57	2,30	6,21	13,03	23,03	35,96	51,19	67,85	85,02	101,9	117,8	132,4	145,3	156,4
5,4	0,58	2,41	6,66	14,21	25,46	40,23	57,83	77,29	97,56	117,7	136,8	154,4	170,1	183,8
5,5	0,59	2,54	7,14	15,50	28,17	45,03	65,37	88,11	112,0	136,0	159,0	180,3	199,4	216,2
5,6	0,61	2,67	7,67	16,92	31,18	50,42	73,93	100,5	128,8	157,3	184,9	210,7	234,0	254,6
5,7	0,62	2,80	8,23	18,48	34,53	56,49	83,66	114,7	148,1	182,0	215,2	246,4	274,8	300,1
5,8	0,64	2,95	8,84	20,19	38,25	63,33	94,73	131,0	170,4	210,9	250,7	288,4	323,1	354,1
5,9	0,65	3,10	9,50	22,07	42,39	71,02	107,3	149,8	196,2	244,4	292,2	337,9	380,2	418,2
6,0	0,67	3,26	10,21	24,13	47,00	79,69	121,6	171,2	226,1	283,5	340,9	396,2	447,7	494,4
6,1	0,68	3,44	10,98	26,39	52,14	89,45	138,0	195,9	260,6	329,0	398,0	464,9	527,7	585,0
6,2	0,70	3,62	11,82	28,87	57,86	100,5	156,5	224,2	300,6	382,1	464,9	546,0	622,5	692,8
6,3	0,72	3,81	12,71	31,60	64,24	112,9	177,7	256,8	347,0	444,0	543,5	641,6	734,9	821,1
6,4	0,73	4,02	13,68	34,60	71,34	126,9	201,7	294,3	400,7	516,3	635,8	754,5	868,3	974,0
6,5	0,75	4,23	14,73	37,90	79,25	142,6	229,2	337,3	463,0	600,6	744,2	887,9	1026,6	1156,3
6,6	0,77	4,46	15,87	41,52	88,07	160,4	260,5	386,9	535,2	699,2	871,6	1045,5	1214,6	1373,8

Table 8 : Function $\Gamma_c [X+1]$

X	$\Gamma_c [X+1]$	X	$\Gamma_c [X+1]$
2,5	3,323	3,3	8,855
2,6	3,717	3,4	10,136
2,7	4,171	3,5	11,632
2,8	4,694	3,6	13,381
2,9	5,299	3,7	15,431
3,0	6,000	3,8	17,838
3,1	6,813	3,9	20,667
3,2	7,757	4,0	24,000

Table 9 : Part of the ship's life in full load condition

Service notation	Coefficient α
Oil tanker ESP Chemical tanker ESP Liquefied gas carrier Tanker Bulk carrier Ore carrier ESP Combination carrier ESP	0,60
Others	0,75

Table 10 : Stress concentration factor K_m for misalignment


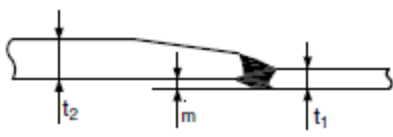
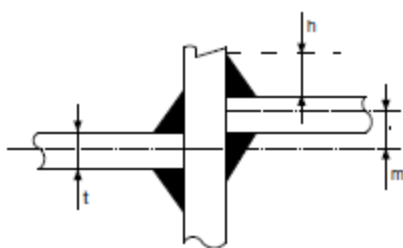









Geometry	K_m (1)
<p>Axial misalignment between flat plates</p> 	$1 + \frac{3(m - m_0)}{t}$
<p>Axial misalignment between flat plates of different thicknesses</p> 	$1 + \frac{6(m - m_0)}{t_1} \frac{t_1^{3/2}}{t_1^{3/2} + t_2^{3/2}}$
<p>Axial misalignment in fillet welded cruciform joints</p> 	$1 + \frac{m - m_0}{t + h}$
<p>(1) When the actual misalignment m is lower than the permissible misalignment m_0, K_m is to be taken equal to 1.</p> <p>Note 1:</p> <p>m : Actual misalignment between two abutting members</p> <p>m_0 : Permissible misalignment for the detail considered, given in Ch 12, Sec 2.</p>	

Table 11 : Weld coefficient λ

Weld configuration				Coefficient λ	Grinding applicable
Type	Description	Stress direction	Figure		
Butt weld		Parallel to the weld		2,10	yes
		Perpendicular to the weld		2,40	yes
Fillet weld	Continuous	Parallel to the weld		1,80	yes
		Perpendicular to the weld (1)		2,15	yes
	Well contoured end	Perpendicular to the weld		2,15	yes
	Not continuous	Parallel to the weld		2,90	yes
	Lap weld (root cracking)	Axial loading out of plane and perpendicular to the weld		4,50	no
Cruciform joint	Full penetration	Perpendicular to the weld		2,10	yes
	Partial penetration	Perpendicular to the weld		Toe cracking: 2,10	yes
				Root cracking: 4,50	no

(1) This case includes the hot spots indicated in the sheets of special structural details in Ch 12, Sec 2 relevant to the connections of longitudinal ordinary stiffeners with transverse primary supporting members.

Table 12 : K_F values

Flame-cut edge description	K_F
Machine gas cut edges, with subsequent machining, dressing or grinding	1,4
Machine thermally cut edges, corners removed, no crack by inspection	1,6
Manually thermally cut edges, free from cracks and severe notches	2,0
Manually thermally cut edges, uncontrolled, no notch deeper than 0,5 mm	2,5

Appendix 2

Det Norske Veritas

Classification Notes – No. 30.7

Table I-3 Load combination for calculation of low cycle fatigue stress range, $\Delta\sigma_{LCF}$				
<i>Location</i>	<i>Load conditions</i>	<i>Tankers with centreline longitudinal bulkhead</i>	<i>Tankers with two longitudinal bulkheads</i>	<i>Vessels without longitudinal bulkhead</i>
Longitudinal flange connections *)	Full load -ballast	$ \sigma_{LC1}-\sigma_{LC2} $	$ \sigma_{LC7}-\sigma_{LC8} $	$ \sigma_{LC13}-\sigma_{LC14} $
Web stiffener on top of longitudinal stiffener	Full load -ballast	$ \sigma_{LC1}-\sigma_{LC2} $	$ \sigma_{LC7}-\sigma_{LC8} $	$ \sigma_{LC13}-\sigma_{LC14} $
Transverse members welded to longitudinals in water ballast tanks, i.e. web stiffener, cutout, lug plate	Full load -ballast	$ \sigma_{LC1}-\sigma_{LC2} $	$ \sigma_{LC7}-\sigma_{LC8} $	$ \sigma_{LC13}-\sigma_{LC14} $
Lower and upper hopper knuckles, lower and upper chamfers *)	Full load -ballast	$ \sigma_{LC1}-\sigma_{LC2} $	$ \sigma_{LC7}-\sigma_{LC8} $	$ \sigma_{LC13}-\sigma_{LC14} $
Horizontal stringer at inner side longitudinal bulkhead *)	Full load -ballast	$ \sigma_{LC1}-\sigma_{LC2} $	$ \sigma_{LC7}-\sigma_{LC8} $	$ \sigma_{LC13}-\sigma_{LC14} $
	Alternate load	$ \sigma_{LC3}-\sigma_{LC4} $	$ \sigma_{LC9}-\sigma_{LC10} $	$ \sigma_{LC15}-\sigma_{LC16} $
Girder connection to transverse bulkhead, inner bottom to lower stool, inner bottom to cofferdam bulkhead *)	Full load -ballast	$ \sigma_{LC1}-\sigma_{LC2} $	$ \sigma_{LC7}-\sigma_{LC8} $	$ \sigma_{LC13}-\sigma_{LC14} $
	Alternate LCs 1 -2	$ \sigma_{LC3}-\sigma_{LC4} $	$ \sigma_{LC9}-\sigma_{LC10} $	$ \sigma_{LC15}-\sigma_{LC16} $
Remark:				
*) hull girder stress should be added to the local bending stress for the corresponding load condition in the trim and stability booklet.				

Appendix 3

Material specification

Chemical composition of mild steel Grade A

Deposit Metal Bostrand LW1



TATA STEEL UK LIMITED
P.O. Box 1, Brigg Road,
Scunthorpe,
North Lincolnshire, DN16 1BP.
Telephone: 01724 404040
Fax: 402353 Telex: 52601

INSPECTION CERTIFICATE

In Accordance with EN10204 3.2
Product manufactured under a Management System approved to ISO 9001

Date	7/ 3/13	Z1
Cert No.	SPLA/13/00243731/1	A3

Customer		A6		A8		A7	
DENT STEEL SERVICES (YORKSHIRE) LTD - BRADFORD LOW MOOR STEEL WORKS NEW WORKS ROAD LOW MOOR BRADFORD (WEST YORKSHIRE) BD120QN		Inspection LLOYD'S REGISTER EMEA		Tata Steel Ref. No. 29416/ 18		Works Order/Item No. 68/ 523/ 8	
Lloyds Register MATERIALS QUALITY SCHEME		A11		Customers Order No. PO033615			
				Specification/Product LLOYDS 2012 A		B1/B2	
				Plate 10000 X 2500 X 16.00mm Piece Weight 3140.0Kg As Rolled.			

B6/A10 PO033615/CAST NO/ TATA STEEL/ EN10025-2:2004/ LLOYDS 2012/DNV 2013 S275JR+AR/A/A

SPLASH RED ON 4 CORNERS

L=Longitudinal		T=Transverse		Z=Through Thickness		S=Sub-Surface		M=Mid-Thickness		Q=Quarter-Thickness		TH=Third-Thickness		BS=Bottom Surface		A=Supply Condition		N=Normalised		SR=Stress Relieved		SA=Strain Aged	
B10	B8	B7	C00 Test Piece No.	C2 D i f f e r e n t i a l	B5 Test Condition	C11 Yield Stress Re	C12 Tensile Strength Rm	C14 Re Rn %	C13 Elong% A Lo = 5.65 / 10	C2 D i f f e r e n t i a l	C1 P o s i t i o n	B5 Test Condition	C40 KV2 10x1.0x2mmV	C41 Units	C42 Joules	C43 Av.	Steelmaking Process:						C70
	B.O.S.																						
Quantity	Cast/Heat No.	Specification	Min Max	T		235 296	400 520 461		22 34	L	S		27 +20C	Av/ 125	19 144	Ind +20C	Other Tests						C50-C69
1	89938	BG247 / 1																					
ANALYSIS %		C71+C92	C	Si	Mn	P	S	Cr	Mo	Ni	Al	Cu	Nb	B	Sn	Ti	N	V					
Specification		Min	.21	.50		.035	.0350	.300	.080	.300		.400	.060	.0008		.050		.100					CEV
Cast / Heat		Max	.15	.32	0.91	.013	.0120	.017	.002	.020	.002	.012	.001	.0001	.002	.001	.003	.003					.40
Specification		Min																					.30
		Max																					

Thickness tolerances to EN 10029 class B
This certificate is issued under the arrangements authorised by Lloyd's Register EMEA in accordance with the requirements of the Materials Quality scheme and certificate number MQS029

On behalf of Tata Steel UK Limited, the manufacturer.
These results are certified by Tata Steel UK Limited and comply with the requirements of the Product Description.

Z1

R. J. Preston

R.J.Preston, Test House Manager, Scunthorpe

All original Inspection Certificates issued by Tata Steel UK Limited will contain either an embossed stamp, or be impregnated with a Tata Steel UK Limited watermarked logo, or a combination of both. Any recipient of a copy of a Tata Steel UK Limited Inspection Certificate without either the stamp or watermarking should ensure from the supplier that it is a true and accurate reproduction of the original. Company Registration Number 02280000.

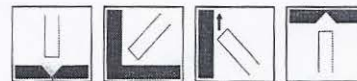
A5

H091s

Solid Wires

Non Alloyed MAG Spooled Wire

Bostrand LW1



Classification Weld Metal

EN ISO 14341-A G 38 2 C G3Si1

EN ISO 14341-A G 42 3 M G3Si1

Classification Wire Electrode

EN ISO 14341-A G3Si1

SFA/AWS A5.18 ER70S-6

Description and applications

Bostrand LW1 is the general purpose mild steel copper coated MAG (metal active gas) wire. De-oxidised with manganese and silicon, it produces quality welds with excellent radiographic and mechanical properties. Bostrand LW1 is ideal for welding most mild and carbon-manganese steels e.g. Lloyds grades A to EH (up to EH32).

Approvals

ABS : 3YSA (M21)

BV : SA3YM (M21)

CE EN 13479

LR : 3S, 3YS

DNV : 111 YMS

Typical all-weld mechanical properties – as welded using Ar/20%CO₂

Yield Stress	480	MPa
Tensile Strength	560	MPa
Elongation	26	%
Charpy V impact value, Typical - 20°C	90	J
- 30°C	70	J

Chemical Composition (wire)

	Min	Max
C	0.06	0.14
Si	0.80	1.00
Mn	1.40	1.60
S		0.025
P		0.025
Cu		0.35

Welding Parameters

Size (mm)	0.6	0.8	1.0	1.2	1.6
Current (amps)	30-100	60-200	80-300	120-380	225-550

Appendix 4

Longitudinal Attachment Type A

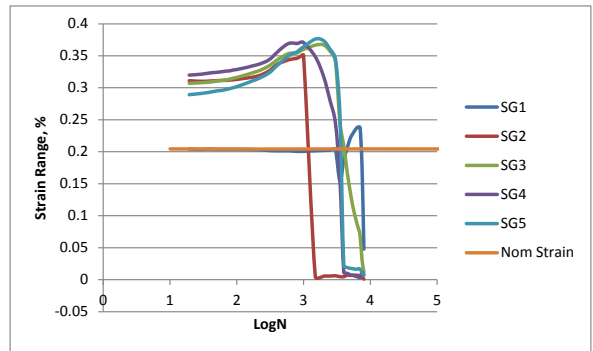
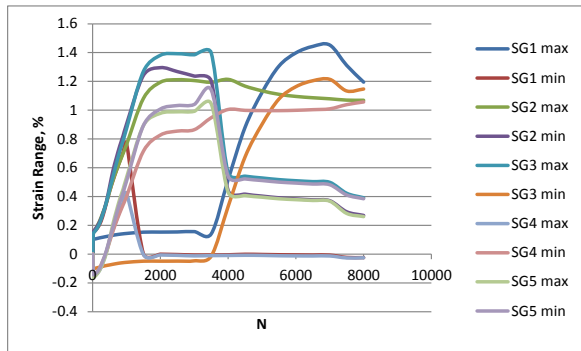
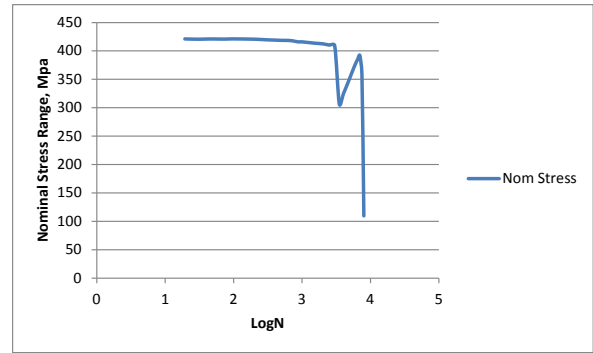
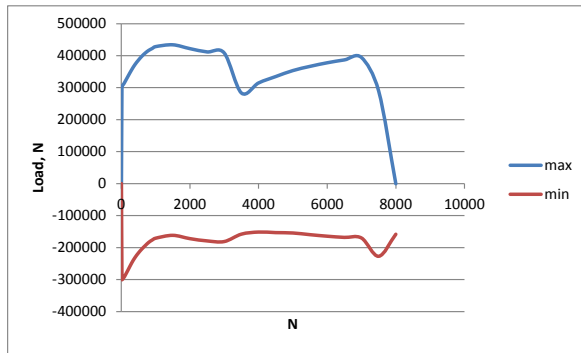
Test Data and Plots

TEST A5

max										
Cycles	logN	SG1 max	SG2 max	SG3 max	SG4 max	SG5 max	Displacem	Load	Nom Stress	Nom Strain
0.36	-0.4437	0	0	0	0	0	-0.004	0	0	0
1.36	0.133539	0	0	0	0	0	-0.004	-19.228	-0.01335	-6.48193E-06
2.36	0.372912	0	0	0	0	0	-0.005	0	0	0
4.36	0.639486	0	0	0	0	0	-0.006	-19.228	-0.01335	-6.48193E-06
19.36	1.286905	0.103904	0.150307	0.1535	0.155652	0.144604	1.09	305693.4	212.2871	0.103051997
29.36	1.467756	0.103904	0.152689	0.157308	0.159943	0.147939	1.087	306328	212.7278	0.103265905
39.36	1.595055	0.104381	0.155071	0.16064	0.16328	0.150797	1.086	307327.9	213.4221	0.103602973
49.36	1.693375	0.104381	0.157453	0.163972	0.166141	0.154132	1.086	308712.3	214.3835	0.104069682
59.36	1.773494	0.104858	0.159835	0.166829	0.169003	0.156515	1.085	309885.2	215.1981	0.104465089
69.36	1.841109	0.105335	0.161741	0.169685	0.171864	0.159374	1.086	311500.4	216.3197	0.105009583
79.36	1.899602	0.105812	0.164124	0.173018	0.174725	0.162233	1.086	313000.2	217.3613	0.105515185
89.36	1.951143	0.106289	0.166506	0.176828	0.178064	0.165092	1.086	315019.2	218.7634	0.106195803
99.36	1.997212	0.106767	0.168889	0.180161	0.181403	0.167951	1.086	316826.7	220.0185	0.106805117
199.36	2.299638	0.112493	0.202735	0.226852	0.221008	0.209908	1.084	336343.5	233.5719	0.113384422
299.36	2.476194	0.117265	0.263334	0.28647	0.281192	0.27673	1.083	355437.4	246.8315	0.11982112
399.38	2.601386	0.122037	0.34887	0.353326	0.35772	0.354164	1.085	372358.4	258.5822	0.125525345
499.38	2.698431	0.126333	0.436468	0.434628	0.467934	0.44753	1.086	386029.8	268.0762	0.130134098
599.38	2.777702	0.131107	0.510303	0.513666	0.580314	0.537229	1.085	398278.3	276.5821	0.134263179
699.38	2.844713	0.134926	0.579442	0.579865	0.668857	0.628531	1.086	408373.2	283.5925	0.137666267
799.38	2.902753	0.138268	0.644346	0.640865	0.751285	0.714218	1.084	416583.8	289.2943	0.140434112
899.02	2.953769	0.141133	0.707888	0.700014	0.822735	0.788951	1.078	422371.5	293.3135	0.142385216
999.02	2.999574	0.14352	0.772476	0.759233	0.902027	0.870078	1.08	428274.6	297.4129	0.144375213
1499.02	3.175807	0.152593	0.0019	1.082063	1.241878	1.269886	1.086	434043.2	301.4189	0.146319835
1999.04	3.300821	0.153071	-0.00047	1.194182	1.295491	1.381561	1.086	422006.2	293.0598	0.142262057
2499.04	3.397773	0.154026	-0.00285	1.211678	1.26819	1.392302	1.08	411757.4	285.9427	0.138807112
2999.08	3.476988	0.156414	-0.00617	1.205845	1.237007	1.384978	1.085	408430.9	283.6326	0.137685713
3499.02	3.543946	0.140178	-0.0057	1.194182	1.202435	1.398651	1.007	283426.9	196.8243	0.095545756
3999.02	3.601954	0.517357	-0.00475	1.214108	0.442036	0.563161	1.11	314711.6	218.5497	0.106092089
4499.02	3.653118	0.880911	-0.00095	1.166979	0.416631	0.54155	1.202	334709.1	232.4369	0.112833445
4999.02	3.698885	1.122797	-0.00237	1.134451	0.403214	0.529068	1.283	353418.4	245.4294	0.119140502
5499.02	3.740285	1.306196	-0.00427	1.110191	0.391238	0.517549	1.355	366570.6	254.5629	0.12357424
5999.02	3.77808	1.398145	-0.00522	1.09564	0.383575	0.50987	1.416	377780.8	262.3478	0.127353289
6499.02	3.812848	1.443203	-0.00617	1.086427	0.37687	0.503633	1.467	386760.5	268.5837	0.130380417
6999.02	3.845037	1.452513	-0.00665	1.079154	0.371125	0.498835	1.505	394221.1	273.7647	0.132895462
7499.02	3.875005	1.311083	-0.02279	1.069944	0.294098	0.422615	1.04	289368.5	200.9504	0.097548717
7999.02	3.903037	1.194907	-0.02422	1.068974	0.268767	0.391489	1.066	-461.482	-0.32047	-0.00015557

min										
Cycles	logN	SG1 min	SG2 min	SG3 min	SG4 min	SG5 min	Displacement	Load	Nom Stress	Nom Strain
0.86	-0.0655	0	0	0	0	0	-0.003	0	0	0
1.86	0.269513	0	0	0	0	0	-0.005	-19.228	-0.01335	-6.5E-06
2.86	0.456366	0	0	0	0	0	-0.005	-19.228	-0.01335	-6.5E-06
4.86	0.686636	0	0	0	0	0	-0.006	-19.228	-0.01335	-6.5E-06
19.86	1.297979	-0.10036	-0.16075	-0.1535	-0.16417	-0.14466	-1.104	-300733	-208.842	-0.10138
29.86	1.47509	-0.09989	-0.15743	-0.15066	-0.16133	-0.14324	-1.102	-299387	-207.907	-0.10093
39.86	1.600537	-0.09989	-0.15554	-0.1483	-0.15991	-0.14229	-1.102	-298771	-207.48	-0.10072
49.86	1.697752	-0.09941	-0.15364	-0.14641	-0.15801	-0.14087	-1.102	-297637	-206.692	-0.10034
59.86	1.777137	-0.09894	-0.15175	-0.14451	-0.15612	-0.13945	-1.102	-296214	-205.704	-0.09986
69.86	1.844229	-0.09846	-0.14986	-0.14262	-0.15422	-0.13803	-1.101	-294503	-204.516	-0.09928
79.86	1.902329	-0.09799	-0.14796	-0.14073	-0.15185	-0.13661	-1.102	-293099	-203.541	-0.09881
89.86	1.953566	-0.09751	-0.14607	-0.13836	-0.14996	-0.13519	-1.102	-291387	-202.352	-0.09823
99.86	1.999392	-0.09704	-0.14417	-0.136	-0.14711	-0.13377	-1.101	-289676	-201.164	-0.09765
199.86	2.300726	-0.09086	-0.11528	-0.0986	-0.11488	-0.10344	-1.101	-269429	-187.103	-0.09083
299.86	2.476919	-0.08468	-0.06265	-0.04743	-0.06222	-0.04605	-1.099	-248777	-172.762	-0.08387
399.88	2.60193	-0.07945	0.01235	0.009966	0.002376	0.019478	-1.099	-231126	-160.504	-0.07791
499.88	2.698866	-0.07517	0.095555	0.085008	0.103714	0.10413	-1.1	-216781	-150.543	-0.07308
599.88	2.778064	-0.07042	0.166506	0.160164	0.210984	0.187018	-1.101	-204379	-141.93	-0.0689
699.88	2.845024	-0.06614	0.234219	0.225422	0.298879	0.274819	-1.099	-193649	-134.479	-0.06528
799.88	2.903025	-0.06233	0.2982	0.28647	0.382138	0.357991	-1.1	-183612	-127.508	-0.0619
899.5	2.954001	-0.05948	0.358914	0.342336	0.451626	0.428364	-1.101	-176459	-122.541	-0.05949
999.5	2.999783	-0.0571	0.421618	0.399222	0.531297	0.506032	-1.101	-170748	-118.575	-0.05756
1499.52	3.175952	-0.04902	-0.00285	0.715414	0.893318	0.893765	-1.101	-161692	-112.286	-0.05451
1999.54	3.30093	-0.04902	-0.00617	0.827203	0.978052	1.008003	-1.101	-172017	-119.457	-0.05799
2499.56	3.397864	-0.04854	-0.00855	0.854707	0.988715	1.03224	-1.099	-179113	-124.384	-0.06038
2999.56	3.477058	-0.04664	-0.01235	0.864361	0.992108	1.039998	-1.097	-181151	-125.799	-0.06107
3499.36	3.543989	-0.01428	-0.01045	0.94746	1.044486	1.13999	-0.64	-158019	-109.736	-0.05327
3999.38	3.601993	0.33057	-0.0095	1.005034	0.43053	0.54107	-0.639	-151462	-105.182	-0.05106
4499.38	3.653153	0.675395	-0.00807	0.998741	0.406568	0.522348	-0.637	-153193	-106.384	-0.05164
4999.4	3.698918	0.901751	-0.00902	0.997289	0.395549	0.51131	-0.638	-154366	-107.198	-0.05204
5499.42	3.740317	1.077538	-0.0114	0.996805	0.384533	0.500275	-0.64	-159634	-110.857	-0.05381
5999.44	3.778111	1.163224	-0.01235	0.999225	0.378307	0.493559	-0.639	-164441	-114.195	-0.05543
6499.46	3.812877	1.204659	-0.01282	1.003582	0.372561	0.486843	-0.64	-168133	-116.759	-0.05668
6999.48	3.845066	1.214414	-0.01282	1.009391	0.367773	0.482047	-0.64	-170095	-118.121	-0.05734
7499.46	3.87503	1.13351	-0.02659	1.038447	0.282626	0.41112	-1.099	-227203	-157.78	-0.07659
7999.5	3.903063	1.147147	-0.02517	1.057343	0.260645	0.384788	-1.102	-158250	-109.896	-0.05335

Range										
log N	Load	SG1	SG2	SG3	SG4	SG5	Nom Stress	Nom Strain	Disp	Pseudo No
1.286905	606426	0.204266	0.311054	0.307003	0.319822	0.289265	421.1291	0.204432	2.194	658.8333
1.467756	605714.5	0.203791	0.310122	0.307973	0.321271	0.291179	420.6351	0.204192	2.189	661.8174
1.595055	606099.1	0.204268	0.31061	0.308939	0.323187	0.29309	420.9021	0.204321	2.188	665.7652
1.693375	606349	0.203793	0.311098	0.310379	0.324153	0.295004	421.0757	0.204406	2.188	667.755
1.773494	606099.1	0.203795	0.311586	0.311343	0.325119	0.295965	420.9021	0.204321	2.187	669.7451
1.841109	606002.9	0.203796	0.311598	0.312307	0.326085	0.297403	420.8354	0.204289	2.187	671.7355
1.899602	606099.1	0.203798	0.312087	0.313748	0.326578	0.298841	420.9021	0.204321	2.188	672.7499
1.951143	606406.7	0.2038	0.312575	0.315191	0.328021	0.300279	421.1158	0.204425	2.188	675.7228
1.997212	606502.9	0.203802	0.313063	0.316158	0.328517	0.301718	421.1825	0.204458	2.187	676.744
2.299638	605772.2	0.20335	0.318013	0.325451	0.335889	0.313348	420.6751	0.204211	2.185	691.9311
2.476194	604214.7	0.201944	0.325987	0.333898	0.343412	0.322782	419.5935	0.203686	2.182	707.4293
2.601386	603484	0.201488	0.33652	0.34336	0.355344	0.334686	419.0861	0.20344	2.184	732.0078
2.698431	602811	0.201505	0.340914	0.34962	0.36422	0.3434	418.6188	0.203213	2.186	750.293
2.777702	602657.2	0.201524	0.343797	0.353502	0.369329	0.350211	418.5119	0.203161	2.186	760.8182
2.844713	602022.6	0.201064	0.345223	0.354443	0.369979	0.353712	418.0713	0.202947	2.185	762.1557
2.902753	600195.9	0.200602	0.346146	0.354395	0.369147	0.356227	416.8027	0.202331	2.184	760.4422
2.953769	598830.7	0.200613	0.348974	0.357678	0.371108	0.360588	415.8547	0.201871	2.179	764.4829
2.999574	599023	0.200623	0.350858	0.360011	0.37073	0.364046	415.9882	0.201936	2.181	763.7044
3.175807	595735	0.20161	0.004749	0.366649	0.34856	0.376121	413.7048	0.200828	2.187	718.033
3.300821	594023.6	0.202088	0.005699	0.366979	0.317439	0.373557	412.5164	0.200251	2.187	653.9243
3.397773	590870.2	0.202568	0.005699	0.356971	0.279476	0.360062	410.3265	0.199188	2.179	575.7195
3.476988	589581.9	0.203053	0.006173	0.341485	0.244899	0.34498	409.4318	0.198753	2.182	504.4924
3.543946	441446.1	0.15446	0.004749	0.246722	0.157949	0.258661	306.5598	0.148815	1.647	325.3749
3.601954	466173.9	0.186787	0.004749	0.209074	0.011506	0.022091	323.7318	0.157151	1.749	23.70236
3.653118	487902	0.205516	0.007124	0.168238	0.010063	0.019202	338.8208	0.164476	1.839	20.72937
3.698885	507784.2	0.221046	0.006648	0.137162	0.007665	0.017758	352.6279	0.171179	1.921	15.7899
3.740285	526205	0.228659	0.007123	0.113385	0.006705	0.017274	365.4201	0.177388	1.995	13.81292
3.77808	542222.3	0.234921	0.007123	0.096414	0.005268	0.016312	376.5432	0.182788	2.055	10.85167
3.812848	554893.8	0.238543	0.006648	0.082845	0.004309	0.01679	385.3429	0.18706	2.107	8.877364
3.845037	564315.7	0.238099	0.006173	0.069763	0.003352	0.016788	391.8859	0.190236	2.145	6.90409
3.875005	516571.5	0.177573	0.003798	0.031496	0.011472	0.011495	358.7302	0.174141	2.139	23.63253
3.903037	157788.4	0.04776	0.000949	0.011632	0.008122	0.006702	109.5753	0.053192	2.168	16.73194

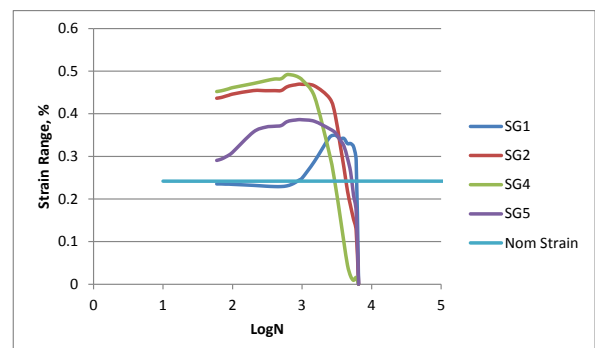
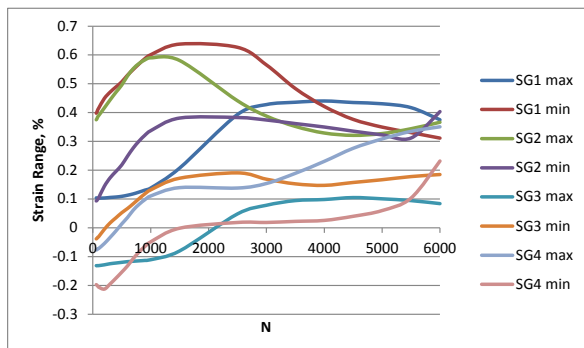
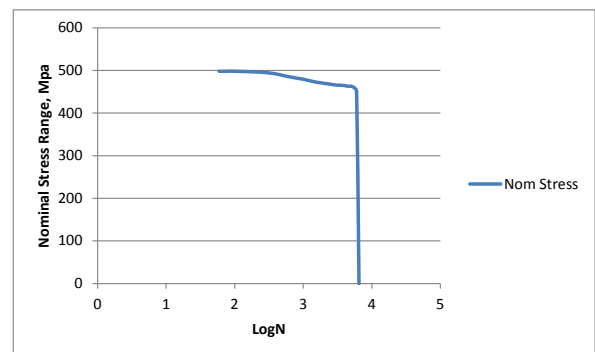
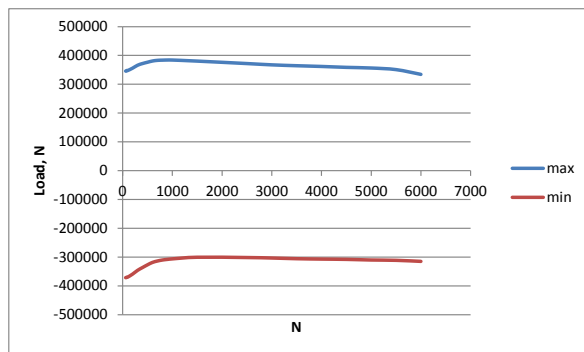


TEST A6

max							
no of Cycles	log N	Load	SG1 max	SG2 max	SG3 max	SG4 max	Nom Stress
59.175	1.77213827	345746.246	0.1039694	0.3979013	0.3750483	0.0931892	240.10156
69.175	1.83994917	345688.561	0.103492	0.4012504	0.3779221	0.0946169	240.061501
79.175	1.89858807	347265.292	0.103492	0.4065137	0.3827121	0.0974724	241.156453
89.175	1.95024312	347880.601	0.103492	0.411299	0.3865444	0.1003281	241.583751
99.175	1.99640221	347457.576	0.1030146	0.414649	0.3889398	0.103184	241.289983
199.175	2.29923483	355841.167	0.103492	0.4491189	0.4162549	0.1441362	247.111922
299.175	2.4759253	365936.089	0.1054017	0.4711537	0.4440645	0.1736806	254.122284
399.175	2.60116333	371896.899	0.106834	0.4888844	0.47045	0.1956119	258.261735
499.175	2.69825283	376396.35	0.1092213	0.5066213	0.4954089	0.21803	261.386354
599.2	2.7775718	380684.288	0.1130412	0.5296407	0.5271055	0.2485728	264.364089
699.2	2.84460142	382953.242	0.1178165	0.5497914	0.5525733	0.2772236	265.939751
799.2	2.90265548	383645.465	0.1240251	0.56899	0.5703603	0.3011118	266.420462
899.2	2.9538563	384087.719	0.1307121	0.5872354	0.5828631	0.3211866	266.727583
999.2	2.99965243	383991.576	0.1378777	0.6006837	0.5900776	0.3369654	266.660817
1499.225	3.17586682	380357.405	0.2071985	0.637685	0.5809394	0.3809809	264.137087
2499.25	3.3978097	371819.986	0.3931641	0.6266298	0.441187	0.3828954	258.208324
2999.275	3.47701629	367339.764	0.4277491	0.5656297	0.3879816	0.3742804	255.097058
3499.275	3.54397807	364320.901	0.4359185	0.4836124	0.3520639	0.3618389	253.000626
3999.3	3.60198398	361782.75	0.440244	0.4213496	0.3290901	0.349879	251.238021
4499.3	3.65314495	358629.289	0.4349574	0.3763768	0.3209561	0.3355307	249.048117
4999.325	3.69891137	356360.335	0.4306323	0.3496037	0.3271761	0.3226209	247.472455
5499.35	3.74031136	350822.549	0.417179	0.3304887	0.3439262	0.3116262	243.62677
5999.35	3.7781042	334266.879	0.3749205	0.3113811	0.3664279	0.4034819	232.129777

min							
no of Cycles	log N	Load	SG1 min	SG2 min	SG3 min	SG4 min	Nom Stress
59.675	1.77579243	-371512.33	-0.1313216	-0.0384311	-0.0769519	-0.1972153	-257.99467
69.675	1.84307698	-371243.13	-0.1317968	-0.0370082	-0.0760026	-0.1991078	-257.80773
79.675	1.90132207	-370166.34	-0.1313216	-0.0346367	-0.0736293	-0.2010003	-257.05996
89.675	1.95267139	-369551.03	-0.1313216	-0.0322651	-0.0722053	-0.2028927	-256.63266
99.675	1.99858624	-369724.09	-0.1313216	-0.0313164	-0.0722053	-0.2057311	-256.75284
199.675	2.30032369	-359110	-0.1284705	-0.0052208	-0.0546386	-0.2128265	-249.38194
299.675	2.47665051	-346150.04	-0.1246687	0.01709	-0.0332654	-0.1948496	-240.38197
399.675	2.60170698	-336305.09	-0.1222924	0.0346607	-0.0109325	-0.1749728	-233.5452
499.675	2.69868762	-326863.94	-0.1199161	0.0522377	0.0133124	-0.154141	-226.98884
599.7	2.77793405	-318538.03	-0.1175396	0.066969	0.0356661	-0.132353	-221.20697
699.7	2.84491187	-313673.24	-0.1161136	0.0836065	0.0613614	-0.1067636	-217.82864
799.7	2.9029271	-310192.9	-0.1146876	0.1012006	0.0813557	-0.0840065	-215.41173
899.7	2.95409772	-308058.54	-0.1132616	0.1178494	0.0975475	-0.0650343	-213.92954
999.7	2.99986969	-306289.53	-0.1108848	0.1316483	0.1104094	-0.0489023	-212.70106
1499.725	3.17601163	-300578.68	-0.0804517	0.1721154	0.13948	-0.001425	-208.7352
2499.75	3.39789658	-301597.79	0.0481425	0.1906936	0.1380499	0.0185289	-209.44291
2999.775	3.47708868	-303251.44	0.0781954	0.1687816	0.1537832	0.0185289	-210.59127
3499.775	3.54404012	-305674.22	0.094422	0.1525919	0.1890818	0.0223306	-212.27376
3999.8	3.60203828	-307000.98	0.0982407	0.1473552	0.2306134	0.0256572	-213.19512
4499.8	3.65319321	-308020.08	0.1049243	0.157353	0.2760034	0.039917	-213.90284
4999.825	3.6989548	-310192.9	0.1006276	0.1668766	0.3085183	0.0598874	-215.41173
5499.85	3.74035084	-311288.92	0.094422	0.177831	0.3348326	0.103184	-216.17286
5999.85	3.77814039	-314942.32	0.0839218	0.1849765	0.3506278	0.2318674	-218.70994

Range									
log N	Load	SG1	SG2	SG4	SG5	Nom Stress	Nom Strai	Disp, mm	Pseudo N
1.77213827	717258.577	0.235291	0.4363324	0.4520002	0.2904045	498.096234	0.241794	0.424	931.1204
1.83994917	716931.694	0.2352888	0.4382586	0.4539247	0.2937247	497.869232	0.241684	-0.378	935.0849
1.89858807	717431.633	0.2348136	0.4411504	0.4563414	0.2984727	498.216412	0.241853	0.426	940.0633
1.95024312	717431.633	0.2348136	0.4435641	0.4587497	0.3032208	498.216412	0.241853	-1.215	945.0244
1.99640221	717181.664	0.2343362	0.4459654	0.4611451	0.3089151	498.042822	0.241768	0.751	949.9589
2.29923483	714951.166	0.2319625	0.4543397	0.4708935	0.3569627	496.493865	0.241016	-1.263	970.0406
2.4759253	712086.132	0.2300704	0.4540637	0.4773299	0.3685302	494.504258	0.240051	1.3	983.2996
2.60116333	708201.99	0.2291264	0.4542237	0.4813825	0.3705847	491.806938	0.238741	-1.282	991.648
2.69825283	703260.286	0.2291374	0.4543836	0.4820965	0.372171	488.375199	0.237075	1.3	993.1188
2.7775718	699222.318	0.2305808	0.4626717	0.4914394	0.3809258	485.571054	0.235714	-1.282	1012.365
2.84460142	696626.481	0.2339301	0.4661849	0.4912119	0.3839872	483.76839	0.234839	1.299	1011.897
2.90265548	693838.36	0.2387127	0.4677894	0.4890046	0.3851183	481.832194	0.233899	-1.283	1007.349
2.9538563	692146.259	0.2439737	0.469386	0.4853156	0.3862209	480.657124	0.233329	1.3	999.7501
2.99965243	690281.101	0.2487625	0.4690354	0.4796682	0.3858677	479.361876	0.2327	-1.282	988.1165
3.17586682	680936.089	0.2876502	0.4655696	0.4414594	0.3824059	472.872284	0.22955	1.3	909.4064
3.3978097	673417.777	0.3450216	0.4359362	0.3031371	0.3643665	467.651234	0.227015	-1.282	624.4624
3.47701629	670591.199	0.3495537	0.3968481	0.2341984	0.3557515	465.688333	0.226062	1.297	482.4487
3.54397807	669995.117	0.3414965	0.3310205	0.1629821	0.3395083	465.274387	0.225861	-1.281	335.7431
3.60198398	668783.727	0.3420033	0.2739944	0.0984767	0.3242218	464.433144	0.225453	1.297	202.862
3.65314495	666649.372	0.3300331	0.2190238	0.0449527	0.2956137	462.950953	0.224733	-1.278	92.60256
3.69891137	666553.23	0.3300047	0.1827271	0.0186578	0.2627335	462.884188	0.224701	1.295	38.43507
3.74031136	662111.464	0.322757	0.1526577	0.0090936	0.2084422	459.799628	0.223204	-1.277	18.73282
3.7781042	649209.194	0.2909987	0.1264046	0.0158001	0.1716145	450.839718	0.218854	1.292	32.54821
3.81284821	0	0	0	0	0	0	0	-1.274	0

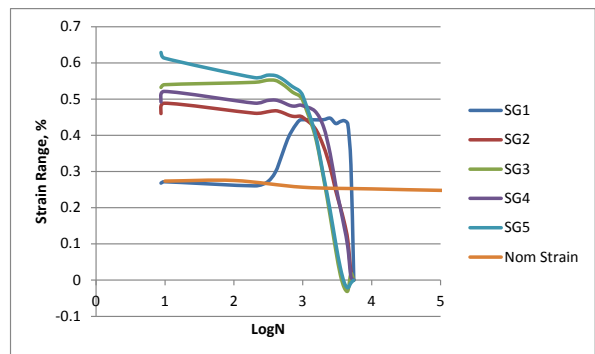
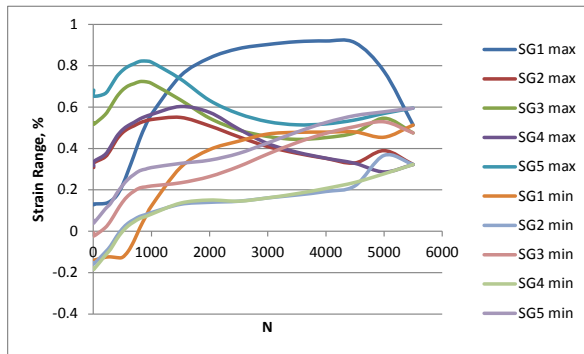
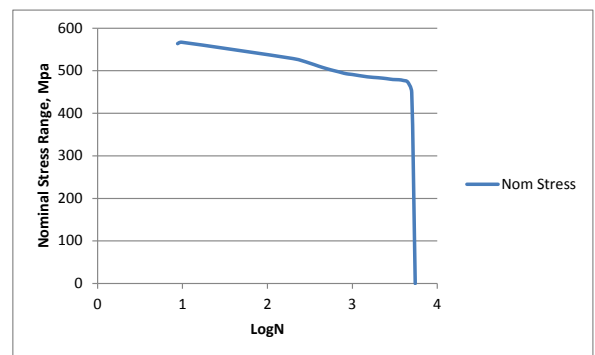
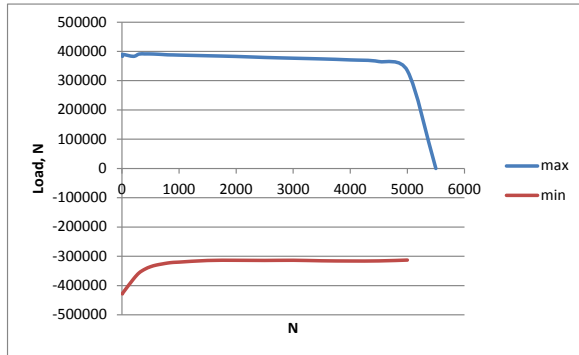


TEST A7

max								
no of Cycles	log N	Load	SG1 max	SG2 max	SG3 max	SG4 max	SG5 max	Nom Stress
8.25	0.91645395	383087.841	0.1279433	0.308244	0.5241529	0.3167567	0.6819838	266.0332229
9.25	0.96614173	389894.702	0.1317676	0.3302317	0.5169554	0.3368297	0.6531418	270.7602097
199.375	2.2996707	383145.526	0.1341579	0.3579691	0.5620772	0.3698244	0.6646766	266.0732819
299.375	2.47621553	390952.265	0.1461111	0.3943379	0.6024331	0.4095423	0.7007399	271.4946285
399.375	2.60138088	391413.747	0.1709829	0.4422317	0.6481128	0.4569579	0.7459757	271.8151021
499.375	2.6984268	391356.062	0.2202846	0.475305	0.6813167	0.4895521	0.7763161	271.7750431
599.375	2.77769862	390683.067	0.2912111	0.495927	0.7025016	0.5106538	0.7965532	271.3076854
699.375	2.8447101	389644.732	0.3660801	0.5093598	0.7130974	0.526006	0.809085	270.5866194
799.4	2.90276414	388394.885	0.4453903	0.523756	0.7232137	0.5428029	0.8211377	269.7186701
899.4	2.95395288	388010.317	0.5113371	0.5333558	0.7227319	0.5548041	0.8225842	269.451609
999.4	2.99973935	387452.692	0.5648319	0.5400768	0.7150242	0.5644071	0.8172805	269.0643694
1499.425	3.17592475	385183.739	0.7508194	0.5501599	0.634645	0.6028376	0.7358663	267.4887076
1999.425	3.30090512	382837.871	0.837526	0.5093598	0.546712	0.5744923	0.6324819	265.8596326
2499.45	3.39784445	379415.212	0.8826336	0.4566087	0.489614	0.4943472	0.5681543	263.4827861
2999.45	3.47704163	376800.147	0.9025326	0.4091801	0.4579741	0.423906	0.5297889	261.6667688
3499.475	3.5440029	374358.137	0.9161267	0.3771073	0.444078	0.3822628	0.5144509	259.9709285
3999.5	3.6020057	370973.935	0.9195258	0.3522291	0.4527027	0.3530853	0.5187643	257.6207882
4499.525	3.65316667	365416.921	0.9112712	0.3302317	0.4761886	0.328226	0.5379391	253.7617507
4999.525	3.69892874	334209.193	0.7726031	0.389551	0.5462319	0.2866621	0.5695935	232.0897174
5499.025	3.74028569	96.142	0.5132638	0.3225828	0.4752297	0.322491	0.5950274	0.066765278

min								
no of Cycles	log N	Load	SG1 min	SG2 min	SG3 min	SG4 min	SG5 min	Nom Stress
8.75	0.942008053	-428466.915	-0.1399801	-0.1517555	-0.0080723	-0.1753759	0.0531548	-297.5464688
9.75	0.989004616	-426563.302	-0.1399801	-0.1583843	-0.0227891	-0.1843651	0.0398608	-296.2245153
199.875	2.300758477	-378030.766	-0.12619	-0.1029595	0.0156735	-0.1190384	0.1054155	-262.5213653
299.875	2.476940261	-356629.533	-0.123812	-0.0702442	0.0503628	-0.0863429	0.1348956	-247.6593979
399.875	2.601924253	-344073.374	-0.1271412	-0.0256411	0.096494	-0.0403436	0.1810525	-238.9398431
499.875	2.698861417	-335497.498	-0.12619	0.0118753	0.1393342	-0.0023741	0.2201049	-232.9843736
599.875	2.778060763	-329959.712	-0.0971707	0.0389616	0.1717266	0.0256469	0.2515595	-229.1386889
699.875	2.845020481	-326306.312	-0.04718	0.0565518	0.1931743	0.0451284	0.273971	-226.6016056
799.875	2.903022123	-322960.567	0.0152596	0.0717699	0.2093854	0.0617649	0.2925754	-224.2781715
899.9	2.954194252	-320730.07	0.0696599	0.0803321	0.2141543	0.071274	0.30021	-222.7292153
999.9	2.999956568	-319826.334	0.1217296	0.0903232	0.2189237	0.0826873	0.3078457	-222.1016208
1499.9	3.176062305	-314230.863	0.3079989	0.1303077	0.2341889	0.1359837	0.3278951	-218.2158771
1999.925	3.301013709	-313577.097	0.3944251	0.1398325	0.2642557	0.1507454	0.3436537	-217.7618729
2499.95	3.397931323	-314077.036	0.4352893	0.1450719	0.3129736	0.1455069	0.3761418	-218.1090528
2999.95	3.477114016	-313538.64	0.4699297	0.1612699	0.37322	0.1612241	0.4268269	-217.7351667
3499.975	3.544064942	-315269.198	0.4781122	0.17509	0.4282699	0.1817115	0.4789998	-218.9369431
4000	3.602059991	-316019.107	0.4790749	0.1922513	0.4733122	0.206975	0.5254746	-219.4577132
4500	3.653212514	-315692.223	0.4800376	0.2194354	0.5059211	0.2360676	0.5590398	-219.2307104
5000	3.698970004	-312827.189	0.454531	0.3665804	0.5289519	0.2775895	0.5772703	-217.2411035
5499.025	3.740285694		0.5132638	0.3225828	0.4752297	0.322491	0.5950274	0.066765278

Range												
log N	Load	SG1	SG2	SG3	SG4	SG5	Nom Stress	Nom Strain	Pseudo Notch			
0.942008053	811554.756	0.2679234	0.4599995	0.5322252	0.4921326	0.628829	563.5796917	0.273582375	1295			
0.989004616	816458.004	0.2717477	0.488616	0.5397445	0.5211948	0.613281	566.984725	0.275235303	1263			
2.300758477	761176.292	0.2603479	0.4609286	0.5464037	0.4888628	0.5592611	528.5946472	0.256599343	1152			
2.476940261	747581.798	0.2699231	0.4645821	0.5520703	0.4958852	0.5658443	519.1540264	0.252016518	1166			
2.601924253	735487.121	0.2981241	0.4678728	0.5516188	0.4973015	0.5649232	510.7549451	0.247939294	1164			
2.698861417	726853.56	0.3464746	0.4634297	0.5419825	0.4919262	0.5562112	504.7594167	0.245028843	1146			
2.778060763	720642.779	0.3883818	0.4569654	0.530775	0.4850069	0.5449937	500.4463743	0.242935133	1123			
2.845020481	715951.044	0.4132601	0.452808	0.5199231	0.4808776	0.535114	497.188225	0.241353507	1102			
2.903022123	711355.452	0.4301307	0.4519861	0.5138283	0.481038	0.5285623	493.9968417	0.239804292	1089			
2.954194252	708740.387	0.4416772	0.4530237	0.5085776	0.4835301	0.5223742	492.1808243	0.23892273	1076			
2.999956568	707279.026	0.4431023	0.4497536	0.4961005	0.4817198	0.5094348	491.1659903	0.238430092	1049			
3.176062305	699414.602	0.4428205	0.4198522	0.4004561	0.4668539	0.4079712	485.7045847	0.235778925	840			
3.301013709	696414.968	0.4431009	0.3695273	0.2824563	0.4237469	0.2888282	483.6215056	0.234767721	595			
3.397931323	693492.248	0.4473443	0.3115368	0.1766404	0.3488403	0.1920125	481.5918389	0.233782446	396			
3.477114016	690338.787	0.4326029	0.2479102	0.0847541	0.2626819	0.102962	479.4019354	0.232719386	212			
3.544064942	689627.335	0.4380145	0.2020173	0.0158081	0.2005513	0.0354511	478.9078715	0.232479549	73			
3.602059991	686993.042	0.4404509	0.1599778	-0.0206095	0.1461103	-0.0067103	477.0785014	0.231591506	-14			
3.653212514	681109.144	0.4312336	0.1107963	-0.0297325	0.0921584	-0.0211007	472.9924611	0.229607991	-43			
3.698970004	647036.382	0.3180721	0.0229706	0.01728	0.0090726	-0.0076768	449.3308208	0.218121758	-16			
3.740285694	96.142	0	0	0	0	0	0	0	0			

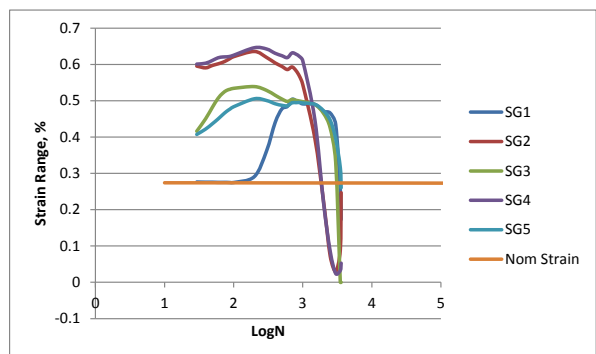
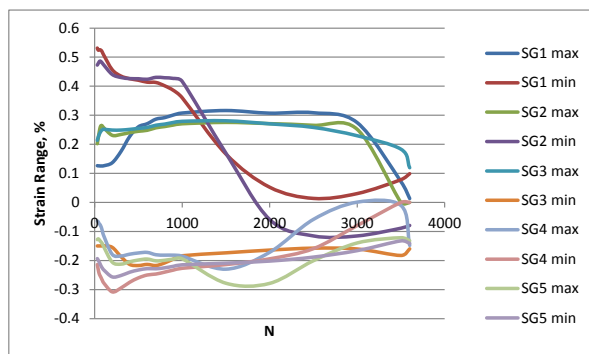
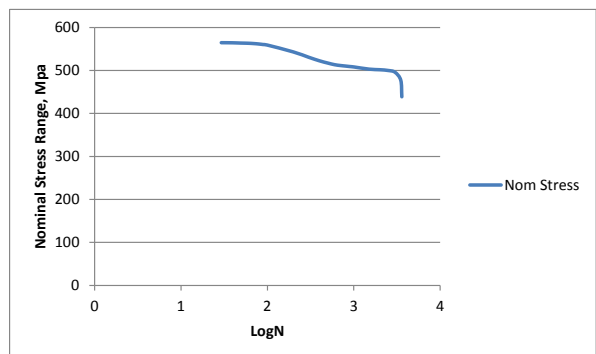
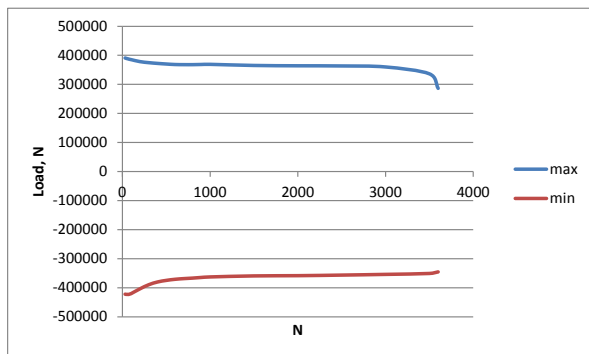


TEST A8

max								
no of Cycl	log N	Load	SG1 max	SG2 max	SG3 max	SG4 max	SG5 max	Nom Stress
29.75	1.473487	390779.2	0.126378	0.531277	0.202015	0.472708	0.213719	271.3745
39.75	1.599337	389933.2	0.1259	0.524079	0.220117	0.477986	0.223737	270.7869
49.75	1.696793	388856.4	0.1259	0.524559	0.238226	0.483264	0.232326	270.0391
59.75	1.776338	388260.3	0.125423	0.525519	0.254911	0.486623	0.239007	269.6252
69.75	1.843544	387125.8	0.125423	0.524079	0.263494	0.485183	0.244257	268.8374
79.75	1.901731	386568.2	0.125423	0.521201	0.264925	0.482304	0.248075	268.4501
89.75	1.953034	385702.9	0.125423	0.515444	0.262064	0.478465	0.250462	267.8492
99.75	1.998913	385164.5	0.1259	0.509208	0.258249	0.474627	0.251894	267.4754
199.75	2.300487	378357.6	0.136406	0.456952	0.231077	0.440576	0.24903	262.7484
299.75	2.476759	374781.2	0.175106	0.434915	0.233937	0.430029	0.24903	260.2647
399.75	2.601788	372204.6	0.226753	0.425816	0.240133	0.426195	0.251417	258.4754
499.75	2.698753	370108.7	0.260256	0.420548	0.244899	0.425716	0.254758	257.0199
599.75	2.777797	368378.1	0.27079	0.413845	0.248236	0.423798	0.2581	255.8181
699.775	2.844958	367955.1	0.286596	0.412888	0.256818	0.430509	0.26574	255.5244
799.775	2.902968	367935.8	0.291865	0.401399	0.26111	0.429071	0.26956	255.511
899.775	2.954134	368551.2	0.300969	0.385607	0.266355	0.426674	0.27529	255.9383
999.775	2.999902	368974.2	0.307677	0.360254	0.270648	0.41661	0.279111	256.2321
1499.8	3.176033	365147.7	0.316304	0.166462	0.275417	0.169471	0.281022	253.5748
1999.8	3.300987	363994	0.307198	0.052257	0.271125	-0.05889	0.270515	252.7736
2499.825	3.39791	363436.4	0.308636	0.013772	0.265402	-0.11535	0.2581	252.3864
2999.85	3.4771	359956.1	0.274622	0.030397	0.251574	-0.11535	0.229463	249.9695
3499.85	3.544049	336305.1	0.071495	0.078406	0	-0.08879	0.1832	233.5452
3599.85	3.556284	286368.9	0.013338	0.098859	0	-0.0793	0.119361	198.8673

min								
no of Cycl	log N	Load	SG1 min	SG2 min	SG3 min	SG4 min	SG5 min	Nom Stress
29.25	1.466126	-422141	-0.14981	-0.06406	-0.21396	-0.12815	-0.19341	-293.153
39.25	1.59384	-422660	-0.14981	-0.06643	-0.23001	-0.12531	-0.19815	-293.514
49.25	1.692406	-422795	-0.14981	-0.07259	-0.24371	-0.12768	-0.2043	-293.607
59.25	1.772688	-422852	-0.14981	-0.07591	-0.25126	-0.13147	-0.21044	-293.647
69.25	1.84042	-422929	-0.14981	-0.0816	-0.25692	-0.13526	-0.21707	-293.701
79.25	1.898999	-422064	-0.14981	-0.08966	-0.26353	-0.13858	-0.22274	-293.1
89.25	1.950608	-421083	-0.14933	-0.10103	-0.26966	-0.14379	-0.227	-292.419
99.25	1.996731	-420006	-0.14886	-0.11193	-0.2758	-0.15042	-0.23125	-291.671
199.25	2.299398	-403701	-0.15456	-0.17869	-0.30786	-0.20535	-0.2563	-280.348
299.25	2.476034	-389568	-0.18636	-0.18436	-0.29466	-0.21245	-0.25158	-270.533
399.25	2.601245	-380146	-0.2134	-0.17821	-0.27485	-0.20441	-0.24023	-263.99
499.25	2.698318	-374666	-0.21719	-0.17395	-0.25975	-0.19825	-0.23267	-260.185
599.25	2.777608	-370878	-0.2134	-0.17206	-0.24984	-0.19494	-0.22794	-257.554
699.275	2.844648	-368532	-0.21719	-0.18011	-0.24654	-0.20109	-0.22841	-255.925
799.275	2.902696	-366782	-0.20818	-0.18152	-0.23993	-0.1992	-0.2251	-254.71
899.275	2.953893	-364513	-0.1949	-0.18152	-0.23285	-0.19494	-0.2199	-253.134
999.275	2.999685	-362763	-0.18351	-0.18484	-0.22671	-0.19399	-0.2147	-251.919
1499.3	3.175889	-359225	-0.17355	-0.22976	-0.21396	-0.27819	-0.20903	-249.462
1999.3	3.300878	-358399	-0.16405	-0.17159	-0.19411	-0.27866	-0.20193	-248.888
2499.325	3.397823	-356418	-0.15741	-0.05837	-0.15914	-0.20062	-0.18821	-247.513
2999.35	3.477027	-353976	-0.16025	0.00095	-0.07963	-0.13952	-0.16596	-245.817
3499.35	3.543987	-350823	-0.18256	-0.01044	0	-0.12151	-0.13234	-243.627
3599.375	3.556227	-345381	-0.15978	-0.14792	0	-0.13194	-0.14087	-239.848

Range									
log N	Load	SG1	SG2	SG3	SG4	SG5	Nom Stress	Nom Strai	Pseudo N
1.466126	812920	0.276185	0.595336	0.415972	0.600857	0.407133	564.5278	0.274043	1237.766
1.59384	812593.1	0.275708	0.590509	0.450131	0.603291	0.421882	564.3008	0.273932	1242.779
1.692406	811650.9	0.275708	0.597153	0.481932	0.610939	0.436621	563.6465	0.273615	1258.534
1.772688	811112.5	0.27523	0.601432	0.506169	0.61809	0.449451	563.2726	0.273433	1273.265
1.84042	810054.9	0.27523	0.605681	0.520416	0.620442	0.461322	562.5382	0.273077	1278.111
1.898999	808632	0.27523	0.61086	0.528453	0.62088	0.470815	561.55	0.272597	1279.014
1.950608	806786.1	0.274756	0.616477	0.531726	0.622255	0.477458	560.2681	0.271975	1281.845
1.996731	805170.9	0.274758	0.621139	0.534044	0.62505	0.483145	559.1465	0.27143	1287.604
2.299398	782058.4	0.290962	0.635637	0.538942	0.64593	0.505332	543.0961	0.263639	1330.617
2.476034	764349	0.361466	0.619278	0.528599	0.642483	0.500606	530.7979	0.257669	1323.514
2.601245	752350.4	0.440153	0.604028	0.514985	0.630603	0.491649	522.4656	0.253624	1299.042
2.698318	744774.4	0.47745	0.594502	0.504653	0.62397	0.487427	517.2045	0.25107	1285.379
2.777608	739255.9	0.48419	0.585907	0.498079	0.61874	0.486041	513.3721	0.24921	1274.604
2.844648	736487	0.503789	0.592993	0.503356	0.631604	0.494154	511.4493	0.248276	1301.103
2.902696	734718	0.500048	0.582924	0.501039	0.628272	0.494664	510.2208	0.24768	1294.241
2.953893	733064.3	0.495869	0.567131	0.499203	0.621615	0.495193	509.0725	0.247123	1280.528
2.999685	731737.6	0.49119	0.545089	0.497356	0.610604	0.493812	508.1511	0.246675	1257.845
3.175889	724373.1	0.48985	0.396219	0.489374	0.447658	0.490047	503.0369	0.244193	922.1761
3.300878	722392.6	0.47125	0.223845	0.465239	0.219766	0.472445	501.6615	0.243525	452.7169
3.397823	719854.4	0.466041	0.07214	0.424537	0.085272	0.446309	499.8989	0.242669	175.6609
3.477027	713932.1	0.434875	0.029448	0.331205	0.024175	0.395427	495.7862	0.240673	49.80112
3.543987	687127.6	0.254058	0.088851	0	0.032722	0.315542	477.172	0.231637	67.40814
3.556227	631749.8	0.173117	0.246783	0	0.05264	0.260229	438.7151	0.212969	108.438

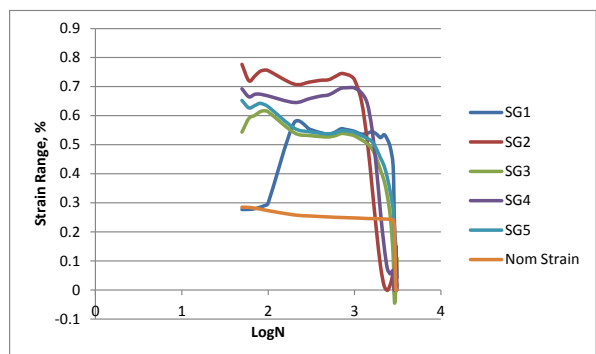
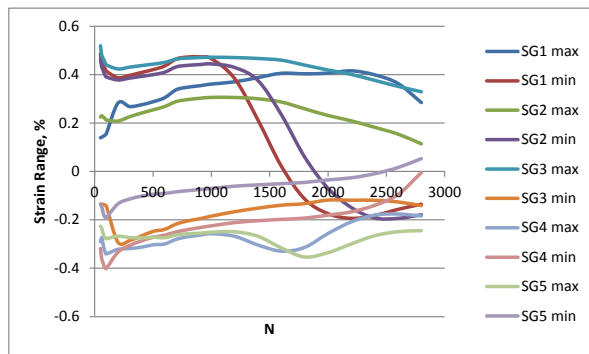
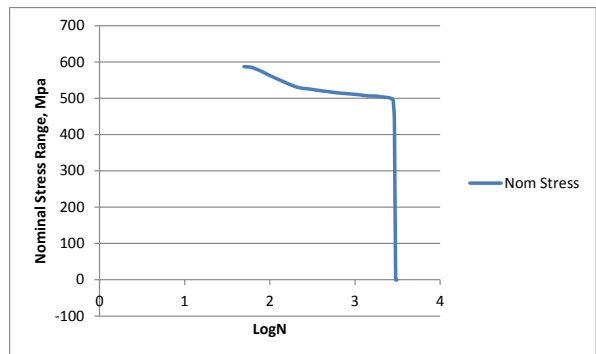
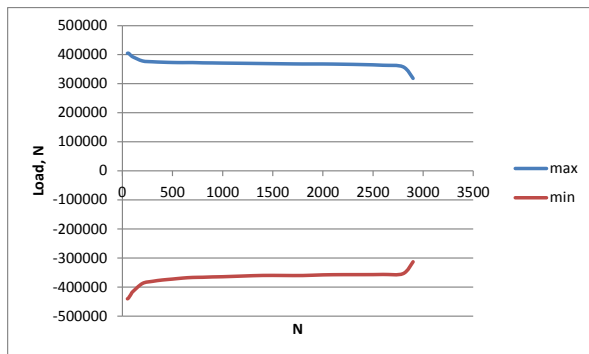


TEST A9

max								
no of Cycles	log N	Load	SG1 max	SG2 max	SG3 max	SG4 max	SG5 max	Nom Stress
49.7	1.69635639	404527.53	0.139	0.4865	0.2247	0.4658	0.519	280.921896
59.7	1.77597433	404989.01	0.1414	0.4467	0.2301	0.4325	0.4812	281.242368
69.7	1.84323278	402181.66	0.1436	0.4409	0.2263	0.4211	0.4697	279.292819
79.7	1.90145832	398720.55	0.1469	0.4322	0.2221	0.407	0.4593	276.889271
89.7	1.95279244	395836.28	0.1505	0.424	0.2178	0.3973	0.449	274.886306
99.7	1.99869516	393086.62	0.1553	0.4146	0.2124	0.3901	0.4402	272.976819
199.7	2.30037806	378338.42	0.2824	0.3868	0.2082	0.3778	0.4233	262.735014
299.7	2.47668674	375550.3	0.268	0.397	0.2261	0.3855	0.4308	260.798819
399.7	2.60173415	374069.71	0.2752	0.4085	0.2409	0.3925	0.4372	259.770632
499.7	2.69870935	373069.83	0.2877	0.4204	0.2543	0.3997	0.4433	259.076271
599.7	2.77793405	372666.04	0.3045	0.4354	0.268	0.4098	0.4502	258.795861
699.725	2.84492739	372800.64	0.3376	0.4646	0.2887	0.432	0.4641	258.889333
799.725	2.90294067	371819.99	0.3481	0.4727	0.297	0.4383	0.4681	258.208326
899.725	2.95410979	371512.33	0.3539	0.4732	0.3021	0.4414	0.4703	257.994674
999.725	2.99988055	370954.71	0.3609	0.4659	0.3058	0.4441	0.4717	257.607438
1199.725	3.07908171	370262.48	0.3702	0.3837	0.3055	0.4294	0.4704	257.126722
1399.725	3.14604272	369435.66	0.3876	0.2122	0.3001	0.3753	0.4665	256.552542
1599.75	3.20405212	368608.84	0.4054	0.0218	0.2868	0.2347	0.4595	255.978361
1799.75	3.25521218	367916.62	0.4033	-0.114	0.2587	0.0594	0.4393	255.497653
1999.75	3.30097571	367916.62	0.406	-0.1745	0.2312	-0.0697	0.4189	255.497653
2199.775	3.34237826	367070.57	0.4155	-0.1939	0.2089	-0.1493	0.4008	254.910118
2399.775	3.38017052	365801.49	0.3991	-0.182	0.1821	-0.1925	0.3761	254.028813
2599.775	3.41493576	363532.54	0.3633	-0.1568	0.1542	-0.1939	0.3514	252.453153
2799.775	3.44712313	358187.03	0.2845	-0.1353	0.1139	-0.1791	0.3289	248.740993
2899.7	3.46235307	318326.52	0.1498	-0.1251	0.0167	-0.1716	0.2849	221.060083
2999.7	3.47707782		0.0541	-0.4537	-0.1703	0.2587	0.000121	0
3099.7	3.49131966		-0.0342	-0.1694	0.2162	0.00012	17.993957	0

min								
no of Cycles	log N	Load	SG1 min	SG2 min	SG3 min	SG4 min	SG5 min	Nom Stress
49.2	1.6919651	-440561.59	-0.1381	-0.2901	-0.3186	-0.2268	-0.1334	-305.94555
59.2	1.77232171	-438100.35	-0.1359	-0.2736	-0.3603	-0.2324	-0.1456	-304.23635
69.2	1.84010609	-432812.54	-0.136	-0.2948	-0.3742	-0.2523	-0.1648	-300.56426
79.2	1.89872518	-427947.75	-0.1375	-0.3196	-0.3908	-0.2672	-0.1832	-297.18594
89.2	1.95036485	-422083.08	-0.1393	-0.3327	-0.3991	-0.2737	-0.1894	-293.11325
99.2	1.99651167	-417026	-0.143	-0.3408	-0.4011	-0.278	-0.1911	-289.60139
199.2	2.29928933	-387683.43	-0.2931	-0.3218	-0.3333	-0.2676	-0.134	-269.2246
299.2	2.47596159	-380376.63	-0.2857	-0.3186	-0.3056	-0.273	-0.1141	-264.15044
399.2	2.60119053	-375684.9	-0.2667	-0.3132	-0.2873	-0.2747	-0.1024	-260.89229
499.2	2.69827458	-372589.12	-0.2479	-0.3032	-0.2724	-0.2718	-0.0943	-258.74244
599.225	2.77758992	-369204.92	-0.2393	-0.2996	-0.2632	-0.2739	-0.091	-256.39231
699.225	2.84461695	-366974.42	-0.2173	-0.2804	-0.2498	-0.2625	-0.0841	-254.84335
799.225	2.90266906	-366397.57	-0.2041	-0.2697	-0.2404	-0.2576	-0.0794	-254.44276
899.225	2.95386837	-365166.95	-0.1956	-0.2636	-0.2322	-0.2554	-0.0751	-253.58816
999.225	2.99966329	-364513.19	-0.1848	-0.2573	-0.2247	-0.2511	-0.0706	-253.13416
1199.225	3.07890067	-362167.32	-0.1664	-0.2681	-0.2114	-0.2494	-0.0609	-251.50508
1399.25	3.14589532	-360090.65	-0.1517	-0.3041	-0.2038	-0.2681	-0.0556	-250.06295
1599.25	3.20391636	-360186.79	-0.1395	-0.3293	-0.1981	-0.3159	-0.0504	-250.12972
1799.25	3.25509151	-360340.62	-0.1331	-0.3139	-0.1928	-0.3537	-0.0455	-250.23654
1999.25	3.3008671	-358090.89	-0.1184	-0.2564	-0.1805	-0.3358	-0.0349	-248.67423
2199.275	3.34227954	-357340.98	-0.119	-0.2083	-0.1669	-0.2995	-0.0264	-248.15346
2399.275	3.38008003	-357283.3	-0.1191	-0.1806	-0.1401	-0.2655	-0.0095	-248.1134
2599.275	3.41485223	-356629.53	-0.1262	-0.1759	-0.0956	-0.249	0.016	-247.6594
2799.275	3.44704557	-353899.1	-0.1412	-0.1841	-0.0046	-0.2446	0.0529	-245.76326
2899.2	3.46227818	-313019.47	-0.0741	-0.1111	0.058	-0.1728	0.0981	-217.37463
2999.2	3.47700543		-0.0966	-0.4514	-0.1746	0.1068	-0.000125	0
3099.2	3.4912496		-0.0758	-0.1888	0.1059	-0.000123	-25.071939	0

Range										
log N	Load	SG1	SG2	SG3	SG4	SG5	Nom Stress	Nom Strai	Pseudo N	
1.69635639	845089.12	0.2771	0.7766	0.5433	0.6926	0.6524	586.867444	0.284887	1599.796	
1.77597433	843089.36	0.2773	0.7203	0.5904	0.6649	0.6268	585.478722	0.284213	1483.818	
1.84323278	834994.2	0.2796	0.7357	0.6005	0.6734	0.6345	579.857083	0.281484	1515.542	
1.90145832	826668.3	0.2844	0.7518	0.6129	0.6742	0.6425	574.075208	0.278677	1548.708	
1.95279244	817919.36	0.2898	0.7567	0.6169	0.671	0.6384	567.999556	0.275728	1558.802	
1.99869516	810112.62	0.2983	0.7554	0.6135	0.6681	0.6313	562.578208	0.273096	1556.124	
2.30037806	766021.85	0.5755	0.7086	0.5415	0.6454	0.5573	531.959618	0.258233	1459.716	
2.47668674	755926.93	0.5537	0.7156	0.5317	0.6585	0.5449	524.949257	0.25483	1474.136	
2.60173415	749754.61	0.5419	0.7217	0.5282	0.6672	0.5396	520.662924	0.252749	1486.702	
2.69870935	745658.95	0.5356	0.7236	0.5267	0.6715	0.5376	517.818715	0.251368	1490.616	
2.77793405	741870.96	0.5438	0.735	0.5312	0.6837	0.5412	515.188167	0.250091	1514.1	
2.84492739	739775.06	0.5549	0.745	0.5385	0.6945	0.5482	513.732681	0.249385	1534.7	
2.90294067	738217.56	0.5522	0.7424	0.5374	0.6959	0.5475	512.651083	0.24886	1529.344	
2.95410979	736679.28	0.5495	0.7368	0.5343	0.6968	0.5454	511.582833	0.248341	1517.808	
2.99988055	735467.9	0.5457	0.7232	0.5305	0.6952	0.5423	510.741597	0.247933	1489.792	
3.07908171	732429.8	0.5366	0.6518	0.5169	0.6788	0.5313	508.631806	0.246909	1342.708	
3.14604272	729526.31	0.5393	0.5163	0.5039	0.6434	0.5221	506.615493	0.24593	1063.578	
3.20405212	728795.63	0.5449	0.3511	0.4849	0.5506	0.5099	506.108076	0.245684	723.266	
3.25521218	728257.24	0.5364	0.1999	0.4515	0.4131	0.4848	505.734194	0.245502	411.794	
3.30097571	726007.51	0.5244	0.0819	0.4117	0.2661	0.4538	504.171882	0.244744	168.714	
3.34237826	724411.55	0.5345	0.0144	0.3758	0.1502	0.4272	503.063576	0.244206	29.664	
3.38017052	723084.79	0.5182	-0.0014	0.3222	0.073	0.3856	502.142215	0.243758	-2.884	
3.41493576	720162.07	0.4895	0.0191	0.2498	0.0551	0.3354	500.112549	0.242773	39.346	
3.44712313	712086.13	0.4257	0.0488	0.1185	0.0655	0.276	494.504257	0.240051	100.528	
3.46235307	631345.99	0.2239	-0.014	-0.0413	0.0012	0.1868	438.434715	0.212832	-28.84	
3.47707782	0	0.1507	-0.0023	0.0043	0.1519	0.000246	0	0	-4.738	

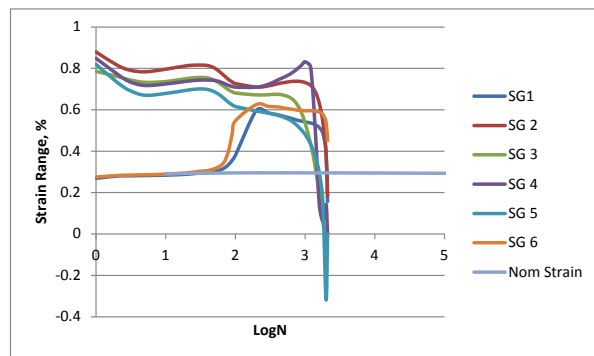
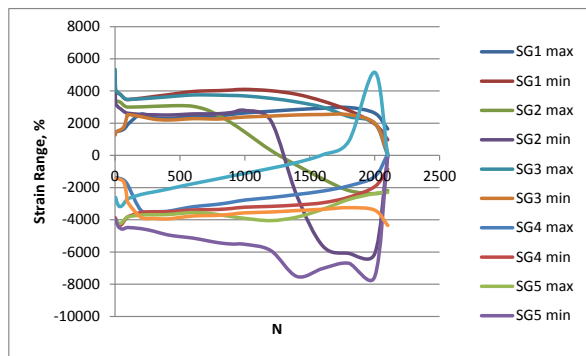
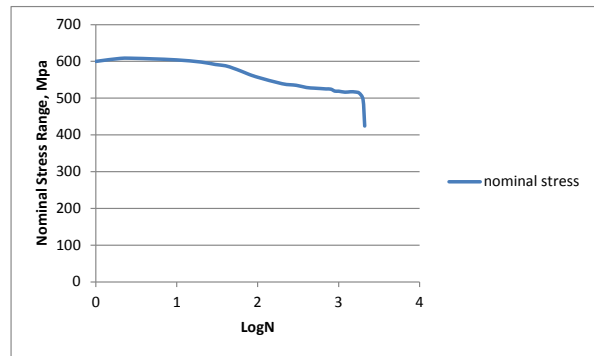
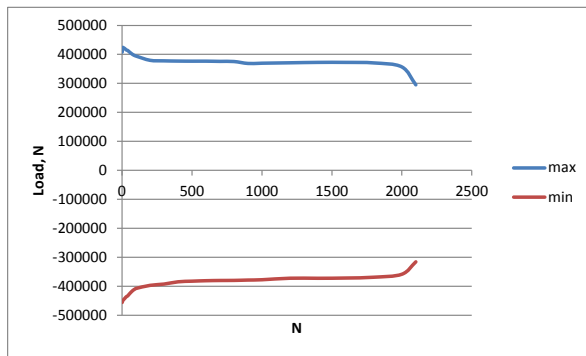


TEST A10

max									
Cycles	logN	SG1 max	SG2 max	SG3 max	SG4 max	SG5 max	SG6 max	Displacement	Load
1	0	1278	4926	3734	4499	5345	1299	1.64	407911.7
2	0.30103	1401	4252	3494	3770	4604	1394	1.64	422217.7
3	0.477121	1418	4019	3380	3417	4311	1418	1.64	423736.7
5	0.69897	1436	3912	3326	3216	4086	1439	1.64	424159.8
10	1	1455	3904	3339	3127	3998	1464	1.64	422929.1
20	1.30103	1484	3892	3367	3047	3927	1510	1.64	419775.7
30	1.477121	1514	3832	3338	2959	3853	1557	1.64	415430.1
40	1.60206	1529	3798	3310	2916	3804	1580	1.64	413488
50	1.69897	1558	3723	3244	2847	3717	1631	1.64	409296.2
60	1.778151	1592	3631	3164	2777	3633	1696	1.64	405354.4
70	1.845098	1647	3550	3093	2714	3558	1811	1.64	401624
80	1.90309	1729	3497	3043	2667	3507	2047	1.64	398412.9
90	1.954243	1829	3471	3014	2636	3484	2355	1.64	395970.9
100	2	1941	3465	3002	2618	3476	2531	1.64	394163.4
200	2.30103	2563	3552	3015	2544	3516	2408	1.63	379530.6
300	2.477121	2344	3658	3048	2524	3572	2248	1.63	377684.7
400	2.60206	2294	3757	3074	2507	3635	2197	1.64	376896.3
500	2.69897	2346	3869	3093	2535	3702	2233	1.64	376550.2
600	2.778151	2418	3970	3050	2579	3754	2284	1.64	376607.9
700	2.845098	2436	4007	2851	2580	3758	2271	1.64	375838.7
800	2.90309	2457	4024	2477	2593	3743	2258	1.64	375338.8
900	2.954243	2547	4063	2000	2668	3723	2322	1.63	368724.2
1000	3	2637	4103	1451	2794	3695	2385	1.63	369551
1200	3.079181	2743	4018	312	2155	3544	2444	1.64	370973.9
1400	3.146128	2850	3794	-616	-2499	3319	2513	1.64	372396.8
1600	3.20412	2927	3373	-1456	-5627	2990	2540	1.64	372377.6
1800	3.255273	2974	2796	-2183	-6086	2411	2527	1.63	370531.7
2000	3.30103	2626	1951	-2376	-6102	1994	1999	1.63	356744.9
2100	3.322219	1643	972	-2184	0	0	158	1.63	294925.5

min									
Cycles	logN	SG1 min	SG2 min	SG3 min	SG4 min	SG5 min	SG6 min	Displacem	Load
1	0	-1412	-3866	-4122	-3987	-2845	-1454	-1.75	-455964
2	0.30103	-1398	-3907	-4120	-3965	-2729	-1432	-1.75	-453464
3	0.477121	-1393	-3902	-4072	-3946	-2631	-1426	-1.75	-452310
5	0.69897	-1388	-3923	-4002	-3958	-2618	-1424	-1.75	-449695
10	1	-1388	-4056	-4026	-4121	-2792	-1426	-1.75	-446869
20	1.30103	-1402	-4236	-4144	-4332	-3018	-1443	-1.74	-441600
30	1.477121	-1426	-4328	-4227	-4474	-3155	-1469	-1.74	-436370
40	1.60206	-1437	-4339	-4230	-4519	-3176	-1483	-1.74	-433332
50	1.69897	-1464	-4295	-4188	-4571	-3151	-1523	-1.74	-427813
60	1.778151	-1497	-4195	-4103	-4576	-3075	-1582	-1.74	-422545
70	1.845098	-1550	-4078	-4008	-4549	-2967	-1700	-1.74	-417718
80	1.90309	-1629	-3964	-3919	-4513	-2849	-1990	-1.74	-413469
90	1.954243	-1734	-3874	-3857	-4491	-2757	-2493	-1.74	-410392
100	2	-1859	-3802	-3809	-4477	-2684	-2936	-1.74	-407662
200	2.30103	-3410	-3546	-3704	-4548	-2426	-3846	-1.74	-396990
300	2.477121	-3491	-3499	-3683	-4711	-2267	-3913	-1.74	-392567
400	2.60206	-3473	-3500	-3677	-4927	-2106	-3946	-1.74	-384761
500	2.69897	-3330	-3446	-3606	-5043	-1928	-3853	-1.74	-382588
600	2.778151	-3190	-3389	-3550	-5135	-1758	-3762	-1.74	-380973
700	2.845098	-3106	-3372	-3581	-5283	-1600	-3738	-1.74	-380184
800	2.90309	-3026	-3354	-3685	-5427	-1441	-3720	-1.74	-379896
900	2.954243	-2906	-3293	-3804	-5507	-1274	-3650	-1.74	-378704
1000	3	-2773	-3215	-3911	-5523	-1116	-3566	-1.74	-377646
1200	3.079181	-2620	-3165	-4049	-5913	-801	-3516	-1.74	-372378
1400	3.146128	-2427	-3081	-3835	-7519	-441	-3425	-1.75	-372570
1600	3.20412	-2214	-2940	-3345	-7021	44	-3346	-1.74	-371705
1800	3.255273	-1892	-2598	-2735	-6699	881	-3245	-1.74	-368916
2000	3.30103	-1309	-1937	-2365	-7528	5164	-3401	-1.74	-358668
2100	3.322219	77	-858	-2299	0	0	-4350	-1.73	-315827

Range												
Cycles	logN	SG1	SG 2	SG 3	SG 4	SG 5	SG 6	Displacement	Load	nominal stress	Nom Strain	Pseudo N
1	0	0.269	0.8792	0.7856	0.8486	0.819	0.2753	3.39	863875.3	599.9134	0.29122	1811.152
2	0.30103	0.2799	0.8159	0.7614	0.7735	0.7333	0.2826	3.39	875681.5	608.1122	0.2952	1680.754
3	0.477121	0.2811	0.7921	0.7452	0.7363	0.6942	0.2844	3.39	876046.9	608.3659	0.295323	1631.726
5	0.69897	0.2824	0.7835	0.7328	0.7174	0.6704	0.2863	3.39	873854.8	606.8436	0.294584	1614.01
10	1	0.2843	0.796	0.7365	0.7248	0.679	0.289	3.39	869797.6	604.0261	0.293217	1639.76
20	1.30103	0.2886	0.8128	0.7511	0.7379	0.6945	0.2953	3.38	861375.6	598.1775	0.290377	1674.368
30	1.477121	0.294	0.816	0.7565	0.7433	0.7008	0.3026	3.38	851799.9	591.5277	0.287149	1680.96
40	1.60206	0.2966	0.8137	0.754	0.7435	0.698	0.3063	3.38	846819.7	588.0692	0.28547	1676.222
50	1.69897	0.3022	0.8018	0.7432	0.7418	0.6868	0.3154	3.38	837109.3	581.3259	0.282197	1651.708
60	1.778151	0.3089	0.7826	0.7267	0.7353	0.6708	0.3278	3.38	827898.9	574.9298	0.279092	1612.156
70	1.845098	0.3197	0.7628	0.7101	0.7263	0.6525	0.3511	3.38	819342.3	568.9877	0.276208	1571.368
80	1.90309	0.3358	0.7461	0.6962	0.718	0.6356	0.4037	3.38	811881.6	563.8067	0.273693	1536.966
90	1.954243	0.3563	0.7345	0.6871	0.7127	0.6241	0.4848	3.38	806363.1	559.9744	0.271832	1513.07
100	2	0.38	0.7267	0.6811	0.7095	0.616	0.5467	3.38	801825.2	556.823	0.270302	1497.002
200	2.30103	0.5973	0.7098	0.6719	0.7092	0.5942	0.6254	3.37	776520.6	539.2504	0.261772	1462.188
300	2.477121	0.5835	0.7157	0.6731	0.7235	0.5839	0.6161	3.37	770252.1	534.8973	0.259659	1474.342
400	2.60206	0.5767	0.7257	0.6751	0.7434	0.5741	0.6143	3.38	761657	528.9285	0.256761	1494.942
500	2.69897	0.5676	0.7315	0.6699	0.7578	0.563	0.6086	3.38	759138.1	527.1792	0.255912	1506.89
600	2.778151	0.5608	0.7359	0.66	0.7714	0.5512	0.6046	3.38	757580.6	526.0976	0.255387	1515.954
700	2.845098	0.5542	0.7379	0.6432	0.7863	0.5358	0.6009	3.38	756023.1	525.016	0.254862	1520.074
800	2.90309	0.5483	0.7378	0.6162	0.802	0.5184	0.5978	3.38	755234.7	524.4685	0.254596	1519.868
900	2.954243	0.5453	0.7356	0.5804	0.8175	0.4997	0.5972	3.37	747428	519.0472	0.251965	1515.336
1000	3	0.541	0.7318	0.5362	0.8317	0.4811	0.5951	3.37	747197.2	518.887	0.251887	1507.508
1200	3.079181	0.5363	0.7183	0.4361	0.8068	0.4345	0.596	3.38	743351.6	516.2164	0.25059	1479.698
1400	3.146128	0.5277	0.6875	0.3219	0.502	0.376	0.5938	3.39	744966.7	517.338	0.251135	1416.25
1600	3.20412	0.5141	0.6313	0.1889	0.1394	0.2946	0.5886	3.38	744082.2	516.7238	0.250837	1300.478
1800	3.255273	0.4866	0.5394	0.0552	0.0613	0.153	0.5772	3.37	739448.2	513.5057	0.249275	1111.164
2000	3.30103	0.3935	0.3888	-0.0011	0.1426	-0.317	0.54	3.37	715412.7	496.8143	0.241172	800.928
2100	3.322219	0.1566	0.183	0.0115	0	0	0.4508	3.36	610752.4	424.1336	0.20589	376.98

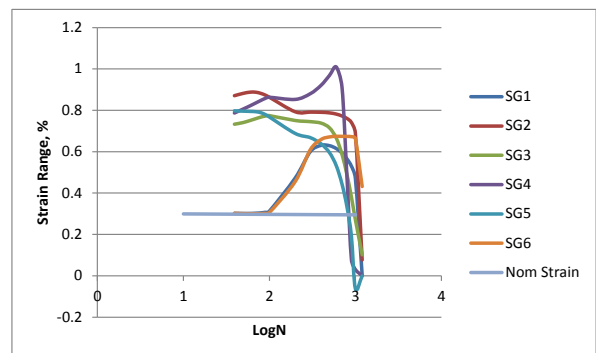
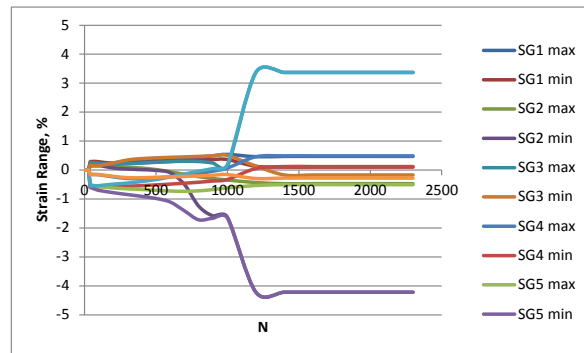
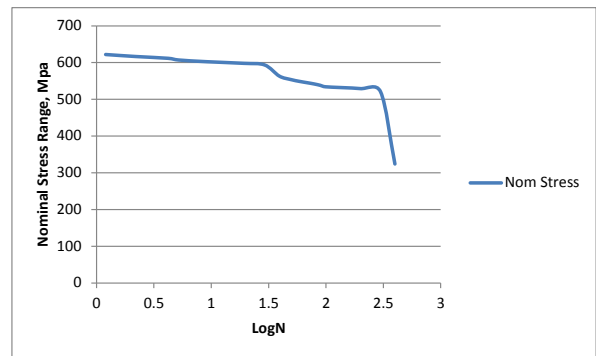
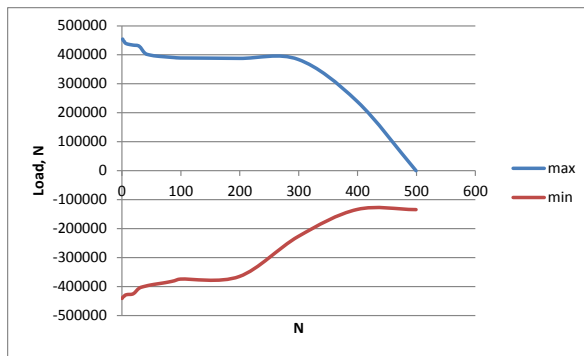


TEST A11

max												
Cycles	logN	SG1 max	SG2 max	SG3 max	SG4 max	SG5 max	SG6 max	Displaceme	Load	Nom Stress	Nom Strain	
0.2	-0.69897	0	0	-0.0002	0	0	0	0	0	0	0	0
1.2	0.07918125	0	0	-0.0002	0	0	0	0	0	0	0	0
2.2	0.34242268	0	0	-0.0002	0	0	0	0	0	0	0	0
4.2	0.62324929	0	0	-0.0003	0.0001	-0.0001	0	0	0	0	0	0
5.2	0.71600334	0	0	-0.0003	0.0001	-0.0001	0	0	6	0.00416667	2.0227E-06	
9.2	0.96378783	0	0	-0.0004	0.0001	-0.0001	0	0	6	0.00416667	2.0227E-06	
19.2	1.28330123	0.0049	0.0037	-0.0043	-0.003	0.003	-0.0048	-0.12	-32	-0.0222222	-1.079E-05	
29.2	1.46538285	0.0048	0.0037	-0.0046	-0.003	0.003	-0.0047	-0.14	-63	-0.04375	-2.124E-05	
39.2	1.59328607	0.1523	0.2834	0.2272	0.1983	0.2567	0.1466	3.43	454444	315.586111	0.15319714	
49.2	1.6919651	0.1502	0.2913	0.2253	0.191	0.254	0.146	3.42	449562	312.195833	0.15155138	
59.2	1.77232171	0.1489	0.2966	0.2243	0.1861	0.2511	0.1461	3.42	445322	309.251389	0.15012203	
69.2	1.84010609	0.1486	0.2988	0.223	0.1819	0.2489	0.146	3.42	441365	306.503472	0.14878809	
79.2	1.89872518	0.1483	0.2964	0.2197	0.1761	0.244	0.1466	3.42	437264	303.655556	0.14740561	
89.2	1.95036485	0.1489	0.2923	0.2148	0.1696	0.2376	0.1477	3.42	433453	301.009028	0.14612089	
99.2	1.99651167	0.1502	0.2869	0.2081	0.1613	0.2308	0.1492	3.42	429755	298.440972	0.14487426	
199.2	2.29928933	0.2382	0.2333	0.133	0.0724	0.2002	0.2404	3.42	405260	281.430556	0.13661677	
299.2	2.47596159	0.3103	0.2351	0.0979	0.0349	0.2179	0.3475	3.41	398645	276.836806	0.1343868	
399.2	2.60119053	0.3377	0.2522	0.0675	0.0133	0.2417	0.3943	3.41	395564	274.697222	0.13334817	
499.2	2.69827458	0.3582	0.274	0.0169	-0.0116	0.2673	0.421	3.41	393756	273.441667	0.13273867	
599.2	2.7775718	0.3789	0.2961	-0.0581	-0.0934	0.2906	0.4396	3.41	392087	272.282639	0.13217604	
699.2	2.84460142	0.4042	0.3173	-0.1477	-0.4968	0.3036	0.4539	3.41	390455	271.149306	0.13162588	
799.2	2.90265548	0.4427	0.3402	-0.23	-1.2477	0.2931	0.4718	3.4	389120	270.222222	0.13117584	
899.2	2.9538563	0.4922	0.3625	-0.2939	-1.5852	0.2421	0.4938	3.4	387727	269.254861	0.13070624	
999.2	2.99965243	0.5402	0.363	-0.3442	-1.6203	0.1212	0.5078	3.4	384136	266.761111	0.12949569	
1199.2	3.07889162	0.4609	0.1286	-0.4315	-4.2182	3.3701	0.1386	3.4	239343	166.210417	0.08068467	
1399.2	3.1458798	0.4711	0.102	-0.4713	-4.2182	3.3701	-0.1708	3.39	-139	-0.0965278	-4.686E-05	
1599.2	3.20390278	0.4712	0.1025	-0.4696	-4.2182	3.3701	-0.1703	3.39	-132	-0.0916667	-4.45E-05	
1799.175	3.25507341	0.4713	0.1028	-0.469	-4.2182	3.3701	-0.17	3.24	-132	-0.0916667	-4.45E-05	
1999.175	3.30085081	0.4713	0.1031	-0.4692	-4.2182	3.3701	-0.1698	3.23	-132	-0.0916667	-4.45E-05	
2199.175	3.34225979	0.4714	0.1031	-0.4705	-4.2182	3.3701	-0.1698	3.21	-126	-0.0875	-4.248E-05	
2299.2	3.36157675	0.4713	0.1031	-0.4706	-4.2182	3.3701	-0.1697	3.36	-120	-0.0833333	-4.045E-05	

min												
Cycles	logN	SG1 min	SG2 min	SG3 min	SG4 min	SG5 min	SG6 min	Displacem	Load	Nom Stres	Nom Strain	
0.7	-0.154902	0	0	-0.0002	0	0	0	0	0	0	0	0
1.7	0.23044892	0	0	-0.0002	0	-0.0001	0	0	0	0	0	0
2.7	0.43136376	0	0	-0.0002	0	-0.0001	0	0	0	0	0	0
4.7	0.67209786	0	0	-0.0003	0.0001	-0.0001	0	0	6	0.004167	2.02265E-06	
5.7	0.75587486	0	0	-0.0003	0.0001	-0.0001	0	0	0	0	0	0
9.7	0.98677173	0	0	-0.0004	0.0001	-0.0001	0	0	0	0	0	0
19.7	1.29446623	0.0049	0.0037	-0.0043	-0.003	0.003	-0.0048	-0.12	-63	-0.04375	-2.1238E-05	
29.7	1.47275645	0.0048	0.0037	-0.0046	-0.003	0.003	-0.0048	-0.14	-63	-0.04375	-2.1238E-05	
39.7	1.59879051	-0.1496	-0.5873	-0.5056	-0.5886	-0.5407	-0.1556	-3.73	-441214	-306.399	-0.14873719	
49.7	1.69635639	-0.1512	-0.5903	-0.5153	-0.6146	-0.542	-0.1547	-3.72	-438247	-304.338	-0.14773699	
59.7	1.77597433	-0.1525	-0.591	-0.5261	-0.6351	-0.5437	-0.1544	-3.72	-435475	-302.413	-0.14680252	
69.7	1.84323278	-0.154	-0.5888	-0.5364	-0.6533	-0.5445	-0.1541	-3.72	-432772	-300.536	-0.14589132	
79.7	1.90145832	-0.1558	-0.5856	-0.5473	-0.6713	-0.5447	-0.1541	-3.72	-430158	-298.721	-0.14501011	
89.7	1.95279244	-0.1581	-0.5816	-0.5573	-0.6878	-0.5424	-0.1544	-3.72	-427638	-296.971	-0.1441606	
99.7	1.99869516	-0.1608	-0.5771	-0.5664	-0.7019	-0.5378	-0.1551	-3.72	-424985	-295.128	-0.14326625	
199.7	2.30037806	-0.234	-0.5597	-0.6178	-0.7803	-0.4881	-0.2147	-3.72	-405859	-281.847	-0.1368187	
299.7	2.47668674	-0.2902	-0.5562	-0.6473	-0.8455	-0.4499	-0.2624	-3.72	-399048	-277.117	-0.13452265	
399.7	2.60173415	-0.2929	-0.5383	-0.6705	-0.9078	-0.3961	-0.2646	-3.71	-394506	-273.963	-0.1329915	
499.7	2.69870935	-0.2709	-0.5137	-0.6984	-0.98	-0.3284	-0.2503	-3.71	-391085	-271.587	-0.13183826	
599.7	2.77793405	-0.2363	-0.4857	-0.7238	-1.1031	-0.2419	-0.2346	-3.71	-388011	-269.452	-0.13080198	
699.7	2.84491187	-0.1888	-0.4552	-0.7345	-1.4073	-0.1392	-0.2202	-3.71	-384432	-266.967	-0.12959547	
799.7	2.9029271	-0.1221	-0.4203	-0.7175	-1.7186	-0.0387	-0.202	-3.71	-380022	-263.904	-0.12810882	
899.7	2.95409772	-0.0376	-0.3785	-0.6741	-1.6632	0.0516	-0.1787	-3.71	-374308	-259.936	-0.12618258	
999.7	2.99986969	0.0686	-0.3269	-0.6158	-1.6508	0.1832	-0.1559	-3.7	-365469	-253.798	-0.12320287	
1199.725	3.07908171	0.4588	0.0522	-0.5331	-4.2182	3.3701	-0.2931	-3.74	-227172	-157.758	-0.07658172	
1399.725	3.14604272	0.4889	0.1192	-0.506	-4.2182	3.3701	-0.2768	-3.74	-133932	-93.0083	-0.04514968	
1599.725	3.20404533	0.4882	0.1187	-0.5039	-4.2182	3.3701	-0.2753	-3.74	-134429	-93.3535	-0.04531722	
1799.725	3.25520615	0.4882	0.1187	-0.5037	-4.2182	3.3701	-0.276	-3.74	-136288	-94.6444	-0.04594391	
1999.725	3.30097028	0.4884	0.119	-0.5048	-4.2182	3.3701	-0.2777	-3.73	-139003	-96.5299	-0.04685916	
2199.725	3.34236839	0.4888	0.1194	-0.5068	-4.2182	3.3701	-0.2788	-3.73	-140326	-97.4486	-0.04730515	
2299.725	3.36167591	0.4891	0.1198	-0.5071	-4.2182	3.3701	-0.2792	-3.73	-140585	-97.6285	-0.04739246	

Range										
log N	Load	SG1	SG2	SG3	SG4	SG5	SG6	Nom Stres	Nom Strai	Pseudo N
-0.69897	0	0	0	0	0	0	0	0	0	0
0.079181	0	0	0	0	0	0.0001	0	0	0	0
0.342423	0	0	0	0	0	0.0001	0	0	0	0
0.623249	-6	0	0	0	0	0	0	-0.00417	-2E-06	0
0.716003	6	0	0	0	0	0	0	0.004167	2.02E-06	0
0.963788	6	0	0	0	0	0	0	0.004167	2.02E-06	0
1.283301	31	0	0	0	0	0	0	0.021528	1.05E-05	0
1.465383	0	0	0	0	0	0	0.0001	0	0	0
1.593286	895658	0.3019	0.8707	0.7328	0.7869	0.7974	0.3022	621.9847	0.301934	1793.642
1.691965	887809	0.3014	0.8816	0.7406	0.8056	0.796	0.3007	616.534	0.299288	1816.096
1.772322	880797	0.3014	0.8876	0.7504	0.8212	0.7948	0.3005	611.6646	0.296925	1828.456
1.840106	874137	0.3026	0.8876	0.7594	0.8352	0.7934	0.3001	607.0396	0.294679	1828.456
1.898725	867422	0.3041	0.882	0.767	0.8474	0.7887	0.3007	602.3764	0.292416	1816.92
1.950365	861091	0.307	0.8739	0.7721	0.8574	0.78	0.3021	597.9799	0.290281	1800.234
1.996512	854740	0.311	0.864	0.7745	0.8632	0.7686	0.3043	593.5694	0.288141	1779.84
2.299289	811119	0.4722	0.793	0.7508	0.8527	0.6883	0.4551	563.2771	0.273435	1633.58
2.475962	797693	0.6005	0.7913	0.7452	0.8804	0.6678	0.6099	553.9535	0.268909	1630.078
2.601191	790070	0.6306	0.7905	0.738	0.9211	0.6378	0.6589	548.6597	0.26634	1628.43
2.698275	784841	0.6291	0.7877	0.7153	0.9684	0.5957	0.6713	545.0285	0.264577	1622.662
2.777572	780098	0.6152	0.7818	0.6657	1.0097	0.5325	0.6742	541.7347	0.262978	1610.508
2.844601	774887	0.593	0.7725	0.5868	0.9105	0.4428	0.6741	538.116	0.261221	1591.35
2.902655	769142	0.5648	0.7605	0.4875	0.4709	0.3318	0.6738	534.1264	0.259285	1566.63
2.953856	762035	0.5298	0.741	0.3802	0.078	0.1905	0.6725	529.191	0.256889	1526.46
2.999652	749605	0.4716	0.6899	0.2716	0.0305	-0.062	0.6637	520.559	0.252699	1421.194
3.078892	466515	0.0021	0.0764	0.1016	0	0	0.4317	323.9688	0.157266	157.384
3.14588	133793	-0.0178	-0.0172	0.0347	0	0	0.106	92.91181	0.045103	-35.432
3.203903	134297	-0.017	-0.0162	0.0343	0	0	0.105	93.26181	0.045273	-33.372
3.255073	136156	-0.0169	-0.0159	0.0347	0	0	0.106	94.55278	0.045899	-32.754
3.300851	138871	-0.0171	-0.0159	0.0356	0	0	0.1079	96.43819	0.046815	-32.754
3.34226	140200	-0.0174	-0.0163	0.0363	0	0	0.109	97.36111	0.047263	-33.578
3.361577	140465	-0.0178	-0.0167	0.0365	0	0	0.1095	97.54514	0.047352	-34.402

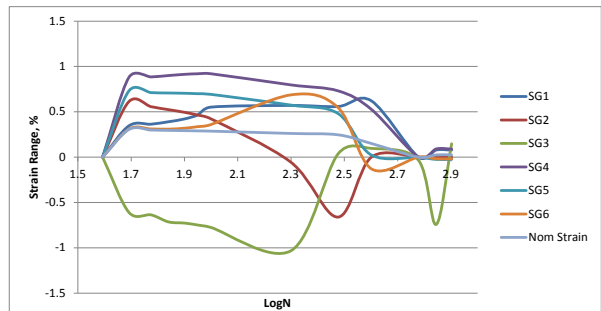
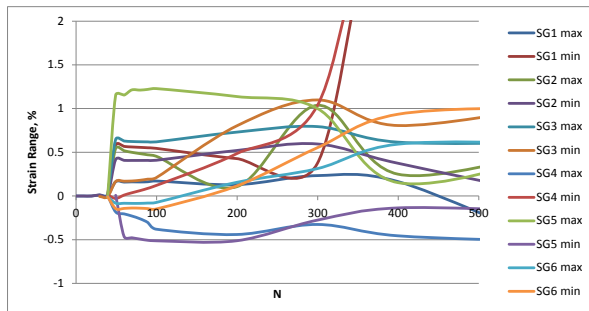
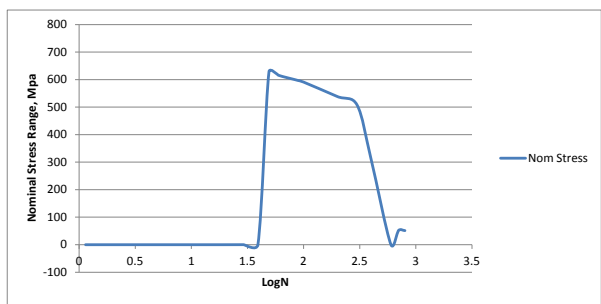
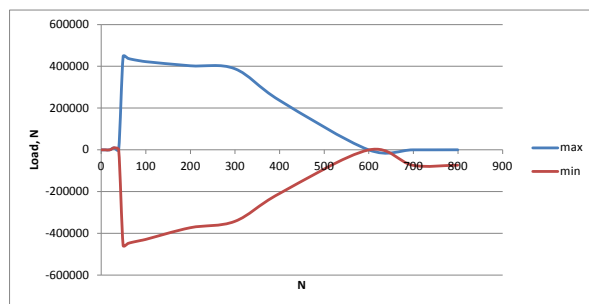


TEST A12

max										
Cycles	LogN	Load	SG1 max	SG2 max	SG3 max	SG4 max	SG5 max	SG6 max	Nom Stress	Nom Strain
0.14	-0.85387	-6	0	0	0	0	0	0	-0.00417	-2E-06
1.14	0.056905	0	0	0	0	0	0	0	0	0
2.14	0.330414	0	0	0	0	0	0	0	0	0
4.14	0.617	0	0	0	0	0	0	0	0	0
9.14	0.960946	0	0	0	0	0	0	0	0	0
19.14	1.281942	0	0	0	0	0	0	0	0	0
29.14	1.46449	9784	0.0114	0.0167	-0.0075	0.0126	-0.0041	-0.0051	6.794444	0.003298
39.14	1.592621	13	0.0082	0.0121	-0.0118	0.008	-0.0084	-0.0081	0.009028	4.38E-06
49.14	1.691435	447495	0.163	0.5849	0.546	0.4174	0.6481	0.1656	310.7604	0.150855
59.54	1.774809	438341	0.1593	0.5672	0.5177	0.4076	0.6289	0.1695	304.4035	0.147769
69.14	1.839729	433213	0.1619	0.561	0.4998	0.4069	0.6233	0.1716	300.8424	0.14604
79.54	1.900586	429011	0.1606	0.5563	0.4844	0.407	0.6205	0.1802	297.9243	0.144623
89.14	1.950073	425660	0.163	0.5516	0.4709	0.4074	0.6192	0.1931	295.5972	0.143494
99.54	1.997998	422384	0.1717	0.5451	0.4546	0.4088	0.6192	0.2099	293.3222	0.142389
199.54	2.30003	402595	0.13	0.4277	0.1063	0.5207	0.7307	0.8026	279.5799	0.135718
299.54	2.476455	388420	0.2335	0.3724	1.0373	0.5952	0.7939	1.0987	269.7361	0.13094
399.54	2.60156	237107	0.1655	3.8725	0.2499	0.3749	0.6161	0.8061	164.6576	0.079931
599.28	2.77763	359	-0.5287	3.8725	0.4636	0.0123	0.6084	1.0178	0.249306	0.000121
699.04	2.844502	6	-0.5282	3.8725	0.1522	0.0119	0.6089	1.0185	0.004167	2.02E-06
799.28	2.902699	284	-0.5275	3.8725	1.3115	0.0116	0.6098	1.0185	0.197222	9.57E-05

min										
Cycles	LogN	Load	SG1 min	SG2 min	SG3 min	SG4 min	SG5 min	SG6 min	Nom Stress	Nom Strain
0.54	-0.26761	0	0	0	0	0	0	0	0	0
1.54	0.187521	6	0	0	0	0	0	0	0.004167	2.02E-06
2.54	0.404834	0	0	0	0	0	0	0	0	0
4.54	0.657056	0	0	0	0	0	0	0	0	0
9.54	0.979548	0	0	0	0	0	0	0	0	0
19.54	1.290925	0	0	0	0	0	0	0	0	0
29.54	1.47041	9608	0.0113	0.0165	-0.0075	0.0125	-0.0042	-0.0051	6.672222	0.003239
39.54	1.597037	0	0.0082	0.0121	-0.0118	0.008	-0.0084	-0.0081	0	0
49.54	1.694956	-458010	-0.1822	-0.0277	1.1548	-0.4623	-0.0825	-0.1446	-318.063	-0.1544
59.94	1.777717	-448472	-0.2044	0.0106	1.1541	-0.4773	-0.0829	-0.1418	-311.439	-0.15118
69.54	1.842235	-442777	-0.2285	0.0367	1.2135	-0.493	-0.0844	-0.1374	-307.484	-0.14926
79.94	1.902764	-437995	-0.2611	0.0619	1.2114	-0.5065	-0.0841	-0.1393	-304.163	-0.14765
89.54	1.952017	-433692	-0.3035	0.0879	1.2196	-0.5124	-0.0806	-0.1437	-301.175	-0.1462
99.94	1.999739	-428942	-0.3797	0.1207	1.2286	-0.5117	-0.0737	-0.1483	-297.876	-0.1446
199.94	2.3009	-372859	-0.4403	0.4849	1.1377	-0.276	0.1566	0.1153	-258.93	-0.12569
299.94	2.477034	-342474	-0.3254	1.0332	1.0014	-0.136	0.3132	0.5523	-237.829	-0.11545
399.96	2.602017	-209330	-0.4552	3.8725	0.1532	-0.1518	0.5929	0.9351	-145.368	-0.07057
599.82	2.778021	-542	-0.5297	3.8725	0.4956	0.0093	0.6107	1.0181	-0.37639	-0.00018
699.16	2.844577	-74012	-0.607	3.8725	0.8943	-0.0786	0.6337	1.0368	-51.3972	-0.02495
799.96	2.903068	-73546	-0.6059	3.8725	1.1639	-0.078	0.6338	1.0367	-51.0736	-0.02479

Range												
LogN	Load	SG1	SG2	SG3	SG4	SG5	SG6	Nom Stress	Nom Strain	Pseudo N		
-0.85387	-6	0	0	0	0	0	0	0	-0.00417	-2.02265E-06	0	
0.056905	-6	0	0	0	0	0	0	0	-0.00417	-2.02265E-06	0	
0.330414	0	0	0	0	0	0	0	0	0	0	0	
0.617	0	0	0	0	0	0	0	0	0	0	0	
0.960946	0	0	0	0	0	0	0	0	0	0	0	
1.281942	0	0	0	0	0	0	0	0	0	0	0	
1.46449	176	1E-04	0.0002	0	1E-04	0.0001	0	0.122222	5.93312E-05	0.206		
1.592621	13	0	0	0	0	0	0	0.009028	4.38242E-06	0		
1.691435	905505	0.3452	0.6126	-0.6088	0.8797	0.7306	0.3102	628.8229	0.305253843	1812.182		
1.774809	886813	0.3637	0.5566	-0.6364	0.8849	0.7118	0.3113	615.8424	0.298952602	1822.894		
1.839729	875990	0.3904	0.5243	-0.7137	0.8999	0.7077	0.309	608.3264	0.295304072	1853.794		
1.900586	867006	0.4217	0.4944	-0.727	0.9135	0.7046	0.3195	602.0875	0.292275485	1881.81		
1.950073	859352	0.4665	0.4637	-0.7487	0.9198	0.6998	0.3368	596.7722	0.289695254	1894.788		
1.997998	851326	0.5514	0.4244	-0.774	0.9205	0.6929	0.3582	591.1986	0.286989617	1896.23		
2.30003	775454	0.5703	-0.0572	-1.0314	0.7967	0.5741	0.6873	538.5097	0.261412487	1641.202		
2.476455	730894	0.5589	-0.6608	0.0359	0.7312	0.4807	0.5464	507.5653	0.246390912	1506.272		
2.60156	446437	0.6207	0	0.0967	0.5267	0.0232	-0.129	310.0257	0.15049791	1085.002		
2.77763	901	0.001	0	-0.032	0.003	-0.0023	-0.0003	0.625694	0.000303735	6.18		
2.844502	74018	0.0788	0	-0.7421	0.0905	-0.0248	-0.0183	51.40139	0.024952131	186.43		
2.902699	73830	0.0784	0	0.1476	0.0896	-0.024	-0.0182	51.27083	0.024888754	184.576		

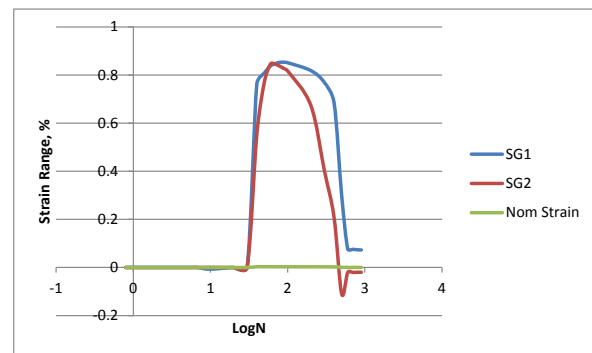
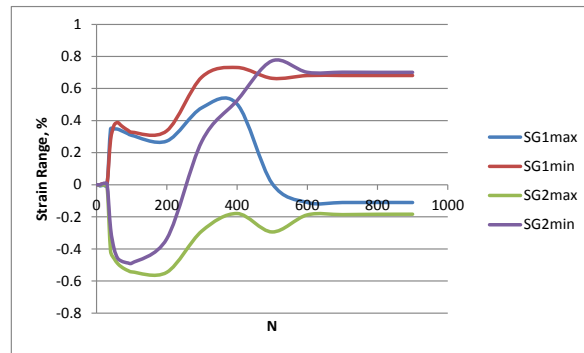
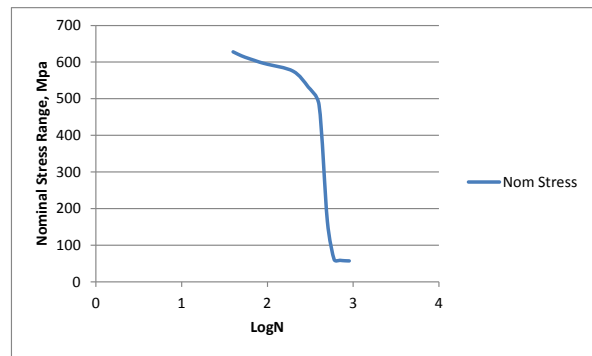
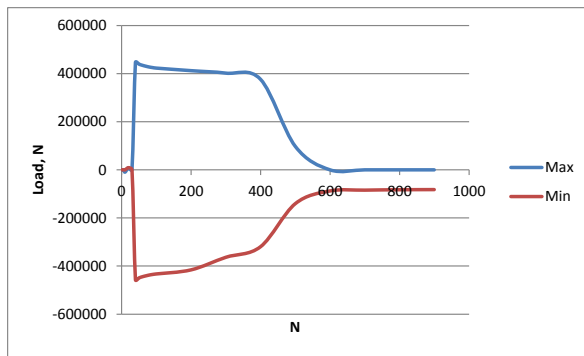


TEST A13

Max						
Cycles	LogN	Load	SG1max	SG2max	Nom Stres	Nom Strain
0.8	-0.09691	-6	0	0	-0.00417	-2E-08
1.8	0.255273	-6	0	0	-0.00417	-2E-08
2.8	0.447158	19	0	0	0.013194	6.41E-08
4.8	0.681241	-6	0	0	-0.00417	-2E-08
5.8	0.763428	0	0	0	0	0
6.8	0.832509	0	0	0	0	0
9.8	0.991226	-9696	-0.007	0.0006	-6.73333	-3.3E-05
19.8	1.296665	8669	-0.0023	0.008	6.020139	2.92E-05
29.8	1.474216	107	-0.0052	0.0053	0.074306	3.61E-07
39.8	1.599883	446790	0.348	0.2795	310.2708	0.001506
49.8	1.697229	439305	0.348	0.3713	305.0729	0.001481
59.8	1.776701	434391	0.347	0.3881	301.6604	0.001464
69.8	1.843855	430529	0.3377	0.3697	298.9785	0.001451
79.8	1.902003	427184	0.328	0.3529	296.6556	0.00144
89.8	1.953276	424740	0.3177	0.339	294.9583	0.001432
99.8	1.999131	422762	0.308	0.3277	293.5847	0.001425
199.8	2.300595	412121	0.2724	0.3362	286.1951	0.001389
299.8	2.476832	401883	0.4803	0.6718	279.0854	0.001355
399.8	2.601843	376160	0.5038	0.7311	261.2222	0.001268
499.775	2.698775	97656	0.0082	0.6637	67.81667	0.000329
599.8	2.778006	-95	-0.1106	0.681	-0.06597	-3.2E-07
699.8	2.844974	-88	-0.1106	0.6812	-0.06111	-3E-07
799.8	2.902981	-82	-0.1104	0.6811	-0.05694	-2.8E-07
899.8	2.954146	-88	-0.1106	0.6812	-0.06111	-3E-07

Min						
Cycles	LogN	Load	SG1min	SG2min	Nom Stres	Nom Strain
0.3	-0.52288	0	0	0	0	0
1.3	0.113943	0	0	0	0	0
2.3	0.361728	0	0	0	0	0
4.3	0.633468	-6	0	0	-0.00417	-2E-08
5.3	0.724276	-6	0	0	-0.00417	-2E-08
6.3	0.799341	-6	0	0	-0.00417	-2E-08
9.3	0.968483	6	0	0.0001	0.004167	2.02E-08
19.3	1.285557	8833	-0.0022	0.008	6.134028	2.98E-05
29.3	1.466868	158	-0.0052	0.0053	0.109722	5.33E-07
39.3	1.594393	-457475	-0.4144	-0.2719	-317.691	-0.00154
49.3	1.692847	-449392	-0.4599	-0.3984	-312.078	-0.00151
59.3	1.773055	-444371	-0.4907	-0.4573	-308.591	-0.0015
69.3	1.840733	-440654	-0.5104	-0.4747	-306.01	-0.00149
79.3	1.899273	-437308	-0.5247	-0.4829	-303.686	-0.00147
89.3	1.950851	-434738	-0.5354	-0.4877	-301.901	-0.00147
99.3	1.996949	-432791	-0.5431	-0.4893	-300.549	-0.00146
199.275	2.299453	-415869	-0.546	-0.3371	-288.798	-0.0014
299.275	2.47607	-363661	-0.2882	0.2713	-252.542	-0.00123
399.3	2.601299	-319637	-0.1793	0.5248	-221.97	-0.00108
499.3	2.698362	-140824	-0.2942	0.7726	-97.7944	-0.00047
599.3	2.777644	-87803	-0.1879	0.7012	-60.9743	-0.0003
699.3	2.844664	-84483	-0.1862	0.7018	-58.6688	-0.00028
799.325	2.902723	-82788	-0.184	0.7009	-57.4917	-0.00028
899.325	2.953917	-82215	-0.1835	0.701	-57.0938	-0.00028

Range					
LogN	Load	SG1	SG2	Nom Stres	Nom Strain
-0.09691	-6	0	0	-0.00417	-2.02265E-08
0.255273	-6	0	0	-0.00417	-2.02265E-08
0.447158	19	0	0	0.013194	6.40507E-08
0.681241	0	0	0	0	0
0.763428	6	0	0	0.004167	2.02265E-08
0.832509	6	0	0	0.004167	2.02265E-08
0.991226	-9702	-0.007	0.0005	-6.7375	-3.27063E-05
1.296665	-164	-1E-04	0	-0.11389	-5.52859E-07
1.474216	-51	0	0	-0.03542	-1.71926E-07
1.599883	904265	0.7624	0.5514	627.9618	0.003048358
1.697229	888697	0.8079	0.7697	617.1507	0.002995877
1.776701	878762	0.8377	0.8454	610.2514	0.002962385
1.843855	871183	0.8481	0.8444	604.9882	0.002936836
1.902003	864492	0.8527	0.8358	600.3417	0.00291428
1.953276	859478	0.8531	0.8267	596.8597	0.002897377
1.999131	855553	0.8511	0.817	594.134	0.002884146
2.300595	827990	0.8184	0.6733	574.9931	0.002791228
2.476832	765544	0.7685	0.4005	531.6278	0.002580717
2.601843	695797	0.6831	0.2063	483.1924	0.002345594
2.698775	238480	0.3024	-0.1089	165.6111	0.000803937
2.778006	87708	0.0773	-0.0202	60.90833	0.000295672
2.844974	84395	0.0756	-0.0206	58.60764	0.000284503
2.902981	82706	0.0736	-0.0198	57.43472	0.000278809
2.954146	82127	0.0729	-0.0198	57.03264	0.000276857

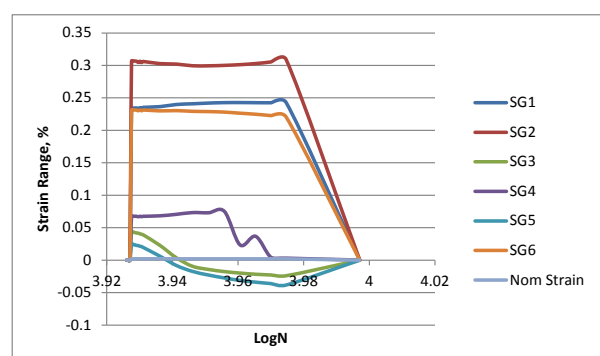
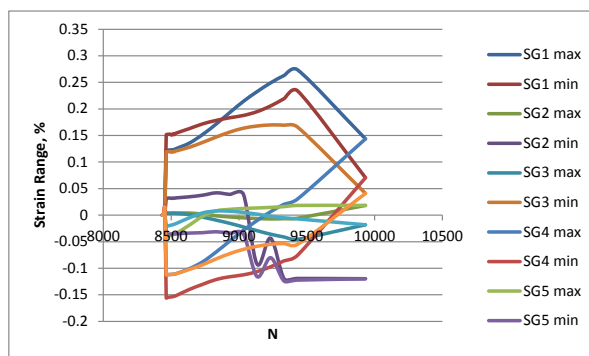
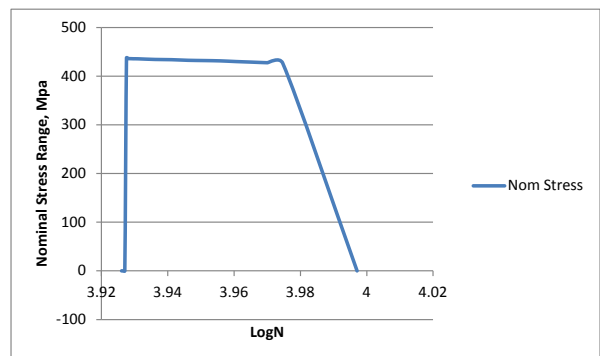
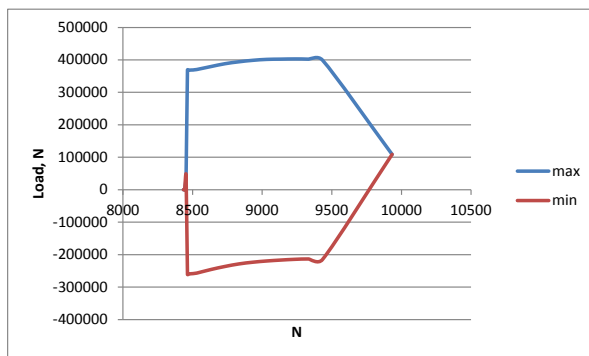


TEST A14

Adjusted Cycles	max Cycles	LogN	Load	SG1 max	SG2 max	SG3 max	SG4 max	SG5 max	SG6 max	Nom Stres	Nom Strain
8434.5	0.5	3.926059	0	0	0	0	0	0	0	0	0
8435.5	1.5	3.926111	0	0	0	0	0	0	0	0	0
8436.5	2.5	3.926162	0	0	0	0	0	0	0	0	0
8438.5	4.5	3.926265	0	0	0	0	0	0	0	0	0
8439.5	5.5	3.926317	0	0	0	0	0	0	0	0	0
8440.5	6.5	3.926368	0	0	0	0	0	0	0	0	0
8443.5	9.5	3.926523	0	0	0	0	0	0	0	0	0
8453.5	19.5	3.927037	44478	0.0141	0.0165	0.0003	0.0038	0.0003	0.0144	30.8875	0.00015
8463.4	29.4	3.927545	369079	0.1213	0.1509	0.0033	0.0314	0.0039	0.1187	256.3049	0.001244
8473.02	39.02	3.928038	368468	0.1222	0.1521	0.0033	0.032	0.0037	0.1194	255.8806	0.001242
8483.42	49.42	3.928571	368588	0.1225	0.1522	0.0034	0.0321	0.0037	0.1194	255.9639	0.001243
8493.02	59.02	3.929062	368871	0.1228	0.1524	0.0035	0.0321	0.0036	0.1195	256.1604	0.001243
8503.4	69.4	3.929593	368947	0.1218	0.1507	0.0037	0.0315	0.0038	0.1184	256.2132	0.001244
8513.02	79.02	3.930084	369514	0.1236	0.153	0.0037	0.0322	0.0036	0.1199	256.6069	0.001246
8523.4	89.4	3.930613	370031	0.123	0.1517	0.0038	0.0317	0.0038	0.1191	256.966	0.001247
8533.02	99.02	3.931103	370629	0.1249	0.1541	0.0039	0.0324	0.0034	0.1207	257.3813	0.001249
8633.02	199.02	3.936163	379625	0.1355	0.1628	0.0039	0.0345	0.0011	0.1277	263.6285	0.00128
8733.02	299.02	3.941164	388250	0.152	0.1719	0.0018	0.0376	-0.0038	0.1371	269.6181	0.001309
8833.02	399.02	3.946109	394216	0.1718	0.1784	-0.0013	0.042	-0.0095	0.1471	273.7611	0.001329
8933.02	499.02	3.950998	398733	0.1934	0.1834	-0.0034	0.0391	-0.0155	0.1565	276.8979	0.001344
9033.02	599.02	3.955833	401606	0.2143	0.1877	-0.0051	0.0391	-0.0223	0.1637	278.8931	0.001354
9133.02	699.02	3.960614	402368	0.2325	0.1948	-0.0064	-0.0923	-0.0293	0.1678	279.4222	0.001356
9233.02	799.02	3.965344	402954	0.249	0.2056	-0.0071	-0.0434	-0.0359	0.1698	279.8292	0.001358
9333.02	899.02	3.970022	402255	0.263	0.2194	-0.0067	-0.1199	-0.0412	0.1693	279.3438	0.001356
9433.02	999.02	3.974651	399294	0.2734	0.2338	-0.0057	-0.1192	-0.0454	0.1656	277.2875	0.001346
9933.02	1499.02	3.997081	108814	0.1436	0.0704	0.0183	-0.1197	-0.0182	0.0409	75.56528	0.000367

Adjusted Cycles	min Cycles	LogN	Load	SG1 min	SG2 min	SG3 min	SG4 min	SG5 min	SG6 min	Nom Stres	Nom Strain
8435	1	3.926085	0	0	0	0	0	0	0	0	0
8436	2	3.926137	-6	0	0	0	0	0	0	-0.00417	-2E-08
8437	3	3.926188	0	0	0	0	0	0	0	0	0
8439	5	3.926291	0	0	0	0	0	0	0	0	0
8440	6	3.926342	0	0	0	0	0	0	0	0	0
8441	7	3.926394	0	0	0	0	0	0	0	0	0
8444	10	3.926548	-6	0.0002	0.0005	0	0.0002	-0.0002	-0.0002	-0.00417	-2E-08
8454	20	3.927062	44491	0.0141	0.0165	0.0003	0.0038	0.0003	0.0145	30.89653	0.00015
8463.8	29.8	3.927565	-260927	-0.1125	-0.1558	-0.041	-0.0362	-0.0214	-0.1124	-181.199	-0.00088
8473.4	39.4	3.928058	-259736	-0.1121	-0.1549	-0.0399	-0.0358	-0.0204	-0.1121	-180.372	-0.00088
8483.8	49.8	3.92859	-259119	-0.1119	-0.1545	-0.0392	-0.0355	-0.0198	-0.1119	-179.944	-0.00087
8493.4	59.4	3.929082	-258703	-0.1117	-0.1541	-0.0384	-0.0355	-0.0192	-0.1118	-179.655	-0.00087
8503.8	69.8	3.929613	-258413	-0.1116	-0.1539	-0.0379	-0.0354	-0.0186	-0.1117	-179.453	-0.00087
8513.4	79.4	3.930103	-257859	-0.1113	-0.1534	-0.037	-0.0354	-0.0179	-0.1114	-179.069	-0.00087
8523.8	89.8	3.930633	-257235	-0.1109	-0.1527	-0.036	-0.0353	-0.0171	-0.111	-178.635	-0.00087
8533.4	99.4	3.931122	-256555	-0.1105	-0.152	-0.0351	-0.0352	-0.0162	-0.1106	-178.163	-0.00086
8633.4	199.4	3.936182	-245706	-0.101	-0.14	-0.019	-0.0338	-0.0051	-0.1023	-170.629	-0.00083
8733.42	299.42	3.941184	-236389	-0.0878	-0.1302	-0.002	-0.033	0.0043	-0.0933	-164.159	-0.0008
8833.42	399.42	3.946129	-228589	-0.0691	-0.1211	0.0081	-0.0313	0.0078	-0.0822	-158.742	-0.00077
8933.42	499.42	3.951018	-223316	-0.0486	-0.116	0.0109	-0.0339	0.0074	-0.0724	-155.081	-0.00075
9033.42	599.42	3.955852	-219530	-0.0284	-0.1124	0.0125	-0.036	0.0051	-0.0644	-152.451	-0.00074
9133.42	699.42	3.960633	-216726	-0.0103	-0.1064	0.0135	-0.1157	0.0019	-0.0586	-150.504	-0.00073
9233.42	799.42	3.965363	-214458	0.0064	-0.0973	0.0146	-0.0802	-0.002	-0.055	-148.929	-0.00072
9333.42	899.42	3.970041	-213368	0.0205	-0.086	0.0161	-0.1243	-0.0051	-0.0534	-148.172	-0.00072
9433.42	999.42	3.974669	-215051	0.0306	-0.0753	0.0183	-0.1223	-0.0071	-0.0549	-149.341	-0.00072
9933.42	1499.42	3.997099	108908	0.1436	0.0704	0.0183	-0.1199	-0.0182	0.0409	75.63056	0.000367

Range												
LogN	Load	SG1	SG2	SG3	SG4	SG5	SG6	Nom Stres	Nom Strain	Pseudo Not		
3.926059	0	0	0	0	0	0	0	0	0	0		
3.926111	6	0	0	0	0	0	0	0.004167	2.02E-08	0		
3.926162	0	0	0	0	0	0	0	0	0	0		
3.926265	0	0	0	0	0	0	0	0	0	0		
3.926317	0	0	0	0	0	0	0	0	0	0		
3.926368	0	0	0	0	0	0	0	0	0	0		
3.926523	6	-0.0002	-0.0005	0	-0.0002	0.0002	0.0002	0.004167	2.02E-08	-1.03		
3.927037	-13	0	0	0	0	0	-1E-04	-0.00903	-4.4E-08	0		
3.927545	630006	0.2338	0.3067	0.0443	0.0676	0.0253	0.2311	437.5042	0.002124	631.802		
3.928038	628204	0.2343	0.307	0.0432	0.0678	0.0241	0.2315	436.2528	0.002118	632.42		
3.928571	627707	0.2344	0.3067	0.0426	0.0676	0.0235	0.2313	435.9076	0.002116	631.802		
3.929062	627574	0.2345	0.3065	0.0419	0.0676	0.0228	0.2313	435.8153	0.002116	631.39		
3.929593	627360	0.2334	0.3046	0.0416	0.0669	0.0224	0.2301	435.6667	0.002115	627.476		
3.930084	627373	0.2349	0.3064	0.0407	0.0676	0.0215	0.2313	435.6757	0.002115	631.184		
3.930613	627266	0.2339	0.3044	0.0398	0.067	0.0209	0.2301	435.6014	0.002115	627.064		
3.931103	627184	0.2354	0.3061	0.039	0.0676	0.0196	0.2313	435.5444	0.002114	630.566		
3.936163	625331	0.2365	0.3028	0.0229	0.0683	0.0062	0.23	434.2576	0.002108	623.768		
3.941164	624639	0.2398	0.3021	0.0038	0.0706	-0.0081	0.2304	433.7771	0.002106	622.326		
3.946109	622805	0.2409	0.2995	-0.0094	0.0733	-0.0173	0.2293	432.5035	0.0021	616.97		
3.950998	622049	0.242	0.2994	-0.0143	0.073	-0.0229	0.2289	431.9785	0.002097	616.764		
3.955833	621136	0.2427	0.3001	-0.0176	0.0751	-0.0274	0.2281	431.3444	0.002094	618.206		
3.960614	619094	0.2428	0.3012	-0.0199	0.0234	-0.0312	0.2264	429.9264	0.002087	620.472		
3.965344	617412	0.2426	0.3029	-0.0217	0.0368	-0.0339	0.2248	428.7583	0.002081	623.974		
3.970022	615623	0.2425	0.3054	-0.0228	0.0044	-0.0361	0.2227	427.516	0.002075	629.124		
3.974651	614345	0.2428	0.3091	-0.024	0.0031	-0.0383	0.2205	426.6285	0.002071	636.746		
3.997081	-94	0	0	0	0.0002	0	0	-0.06528	-3.2E-07	0		

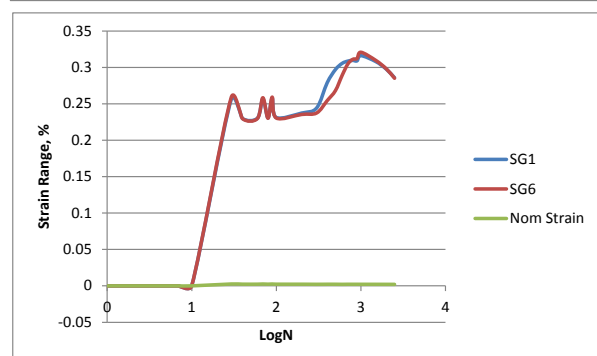
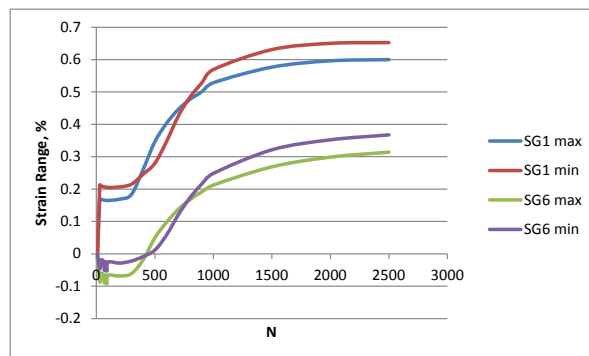
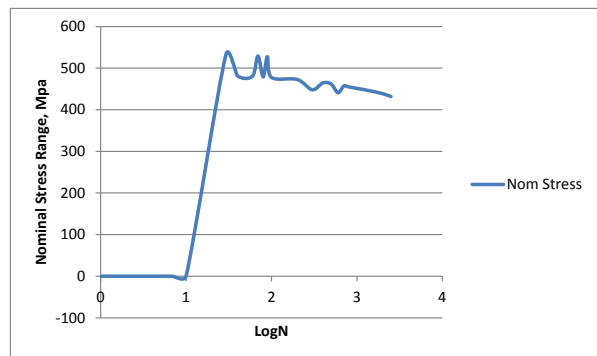
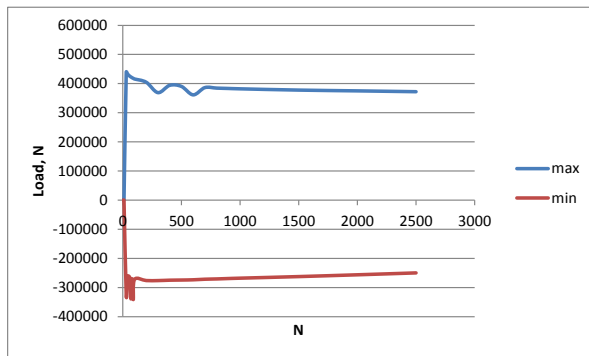


TEST A15

max						
Cycles	LogN	Load	SG1 max	SG6 max	Nom Stres	Nom Strain
1	0	19	0	0	0.013194	6.40507E-08
2	0.30103	19	0	0	0.013194	6.40507E-08
3	0.477121	13	0	0	0.009028	4.38242E-08
5	0.69897	13	0	0	0.009028	4.38242E-08
6	0.778151	19	0	0	0.013194	6.40507E-08
7	0.845098	19	0	0	0.013194	6.40507E-08
9.98	0.999131	13	0	0	0.009028	4.38242E-08
29.28	1.466571	439942	0.1705	0.2127	305.5153	0.001483084
39.68	1.598572	433175	0.1684	0.2103	300.816	0.001460272
59.68	1.775829	425263	0.1664	0.2076	295.3215	0.0014336
69.28	1.840608	422780	0.1659	0.2068	293.5972	0.001425229
79.68	1.901349	420002	0.1654	0.206	291.6681	0.001415864
89.28	1.950754	418093	0.1651	0.2056	290.3424	0.001409429
99.68	1.998608	415844	0.1647	0.2049	288.7806	0.001401847
199.68	2.300335	404662	0.1689	0.2068	281.0153	0.001364152
299.74	2.476745	369004	0.1832	0.2152	256.2528	0.001243946
399.68	2.601712	394078	0.2605	0.246	273.6653	0.001328472
499.68	2.698692	390304	0.3462	0.2794	271.0444	0.00131575
599.74	2.777963	361393	0.403	0.3471	250.9674	0.001218288
699.68	2.844899	386266	0.446	0.425	268.2403	0.001302137
799.68	2.902916	384527	0.4771	0.4841	267.0326	0.001296275
899.68	2.954088	383311	0.5002	0.5274	266.1882	0.001292176
999.7	2.99987	382076	0.5285	0.5693	265.3306	0.001288012
1499.7	3.176004	377691	0.5768	0.631	262.2854	0.00127323
1999.7	3.300965	375045	0.5963	0.6503	260.4479	0.00126431
2499.7	3.397888	372179	0.6	0.6526	258.4576	0.001254649

min						
Cycles	LogN	Load	SG1 min	SG6 min	Nom Stres	Nom Strain
0.5	-0.30103	13	0	0	0.009028	4.38E-08
1.5	0.176091	19	0	0	0.013194	6.41E-08
2.5	0.39794	19	0	0	0.013194	6.41E-08
4.5	0.653213	19	0	0	0.013194	6.41E-08
5.5	0.740363	13	0	0	0.009028	4.38E-08
6.5	0.812913	13	0	0	0.009028	4.38E-08
10	1	13	0	0	0.009028	4.38E-08
29.68	1.472464	-327638	-0.0855	-0.046	-227.526	-0.0011
40	1.60206	-261104	-0.0616	-0.0194	-181.322	-0.00088
60	1.778151	-266622	-0.0638	-0.0221	-185.154	-0.0009
69.68	1.843108	-339148	-0.0907	-0.0516	-235.519	-0.00114
80	1.90309	-269873	-0.0653	-0.0241	-187.412	-0.00091
89.68	1.952696	-341460	-0.0924	-0.0536	-237.125	-0.00115
100	2	-272122	-0.0665	-0.0256	-188.974	-0.00092
200	2.30103	-276085	-0.0684	-0.0286	-191.726	-0.00093
300	2.477121	-276173	-0.0611	-0.0222	-191.787	-0.00093
400	2.60206	-274838	-0.0185	-0.0084	-190.86	-0.00093
500	2.69897	-274315	0.0492	0.0113	-190.497	-0.00092
600	2.778151	-273483	0.0975	0.0581	-189.919	-0.00092
700	2.845098	-271505	0.1374	0.1204	-188.545	-0.00092
800	2.90309	-270528	0.1675	0.1731	-187.867	-0.00091
900	2.954243	-269123	0.1912	0.2152	-186.891	-0.00091
1000	3	-267901	0.2124	0.2485	-186.042	-0.0009
1500	3.176091	-262452	0.2688	0.3214	-182.258	-0.00088
2000	3.30103	-256309	0.2988	0.3523	-177.992	-0.00086
2500	3.39794	-249795	0.3142	0.3675	-173.469	-0.00084

Range					
LogN	Load	SG1	SG6	Nom Stress	Nom Strain
0	6	0	0	0.004167	2.02265E-08
0.30103	0	0	0	0	0
0.477121	-6	0	0	-0.00417	-2.02265E-08
0.69897	-6	0	0	-0.00417	-2.02265E-08
0.778151	6	0	0	0.004167	2.02265E-08
0.845098	6	0	0	0.004167	2.02265E-08
0.999131	0	0	0	0	0
1.466571	767580	0.256	0.2587	533.0417	0.002587581
1.598572	694279	0.23	0.2297	482.1382	0.002340477
1.775829	691885	0.2302	0.2297	480.4757	0.002332406
1.840608	761928	0.2566	0.2584	529.1167	0.002568528
1.901349	689875	0.2307	0.2301	479.0799	0.00232563
1.950754	759553	0.2575	0.2592	527.4674	0.002560521
1.998608	687966	0.2312	0.2305	477.7542	0.002319195
2.300335	680747	0.2373	0.2354	472.741	0.002294859
2.476745	645177	0.2443	0.2374	448.0396	0.002174949
2.601712	668916	0.279	0.2544	464.525	0.002254976
2.698692	664619	0.297	0.2681	461.541	0.00224049
2.777963	634876	0.3055	0.289	440.8861	0.002140224
2.844899	657771	0.3086	0.3046	456.7854	0.002217405
2.902916	655055	0.3096	0.311	454.8993	0.002208249
2.954088	652434	0.309	0.3122	453.0792	0.002199413
2.99987	649977	0.3161	0.3208	451.3729	0.002191131
3.176004	640143	0.308	0.3096	444.5438	0.002157979
3.300965	631354	0.2975	0.298	438.4403	0.002128351
3.397888	621974	0.2858	0.2851	431.9264	0.00209673



Appendix 5

Position Paper

Representative Operational Loading Conditions for Low Cycle Fatigue Assessment of FPSO

Ahmed Megharbi, Dr. Helena Polezhayeva, Dr. Mohammed Sarumi and Dr Manoj Kumar
Lloyd's Register Energy
Aberdeen, London UK

ABSTRACT

For Floating Production Storage and Offloading (FPSO) units fatigue cyclic loadings are mainly due to loading/offloading of cargo and wave induced loads. Combinations of hull draughts and tank filling patterns (loading conditions) are the main contributors to low cycle fatigue damage. In this paper, representative loading conditions used by different classification societies in their rules for assessing low cycle fatigue damage are compared. Loading manuals for FPSOs approved by Lloyd's Register are reviewed. A record of two years draught during loading and offloading is analyzed for two FPSOs operating in the North Sea. The representative loading conditions and percentage of operational service life in each loading condition are proposed for low cycle fatigue assessments.

KEY WORDS: Low cycle fatigue, FPSO, loading, offloading, representative loading conditions, hull draughts, tank fillings.

INTRODUCTION

Fatigue damage is caused by repeated loads due to wave loads and loading /offloading of cargo. Damage caused by wave loads is normally termed as high cycle fatigue (HCF) damage, where stress levels remain significantly lower than yield stress of the material used in construction. Damage caused by continuous loading and periodic offloading of cargo is referred as low cycle fatigue (LCF) damage where the stress levels lead to plastic deformation in the material. Unlike tankers, FPSOs are designed to operate at a fixed location for longer time with limited scope of surveys, repairs and dry docking. However, industry experience shows fatigue damage and subsequent costly repairs for many FPSOs and lost production (Kaminski 2007). Hence, a reliable fatigue design is crucial for economic operation of FPSOs. An important step toward this is understanding and quantification of uncertainties in the fatigue design process. Among them, one such uncertainty is representative loading condition. In FPSOs, quasi-static loading due to frequent loading and offloading of cargo and ballast is the single most significant load case contributing to low cycle fatigue damage. The loading time of a FPSO is generally between 10 to 14 days, while offloading is carried out within 20 to 24 hours. The sequence and timing of loading and offloading cargo

depends entirely on the operator of the FPSO (Raji, Incecik et al. 2009). By default, Bureau Veritas (BV) considers this cycle once per week (BV-Part-D-Ch1-Sec7 (2013)). Det Norske Veritas (DNV) specify different numbers of cycles for low cycle fatigue assessment for different vessel types (DNV-CN-30.7 2010). The number of loading and offloading cycles could be 1000 in 20 years, which is significantly more than those of tankers (Kaminski 2007). During this process, loading conditions change continuously. Each of these loading conditions contributes to low cycle fatigue damage. Hence, a set of representative loading conditions must be identified and their contribution to total damage must be quantified. Classification societies specify a minimum number of required loading conditions for fatigue design assessment in their Rules.

Lloyd's Register has various recommendations for the representative loading conditions for Ship-shaped FPSO hulls. Two to seven loading conditions may be required. These are selected on a case by case basis. For example, in a life extension study (LR-Report 2009) only two loading conditions were considered: the ballast and full load conditions. In (LR-Report 2003) three loading conditions are considered, namely: ballast condition (light load), 50% load and full load condition with a specified amount of time at each condition. For a conversion from tanker to FPSO (LR-Report 2008), four loading conditions were considered as given in Table 1 for spectral fatigue analysis. For this FPSO, length between perpendiculars, moulded breadth and depth are 232.0 m, 41.6 m and 23.5 m respectively.

Table 1: Loading conditions for conversion FPSO service (LR-Report 2008)

Loading Condition	Mean Draught (m)	% of Operation
Draught 1	9.746	10
Draught 2	10.247	40
Draught 3	11.649	40
Draught 4	14.434	10

Three onsite representative loading conditions were used for spectral fatigue assessment of Agbami FPSO in moderate sea environment in the west offshore Nigeria off the Central Niger Delta (Hwang, Kwon et al. 2007). These were ballast, intermediate and full loading conditions with each contributing 33% to the fatigue damage at onsite. One additional transit loading condition and seagoing loading conditions

were also used in this assessment as per the American Bureau of Shipping (ABS) Spectral Fatigue Analysis (SFA) guidance (ABS-SFA 2002). It was found that the seagoing condition is more dominant for fatigue damage in this case. However, low cycle fatigue was not considered explicitly.

In this paper, representative loading conditions selected for assessing LCF by classification societies will be reviewed. This will be complemented by a review of FPSO loading manuals for typical tank loading patterns and hull draughts. Comparison will be made with data recorded for two FPSOs operating in the North Sea. The data will be used to extract draughts observed at Afterward (Aft) and Forward (Fwd) positions over a period of two years during loading and offloading cycles.

The objective of this paper is to identify the most onerous loading condition(s) for LCF assessment and therefore identify representative loading conditions in terms of percent of scantling draught and percent of operation in the selected loading conditions. These data are inputs in spectral fatigue analysis using Lloyd's Register Fatigue Design procedure implemented in ShipRight software for Fatigue Design Assessment (FDA) Levels 2 and 3 (FDA2 and FDA3).

CASE STUDY

Draught data collected from two FPSOs operating in the North Sea have been used in this case study to quantify the most frequent draughts during loading and offloading of cargo. The FPSO's general particulars are given in Table 2.

Table 2: General particulars of FPSOs.

Item	FPSO I	FPSO II
Overall Length (<i>m</i>)	217.2	257.6
Beam (<i>m</i>)	38.0	41.0
Depth (<i>m</i>)	23.0	23.6
Scantling draught (<i>m</i>)	17.0	16.5

FPSO I: In (Client-Report-G3 2002) loading and offloading data in the form of draughts at Fwd and Aft ends during loading and after offloading were reviewed for a period of 28 months. During this period, there were 27 loading and offloading cycles, i.e. nearly one loading/offloading cycle every month. The number of occurrence of draughts at Aft and Fwd ends during are presented against percentage of scantling draught in Table 3 and Table 4 as well as Figures 1-4.

Table 3: Observed draughts for FPSO I before discharge

Range of Draughts (m)	Number of Occurrence	
	Fwd	Aft
10.00 – 10.99	0	0
11.00 – 11.99	3	0
12.00 – 12.99	10	1
13.00 – 13.99	3	5
14.00 – 14.99	6	9
15.00 – 15.99	3	4
16.00 – 16.99	2	8

Table 4: Observed draughts for FPSO I after discharge

Range of Draughts (m)	Number of Occurrence	
	Fwd	Aft
10.00 – 10.99	1	0
11.00 – 11.99	16	0
12.00 – 12.99	5	14
13.00 – 13.99	0	5
14.00 – 14.99	0	3
15.00 – 15.99	0	0
16.00 – 16.99	0	0

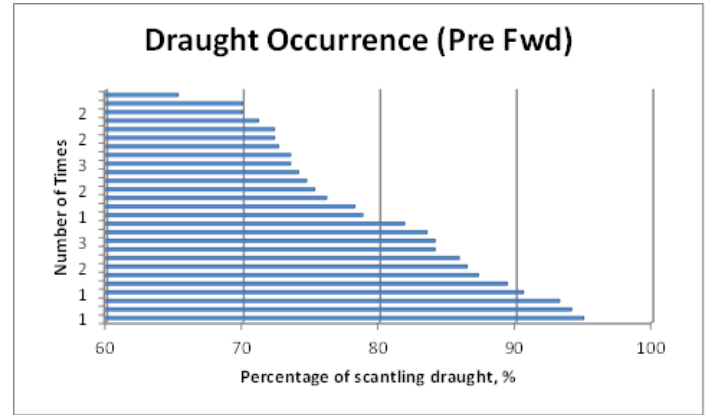


Fig. 1: Frequency of observed draughts at Fwd end for FPSO I during loading (Pre Discharge)

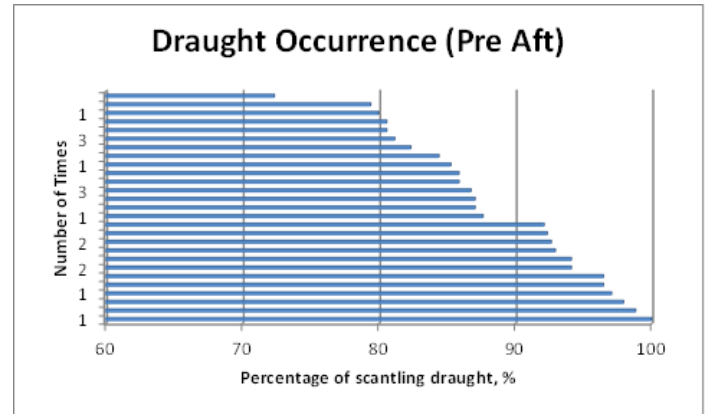


Fig. 2: Frequency of observed draughts at Aft end for FPSO I during loading (Pre Discharge)

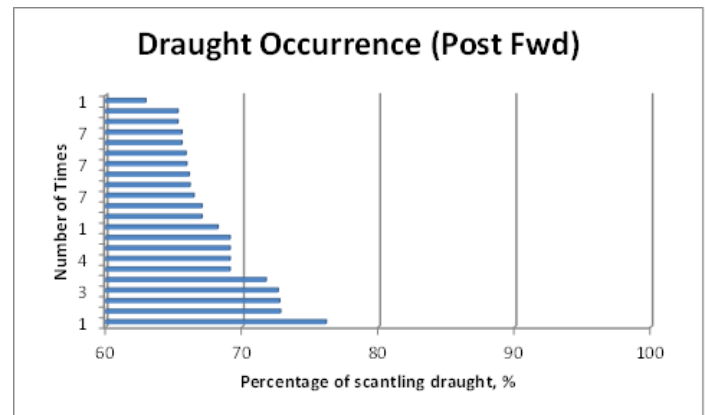


Fig. 3: Frequency of observed draughts at Fwd end for FPSO I

after offloading (Post- Discharge)

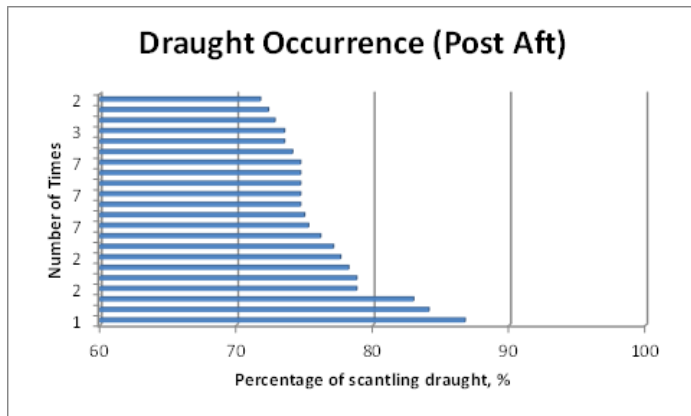


Fig. 4: Frequency of observed draughts at Aft end for FPSO I after offloading (Post- Discharge)

From Figure 1, it is clear that the minimum recorded draught of 11.1m (65.0% of scantling draught) was only recorded once as well as the maximum recorded draught of 16.15m (95.0% of scantling draught). The most repeated draughts were 12.3m and 12.35m (72% to 73% of scantling draught).

From Figure 2, it is clear that the minimum recorded draught of 12.3m (72.0% of scantling draught) was only recorded once as well as the maximum recorded draught of 17.8m (more than 100% of scantling draught). The most repeated draughts were 14.75, 14.8m, 15.66m, 15.7 and 15.75m (87.0%, 88.0%, 92.0% and 93.0% of scantling draught).

From Figure 3, it is clear that the minimum recorded draught of 10.7m (63.0% of scantling draught) was only recorded once as well as the maximum recorded draught of 12.95m (76.0% of scantling draught). The most repeated draughts were 11.1m and 11.2m (65.0% to 66.0% of scantling draught).

From Figure 4, it is clear that the minimum recorded draught of 12.2m (72.0% of scantling draught) was only recorded once as well as the maximum recorded draught of 14.75m (87.0% of scantling draught). The most repeated draughts were 12.7m and 12.75m (about 75.0% of scantling draught).

FPSO II: In (Client-Report-G 2009), Loading and offloading data such as Fwd and Aft draughts, bending moment and shear force were reviewed for a period of 21 months (about 40 loading cycles). The loading and offloading occurrence percentages for Aft and Fwd draught are presented in Table 5 as well as Figures 5 and 6.

Table 5: FPSO II Range of Draught Occurrence

Range of Draughts (m)	Number of Occurrence	
	Fwd	Aft
10.00 – 10.99	7	1
11.00 – 11.99	37	19
12.00 – 12.99	20	21
13.00 – 13.99	10	22
14.00 – 14.99	4	15

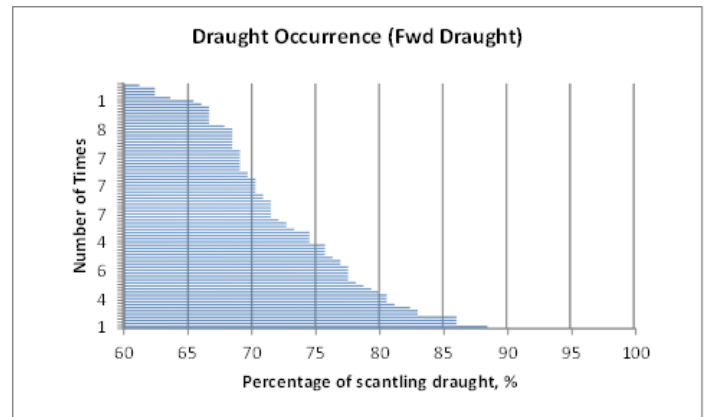


Fig. 5: Frequency of observed draughts at Fwd end for FPSO II during loading/offloading

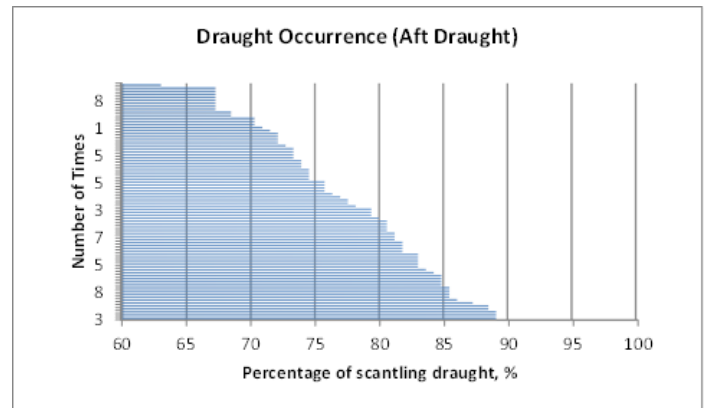


Fig. 6: Frequency of observed draughts at Aft end for FPSO II during loading/offloading

From Figure 5, it is clear that the minimum recorded draught of 10.1m (61.0% of scantling draught) was only recorded once as well as the maximum recorded draught of 14.6m (88.0% of scantling draught). The most repeated draughts were 11.3m and 11.4m (68.0% and 69.0% of scantling draught).

From Figure 6, it is clear that the minimum recorded draught of 10.4m (63.0% of scantling draught) was only recorded once; the maximum recorded draught of 14.7m (89.0% of scantling draught) was recorded three times. The most repeated draught was 11.1m (67.0% of scantling draught).

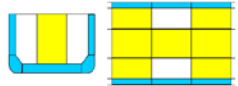
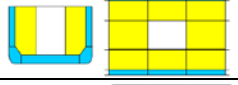




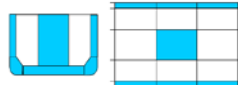
REPRESENTATIVE LOADING CONDITIONS IN CLASS SOCIETY RULES

Fatigue assessment is mandatory for design review of FPSOs according to the Rules of classification societies. The number of loading conditions in this assessment is selected on case by case basis and kept to a minimum. Normally, this number is in the range of two to seven. The typical tank loading patterns and hull draught conditions found in FPSO's Loading Manuals and Trim and Stability Booklet are five to eight representative conditions including major transportation phase(s) for the FPSO (ABS-DLA 2001).

Lloyd's Register (LR)

In (LR-Report 2007) seven loading conditions were considered as shown in Table 6, for conversion of a relatively new tanker to FPSO.

Table 6: Design Load Combinations Static & Dynamic (Sea-going load cases) (LR-Report 2007)

Loading Condition	Transverse metacentric height and Radius of Gyration	Tank Arrangements
CSR A I - Mid Side Tanks Empty (0.9 Tsc) & Ballast Tanks Full	GM 10.16m RoG 20.3m	
CSR A2 - Mid Centre Tank Empty (0.9 Tsc) & Ballast Tanks Full	GM 9.60m RoG 20.3m	
CSR A3 - Mid All Tanks Abreast Empty (0.55 Tsc)	GM 13.9m RoG 23.2m	
CSR A4 - Diagonal Mid Centre Tank Empty (0.6 Tsc) & Ballast Tanks Full	GM 8.58m RoG 21.04m	
CSR AS- Mid All Tanks Abreast Full (0.8 Tsc)	GM 9.28m RoG 20.9m	
CSR A6 - Diagonal Mid Centre Tank Full (0.6 Tsc) & Ballast Tanks Full	GM 8.58m RoG 21.04m	
CSR A7- Asym. Centre & Side Tanks Empty (Tic)	Not Applicable	
CSR AS- Heavy Ballast Condition (Thb)	GM 13.6m RoG 26.1m	

American Bureau Of Shipping (ABS-FPI 2009)

Four loading conditions may be considered for LCF assessment of FPSO with double hull or double side single bottom; these are:

1. Loading condition 1, Figure 7; 0.4 x scantling draught or actual minimum onsite operating ballast draught if greater than 0.4 x scantling draught but not to exceed 0.6 x scantling draught. This condition is also used for transit condition with actual transit draught between 0.1 x scantling draught and 0.6 x scantling draught.
2. Loading condition 2, Figure 8; 0.57 x scantling draught.
3. Loading condition 3, Figure 9; 0.73 x scantling draught.
4. Loading condition 4, Figure 10; 0.9 x scantling draught or actual maximum onsite operating full load draught if greater than 0.9 x scantling draught.

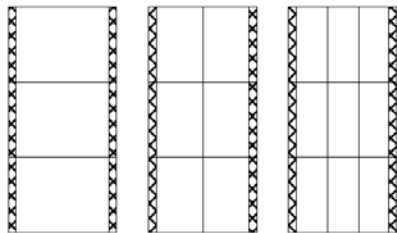


Fig. 7: Loading condition 1

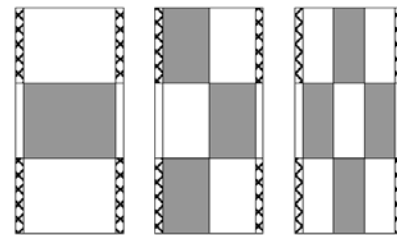


Fig. 8: Loading condition 2

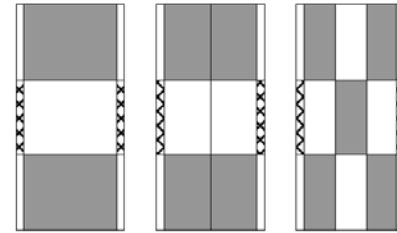


Fig. 9: Loading condition 3

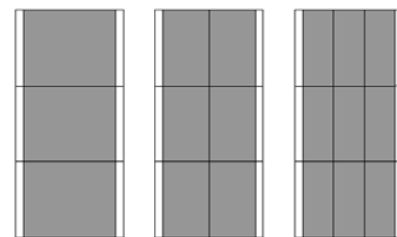


Fig. 10: Loading condition 4

Det Norske Veritas (DNV-CN-30.7 2010)

Six load conditions may be considered for low cycle fatigue assessment for vessels with one centreline bulkhead, these are:

1. Loading Condition 1, Figure 11; full load T_s , σ_{LC1} ,
2. Loading Condition 2, Figure 12; ballast T_{ball} , σ_{LC2} ,
3. Loading Condition 3, Figure 13; alternate 1, T_{act} , σ_{LC3} ,
4. Loading Condition 4, Figure 14; alternate 2, T_{act} , σ_{LC4} ,
5. Loading Condition 5, Figure 15; alternate 3, T_{act} , σ_{LC5} ,
6. Loading Condition 6, Figure 16; alternate 4, T_{act} , σ_{LC6} ,

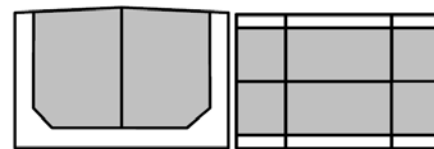


Fig. 11: Loading Condition 1

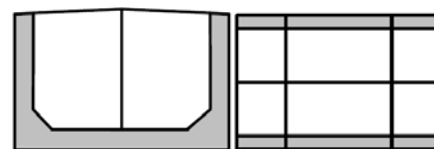


Fig. 12: Loading Condition 2

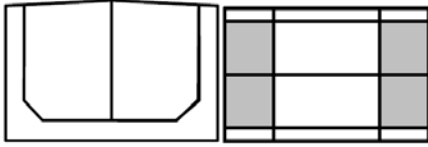


Fig. 13: Loading Condition 3

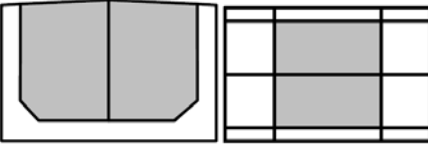


Fig. 14: Loading Condition 4

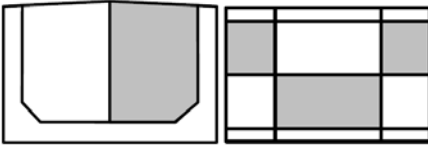


Fig. 15: Loading Condition 5

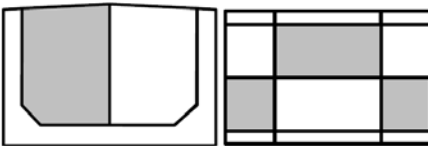


Fig. 16: Loading Condition 6

Six load conditions may be considered for low cycle fatigue assessment for the vessel with two longitudinal bulkheads, these are:

1. Loading Condition 7, Figure 17; full load T_s , σ_{LC7} ,
2. Loading Condition 8, Figure 18; ballast T_{ball} , σ_{LC8} ,
3. Loading Condition 9, Figure 19; T_{act} , σ_{LC9} ,
4. Loading Condition 10, Figure 20; T_{act} , σ_{LC10} ,
5. Loading Condition 11, Figure 21; T_{act} , σ_{LC11} ,
6. Loading Condition 12, Figure 22; T_{act} , σ_{LC12} ,

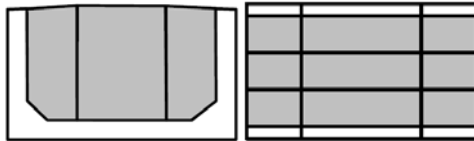


Fig. 17: Loading Condition 7

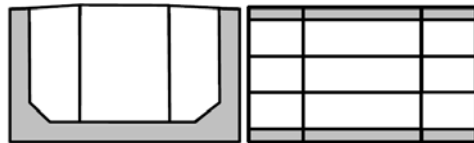


Fig. 18: Loading Condition 8

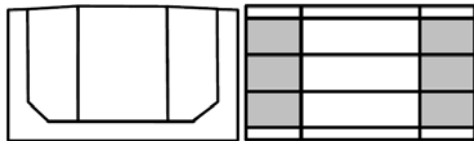


Fig. 19: Loading Condition 9

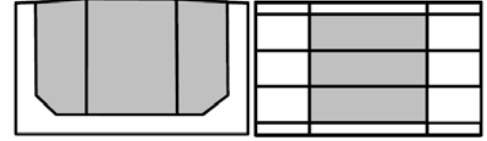


Fig. 20: Loading Condition 10

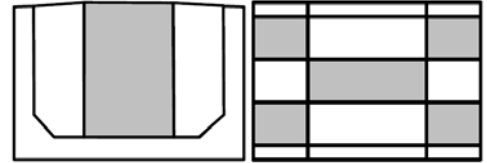


Fig. 21: Loading Condition 11

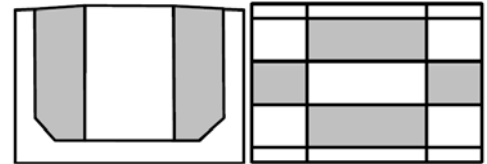


Fig. 22: Loading Condition 12

Four load conditions may be considered for low cycle fatigue for vessels without longitudinal bulkhead, these are:

1. Loading Condition 13, Figure 23; full load T_s , σ_{LC13} ,
2. Loading Condition 14, Figure 24; ballast T_{ball} , σ_{LC14} ,
3. Loading Condition 15, Figure 25; T_{act} , σ_{LC15} ,
4. Loading Condition 16, Figure 26; T_{act} , σ_{LC16} ,

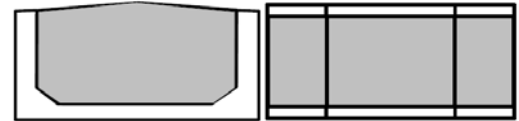


Fig. 23: Loading Condition 13



Fig. 24: Loading Condition 14



Fig. 25: Loading Condition 15

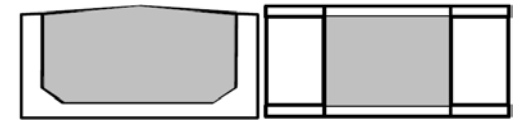


Fig. 26: Loading Condition 16

Bureau Veritas (BV-PART-D-CH1-SEC7 2007)

For on-site condition, four loading conditions are specified for units fitted with one central longitudinal bulkhead and three are specified for units fitted with two central longitudinal bulkheads. These are:

1. Loading condition 1, Figure 27 and Figure 28; minimum draught T_{mini} ,

2. Loading condition 2, Figure 29 and Figure 30; 0.75 x scantling draught,
3. Loading condition 3, Figure 31; 0.9 x scantling draught (not considered for units fitted with two central longitudinal bulkhead,
4. Loading condition 4, Figure 32 and Figure 33; maximum draught T.

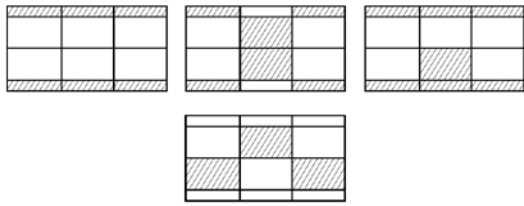


Fig. 27: Loading condition 1 for one Centerline longitudinal bulkhead

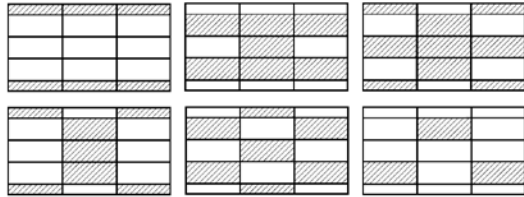


Fig. 28: Loading condition 1 for two Centerline longitudinal bulkheads

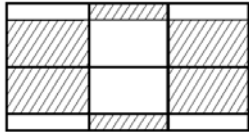


Fig. 29: Loading condition 2 for one Centerline longitudinal bulkhead

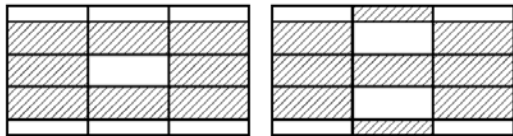


Fig. 30: Loading condition 2 for two Centerline longitudinal bulkheads

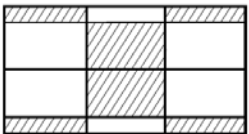


Fig. 31: Loading condition 3 for one Centerline longitudinal bulkhead

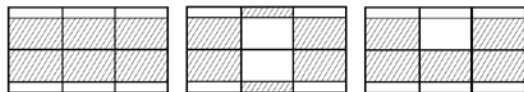


Fig. 32: Loading condition 4 for one Centerline longitudinal bulkhead

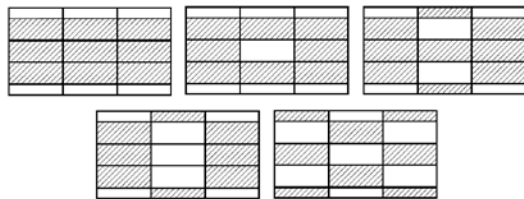


Fig. 33: Loading condition 4 for two Centerline longitudinal bulkheads

SUMMARY OF OPERATIONAL (HULL) LOADING

CONDITIONS CONSIDERED FOR LCF ACCORDING TO CLASS SOCIETIES

The common representative loading conditions recommended by class societies for FPSOs are as follows:

1. Ballast condition; this is considered the minimum draught condition where all cargo tanks are empty. ABS considers 0.4 times the scantling draught (ABS-FPI 2009). DNV considers 0.35 times the scantling draught.
2. Full load condition at scantling draught or before offloading where all tanks are full. ABS considers more than 0.9 times the scantling draught (ABS-FPI 2009).
3. Intermediate loading:
For the selection of the intermediate loading case(s). Different class societies have different recommendations for intermediate loading; ABS considers 3 load cases, DNV considers 4 load cases, BV considers 4 load cases and LR considers 2 to 7 load cases but only the most representative are mentioned as follows:
 - a. loading condition at 90% of maximum draught (BV)
 - b. loading condition at 75% of maximum draught (BV)
 - c. 0.73*Scantling Draught (ABS-FPI 2009)
 - d. where tanks are 50% filled (LR and ABS)
 - e. 0.57*Scantling Draught (ABS-FPI 2009)

SUMMARY OF OPERATIONAL (HULL) LOADING CONDITIONS ACCORDING TO CASE STUDY

It is clear that the minimum draught condition considered by class societies is not the case in the investigated two FPSOs where minimum draught was always not less than 61.0% of scantling draught. However, it is important to note that contribution of intermediate loading condition in the calculation of fatigue damage is significantly more than those of the ballast and full loading conditions. ABS (ABS-FPI, 2009) recommends contributions of 15%, 35%, 35% and 15% to the fatigue damage for ballast, two intermediate and full loading conditions respectively.

CONCLUSION

The number of recommended loading conditions to be considered for LCF assessment of an FPSO should be at least four loading conditions. These are:

1. Ballast condition at 10% of operation
2. Full load condition at 10% of operation
3. Loading condition at the most frequent draught below 50% at 40% of operation
4. Loading condition at the most frequent draught above 50% at 40% of operation

REFERENCES

- ABS-DLA (2001). "Guidance Notes on Safehull-Dynamic Loading Approach for FPSO Systems."
- ABS-FPI (2009). "Floating production installations." ABS - Guide Notes Part 5A, Ch. 3 and Appendix 2.
- ABS-SFA (2002). "Guidance Notes on Spectral-based Fatigue Analysis for Floating Production, Storage and Offloading (FPSO) System."

BV-Part-D-Ch1-Sec7 (2007). "HULL SCANTLINGS."

Client-Report-G3 (2002). "FPSO Stability Manual."

Client-Report-G (2009). "FPSO Cargo Offload Operations."

DNV-CN-30.7 (2010). "FATIGUE ASSESSMENT OF SHIP STRUCTURES."

Hwang, O., et al. (2007). Spectral Fatigue Assessment of AGBAMI FPSO hull for Onsite and Seagoing as per ABS's SFA Guidance. 26th International Conference on Offshore Mechanics and Arctic Engineering, San Diego, California, USA.

Kaminski, M. L. (2007). Sensing and Understanding Fatigue Lifetime of New and Converted FPSOs. Offshore Technology Conference. Houston, Texas, U.S.A.

LR-Report (2003). "Ship-Type FPSO Hull Structural Appraisal."

LR-Report (2007). "Anonymous FPSO Hull Strength Assessment for FPSO Specific Loading Conditions".

LR-Report (2008). "FDA2 Fatigue Assessment of the FPSO " Anonymous ".

LR-Report (2009). "Anonymous Structural Life Extension Study."

Raji, H., et al. (2009). Low cycle fatigue assessment of an FPSO. 1st International Conference Integrating Structural Analysis, Risk and Reliability. Glasgow.

Lloyd's Register and variants of it are trading names of Lloyd's Register Group Limited, its subsidiaries and affiliates. Copyright © Lloyd's Register Group Limited. 2014. A member of the Lloyd's Register group.

Lloyd's Register Group Limited, its subsidiaries and affiliates and their respective officers, employees or agents are, individually and collectively, referred to in this clause as 'Lloyd's Register'. Lloyd's Register assumes no responsibility and shall not be liable to any person for any loss, damage or expense caused by reliance on the information or advice in this document or howsoever provided, unless that person has signed a contract with the relevant Lloyd's Register entity for the provision of this information or advice and in that case any responsibility or liability is exclusively on the terms and conditions set out in that contract.